REPORT DOCUMENTATION PAGE

Form Approved OMB NO. 0704-0188

1. REPORT DATE (DD-MM-YYYY)	2. REPORT TYPE	3. DATES COVERED (From - To)
04-02-2015	Final Report	16-Sep-2011 - 15-Sep-2014

4. TITLE AND SUBTITLE

A New Mathematical and Computational Framework for BVPs and IVPs in Solids, Fluids, Gases and their Interactions

5a. CONTRACT NUMBER
W911NF-11-1-0471

5b. GRANT NUMBER

5c. PROGRAM ELEMENT NUMBER
611102

6. AUTHORS

K. S. Surana, J. N. Reddy, D. Nunez

5d. PROJECT NUMBER

5e. TASK NUMBER

5f. WORK UNIT NUMBER

7. PERFORMING ORGANIZATION NAMES AND ADDRESSES

University of Kansas
2385 Irving Hill Road

Lawrence, KS 66044 -7552

8. PERFORMING ORGANIZATION REPORT NUMBER

9. SPONSORING/MONITORING AGENCY NAME(S) AND ADDRESS (ES)

U.S. Army Research Office
P.O. Box 12211
Research Triangle Park, NC 27709-2211

10. SPONSOR/MONITOR'S ACRONYM(S)
ARO

11. SPONSOR/MONITOR'S REPORT NUMBER(S)
56445-MA.27

12. DISTRIBUTION AVAILIBILITY STATEMENT

Approved for Public Release; Distribution Unlimited

13. SUPPLEMENTARY NOTES

The views, opinions and/or findings contained in this report are those of the author(s) and should not contrued as an official Department of the Army position, policy or decision, unless so designated by other documentation.

14. ABSTRACT

During this three year time period of the grant, five major areas listed under I-V have been investigated. Summary and conclusions resulting from this research, its impact and significance have been described at the end of each section in italics. Comments and in some cases, preliminary details, are also provided for future research. In each of the five major areas of research, model problems and their numerical solutions are presented to illustrate the features of the mathematical models and their applications. Computational mathematics frame for obtaining numerical solutions of the BVPs and IVPs in these areas is based on hpk finite element method with variationally

15. SUBJECT TERMS

Fluid-solid interaction, Mathematical model, Lagrangian, Eulerian, Least-squares processes, Ordered rate constitutive theories, Phase transition

16. SECURITY CLASSIFICATION OF:			17. LIMITATION OF ABSTRACT	15. NUMBER OF PAGES	19a. NAME OF RESPONSIBLE PERSON
a. REPORT	b. ABSTRACT	c. THIS PAGE			Karan Surana
UU	UU	UU	UU		19b. TELEPHONE NUMBER: 785-864-2988

Report Title

A New Mathematical and Computational Framework for BVPs and IVPs in Solids, Fluids, Gases and their Interactions

ABSTRACT

During this three year time period of the grant, five major areas listed under I-V have been investigated. Summary and conclusions resulting from this research, its impact and significance have been described at the end of each section in italics. Comments and in some cases, preliminary details, are also provided for future research. In each of the five major areas of research, model problems and their numerical solutions are presented to illustrate the features of the mathematical models and their applications. Computational mathematics frame for obtaining numerical solutions of the BVPs and IVPs in these areas is based on hpk finite element method with variationally consistent integral forms in which the space or space-time local approximations are in scalar product spaces. These spaces permit higher order global differentiability local approximations that are necessary to ensure integrals over the discretizations in the Riemann sense, so that when the integrated sum of squares of the residuals approaches zero for the whole discretization we are ensured that the GDEs are satisfied in the pointwise sense. Variationally consistent integral forms (in space or space-time) yield unconditionally stable computational processes for all BVPs and IVPs.

Enter List of papers submitted or published that acknowledge ARO support from the start of the project to the date of this printing. List the papers, including journal references, in the following categories:

(a) Papers published in peer-reviewed journals (N/A for none)

Received	Paper
02/04/2015 21.00	K. S. Surana, B. Blackwell, M. Powell, J. N. Reddy. Mathematical Models for Fluid-Solid Interaction and their Numerical Solutions, Journal of Fluids and Structures, Journal of Fluids and Structures, (10 2014): 184. doi:
02/04/2015 26.00	Karan Surana, J.N. Reddy, Daniel Nunez. Ordered Rate Constitutive Theories for Thermoviscoelastic Solids with Memory in Lagrangian Description using Gibbs Potential, Continuum Mechanics and Thermodynamics, (02 2015): 0. doi:
02/04/2015 25.00	Karan Surana, J.N. Reddy, Daniel Nunez. Ordered Rate Constitutive Theories for Thermoviscoelastic Solids without Memory in Lagrangian Description using Gibbs Potential, Continuum Mechanics and Thermodynamics, (03 2015): 0. doi:
02/04/2015 24.00	Karan Surana, T. Moody, J.N. Reddy. Ordered Rate Constitutive Theories in Lagrangian Description for Thermoviscoelastic Solids with Memory, Acta Mechanica, (01 2015): 157. doi:
02/04/2015 22.00	Karan Surana, K.P.J. Reddy, Aaron Joy, J.N. Reddy. Riemann Shock Tube: 1D Normal Shocks in Air, Simulation and Experiments, International Journal of Computational Fluid Dynamics, (10 2014): 251. doi:
02/04/2015 23.00	Karan Surana, A.D. Joy, L.A. Quiros, J.N. Reddy. Mathematical Models and Numerical Solutions of Liquid-Solid and Solid-Liquid Phase Change, Journal of Thermal Engineering, (01 2015): 61. doi:
08/26/2014 13.00	K. S. Surana, B. Blackwell, M. Powell, J. N. Reddy. Mathematical Models for Fluid-Solid Interaction and Their Numerical Solutions, Journal of Fluids and Structures, (09 2014): 0. doi:
08/26/2014 14.00	K.S. Surana, K.P.J. Reddy, A.D. Joy, J.N. Reddy. Riemann shock tube: 1D normal shocks in air, simulations and experiments, International Journal of Computational Fluid Dynamics, (04 2014): 0. doi:
08/26/2014 15.00	K.S. Surana, A.D. Joy, L.A. Quiros, J.N. Reddy. Mathematical models and numerical solutions of liquid-solid and solid-liquid phase change, Journal of Thermal Engineering, (10 2014): 0. doi:
08/26/2014 16.00	K.S. Surana, T. Moody, J.N. Reddy. Ordered rate constitutive theories in Lagrangian description for thermoviscoelastic solids with memory, Acta Mechanica, (06 2014): 0. doi:
08/26/2014 18.00	K.S. Surana, Daniel Nunez, J.N. Reddy. Giesekus Constitutive Model for Thermoviscoelastic Fluids based on Ordered Rate Constitutive Theories, Journal of Research Updates in Polymer Science, (12 2013): 232. doi:
08/26/2014 19.00	K. S. Surana, J. N. Reddy, D. Nunez. Ordered rate constitutive theories for thermoviscoelastic solids without memory in Lagrangian description using Gibbs potential, Continuum Mechanics and Thermodynamics, (06 2014): 0. doi: 10.1007/s00161-014-0366-5

08/27/2013 1.00 K. S. Surana, M. Powell, J. N. Reddy. A simple mixture theory for v Newtonian and generalized Newtonian constituents,
Continuum Mechanics and Thermodynamics, (12 2012): 0. doi: 10.1007/s00161-012-0274-5

08/27/2013 2.00 K. S. Surana, T. Moody, J. N. Reddy. Ordered rate constitutive theories in Lagrangian description for thermoviscoelastic solids without memory,
Acta Mechanica, (06 2013): 0. doi: 10.1007/s00707-013-0893-3

08/27/2013 3.00 K. S. Surana, Y. Mendoza, J. N. Reddy. Constitutive theories for thermoelastic solids in Lagrangian description using Gibbs potential,
Acta Mechanica, (01 2013): 0. doi: 10.1007/s00707-012-0805-y

08/27/2013 4.00 K.S. Surana, T. Moody, J.N. Reddy. Ordered Rate Constitutive Theories of Order Zero in Lagrangian Description for Thermoelastic Solids,
Mechanics of Advanced Materials and Structures, (2013): 0. doi:

08/27/2013 7.00 K.S. Surana, T. Moddy, J.N. Reddy. Ordered Rate Constitutive Theories in Lagrangian Description for Thermoviscoelastic Solids with Memory,
Acta Mechanica, (08 2013): 0. doi:

TOTAL: **17**

Number of Papers published in peer-reviewed journals:

(b) Papers published in non-peer-reviewed journals (N/A for none)

Received Paper

TOTAL:

Number of Papers published in non peer-reviewed journals:

(c) Presentations

Number of Presentations: 0.00

Non Peer-Reviewed Conference Proceeding publications (other than abstracts):

Received Paper

TOTAL:

Number of Non Peer-Reviewed Conference Proceeding publications (other than abstracts):

Peer-Reviewed Conference Proceeding publications (other than abstracts):

Received	Paper

TOTAL:

Number of Peer-Reviewed Conference Proceeding publications (other than abstracts):

(d) Manuscripts

Received	Paper
08/26/2014 17.00	K.S. Surana, Daniel Nunez, J.N. Reddy. First and Second Laws of Thermodynamics and Constitutive Theories for Thermoelastic Solids, Annals of Solids and structural mechanics (06 2014)
08/26/2014 20.00	K.S. Surana, J.N. Reddy, Daniel Nunez. Ordered rate constitutive theories for Thermoviscoelastic Solids with Memory in Lagrangian Description using Gibbs Potential, Continuum Mechanics and Thermodynamics (06 2014)
TOTAL:	**2**

Number of Manuscripts:

Books

Received	Book

TOTAL:

Received	Book Chapter

TOTAL:

Patents Submitted

Patents Awarded

Awards

Graduate Students

NAME	PERCENT_SUPPORTED	Discipline
Stone, Tyler	0.50	
Mysore, Dhaval	0.00	
Mohammadi, Fariba	0.00	
Sepehri, Shilan	0.00	
Knight, Jason	0.00	
Yang, Shin	0.00	
Kedari, Sayali	0.00	
Khadka, Dipin	0.00	
Long, Stephen	0.00	
Mule, Pateek Reddy	0.00	
Selvaraj, Deeptesh	0.00	
Shanbhag, Rajat Ramdas	0.00	
Powel, Michael	0.00	
FTE Equivalent:	**0.50**	
Total Number:	**13**	

Names of Post Doctorates

NAME	PERCENT_SUPPORTED
Daniel Nunez	1.00
FTE Equivalent:	**1.00**
Total Number:	**1**

Names of Faculty Supported

NAME	PERCENT_SUPPORTED

FTE Equivalent:
Total Number:

Names of Under Graduate students supported

NAME	PERCENT_SUPPORTED

FTE Equivalent:
Total Number:

Student Metrics

This section only applies to graduating undergraduates supported by this agreement in this reporting period

The number of undergraduates funded by this agreement who graduated during this period: 0.00

The number of undergraduates funded by this agreement who graduated during this period with a degree in science, mathematics, engineering, or technology fields:..... 0.00

The number of undergraduates funded by your agreement who graduated during this period and will continue to pursue a graduate or Ph.D. degree in science, mathematics, engineering, or technology fields:..... 0.00

Number of graduating undergraduates who achieved a 3.5 GPA to 4.0 (4.0 max scale):..... 0.00

Number of graduating undergraduates funded by a DoD funded Center of Excellence grant for Education, Research and Engineering:..... 0.00

The number of undergraduates funded by your agreement who graduated during this period and intend to work for the Department of Defense 0.00

The number of undergraduates funded by your agreement who graduated during this period and will receive scholarships or fellowships for further studies in science, mathematics, engineering or technology fields: 0.00

Names of Personnel receiving masters degrees

NAME

Total Number:

Names of personnel receiving PHDs

NAME

Total Number:

Names of other research staff

NAME	PERCENT_SUPPORTED

FTE Equivalent:
Total Number:

Sub Contractors (DD882)

Inventions (DD882)

Scientific Progress

please see attached pdf document

Technology Transfer

N/A

REPORT DOCUMENTATION PAGE

Form Approved
OMB No. 0704-0188

1. REPORT DATE *(DD-MM-YYYY)*	2. REPORT TYPE	3. DATES COVERED *(From - To)*
04-02-2015	Final Progress Report	Sept. 2011 - Sept. 2014 ; Feb. 2015

4. TITLE AND SUBTITLE

A new mathematical and computational framework for BVPs and IVPs for solids, liquids and gases and their interactions

5a. CONTRACT NUMBER

5b. GRANT NUMBER

W-911NF-11-1-0471 ; FED0061541

5c. PROGRAM ELEMENT NUMBER

---

6. AUTHOR(S)

Surana, Karan, S.

Reddy, Junuthula, N.

Nunez, Daniel, S.

5d. PROJECT NUMBER

5e. TASK NUMBER

5f. WORK UNIT NUMBER

---

7. PERFORMING ORGANIZATION NAME(S) AND ADDRESS(ES)

The University of kansas, Department of Mechanical Engineering, Lawrence, KS, 66046, USA
Texas A&M University, Department of Mechanical Engineering, College Station, TX, 77843, USA

8. PERFORMING ORGANIZATION REPORT NUMBER

---

9. SPONSORING/MONITORING AGENCY NAME(S) AND ADDRESS(ES)

---

10. SPONSOR/MONITOR'S ACRONYM(S)

ARO

11. SPONSOR/MONITOR'S REPORT NUMBER(S)

---

12. DISTRIBUTION/AVAILABILITY STATEMENT

---

13. SUPPLEMENTARY NOTES

---

14. ABSTRACT

During this three year time period of the grant, five major areas listed under I--V have been investigated. Summary and conclusions resulting from this research, its impact and significance have been described at the end of each section in italics. Comments and in some cases, preliminary details, are also provided for future research. In each of the five major areas of research, model problems and their numerical solutions are presented to illustrate the features of the mathematical models and their applications. Computational mathematics frame for obtaining numerical solutions of the BVPs and IVPs in these areas is based on hpk finite element method with variationally consistent integral forms in which the space or space-time local approximations are in scalar product spaces. These spaces permit higher order global differentiability local approximations that are necessary to ensure integrals over the discretizations in the Riemann sense, so that when the integrated sum of squares of the residuals approaches zero for the whole discretization we are ensured that the GDEs are satisfied in the pointwise sense. Variationally consistent integral forms (in space or space-time) yield unconditionally stable computational processes for all BVPs and IVPs.

15. SUBJECT TERMS

Fluid-solid interaction, Mathematical model, Lagrangian, Eulerian, Least-squares processes, Ordered rate constitutive theories, liquid-solid, solid-liquid, phase change, space-time methods, time marching, shock tube, 1D normal shock, Reddy tube, shock evolution, Riemann shock tube

16. SECURITY CLASSIFICATION OF:			17. LIMITATION OF ABSTRACT	18. NUMBER OF PAGES	19a. NAME OF RESPONSIBLE PERSON
a. REPORT	b. ABSTRACT	c. THIS PAGE			Prof. Karan S. Surana
U	U	U	UU	214	19b. TELEPHONE NUMBER *(Include area code)* 785-864-2988

Publications under ARO sponsorship during this reporting period:

(a) Papers published in peer-reviewed journals:

1. K. S. Surana, B. Blackwell, M. Powell and J. N. Reddy, *Mathematical Models for Fluid-Solid Interaction and their Numerical Solutions*, Journal of Fluids and Structures, Vol. 50, pp. 184-216, 2014.
2. K. S. Surana, K. P. J. Reddy, A. Joy and J. N. Reddy, *Riemann Shock Tube: 1D Normal Shocks in Air, Simulation and Experiments*, International Journal of Computational Fluid Dynamics, Vol. 28(6-10), pp. 251-271, 2014.
3. K. S. Surana, A. D. Joy, L. A. Quiros and J. N. Reddy, *Mathematical Models and Numerical Solutions of Liquid-Solid and Solid-Liquid Phase Change*, Journal of Thermal Engineering, Vol. 1(2), pp. 61-98, 2015.
4. K. S. Surana, T. Moody and J. N. Reddy, *Ordered Rate Constitutive Theories in Lagrangian Description for Thermoviscoelastic Solids with Memory*, Acta Mechanica, Vol., pp. N/A yet, (already published online) DOI: 10.1007/s00707-014-1173-6
5. K. S. Surana, J. N. Reddy and D. Nunez, *Ordered Rate Constitutive Theories for Thermoviscoelastic Solids without Memory in Lagrangian Description using Gibbs Potential*, Journal of Continuum Mechanics and Thermodynamics, Vol., pp. N/A yet, (already published online) DOI: 10.1007/s00161-014-0366-5
6. K. S. Surana, J. N. Reddy and D. Nunez, *Ordered Rate Constitutive Theories for Thermoviscoelastic Solids with Memory in Lagrangian Description using Gibbs Potential*, Journal of Continuum Mechanics and Thermodynamics, Vol., pp. N/A yet, (already published online) DOI: 10.1007/s00161-014-0395-0

Papers under review in peer-reviewed journals:

K. S. Surana, D. Nunez and J. N. Reddy, *First and Second Laws of Thermodynamics and Constitutive Theories for Thermoelastic Solids*, Annals of Solids and Structural Mechanics (under review, 2015).

(b) Papers published in non-peer-reviewed journals: Not applicable

(c) Presentations: Not applicable

(d) Manuscripts: Not applicable

(e) Books:

K. S. Surana, *Advanced Mechanics of Continua*, Taylor & Francis - CRC Press, 2014

(f) Honor and awards: Not applicable

(g) Title of patents disclosed during the reporting period: Not applicable

(h) Patents awarded during the reporting period: Not applicable

Student/personnel metrics for this reporting period:

(a) Graduate students:

	Students supervised	Degree	% FTE	
1.	Stone, Tyler	Ph.D.	50%	
2.	Mysore, Dhaval	Ph.D.	–	
3.	Mohammadi, Fariba	Ph.D.	–	
4.	Sepehri, Shilan	M.S.	–	
5.	Knight, Jason	M.S.	–	
6.	Yang, Shin	M.S.	–	
7.	Kedari, Sayali	M.S.	–	
8.	Khadka, Dipin	M.S.	–	
9.	Long, Stephen	M.S.	–	
10.	Mule, Pateek Reddy	M.S.	–	
11.	Selvaraj, Deeptesh	M.S.	–	
12.	Shanbhag, Rajat Ramdas	M.S.	–	
13.	Powell, Michael	Ph.D.	50%	Texas A&M, College Station Prof. J. N. Reddy, Advisor

(b) Post doctorates: Nunez, Daniel

(c) Faculty: Not applicable

(d) Undergraduate students: Not applicable

(e) Graduating undergraduate metrics: Not applicable

(f) Master degrees awarded: Not Applicable

(g) Ph.D. degrees awarded: Not Applicable

(h) Other research staff: Not applicable

Technology transfer: Not applicable

Scientific progress and accomplishments:

A New Mathematical and Computational Framework for BVPs and IVPs for Solids, Liquids and Gases and their Interactions

Final Report

Under the Grant number: W-911NF-11-1-0471(FED0061541)
PI: Karan S. Surana, *The University of Kansas*
Co-PI: J. N. Reddy, *Texas A&M University*

Abstract

In the three year duration of the research grant, the research has been concentrated in five major areas:

(I) Ordered rate constitutive theories in Lagrangian description

(II) Mathematical models and their numerical solutions for fluid-solid interaction

(III) Mathematical models and their numerical solutions for solid-liquid and liquid-solid phase transition

(IV) A mixture theory for ν component incompressible fluids

(V) 1D normal shocks (Riemann shock tube): numerical simulations and comparisons with experiments

(I) Ordered rate constitutive theories in Lagrangian description: Ordered rate constitutive theories in Lagrangian description for thermoelastic solids, thermoviscoelastic solids without memory and thermoviscoelastic solids with memory using entropy inequality expressed in terms of Helmholtz free energy density Φ as well as Gibbs potential Ψ for isotropic, homogeneous, compressible as well as incompressible solid matter experiencing finite deformation and finite strains have been derived. In case of thermoelastic solids, the first and second law of thermodynamics are derived from fundamental principles in which the mechanical work does not result in rate of entropy production and hence cannot influence entropy. For such matter, the resulting entropy inequality provides no mechanism to derive constitutive theories for the stress tensor. The research work during this grant presents a number of alternatives, the associated constitutive theories, their usefulness and limitations. The constitutive theories for the stress tensor as well as heat vector are presented for thermoelastic solids. The ordered rate constitutive theories for thermoviscoelastic solids (for stress tensor and heat vector) with and without memory are derived using entropy inequality expressed in terms of Φ and Ψ in conjunction with the theory of generators and invariants. Although the two forms of the entropy inequality using Φ and Ψ are precisely equivalent, their equivalence may or may not exist in the constitutive theories resulting from these two approaches. This report presents developments and derivations of ordered rate constitutive theories in Lagrangian description for solid matter for homogeneous, isotropic, compressible and incompressible: (i) thermoelastic solids (ii) thermoviscoelastic solids without memory and (iii) thermoviscoelastic solid matter with memory experiencing finite deformation. To ensure thermodynamics equilibrium in the deforming solid matter, the rate constitutive theories are derived using the second law of thermodynamics i.e. entropy inequality derived and expressed (a) using Helmholtz free energy density Φ and (b) using Gibbs potential Ψ. This research work provides a consistent and rigorous continuum mechanics framework for the derivations of broad range of constitutive theories that enable varied physics in the mathematical models for finite deformation of solid matter. Comparisons with currently used constitutive theories explain and illustrate (1) various assumptions employed in their derivations and their severe limitations for finite deformation (2) total lack of continuum mechanics foundation in many cases. The ordered rate constitutive theories derived here, when incorporated with the conservation and balance laws, result in mathematical models that ensure thermodynamic equilibrium during the entire evolution and allow us to incorporate complex material behaviors in the mathematical models. In high temperature applications, melting and subsequent solidification may occur in solids. In such cases, mathematical models for the transition zone, a mixture of solid and liquid, is critical. Use of mixture theory based on continuum mechanics principles and thermodynamics is being investigated. Preliminary work for mixture theory for Newtonian and generalized Newtonian fluids is quite promising and is being extended for solid-liquid mixtures.

(II) Mathematical models and their numerical solutions for fluid-solid interaction: The second area of research during this grant considers development of mathematical models and possibility of obtaining their numerical solutions for fluid-solid interaction (FSI) processes. A number of alternate mathematical models are derived using conservation and balance laws in Lagrangian and Eulerian descriptions including currently used ALE (Arbitrary Lagrangian Eulerian) approach to demonstrate that ALE methodologies do not permit discretized solid and fluid domains to coexists and interact with each other during the solution process. This is primarily due to the fact that solids employ Lagrangian description in which displacements of material points are intrinsic in the mathematical models. In case of fluids, we monitor the evolving state of the fluid at fixed locations, hence displacements of the material points are not measured. The development of conservation and balance laws follows based on velocities at each fixed location that corresponds to different material points during the evolution. Thus, for fluids in the current thermodynamic framework, displacements are not available and also cannot be obtained using velocities at fixed locations as these are velocities of different material points during the evolution. Thus, we realize that mathematical description for fluids are not Eulerian as for a true Eulerian description, its counter part, Lagrangian description, exists. Mathematical description for fluids over a fixed grid suggests that this grid should not be moved, otherwise the validity of the associated mathematical descriptions may be in question. In summary, the mathematical description for solids and fluids are two entirely different mathematical models with nothing in common. When the mathematical models for fluids and solids are derived using same dependent variables, same physics and the same description, their interaction is transparent as it is intrinsic in the mathematical description. In the present work we show that in the case of hypo-elastic solids and fluids (like polymers), the mathematical models are based on same dependent variables and hence exactly same basis for their derivations, hence permit interaction and computations using discretizations for both solid and fluid with transparent interaction at the common boundary. It is shown that presently used ALE methodologies for FSI have no continuum mechanics basis and hence produce results in the numerical simulations that are not solutions of the associated mathematical models.

(III) Mathematical models and their numerical solutions for solid-liquid and liquid-solid phase transition: In the third area of research we consider development of mathematical models in Lagrangian and Eulerian description and their numerical simulation for solid-liquid and liquid-solid phase transition processes. The mathematical models are derived by assuming a smooth interface or transition region between the solid and liquid phases in which the specific heat, density, thermal conductivity, and latent heat of fusion are continuous and differentiable functions of temperature. In the derivations of the mathematical models we assume the matter to be homogeneous, isotropic, and incompressible in all phases. The change in volume due to change in density during phase transition is neglected in all mathematical models considered. This research describes various approaches of deriving mathematical models that incorporate phase transition physics in various ways, hence results in different mathematical models. In the present work we only consider the following two types of mathematical models: (i) We assume the velocity field to be zero i.e. no flow assumption, and free boundaries i.e. zero stress field in all phases. Under these assumptions the mathematical models reduce to first law of thermodynamics i.e. the energy equation, a nonlinear diffusion equation in temperature if we assume Fourier heat conduction law relating temperature gradient to the heat vector. These mathematical models are invariant of the type of description i.e. Lagrangian or Eulerian due to absence of velocities and stress field. (ii) The second class of mathematical models are derived with the assumption that stress field and velocity field are nonzero in the fluid region but in the solid region stress field is assumed constant and the velocity field is assumed zero. In the transition region the stress field and the velocity field transition in a continuous and differentiable manner from nonzero at the liquid state to constant and zero in the solid state based on temperature in the transition zone. Both of these models are consistent with the principles of continuum mechanics, hence provide correct interaction between the regions and are shown to work well in the numerical simulations of phase transition applications with flow. Details of other mathematical models, problems associated with them, and their limitations are also discussed. Numerical solutions of phase transition model problems in $\mathbb{R}^1$ and $\mathbb{R}^2$ are presented using these two types of mathematical models. Numerical solutions are obtained using h, p, k space-time finite element processes based on residual functional for an increment of time with time marching in which variationally consistent space-time integral forms ensure unconditionally stable computations during the entire evolution.

(IV) A mixture theory for ν component incompressible fluids: The fourth area of research consists of development of mixture theory for ν constituent incompressible fluids. Development of mathematical models based on conservation laws for a saturated mixture of ν homogeneous, isotropic, and incompressible constituents for isothermal flows. The constituents and the mixture are assumed to be Newtonian or generalized Newtonian fluids. Power law and Carreau-Yasuda models are considered for generalized Newtonian shear thinning fluids. The mathematical model is derived for a ν constituent mixture with volume fractions ϕ_α using principles of continuum mechanics: conservation of mass, balance of momenta, first and second laws of thermodynamics, and principles of mixture theory yielding continuity equations, momentum equations, energy equation, and constitutive theories for mechanical pressures and deviatoric Cauchy stress tensors in terms of the dependent variables related to the constituents. It is shown that for Newtonian fluids with constant transport properties, the mathematical models for constituents are decoupled. In this case one could use individual constituent models to obtain constituent deformation fields, and then use mixture theory to obtain the deformation field for the mixture. In the case of generalized Newtonian fluids, the dependence of viscosities on deformation field does not permit decoupling. Numerical studies are also presented to demonstrate this aspect. Using fully developed flow of Newtonian and generalized Newtonian fluids between parallel plates as a model problem, it is shown that partial pressures p_α of the constituents must be expressed in terms of the mixture pressure p. In this work we propose $p_\alpha = \phi_\alpha p$ and $\sum_\alpha^\nu p_\alpha = p$ which implies $\sum_\alpha^\nu \phi_\alpha = 1$ which obviously holds. This rule for partial pressure is shown to be valid for a mixture of Newtonian and generalized Newtonian constituents yielding Newtonian and generalized Newtonian mixture. Modifications of the currently used constitutive theories for deviatoric Cauchy stress tensor are proposed. These modifications are demonstrated to be essential in order for the mixture theory for ν constituents to yield a valid mathematical model when the constituents are the same. Dimensionless form of the mathematical models are derived and used to present numerical studies for boundary value problems using finite element processes based on a residual functional i.e. least squares finite element processes in which local approximations are considered in $H^{k,p}\left(\bar{\Omega}^e\right)$ scalar product spaces. Fully developed flow between parallel plates and 1:2 asymmetric backward facing step are used as model problems for a mixture of two constituents.

(V) 1D normal shocks (Riemann shock tube): numerical simulations and comparisons with experiments: We consider numerical simulation of the evolution of one-dimensional normal shocks, their propagation, reflection, and interaction in air using a single diaphragm Riemann shock tube and validate them using experimental results. Mathematical model is derived for one-dimensional compressible flow of viscous and conducting medium. Dimensionless form of the mathematical model is used to construct space-time finite element processes based on minimization of the space-time residual functional. The space-time local approximation functions for space-time p-version hierarchical finite elements are considered in higher order $H^{k,p}(\bar{\Omega}^e_{xt})$ spaces that permit desired order of global differentiability of local approximations in space and time. The resulting algebraic systems from this approach yield unconditionally positive-definite coefficient matrices, hence ensure unique numerical solution. The evolution is computed for a space-time strip corresponding to a time increment Δt and then time march to obtain the evolution up to any desired value of time. Numerical studies are designed using recently invented hand-driven shock tube (Reddy tube) parameters, high/low side densities and pressure values, high and low pressure side shock tube lengths, so that numerically computed results can be compared with actual experimental measurements.

Motivation

In obtaining accurate numerical solutions of boundary value problems (BVPs) and initial value problems (IVPs) describing the stationary and time dependent physical processes, there are two significant aspects: (i) Derivations of mathematical models that incorporate the desired physics and ensure thermodynamic equilibrium during the entire evolution (IVPs) or their stationary states (BVPs) (ii) accurate numerical solutions of the BVPs and IVPs resulting from the mathematical models regardless of their complexity with built-in intrinsic measures of error in the computed evolution without the knowledge of the theoretical solutions and inherent mechanism(s) of adaptivity for reducing the error in the computed solution to the desired level.

Recent and ongoing developments in computational mathematics (Surana et al. [1–7]) have lead to the new generation of finite element processes for BVPs and IVPs that are highly meritorious and can provide numerical solutions that are as good as their theoretical solutions. The h, p, k finite element processes based on variationally consistent (VC) integral forms

resulting from these recent developments indeed have all desired features. Variationally consistent integral forms ensure unconditionally stable computational processes regardless of the choice of h, p and k and the nature of the differential operator, thus avoiding the use of stabilizing methods such as SUPG, SUPG/DC, SUPG/DC/LS [8, 9] used currently that lack mathematical basis in almost all aspects. The h, p, k framework permits variable element size (h), choice of the degrees (p) of local approximation in spatial directions as well as time, and higher order global differentiability in space and time due to k, the order of the approximation space. With the advent of k (or k-version of the finite element method), it is now possible to incorporate desired physics in the computational processes. The use of k allows the integrals in the finite element processes to be in the Riemann sense, permitting precise computations of the integrated sums of squares of the residuals as a quantitative measure of error which also provides basis for adaptive refinements. In summary, the h, p, k framework with VC integral forms developed by Surana et al. [10–12] and being further developed during the current grant ensures numerical solutions (upon convergence) that are as good as the theoretical solution in almost all aspects is the basis for all numerical computations in the research being performed under the current grant.

When the numerical solutions for a mathematical model (BVP or IVP) are computed using h, p, k framework with VC integral forms and when there is a lack of agreement between the computed solutions and the experimental or observed behavior, this disagreement cannot be attributed to the h, p, k finite element computational process. In such situations, if the experimental or observed behavior is the right behavior, then the lack of agreement between the numerically computed solution and experimental or observed behavior is undoubtedly due to lack of desired physics in the mathematical model used in the computational process.

The mathematical models for homogeneous isotropic, compressible and incompressible solid media experiencing finite deformation can be derived using conservation and balance laws in Lagrangian description, preferred for solid matter as it provides ability to monitor material particle displacements. Conservation of mass, balance of momenta and first law of thermodynamics are independent of the constitution of the matter and hence hold for all deforming matter regardless of whether it is solid, liquid or gas. In the conservation laws, we assume existence of stress field and heat vector without regard to how these are arrived at. Determination of the dependence of the stress tensor and heat vector on the kinematic of deforming matter is referred to as constitutive theory. For the deforming matter to be in thermodynamic equilibrium, in addition to these three conservation laws, the second law of thermodynamics must also be satisfied during evolution of the deforming matter. Thus, if the constitutive theories are derived using the second law of thermodynamics (entropy inequality), then we are assured that the resulting mathematical model will undoubtedly satisfy thermodynamic equilibrium during the evolution of deforming matter. Conservation of mass, balance of momenta and first law of thermodynamics or balance of energy are well established and hold regardless of the constitution of the matter. Thus, if the mathematical models of the deforming matter used in obtaining numerical solutions using h, p, k framework with VC integral forms are unable to yield numerical solutions that are in agreement with observed behavior, then undoubtedly the problem in the mathematical models must arise due to the use of less than adequate constitutive theories. Unless the derivations of the constitutive theories based on entropy inequality and the assumptions employed in their derivations are clearly understood, the adequacy of the mathematical models for the desired physics cannot be ensured. The currently used constitutive theories in some cases have rigorous derivations based on entropy inequality but in most cases are simple ad hoc extensions of simple one dimensional phenomenological models. Such theories lack thermodynamic foundation and could be in violation of the axioms of constitutive theory in continuum mechanics. Thus, the motivation for addressing constitutive theories for solid matter is to ensure that the resulting mathematical model will yield thermodynamic equilibrium in the deforming matter during evolutions and will permit desired and varied physics associated with finite deformation of complex materials. Such mathematical models, when used in conjunction with h, p, k framework with VC integral forms, have extremely high likelihood of simulating the observed behaviors during the evolution of deforming matter.

In the following we consider each of the five areas of research and present: scientific approach, research details, findings, merits, summary, concluding remarks, significance and impact of the research.

I Ordered rate constitutive theories for solid matter using second law of thermodynamics in Helmholtz free energy Φ and Gibbs potential Ψ

In order to ensure thermodynamic equilibrium in the deforming matter, the constitutive theories for stress tensor and heat vector (for simple matter) must satisfy conservation and balance laws. Conservation of mass, balance of momenta and first law of thermodynamics simply use the stress tensor and heat vector but have no mechanism for deriving constitutive theories for these. Hence, we must some how employ the second law of thermodynamics (entropy inequality) in the derivation of the constitutive theories or ensure that the conditions resulting from the entropy inequality are satisfied by the constitutive theories we choose. When constitutive theories are derived using entropy inequality, then it is obviously satisfied, hence thermodynamic equilibrium is ensured during deformation. If other measures are employed to derive the constitutive theories, then we must ensure that these constitutive theories do not violate the restrictions imposed by the entropy inequality. In cases where the entropy inequality neither has any mechanism for deriving constitutive theories nor places any restrictions, the choice of constitutive theories can be independent of conservation and balance laws. This is indeed the case for thermoelastic solids.

The entropy inequality can be expressed either in terms of Helmholtz free energy density Φ or Gibbs potential Ψ. The two forms of entropy inequality are exactly equivalent but the resulting constitutive theories from these two forms may not always be equivalent. In the research conducted here, we consider derivations of the ordered rate constitutive theories using both forms of the entropy inequality and establish when there is equivalence between the resulting constitutive theories. Regardless of whether we consider entropy inequality in terms of Φ or Ψ, the basic principles and the axioms of continuum mechanics in the derivations of constitutive theories remain almost the same for the three types of solids considered in the present work. We describe these in the following.

Let $\boldsymbol{\sigma}$ and $\boldsymbol{\varepsilon}$ represent conjugate stress and strain (measure of finite strain i.e. Green's strain) tensors in Lagrangian description and η, θ, $\boldsymbol{g}$ and $\boldsymbol{q}$ be specific entropy, temperature (absolute), temperature gradient and heat vector.

Entropy inequality in Helmholtz free energy Φ

(1) Using entropy inequality in Lagrangian description expressed in terms of Φ and other three conservation laws, Φ, η, $\boldsymbol{\sigma}$ and $\boldsymbol{q}$ are established as dependent variables in the constitutive theories.

(2) The argument tensors of these dependent variables are established based on the desired physics i.e. thermoelastic solids, thermoviscoelastic solids without memory and thermoviscoelastic solids with memory.

(3) Using the argument tensors in (2) for Φ we obtain material derivative of Φ i.e. $\frac{D\Phi}{Dt}$ or $\dot{\Phi}$ which is $\frac{\partial \Phi}{\partial t}$ in Lagrangian description and substitute this in the entropy inequality. From the resulting form of the entropy inequality: (i) η is eliminated as a dependent variable (ii) reduced argument tensors of Φ are established. Thus, now Φ, $\boldsymbol{\sigma}$ and $\boldsymbol{q}$ remain as dependent variables in the constitutive theories with their argument tensors defined.

(4) At this stage, if the conditions resulting from the entropy inequality permit, the constitutive theory for $\boldsymbol{\sigma}$ is derived directly using these. This is indeed the case for thermoelastic solids. The result is a rate constitutive theory of order zero for $\boldsymbol{\sigma}$.

(5) If the conditions resulting from the entropy inequality do not permit derivation of the constitutive theories for $\boldsymbol{\sigma}$, then $\boldsymbol{\sigma}$ is decomposed into equilibrium stress ${}_e\boldsymbol{\sigma}$ and deviatoric stress ${}_d\boldsymbol{\sigma}$ i.e. the total stress is $\boldsymbol{\sigma} = {}_e\boldsymbol{\sigma} + {}_d\boldsymbol{\sigma}$. The conditions resulting from the entropy inequality permit derivation of the constitutive theory for ${}_e\boldsymbol{\sigma}$ as thermodynamic pressure $\boldsymbol{p} = p(\rho, \theta)\boldsymbol{I}$ for compressible case and mechanical pressure $\boldsymbol{p} = p(\theta)\boldsymbol{I}$ (after inserting incompressibility constraint in the entropy inequality) for incompressible case. Additionally, another inequality due to the decomposition of $\boldsymbol{\sigma}$ requires the work expanded due to ${}_d\boldsymbol{\sigma}$ to be positive, but the entropy inequality provides no mechanism for deriving constitutive theories for ${}_d\boldsymbol{\sigma}$. In the present work, we use the theory of generators and invariants [13–30] to derive constitutive theories for ${}_d\boldsymbol{\sigma}$, keeping in mind that the entropy inequality requires work expanded due to ${}_d\boldsymbol{\sigma}$ to be positive for thermodynamic equilibrium to hold. In this approach, we determine the combined generators of the argument tensors of ${}_d\boldsymbol{\sigma}$. These form a basis or integrity, hence ${}_d\boldsymbol{\sigma}$ can be expressed as a linear combination of the combined generators. The coefficients in the linear combination are functions of the combined invariants of the argument tensors of ${}_d\boldsymbol{\sigma}$ and others. For thermoviscoelastic solids without memory and thermoviscoelastic solids with memory, we use this approach to derive ordered rate constitutive theories for ${}_d\boldsymbol{\sigma}$.

(6) The rate constitutive theories for $\boldsymbol{q}$ are derived to be consistent with the rate constitutive theories for $\boldsymbol{\sigma}$ in the sense of argument tensors and use of integrity. The rate constitutive theories for $\boldsymbol{q}$ derived using the theory of generators and invariants are much more comprehensive. These demonstrate influence of various kinematic measures of deformation on the heat vector. Using the rate constitutive theories for $\boldsymbol{q}$ based on integrity, many simplified forms are possible with appropriate assumptions based on the desired physics. The simplest possible case results in Fourier heat conduction law which also can be derived directly using the inequality resulting from the entropy inequality with the assumption that $\boldsymbol{q}$ is proportional to the temperature gradient $\boldsymbol{g}$.

(7) It is shown that all constitutive theories for the three types of solids considered here are indeed ordered rate constitutive theories for $\boldsymbol{\sigma}$ (or ${}_d\boldsymbol{\sigma}$) and $\boldsymbol{q}$.

Entropy inequality in Gibbs potential Ψ

(1) Using entropy inequality in Lagrangian description expressed in terms of Ψ and the other three conservation laws, Ψ, η, $\boldsymbol{\varepsilon}$ and $\boldsymbol{q}$ are established as dependent variables in the constitutive theories.

(2) The argument tensors of these dependent variables are established based on the desired physics i.e. thermoelastic solids, thermoviscoelastic solids without memory and thermoviscoelastic solids with memory.

(3) Using the argument tensors in (2) for Ψ we obtain material derivative of Ψ i.e. $\frac{D\Psi}{Dt}$ or $\dot{\Psi}$ which is $\frac{\partial\Psi}{\partial t}$ in Lagrangian description and substitute this in the entropy inequality. From the resulting form of the entropy inequality: (i) η is eliminated as a dependent variable (ii) reduced argument tensors of Ψ are established. Thus, now Ψ, $\boldsymbol{\varepsilon}$ and $\boldsymbol{q}$ remain as dependent variables in the constitutive theories with their argument tensors defined.

(4) At this stage, if the conditions resulting from the entropy inequality permit, the constitutive theory for $\boldsymbol{\varepsilon}$ is derived directly using these. This is indeed the case for thermoelastic solids. The result is a rate constitutive theory of order zero for $\boldsymbol{\varepsilon}$.

(5) If the conditions resulting from the entropy inequality do not permit derivation of the constitutive theories for $\boldsymbol{\varepsilon}$, then $\boldsymbol{\sigma}$ is decomposed into equilibrium stress ${}_e\boldsymbol{\sigma}$ and deviatoric stress ${}_d\boldsymbol{\sigma}$ i.e. the total stress is $\boldsymbol{\sigma} = {}_e\boldsymbol{\sigma} + {}_d\boldsymbol{\sigma}$. The entropy inequality in Ψ has no mechanism for the constitutive theories for ${}_e\boldsymbol{\sigma}$, but ${}_e\boldsymbol{\sigma}$ describes fixed physics, hence the constitutive theories for ${}_e\boldsymbol{\sigma}$ derived using entropy inequality in Φ remain valid here as well i.e. thermodynamic pressure $\boldsymbol{p} = p(\rho,\theta)\boldsymbol{I}$ for compressible case and mechanical pressure $\boldsymbol{p} = p(\theta)\boldsymbol{I}$ for incompressible case. In this case also (as in the case of Φ), the inequality from entropy inequality requires work expanded to be positive, but the entropy inequality provides no mechanism for deriving constitutive theories for $\boldsymbol{\varepsilon}$. Due to the decomposition $\boldsymbol{\sigma} = {}_e\boldsymbol{\sigma} + {}_d\boldsymbol{\sigma}$, we can establish that Ψ must contain ${}_d\boldsymbol{\sigma}$ as an argument tensor instead of $\boldsymbol{\sigma}$, and likewise, due to the axiom of equipresence, ${}_d\boldsymbol{\sigma}$ must also be an argument tensor of all other dependent variables instead of the total stress $\boldsymbol{\sigma}$. In the present work, we use the theory of generators and invariants [13–30] to derive constitutive theories for $\boldsymbol{\varepsilon}$, keeping in mind that the entropy inequality requires work expanded due to the total stress $\boldsymbol{\sigma}$ to be positive for thermodynamic equilibrium to hold. In this approach, we determine the combined generators of the argument tensors of $\boldsymbol{\varepsilon}$. These form a basis or integrity, hence $\boldsymbol{\varepsilon}$ can be expressed as a linear combination of the combined generators. The coefficients in the linear combination are functions of the combined invariants of the argument tensors of $\boldsymbol{\varepsilon}$ and others. For thermoviscoelastic solids without memory and thermoviscoelastic solids with memory, we use this approach to derive ordered rate constitutive theories for $\boldsymbol{\varepsilon}$.

(6) The rate constitutive theories for $\boldsymbol{q}$ are derived to be consistent with the rate constitutive theories for $\boldsymbol{\varepsilon}$ in the sense of argument tensors and use of integrity. The rate constitutive theories for $\boldsymbol{q}$ derived using the theory of generators and invariants are much more comprehensive. These demonstrate influence of various kinematic measures of deformation on the heat vector. Using the rate constitutive theories for $\boldsymbol{q}$ based on integrity, many simplified forms are possible with appropriate assumptions based on the desired physics. The simplest possible case results in Fourier heat conduction law which also can be derived directly using the inequality resulting from the entropy inequality with the assumption that $\boldsymbol{q}$ is proportional to the temperature gradient $\boldsymbol{g}$.

(7) It is shown that all constitutive theories for the three types of solids considered here are indeed ordered rate constitutive theories for $\boldsymbol{\varepsilon}$ and $\boldsymbol{q}$.

Remarks

The material coefficients in both approaches are determined by considering Taylor series expansions of the coefficients in the linear combinations about a known configuration. This allows the material coefficients to be functions of combined invariants and temperature θ in the known configuration, thus permitting complex material behaviors that is deformation dependent during the evolution.

I.1 Constitutive theories for thermoelastic solids

In thermoelastic solids both compressible and incompressible, the mechanical deformation by definition is reversible, hence such solids do not have any mechanism of conversion of mechanical energy into any other forms. Thus, for such solids, the rate of mechanical work cannot contribute to entropy production, hence thermal changes in the matter purely due to mechanical work are not possible in thermoelastic solids. The consequence of this is that the rate of applied mechanical work to a volume of matter can only cause rate of change of kinetic energy and rate of change of strain energy but cannot influence internal energy as this would require entropy production and associated thermal changes due to rate of mechanical work which are not possible for thermoelastic solids. Thus, for thermoelastic solids, rate of mechanical work equilibrates with the rate of kinetic energy and rate of strain energy. In this section, this aspect of the physics is utilized to (i) derive energy equation based on the first law of thermodynamics (ii) derive entropy inequality based on the second law of thermodynamics. The entropy inequality and other approaches are examined from the point of view of possibilities for establishing dependent variables and their arguments for deriving constitutive theories for such solids in Lagrangian description. The solid matter is assumed to be homogeneous, isotropic, compressible as well as incompressible but the deformation and the strains can be finite.

Introduction

In the derivations of the energy equation and entropy inequality using first and second laws of thermodynamics for solid matter we generally do not make a distinction between the matter specific limited physics that may warrant a different approach and may also result in different final mathematical expressions. If we consider Lagrangian description, homogeneous and isotropic solid matter with finite deformation and strains, then general derivations of energy equation and entropy inequality are assumed to hold regardless of other matter specific physics, i.e. thermoelastic, thermoviscoelastic without memory, thermoviscoelastic with memory etc. The same forms of energy equation and entropy inequality is assumed to hold for all solid matter. Only a closer examination of the derivation can reveal if this is indeed always the case. In this section, we consider thermoelastic solids. The matter is assumed to be homogeneous, isotropic, compressible as well as incompressible but can experience finite deformation and strain. By definition, the mechanical deformation in thermoelastic solids is reversible. Hence in such solids there is no mechanism of conversion of mechanical energy into any other form as the mechanical deformation is reversible. Thus, the rate of mechanical work can not contribute to entropy production and hence cannot influence the thermal field. In such solids, the rate of mechanical work results in motion of material particles, i.e. rate of change of kinetic energy and rate of change of strain energy, but the internal energy remains unaffected by the rate of mechanical work since it does not contribute to entropy production and hence the thermal field also remains unaffected by the rate of mechanical work. This aspect of the physics is instrumental in influencing the derivations of the energy equation and the entropy inequality as shown in this section. Since the derivations of the constitutive theories are based on entropy inequality (or the conditions resulting from the entropy inequality), these are also likely to be affected as explored.

First and second laws of thermodynamics

For thermoelastic solids, the first and second laws of thermodynamics have been derived in reference [31] in Lagrangian description and given below.

$$\begin{aligned} &\rho_0 \frac{De}{Dt} + \boldsymbol{\nabla} \cdot \boldsymbol{q} = 0 \\ \text{or} \qquad &\rho_0 \frac{\partial e}{\partial t} + \boldsymbol{\nabla} \cdot \boldsymbol{q} = 0 \end{aligned} \tag{I.1}$$

$$\begin{aligned} &\rho_0 \Big(\frac{D\Phi}{Dt} + \eta \frac{D\theta}{Dt} \Big) + \frac{1}{\theta} \boldsymbol{q} \cdot \boldsymbol{g} \leq 0 \\ \text{or} \qquad &\rho_0 \Big(\frac{\partial \Phi}{\partial t} + \eta \frac{\partial \theta}{\partial t} \Big) + \frac{1}{\theta} \boldsymbol{q} \cdot \boldsymbol{g} \leq 0 \end{aligned} \tag{I.2}$$

Remarks

(1) We note that (I.1) is a simple linear or non-linear heat conduction equation. In (I.1) the rate of mechanical work does not contribute to the energy equation.

(2) The derivation of the energy equation for solid matter in published works contains an additional term [18,19] $-(\boldsymbol{\sigma}^{[0]} : \dot{\boldsymbol{\varepsilon}}_{[0]})$ in (I.1) resulting due to rate of mechanical work, in which $\boldsymbol{\sigma}^{[0]}$ is the second Piola-Kirchhoff stress tensor and $\dot{\boldsymbol{\varepsilon}}_{[0]}$ is the material derivative of the Green's strain tensor. This term represents dissipation, i.e. conversion of mechanical energy into heat, and hence entropy production which is not possible for thermoelastic solids and hence is absent in the derivation presented here that results in (I.1).

(3) Since for such solids there is no entropy production due to rate of mechanical work, the term $-(\boldsymbol{\sigma}^{[0]} : \dot{\boldsymbol{\varepsilon}}_{[0]})$ reflecting this physics is absent in the entropy inequality derived here. In published works [18, 19] the entropy inequality contains the expression $-(\boldsymbol{\sigma}^{[0]} : \dot{\boldsymbol{\varepsilon}}_{[0]})$ as additional term on the left side of (I.2) for solid matter.

(4) For thermoelastic solids, the rate of mechanical work resulting in motions of material points, stress and strain makes no contribution to the energy equation (I.1) and entropy inequality (I.2). This is obvious due to the absence of velocities, stresses and strains in (I.1) and (I.2). Thus, as it appears the thermodynamics described by the energy equation and entropy inequality is completely unaffected by the strains and stresses and their rates created in the deforming matter due to rate of mechanical work.

Constitutive theories for thermoelastic solids in Lagrangian description

In this section we follow the standard line of thinking that is *since conservation of mass, balance of momenta and the energy equation do not provide any mechanism for deriving constitutive theories, the entropy inequality must be explored for their derivations to ensure thermodynamic equilibrium in the deforming matter during evolution*. If we examine the equations resulting from the conservation and balance laws (for finite deformation) then it is straight forward to conclude that the second Piola-Kirchhoff stress tensor $\boldsymbol{\sigma}^{[0]}$, heat vector $\boldsymbol{q}$, Helmholtz free energy density Φ and specific entropy η as possible choice of dependent variables in describing the constitution of the matter. Based on entropy inequality we can easily conclude that $\Phi = \Phi(\theta)$, $\eta = \eta(\theta)$ and we know that $\boldsymbol{q} = \boldsymbol{q}(\boldsymbol{g}, \theta)$ must certainly be considered, hence at the onset we could assume that Φ, η and $\boldsymbol{q}$ are all functions of $\boldsymbol{g}$ and θ. The stress tensor $\boldsymbol{\sigma}^{[0]}$ on the other hand must certainly be a function of deformation, i.e. say Green's strain tensor $\boldsymbol{\varepsilon}_{[0]}$ (with $\boldsymbol{\sigma}^{[0]}$ and $\boldsymbol{\varepsilon}_{[0]}$ as *conjugate pair* [31]) and and θ as the matter is thermoelastic. Thermal expansion and contraction, and the strain and stress field associated with these is accounted for by temperature θ. The stress and strain field associated with the mechanical work is independent of $\boldsymbol{q}$, thus at this stage, it appears appropriate to have $\boldsymbol{\varepsilon}_{[0]}$ and θ as the only argument tensors of $\boldsymbol{\sigma}^{[0]}$. As mentioned before, in case of the heat vector $\boldsymbol{q}$, temperature θ and temperature gradient $\boldsymbol{g}$ are obvious choices as argument tensors of $\boldsymbol{q}$. In case of finite deformation, the presence of strain field responsible for influencing mean free path can certainly influence the heat transfer, thus $\boldsymbol{\varepsilon}_{[0]}$, $\boldsymbol{g}$ and θ as argument tensors of $\boldsymbol{q}$ is an appropriate choice even though not obvious from energy equation and

entropy inequality or the conditions resulting from it. In case of Φ and η, consideration of $\boldsymbol{\varepsilon}_{[0]}$ as argument tensor in addition to $\boldsymbol{g}$ and θ is not supported by entropy inequality as deformation measure, i.e. $\boldsymbol{\varepsilon}_{[0]}$, is totally absent in the entropy inequality. Thus, at this stage we conclude the following for the argument tensors of Φ, η, $\boldsymbol{\sigma}^{[0]}$ and $\boldsymbol{q}$.

$$\begin{aligned}
&\Phi = \Phi(\ \boldsymbol{g}\ ,\ \theta\ ) \\
&\eta = \eta(\ \boldsymbol{g}\ ,\ \theta\ ) \\
&\boldsymbol{\sigma}^{[0]} = \boldsymbol{\sigma}^{[0]}(\ \boldsymbol{\varepsilon}_{[0]}\ ,\ \theta\ ) \\
&\boldsymbol{q} = \boldsymbol{q}(\ \boldsymbol{\varepsilon}_{[0]}\ ,\ \boldsymbol{g}\ ,\ \theta\ )
\end{aligned} \tag{I.3}$$

Using (I.3) we can obtain

$$\dot{\Phi} = \frac{\partial \Phi}{\partial \boldsymbol{g}} \cdot \dot{\boldsymbol{g}} + \frac{\partial \Phi}{\partial \theta}\dot{\theta} \tag{I.4}$$

Substituting from (I.4) into entropy inequality (I.2)

$$\rho_{_0}\Big(\frac{\partial \Phi}{\partial \boldsymbol{g}} \cdot \dot{\boldsymbol{g}} + \frac{\partial \Phi}{\partial \theta}\dot{\theta} + \eta\dot{\theta}\Big) + \frac{1}{\theta}\boldsymbol{q}\cdot\boldsymbol{g} \leq 0 \tag{I.5}$$

$$\text{or} \quad \rho_{_0}\Big(\frac{\partial \Phi}{\partial \theta} + \eta\Big)\dot{\theta} + \rho_{_0}\frac{\partial \Phi}{\partial \boldsymbol{g}} \cdot \dot{\boldsymbol{g}} + \frac{1}{\theta}\boldsymbol{q}\cdot\boldsymbol{g} \leq 0 \tag{I.6}$$

For (I.6) to hold for arbitrary but admissible $\dot{\theta}$ and $\dot{\boldsymbol{g}}$ the following must hold.

$$\rho_{_0}\Big(\frac{\partial \Phi}{\partial \theta} + \eta\Big) = 0 \ \ ; \ \ \rho_{_0}\frac{\partial \Phi}{\partial \boldsymbol{g}} = 0 \ \ ; \ \ \frac{\boldsymbol{q}\cdot\boldsymbol{g}}{\theta} \leq 0 \tag{I.7}$$

and since $\rho_{_0}$ is constant and $\theta > 0$, we can write

$$\frac{\partial \Phi}{\partial \theta} + \eta = 0 \tag{I.8}$$

$$\frac{\partial \Phi}{\partial \boldsymbol{g}} = 0 \tag{I.9}$$

$$\boldsymbol{q}\cdot\boldsymbol{g} \leq 0 \tag{I.10}$$

Equation (I.8) implies that $\eta = -\partial\Phi/\partial\theta$, i.e. if Φ is known as a function of θ then η is deterministic, thus η cannot be a dependent variable in the constitutive theories. Equation (I.9) implies that Φ cannot be a function of $\boldsymbol{g}$. We note that the conditions resulting from the entropy inequality ((I.8) - (I.10)) give us no further information regarding the argument tensors of $\boldsymbol{\sigma}^{[0]}$ and $\boldsymbol{q}$ as used in (I.3) except the fact that the constitutive theory for $\boldsymbol{q}$ must satisfy (I.10). Thus, finally we have the following for the constitutive dependent variables and their argument tensors for thermoelastic solids.

$$\Phi = \Phi(\ \theta\ ) \tag{I.11}$$

$$\boldsymbol{\sigma}^{[0]} = \boldsymbol{\sigma}^{[0]}(\ \boldsymbol{\varepsilon}_{[0]}\ ,\ \theta\ ) \tag{I.12}$$

$$\boldsymbol{q} = \boldsymbol{q}(\ \boldsymbol{\varepsilon}_{[0]}\ ,\ \boldsymbol{g}\ ,\ \theta\ ) \tag{I.13}$$

with the following condition

$$\boldsymbol{q}\cdot\boldsymbol{g} \leq 0 \tag{I.14}$$

Remarks

(1) We note that entropy inequality provides no conditions or mechanism for deriving constitutive theories for the stress tensor $\boldsymbol{\sigma}^{[0]}$. This is to be expected as entropy inequality is completely independent of $\boldsymbol{\sigma}^{[0]}$ and strain tensor $\boldsymbol{\varepsilon}_{[0]}$.

(2) We also know note that energy equation is independent of $\boldsymbol{\sigma}^{[0]}$ and strain tensor $\boldsymbol{\varepsilon}_{[0]}$.

(3) From remarks (1) and (2) we conclude that both laws of thermodynamics are independent of the mechanical deformation, i.e. $\boldsymbol{\sigma}^{[0]}$ and $\boldsymbol{\varepsilon}_{[0]}$. Thus *the derivations of the constitutive theories for* $\boldsymbol{\sigma}^{[0]}$ *do not have any thermodynamic restrictions*. In other words, any constitutive theory for $\boldsymbol{\sigma}^{[0]}$ will suffice as far as thermodynamic equilibrium of the deforming solid matter is concerned.

(4) In the derivations of the constitutive theories for $\boldsymbol{\sigma}^{[0]}$ presented here, we consider (I.12) to hold.

(5) In deriving the constitutive theories for $\boldsymbol{q}$ we also consider (I.13) to hold.

(6) Thus the constitutive theories for thermoelastic solids reduce to determining expressions for:

(i) $\boldsymbol{\sigma}^{[0]}$ as function of $\boldsymbol{\varepsilon}_{[0]}$, θ based on (I.12).

(ii) $\boldsymbol{q}$ as function of $\boldsymbol{\varepsilon}_{[0]}$, $\boldsymbol{g}$, θ based on (I.13) keeping in mind that the final constitutive theory for $\boldsymbol{q}$ must satisfy condition (I.14) resulting from the entropy inequality.

I.1.1 Constitutive theories based on $\boldsymbol{\sigma}^{[0]} = \boldsymbol{\sigma}^{[0]}(\boldsymbol{\varepsilon}_{[0]}, \theta)$ using theory of generators and invariants: Lagrangian description

Based on the material presented so far, it is clear that derivations of the constitutive theories for $\boldsymbol{\sigma}^{[0]}$ are indeed independent of entropy inequality or the conditions resulting from it. In the derivation of constitutive theories that follow, we consider (I.12) and use the theory of generators and invariants [13–17, 20–30, 32] but other possibilities are admissible too as there are no thermodynamic restrictions. Let ${}^{\sigma}\underset{\sim}{\boldsymbol{G}}^{i}\ ; i = 1, 2, \ldots, N$ be combined generators of the arguments $\boldsymbol{\varepsilon}_{[0]}$ and θ that are symmetric tensors of rank two, then $\boldsymbol{\sigma}^{[0]}$, a symmetric tensor of rank two can be expressed by a linear combination of $\boldsymbol{I}$ and ${}^{\sigma}\underset{\sim}{\boldsymbol{G}}^{i}\ ; i = 1, 2, \ldots, N$. Generators ${}^{\sigma}\underset{\sim}{\boldsymbol{G}}^{i}\ ; i = 1, 2, \ldots, N$ form *integrity*, i.e. they satisfy the *complete basis principle*.

$$[\sigma^{[0]}] = {}^{\sigma}\tilde{\alpha}_{0}[I] + \sum_{i=1}^{N} {}^{\sigma}\tilde{\alpha}_{i}\ [{}^{\sigma}\underset{\sim}{G}^{i}] \tag{I.15}$$

where

$${}^{\sigma}\tilde{\alpha}_{i} = {}^{\sigma}\tilde{\alpha}_{i}\big({}^{\sigma}\underset{\sim}{I}^{j}\ ;\ j = 1, 2, \ldots, M\ ,\ \theta\big) \tag{I.16}$$

in which $i = 0, 1, \ldots, N$ and ${}^{\sigma}\underset{\sim}{I}^{j}\ ; j = 1, 2, \ldots, M$ are the combined invariants of the argument tensors $\boldsymbol{\varepsilon}_{[0]}$ and θ. The constitutive theory for $\boldsymbol{\sigma}^{[0]}$ is in the current configuration, hence ${}^{\sigma}\tilde{\alpha}_{i}\ ; i = 0, 1, \ldots, N$ are also functions of the invariants and temperature θ in the current configuration. For $\boldsymbol{\varepsilon}_{[0]}$ and θ as argument tensors of $\boldsymbol{\sigma}^{[0]}$ we have

$$[{}^{\sigma}\underset{\sim}{G}^{1}] = [\varepsilon_{[0]}]\ ,\ [{}^{\sigma}\underset{\sim}{G}^{2}] = [\varepsilon_{[0]}]^{2} \quad ; \quad N = 2 \tag{I.17}$$

and the invariants are

$$\begin{aligned} &{}^{\sigma}\underset{\sim}{I}^{1} = \text{tr}([\varepsilon_{[0]}]) = i_{\varepsilon_{[0]}}\ \ ,\ \ {}^{\sigma}\underset{\sim}{I}^{2} = \text{tr}([\varepsilon_{[0]}]^{2}) = \ddot{\imath}_{\varepsilon_{[0]}} \\ &{}^{\sigma}\underset{\sim}{I}^{3} = \det([\varepsilon_{[0]}]) = \dddot{\imath}_{\varepsilon_{[0]}} \qquad ; \qquad M = 3 \end{aligned} \tag{I.18}$$

and if we choose the *invariants from the characteristic equation of* $\boldsymbol{\varepsilon}_{[0]}$ then

$$\begin{aligned} &{}^{\sigma}\underset{\sim}{I}^{1} = \text{tr}([\varepsilon_{[0]}]) = I_{\varepsilon_{[0]}} \\ &{}^{\sigma}\underset{\sim}{I}^{2} = \frac{1}{2}\Big((\text{tr}([\varepsilon_{[0]}]))^{2} - \text{tr}([\varepsilon_{[0]}]^{2})\Big) = II_{\varepsilon_{[0]}} \\ &{}^{\sigma}\underset{\sim}{I}^{3} = \text{tr}([\varepsilon_{[0]}]^{3}) = III_{\varepsilon_{[0]}} \quad ; \quad M = 3 \end{aligned} \tag{I.19}$$

In the following we consider the invariants from the characteristic equation of $\boldsymbol{\varepsilon}_{[0]}$, hence

$$[\sigma^{[0]}] = {}^{\sigma}\tilde{\alpha}_{0}[I] + {}^{\sigma}\tilde{\alpha}_{1}[\varepsilon_{[0]}] + {}^{\sigma}\tilde{\alpha}_{2}[\varepsilon_{[0]}]^{2} \tag{I.20}$$

in which

$$ {}^{\sigma}\tilde{\alpha}_i = {}^{\sigma}\tilde{\alpha}_i \left(I_{\varepsilon_{[0]}} \, , \, II_{\varepsilon_{[0]}} \, , \, III_{\varepsilon_{[0]}} \, , \, \theta \right) \, ; \, i = 0, 1, 2 \tag{I.21} $$

We note that ${}^{\sigma}\tilde{\alpha}_i \, ; \, i = 0, 1, 2$ are in the current configuration and hence unknown. In the following section we determine material coefficients in the constitutive theory for $\boldsymbol{\sigma}^{[0]}$. The material coefficients can be derived using standard procedure of Taylor series expansion [31].

I.1.2 Constitutive theories for $\boldsymbol{\sigma}^{[0]}$ in terms of $\boldsymbol{\varepsilon}_{[0]}$ based on strain energy density function π: Lagrangian description

(a) Approach I: considering $\pi = \pi(I_{\varepsilon_{[0]}}, II_{\varepsilon_{[0]}}, III_{\varepsilon_{[0]}}, \theta)$ and using $[\sigma^{[0]}]^T = [\sigma^{[0]}] = \rho_0 \frac{\partial \pi}{\partial [\varepsilon_{[0]}]}$

In this derivation we consider π as a function of $\boldsymbol{\varepsilon}_{[0]}$ and θ and then use $[\sigma^{[0]}]^T = [\sigma^{[0]}] = \rho_0 \frac{\partial \pi}{\partial [\varepsilon_{[0]}]}$. The *principle of frame invariance* requires that instead of $\boldsymbol{\varepsilon}_{[0]}$ and θ, π must be a function of the invariants of $\boldsymbol{\varepsilon}_{[0]}$ and θ. If we choose *invariants from the characteristic equation of* $\boldsymbol{\varepsilon}_{[0]}$, then we have

$$ \pi = \pi(I_{\varepsilon_{[0]}}, II_{\varepsilon_{[0]}}, III_{\varepsilon_{[0]}}, \theta) \tag{I.22} $$

Using $[\sigma^{[0]}]^T = [\sigma^{[0]}] = \rho_0 \frac{\partial \pi}{\partial [\varepsilon_{[0]}]}$ we can derive constitutive theories for the stress tensor [31].

(b) Approach II: expanding $\pi = \pi(\boldsymbol{\varepsilon}_{[0]}, \theta)$ in Taylor series about a known configuration and using $[\sigma^{[0]}]^T = [\sigma^{[0]}] = \rho_0 \frac{\partial \pi}{\partial [\varepsilon_{[0]}]}$

We consider $\pi = \pi(\boldsymbol{\varepsilon}_{[0]}, \theta)$ and based on the *principle or axiom of smooth neighborhood* we expand π in $\boldsymbol{\varepsilon}_{[0]}$ using Taylor series about a known configuration $\underline{\Omega}$ and then use $[\sigma^{[0]}]^T = [\sigma^{[0]}] = \rho_0 \frac{\partial \pi}{\partial [\varepsilon_{[0]}]}$ to derive constitutive theory for $[\sigma^{[0]}]$. See [31] for details. The final form (using symmetry of the material coefficients) is given by

$$ \begin{aligned} \sigma^{[0]}_{mn} =& (\sigma^{[0]}_{mn})_{\underline{\Omega}} + \underline{\underline{C}}_{mnij} (\varepsilon_{[0]})_{ij} \\ &+ \overline{\overline{C}}_{mnijkl} (\varepsilon_{[0]})_{ij} (\varepsilon_{[0]})_{kl} + \cdots \end{aligned} \tag{I.23} $$

I.1.3 Constitutive theories for $\boldsymbol{\sigma}^{[0]}$ in terms of $\boldsymbol{C}_{[0]}$ based on π: Lagrangian description

(a) Approach I: considering $\pi = \pi(I_{C_{[0]}}, II_{C_{[0]}}, III_{C_{[0]}}, \theta)$ and using $[\sigma^{[0]}]^T = [\sigma^{[0]}] = 2\rho_0 \frac{\partial \pi}{\partial [C_{[0]}]}$

Following derivations similar to section I.1.2 we can derive the following

$$ [\sigma^{[0]}] = \mathfrak{a}_0 [I] + \mathfrak{a}_1 [C_{[0]}] + \mathfrak{a}_{-1} [C_{[0]}]^{-1} \tag{I.24} $$

and using Hamilton-Cayley theorem

$$ [\sigma^{[0]}] = \tilde{\mathfrak{a}}_0 [I] + \tilde{\mathfrak{a}}_1 [C_{[0]}] + \tilde{\mathfrak{a}}_2 [C_{[0]}]^2 \tag{I.25} $$

Material coefficients in these constitutive theories are determined using same procedure as in section I.1.2, i.e. Taylor series expansion of the coefficients in (I.24) or (I.25) in the invariants of the Cauchy strain tensor $\boldsymbol{C}_{[0]}$ and temperature θ about a known configuration $\underline{\Omega}$, and their substitution in (I.24) or (I.25). Details are straight forward and not repeated.

(b) Approach II: expanding $\pi = \pi(\boldsymbol{C}_{[0]}, \theta)$ in Taylor series about a known configuration and using $[\sigma^{[0]}]^T = [\sigma^{[0]}] = 2\rho_0 \frac{\partial \pi}{\partial [C_{[0]}]}$

Similar to section I.1.2 we can expand π in Taylor series in the components of the Cauchy strain tensor $\boldsymbol{C}_{[0]}$ about a known configuration $\underline{\Omega}$ and then substitute the resulting expression to obtain the appropriate constitutive theory for $\boldsymbol{\sigma}^{[0]}$. The resulting constitutive theory is similar to (I.23).

I.1.4 Constitutive theory for $\boldsymbol{\varepsilon}_{[0]}$ in terms of $\boldsymbol{\sigma}^{[0]}$ using theory of generators and invariants

In this case we can derive

$$[\varepsilon_{[0]}] = {}^{\varepsilon}\tilde{\alpha}^0[I] + {}^{\varepsilon}\tilde{\alpha}^1[\sigma^{[0]}] + {}^{\varepsilon}\tilde{\alpha}^2[\sigma^{[0]}]^2 \tag{I.26}$$

in which

$${}^{\varepsilon}\tilde{\alpha}^i = {}^{\varepsilon}\tilde{\alpha}^i(I_{\sigma^{[0]}}, I\!I_{\sigma^{[0]}}, I\!I\!I_{\sigma^{[0]}}, \theta)\ ;\ i = 0, 1, 2 \tag{I.27}$$

We note that ${}^{\varepsilon}\tilde{\alpha}^i\ ; i = 0, 1, 2$ are in the current configuration and hence unknown. In the following section we determine material coefficients in the constitutive theory for $\boldsymbol{\varepsilon}_{[0]}$. Material coefficients from these can be derived using the standard procedure.

I.1.5 Constitutive theories for $\boldsymbol{\varepsilon}_{[0]}$ in terms of $\boldsymbol{\sigma}^{[0]}$ based on complementary strain energy density function π^c

Similar to the material in previous sections we begin with

$$\pi^c(\boldsymbol{\sigma}^{[0]}) = \frac{1}{\rho_0}\int_0^{\boldsymbol{\sigma}^{[0]}} (\varepsilon_{[0]})_{ij}\ d\sigma^{[0]}_{ij} \tag{I.28}$$

in which π^c is the *complementary strain energy density function*. From (I.28) we can obtain (fundamental theorem of calculus)

$$[\varepsilon_{[0]}]^T = [\varepsilon_{[0]}] = \rho_0 \frac{\partial \pi^c(\boldsymbol{\sigma}^{[0]})}{\partial [\sigma^{[0]}]} \tag{I.29}$$

The *complementary strain energy density function* π^c and the *strain energy density function* π are obviously related.

(a) Approach I: considering $\pi^c = \pi^c(I_{\sigma^{[0]}}, II_{\sigma^{[0]}}, III_{\sigma^{[0]}}, \theta)$ and using (I.29)

In this approach we consider π^c to be a function of the invariants $I_{\sigma^{[0]}}$, $I\!I_{\sigma^{[0]}}$, $I\!I\!I_{\sigma^{[0]}}$ (based on characteristic equation for $\boldsymbol{\sigma}^{[0]}$) of $\boldsymbol{\sigma}^{[0]}$ and temperature θ in the current configuration and then use (I.29) to determine the constitutive theory for strain tensor $\boldsymbol{\varepsilon}_{[0]}$.

$$\pi = \pi(I_{\sigma^{[0]}}, I\!I_{\sigma^{[0]}}, I\!I\!I_{\sigma^{[0]}}, \theta) \tag{I.30}$$

We can derive

$$[\varepsilon_{[0]}] = {}^{\varepsilon}\tilde{\alpha}^0[I] + {}^{\varepsilon}\tilde{\alpha}^1[\sigma^{[0]}] + {}^{\varepsilon}\tilde{\alpha}^2[\sigma^{[0]}]^2 \tag{I.31}$$

in which

$${}^{\varepsilon}\tilde{\alpha}^i = {}^{\varepsilon}\tilde{\alpha}^i\big(\rho_0, I_{\sigma^{[0]}}, I\!I_{\sigma^{[0]}}, I\!I\!I_{\sigma^{[0]}}, \theta\big)\ ;\ i = 0, 1, 2 \tag{I.32}$$

and then establish material coefficients using ${}^{\varepsilon}\tilde{\alpha}^i$ and their Taylor series expansion.

(b) Approach II: expanding $\pi^c = \pi^c(\boldsymbol{\sigma}^{[0]}, \theta)$ in Taylor series about a known configuration and using (I.29)

We consider $\pi = \pi(\boldsymbol{\sigma}^{[0]}, \theta)$ and expand π in $\boldsymbol{\sigma}^{[0]}$ using Taylor series about a known configuration $\underline{\Omega}$.

$$\begin{aligned}(\varepsilon_{[0]})_{mn} =& (\varepsilon^0_{mn})_{\underline{\Omega}} + (\underline{\underline{C}}_{mnij})_{\underline{\Omega}}\sigma^{[0]}_{ij} \\ &+ (\underline{\underline{\tilde{C}}}_{mnijkl})_{\underline{\Omega}}\sigma^{[0]}_{ij}\sigma^{[0]}_{kl} + \dots\end{aligned} \tag{I.33}$$

I.1.6 Constitutive theories for the heat vector $\boldsymbol{q}$: Lagrangian description

The conditions resulting from the entropy inequality require that

$$\boldsymbol{q} \cdot \boldsymbol{g} \leq 0 \tag{I.34}$$

be satisfied by the constitutive theories for $\boldsymbol{q}$ regardless of how they are derived. We can take two approaches to derive constitutive theory for $\boldsymbol{q}$. In the first approach [18, 19], we strictly use (I.34) to derive the constitutive theory for $\boldsymbol{q}$. Such constitutive theory for $\boldsymbol{q}$ will naturally satisfy the entropy inequality as it is derived using the conditions resulting from it. In the second approach we use the argument tensors of $\boldsymbol{q}$ and then use theory of generators and invariants [13–17, 20–30, 32]. The constitutive theories derived using this approach must ensure that the constitutive theories for $\boldsymbol{q}$ satisfy (I.34) so that the deforming matter will be in thermodynamic equilibrium during evolution. We present the derivation of the constitutive theories for $\boldsymbol{q}$ using both approaches and present comparisons of the resulting constitutive theories, discuss assumptions, and make some remarks regarding their merits and shortcomings.

I.1.7 Constitutive theory for $\boldsymbol{q}$ using entropy inequality

This derivation based on (I.34) is fundamental and can be found in any textbook on continuum mechanics [18, 19]. We present details in the following to point out the assumptions used in the derivation as they play a significant role when comparing this constitutive theory with the theories resulting from the theory of generators and invariants. Following references [18, 19], we begin with (I.34). Equation (I.34) implies that

$$\boldsymbol{q} \cdot \boldsymbol{g} = \beta \leq 0 \tag{I.35}$$

Using equality, we obtain

$$\frac{\partial \beta}{\partial \boldsymbol{g}} = \boldsymbol{q} \tag{I.36}$$

β has a maximum value at $\boldsymbol{g} = 0$ [18, 19], hence

$$\frac{\partial \beta}{\partial \boldsymbol{g}}\Big|_{\boldsymbol{g}=0} = \boldsymbol{q}\Big|_{\boldsymbol{g}=0} = 0 \tag{I.37}$$

That is, *heat flux vanishes in the absence of temperature gradient*. Thus, the constitutive theory for $\boldsymbol{q}$ must be a function of $\boldsymbol{g}$. At this stage, many possibilities exist; the simplest of course is assuming that $\boldsymbol{q}$ is proportional to $-\boldsymbol{g}$, i.e. $\boldsymbol{q}$ is a linear function of $-\boldsymbol{g}$.

$$\boldsymbol{q} = -\boldsymbol{k}(\theta) \cdot \boldsymbol{g} \qquad \text{or} \qquad q_i = -k_{ij}(\theta) g_j \tag{I.38}$$

from which we define

$$\frac{\partial \boldsymbol{q}}{\partial \boldsymbol{g}} = -\boldsymbol{k}(\theta) \qquad \text{or} \qquad \frac{\partial q_i}{\partial g_j} = -k_{ij}(\theta) \tag{I.39}$$

Also, from (I.36)

$$\begin{aligned} \frac{\partial^2 \beta}{\partial^2 \boldsymbol{g}} = \frac{\partial \boldsymbol{q}}{\partial \boldsymbol{g}} = -\boldsymbol{k}(\theta) \leq 0 \\ \text{or} \quad \frac{\partial^2 \beta}{\partial g_j \partial g_i} = \frac{\partial q_i}{\partial g_j} = -k_{ij}(\theta) \leq 0 \end{aligned} \tag{I.40}$$

From (I.40), we conclude that the matrix $[k]$ is positive-semidefinite and all its eigenvalues are non-negative. Equation (I.38) is the *Fourier heat conduction law* in Lagrangian description. Thermal conductivity matrix $[k]$ does not have to be symmetric but is often assumed to be. In general, in this constitutive theory for $\boldsymbol{q}$, the coefficients of $[k]$ can be functions of temperature θ. This constitutive theory is based on the assumption that $\boldsymbol{q}$ is a linear function of $\boldsymbol{g}$.

I.1.8 Constitutive theories for $\boldsymbol{q}$ using theory of generators and invariants

In this approach, the heat vector $\boldsymbol{q}$, a tensor of rank one, is expressed as a linear combination of the combined generators (only tensors of rank one) of its argument tensors. The material coefficients in the linear combination are assumed to be functions of the combined invariants of the argument tensors and temperature θ. The material coefficients are derived by expanding each coefficient in the linear combination in Taylor series about a known configuration. In this approach it is obvious that the explicit form of the constitutive theory for $\boldsymbol{q}$ depends on the argument tensors of $\boldsymbol{q}$ and the terms retained in the Taylor series expansion of the coefficients in the linear combination. We present derivations of two constitutive theories for $\boldsymbol{q}$ using this approach.

(a) Approach I

In this derivation, we assume that

$$\boldsymbol{q} = \boldsymbol{q}(\boldsymbol{g}, \theta) \tag{I.41}$$

$\boldsymbol{q}$ and $\boldsymbol{g}$ are tensors of rank one and θ is a tensor of rank zero. The only combined generator of rank one of the argument tensors $\boldsymbol{g}$ and θ is $\boldsymbol{g}$, hence based on the theory of generators and invariants, we can write

$$\boldsymbol{q} = -{}^{q}\alpha \boldsymbol{g} \tag{I.42}$$

The coefficient ${}^{q}\alpha$ is a function of the combined invariants of $\boldsymbol{g}$, θ, i.e. $\{g\}^T\{g\}$ and temperature θ. Then

$$\boldsymbol{q} = -k\boldsymbol{g} - k_1\{g\}^T\{g\}\boldsymbol{g} - k_2(\theta - \theta_{\underset{\sim}{\Omega}})\boldsymbol{g} \tag{I.43}$$

This is the simplest possible constitutive theory based on theory of generators and invariants using (I.41). The only assumption in this theory beyond (I.41) is the truncation of the Taylor series beyond linear terms in ${}^{q}\underset{\sim}{I}$ and θ.

(b) Approach II

In this case, we consider

$$\boldsymbol{q} = \boldsymbol{q}(\boldsymbol{\varepsilon}_{[0]}, \boldsymbol{g}, \theta) \tag{I.44}$$

This is a more general case due to dependence of $\boldsymbol{q}$ on $\boldsymbol{g}$, θ, as well as $\boldsymbol{\varepsilon}_{[0]}$. The heat vector $\boldsymbol{q}$ is a tensor of rank one, whereas $\boldsymbol{\varepsilon}_{[0]}$, $\boldsymbol{g}$, and θ are symmetric tensor of rank two, tensor of rank one, and tensor of rank zero respectively. Justification for retaining $\boldsymbol{\varepsilon}_{[0]}$ as an argument tensor of $\boldsymbol{q}$ (over and beyond the *principle of equipresence*) will be discussed after we present the details of the constitutive theory for $\boldsymbol{q}$ based on (I.44) by using the theory of generators and invariants. The combined generators of rank one of the argument tensors $\boldsymbol{\varepsilon}_{[0]}$, $\boldsymbol{g}$, and θ are

$${}^{q}\underset{\sim}{\boldsymbol{G}}^1 = \boldsymbol{g} \quad ; \quad {}^{q}\underset{\sim}{\boldsymbol{G}}^2 = \boldsymbol{\varepsilon}_{[0]} \cdot \boldsymbol{g} \quad ; \quad {}^{q}\underset{\sim}{\boldsymbol{G}}^3 = (\boldsymbol{\varepsilon}_{[0]} \cdot \boldsymbol{\varepsilon}_{[0]}) \cdot \boldsymbol{g} \tag{I.45}$$

The combined invariants of $\boldsymbol{\varepsilon}_{[0]}$, $\boldsymbol{g}$, and θ are

$$\begin{aligned} &{}^{q}\underset{\sim}{I}^1 = \mathrm{tr}([\varepsilon_{[0]}]) \quad ; \quad {}^{q}\underset{\sim}{I}^2 = \mathrm{tr}([\varepsilon_{[0]}]^2) \\ &{}^{q}\underset{\sim}{I}^3 = \mathrm{tr}([\varepsilon_{[0]}]^3) \quad ; \quad {}^{q}\underset{\sim}{I}^4 = \{g\}^T\{g\} \\ &{}^{q}\underset{\sim}{I}^5 = \{g\}^T[\varepsilon_{[0]}]\{g\} \; ; \; {}^{q}\underset{\sim}{I}^6 = \{g\}^T[\varepsilon_{[0]}]^2\{g\} \end{aligned} \tag{I.46}$$

We note that for ${}^{q}\underset{\sim}{I}^j \; ; j = 1, 2, 3$, we could have also used $I_{\varepsilon_{[0]}}$, $II_{\varepsilon_{[0]}}$, and $III_{\varepsilon_{[0]}}$. As the two sets of invariants are related, the resulting constitutive theory remains unaffected. Using the generators in (I.45), we can write

$$\boldsymbol{q} = -\sum_{i=1}^{3} {}^{q}\tilde{\alpha}^i \; {}^{q}\underset{\sim}{\boldsymbol{G}}^i \tag{I.47}$$

The coefficients ${}^q\tilde{\alpha}^i$ in the linear combination are functions of the invariants ${}^q\underset{\sim}{I}^j$; $j = 1, 2, \ldots, 6$ and θ in the current configuration. To determine the material coefficients from ${}^q\tilde{\alpha}^i$; $i = 1, 2, 3$ in (I.47), we consider Taylor series expansion of ${}^q\tilde{\alpha}^i$; $i = 1, 2, 3$ in ${}^q\underset{\sim}{I}^j$; $j = 1, 2, \ldots, 6$ and θ about a known configuration $\underline{\Omega}$ and retain only up to linear terms in the invariants and θ. This gives

$$\begin{aligned}\boldsymbol{q} = &-{}^q\tilde{a}_1\boldsymbol{g} - {}^q\tilde{a}_2\boldsymbol{\varepsilon}_{[0]}\cdot\boldsymbol{g} - \tilde{b}_{11}\mathrm{tr}([\varepsilon_{[0]}])\boldsymbol{g}\\ &- \tilde{b}_{14}\{g\}^T\{g\}\boldsymbol{g} - \tilde{b}_{15}\{g\}^T[\varepsilon_{[0]}]\{g\}\boldsymbol{g}\\ &- \tilde{b}_{24}\{g\}^T\{g\}\,\boldsymbol{\varepsilon}_{[0]}\cdot\boldsymbol{g} - {}^q\tilde{c}_1(\theta-\theta_{\underline{\Omega}})\boldsymbol{g}\\ &- {}^q\tilde{c}_2(\theta-\theta_{\underline{\Omega}})\boldsymbol{\varepsilon}_{[0]}\cdot\boldsymbol{g}\end{aligned} \tag{I.48}$$

This constitutive theory requires eight material coefficients. If we remove the dependence of $\boldsymbol{q}$ on $\boldsymbol{\varepsilon}_{[0]}$ in (I.48), then

$$\boldsymbol{q} = -{}^q\tilde{a}_1\boldsymbol{g} - \tilde{b}_{14}\big(\{g\}^T\{g\}\big)\boldsymbol{g} - {}^q\tilde{c}_1(\theta-\theta_{\underline{\Omega}})\boldsymbol{g} \tag{I.49}$$

This constitutive theory for $\boldsymbol{q}$ is the same as derived earlier (equation (I.43)). The coefficients in (I.49) are functions of $\theta_{\underline{\Omega}}$ and $(\{g\}^T\{g\})_{\underline{\Omega}}$.

(c) Approach III

In this case, we consider

$$\boldsymbol{q} = \boldsymbol{q}(\boldsymbol{\sigma}^{[0]}, \theta, \boldsymbol{g}) \tag{I.50}$$

This is a more general case due to dependence of $\boldsymbol{q}$ on $\boldsymbol{g}$, θ as well as $\boldsymbol{\sigma}^{[0]}$. $\boldsymbol{q}$ is a tensor of rank one, whereas $\boldsymbol{\sigma}^{[0]}$, $\boldsymbol{g}$ and θ are symmetric tensor of rank two, tensor of rank one, and tensor of rank zero, respectively. Justification for retaining $\boldsymbol{\sigma}^{[0]}$ as an argument tensor of $\boldsymbol{q}$ will be discussed after we present details of the constitutive theory for $\boldsymbol{q}$ based on (I.50) by using the theory of generators and invariants. The combined generators of rank one of the argument tensors $\boldsymbol{\sigma}^{[0]}$, $\boldsymbol{g}$ and θ are

$$\begin{aligned}&{}^q\underset{\sim}{\boldsymbol{G}}^1 = \boldsymbol{g} \quad ; \quad {}^q\underset{\sim}{\boldsymbol{G}}^2 = \boldsymbol{\sigma}^{[0]}\cdot\boldsymbol{g}\\ &{}^q\underset{\sim}{\boldsymbol{G}}^3 = (\boldsymbol{\sigma}^{[0]}\cdot\boldsymbol{\sigma}^{[0]})\cdot\boldsymbol{g}\end{aligned} \tag{I.51}$$

The combined invariants of the argument tensors $\boldsymbol{\sigma}^{[0]}$, $\boldsymbol{g}$ and θ are

$$\begin{aligned}&{}^q\underset{\sim}{I}^1 = \mathrm{tr}([\sigma^{[0]}]) \quad ; \quad {}^q\underset{\sim}{I}^2 = \mathrm{tr}([\sigma^{[0]}]^2)\\ &{}^q\underset{\sim}{I}^3 = \mathrm{tr}([\sigma^{[0]}]^3) \quad ; \quad {}^q\underset{\sim}{I}^4 = \{g\}^T\{g\}\\ &{}^q\underset{\sim}{I}^5 = \{g\}^T[\sigma^{[0]}]\{g\} \quad ; \quad {}^q\underset{\sim}{I}^6 = \{g\}^T[\sigma^{[0]}]^2\{g\}\end{aligned} \tag{I.52}$$

We note that for ${}^q\underset{\sim}{I}^j$; $j = 1, 2, 3$ we could have also used $I_{\sigma^{[0]}}$, $I\!I_{\sigma^{[0]}}$ and $I\!I\!I_{\sigma^{[0]}}$. As the two sets of invariants are related, the resulting constitutive theory remains unaffected. Using (I.51), we can write

$$\boldsymbol{q} = -\sum_{i=1}^{3} {}^q\alpha^i\ {}^q\underset{\sim}{\boldsymbol{G}}^i \tag{I.53}$$

The coefficients ${}^q\alpha^i$; $i = 1, 2, 3$ are functions of invariants ${}^q\underset{\sim}{I}^j$; $j = 1, 2, \ldots, 6$ and temperature θ in the current configuration. To determine the material coefficients from ${}^q\alpha^i$; $i = 1, 2, 3$ in (I.53), we consider Taylor series expansion of ${}^q\alpha^i$; $i = 1, 2, 3$ in ${}^q\underset{\sim}{I}^j$; $j = 1, 2, \ldots, 6$ and θ about a known configuration $\underline{\Omega}$ and retain only up to linear terms in θ and the invariants. The final form is given below.

$$\begin{aligned}\boldsymbol{q} = &-\sum_{i=1}^{3} {}^q a_i\ {}^q\underset{\sim}{\boldsymbol{G}}^i - \sum_{i=1}^{3}\sum_{j=1}^{6} {}^q b_{ij}\,{}^q\underset{\sim}{I}^j\ {}^q\underset{\sim}{\boldsymbol{G}}^i\\ &- \sum_{i=1}^{3} {}^q c_i(\theta-\theta_{\underline{\Omega}})\ {}^q\underset{\sim}{\boldsymbol{G}}^i\end{aligned} \tag{I.54}$$

Remarks

(1) With some assumptions the constitutive theory (I.54) for $\boldsymbol{q}$ can be simplified to yield an approximate constitutive theory in which the material coefficients may not be as many as in (I.54). This will undoubtedly limit the physics. If we limit the constitutive theory to be linear in $\boldsymbol{\sigma}^{[0]}$, that is, we neglect generator ${}^{q}\underset{\sim}{\boldsymbol{G}}^{3} = (\boldsymbol{\sigma}^{[0]} \cdot \boldsymbol{\sigma}^{[0]}) \cdot \boldsymbol{g}$ and invariants ${}^{q}\underset{\sim}{I}^{2}$, ${}^{q}\underset{\sim}{I}^{3}$ and ${}^{q}\underset{\sim}{I}^{6}$, the constitutive theory (I.54) for $\boldsymbol{q}$ reduces to

$$\begin{aligned}\boldsymbol{q} = &- {}^{q}a_1\boldsymbol{g} - {}^{q}a_2\boldsymbol{\sigma}^{[0]} \cdot \boldsymbol{g} - {}^{q}b_{11}\mathrm{tr}([\sigma^{[0]}])\boldsymbol{g} \\ &- {}^{q}b_{14}\{g\}^{T}\{g\}\boldsymbol{g} - {}^{q}b_{15}\{g\}^{T}[\sigma^{[0]}]\{g\}\boldsymbol{g} \\ &- {}^{q}b_{21}\mathrm{tr}([\sigma^{[0]}])\boldsymbol{\sigma}^{[0]} \cdot \boldsymbol{g} - {}^{q}b_{24}\{g\}^{T}\{g\}\boldsymbol{\sigma}^{[0]} \cdot \boldsymbol{g} \\ &- {}^{q}b_{25}\{g\}^{T}[\sigma^{[0]}]\{g\}\boldsymbol{\sigma}^{[0]} \cdot \boldsymbol{g} \\ &- {}^{q}c_1(\theta - \theta_{\underline{\Omega}})\boldsymbol{g} - {}^{q}c_2(\theta - \theta_{\underline{\Omega}})\boldsymbol{\sigma}^{[0]} \cdot \boldsymbol{g}\end{aligned} \tag{I.55}$$

This constitutive theory still requires ten material coefficients. If we further assume that the constitutive theory for $\boldsymbol{q}$ is linear in the components of $\boldsymbol{\sigma}^{[0]}$, then terms containing material coefficients ${}^{q}b_{21}$ and ${}^{q}b_{25}$ can be removed from (I.55).

$$\begin{aligned}\boldsymbol{q} = &- {}^{q}a_1\boldsymbol{g} - {}^{q}a_2\boldsymbol{\sigma}^{[0]} \cdot \boldsymbol{g} - {}^{q}b_{11}\mathrm{tr}([\sigma^{[0]}])\boldsymbol{g} \\ &- {}^{q}b_{14}\{g\}^{T}\{g\}\boldsymbol{g} - {}^{q}b_{15}\{g\}^{T}[\sigma^{[0]}]\{g\}\boldsymbol{g} \\ &- {}^{q}b_{24}\{g\}^{T}\{g\}\,\boldsymbol{\sigma}^{[0]} \cdot \boldsymbol{g} - {}^{q}c_1(\theta - \theta_{\underline{\Omega}})\boldsymbol{g} \\ &- {}^{q}c_2(\theta - \theta_{\underline{\Omega}})\boldsymbol{\sigma}^{[0]} \cdot \boldsymbol{g}\end{aligned} \tag{I.56}$$

This constitutive theory requires eight material coefficients.

(2) If we remove dependence of $\boldsymbol{q}$ on $\boldsymbol{\sigma}^{[0]}$ in (I.56), then

$$\boldsymbol{q} = -{}^{q}a_1\boldsymbol{q} - {}^{q}b_{14}\{g\}^{T} \cdot \{g\}\boldsymbol{q} - {}^{q}c_1(\theta - \theta_{\underline{\Omega}})\boldsymbol{q} \tag{I.57}$$

This constitutive theory for $\boldsymbol{q}$ is the same as derived earlier. The coefficients in (I.57) are functions of $\theta_{\underline{\Omega}}$ and $(\{g\}^{T}\{g\})_{\underline{\Omega}}$.

I.1.9 Summary and conclusions

In this section, constitutive theories for thermoelastic solids are presented in Lagrangian description. For such solid matter, the external work applied to a volume of matter does not contribute to entropy production and hence the thermal field and internal energy are not affected by the external work. It is shown that for such matter, the entropy inequality has no mechanism for deriving constitutive theories for $\boldsymbol{\sigma}^{[0]}$ or $\boldsymbol{\varepsilon}_{[0]}$ as the first and the second law of thermodynamics are independent of the rate of mechanical work. Constitutive theories for $\boldsymbol{\sigma}^{[0]}$ or $\boldsymbol{\varepsilon}_{[0]}$ are presented using the theory of generators and invariants. First, general derivations (such as those based on integrity) are presented which are subsequently simplified to obtain simpler constitutive theories for finite as well as infinitesimal deformation. It is also shown that for such matter, strain energy density function or its complement can be used to derive constitutive theories for $\boldsymbol{\sigma}^{[0]}$ or $\boldsymbol{\varepsilon}_{[0]}$ in addition to constitutive theories for $\boldsymbol{\sigma}^{[0]}$ in terms of $\boldsymbol{C}_{[0]}$ in Lagrangian description. Since there are no thermodynamic restrictions on the constitutive theories for the stress tensor or strain tensor for the solids considered here, all of the theories presented here are valid. The constitutive theories for the heat vector in Lagrangian description are derived using the conditions resulting from the entropy inequality as well as using the theory of generators and invariants with various choices of argument tensors. Simplifications of these theories are also presented.

I.2 Ordered rate constitutive theories for thermoviscoelastic solids without memory

In this section, we consider ordered rate constitutive theories for isotropic, homogeneous, compressible and incompressible thermoviscoelastic solids in Lagrangian description with finite deformation but without memory. The rate constitutive theories are derived using the entropy inequality expressed in terms of Helmholtz free energy density Φ as well as Gibbs potential Ψ.

Thermoviscoelastic solids are naturally elastic (linear or nonlinear) but also contain thermal effects. In addition, such solids also contain a mechanism of dissipation of mechanical energy, i.e. some part of the mechanical energy applied to the matter is converted into entropy, which results in heat, hence affects internal energy. Derivations of the constitutive theories for such solid matter are considered.

I.2.1 Ordered rate constitutive theories for thermoviscoelastic solids without memory using Φ

We consider basic form [18,19,31] of the entropy inequality (Clausius-Duhem inequality) expressed in terms of Φ and conjugate pair $\boldsymbol{\sigma}^{[0]}$ and $\boldsymbol{\varepsilon}^{[0]}$

$$\rho_0 \dot{\Phi} + \eta \dot{\theta} + \frac{q_i g_i}{\theta} - \sigma^*_{ki} \dot{J}_{ik} \leq 0 \tag{I.58}$$

in which ρ_0 is density in the reference configuration and $|J|$ is determinate of the Jacobian of deformation. This allows us (in conjunction with other conservation laws) to conclude that at the onset Φ, η $\boldsymbol{\sigma}^{[0]}$ and $\boldsymbol{q}$ must be dependent variables in the constitutive theory. Following the material presented in the previous section, it is straightforward to conclude the following argument tensors of the dependent variables

$$\begin{aligned} \Phi &= \Phi\big(\boldsymbol{\varepsilon}^{[0]}, \boldsymbol{g}, \theta\big) \\ \eta &= \eta\big(\boldsymbol{\varepsilon}^{[0]}, \boldsymbol{g}, \theta\,\big) \\ \boldsymbol{\sigma}^{[0]} &= \boldsymbol{\sigma}^{[0]}\big(\boldsymbol{\varepsilon}^{[0]}, \boldsymbol{g}, \theta\big) \\ \boldsymbol{q} &= \boldsymbol{q}\big(\boldsymbol{\varepsilon}^{[0]}, \boldsymbol{g}, \theta\big) \end{aligned} \tag{I.59}$$

In thermoviscoelastic solids without memory, the mechanism of dissipation must be incorporated in the constitutive theories. This requires that at least $\boldsymbol{\varepsilon}^{[1]}$, the material derivative of order one must be an argument tensor of $\boldsymbol{\sigma}^{[0]}$ and hence of all other dependent variables due to the principle of equipresence. Since $\boldsymbol{\varepsilon}^{[i]}\,; i = 1, 2, \ldots, n$, the material derivatives of upto orders n of $\boldsymbol{\varepsilon}$, are fundamental kinematic tensors, we can generalize the choice of $\boldsymbol{\varepsilon}^{[1]}$ as argument tensor by replacing it with $\boldsymbol{\varepsilon}^{[i]}\,; i = 1, 2, \ldots, n$. Thus (I.59) now becomes

$$\begin{aligned} \Phi &= \Phi\big(\,\boldsymbol{\varepsilon}^{[i]}(x_i, t)\,;\; i = 0, 1, \ldots, n\;,\; \theta(x_i, t)\,\big) \\ \boldsymbol{\sigma}^{[0]} &= \boldsymbol{\sigma}^{[0]}\big(\,\boldsymbol{\varepsilon}^{[i]}(x_i, t)\,;\; i = 0, 1, \ldots, n\;,\; \theta(x_i, t)\,\big) \\ \boldsymbol{q} &= \boldsymbol{q}\big(\,\boldsymbol{\varepsilon}^{[i]}(x_i, t)\,;\; i = 0, 1, \ldots, n\;,\; \boldsymbol{g}(x_i, t)\;,\; \theta(x_i, t)\,\big) \end{aligned} \tag{I.60}$$

The conditions resulting from the entropy inequality in this case do not permit derivation of constitutive theories for $\boldsymbol{\sigma}^{[0]}$. We perform decomposition of $\boldsymbol{\sigma}^{[0]}$ into equilibrium stress ${}_e\boldsymbol{\sigma}^{[0]}$ and deviatoric stress ${}_d\boldsymbol{\sigma}^{[0]}$ and substitute it in the entropy inequality. The resulting conditions permit derivation of ${}_e\boldsymbol{\sigma}^{[0]}$ in terms of thermodynamic pressure $p(\rho, \theta)\boldsymbol{I}$ for compressible case and in terms of mechanical pressure $p(\theta)\boldsymbol{I}$ for incompressible case (derived by incorporating incompressibility condition in the entropy inequality). Additionally, the entropy inequality requires the work expanded due to ${}_d\boldsymbol{\sigma}^{[0]}$ to be positive if we assume

$$\frac{q_i g_i}{\theta} \leq 0 \qquad \text{or} \qquad q_i g_i \leq 0 \tag{I.61}$$

but provides no mechanism to derive constitutive theories for ${}_d\boldsymbol{\sigma}^{[0]}$. At this stage we have

$$\begin{aligned} \boldsymbol{\sigma}^{[0]} &= {}_e\boldsymbol{\sigma}^{[0]} + {}_d\boldsymbol{\sigma}^{[0]}\big(\,\boldsymbol{\varepsilon}^{[0]}\;,\; \boldsymbol{\varepsilon}^{[i]}(x_i, t)\,;\; i = 1, 2, \ldots, n\;,\; \theta(x_i, t)\,\big) \\ \boldsymbol{q} &= \boldsymbol{q}\big(\,\boldsymbol{\varepsilon}^{[0]}\;,\; \boldsymbol{\varepsilon}^{[i]}(x_i, t)\,;\; i = 1, 2, \ldots, n\;,\; \boldsymbol{g}(x_i, t)\;,\; \theta(x_i, t)\,\big) \end{aligned} \tag{I.62}$$

in which

$$\begin{aligned} {}_e\boldsymbol{\sigma}^{(0)} &= p(\rho, \theta)\boldsymbol{I} \qquad ; \qquad \text{compressible case} \\ {}_e\boldsymbol{\sigma}^{(0)} &= p(\theta)\boldsymbol{I} \qquad ; \qquad \text{incompressible case} \end{aligned} \tag{I.63}$$

We transfor ${}_e\boldsymbol{\sigma}^{(0)}$ to obtain ${}_e\boldsymbol{\sigma}^{[0]}$ for both compressible and incompressible case.

(a) Rate constitutive theories for ${}_d\boldsymbol{\sigma}^{[0]}$ of order n: We derive constitutive theories for ${}_d\boldsymbol{\sigma}^{[0]}$ using the theory of generators and invariants. If $[{}^{\sigma}\underset{\sim}{G}^i]\ ; i = 1, 2, \ldots, N$ are the combined generators of the argument tensors of ${}_d\boldsymbol{\sigma}^{[0]}$ in (I.62) that are symmetric tensors of rank two and if ${}^{q\sigma}\underset{\sim}{I}^j\ ; j = 1, 2, \ldots, M$ are the combined invariants of the same argument tensors, then

$$ {}_d\boldsymbol{\sigma}^{[0]} = {}^{\sigma}\tilde{\alpha}^0 + \sum_{i=1}^{N} {}^{\sigma}\tilde{\alpha}^i [{}^{\sigma}\underset{\sim}{G}^i] \tag{I.64} $$

$$ {}^{\sigma}\tilde{\alpha}^i = {}^{\sigma}\tilde{\alpha}^i \big({}^{q\sigma}\underset{\sim}{I}^j\ ;\ j = 1, 2, \ldots, M\ ,\ \theta \big) \qquad ; \qquad i = 1, 2, \ldots, N \tag{I.65} $$

The material coefficients are derived by expanding ${}^{\sigma}\tilde{\alpha}^i\ ; i = 0, 1, \ldots, N$ in ${}^{q\sigma}\underset{\sim}{I}^j\ ; j = 1, 2, \ldots, M$ and θ about a known configuration $\underline{\Omega}$ and retaining only upto linear terms in ${}^{q\sigma}\underset{\sim}{I}^j\ ; 1, 2, \ldots, M$ and θ. This gives us

$$ \boldsymbol{\sigma}^{[0]} = \underline{\sigma}^0\big|_{\underline{\Omega}}[I] + \sum_{j=1}^{M} {}^{\sigma}\underline{a}_j\, {}^{q\sigma}\underset{\sim}{I}^j[I] + \sum_{i=1}^{N} {}^{\sigma}\underline{b}_i [{}^{\sigma}\underset{\sim}{G}^i] + \sum_{i=1}^{N}\sum_{j=1}^{M} {}^{\sigma}\underline{c}_{ij}\, {}^{q\sigma}\underset{\sim}{I}^j [{}^{\sigma}\underset{\sim}{G}^i] + \sum_{i=1}^{N} {}^{\sigma}\underline{d}_i (\theta - \theta_{\underline{\Omega}})[{}^{\sigma}\underset{\sim}{G}^i] - (\alpha_{tm})_{\underline{\Omega}}(\theta - \theta_{\underline{\Omega}})[I] \tag{I.66} $$

$\underline{\sigma}^0\big|_{\underline{\Omega}}$ is the initial stress in the configuration $\underline{\Omega}$. This constitutive theory for ${}_d\boldsymbol{\sigma}^{[0]}$ requires $(M + N + MN + N + 1)$ material coefficients. The material coefficients defined in (I.66) are functions of $\theta_{\underline{\Omega}}$ and $({}^{q\sigma}\underset{\sim}{I}^j)_{\underline{\Omega}}\ ; j = 1, 2, \ldots, M$ in the known configuration $\underline{\Omega}$. This constitutive theory is based on integrity and hence is complete. See reference [33] for definitions of material coefficients.

(b) Rate constitutive theories for $\boldsymbol{q}$ of order n: In this derivation we consider the argument tensors of $\boldsymbol{q}$ in (I.62). We express $\boldsymbol{q}$ as a linear combination of the combined generators of the argument tensors of $\boldsymbol{q}$. As in the case of ${}_d\boldsymbol{\sigma}^{[0]}$, here also the coefficients in the linear combination are functions of the combined invariants of the argument tensors of $\boldsymbol{q}$. The material coefficients in this case are also derived using a Taylor series expansion of each coefficient in the linear combination about a known configuration. $\boldsymbol{q}$ is a tensor of rank one, but $\boldsymbol{\varepsilon}^{[0]}, \boldsymbol{\varepsilon}^{[m]}\ ; m = 1, 2, \ldots, n$ are symmetric tensors of rank two and $\boldsymbol{g}$, θ are tensors of rank one and zero. Let $\{{}^{q}\underset{\sim}{G}^i\}\ ; i = 1, 2, \ldots, \widetilde{N}$ be the combined generators of the argument tensors of $\boldsymbol{q}$ that are tensors of rank one and let ${}^{q\sigma}\underset{\sim}{I}^j\ ; j = 1, 2, \ldots, M$ be the combined invariants of the same argument tensors of $\boldsymbol{q}$, which are the same as those for ${}_d\boldsymbol{\sigma}^{[0]}$. Then, we can express $\boldsymbol{q}$ in the current configuration as a linear combination of $\{{}^{q}\underset{\sim}{G}^i\}\ ; i = 1, 2, \ldots, \widetilde{N}$:

$$ \boldsymbol{q} = -\sum_{i=1}^{\widetilde{N}} {}^{q}\tilde{\alpha}^i \{{}^{q}\underset{\sim}{G}^i\} \tag{I.67} $$

$$ {}^{q}\tilde{\alpha}^i = {}^{q}\tilde{\alpha}^i \big({}^{q\sigma}\underset{\sim}{I}^j\ ;\ j = 1, 2, \ldots, M, \theta \big) \tag{I.68} $$

To determine the material coefficients from ${}^{q}\tilde{\alpha}^i\ ; i = 1, 2, \ldots, \widetilde{N}$, we consider a Taylor series expansion of each ${}^{q}\tilde{\alpha}^i\ ; i = 1, 2, \ldots, \widetilde{N}$ about a known configuration $\underline{\Omega}$ in invariants ${}^{q\sigma}\underset{\sim}{I}^j\ ; j = 1, 2, \ldots, M$ and temperature θ and retain only up to linear terms in the invariants and the temperature θ. By substituting these in (I.67) we obtain

$$ \boldsymbol{q} = -\sum_{i=1}^{\widetilde{N}} {}^{q}\underline{b}_i \{{}^{q}\underset{\sim}{G}^i\} - \sum_{i=1}^{\widetilde{N}}\sum_{j=1}^{M} {}^{q}\underline{c}_{ij}\, {}^{q\sigma}\underset{\sim}{I}^j \{{}^{q}\underset{\sim}{G}^j\} - \sum_{i=1}^{\widetilde{N}} {}^{q}\underline{d}_i (\theta - \theta_{\underline{\Omega}}) \{{}^{q}\underset{\sim}{G}^i\} \tag{I.69} $$

This constitutive theory for $\boldsymbol{q}$ requires $(\widetilde{N} + \widetilde{N}M + \widetilde{N})$ material coefficients (see reference [33] for their definition). These material coefficients defined are functions of invariants $({}^{q\sigma}\underset{\sim}{I}^j)_{\underline{\Omega}}\ ; j = 1, 2, \ldots, M$ and temperature $\theta_{\underline{\Omega}}$ in the known configuration $\underline{\Omega}$. This constitutive theory is also based on integrity, hence is complete.

Remarks:

(1) Using the general derivations presented for rate theories of order n for ${}_d\boldsymbol{\sigma}^{[0]}$ and $\boldsymbol{q}$, constitutive theories of any desired order can be obtained.

(2) Constitutive theory for $\boldsymbol{q}$ is consistent with the constitutive theory for ${}_d\boldsymbol{\sigma}^{[0]}$ as it uses the same argument tensors as in the case of ${}_d\boldsymbol{\sigma}^{[0]}$. At this stage, there is no rational to alter the argument tensors of $\boldsymbol{q}$. The constitutive theory for $\boldsymbol{q}$ demonstrates the influence of $\boldsymbol{\varepsilon}$ and $\boldsymbol{\varepsilon}^{[m]}\ ; m = 1, 2, \ldots, n$ as well as their interaction with $\boldsymbol{g}$ on heat conduction.

(3) Simplified rate theories can be derived using the rate theories of order n derived here for ${}_d\boldsymbol{\sigma}^{[0]}$ and $\boldsymbol{q}$. These are presented in reference [33] along with comparisons with current theories.

(4) Comparisons of constitutive theories for ${}_d\boldsymbol{\sigma}^{[0]}$ with Kelvin-Voigt model are given in reference [33] to demonstrate that Kelvin-Voigt model does not have thermodynamic basis and cannot be extended to 2-d or 3-d. The theories derived here use ${}_d\boldsymbol{\sigma}^{[0]}$ and $\boldsymbol{\varepsilon}^{[i]}$; $i = 1, 2, \ldots, n$ that are measures of finite deformation, whereas Kelvin-Voigt model uses $\boldsymbol{\sigma}$, total stress for infinitesimal deformation. Many other differences are also illustrated in reference [33].

(5) For elastic materials, the strain rate in one direction must be accompanied by the strain rate in the two mutually orthogonal directions as well, due to Poisson's effect. This is evident in the composition of the coefficient matrix in which the (3×3) portion of the coefficient matrix associated with normal strain rates is fully populated, (i.e. not diagonal).

(6) Thus, we see that the mathematical model associated with strain rate dependent dissipation requires two material coefficients (just like strain dependent elasticity).

(7) When we consider the 1-d case for incompressible viscoelastic solid matter and compare with the Kelvin-Voigt model, we shall observe that dissipation is due to strain rate of order one.

(8) We note that if we ignore the elastic part, then this theory is a counterpart to Newton's law of viscosity, but in Lagrangian description, which confirms that the mechanism of dissipation in the theories presented here is the same as in viscous fluids.

(9) The simple first order rate theory when simplified and applied to 1-d incompressible viscoelastic solid yields a constitutive theory for deviatoric axial stress that is similar in appearance to the Kelvin-Voigt model but is quite different due to the fact that in the Kelvin-Voigt model, the constitutive theory is for total axial stress.

(10) The derivation of the n^{th} order rate theory shows that when strain and strain rate tensors are arguments of the stress tensor, decomposition of the stress tensor into equilibrium and deviatoric tensors is essential. The constitutive theories for equilibrium stress tensor for compressible as well as incompressible cases are derived using the conditions resulting from the entropy inequality, while the constitutive theory for deviatoric stress tensor is derived using theory of generators and invariants. These derivations are consistent with the axioms and principles of continuum mechanics.

(11) Based on (10) and the derivation presented for the simplified 1-d case, it is straightforward to conclude that the 1-d Kelvin-Voigt model for viscoelastic solids is not supported by the rate theories presented in this work and the thermodynamic principles.

(12) For the 1-d linear elastic incompressible case with infinitesimal deformation, the momentum equation or equilibrium equation resulting from the presented theory and the Kelvin-Voigt model are the same, provided the material coefficients are assumed to be identical, which is not the case.

(13) In the 1-d Kelvin-Voigt model, a single material coefficient describes the mechanism of dissipation (damping coefficient for the dash-pot). From the derivation presented here and the physics, it is quite clear that the mechanism of dissipation in viscoelastic solids requires two material coefficients.

(14) The 1-d spring and dash-pot in parallel has no mechanism for its extension: (i) to 2-d or 3-d or continuous media in general, (ii) for compressible matter, (iii) for finite deformation and finite strain, whereas the derivations presented in this work are for finite deformation and are consistent with the axioms of constitutive theory in continuum mechanics.

(15) Simplified constitutive theories for $\boldsymbol{q}$ can be easily derived using (I.69) with the appropriate assumption and by following the details in previous section and reference [33, 34]. The details are omitted for the sake of brevity.

I.2.2 Ordered rate constitutive theories for thermoviscoelastic solids without memory [35] using Ψ

The rate constitutive theories presented in the following section are derived using entropy inequality expressed in terms of Gibbs potential Ψ and the conditions resulting from it in conjunction with the theory of generators and invariants. In this approach Ψ, $\boldsymbol{\varepsilon}$ and $\boldsymbol{q}$ always emerge as dependent variables for the type of solids considered in this work. Thus the objective of the constitutive theories is to establish dependence of $\boldsymbol{\varepsilon}$ and $\boldsymbol{q}$ on the kinematics of the deforming solid during evolution. The argument tensors of Φ, $\boldsymbol{\varepsilon}$ and $\boldsymbol{q}$ depend upon the physics under consideration i.e. the type of solid matter. As in case of Helmholtz free energy density Φ, here also, we choose $\boldsymbol{\sigma}^{[0]}$ and $\boldsymbol{\varepsilon}$ as conjugate pair in the derivations of the rate constitutive theories. For some types of solids such as thermoviscoelastic, the conditions resulting from the entropy inequality are sufficient to derive the constitutive theories for $\boldsymbol{\varepsilon}$ and $\boldsymbol{q}$. However, it is shown that the theory of generators and invariants in some cases provides much more comprehensive theories. This approach also becomes necessary in many instances when the entropy inequality fails to provide mechanism of deriving constitutive theories. In the work performed during this period of the grant, various approaches are explored and the resulting constitutive theories are compared for their merits and shortcomings. These theories are also compared with those used currently to demonstrate the differences and limitations of the current theories that in many cases are significant and are of major concern.

The derivations of these rate theories follow details similar to those already presented in earlier sections once the dependent variables and their argument tensors are established, hence, in the following, we only presents basic steps and outline of the derivations.

We consider the derivations of the constitutive theories in Lagrangian description for homogeneous, isotropic, compressible and incompressible thermoviscoelastic solids without memory undergoing finite deformation based on the second law of thermodynamics expressed in terms of Gibbs potential Ψ and conjugate stress and strain measures: $\boldsymbol{\sigma}^{[0]}$, $\boldsymbol{\varepsilon}$. The entropy inequality is derived in Lagrangian description using Gibbs potential Ψ and conjugate pair $\boldsymbol{\sigma}^{[0]}$, $\boldsymbol{\varepsilon}$ and the possible choice of dependent variables: $\Psi, \boldsymbol{\varepsilon}, \eta$ (entropy inequality) and $\boldsymbol{q}$ is established. In the rate theories considered here, the constitutive theories for $\boldsymbol{\varepsilon}$ is derived by considering $\boldsymbol{\varepsilon}^{[n]}$ as a dependent variable in the constitutive theory. At the onset, $\boldsymbol{\varepsilon}^{[i]}$; $i = 0, 1 \ldots, n-1$, $\boldsymbol{\sigma}^{[0]}$, $\boldsymbol{g}$ and θ are considered as argument tensors of Ψ, $\boldsymbol{\varepsilon}^{[n]}$, η and $\boldsymbol{q}$. With this choice of argument tensors for Ψ, when $\dot{\Psi}$ (obtained using chain rule of differentiation) is substituted in the entropy inequality, the resulting conditions show that Ψ cannot be a function of $\boldsymbol{\varepsilon}^{[i]}$; $i = 0, 1 \ldots, n-1$ and $\boldsymbol{g}$. Additionally Ψ cannot be a function of $\boldsymbol{\sigma}^{[0]}$. This requires decomposition of $\boldsymbol{\sigma}^{[0]}$ into ${}_e\boldsymbol{\sigma}^{[0]}$, equilibrium stress, and ${}_d\boldsymbol{\sigma}^{[0]}$, deviatoric stress. This permits Ψ to be a function of ${}_d\boldsymbol{\sigma}^{[0]}$. The conditions resulting from the entropy also show that η cannot be a dependent variable in the rate constitutive theories. Thus, finally we have Ψ, $\boldsymbol{\varepsilon}^{[n]}$ and $\boldsymbol{q}$ as dependent variables in the rate constitutive theory. The argument tensors of Ψ are ${}_d\boldsymbol{\sigma}^{[0]}$ and θ whereas as the argument tensors of $\boldsymbol{\varepsilon}^{[n]}$ and $\boldsymbol{q}$ are $\boldsymbol{\varepsilon}^{[i]}$; $i = 0, 1 \ldots, n-1$, ${}_d\boldsymbol{\sigma}^{[0]}$, $\boldsymbol{g}$ and θ. The constitutive theory for ${}_e\boldsymbol{\sigma}^{[0]}$ is well established [18, 19, 31] in terms of thermodynamic pressure for compressible case and mechanical pressure when the matter is incompressible. The remaining last inequality resulting from the entropy inequality places some restrictions on the constitutive theories for $\boldsymbol{\sigma}^{[0]}$, $\boldsymbol{\varepsilon}$ and $\boldsymbol{q}$ but provides no mechanism to derive constitutive theories for $\boldsymbol{\varepsilon}$ and $\boldsymbol{q}$. In the present work, we use the theory of generators and invariants to derive the constitutive theories for $\boldsymbol{\varepsilon}$ and $\boldsymbol{q}$ using $\boldsymbol{\varepsilon}^{[n]}$ and $\boldsymbol{q}$ as dependent variables in the constitutive theories. These rate theories are of order n due to the fact they utilize material derivatives upto order n of $\boldsymbol{\varepsilon}$. The constitutive theories presented here for $\boldsymbol{\varepsilon}$ and $\boldsymbol{q}$ are consistent as they use the same argument tensors and are complete as they are based on integrity.

Many simplified forms of these rate theories of order n are also considered. The most obvious is the constitutive theory of order one. It is shown that even this theory contain too many material coefficients to be of use in practical applications. Further simplifications of these theories are also considered and compared with those that are currently used. The constitutive theories for heat vector include influence of strain, strain rate and stress field in addition to temperature gradient as well as their interactions. Many simplified forms of the n^{th} ordered theory are presented. The most simplified form of the first order rate theory for the heat vector is shown to result in Fourier heat conduction law.

I.2.3 Numerical studies

In this section, we present some numerical studies using the constitutive theory presented here and comparisons with the currently and commonly used model for dissipation in solids in which dissipation is proportional to velocity. We consider the 1D case with infinitesimal strain tensor. As shown earlier for this particular 1D case, the momentum equation resulting from the

constitutive theory presented here and using the *Kelvin-Voigt 1D model* is the same.

$$\rho_0 \frac{\partial^2 u_{x_1}}{\partial t^2} - c_1 \frac{\partial^2 u_{x_1}}{\partial x_1^2} - c_2 \frac{\partial}{\partial t}\Big(\frac{\partial^2 u_{x_1}}{\partial x_1^2}\Big) = 0 \qquad \forall (x_1, t) \in \Omega_{x_1,t} \tag{I.70}$$

in which $\Omega_{x_1,t} = \Omega_{x_1} \times \Omega_t = \Omega_{x_1} \times [0, \tau]$. If we assume dissipation is proportional to velocity (a commonly used mechanism for structural damping in solids [40]), then the momentum equation becomes

$$\rho_0 \frac{\partial^2 u_{x_1}}{\partial t^2} - c_1 \frac{\partial^2 u_{x_1}}{\partial x_1^2} + \underset{\sim}{c}_2 \frac{\partial u_{x_1}}{\partial t} = 0 \qquad \forall (x_1, t) \in \Omega_{x_1,t} \tag{I.71}$$

We remark that in the derivation of (I.71) we only have the constitutive theory for elastic behavior; the damping or dissipation is directly through the momentum equation (rate of change of momentum must be equal to the sum of the forces acting on the volume of matter) in terms of a dissipative force (the third term in (I.71)).

Using (I.70) and (I.71) as mathematical models we present some numerical studies for 1D wave propagation using space-time least squares finite element processes based on a space-time strip $\Omega_{x_1} \times \Delta t$ for an increment with time marching. The local approximations for a space-time element are considered in higher order space-time scalar product spaces that permit higher-order global differentiability approximations in space and time.

First, derive the dimensional form of the PDEs (I.70) and (I.71). Consider PDE (I.70). We rewrite (I.70) by introducing a hat $(\widehat{\ })$ on all quantities signifying that all quantities have their usual dimensions.

$$\widehat{\rho}_0 \frac{\partial^2 \widehat{u}_{x_1}}{\partial \widehat{t}^2} - \widehat{c}_1 \frac{\partial^2 \widehat{u}_{x_1}}{\partial \widehat{x}_1^2} - \widehat{c}_2 \frac{\partial}{\partial \widehat{t}}\Big(\frac{\partial^2 \widehat{u}_{x_1}}{\partial \widehat{x}_1^2}\Big) = 0 \quad \forall (\widehat{x}_1, \widehat{t}) \in \Omega_{\widehat{x}_1,\widehat{t}} \tag{I.72}$$

in which $\Omega_{\widehat{x}_1,\widehat{t}} = \Omega_{\widehat{x}_1} \times \Omega_{\widehat{t}} = (0, \widehat{L}) \times (0, \widehat{\tau})$. We choose reference quantities with subscript $_0$ or $_{ref}$ and define dimensionless variables using these. Let

$$\rho_0 = \frac{\widehat{\rho}_0}{(\rho_0)_{ref}} \quad , \quad u_{x_1} = \frac{\widehat{u}_{x_1}}{u_0} \ , \ v_{x_1} = \frac{\widehat{v}_{x_1}}{v_0} \ , \ x_1 = \frac{\widehat{x}_1}{L_0} \ , \ t = \frac{\widehat{t}}{t_0} \tag{I.73}$$

L_0 is a reference length, hence $u_0 = L_0$, and if we choose v_0 as a reference velocity (generally the speed of sound using reference quantities), then $t_0 = u_0/v_0 = L_0/v_0$. Hence

$$\rho_0 \frac{\partial^2 u_{x_1}}{\partial t^2} - \Big(\frac{\widehat{c}_1}{(\rho_0)_{ref} v_0^2}\Big) \frac{\partial^2 u_{x_1}}{\partial x_1^2} - \Big(\frac{\widehat{c}_2}{L_0 (\rho_0)_{ref} v_0}\Big) \frac{\partial}{\partial t}\Big(\frac{\partial^2 u_{x_1}}{\partial x_1^2}\Big) = 0 \tag{I.74}$$

$\forall (x_1, t) \in \Omega_{x_1,t}$. The term $(\rho_0)_{ref} v_0^2$ has dimensions of stress; we generally define $\tau_0 = (\rho_0)_{ref} v_0^2$ as the reference stress based on characteristic kinetic energy. Likewise, $L_0 (\rho_0)_{ref} v_0$ has units of viscosity and is essentially the Reynolds number with a unit reference viscosity. We define $c_1^d = \frac{\widehat{c}_1}{(\rho_0)_{ref} v_0^2}$ and $c_2^d = \frac{\widehat{c}_2}{L_0 (\rho_0)_{ref} v_0}$. Then the dimensionless form of (I.70) using (I.74) becomes

$$\rho_0 \frac{\partial^2 u_{x_1}}{\partial t^2} - c_1^d \frac{\partial^2 u_{x_1}}{\partial x_1^2} - c_2^d \frac{\partial}{\partial t}\Big(\frac{\partial^2 u_{x_1}}{\partial x_1^2}\Big) = 0 \ \forall (x_1, t) \in \Omega_{x_1,t} \ : \text{ Model A} \tag{I.75}$$

Following the same procedure, we can also derive the following dimensionless form of (I.71):

$$\rho_0 \frac{\partial^2 u_{x_1}}{\partial t^2} - c_1^d \frac{\partial^2 u_{x_1}}{\partial x_1^2} + \underset{\sim}{c}_2^d \frac{\partial u_{x_1}}{\partial t} = 0 \quad \forall (x_1, t) \in \Omega_{x_1,t} \ : \text{ Model B} \tag{I.76}$$

in which $\underset{\sim}{c}_2^d = \frac{\underset{\sim}{c}_2 L_0}{(\rho_0)_{ref} v_0}$. In the numerical studies, we consider an axial rod of dimensionless length one unit and choose $(\rho_0)_{ref} = \widehat{\rho}_0$ so that ρ_0 in (I.75) and (I.76) becomes unity. The spatial domain $[0, 1]$ for an increment of time $\Delta t = 0.1$, i.e. the space-time strip $[0, L] \times [0, \Delta t]$, is discretized using a uniform mesh of eight nine-node, p-version, higher order global differentiability, space-time

finite elements [41–45]. Figure 1 shows details of the space-time domain for a time increment $\Delta t = t_{n+1} - t_n$ and boundary conditions as well as the initial conditions.

The left end of the rod is clamped (impermeable boundary) and the right end is subjected to a compressive piecewise-quintic strain distribution, such that the strain is twice continuously differentiable with respect to time, over a time period of $2\Delta t$. For $t \geq 2\Delta t$, the applied strain at the right end of the rod is zero. We choose a p-level of 9 in space and time and a local approximation of class $C^{11}(\bar{\Omega}^e_{x_1,t})$, i.e. of class C^1 in space and time. The finite element formulations used for computing numerical solutions for both models (models A and B) use the space-time least squares process constructed using residual functionals [41–45].

The resulting computational process is unconditionally stable. Evolutions are computed using a space-time strip with time marching [41–45]. For the choice of local approximation ($C^{11}(\bar{\Omega}^e_{x_1,t})$), the integrals in the finite element processes are Lebesgue, but due to the smoothness of the evolution for the 8-element discretization with a p-level of 9, the residual functionals are on the order of $O(10^{-6})$ or lower for all space-time strips for both model problems, confirming good accuracy of evolution. For both model problems, the evolutions are completed for $0 \leq t \leq 2.0$. In both model problems, we choose $c_1^d = 1.0$. Since c_2^d, $\underset{\sim}{c}{}_2^d$ in model problems A and B do not have the same meaning (i.e. physics), a direct comparison of the evolutions for the same values of c_2^d and $\underset{\sim}{c}{}_2^d$ is not meaningful. For this reason, we choose a range of values for c_2^d and $\underset{\sim}{c}{}_2^d$ to show behaviors of dissipation in models A and B. Figures 2 and 3 show plots of strain $\varepsilon_{x_1x_1}$ versus x_1 for different values of time for $c_2^d = 0$, 0.1, and 0.5 for model A. From Figures 2 and 3 for model A, we note that when $c_2^d = 0$, we have pure elastic strain wave propagation. Reflections of the strain wave at the fixed and free boundaries are simulated perfectly. Since in this case there is no dissipation, the wave shape is preserved during propagation, i.e. no amplitude decay or base elongation is observed.

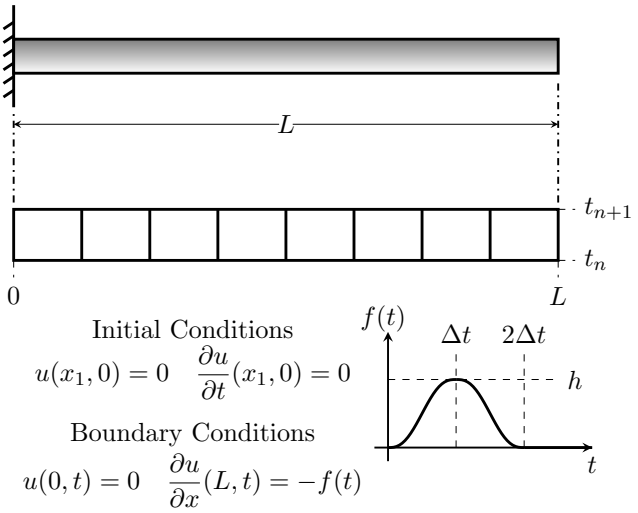

Figure 1: Schematic diagram for the studied problem

At the fixed boundary, the amplitude of the strain wave doubles as expected, and the reflected wave at the free boundary returns as a tensile wave. When c_2^d is nonzero, we observe amplitude decay and base elongation of the strain wave during the evolution. Progressively increasing values of c_2^d result in large amplitude decay and base elongation, due to increased dissipation. This mechanism of dissipation is exactly the same as viscous dissipation in fluids (as discussed earlier).

Figures 4 and 5 show plots of strain $\varepsilon_{x_1x_1}$ versus x_1 for model B for different values of time using $\underset{\sim}{c}{}_2^d = 0$, 1.0, and 2.0. From Figures 4 and 5, for model B, we note that for $\underset{\sim}{c}{}_2^d = 0$, we have exactly the same behavior as in Figures 2 and 3 as in this case, the two models are identical. For nonzero values of $\underset{\sim}{c}{}_2^d$, the evolutions in figures 4 and 5 show amplitude decay of the strain wave, but the base of the wave is preserved during the evolution, regardless of the values of $\underset{\sim}{c}{}_2^d$.

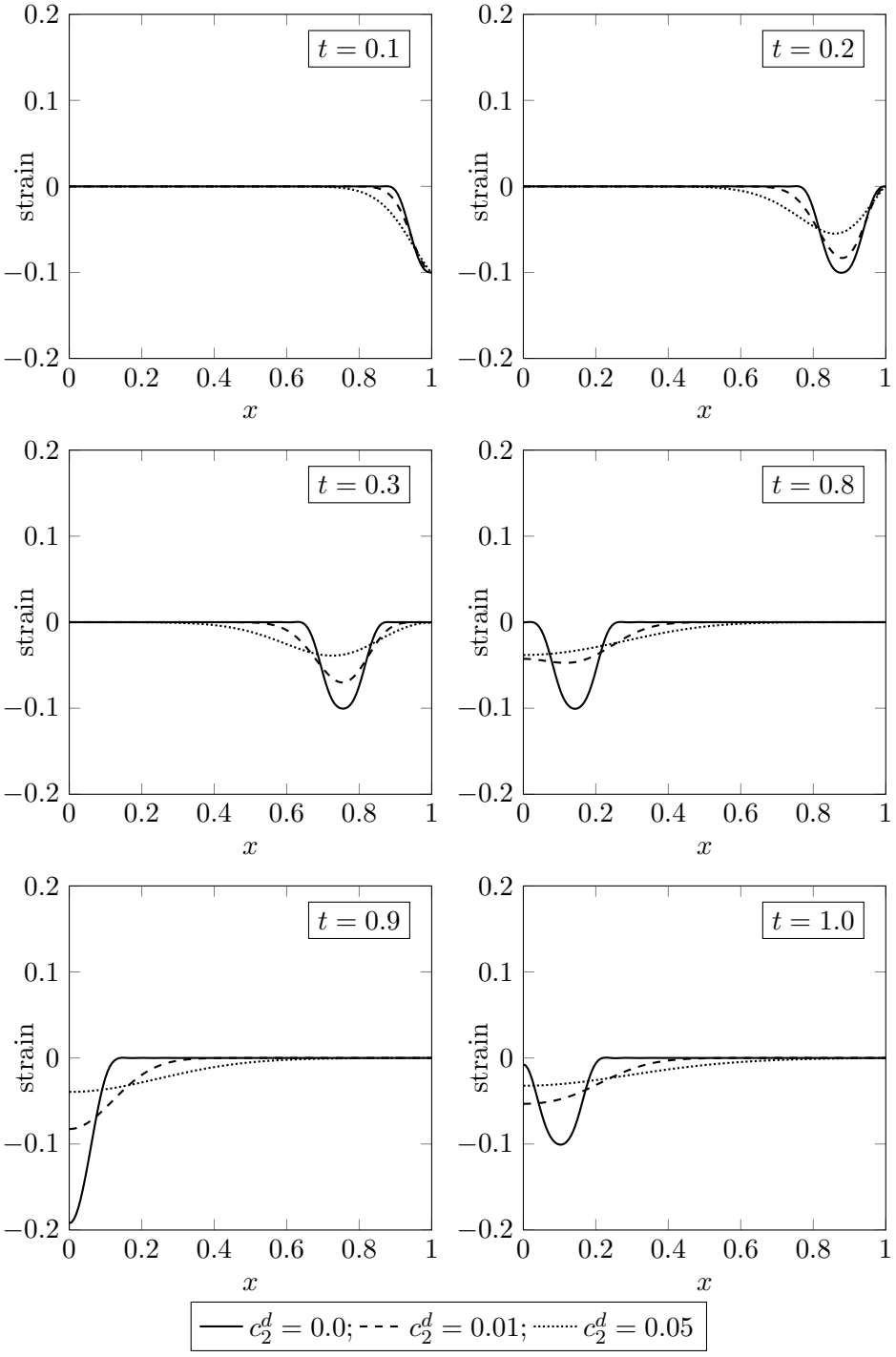

Figure 2: Time evolution of the propagation of an applied strain pulse in a one-dimensional axially deforming rod with dissipation based on strain rate (model A: **strain rate-based damping**)

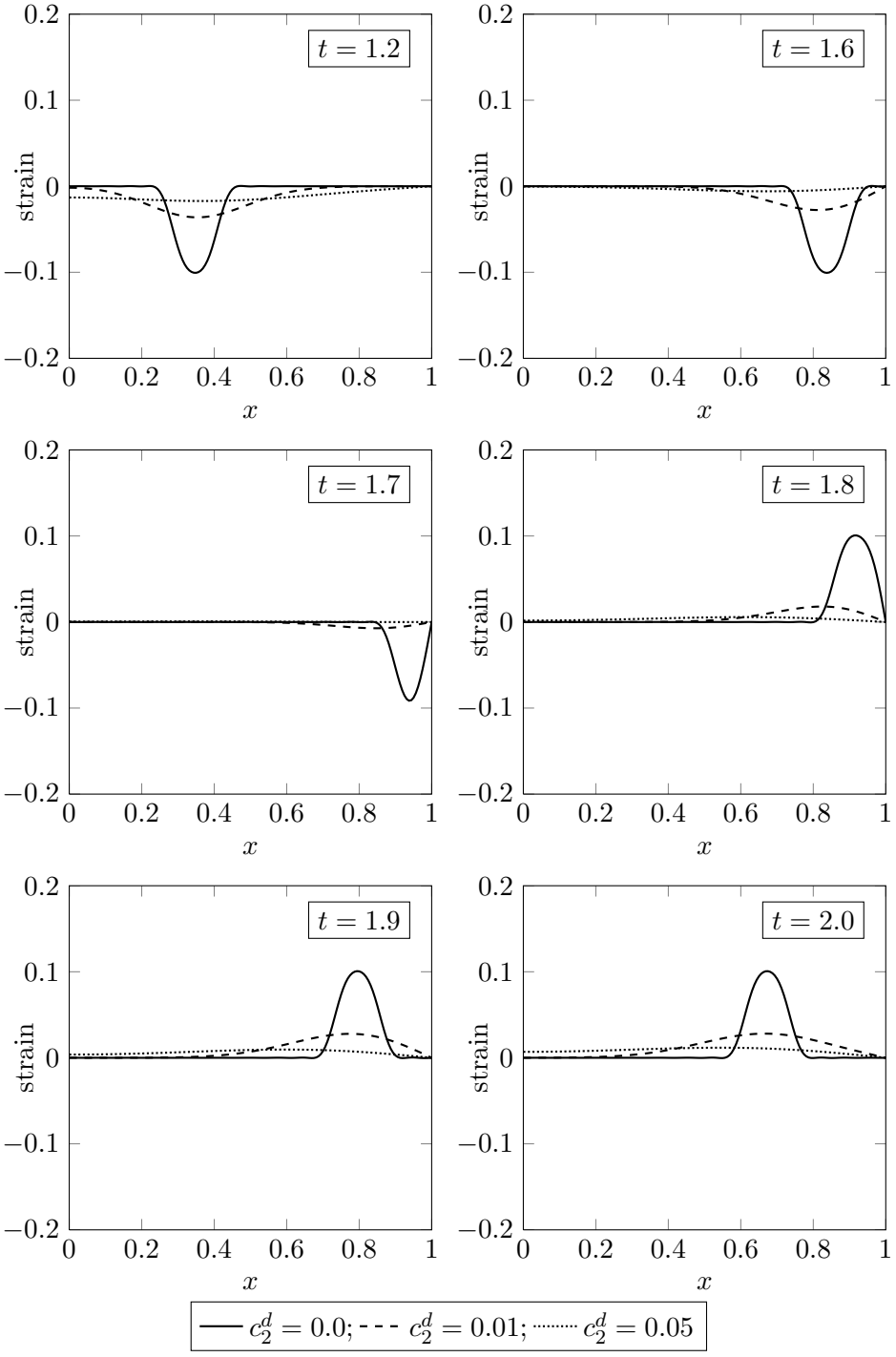

Figure 3: Continued time evolution of the propagation of an applied strain pulse in a one-dimensional axially deforming rod with dissipation based on strain rate (model A: **strain rate-based damping**)

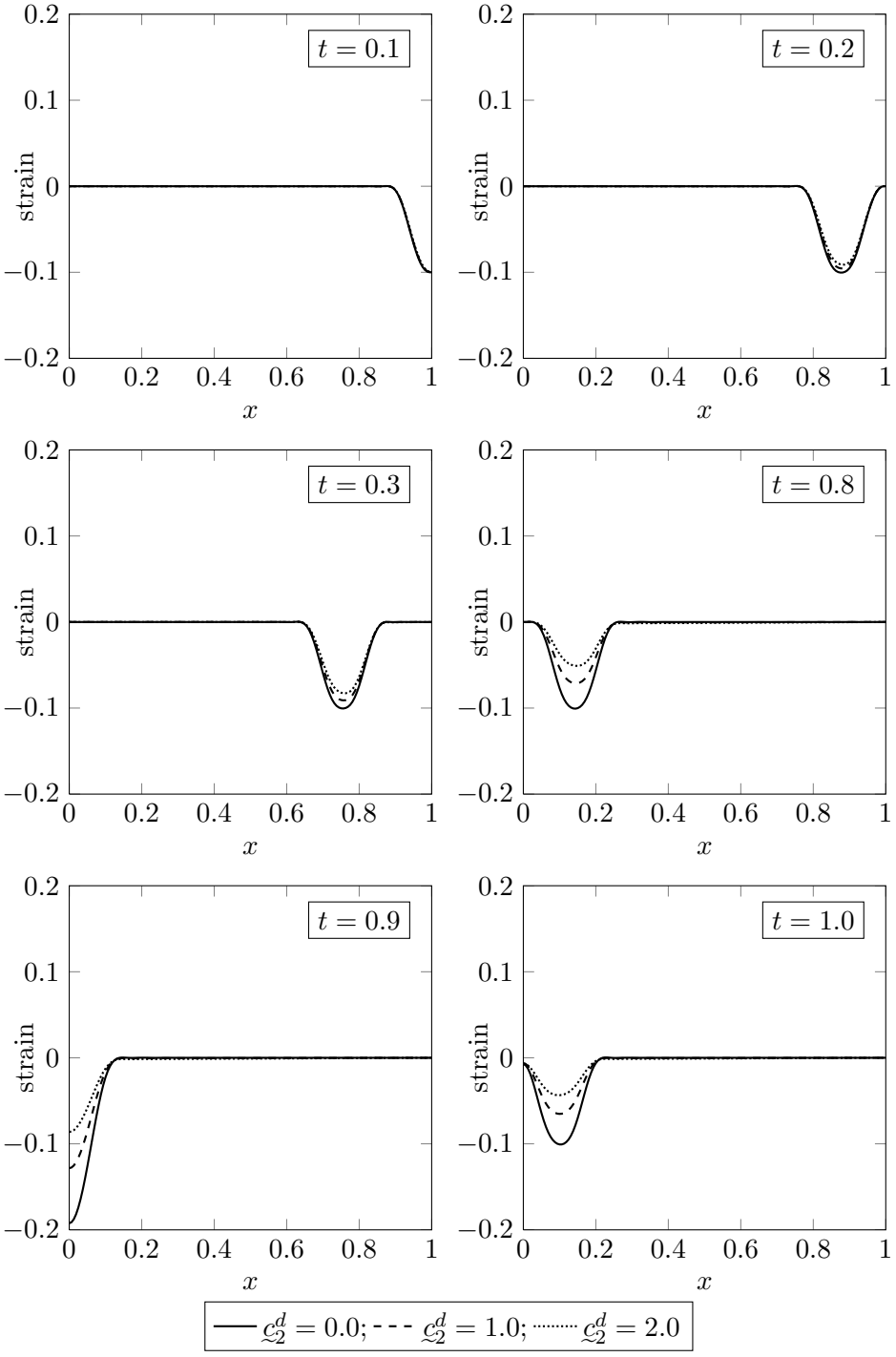

Figure 4: Continued time evolution of the propagation of an applied strain pulse in a one-dimensional axially deforming rod with dissipation based on velocity (model B: **velocity-based damping**)

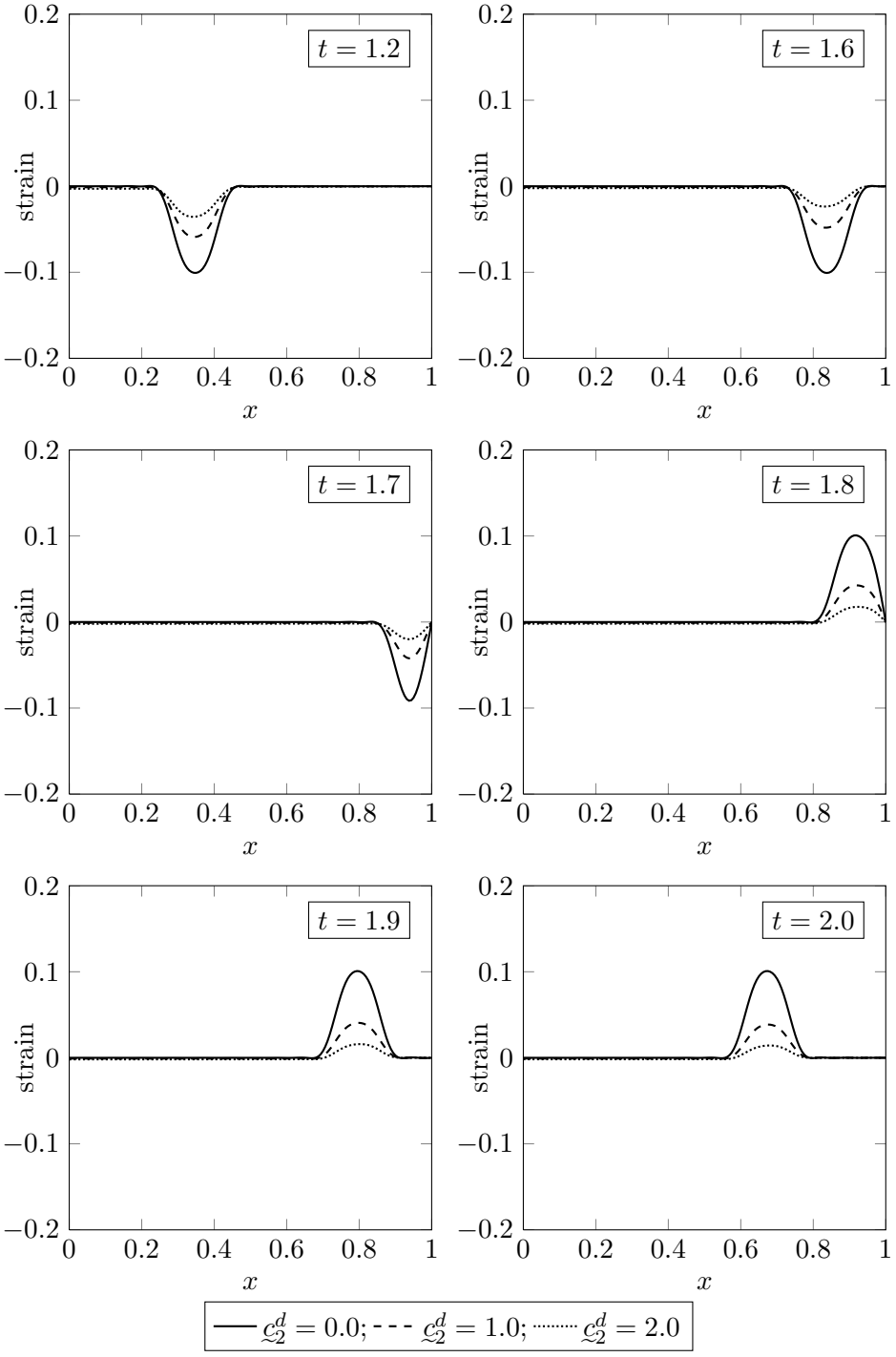

Figure 5: Continued time evolution of the propagation of an applied strain pulse in a one-dimensional axially deforming rod with dissipation based on velocity (model B: **velocity-based damping**)

Thus, this mechanism of dissipation is quite different in model B from the case of model A. As expected, progressively increasing values of $\underset{\sim}{c}_2^d$ result in progressively decaying amplitudes of the strain wave, indicating progressively increased dissipation, but the base of the strain wave remains unaltered during the entire evolution.

I.3 Ordered rate constitutive theories for thermoviscoelastic solids with memory

I.3.1 Ordered rate constitutive theories for thermoviscoelastic solids with memory using Φ

We consider basic form [18,19,31] of the entropy inequality (Clausius-Duhem inequality) expressed in terms of Φ and conjugate pair $\boldsymbol{\sigma}^{[0]}$ and $\boldsymbol{\varepsilon}^{[0]}$

$$\rho_0 \dot{\Phi} + \eta \dot{\theta} + \frac{|J| q_i g_i}{\theta} - \sigma^*_{ki} \dot{J}_{ik} \leq 0 \tag{I.77}$$

in which ρ_0 is density in the reference configuration and $|J|$ is determinate of the Jacobian of deformation. This allows us (in conjunction with other conservation laws) to conclude that at the onset Φ, η $\boldsymbol{\sigma}^{[0]}$ and $\boldsymbol{q}$ must be dependent variables in the constitutive theory. Following the material presented in previous sections, it is straightforward to conclude the following argument tensors of the dependent variables

$$\begin{aligned}
\Phi &= \Phi\big(\boldsymbol{\varepsilon}^{[0]}, \boldsymbol{g}, \theta\big) \\
\eta &= \eta\big(\boldsymbol{\varepsilon}^{[0]}, \boldsymbol{g}, \theta\big) \\
\boldsymbol{\sigma}^{[0]} &= \boldsymbol{\sigma}^{[0]}\big(\boldsymbol{\varepsilon}^{[0]}, \boldsymbol{g}, \theta\big) \\
\boldsymbol{q} &= \boldsymbol{q}\big(\boldsymbol{\varepsilon}^{[0]}, \boldsymbol{g}, \theta\big)
\end{aligned} \tag{I.78}$$

In thermoviscoelastic solids without memory, the mechanism of dissipation must be incorporated in the constitutive theories. This requires that at least $\boldsymbol{\varepsilon}^{[1]}$, the material derivative of order one must be an argument tensor of $\boldsymbol{\sigma}^{[0]}$ and hence of all other dependent variables due to the principle of equipresence. Since $\boldsymbol{\varepsilon}^{[i]}\ ; i = 1, 2, \ldots, n$, the material derivatives of upto orders n of $\boldsymbol{\varepsilon}$, are fundamental kinematic tensors, we can generalize the choice of $\boldsymbol{\varepsilon}^{[1]}$ as argument tensor by replacing it with $\boldsymbol{\varepsilon}^{[i]}\ ; i = 1, 2, \ldots, n$.

From the development of the constitutive theories in Eulerian description for thermoviscoelastic fluids [36] and their simplifications resulting in Maxwell model, Oldroyd-B model, and Giesekus model [37], we know that for such fluids to have memory, at the very least, the constitutive theory must consider the first convected time derivative of the stress tensor as a dependent variable with stress and strain rate as its arguments (in addition to others). The generalization of this concept leads to the (m, n) ordered rate theories for thermoviscoelastic fluids [36, 37] in Eulerian description. In the case of solids, we utilize a similar concept but in Lagrangian description. This leads to the material derivatives upto orders m of the conjugate stress tensor as a dependent variable in the constitutive theory as opposed to the stress tensor, and in addition to $\boldsymbol{\varepsilon}^{[i]}\ ;\ i = 0, 1, \ldots, n$ as arguments of all dependent variables, we now also consider stress tensor and its material derivatives up to order $m-1$ as arguments of the dependent variables in the constitutive theories. Additionally, we also consider θ and $\boldsymbol{g}$ as arguments of all dependent variables in the constitutive theories. Thus, in the rate constitutive theories considered here, the possible dependent variables at this stage are $\boldsymbol{\sigma}^{[m]}$, $\boldsymbol{q}$, Φ, and η, and their argument tensors are $\boldsymbol{\varepsilon}^{[i]}\ ; i = 0, 1, \ldots, n$, $\boldsymbol{\sigma}^{[j]}\ ; j = 0, 1, \ldots, m-1$, $\boldsymbol{g}$ and θ.

$$\begin{aligned}
\Phi &= \Phi\big(\boldsymbol{\sigma}^{[j]}\ ;\ j = 0, 1, \ldots, m-1\ ,\ \boldsymbol{\varepsilon}^{[i]}\ ;\ i = 0, 1, \ldots, n\ ,\ \boldsymbol{g}\ ,\ \theta\big) \\
\boldsymbol{q} &= \boldsymbol{q}\big(\boldsymbol{\sigma}^{[j]}\ ;\ j = 0, 1, \ldots, m-1\ ,\ \boldsymbol{\varepsilon}^{[i]}\ ;\ i = 0, 1, \ldots, n\ ,\ \boldsymbol{g}\ ,\ \theta\big) \\
\eta &= \eta\big(\boldsymbol{\sigma}^{[j]}\ ;\ j = 0, 1, \ldots, m-1\ ,\ \boldsymbol{\varepsilon}^{[i]}\ ;\ i = 0, 1, \ldots, n\ ,\ \boldsymbol{g}\ ,\ \theta\big) \\
\boldsymbol{\sigma}^{[m]} &= \boldsymbol{\sigma}^{[m]}\big(\boldsymbol{\sigma}^{[j]}\ ;\ j = 0, 1, \ldots, m-1\ ,\ \boldsymbol{\varepsilon}^{[i]}\ ;\ i = 0, 1, \ldots, n\ ,\ \boldsymbol{g}\ ,\ \theta\big)
\end{aligned} \tag{I.79}$$

Using Φ in (I.79) with its argument tensors defined, we obtain $\dot{\Phi}$ using chain rule of differentiation and substitute it in entropy inequality (I.77). From this form of entropy inequality we can conclude that:

(1) $\eta = -\frac{\partial \Phi}{\partial \theta}$, hence η is deterministic from Φ, therefore η is not a dependent variable in the constitutive theories

(2) Φ is not a function of $\boldsymbol{\varepsilon}^{[i]}$; $i = 0, 1, \ldots, n$

(3) Φ is not a function of $\boldsymbol{\sigma}^{[j]}$; $j = 0, 1, \ldots, m-1$ either

(4) Φ is not a function of $\boldsymbol{g}$ also

(5) and a remaining inequality (see reference [38]) that must be satisfied

Thus, now we have

$$\begin{aligned}
&\Phi = \Phi\big(|J| \ , \ \theta\big) \\
&\boldsymbol{\sigma}^{[m]} = \boldsymbol{\sigma}^{[m]}\big(\boldsymbol{\sigma}^{[j]} \ ; \ j = 0, 1, \ldots, m-1 \ , \ \boldsymbol{\varepsilon}^{[i]} \ ; \ i = 0, 1, \ldots, n \ , \ \boldsymbol{g} \ , \ \theta\big) \\
&\boldsymbol{q} = \boldsymbol{q}\big(\boldsymbol{\sigma}^{[j]} \ ; \ j = 0, 1, \ldots, m-1 \ , \ \boldsymbol{\varepsilon}^{[i]} \ ; \ i = 0, 1, \ldots, n \ , \ \boldsymbol{g} \ , \ \theta\big)
\end{aligned} \tag{I.80}$$

Thus the constitutive theories for these solids reduce to determination of $\boldsymbol{\sigma}^{[m]}$ and $\boldsymbol{q}$. The conditions resulting from the entropy inequality in this case do not permit derivation of constitutive theories for $\boldsymbol{\sigma}^{[0]}$. We perform decomposition of $\boldsymbol{\sigma}^{[0]}$ into equilibrium stress ${}_e\boldsymbol{\sigma}^{[0]}$ and deviatoric stress ${}_d\boldsymbol{\sigma}^{[0]}$ and substitute it in the entropy inequality. The resulting conditions permit derivation of ${}_e\boldsymbol{\sigma}^{[0]}$ in thermodynamic pressure $p(\rho, \theta)\boldsymbol{I}$ for compressible case and mechanical pressure $p(\theta)\boldsymbol{I}$ for incompressible case (derived by incorporating incompressibility condition in the entropy inequality). Additionally, the entropy inequality requires the work expanded due to ${}_d\boldsymbol{\sigma}^{[0]}$ to be positive if we assume

$$\frac{|J| q_i g_i}{\theta} \leq 0 \qquad \text{or} \qquad q_i g_i \leq 0 \tag{I.81}$$

but provides no mechanism to derive constitutive theories for ${}_d\boldsymbol{\sigma}^{[0]}$. At this stage we have

$$\begin{aligned}
&\boldsymbol{\sigma}^{[0]} = {}_e\boldsymbol{\sigma}^{[0]} + {}_d\boldsymbol{\sigma}^{[0]} \\
&{}_d\boldsymbol{\sigma}^{[m]} = {}_d\boldsymbol{\sigma}^{[m]}\big(\boldsymbol{\sigma}^{[j]} \ ; \ j = 0, 1, \ldots, m-1 \ , \ \boldsymbol{\varepsilon}^{[i]} \ ; \ i = 0, 1, \ldots, n \ , \ \boldsymbol{g} \ , \ \theta\big) \\
&\boldsymbol{q} = \boldsymbol{q}\big(\boldsymbol{\sigma}^{[j]} \ ; \ j = 0, 1, \ldots, m-1 \ , \ \boldsymbol{\varepsilon}^{[i]} \ ; \ i = 0, 1, \ldots, n \ , \ \boldsymbol{g} \ , \ \theta\big)
\end{aligned} \tag{I.82}$$

in which

$$\begin{aligned}
&{}_e\boldsymbol{\sigma}^{[0]} = p(\rho, \theta)\boldsymbol{I} \qquad ; \qquad \text{compressible case} \\
&{}_e\boldsymbol{\sigma}^{[0]} = p(\theta)\boldsymbol{I} \qquad ; \qquad \text{incompressible case}
\end{aligned} \tag{I.83}$$

(a) Rate constitutive theories for ${}_d\boldsymbol{\sigma}^{[0]}$ of orders (m, n): We derive constitutive theories for ${}_d\boldsymbol{\sigma}^{[0]}$ using the theory of generators and invariants. If $[{}^{\sigma}\underset{\sim}{G}^i]$; $i = 1, 2, \ldots, N$ are the combined generators of the argument tensors of ${}_d\boldsymbol{\sigma}^{[m]}$ in (I.82) that are symmetric tensors of rank two and if ${}^{q\sigma}\underset{\sim}{I}^j$; $j = 1, 2, \ldots, M$ are the combined invariants of the same argument tensors, then

$${}_d\boldsymbol{\sigma}^{[m]} = {}^{\sigma}\tilde{\alpha}^0 + \sum_{i=1}^{N} {}^{\sigma}\tilde{\alpha}^i [{}^{\sigma}\underset{\sim}{G}^i] \tag{I.84}$$

$${}^{\sigma}\tilde{\alpha}^i = {}^{\sigma}\tilde{\alpha}^i\big({}^{q\sigma}\underset{\sim}{I}^j \ ; \ j = 1, 2, \ldots, M \ , \ \theta\big) \qquad ; \qquad i = 1, 2, \ldots, N \tag{I.85}$$

The material coefficients are derived by expanding ${}^{\sigma}\tilde{\alpha}^i$; $i = 0, 1, \ldots, N$ in ${}^{q\sigma}\underset{\sim}{I}^j$; $j = 1, 2, \ldots, M$ and θ about a known configuration $\underline{\Omega}$ and retaining only upto linear terms in ${}^{q\sigma}\underset{\sim}{I}^j$; $1, 2, \ldots, M$ and θ. This gives us

$$\boldsymbol{\sigma}^{[m]} = \underline{\sigma}^0\big|_{\underline{\Omega}}[I] + \sum_{j=1}^{M} {}^{\sigma}\underline{a}_j \, {}^{q\sigma}\underset{\sim}{I}^j[I] + \sum_{i=1}^{N} {}^{\sigma}\underline{b}_i [{}^{\sigma}\underset{\sim}{G}^i] + \sum_{i=1}^{N}\sum_{j=1}^{M} {}^{\sigma}\underline{c}_{ij} \, {}^{q\sigma}\underset{\sim}{I}^j [{}^{\sigma}\underset{\sim}{G}^i] + \sum_{i=1}^{N} {}^{\sigma}\underline{d}_i (\theta - \theta_{\underline{\Omega}})[{}^{\sigma}\underset{\sim}{G}^i] - (\alpha_{tm})_{\underline{\Omega}}(\theta - \theta_{\underline{\Omega}})[I] \tag{I.86}$$

$\underline{\sigma}^0\big|_{\underline{\Omega}}$ is the initial stress in the configuration $\underline{\Omega}$. This constitutive theory for ${}_d\boldsymbol{\sigma}^{[0]}$ requires $(M + N + MN + N + 1)$ material coefficients. The material coefficients defined in (I.86) are functions of $\theta_{\underline{\Omega}}$ and $({}^{q\sigma}\underset{\sim}{I}^j)_{\underline{\Omega}}$; $j = 1, 2, \ldots, M$ in the known configuration

$\underline{\Omega}$. This constitutive theory is based on integrity and hence is complete. See reference [38] for definitions of material coefficients.

(b) Rate constitutive theories for $\boldsymbol{q}$ of orders (m, n): In this derivation we consider the argument tensors of $\boldsymbol{q}$ in (I.82). These are in agreement with those for ${}_d\boldsymbol{\sigma}^{[m]}$, hence this constitutive theory is consistent with the rate constitutive theory for deviatoric second Piola-Kirchhoff stress tensor in section (a). We express $\boldsymbol{q}$ as a linear combination of the combined generators of the argument tensors of $\boldsymbol{q}$. As in the case of ${}_d\boldsymbol{\sigma}^{[m]}$, here also the coefficients in the linear combination are functions of the combined invariants of the argument tensors of $\boldsymbol{q}$. The material coefficients in this case are also derived using a Taylor series expansion of each coefficient in the linear combination about a known configuration $\underline{\Omega}$. Since $\boldsymbol{q}$ is a tensor of rank one, the combined generators of the argument tensors of $\boldsymbol{q}$ must also be tensors of rank one. We keep in mind that $\boldsymbol{\varepsilon}^{[k]}\ ; k = 0, 1, \ldots, n$ and ${}_d\boldsymbol{\sigma}^{[l]}\ ; l = 0, 1, \ldots, m$ are symmetric tensors of rank two, while $\boldsymbol{g}$, θ are tensors of rank one and zero respectively. Let $\{{}^q\underset{\sim}{G}^i\}\ ; i = 1, 2, \ldots, \widetilde{N}$ be the combined generators of the argument tensors of $\boldsymbol{q}$ that are tensors of rank one and let ${}^{q\sigma}\underset{\sim}{I}^j\ ; j = 1, 2, \ldots, M$ be the combined invariants of the same argument tensors of $\boldsymbol{q}$, which are the same as those for ${}_d\boldsymbol{\sigma}^{[m]}$. Then, we can express $\boldsymbol{q}$ in the current configuration as a linear combination of $\{{}^q\underset{\sim}{G}^i\}\ ; i = 1, 2, \ldots, \widetilde{N}$:

$$\boldsymbol{q} = -\sum_{i=1}^{\widetilde{N}} {}^q\tilde{\alpha}^i \{{}^q\underset{\sim}{G}^i\} \tag{I.87}$$

$${}^q\tilde{\alpha}^i = {}^q\tilde{\alpha}^i\big({}^{q\sigma}\underset{\sim}{I}^j\ ;\ j = 1, 2, \ldots, M, \theta\big) \tag{I.88}$$

To determine the material coefficients from ${}^q\tilde{\alpha}^i\ ; i = 1, 2, \ldots, \widetilde{N}$, we consider a Taylor series expansion of each ${}^q\tilde{\alpha}^i\ ; i = 1, 2, \ldots, \widetilde{N}$ about a known configuration $\underline{\Omega}$ in invariants ${}^{q\sigma}\underset{\sim}{I}^j\ ; j = 1, 2, \ldots, M$ and temperature θ and retain only up to linear terms in the invariants and the temperature θ. By substituting these in (I.87) we obtain

$$\boldsymbol{q} = -\sum_{i=1}^{\widetilde{N}} {}^q\underline{b}_i \{{}^q\underset{\sim}{G}^i\} - \sum_{i=1}^{\widetilde{N}}\sum_{j=1}^{M} {}^q\underline{c}_{ij}\, {}^{q\sigma}\underset{\sim}{I}^j \{{}^q\underset{\sim}{G}^j\} - \sum_{i=1}^{\widetilde{N}} {}^q\underline{d}_i(\theta - \theta_{\underline{\Omega}})\{{}^q\underset{\sim}{G}^i\} \tag{I.89}$$

This constitutive theory for $\boldsymbol{q}$ requires $(\widetilde{N} + \widetilde{N}M + \widetilde{N})$ material coefficients (see reference [38] for their definition). These defined material coefficients are functions of invariants ${}^{q\sigma}\underset{\sim}{I}^j_{\underline{\Omega}}\ ; j = 1, 2, \ldots, M$ and temperature $\theta_{\underline{\Omega}}$ in the known configuration $\underline{\Omega}$. This constitutive theory is also based on integrity, hence is complete.

Remarks:

(1) Using the general derivations presented for rate theories of orders (m, n) for ${}_d\boldsymbol{\sigma}^{[0]}$ and $\boldsymbol{q}$, constitutive theories of any desired order can be obtained.

(2) Constitutive theory for $\boldsymbol{q}$ is consistent with the constitutive theory for ${}_d\boldsymbol{\sigma}^{[0]}$ as it uses the same argument tensors as in the case of ${}_d\boldsymbol{\sigma}^{[0]}$. At this stage, there is no rational to alter the argument tensors of $\boldsymbol{q}$. The constitutive theory for $\boldsymbol{q}$ demonstrates the influence of $\boldsymbol{\varepsilon}^{[0]}$ and $\boldsymbol{\varepsilon}^{[m]}\ ; m = 1, 2, \ldots, n$ as well as their interaction with $\boldsymbol{g}$ on heat conduction.

(3) Using the general derivations presented for rate theories of orders (m, n) for the deviatoric second Piola-Kirchhoff stress tensor and the heat vector, the constitutive theories of any desired order can be obtained.

(4) The rate constitutive theories for deviatoric second Piola-Kirchhoff stress tensor and heat vector are consistent with each other as they use the same argument tensors. The constitutive theory for $\boldsymbol{q}$ demonstrates the influence of $\boldsymbol{\varepsilon}^{[k]}\ ; k = 0, 1, \ldots, n$ and ${}_d\boldsymbol{\sigma}^{[l]}\ ; l = 0, 1, \ldots, m-1$ on $\boldsymbol{q}$ as well as their interaction with temperature gradient $\boldsymbol{g}$. In a later section we consider much simplified constitutive theory for $\boldsymbol{q}$ to demonstrate this point more clearly.

For the rate constitutive theories of orders $(m = 1, n)$, we have

$${}_d\boldsymbol{\sigma}^{[1]} = {}_d\boldsymbol{\sigma}^{[1]}\big({}_d\boldsymbol{\sigma}^{[0]}, \boldsymbol{\varepsilon}^{[i]}\ ;\ i = 0, 1, \ldots, n\ ,\ \boldsymbol{g}\ ,\ \theta\big)$$

Consider simplified constitutive theories based on the following assumptions:

(i) The constitutive theories are linear in the components of the argument tensors.

(ii) We neglect all product terms (in the current configuration) related to the argument tensors.

Based on these assumptions, we only have ${}_d\boldsymbol{\sigma}^{[0]}$, $\boldsymbol{\varepsilon}^{[i]}$; $i = 0, 1, \ldots, n$ as generators, and the only invariants to be considered are $\text{tr}({}_d\boldsymbol{\sigma}^{[0]})$ and $\text{tr}(\boldsymbol{\varepsilon}^{[i]})$; $i = 0, 1, \ldots, n$. The resulting simplified rate theories of order $(1, n)$ are given by

$$ {}_d\boldsymbol{\sigma}^{[1]} = \underline{\sigma}^0|_{\underline{\Omega}} - c_1 {}_d\boldsymbol{\sigma}^{[0]} - c_2 \,\text{tr}\big({}_d\boldsymbol{\sigma}^{[0]}\big)[I] + \sum_{i=0}^{n} a_i^1 \boldsymbol{\varepsilon}^{[i]} + \sum_{i=0}^{n} a_i^2 \,\text{tr}\big(\boldsymbol{\varepsilon}^{[i]}\big)[I] - \underline{\alpha}_{tm}(\theta - \theta_{\underline{\Omega}})[I] \tag{I.90} $$

The material coefficients c_1, c_2, a_i^1, a_i^2, and $\underline{\alpha}_{tm}$ are functions of the invariants and temperature θ in the known configuration $\underline{\Omega}$. We can write (I.90) in matrix and vector form using Voigt's notation (in the absence of the first and last terms in (I.90) without loss of generality)

$$ \{{}_d\sigma^{[1]}\} + [\underset{\sim}{c}]\{{}_d\sigma^{[0]}\} = [\underset{\sim}{a}_0]\{\varepsilon^{[0]}\} + \sum_{i=1}^{n} [\underset{\sim}{a}_i]\{\varepsilon^{[i]}\} \tag{I.91} $$

Remarks:

1. The coefficients of the matrix $[\underset{\sim}{a}_0]$ are completely defined using material coefficients a_0^1 and a_0^2. For linear elastic solids, $(\underset{\sim}{a}_0)_{ij}$ of $[\underset{\sim}{a}_0]$ are functions of the modulus of elasticity and Poisson's ratio, or Lamé's constants.

2. The dissipation mechanism is due to $[\underset{\sim}{a}_i]\{\varepsilon^{[i]}\}$; $i = 1, 2, \ldots, n$ terms in (I.91). Each $\{\varepsilon^{[i]}\}$; $i = 1, 2, \ldots, n$ requires two material constants.

3. Using (I.91), various order rate theories can be obtained by choosing appropriate values of n. For all these theories, m remains one.

4. Derivation of memory modulus for finite deformation can be found in reference [38].

5. Equation (I.91) is a first-order partial differential equation in ${}_d\boldsymbol{\sigma}^{[0]}$, hence it can be integrated in time to obtain an integral expression for ${}_d\boldsymbol{\sigma}^{[0]}$. The integrand in this expression is an exponentially decaying function and is called the memory modulus. Such materials, upon cessation of a disturbance, require a finite amount of time to achieve a relaxed or stress-free state (stress relaxation). Such materials are referred to as materials with memory.

6. It is important to reiterate that (I.91) holds for finite deformation as the conjugate stress and strain measures are for finite deformation.

7. When the linear 1-d constitutive theory is reduced to incompressible small deformation case, the constitutive model for ${}_d\boldsymbol{\sigma}^{[0]}$ resembles Zener model but differs due to the fact that the model derived here uses ${}_d\sigma_{x_1x_1}$, whereas the Zener model uses ${}_d\sigma_{x_1x_1}$. Based on the derivations presented here, the Zener model does not have a continuum mechanics and thermodynamic basis.

8. Simplified constitutive theories for $\boldsymbol{q}$ can be easily derived using (I.89) with appropriate assumptions and by following the details in previous section and reference [38]. The details are omitted for the sake of brevity.

I.3.2 Ordered rate constitutive theories for thermoviscoelastic solids with memory [39] using Ψ

The derivations of these rate theories follow similar details as presented in earlier sections once the dependent variables and their argument tensors are established, hence in in the following, we only present basic steps and the outline of the derivations.

We consider the derivations of the constitutive theories in Lagrangian description for homogeneous, isotropic, compressible and incompressible thermoviscoelastic solids with memory undergoing finite deformation based on the second law of thermodynamics expressed in terms of Gibbs potential Ψ and conjugate stress and strain measures: $\boldsymbol{\sigma}^{[0]}$, $\boldsymbol{\varepsilon}$. The entropy inequality is derived in Lagrangian description using Gibbs potential Ψ and conjugate pair $\boldsymbol{\sigma}^{[0]}$, $\boldsymbol{\varepsilon}$ and the possible choice of dependent variables: Ψ, $\boldsymbol{\varepsilon}$, η (entropy inequality) and $\boldsymbol{q}$ is established. In the rate theories considered here, the constitutive theories for $\boldsymbol{\varepsilon}$ is derived by

considering $\boldsymbol{\varepsilon}^{[n]}$ as a dependent variable in the constitutive theory. At the onset, $\boldsymbol{\varepsilon}^{[i]}\ ; i = 0, 1, 2, \ldots, n-1$, $\boldsymbol{\sigma}^{[j]}\ ; j = 0, 1, \ldots, m$, $\boldsymbol{g}$ and θ are considered as argument tensors of Ψ, $\boldsymbol{\varepsilon}^{[n]}$, η and $\boldsymbol{q}$. With this choice of argument tensors for Ψ, when $\dot{\Psi}$ (obtained using chain rule of differentiation) is substituted in the entropy inequality, the resulting conditions show that Ψ cannot be a function of $\boldsymbol{\sigma}^{[j]}\ ; j = 0, 1, \ldots, m$, $\boldsymbol{\varepsilon}^{[i]}\ ; i = 0, 1, \ldots, n-1$ and $\boldsymbol{g}$. Additionally Ψ cannot be a function of $\boldsymbol{\sigma}^{[0]}$. This requires decomposition of $\boldsymbol{\sigma}^{[0]}$ into ${}_e\boldsymbol{\sigma}^{[0]}$, equilibrium stress, and ${}_d\boldsymbol{\sigma}^{[0]}$, deviatoric stress. With the stress decomposition, it is established that Ψ can be a function of ${}_d\boldsymbol{\sigma}^{[j]}$. The conditions resulting from the entropy also show that η cannot be a dependent variable in the rate constitutive theories. Thus, finally we have Ψ, $\boldsymbol{\varepsilon}^{[n]}$ and $\boldsymbol{q}$ as dependent variables in the rate constitutive theory. The argument tensors of Ψ are ${}_d\boldsymbol{\sigma}^{[j]}\ ; j = 0, 1, \ldots, m$ and θ whereas as the argument tensors of $\boldsymbol{\varepsilon}^{[n]}$ and $\boldsymbol{q}$ are $\boldsymbol{\varepsilon}^{[i]}\ ; i = 0, 1, \ldots, n-1$, ${}_d\boldsymbol{\sigma}^{[j]}\ ; j = 0, 1, \ldots, m$, $\boldsymbol{g}$ and θ. The constitutive theory for ${}_e\boldsymbol{\sigma}^{[0]}$ is well established [18, 19, 31] in terms of thermodynamic pressure for compressible case and mechanical pressure when the matter is incompressible. The remaining last inequality resulting from the entropy inequality places some restrictions on the constitutive theories for ${}_d\boldsymbol{\sigma}^{[0]}$, $\boldsymbol{\varepsilon}$ and $\boldsymbol{q}$ but provide no mechanism to derive constitutive theories for $\boldsymbol{\varepsilon}$ and $\boldsymbol{q}$. In the present work, we use the theory of generators and invariants to derive the constitutive theories for $\boldsymbol{\varepsilon}$ and $\boldsymbol{q}$ using $\boldsymbol{\varepsilon}^{[n]}$ and $\boldsymbol{q}$ as dependent variables in the constitutive theories. These rate theories are of orders (m, n) due to the fact they utilize material derivatives upto order m of the second Piola-Kirchhoff stress tensor, and material derivatives upto order n of $\boldsymbol{\varepsilon}$. The constitutive theories presented here for $\boldsymbol{\varepsilon}$ and $\boldsymbol{q}$ are consistent as they use the same argument tensors and are complete as they are based on integrity.

Many simplified forms of these rate theories of orders (m, n) are also considered. The most obvious is the constitutive theory of orders one $(1, 1)$. It is shown that even this theory contain too many material coefficients to be of use in practical applications. Further simplifications of these theories are also considered and compared with those that are currently used. The constitutive theories for heat vector include influence of strain, strain rate and stress field in addition to temperature gradient as well as their interactions. Many simplified forms of the (m, n) ordered theories are presented. The most simplified form of the first order rate theory for the heat vector is shown to result in Fourier heat conduction law. The rate constitutive theories derived here are compared for equivalence with those resulting from Helmholtz free energy density. Derivation of memory modulus is presented to show that the materials characterized by these theories have fading memory.

I.3.3 Numerical studies

In this section, we present some numerical studies using the constitutive theory for stress tensor presented in this work. We consider the 1D case with infinitesimal deformation and strain. We assume the material to be incompressible. For this case, the momentum and constitutive equations (in the absence of body forces) in the x_1-coordinate direction are

$$\rho_0 \frac{\partial^2 u_{x_1}}{\partial t^2} + \frac{\partial p}{\partial x_1} - \frac{\partial({}_d\sigma_{x_1x_1})}{\partial x_1} = 0 \tag{I.92}$$

$${}_d\sigma_{x_1x_1} + \lambda \frac{\partial({}_d\sigma_{x_1x_1})}{\partial t} = e_1 \frac{\partial u_{x_1}}{\partial x_1} + n_1 \frac{\partial}{\partial t}\left(\frac{\partial u_{x_1}}{\partial x_1}\right) \tag{I.93}$$

For the incompressible case

$$p = -\frac{1}{2}\,{}_d\sigma_{x_1x_1}$$

Hence, (I.92) in this case can be written as

$$\rho_0 \frac{\partial^2 u_{x_1}}{\partial t^2} - \frac{3}{2}\frac{\partial({}_d\sigma_{x_1x_1})}{\partial x_1} = 0 \tag{I.94}$$

Equations (I.93) and (I.94) constitute the mathematical model for the 1D case used in the numerical studies presented in this section. In this mathematical model, ${}_d\sigma_{x_1x_1}$ must be maintained as a dependent variable as the substitution of ${}_d\sigma_{x_1x_1}$ from (I.93) into (I.94) is not possible. The mathematical model for incompressible thermoviscoelastic solids without memory for the 1D case

consists of

$$\rho_0 \frac{\partial^2 u_{x_1}}{\partial t^2} - \frac{3}{2}\frac{\partial({}_d\sigma_{x_1x_1})}{\partial x_1} = 0 \tag{I.95}$$

$${}_d\sigma_{x_1x_1} = \widetilde{a}_{11}\frac{\partial u_{x_1}}{\partial x_1} + \widetilde{b}_{11}\frac{\partial}{\partial t}\left(\frac{\partial u_{x_1}}{\partial x_1}\right) \tag{I.96}$$

First we derive dimensionless forms of (I.93), (I.94), (I.95) and (I.96). We rewrite these by introducing '$\widehat{\ }$' (hat) on all quantities signifying that all quantities have their usual dimensions or units.

$$\widehat{\rho}_0 \frac{\partial^2 \widehat{u}_{x_1}}{\partial \widehat{t}^2} - \frac{3}{2}\frac{\partial({}_d\widehat{\sigma}_{x_1x_1})}{\partial \widehat{x}_1} = 0 \tag{I.97}$$

$${}_d\widehat{\sigma}_{x_1x_1} + \widehat{\lambda}\frac{\partial({}_d\widehat{\sigma}_{x_1x_1})}{\partial \widehat{t}} = \widehat{e}_1\frac{\partial \widehat{u}_{x_1}}{\partial \widehat{x}_1} + \widehat{n}_1\frac{\partial}{\partial \widehat{t}}\left(\frac{\partial \widehat{u}_{x_1}}{\partial \widehat{x}_1}\right) \tag{I.98}$$

$$\widehat{\rho}_0 \frac{\partial^2 \widehat{u}_{x_1}}{\partial \widehat{t}^2} - \frac{3}{2}\frac{\partial({}_d\widehat{\sigma}_{x_1x_1})}{\partial \widehat{x}_1} = 0 \tag{I.99}$$

$${}_d\widehat{\sigma}_{x_1x_1} = \widehat{\widetilde{a}}_{11}\frac{\partial \widehat{u}_{x_1}}{\partial \widehat{x}_1} + \widehat{\widetilde{b}}_{11}\frac{\partial}{\partial \widehat{t}}\left(\frac{\partial \widehat{u}_{x_1}}{\partial \widehat{x}_1}\right) \tag{I.100}$$

We choose reference quantities with subscript zero or ref and define dimensionless variables using these

$$\rho_0 = \frac{\widehat{\rho}_0}{(\rho_0)_{\text{ref}}} \quad , \quad u_{x_1} = \frac{\widehat{u}_{x_1}}{u_0} \quad , \quad v_{x_1} = \frac{\widehat{v}_{x_1}}{v_0}x_1 = \frac{\widehat{x}_1}{L_0} \quad , \quad t = \frac{\widehat{t}}{t_0} \quad , \quad {}_d\sigma_{x_1x_1} = \frac{{}_d\widehat{\sigma}_{x_1x_1}}{\tau_0} \tag{I.101}$$

L_0 is a reference length, hence $u_0 = L_0$ and if we choose v_0 as a reference velocity (generally the speed of sound using reference quantities, i.e. the reference speed of sound), then $t_0 = \frac{u_0}{v_0} = \frac{L_0}{v_0}$. τ_0 is a reference stress. We choose $\tau_0 = (\rho_0)_{\text{ref}}v_0^2$, the characteristic kinetic energy (which has the same dimension as stress). The dimensionless forms of (I.97) to (I.100) become

$$\rho_0 \frac{\partial^2 u_{x_1}}{\partial t^2} - \frac{3}{2}\frac{\partial({}_d\sigma_{x_1x_1})}{\partial x_1} = 0 \tag{I.102}$$

$${}_d\sigma_{x_1x_1} + \text{De}\,\frac{\partial({}_d\sigma_{x_1x_1})}{\partial t} = e_1^d\frac{\partial u_{x_1}}{\partial x_1} + n_1^d\frac{\partial}{\partial t}\left(\frac{\partial u_{x_1}}{\partial x_1}\right) \tag{I.103}$$

$$\rho_0 \frac{\partial^2 u_{x_1}}{\partial t^2} - \frac{3}{2}\frac{\partial({}_d\sigma_{x_1x_1})}{\partial x_1} = 0 \tag{I.104}$$

$${}_d\sigma_{x_1x_1} = a_{11}^d\frac{\partial u_{x_1}}{\partial x_1} + b_{11}^d\frac{\partial}{\partial t}\left(\frac{\partial u_{x_1}}{\partial x_1}\right) \tag{I.105}$$

where

$$\text{De} = \frac{\widehat{\lambda}v_0}{L_0} \quad , \quad e_1^d = \frac{\widehat{e}_1}{\tau_0} \quad , \quad n_1^d = \frac{\widehat{n}_1}{(\rho_0)_{\text{ref}}v_0L_0} \quad , \quad a_{11}^d = \frac{\widehat{\widetilde{a}}_{11}}{\tau_0} \quad , \quad b_{11}^d = \frac{\widehat{\widetilde{b}}_{11}}{(\rho_0)_{\text{ref}}v_0L_0} \tag{I.106}$$

Clearly $e_1^d = a_{11}^d$ and $n_1^d = b_{11}^d$, hence a_{11}^d and b_{11}^d in (I.105) can be replaced by e_1^d and n_1^d. De is called the Deborah number. By substituting (I.105) into (I.104), we can obtain a single PDE in u_{x_1}

$$\rho_0 \frac{\partial^2 u_{x_1}}{\partial t^2} - c_1^d\frac{\partial^2 u_{x_1}}{\partial x_1^2} - c_2^d\frac{\partial}{\partial t}\left(\frac{\partial^2 u_{x_1}}{\partial x_2^2}\right) = 0 \tag{I.107}$$

in which

$$c_1^d = \frac{3}{2}e_1^d \quad , \quad c_2^d = \frac{3}{2}n_1^d \quad \text{or} \quad e_1^2 = \frac{2}{3}c_1^d \quad , \quad n_1^d = \frac{2}{3}c_2^d \tag{I.108}$$

In the numerical studies presented here, we consider the mathematical model given by (I.102) and (I.103), in which we choose e_1^d and n_1^d using (I.108) with the equivalent values of c_1^d and c_2^d as used in reference [33] so that these studies can be compared with those in reference [33] to illustrate the influence of rheology.

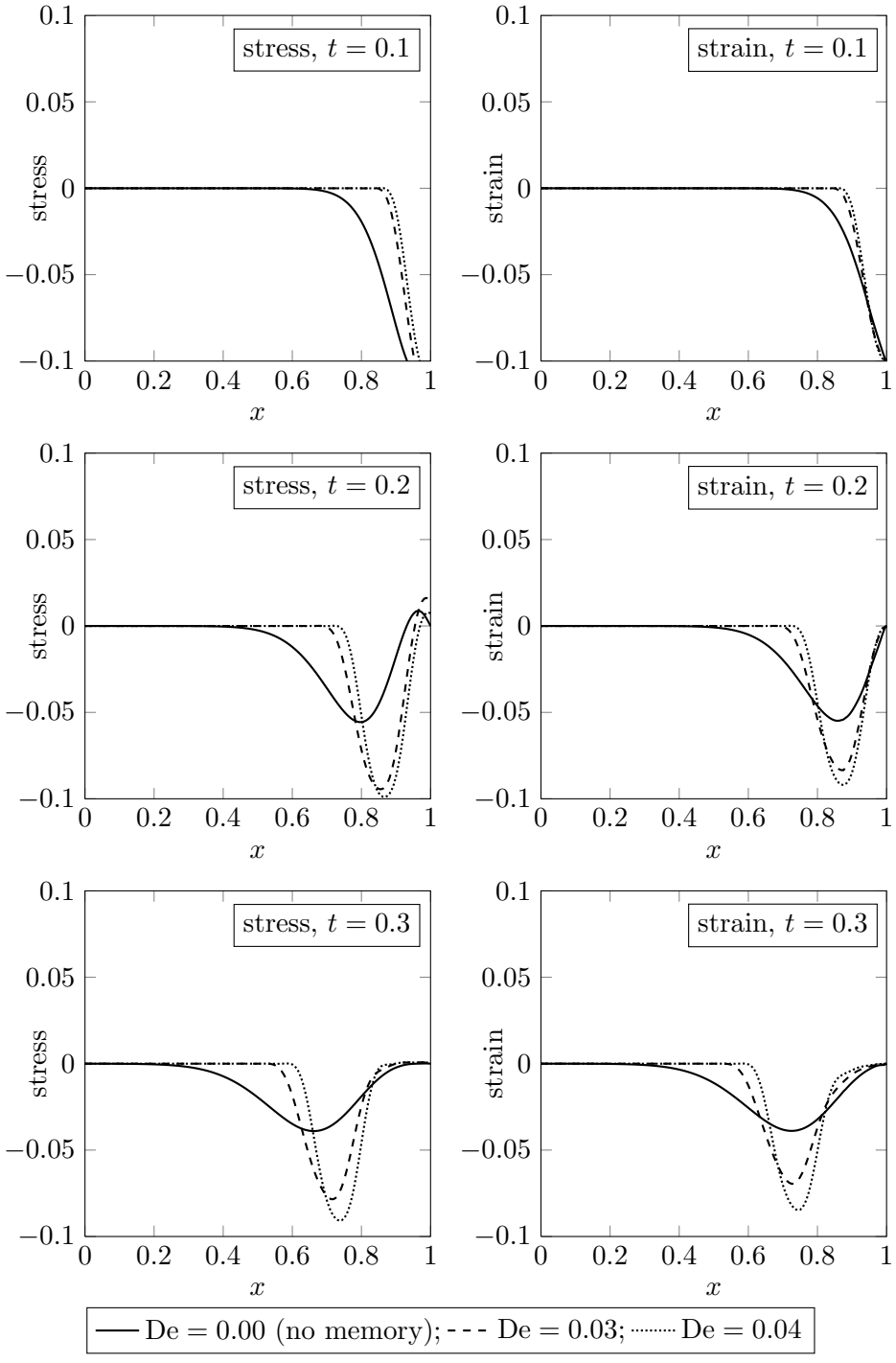

Figure 6: Evolutions of stress and strain for $e_1^d = 1.0$, $\eta_1^d = 0.05$ (with memory); $c_1^d = \frac{3}{2}e_1^d = 1.5$, $c_2^d = \frac{3}{2}\eta_1^d = 0.075$ (no memory)

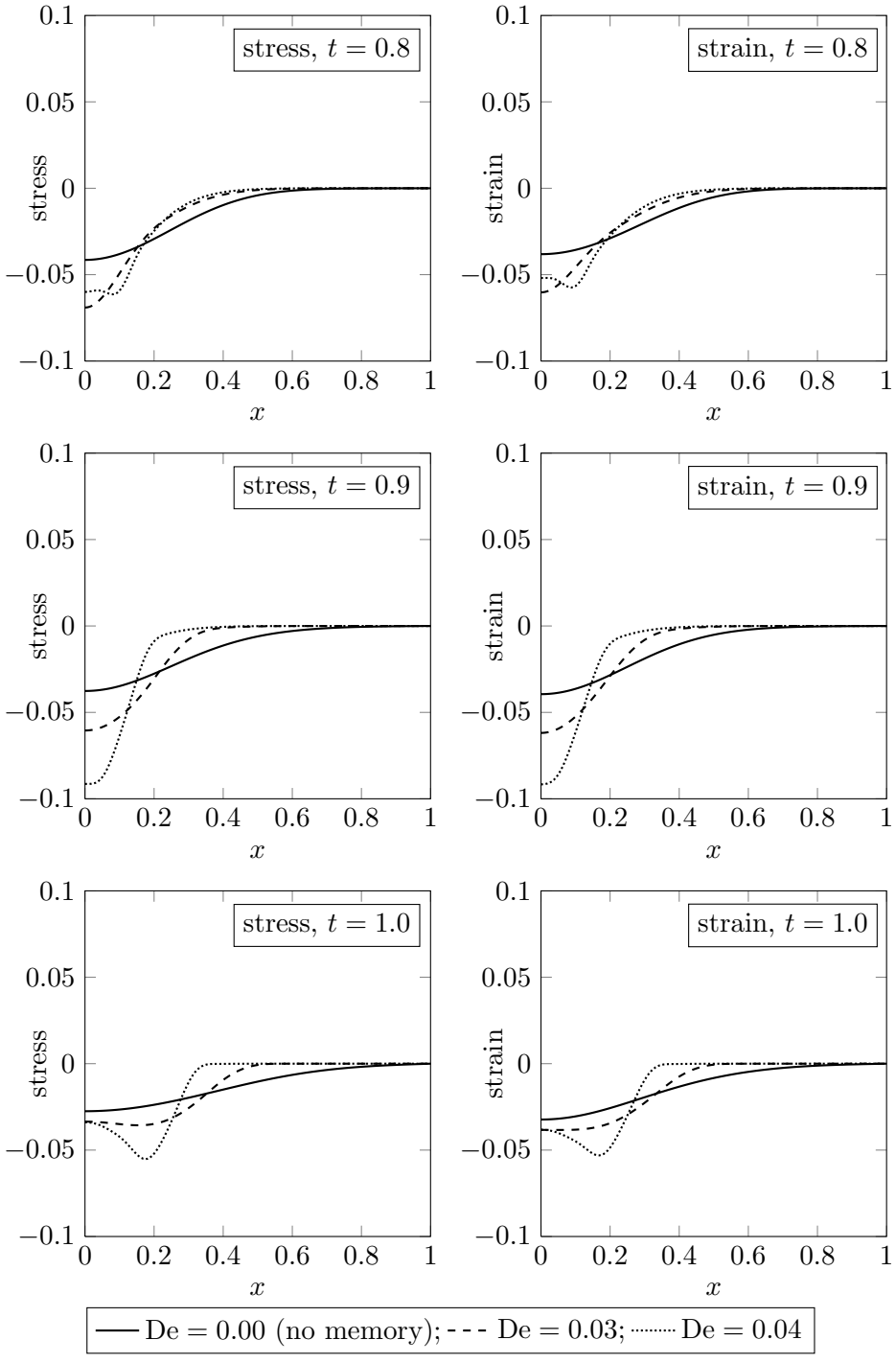

Figure 7: Evolutions of stress and strain for $e_1^d = 1.0$, $\eta_1^d = 0.05$ (with memory); $c_1^d = \frac{3}{2}e_1^d = 1.5$, $c_2^d = \frac{3}{2}\eta_1^d = 0.075$ (no memory)

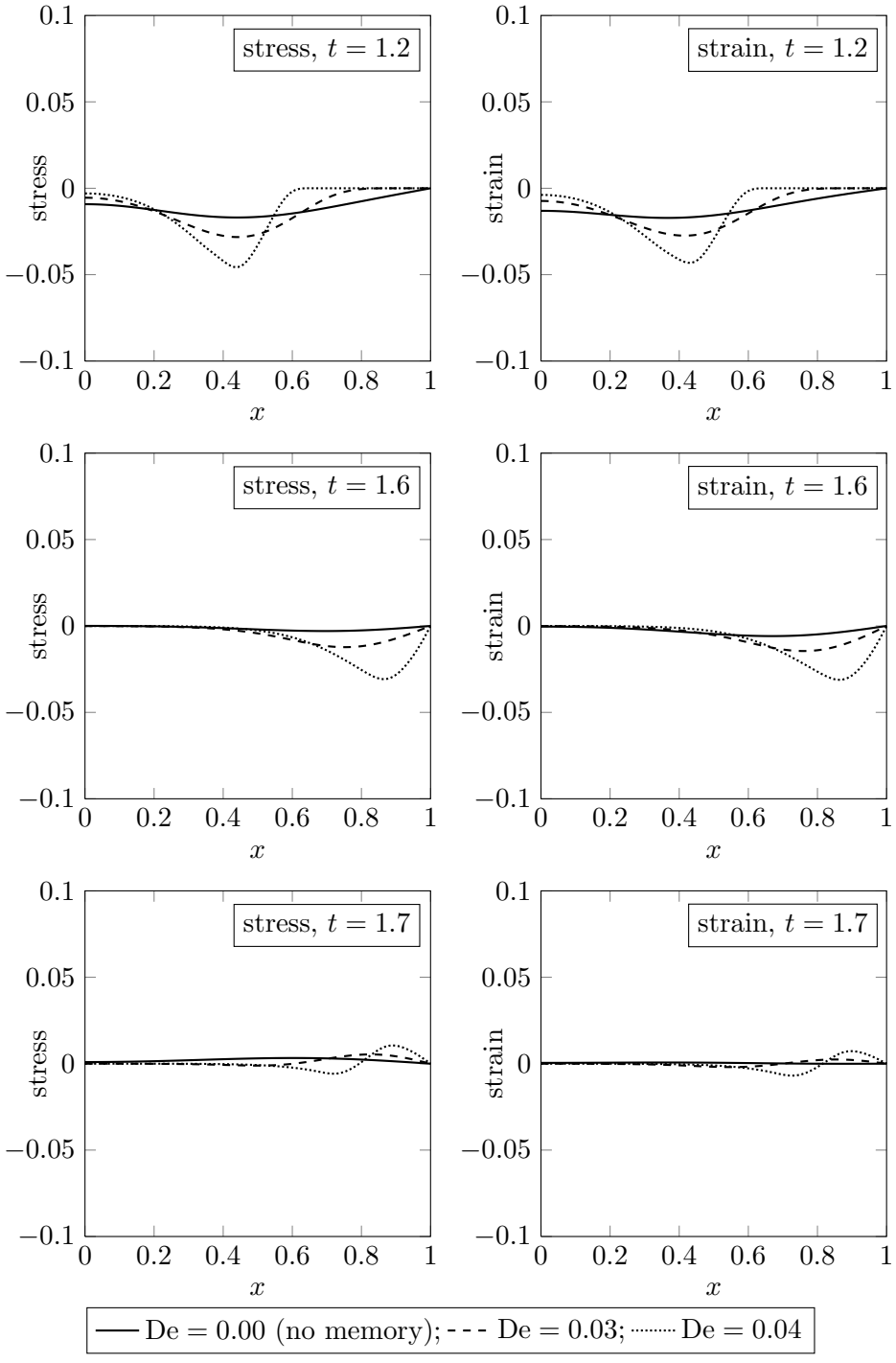

Figure 8: Evolutions of stress and strain for $e_1^d = 1.0$, $\eta_1^d = 0.05$ (with memory); $c_1^d = \frac{3}{2}e_1^d = 1.5$, $c_2^d = \frac{3}{2}\eta_1^d = 0.075$ (no memory)

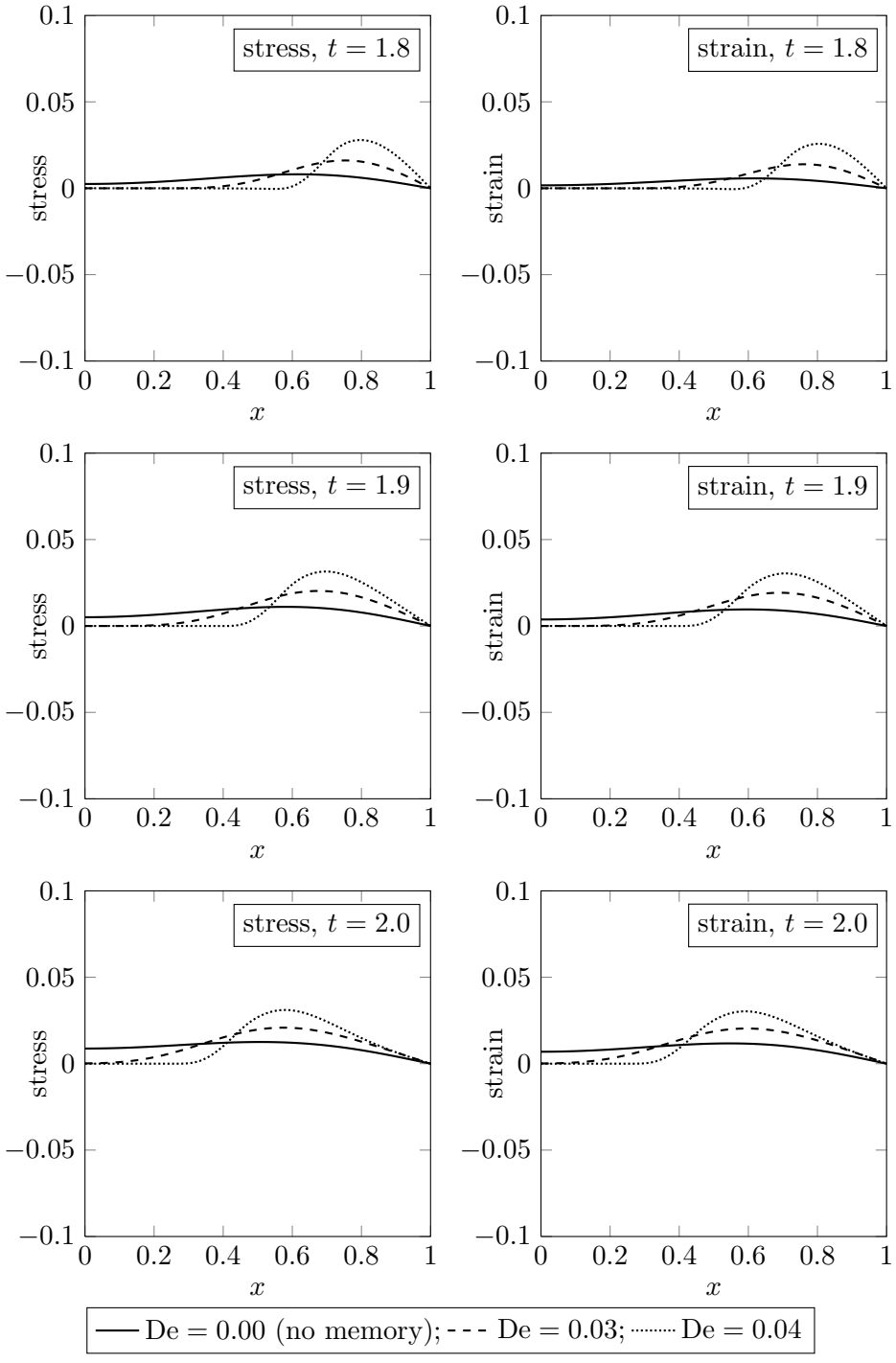

Figure 9: Evolutions of stress and strain for $e_1^d = 1.0$, $\eta_1^d = 0.05$ (with memory); $c_1^d = \frac{3}{2}e_1^d = 1.5$, $c_2^d = \frac{3}{2}\eta_1^d = 0.075$ (no memory)

In the numerical studies we consider an axial rod of dimensionless length one unit and choose $(\rho_{_0})_{\text{ref}} = \widehat{\rho}_0$ so that $\rho_{_0} = 1$. The spatial domain $[0,1]$ for an increment of time $\Delta t = t_{n+1} - t_n$, i.e. the n^{th} space-time strip $[0,1] \times [t_n, t_{n+1}]$, is discretized using a uniform mesh of eight space-time p-version finite elements with higher order global differentiability.

Figure 1 shows details of the space-time domain for an increment of time $\Delta t = t_{n+1} - t_n$, boundary conditions, as well as initial conditions. The left end of the rod is clamped (impermeable boundary) and the right end is subjected to a continuous and differentiable compressive piecewise-cubic strain distribution over a time period of $2\Delta t$. For $t \geq 2\Delta t$, the applied strain at the right end of the rod is zero. We choose p-level of 9 in space and time, and the local approximation is of class $C^{11}(\bar{\Omega}_{x_1 t})$, i.e. C^1 in space and time. The finite element formulation used for computing numerical solutions is based on space-time least squares process constructed using residual functionals. The resulting computational processes are unconditionally stable. Evolutions are computed using a space-time strip with time marching [41–45]. For the choice of local approximation $C^{11}(\bar{\Omega}_{x_1 t})$, the integrals in the finite element processes are Lebesgue, but due to the smoothness of the evolution, for the eight-element discretization with p-level of 9, the residual functionals are on the order of $O(10^{-8})$ for all space-time strips, confirming good accuracy of the evolution.

Figures 6–9 show evolution of stress and strain for De = 0.0, 0.03 and 0.04 for $0 \leq t \leq 2.0$. When De $= 0.0$, we use mathematical model (I.107) for computations as for this case, (I.93) loses its time term and hence is not a valid differential constitutive model. Figure 6 shows the evolution of stress and strain for $0 \leq t \leq 0.3$. The evolutions of stress and strain for $0.3 \leq t \leq 1.0$, $1.2 \leq t \leq 1.7$ and $1.8 \leq t \leq 2.0$ are shown in Figures 7, 8 and 9. Numerical values of the material coefficients are also shown in the captions of the figures. When De $= 0.0$, the behavior is thermoviscoelastic but without memory. As time elapses, the stress and strain waves experience base elongation and amplitude decay due to dissipation as shown in the figures. At time $t = 2.0$, waves show almost complete amplitude decay. For nonzero Deborah number, the stress and strain amplitude are higher than for De $= 0.0$ throughout the evolution, due to rheology. Increasing Deborah numbers produce increasing values of stress and strain during evolution. Peak stress and strain values for De $= 0.04$ are higher than those for De $= 0.03$ throughout the evolution.

I.4 Summary, concluding remarks, significance and impact of this research

In this section we present a brief summary of the research work presented here and provide some concluding remarks:

(1) The ordered rate theories presented here in Lagrangian description for thermoelastic solids, thermoviscoelastic solids without memory and thermoviscoelastic solids with memory are derived using second law of thermodynamics (entropy inequality) expressed in terms of Helmholtz free energy density Φ as well as Gibbs potential Ψ. The solid matter is assumed to be homogeneous, isotropic but can have finite deformation.

(2) Even though the two forms of entropy inequality resulting from the Helmholtz free energy density Φ and Gibbs potential Ψ are equivalent, the equivalence between the constitutive theories derived using these two forms of the entropy inequality may or may not exist.

(3) Using Helmholtz free energy density Φ, the dependent variables in the constitutive theories are stress tensor $\boldsymbol{\sigma}^{[0]}$ and heat vector $\boldsymbol{q}$ ($\boldsymbol{\sigma}^{[0]}$, the second Piola-Kirchhoff stress tensor and $\boldsymbol{\varepsilon}$, Green's strain tensor, measure of finite strain) whereas when using Gibbs potential, $\boldsymbol{\varepsilon}$ and $\boldsymbol{q}$ are dependent variables in the constitutive theories.

(4) We use notation G and H for Gibbs potential and Helmholtz free energy density to list dependent variables and their argument tensors in the two approaches:

(I) Thermoelastic solids

$$\left.\begin{aligned} \boldsymbol{\sigma}^{[0]} &= \boldsymbol{\sigma}^{[0]}(\boldsymbol{\varepsilon}, \theta) = \boldsymbol{\sigma}^{[0]}(\boldsymbol{\varepsilon}^{[0]}, \theta) \\ \boldsymbol{q} &= \boldsymbol{q}(\boldsymbol{\varepsilon}, \boldsymbol{g}, \theta) \end{aligned}\right\} \quad H$$

$$\left.\begin{aligned} \boldsymbol{\varepsilon} &= \boldsymbol{\varepsilon}(\boldsymbol{\sigma}^{[0]}, \theta) \\ \boldsymbol{q} &= \boldsymbol{q}(\boldsymbol{\sigma}^{[0]}, \boldsymbol{g}, \theta) \end{aligned}\right\} \quad G \tag{I.109}$$

The derivation of the constitutive theories in both cases can be done using (i) condition resulting from entropy inequality, (ii) using the theory of generators and invariants (iii) Taylor series expansion. We have shown that (i) and (ii) result in identical theories for H as well as G which are meritorious over the theories resulting from (iii). The equivalence between the theories due to H and G only exist if the theories are linear.

(II) Thermoviscoelastic solids without memory

$$\left.\begin{aligned} \boldsymbol{\sigma}^{[0]} &= {}_e\boldsymbol{\sigma}^{[0]} + {}_d\boldsymbol{\sigma}^{[0]} \\ {}_d\boldsymbol{\sigma}^{[0]} &= {}_d\boldsymbol{\sigma}^{[0]}(\ \boldsymbol{\varepsilon}^{[i]}\ ;\ i=0,1,\ldots,n\ ,\ \boldsymbol{g}\ ,\ \theta\ ) \\ \boldsymbol{q} &= \boldsymbol{q}(\ \boldsymbol{\varepsilon}^{[i]}\ ;\ i=0,1,\ldots,n\ ,\ \boldsymbol{g}\ ,\ \theta\ ) \end{aligned}\right\}\quad H$$

$$\left.\begin{aligned} \boldsymbol{\sigma}^{[0]} &= {}_e\boldsymbol{\sigma}^{[0]} + {}_d\boldsymbol{\sigma}^{[0]} \\ \boldsymbol{\varepsilon}^{[n]} &= \boldsymbol{\varepsilon}^{[n]}(\ {}_d\boldsymbol{\sigma}^{[0]}\ ,\ \boldsymbol{\varepsilon}^{[i]}\ ;\ i=0,1,\ldots,n-1\ ,\ \boldsymbol{g}\ ,\ \theta\ ) \\ \boldsymbol{q} &= \boldsymbol{q}(\ {}_d\boldsymbol{\sigma}^{[0]}\ ,\ \boldsymbol{\varepsilon}^{[i]}\ ;\ i=0,1,\ldots,m-1\ ,\ \boldsymbol{g}\ ,\ \theta\ ) \end{aligned}\right\}\quad G \tag{I.110}$$

where ${}_e\boldsymbol{\sigma}^{[0]} = p(\rho,\theta)\boldsymbol{I}$ and ${}_e\boldsymbol{\sigma}^{[0]} = p(\theta)\boldsymbol{I}$ for compressible and incompressible cases for both H and G. In this case, the use the theory of generators and invariants to derive the rate constitutive theories. These are rate theories of order n. Dissipation mechanism is due to $\boldsymbol{\varepsilon}^{[i]}\ ;\ i=0,1,\ldots,n$. The resulting theories of order n from G and H have no equivalence. Simplified linear rate theories of order one ($n=1$) show equivalence between H and G. This mechanism of dissipation in these rate theories is not the same as velocity dependent damping commonly used for solids which has continuum mechanics basis. The linear rate theories using H and G both show that inclusion of each strain rate $\boldsymbol{\varepsilon}^{[i]}$; ; $i=0,1,\ldots,m-1$ requires two material coefficients. This is consistent with the purely elastic behavior. Simplified form of linear first order rate theory in $\mathbb{R}^1$ for incompressible solid with infinitesimal deformation can be compared with Kelvin-Voigt model. The two theories look alike but the significant difference is that the theory derived here uses ${}_d\boldsymbol{\sigma}^{[0]}$ whereas Kelvin-Voigt model uses total stress $\boldsymbol{\sigma}$. From the work presented here, it is straight forward to conclude that (i) Kelvin-Voigt does not have continuum mechanics basis (ii) its extension to $\mathbb{R}^2$ and $\mathbb{R}^3$ (only for infinitesimal deformation) is ad-hoc as it would still contain one material coefficient for dissipation mechanism which is non-physical based on this work (iii) use of Kelvin-Voigt model in the mathematical models of deforming thermoviscoelastic solids is not ensured to yield thermodynamic equilibrium during evolution. It is shown that the rate theories derived here have no mechanism of fading memory. This is consistent with the assumed physics. Rate theories of upto orders n for $\boldsymbol{q}$ using H and G are presented. These are consistent with those for $\boldsymbol{\sigma}^{[0]}$ and $\boldsymbol{\varepsilon}^{[0]}$ in the sense of argument tensors.

(III) Thermoviscoelastic solids with memory

$$\left.\begin{aligned} \boldsymbol{\sigma}^{[0]} &= {}_e\boldsymbol{\sigma}^{[0]} + {}_d\boldsymbol{\sigma}^{[0]} \\ {}_d\boldsymbol{\sigma}^{[m]} &= {}_d\boldsymbol{\sigma}^{[m]}(\ {}_d\boldsymbol{\sigma}^{[j]}\ ;\ j=0,1,\ldots,m-1\ ,\ \boldsymbol{\varepsilon}^{[i]}\ ;\ i=0,1,\ldots,n\ ,\ \boldsymbol{g}\ ,\ \theta\ ) \\ \boldsymbol{q} &= \boldsymbol{q}(\ {}_d\boldsymbol{\sigma}^{[j]}\ ;\ j=0,1,\ldots,m-1\ ,\ \boldsymbol{\varepsilon}^{[i]}\ ;\ i=0,1,\ldots,n\ ,\ \boldsymbol{g}\ ,\ \theta\ ) \end{aligned}\right\}\quad H$$

$$\left.\begin{aligned} \boldsymbol{\sigma}^{[0]} &= {}_e\boldsymbol{\sigma}^{[0]} + {}_d\boldsymbol{\sigma}^{[0]} \\ \boldsymbol{\varepsilon}^{[n]} &= \boldsymbol{\varepsilon}^{[n]}(\ {}_d\boldsymbol{\sigma}^{[j]}\ ;\ j=0,1,\ldots,m\ ,\ \boldsymbol{\varepsilon}^{[i]}\ ;\ i=0,1,\ldots,n-1\ ,\ \boldsymbol{g}\ ,\ \theta\ ) \\ \boldsymbol{q} &= \boldsymbol{q}(\ {}_d\boldsymbol{\sigma}^{[j]}\ ;\ j=0,1,\ldots,m\ ,\ \boldsymbol{\varepsilon}^{[i]}\ ;\ i=0,1,\ldots,n-1\ ,\ \boldsymbol{g}\ ,\ \theta\ ) \end{aligned}\right\}\quad G \tag{I.111}$$

where ${}_e\boldsymbol{\sigma}^{[0]} = p(\rho,\theta)\boldsymbol{I}$ and ${}_e\boldsymbol{\sigma}^{[0]} = p(\theta)\boldsymbol{I}$ for compressible and incompressible cases for both H and G. In this case, the use the theory of generators and invariants to derive the rate constitutive theories of orders (m,n). Existence of memory modulus requires $m \geq 1$. The resulting constitutive theories of orders (m,n) from H and G have no equivalence. Simplified linear rate theories or orders $(1,1)$ show equivalence between H and G. The mechanism of dissipation in these materials is also due to strain rates $\boldsymbol{\varepsilon}^{[i]}$; $i = 0,1,\ldots,n$. Inclusion of each $\boldsymbol{\varepsilon}^{[i]}$ requires two material coefficients, as described in (II).

Simplified linear rate theory of orders $(1,1)$ in $\mathbb{R}^1$ for incompressible solid with infinitesimal deformation can be compared with Fourier model. The theories look alike but the most significant difference is that the theories derived here use ${}_d\boldsymbol{\sigma}^{[0]}$ where as the Fourier model uses total stress $\boldsymbol{\sigma}$. From the work presented here we conclude that (i) Fourier model used currently for thermoviscoelastic solids with memory has no continuum mechanics basis (ii) its extensions to $\mathbb{R}^2$ and $\mathbb{R}^3$ (only for infinitesimal deformation) is ad-hoc for reasons similar to those in (II) for Kelvin-Voigt model (iii) use of Fourier model may violate thermodynamic equilibrium during evolution. It is shown that rate theories derived here have mechanism of fading memory. Rate theories of orders upto (m,n) are also presented for $\boldsymbol{q}$. These are consistent with the corresponding rate theories for $\boldsymbol{\sigma}^{[0]}$ and $\boldsymbol{\varepsilon}$ using H and G.

(5) All rate theories presented here for $\boldsymbol{\sigma}$, $\boldsymbol{q}$ or $\boldsymbol{\varepsilon}$, $\boldsymbol{q}$ are consistent in the choice of argument tensors, they are valid for finite strains and are in strict adherence with the principles and axioms of continuum mechanics.

(6) The two approaches of deriving rate theories using Helmholtz free energy density Φ and Gibbs potential Ψ are two viable but alternate approaches that may have merits in specific applications for advanced newer materials.

(7) Rate theories for thermoelastic solids using Helmholtz free energy density is meritorious in the sense that these theories yield explicit expressions for $\boldsymbol{\sigma}^{[0]}$ in terms of gradients of displacements, hence permit elimination of $\boldsymbol{\sigma}^{[0]}$ as dependent variables from the mathematical models resulting from the conservation laws. Such mathematical models with reduced number of dependent variables are computationally more efficient.

(8) The rate theories presented in this work provide rigorous, consistent and versatile framework for complex material behaviors in applications where finite strains are important to consider in the development of the complete mathematical models based on conservation laws.

(9) When the mathematical models derived using the rate theories presented here have desired physics, their numerical solutions using h,p,k finite element processes with variationally consistent integral forms are ensured to yield numerical solutions (upon convergence) that are as good as theoretical solutions in all aspects.

(10) In high temperature applications, melting and subsequent solidification may occur in solids. In such cases, mathematical models for the transition zone, a mixture of solid and liquid, is critical. Use of mixture theory based on continuum mechanics principles and thermodynamics is being investigated. Preliminary work for mixture theory for Newtonian and generalized Newtonian fluids is quite promising and is being extended for solid-liquid mixtures.

This work presents the most complete constitutive theories for thermoelastic solids and thermoviscoelastic solids with and without memory using strain energy density function and complementary strain energy density function and with entropy inequality in Helmholtz free energy density and Gibbs potential. In all derivations, finite deformation and finite strains are considered. This work provides the most comprehensive constitutive theory framework to accommodate complex solid material behaviors in which currently used constitutive theories for solids (if based on continuum mechanics axioms and principles) are a subset. The significance and importance of this work is that all constitutive theories presented here are based on integrity, hence complete and thus shows influence of various argument tensors on the constitutive behaviors. Choices of the various terms in the constitutive theories can be made based on desired physics.

II Mathematical Models for Fluid-Solid Interaction and their Numerical Solutions

This work considers various approaches used currently for the fluid-solid interaction problem and associated computational methodologies. The validity of the mathematical models for fluid-solid interaction is established based on the consistency in the

use of continuum mechanics principles and whether the interaction between the solid and the fluid is inherent in the mathematical model or is established external to the mathematical model through interface constraint equations. Computational methodologies are considered from the point of view of unconditional stability, accuracy, and adaptivity of the numerical schemes employed. In particular, the work establishes that fluid-solid interaction physics must be intrinsic in the mathematical model(s), the mathematical models for fluid and solid must have the same description, either Eulerian with transport, Lagrangian, or Eulerian without transport. Since fluids require the Eulerian description with transport, a similar description for solid matter (hypo-elastic solid) indeed provides a mathematical model for fluid-solid interaction in which the fluid-solid interaction is intrinsic in the mathematical model. The mathematical models for solid matter in the Lagrangian description or in the Eulerian description without transport and for fluids in the Eulerian description with transport can never interact due to fundamental differences in their derivations and the basic assumptions employed. For example, the Eulerian description with transport for fluids precludes material point displacements, which are intrinsically present in the Lagrangian description and the Eulerian description without transport, and they are needed for interaction of the fluid with the solid. The mathematical models for solid matter in the Lagrangian description, the Eulerian description without transport, and for fluids in the Eulerian description with transport are presented to illustrate why fluid-solid interaction is not possible with these mathematical models. The ALE methodologies using the mathematical models in Lagrangian and Eulerian descriptions have been carefully evaluated and are demonstrated to be invalid for a consistent formulation of a fluid-solid interaction problem. Some numerical studies for simple model problems are presented to demonstrate various issues discussed here. The present study establishes the possible mathematical models and their limitations within the current knowledge of continuum mechanics that provide correct model for fluid-solid interaction.

II.1 Introduction

Mathematical modeling and numerical simulations of fluid-solid interaction have long been subject of interest. The most challenging and interesting class of applications are those in which the fluid-solid interface experiences finite motion and/or deformation. If one uses a mathematical modeling approach based strictly on the principles of continuum mechanics, then the derivation(s) of the mathematical model(s) for solid matter using Lagrangian description with appropriate measures of finite strain and stress are most natural and useful. In this description the locations $\boldsymbol{x}$ or $\bar{\boldsymbol{x}}$ are indeed locations of the material point in the reference and current configurations and $\bar{\boldsymbol{x}} = \boldsymbol{x} + \boldsymbol{u}(\boldsymbol{x}, t)$ holds. The displacements of material point $\boldsymbol{u}(\boldsymbol{x}, t)$ are monitored during the entire evolution. The physics of deformation for solid matter necessitates this, so that kinematic relations and the associated constitutive theories can be derived. Thus, for solid matter we follow each material point during evolution through its displacement. In the case of fluids, the physics of motion and deformation is quite different than in solid matter.

Consider a simple but common occurrence of flow past an impermeable boundary. Fluid particles attached to the impermeable boundary are immobile, where as the location next to them in the fluid domain are occupied by different fluid particles during the evolution. That is, as the evolution proceeds, different fluid particles rub against these stationary fluid particles attached to the impermeable boundary and move on. In the flow domain away from the impermeable boundaries similar phenomenon exists but the particles rubbing against each other may also be experiencing rigid body motion, that is, they may have their own velocities. As well known, this phenomenon of fluid particles rubbing against each other collectively leads to conversion of mechanical energy into entropy production, which is the basis of Newton's law of viscosity. Thus in fluids: (a) motion of the material points may be so complex that a Lagrangian description may not be possible to describe it and (b) the strains are relatively small and do not play a significant role in the constitutive theory, instead velocity gradients are largely responsible for the stress field. We note that complex motion of fluid particles is difficult to monitor, but fortunately it is not required in the mathematical description of fluids as the strains are negligible.

This short description of the physics of the fluid motion suggests that we can entertain an alternate approach for deriving the mathematical model for fluid motion in which we consider fixed location in the flow domain and monitor the state of the fluid at these locations during evolution. In this approach, the fixed spatial locations are occupied by different fluid particles during the evolution. Thus, these fixed locations are indeed current positions of some fluid particles. Hence it is appropriate to designate them by $\bar{\boldsymbol{x}}$. At a fixed location we can monitor velocities, temperature, stresses, etc. but not the displacements (and they are not needed in the kinematic description of fluid motion). At a fixed location $\bar{\boldsymbol{x}}$ we do not know which fluid particle it is at time t, nor do we know where it is going or came from. This, of course, is all due to the fact that we gave up monitoring displacements of the material points. In deriving the details of the mathematical model for such physics we must consider $\bar{x}_i$ locations and

material particle transport as the particles arriving at the location $\bar{\boldsymbol{x}}$ are due to the transport. We refer to such description as an the Eulerian description (due to $\bar{\boldsymbol{x}}$) with transport. We remark that this is quite different than the Eulerian description of solids in which $\bar{\boldsymbol{x}} = \boldsymbol{x} + \boldsymbol{u}$ holds and thus the mathematical models can either be derived using $(\boldsymbol{x}t)$, the Lagrangian description or $(\bar{\boldsymbol{x}}t)$, the Eulerian description. The two descriptions are equivalent due to uniqueness of displacements $\boldsymbol{u}$. In fluids we are obviously stuck with fixed location $\bar{\boldsymbol{x}}$, the current position of some material particle and material transport but without knowledge of displacements $\boldsymbol{u}$. There is no alternative to this description based on the currently used principles and concepts of continuum mechanics for deriving mathematical model of fluid motion.

From the point of view of this work, an important question is: do these two approaches of deriving the mathematical model for fluid and solid provide the ability of interaction between them? We provide an answer to this question in this section.

A large majority of the recently published literature and on going research work in the area of fluid-solid interaction uses the Arbitrary Lagrangian Eulerian (ALE) approach for mathematical models as a starting point for designing various computational strategies for numerical calculations of the fluid-solid interaction evolution. The ALE concept was first published by Hirt et. al [46] based on the work of Noh [47] and subsequently by Donea et al. [48] and W. K. Liu [49, 50]. In this approach the fluid and solid descriptions are Lagrangian and Eulerian. Based on [48], "ALE has no basic dependence on particles and treats the computational mesh as a reference frame which may be moving with arbitrary velocity $\tilde{v}$." It is claimed that, based on the choice of $\tilde{v}$, Lagrangian and Eulerian descriptions are recoverable from a single mathematical model, which is subsequently utilized for numerical computations. Hughes et al. [51] used ALE approach for modeling fluid sub-domains of many fluid-solid interaction and free surface problems. Tezduyar et al. [52, 53] presented DSD/SST (deforming-spatial-domain/stabilized space-time) procedure developed in reference [53] for finite element computations involving moving boundaries and interfaces. Mesh moving techniques in fluid-solid interactions using DSD/SST are presented by Stein et al. [54]. In chapter 14 of *The Encyclopedia of Computational Mechanics,* Donea et al. [55] presents details of ALE published in their previous papers including numerical studies. In reference [56], Tezduyar et al. considered fluid-solid interaction using a solid-extension mesh moving technique (SEMMT).

In reference [57] Liu et al. presented ALE Petrov-Galerkin finite element formulation for nonlinear continua and presented numerical examples. In a subsequent paper, Liu et al. [58] presented adaptive ALE finite elements with particular reference to external work rate on a frictional interface. Design and evaluation of staggered partitioned procedures for fluid-structure interaction simulations are presented by Piperno et al. [59]. ALE formulation for large deformation are considered in reference [60] by Souli et al. A dual-primal finite element tearing and interconnecting (FETI) method for solving a class of fluid-solid interaction problems in the frequency domain are considered by Li et al. [61]. A level set approach to Eulerian–Lagrangian coupling in fluid-solid interaction is presented by Arienti et al. [62]. Development of what are claimed as coupled and unified solution method for fluid-structure interactions are considered by Sankaran et al. [63]. Various time integration schemes for fluid-solid interaction problems are investigated by Farhat et al. [64]. Algorithms for interface treatment and load computation in embedded boundary methods for fluid and fluid-structure interaction problems are presented by Wang et al. [65]. Numerically stable fluid-structure interactions between compressible flow and solid structures are considered by Gretarsson et al. [66]. Stability of linearized reduced-order models with application to fluid-structure interaction are presented by Amsallem et al. [67]. Computational algorithms for tracking dynamic fluid-structure interfaces in embedded boundary methods are considered by Wang et al. [68].

The present study evaluates mathematical models for solids in the Lagrangian description or in the Eulerian description without transport and for fluids in the Eulerian description with transport to determine whether the interaction between the solid and the fluid is intrinsic in these mathematical models. If the interaction is intrinsic in these mathematical models, then the computation of evolution of their interaction can proceed without any further regard or consideration of the interface between the fluid and the solid. On the other hand, if we establish that the physics of the fluid-solid interaction is not intrinsic or inherent in these mathematical models, then regardless of the type of constraint equations describing interface behavior or any other means employed at the interface, the correct physics of interaction can not be resolved through any justifiable computational means. The results presented demonstrates the following aspects: (i) when the mathematical models for solid are in the Lagrangian description or in the Eulerian description without transport and for the fluid in the Eulerian description with transport, the fluid-solid interaction is not intrinsic in these mathematical models regardless of the magnitude of deformation or motion. The correct interaction physics cannot be defined using these models through any mathematically justifiable means (ii) ALE approaches for fluid-solid interaction result in failure even in the case of infinitesimal deformation and are not justifiable based on continuum mechanics (iii) when the fluid-solid interaction is inherent in the mathematical model, computation of evolution for the fluid-solid interaction problems is a straight forward matter using space-time coupled or space-time decoupled approaches. In all cases, numerical studies are also presented to

demonstrate failure or success of the methodology under consideration.

II.2 Mathematical models for fluid-solid interaction: introduction

Here we consider mathematical models for solid matter in the Lagrangian description and in the Eulerian description without transport, and for fluids in the Eulerian description with transport. From the point of view of the investigation of the interaction physics between a solid and fluid, the specific type of physics we choose for each is not important. Therefore, we choose the simplest possible solid and fluid behaviors. In particular, we consider both solid and fluid to be isotropic, homogeneous, and incompressible, and the processes to be isothermal. Addition of energy equation and considerations of temperature changes and fluxes for non-isothermal cases neither brings in new considerations from the point of view of interaction nor poses any special problems. For the fluid, we consider polymeric liquids such as Maxwell fluid, Oldroyd-B fluid, and Giesekus fluid, etc. In this work, incompressible Newtonian fluids are avoided as the speed of wave propagation in such fluids is infinity. On the other hand, in polymeric liquids the speed of wave propagation is finite, and these are suited for wave propagation studies. In case of solid matter, we further restrict ourselves to thermoelastic solids. Initially we consider the mathematical models for both solid and polymers for non-isothermal case but in numerical studies we consider isothermal behavior only.

II.3 Mathematical model for solid matter

II.3.1 Lagrangian description: finite deformation

For solid matter we consider incompressible thermoelastic solids with finite deformation as well as infinitesimal deformation. If we choose the second Piola–Kirchhoff stress tensor $\boldsymbol{\sigma}^{[0]}$ and Green's strain $\boldsymbol{\varepsilon}_{[0]}$ as a conjugate pair [31], then we can obtain the following mathematical model in the Lagrangian description using conservation and balance laws [31]. We note that for incompressible matter, the determinant of the Jacobian of deformation $[J]$ is $|J| = 1$, then $\rho = |J|\rho_0 = \rho_0$, that is, the continuity equation is identically satisfied. For non-isothermal behavior we need continuity equation, momentum equations, energy equation and the constitutive equations for finite deformation. For hyper-thermoelastic solids [31] we have the following from conservation and balance laws in the Lagrangian description:

$$\rho = |J|\rho_0 = \rho_0 \tag{II.1}$$

$$\rho_0 \frac{\partial v_i}{\partial t} - \rho_0 F_i^b - \frac{\partial \sigma^*_{ji}}{\partial x_j} = 0 \tag{II.2}$$

$$\rho \frac{\partial e}{\partial t} + \boldsymbol{\nabla} \cdot \boldsymbol{q} = 0 \tag{II.3}$$

$$[\sigma^{[0]}] = (\sigma_0)_{\underline{\Omega}}[I] + \lambda_{\underline{\Omega}} \mathrm{tr}([\varepsilon_{[0]}])[I] + 2\mu_{\underline{\Omega}}[\varepsilon_{[0]}] - (\alpha_{tm})_{\underline{\Omega}}(\theta - \theta_{\underline{\Omega}})[I] \tag{II.4}$$

$$\{v\} = \frac{\partial \{u\}}{\partial t} \; ; \quad \{q\} = -k\{g\} \; ; \quad \{g\} = \{\bigtriangledown\}\theta \; ; \quad [\sigma^*]^T = [J][\sigma^{[0]}]^T \tag{II.5}$$

where $\boldsymbol{u}, \boldsymbol{v}$ are displacements and velocities; $\boldsymbol{q}$ and θ are heat flux and temperature; $\boldsymbol{\sigma}^*$ and $\boldsymbol{\sigma}^{[0]}$ are the first Piola–Kirchhoff stress tensor and second Piola–Kirchhoff stress tensor (contravariant); $\boldsymbol{\varepsilon}_{[0]}$ is Green's strain tensor; $\mathbf{F}^b$ is the body force vector (measured per unit mass) in the x-frame; $\boldsymbol{x}$ is a location of a material point in the reference configuration (undeformed configuration); and $\boldsymbol{u}(\boldsymbol{x}, t)$, $\boldsymbol{v}(\boldsymbol{x}, t)$, $\boldsymbol{\sigma}^{[0]}(\boldsymbol{x}, t)$, $\boldsymbol{q}(\boldsymbol{x}, t)$, $\theta(\boldsymbol{x}, t)$, $\boldsymbol{\varepsilon}_{[0]}(\boldsymbol{x}, t)$ are all related to a material point located at $\boldsymbol{x}$ in the reference configuration. As time elapses, these quantities naturally change as they are function of time but $\boldsymbol{x}$ remains the same indicating the identity of the material point in the reference configuration. In this mathematical model displacements $\boldsymbol{u}$ of a material point located at $\boldsymbol{x}$ at the commencement of the evolution are measured (and are essential in the mathematical model) during the evolution. e is specific internal energy, $\boldsymbol{q}$ is heat vector, θ is temperature and k is thermal conductivity. $\lambda_{\underline{\Omega}}$, $\mu_{\underline{\Omega}}$ and $(\alpha_{tm})_{\underline{\Omega}}$ are material coefficients [31] defined in a known configuration $\underline{\Omega}$ and are functions of the invariants of $[\varepsilon_{[0]}]$ and θ in $\underline{\Omega}$ and $(\sigma_0)_{\underline{\Omega}}[I]$ is initial stress tensor in $\underline{\Omega}$.

II.3.2 Lagrangian description: infinitesimal deformation

For this case $\bar{\boldsymbol{x}} \simeq \boldsymbol{x}$ and hence Jacobian of deformation $[J] = [I], |J| = 1$ and the distinction between different stress measures disappear, thus we can use $\boldsymbol{\sigma}$, Cauchy stress in place of $\boldsymbol{\sigma}^{[0]}$. Further more the Green's strain measure $\boldsymbol{\varepsilon}_{[0]}$ for this case simply reduces to the symmetric part of the displacement gradient tensor i.e.

$$(\varepsilon_{[0]})_{ij} = \frac{1}{2}\left(\frac{\partial u_i}{\partial x_j} + \frac{\partial u_j}{\partial x_i}\right) \tag{II.6}$$

For this case the momentum and energy equations and the constitutive theory for the stress tensor reduce to the following:

$$\rho_0 \frac{\partial v_i}{\partial t} - \rho_0 F_i^b - \frac{\partial \sigma_{ji}}{\partial x_j} = 0 \tag{II.7}$$

$$\rho_0 \frac{\partial e}{\partial t} + \boldsymbol{\nabla} \cdot \boldsymbol{q} = 0 \tag{II.8}$$

$$[\sigma] = (\sigma_0)_{\underline{\Omega}}[I] + \lambda_{\underline{\Omega}}\, \mathrm{tr}([\varepsilon_{[0]}])[I] + 2\mu_{\underline{\Omega}}[\varepsilon_{[0]}] - (\alpha_{tm})_{\underline{\Omega}}(\theta - \theta_{\underline{\Omega}})[I] \tag{II.9}$$

$$\{v\} = \frac{\partial\{u\}}{\partial t}\ ; \quad \{q\} = -k\{g\}\ ; \quad \{g\} = \{\bigtriangledown\}\theta \tag{II.10}$$

If we choose constant material coefficients then, $\lambda_{\underline{\Omega}}$ and $\mu_{\underline{\Omega}}$ are Lam$\acute{e}$'s constants that can be defined using modulus of elasticity, E, and Poisson's ratio, ν:

$$\lambda_{\underline{\Omega}} = \frac{\nu E}{(1+\nu)(1-2\nu)} \tag{II.11}$$

$$\mu_{\underline{\Omega}} = \frac{E}{2(1+\nu)} \tag{II.12}$$

II.3.3 Eulerian description without transport: finite deformation

Here we consider the Eulerian description without transport to present mathematical model for homogeneous, isotropic incompressible thermo-elastic solid matter using $\bar{\boldsymbol{\sigma}}^{[0]}$, the contravariant second Piola-Kirchhoff stress tensor in the Eulerian description, Green's strain tensor $\bar{\boldsymbol{\varepsilon}}_{[0]}$ [31], deformed material point coordinate $\bar{\boldsymbol{x}} = \boldsymbol{x} + \boldsymbol{u}$ and time t. $\boldsymbol{u}$ are the displacements of the material point at $\boldsymbol{x}$ in the reference configuration. We use over bar ($^-$) over all quantities to signify the Eulerian description.

$$\rho_0 = |[\bar{J}\,]^{-1}|\bar{\rho}(\bar{\boldsymbol{x}},t) \tag{II.13}$$

$$\bar{\rho}\frac{D\bar{v}_i}{Dt} - \bar{\rho}F_i^b - \frac{\partial \bar{\sigma}^*_{ji}}{\partial \bar{x}_j} = 0 \tag{II.14}$$

$$\bar{\rho}\frac{D\bar{e}}{Dt} + \bar{\bigtriangledown} \cdot \bar{\boldsymbol{q}} = 0 \tag{II.15}$$

$$[\bar{\sigma}^{[0]}] = (\bar{\sigma}_0)_{\underline{\Omega}}[I] + \bar{\lambda}_{\underline{\Omega}}\mathrm{tr}([\bar{\varepsilon}_{[0]}])[I] + 2\bar{\mu}_{\underline{\Omega}}[\bar{\varepsilon}_{[0]}] - (\bar{\alpha}_{tm})_{\underline{\Omega}}(\bar{\theta} - \bar{\theta}_{\underline{\Omega}})[I] \tag{II.16}$$

$$\{\bar{q}\} = -\bar{k}\{\bar{g}\}\ ; \quad \{\bar{g}\} = \{\bar{\bigtriangledown}\}\bar{\theta}\ ; \quad [\bar{\sigma}^*]^T = [\bar{J}]^{-1}[\bar{\sigma}^{[0]}]^T\ ; \quad [\bar{J}] = [J]^{-1} \tag{II.17}$$

All quantities in (II.13)-(II.17) have similar meaning as in (II.1)-(II.5) except that in (II.13)-(II.17) the description is Eulerian. For example, numerical values of $\boldsymbol{\sigma}^*$ and $\bar{\boldsymbol{\sigma}}^*$ are same but the expressions are different due to the fact that $\boldsymbol{\sigma}^*$ is a Lagrangian description whereas $\bar{\boldsymbol{\sigma}}^*$ is Eulerian description.

We remark that constitutive theory for $\bar{\boldsymbol{\sigma}}^{[0]}$ can also be presented using strain measures $\bar{\boldsymbol{C}}_{[0]}$ or $\bar{\boldsymbol{B}}_{[0]}$ [31]. The mathematical models (II.1)-(II.5) and (II.13)-(II.17) are precisely equivalent due to $\bar{\boldsymbol{x}} = \boldsymbol{x} + \boldsymbol{u}$. Thus, for the solid matter we can use either one of these. It is important to point out that during evolution due to the fact that $\bar{\boldsymbol{x}} = \boldsymbol{x} + \boldsymbol{u}$ and the displacements $\bar{\boldsymbol{u}}(\boldsymbol{x}, t)$ of material point $\bar{x}$ evolve as time elapses. We also note that in this mathematical model there is no transport which is same as in case of the Lagrangian description in section II.3.1.

II.3.4 Eulerian description without transport:infinitesimal deformation

In this case $\bar{\boldsymbol{x}} \simeq \boldsymbol{x}$, $[J] = [I]$, $|J| = 1$ and all stress measures are same, hence (II.13)-(II.17) naturally reduces to (II.6)-(II.12). Thus for infinitesimal deformation, the Lagrangian and Eulerian descriptions are the same, as expected.

II.4 Mathematical model for incompressible fluids: polymeric liquids

For simplicity, we consider homogeneous isotropic incompressible polymeric liquids such as Maxwell fluid, Oldroyd-B fluid, Giesekus fluid, etc., but non-isothermal case. It is well known the mathematical models for fluids must be derived in the Eulerian description with transport. This is necessitated due to the physics of fluid flows. In this approach we choose fixed locations in the spatial domain at which we monitor the state of the fluid during evolution. These locations are occupied by different fluid particles at different times. When a fluid particle arrives at a location $\boldsymbol{x}$ at time t, we monitor its state, that is, velocities, temperature, and so on. In this process we do not know which particle it is at location $\boldsymbol{x}$ at time t nor do we know where it came from or where it is going. This is a direct consequence of discarding material particle displacements at the onset of the derivations as these would be too complex to describe using $\boldsymbol{x}$ and t. The positions $\boldsymbol{x}$ in this approach are in fact current positions of some fluid particle at time t. Thus instead of $\boldsymbol{x}$ we use $\bar{\boldsymbol{x}}$ in the derivations of the mathematical models to emphasize this fact. Following [31] we only consider contravariant basis and hence the contravariant Cauchy stress tensor $\bar{\boldsymbol{\sigma}}^{(0)}$ in the description of the mathematical model as covariant, and Jaumann measures become non-physical [31] when deformation is finite. Details of continuity equation, momentum equations, energy equation and the constitutive equations are given in the following [31] using Einstein's notation:

$$\bar{\rho}\frac{\partial \bar{v}_i}{\partial \bar{x}_i} = 0 \tag{II.18}$$

$$\bar{\rho}\left(\frac{\partial \bar{v}_i}{\partial t} + \bar{v}_j\frac{\partial \bar{v}_i}{\partial \bar{x}_j}\right) + \frac{\partial \bar{p}}{\partial \bar{x}_i} - \frac{\partial_d \bar{\sigma}^{(0)}_{ji}}{\partial \bar{x}_j} - \bar{\rho}\bar{F}^b_i = 0 \tag{II.19}$$

$$\bar{\rho}\left(\frac{\partial \bar{e}}{\partial t} + \bar{\boldsymbol{v}}\cdot\bar{\boldsymbol{\nabla}}\bar{e}\right) + \bar{\boldsymbol{\nabla}}\cdot\bar{\boldsymbol{q}} - {}_d\bar{\sigma}^{(0)}_{ji}\bar{D}_{ij} = 0 \tag{II.20}$$

$$\bar{q}_i = -kg_i \ ; \quad \bar{g}_i = \bar{\theta}_{,i} \tag{II.21}$$

In (II.19) we have considered decomposition of the Cauchy stress tensor with equilibrium and deviatoric stresses ${}_e\bar{\boldsymbol{\sigma}}^{(0)}$ and ${}_d\bar{\boldsymbol{\sigma}}^{(0)}$ following [31]. The equilibrium stress ${}_e\bar{\boldsymbol{\sigma}}^{(0)}$ for incompressible matter results in mechanical pressure $\bar{p}$. In (II.23) compressive pressure is considered positive.

$$\bar{\boldsymbol{\sigma}}^{(0)} = {}_e\bar{\boldsymbol{\sigma}}^{(0)} + {}_d\bar{\boldsymbol{\sigma}}^{(0)} \tag{II.22}$$

$${}_e\bar{\boldsymbol{\sigma}}^{(0)} = -\bar{p}\,\boldsymbol{I} \tag{II.23}$$

Constitutive equations for the stress tensor ${}_d\bar{\boldsymbol{\sigma}}^{(0)}$ for the Maxwell, Oldroyd-B, and Giesekus fluid with constant material coefficients are given by [31, 69]:

Maxwell Model

$$[{}_d\bar{\sigma}^{(0)}] + \lambda_1[{}_d\bar{\sigma}^{(1)}] = 2\eta[\gamma_{(1)}] \tag{II.24}$$

Oldroyd-B Model

$$[{}_d\bar{\sigma}^{(0)}] + \lambda_1[{}_d\bar{\sigma}^{(1)}] = 2\eta[\gamma_{(1)}] + \eta\lambda_2[\gamma_{(2)}] \tag{II.25}$$

Giesekus Model

$$\begin{aligned}&[{}_d\bar{\sigma}^{(0)}]_p + \lambda_1[{}_d\bar{\sigma}^{(1)}]_p = 2\eta[\gamma_{(1)}] + \frac{\lambda_1}{\eta}\alpha[{}_d\bar{\sigma}^{(0)}]^2_p\\ &[{}_d\bar{\sigma}^{(0)}] = [{}_d\bar{\sigma}^{(0)}]_s + [{}_d\bar{\sigma}^{(0)}]_p\end{aligned} \tag{II.26}$$

in which $\bar{\boldsymbol{\sigma}}^{(1)}$ is the first convected time derivative of the contravariant Cauchy stress tensor $\bar{\boldsymbol{\sigma}}^{(0)}$. $\boldsymbol{\gamma}_{(1)}$ is the first convected time derivative of the Green's strain tensor, same as symmetric part of the velocity gradient tensor. $\boldsymbol{\gamma}_{(2)}$ is the second convected time derivative of the Green's strain tensor. $\bar{\rho}$, λ_1, η, λ_2 and α are density, relaxation time, viscosity, retardation time and mobility factor. $[{}_d\bar{\sigma}^{(0)}]_s$ and $[{}_d\bar{\sigma}^{(0)}]_p$ refer to solvent and polymer deviatoric stresses. Solvent deviatoric stress is based on Newton's law of viscosity. $\boldsymbol{\gamma}_{(1)}$, $\bar{\boldsymbol{\sigma}}^{(1)}$ and $\boldsymbol{\gamma}_{(2)}$ are defined as

$$(\gamma_{(1)})_{ij} = \bar{D}_{ij} = \frac{1}{2}\left(\frac{\partial \bar{v}_i}{\partial \bar{x}_j} + \frac{\partial \bar{v}_j}{\partial \bar{x}_i}\right) \tag{II.27}$$

$$(\sigma^{(1)})_{ij} = \frac{D(\bar{\sigma}^{(0)})_{ij}}{Dt} - \bar{L}_{ik}(\bar{\sigma}^{(0)})_{kj} - (\bar{\sigma}^{(0)})_{ik}\bar{L}_{jk} + (\bar{\sigma}^{(0)})_{ij}(\bar{L})_{kk} \tag{II.28}$$

$$(\gamma_{(2)})_{ij} = \frac{D(\gamma_{(1)})_{ij}}{Dt} + \bar{L}_{ki}(\gamma_{(1)})_{kj} + (\gamma_{(1)})_{ik}\bar{L}_{kj} \tag{II.29}$$

We note that $\bar{\boldsymbol{x}}$ in this mathematical model does not have the same meaning as $\bar{\boldsymbol{x}}$ in section 2.2.3. Here $\bar{\boldsymbol{x}}$ are fixed locations that are deformed positions of the material points during evolution as the material points occupy these due to transport. Where as $\bar{\boldsymbol{x}}$ in section 2.2.3 are true deformed positions of individual material points.

II.5 Mathematical models in ALE description

In this section we present basic equations describing the mathematical model used in ALE description. Donea et al. [55] presented the first derivation of ALE equations. The derivation is based on the Lagrangian description for solid matter and the Eulerian description with transport for fluid matter as stated in [55]. In our view the derivation has many issues that appear unresolved, but at his stage we do not take issues with these but rather present the final form of the equations describing the mathematical model. Based on Donea et al. [48], the Eulerian description with transport in section 2.3 is converted to ALE form by replacing velocity $\bar{\boldsymbol{v}}$ (velocity at a fixed location $\bar{\boldsymbol{x}}$) in the convective terms with convective velocity $\bar{\boldsymbol{C}}$. The resulting mathematical model is given by

$$\bar{\boldsymbol{C}} = \bar{\boldsymbol{v}} - \hat{\boldsymbol{v}} \tag{II.30}$$

$$\bar{\rho}\frac{\partial \bar{v}_i}{\partial \bar{x}_i} = 0 \tag{II.31}$$

$$\bar{\rho}\frac{\partial \bar{v}_i}{\partial t} + \bar{\rho}\bar{C}_j\frac{\partial \bar{v}_i}{\partial \bar{x}_j} + \frac{\partial \bar{p}}{\partial \bar{x}_j} - \frac{\partial_d \bar{\sigma}^{(0)}_{ji}}{\partial \bar{x}_j} - \bar{\rho}\bar{F}^b_i = 0 \tag{II.32}$$

$$\bar{\rho}\left(\frac{\partial \bar{e}}{\partial t} + \bar{\boldsymbol{C}}\cdot\bar{\boldsymbol{\nabla}}\bar{e}\right) + \bar{\boldsymbol{\nabla}}\cdot\bar{\boldsymbol{q}} - \bar{\sigma}^{(0)}_{ji}\bar{D}_{ij} = 0 \tag{II.33}$$

In (II.30), $\hat{\boldsymbol{v}}$ is referred to as the mesh velocity [48]. We note that in this mathematical model (based on [48]) if we choose $\bar{\boldsymbol{C}} = \bar{\boldsymbol{v}}$ then (II.30) - (II.33) reduce to the Eulerian description with transport as in section 2.3. If $\bar{\boldsymbol{C}} = 0$ then: (i) this mathematical model does not reduce to (II.1) - (II.3), the mathematical model in the Lagrangian description for solid matter that accounts for finite deformation. In this respect we note three important points, first stress measures in (II.30) - (II.33) are not the same as the stress measure in (II.1) - (II.3). Secondly, the velocity $\boldsymbol{v}$ is the material point velocity which is the same as the velocities of the material points during evolution at a fixed location in the absence of transport. Thirdly, for thermoelastic solids the velocity field is not divergence free i.e. (II.31) is not continuity equation for thermoelastic solids. This is obvious from (II.1). (ii) The mathematical model in fact reduces to (II.7) and (II.8), the mathematical model for infinitesimal deformation. In this case also, the continuity equation (II.31) is not admissible. It is advocated that by choosing $\hat{\boldsymbol{v}}$ appropriately, this mathematical model permits simulation of finite motion of the fluid-solid boundaries in spite of the fact that for $\bar{\boldsymbol{C}} = 0$, the mathematical model (II.30) - (II.33) does not have physics of finite deformation. We also remark that in ALE model (II.30) - (II.33), we have not addressed constitutive theories which vary in the published works.

II.5.1 ALE mathematical model for special case of infinitesimal deformation and infinitesimal motion in solid medium

For this case, there is no need to consider a moving frame or moving mesh as the motion or deformation of the interface is infinitesimal. Thus, the mathematical model (II.30) - (II.33) reduces to the following for solid and fluid media.

(a) Solid (thermoelastic solid): Lagrangian description

In the following we have replaced $\bar{\boldsymbol{x}}$ with x (however, this makes no difference as deformation is infinitesimal) and the continuity equation is given for solid matter in which velocity field is not divergence free.

$$\rho = \rho_0 |J| = \rho_0 \quad as \;\; |J| = 1 \tag{II.34}$$

$$\rho_0 \frac{\partial v_i}{\partial t} - \rho_0 F_i^b - \frac{\partial \sigma_{ji}}{\partial x_j} = 0 \tag{II.35}$$

$$v_i = \frac{\partial u_i}{\partial t} \tag{II.36}$$

$$\rho_0 \frac{\partial e}{\partial t} + \boldsymbol{\nabla} \cdot \boldsymbol{q} = 0 \tag{II.37}$$

In (II.35) $\boldsymbol{\sigma}$ is used for the stress tensor as for infinitesimal deformation all stress measures are the same. The definition of $\boldsymbol{q}$ remains same as before.

(b)Fluid (polymer): Eulerian description with transport

$$\bar{\rho} \frac{\partial \bar{v}_i}{\partial \bar{x}_i} = 0 \tag{II.38}$$

$$\bar{\rho} \frac{\partial \bar{v}_i}{\partial t} + \bar{\rho} \bar{v}_j \frac{\partial \bar{v}_i}{\partial \bar{x}_j} + \frac{\partial \bar{p}}{\partial \bar{x}_i} - \frac{\partial_d \bar{\sigma}_{ji}^{(0)}}{\partial \bar{x}_j} - \bar{\rho} \bar{F}_i^b = 0 \tag{II.39}$$

$$\bar{\rho} \left(\frac{\partial \bar{e}}{\partial t} + \bar{\boldsymbol{v}} \cdot \bar{\boldsymbol{\nabla}} \bar{e} \right) + \bar{\boldsymbol{\nabla}} \cdot \bar{\boldsymbol{q}} - {}_d\bar{\sigma}_{ji}^{(0)} \bar{D}_{ij} = 0 \tag{II.40}$$

The constitutive equations (II.24) - (II.26) remain unaffected. Definition of $\boldsymbol{q}$ remains same as before. $\bar{\boldsymbol{\sigma}}^{(0)}$ is the contravariant Cauchy stress tensor in the Eulerian description. Decomposition of $\bar{\boldsymbol{\sigma}}^{(0)}$ into the equilibrium Cauchy stress tensor ${}_e\bar{\boldsymbol{\sigma}}^{(0)}$ and the deviatoric Cauchy stress tensor ${}_d\bar{\boldsymbol{\sigma}}^{(0)}$ gives

$$\bar{\boldsymbol{\sigma}}^{(0)} = {}_e\bar{\boldsymbol{\sigma}}^{(0)} + {}_d\bar{\boldsymbol{\sigma}}^{(0)} \tag{II.41}$$

$${}_e\bar{\boldsymbol{\sigma}}^{(0)} = -\bar{p}(\bar{\boldsymbol{x}}, t)\boldsymbol{I} \tag{II.42}$$

$\bar{p}(\bar{\boldsymbol{x}}, t)$ is mechanical pressure for incompressible fluid. $\bar{p}$ is dependent on $\bar{\theta}$ only.

Remarks:

(1) It is important to distinguish in these mathematical models the presence or absence of transport. First, we note that the convective term $\bar{v}_j \frac{\partial \bar{v}_i}{\partial \bar{x}_j}$ in the momentum equation does not represent transport. This term is due to the material derivative in the Eulerian description, hence it obviously appears in the momentum equation whenever the description is Eulerian regardless of whether there is transport or not. The presence or the absence of transport in the mathematical model is in the constitutive theory.

   (a) For solid matter, the dependence of the stress tensor on the strain tensor only, precludes transport as the material particles must remain connected to their neighbors. Thus thermoelastic solids can not have transport.

(b) In the case of thermo-viscoelastic solids with or without memory the deviatoric stress tensor depends on strain tensor as well as its rates. The dependence of the deviatoric stress tensor on strain tensor precludes transport even though its dependence on strain rate tensors allows transport. Thus, such solids can not have transport either otherwise the dependence of the stress tensor on the strain tensor will not hold.

(c) In the case of fluids the deviatoric stress tensor or its convected time derivatives only depend upon the convected time derivatives of conjugate strain tensor but not on strain tensor itself. This permits the fluids to have transport.

(d) Based on (a)-(c) it is clear that solids do not have transport and fluids do. The presence or absence of transport is in the constitutive theory for the stress tensor.

(e) We note that it is the presence of transport in the fluid that permits arbitrarily large and complex motion of fluid particles.

(f) Study of fluid motion on a fixed grid or fixed spatial locations is meritorious as in this case we do not monitor complex motion of fluid particles i.e. their displacements. Lack of the knowledge of fluid particle displacements precludes measure of strain, but this is okay as the strain measures are not needed in the constitutive theories for fluids.

(2) We note that for infinitesimal deformation and motion in the solid matter, the deformation and motion of the interface is also infinitesimal, hence for this case there is no need for moving mesh or moving frame.

(3) In the mathematical model for solid matter ((II.1) - (II.3)) $\boldsymbol{v}(\boldsymbol{x}, t)$ are velocities of the material point located at $\boldsymbol{x}$ in the reference frame. For this case these are time derivatives of the material point displacement at locations $\boldsymbol{x}$ in the reference configuration i.e.

$$\boldsymbol{v}(\boldsymbol{x}, t) = \frac{\partial \boldsymbol{u}(\boldsymbol{x}, t)}{\partial t} \tag{II.43}$$

(4) In the mathematical model for fluid ((II.38) - (II.40)) $\bar{\boldsymbol{x}}$ is a fixed location and velocities $\bar{\boldsymbol{v}}(\bar{\boldsymbol{x}}, t)$ are the velocities of some material point at this location for time t but we do not know which material point it is. In this description (the Eulerian description with transport) material points are not identified and their displacements are not monitored. This is by choice as explained earlier. Nonetheless the consequence is that the mathematical description for fluid is drastically different than that for solid matter in which we follow material points and hence their displacements are known.

(5) In the derivations of the mathematical models for solid matter and fluid we only consider the desired physics for each case without any consideration regarding the ability of these mathematical models to permit fluid-solid interaction in a combined problem.

(6) ALE description for solid and fluid are no different than the standard Lagrangian and Eulerian descriptions when the deformation and motion of the solid matter is infinitesimal as in sections 2.4.1 (a) and (b).

II.6 Fluid-solid interaction in ALE description

In order to demonstrate the fundamental issues in ALE descriptions for fluid-solid interaction, we consider finite deformation and motion of the solid medium. Fig. 10(a) shows a solid medium in contact with a fluid medium in reference configuration at the commencement of the evolution with common boundary AB. We consider the Lagrangian description for the solid medium and the Eulerian description with transport for the fluid medium. We recall that in the Lagrangian description the locations (or grid points) identify material points, thus any disturbance applied to the system in Fig. 10(a) will result in the motion of the solid domain boundary (material points on the boundary) as well as its interior material points. In the case of the Eulerian description with transport as used for deriving mathematical models for fluids, the boundary of the fluid domain and its interior points (grid points and not the material points) do not move. Instead, as the fluid particles pass through these locations, we monitor their state. Thus, based on these mathematical models, the common boundary AB for solid experiences deformation and motion to occupy a new location $A_s - B_s$ in the current configuration at time t as shown in Fig. 10(b) while the boundary AB for the fluid remains the same as it is in the reference configuration in Fig. 10(a). This illustration is of significance in understanding that the interaction between the solid and the fluid is not intrinsic in the mathematical model otherwise the solid boundary would not deform independent of the

fluid boundary. This is not surprising as the derivations of the mathematical models for solid and fluid are based on specific physics of interest. In the case of solid matter, motion of the material particles is intrinsically important in the kinematic description of the deforming matter and hence the Lagrangian description is essential where as in case of the fluids the displacements of the material points are not needed in the kinematics of the fluid motion and hence are not considered in the derivation of the mathematical model for the fluid. These are the choices made for the solid matter and for the fluid. These mathematical models for solid and fluid, when used in a combined problem, will result in the interface behaviors shown in Fig. 10(b) (as an illustration). This is unavoidable as long as we use the Lagrangian description for the solid and the Eulerian descriptions with transport for fluids.

In published works on ALE, the solid and fluid domain are discretized and integral forms are constructed using the Lagrangian and the Eulerian (with transport) descriptions (presented here) for the respective domains. It is advocated to introduce a "moving mesh" and the two discretizations are mapped on to the moving mesh resulting in the movement of the mesh in the fluid domain such that the separation between the fluid and solid domain boundaries as shown in Fig. 10 (b) does not occur. There are of course numerous strategies and details associated with how this is accomplished. These are not important from the point of view of the present work. It is sufficient to note that currently used mathematical models do not permit interaction between solids and fluids. The current ALE methodologies are based on this basic concept of moving mesh, details of how this is accomplished precisely differ in different papers.

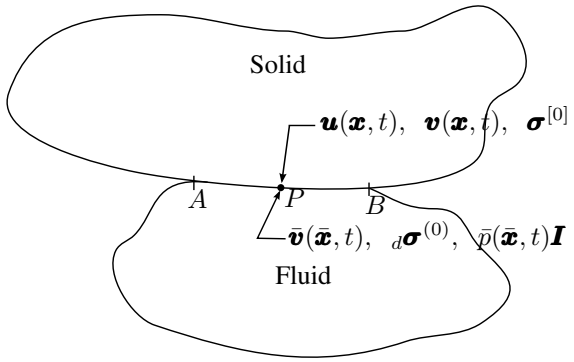

(a) Fluid-solid interaction through boundary AB, reference configuration

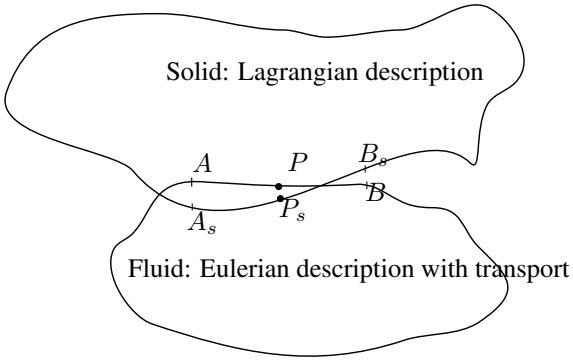

(b) Fluid-solid interaction with boundary AB at time t, current configuration

Figure 10: Fluid-solid interaction

Remarks:

(1) First, we note that the mathematical models used in ALE for solid and fluid that are the standard Lagrangian and Eulerian with transport descriptions produce the behavior shown in Fig. 10(b) (as an illustration) at the solid-fluid interface during

evolution. This is unavoidable when these mathematical descriptions are used. Thus with these mathematical models there is no interaction between solid and fluid.

(2) The ALE approach does nothing to the mathematical models to correct this situation.

(3) Forcing the interaction between solid and fluid by: (a) using discretized forms of the mathematical models (b) mapping the discretized forms on to a moving mesh so that the fluid and solid interfaces never separate even though mathematical models allow separation between the two media lacks rationale and justification.

(4) It is clear that at a fluid-solid interface the mathematical models based on the Lagrangian and Eulerian descriptions with transport do not allow communication between the two media as the dependent variables in the two mathematical models do not have the same physical meaning. For example velocities in the Lagrangian description at each point $\boldsymbol{x}$ (the grid points and material points) is the time rate of change of displacement of the material point located at position $\boldsymbol{x}$ in the reference configuration. Where the velocity $\bar{\boldsymbol{v}}(\bar{\boldsymbol{x}}, t)$ at fixed location $\bar{\boldsymbol{x}}$ is velocity of some material point at time t. The location $\bar{\boldsymbol{x}}$ is occupied by different material particles for different values of time during the evolution. Clearly velocities $\boldsymbol{v}(\boldsymbol{x}, t)$ and $\bar{\boldsymbol{v}}(\bar{\boldsymbol{x}}, t)$ for solid and fluid are physically different quantities. At a common grid point if $\boldsymbol{v}$ and $\bar{\boldsymbol{v}}$ are forced to be equal (for example during finite element computations) then erroneous evolution is bound to occur. Likewise stress measure $\boldsymbol{\sigma}^{[0]}$ and $\bar{\boldsymbol{\sigma}}^{[0]}$ or ${}_d\boldsymbol{\sigma}^{(0)}$ and ${}_d\bar{\boldsymbol{\sigma}}^{(0)}$ have drastically different meanings as well when the solid deformation and motion is finite.

(5) Based on the remarks and discussion presented here, we conclude that fluid-solid interaction is not intrinsic in the mathematical model for solid matter using the Lagrangian description or the Eulerian description without transport and the mathematical model for fluid matter using the Eulerian description with transport. Forcing the meshes in the discretized model at the interface to stay in contact using moving mesh strategies are ad hoc and have no basis as these techniques have no correspondence to the original mathematical models or their modified form (if such forms exist). Thus, in our view ALE descriptions and computational approaches used for fluid-solid interaction have no justification based on the mathematical models derived from continuum mechanics principles.

II.7 When do the mathematical models for solid and fluid contain interaction physics between solid and fluid?

From the discussion presented so far it is clear that the main source of problem in fluid-solid interaction is that the mathematical models for solid matter do not have transport where as the mathematical models for fluid have transport. Thus, we can address this problem of lack of interaction in the mathematical models in a couple of alternative approaches.

(1) Construct mathematical models for fluid in the Eulerian description but without transport, that is derive constitutive theory for the deviatoric stress tensor in terms of strain tensor and its convected time derivatives. Thus, now we have both solid and fluid mathematical models without transport and if we carefully choose the same dependent variables in the two mathematical models then these mathematical models will contain fluid-solid interaction physics. unfortunately, the constitutive theories for fluid without transport are nonphysical, hence this option must be ruled out.

(2) Construct mathematical models for solid matter in the Eulerian description with transport. This requires that in the constitutive theory for the solid matter we express the stress tensor (or the deviatoric stress tensor) or its convected time derivatives as a function of the convected time derivatives of the conjugate strain tensor but not including the strain tensor itself. Such solid matter is called hypo-elastic solid. obviously due to lack of dependence of the stress tensor or the deviatoric stress tensor on the strain tensor, such constitutive theories are not able to describe the physics of commonly encountered solids such as metals (hyper-elastic). Nonetheless, such a mathematical model for solid matter will provide interaction with fluids intrinsically through the mathematical model without the use of any other means. We use such mathematical description for solid matter (hypo-elastic solid) in the numerical studies to demonstrate its effectiveness in fluid-solid interaction. We can generalize these concepts to provide some clear guidelines that can be used to determine if the mathematical models for fluid and solid adequately contain interaction physics.

Based on the material presented above, it is straight forward to see that for the fluid-solid interaction to be intrinsic in the mathematical model(s) there are two basic requirements: (i) the mathematical models for the solid and the fluid must be derived using the same description (ii) the mathematical models must employ the same dependent variables that have the same physical meaning. We note that it is essential to use the Eulerian description with transport for deriving mathematical models for fluids. We have seen in the ALE description that the Lagrangian description or the Eulerian description without transport for solid fails to provide interaction with the fluid. The mathematical model for solid based on the Eulerian description with transport (hence the same description as used for fluids) referred to as hypo-elastic solids does provide desired interaction physics with fluids.

II.8 Mathematical models for one dimensional wave propagation in solids and fluids

To illustrate if the fluid-solid interaction physics is possible using the Eulerian description with transport for fluids and the Lagrangian as well as the Eulerian descriptions with transport for solid matter (hypo-elastic solids), we consider a simple one dimensional wave propagation problem. In the following we present various forms of the mathematical models for fluids and solids using quantities with hat ($\hat{}$) have their usual dimensions and those without hat ($\hat{}$) are dimensionless. For the solid matter we only consider infinitesimal isothermal deformation. Thus all stress measures are the same and we can use $\boldsymbol{\sigma}$ for stress measure. Quantities without over-bar imply the Lagrangian description and those with over-bar are in the Eulerian description with transport. We choose a set of reference quantities denoted by subscript '0'. We divide the quantities with dimension by the reference quantities to non-dimensionalize them. These are then introduced in each equation of the mathematical model. We choose the following reference quantities and the dimensionless variables.

$$
\begin{aligned}
&L=\hat{L}/L_0,\ x_i=\hat{x}_i/L_0\ ,\ F=\hat{F}/F_0\ \ v_i=\hat{v}_i/v_0\ ,\ \tau_{ij}=\hat{\tau}_{ij}/\tau_0\ , \sigma_{ij}=\hat{\sigma_{ij}}/\sigma_0\ p=\hat{p}/p_0\ ;\\
&E=\hat{E}/E_0\ , \rho=\hat{\rho}/\rho_0\ k_{ij}=\hat{k}_{ij}/k_0,\ \ \mu=\hat{\mu}/\mu_0\ ,\ \eta=\hat{\eta}/\mu_0\ ,\ \eta_s=\hat{\eta}_s/\mu_0\ \ \eta_p=\hat{\eta}_p/\mu_0\ ;\\
&\eta=(\hat{\eta}_p+\hat{\eta}_s)/\mu_0\ ,\ \lambda=\hat{\lambda}/\lambda_0\ t=\hat{t}/t_0\ ,\ t_0=L_0/v_0\ C_v=\hat{C}_v/C_{v0}\ ,\ e=\hat{e}/e_0\ ,\ e_0=C_0T_0
\end{aligned}
$$

We note that τ_0, p_0 and E_0 all have the same dimensions $(force/(length)^2)$ and hence, care must be taken in their selections to ensure that $\tau_0 = p_0 = E_0$ always holds. For example we can choose $\tau_0 = p_0 = E_0 = \rho_0 {v_0}^2$, characteristic kinetic energy. Then, if we choose $E_0 = \hat{E} = \rho_0 {v_0}^2$ we have $v_0 = \sqrt{E_0/\rho_0}$ and $E = 1$ and τ_0, p_0 are now automatically defined. We can also choose $\tau_0 = p_0 = E_0 = \mu_0 v_0/L_0$, characteristic viscous stress, hence if we chose $E_0 = \hat{E} = \mu_0 v_0/L_0$ we have $v_0 = E_0 L_0/\mu_0$. We choose $\boldsymbol{x}$ to denote axial direction and the contravariant Cauchy stress tensor [70] in the Eulerian description for the mathematical models for fluids in the Eulerian description with transport.

II.8.1 Solid matter: 1D axial behavior

(A) Hyper-elastic solid

This mathematical model is based on the Lagrangian description. The constitutive theories for the stress tensor for these solids can be derived using strain energy density function. The momentum equation (in the absence of body forces) and constitutive equations are given (using the deviatoric stress) by:

$$
\begin{aligned}
&\hat{\rho}\frac{\partial \hat{v}}{\partial \hat{t}} - 1.5\frac{\partial_d \hat{\sigma}_{xx}}{\partial \hat{x}} = 0\\
&{}_d\hat{\sigma}_{xx} - \frac{2}{3}\hat{E}\frac{\partial \hat{u}}{\partial \hat{x}} = 0\\
&\hat{v} = \frac{\partial \hat{u}}{\partial \hat{t}}
\end{aligned}
\tag{II.44}
$$

The dimensionless form of (II.44) is given by:

$$\begin{aligned}
&\rho\frac{\partial v}{\partial t} - 1.5\left(\frac{\tau_0}{\rho_0 {v_0}^2}\right)\frac{\partial {}_d\sigma_{xx}}{\partial x} = 0\\
&{}_d\sigma_{xx} - \left(\frac{E_0}{\tau_0}\right)\frac{2}{3}E\frac{\partial u}{\partial x} = 0\\
&v = \frac{\partial u}{\partial t}
\end{aligned} \tag{II.45}$$

(B) Hypo-elastic solid

This mathematical model is based on the Eulerian description with transport. The constitutive theory in this case is the first order rate theory in terms of convected time derivatives of the conjugate stress and strain tensors. We only consider the contravariant Cauchy stress tensor $\bar{\boldsymbol{\sigma}}^{(0)}$ [31] and its convected time derivative $\bar{\boldsymbol{\sigma}}^{(1)}$ and the convected time derivative of the Green's strain tensor.

$$\begin{aligned}
&\hat{\rho}\frac{\partial \hat{v}}{\partial \hat{t}} + \hat{\rho}\hat{v}\frac{\partial \hat{v}}{\partial \hat{x}} - 1.5\frac{\partial {}_d\hat{\bar{\sigma}}^{(0)}_{xx}}{\partial \hat{x}} = 0\\
&\frac{\partial {}_d\hat{\bar{\sigma}}^{(0)}_{xx}}{\partial \hat{t}} + \hat{v}\frac{\partial {}_d\hat{\bar{\sigma}}^{(0)}_{xx}}{\partial \hat{x}} - 2.0\frac{\partial \hat{v}}{\partial \hat{x}} = \hat{E}\frac{\partial \hat{v}}{\partial \hat{x}}
\end{aligned} \tag{II.46}$$

The dimensionless form of (II.46) is given by:

$$\begin{aligned}
&\bar{\rho}\frac{\partial \bar{v}}{\partial \bar{t}} + \bar{\rho}\bar{v}\frac{\partial \bar{v}}{\partial \bar{x}} - 1.5\left(\frac{\tau_0}{\rho_0 {v_0}^2}\right)\frac{\partial {}_d\bar{\sigma}^{(0)}_{xx}}{\partial \bar{x}} = 0\\
&\frac{\partial {}_d\bar{\sigma}^{(0)}_{xx}}{\partial \bar{t}} + \bar{v}\frac{\partial {}_d\bar{\sigma}^{(0)}_{xx}}{\partial \bar{x}} - 2.0\frac{\partial \bar{v}}{\partial \bar{x}} = \left(\frac{E_0}{\tau_0}\right)\bar{E}\frac{\partial \bar{u}}{\partial \bar{x}}
\end{aligned} \tag{II.47}$$

In (II.46) and (II.47) ${}_d\hat{\bar{\sigma}}^{(0)}_{xx}$ and ${}_d\bar{\sigma}^{(0)}_{xx}$ are the deviatoric axial Cauchy stresses with and without dimensions.

II.8.2 Viscoelastic polymeric liquids: 1D axial behavior

We consider incompressible viscoelastic polymeric liquids. These are ideal to investigate fluid-solid interaction in wave propagation as the speed of wave propagation in these liquids is finite. We consider the Maxwell, Oldroyd-B and Giesekus fluids and present mathematical models (in the absence of body forces) for 1D wave propagation.

(A) Maxwell fluid

Momentum and constitutive equations are given by:

$$\begin{aligned}
&\hat{\rho}\frac{\partial \hat{v}}{\partial \hat{t}} + \hat{\rho}\hat{v}\frac{\partial \hat{v}}{\partial \hat{x}} + \frac{\partial \hat{p}}{\partial \hat{x}} - \frac{\partial {}_d\hat{\bar{\sigma}}^{(0)}_{xx}}{\partial \hat{x}} = 0\\
&{}_d\hat{\bar{\sigma}}^{(0)}_{xx} + \hat{\bar{\lambda}}_1\left(\frac{\partial {}_d\hat{\bar{\sigma}}^{(0)}_{xx}}{\partial \hat{t}} + \hat{v}\frac{\partial {}_d\hat{\bar{\sigma}}^{(0)}_{xx}}{\partial \hat{x}} - 2\frac{\partial \hat{v}}{\partial \hat{x}}\,{}_d\hat{\bar{\sigma}}^{(0)}_{xx}\right) = 2\hat{\eta}\frac{\partial \hat{v}}{\partial \hat{x}}
\end{aligned} \tag{II.48}$$

$\hat{\bar{\lambda}}_1$ is relaxation time and $\hat{\eta}$ is viscosity. The dimensionless form of (II.48) is given by:

$$\begin{aligned}
&\bar{\rho}\frac{\partial \bar{v}}{\partial \bar{t}} + \bar{\rho}\bar{v}\frac{\partial \bar{v}}{\partial \bar{x}} + \left(\frac{p_0}{\rho_0 {v_0}^2}\right)\frac{\partial \bar{p}}{\partial \bar{x}} - \left(\frac{\tau_0}{\rho_0 {v_0}^2}\right)\frac{\partial {}_d\bar{\sigma}^{(0)}_{xx}}{\partial \bar{x}} = 0\\
&{}_d\bar{\sigma}^{(0)}_{xx} + De\left(\frac{\partial {}_d\bar{\sigma}^{(0)}_{xx}}{\partial \bar{t}} + \bar{v}\frac{\partial {}_d\bar{\sigma}^{(0)}_{xx}}{\partial \bar{x}} - 2\frac{\partial \bar{v}}{\partial \bar{x}}\,{}_d\bar{\sigma}^{(0)}_{xx}\right) = \left(\frac{\mu_o v_0}{\tau_0 L_0}\right)2\eta\frac{\partial \bar{v}}{\partial \bar{x}}
\end{aligned} \tag{II.49}$$

In this case pressure gradient $\partial\bar{p}/\partial\bar{x}$ is known depending upon whether the flow is pressure driven or not, hence mechanical pressure $\bar{p}$ is not a dependent variable in the mathematical model. De is Deborah number defined as $De = \hat{\bar{\lambda}}_1 v_0/L_0$. This constitutive model is generally used for dilute polymeric liquids.

(B) Oldroyd-B fluid

Momentum and constitutive equations are given by:

$$\begin{aligned}
&\hat{\bar{\rho}}\frac{\partial\hat{\bar{v}}}{\partial\hat{\bar{t}}} + \hat{\bar{\rho}}\hat{\bar{v}}\frac{\partial\hat{\bar{v}}}{\partial\hat{\bar{x}}} + \frac{\partial\hat{\bar{p}}}{\partial\hat{\bar{x}}} - \frac{\partial_d\hat{\bar{\sigma}}^{(0)}_{xx}}{\partial\hat{\bar{x}}} = 0 \\
&{}_d\hat{\bar{\sigma}}^{(0)}_{xx} + \hat{\bar{\lambda}}_1\left(\frac{\partial_d\hat{\bar{\sigma}}^{(0)}_{xx}}{\partial\hat{\bar{t}}} + \hat{\bar{v}}\frac{\partial_d\hat{\bar{\sigma}}^{(0)}_{xx}}{\partial\hat{\bar{x}}} - 2.0\frac{\partial\hat{\bar{v}}}{\partial\hat{\bar{x}}}\,{}_d\hat{\bar{\sigma}}^{(0)}_{xx}\right) = 2\hat{\eta}\frac{\partial\hat{\bar{v}}}{\partial\hat{\bar{x}}} + \hat{\bar{\lambda}}_2\hat{\eta}\left(\frac{\partial^2\hat{\bar{v}}}{\partial\hat{\bar{t}}\partial\hat{\bar{x}}} + \hat{\bar{v}}\frac{\partial^2\hat{\bar{v}}}{\partial\hat{\bar{x}}^2} - 2\left(\frac{\partial\hat{\bar{v}}}{\partial\hat{\bar{x}}}\right)^2\right)
\end{aligned} \tag{II.50}$$

$\hat{\bar{\lambda}}_1$ is relaxation time and $\hat{\bar{\lambda}}_2$ is retardation time.
The dimensionless form of (II.50) is given by:

$$\begin{aligned}
&\bar{\rho}\frac{\partial\bar{v}}{\partial\bar{t}} + \bar{\rho}\bar{v}\frac{\partial\bar{v}}{\partial\bar{x}} + \left(\frac{p_0}{\rho_0{v_0}^2}\right)\frac{\partial\bar{p}}{\partial\bar{x}} - \left(\frac{\tau_0}{\rho_0{v_0}^2}\right)\frac{\partial_d\bar{\sigma}^{(0)}_{xx}}{\partial\bar{x}} = 0 \\
&{}_d\bar{\sigma}^{(0)}_{xx} + De_1\left(\frac{\partial_d\bar{\sigma}^{(0)}_{xx}}{\partial\bar{t}} + \bar{v}\frac{\partial_d\bar{\sigma}^{(0)}_{xx}}{\partial\bar{x}} - 2.0\frac{\partial\bar{v}}{\partial\bar{x}}\,{}_d\bar{\sigma}^{(0)}_{xx}\right) = \left(\frac{\mu_o v_0}{\tau_0 L_0}\right)\eta\left(2\frac{\partial\bar{v}}{\partial\bar{x}} + De_2\left(\frac{\partial^2\bar{v}}{\partial\bar{t}\partial\bar{x}} + \bar{v}\frac{\partial^2\bar{v}}{\partial\bar{x}^2} - 2\left(\frac{\partial\bar{v}}{\partial\bar{x}}\right)^2\right)\right)
\end{aligned} \tag{II.51}$$

Deborah numbers De_1 and De_2 are defined as $De_1 = \hat{\bar{\lambda}}_1 v_0/L_0$ and $De_2 = \hat{\bar{\lambda}}_2 v_0/L_0$. This constitutive model is also generally used for dilute polymeric liquids.

(C) Giesekus fluid

Giesekus constitutive model is generally used for dense polymeric liquids in which the behavior is elastically dominated. We consider the Giesekus fluid behavior as elastically dominated. We consider the Giesekus constitutive model used in the published work [69, 71] as opposed to the model reported in [37] by Surana et. al.

$$\begin{aligned}
&\hat{\bar{\rho}}\frac{\partial\hat{\bar{v}}}{\partial\hat{\bar{t}}} + \hat{\bar{\rho}}\hat{\bar{v}}\frac{\partial\hat{\bar{v}}}{\partial\hat{\bar{x}}} + \frac{\partial\hat{\bar{p}}}{\partial\hat{\bar{x}}} - \frac{\partial_d\hat{\bar{\sigma}}^{(0)}_{xx}}{\partial\hat{\bar{x}}} = 0 \\
&{}_d\hat{\bar{\sigma}}^{(0)}_{xx} + \hat{\bar{\lambda}}_1\left(\frac{\partial_d\hat{\bar{\sigma}}^{(0)}_{xx}}{\partial\hat{\bar{t}}} + \hat{\bar{d}}v\frac{\partial_d\hat{\bar{\sigma}}^{(0)}_{xx}}{\partial\hat{\bar{x}}} - 2.0\frac{\partial\hat{\bar{v}}}{\partial\hat{\bar{x}}}{}_d\hat{\bar{\sigma}}^{(0)}_{xx}\right) - 2\hat{\eta}_s\hat{\bar{\lambda}}_1\left(\frac{\partial^2\hat{\bar{v}}}{\partial\hat{\bar{t}}\partial\hat{\bar{x}}} + \hat{\bar{v}}\frac{\partial^2\hat{\bar{v}}}{\partial\hat{\bar{x}}^2} - 2.0\left(\frac{\partial\hat{\bar{v}}}{\partial\hat{\bar{x}}}\right)^2\right) \\
&- \alpha\frac{\hat{\bar{\lambda}}_1}{\hat{\eta}_p}\left({}_d\hat{\bar{\sigma}}^{(0)}_{xx} - 2\hat{\eta}_s\frac{\partial\hat{\bar{v}}}{\partial\hat{\bar{x}}}\right)\left({}_d\hat{\bar{\sigma}}^{(0)}_{xx} - 2\hat{\eta}_s\frac{\partial\hat{\bar{v}}}{\partial\hat{\bar{x}}}\right) = 2\hat{\eta}\frac{\partial\hat{\bar{v}}}{\partial\hat{\bar{x}}}
\end{aligned} \tag{II.52}$$

The dimensionless form of (II.52) is given by:

$$\begin{aligned}
&\bar{\rho}\frac{\partial\bar{v}}{\partial\bar{t}} + \bar{\rho}\bar{v}\frac{\partial\bar{v}}{\partial\bar{x}} + \frac{\partial\bar{p}}{\partial\bar{x}} - \frac{\partial_d\bar{\sigma}^{(0)}_{xx}}{\partial\bar{x}} = 0 \\
&{}_d\bar{\sigma}^{(0)}_{xx} + De\left(\frac{\partial_d\bar{\sigma}^{(0)}_{xx}}{\partial\bar{t}} + \hat{\bar{v}}\frac{\partial_d\bar{\sigma}^{(0)}_{xx}}{\partial x} - 2.0\frac{\partial\bar{v}}{\partial\bar{x}}{}_d\bar{\sigma}^{(0)}_{xx}\right) - 2\eta_s De\left(\frac{\mu_0 v_0}{\tau_0 L_0}\right)\left(\frac{\partial^2\bar{v}}{\partial\bar{t}\partial\bar{x}} + \bar{v}\frac{\partial^2\bar{v}}{\partial\bar{x}^2} - 2.0\left(\frac{\partial\bar{v}}{\partial\bar{x}}\right)^2\right) \\
&- \alpha\frac{De}{\eta_p}\left(\frac{\tau_0 L_0}{\mu_0 v_0}\right)\left({}_d\bar{\sigma}^{(0)}_{xx} - 2\eta_s\left(\frac{\mu_0 v_0}{\tau_0 L_0}\right)\frac{\partial\bar{v}}{\partial\bar{x}}\right)\left({}_d\bar{\sigma}^{(0)}_{xx} - 2\eta_s\left(\frac{\mu_0 v_0}{\tau_0 L_0}\right)\frac{\partial\bar{v}}{\partial\bar{x}}\right) = 2\eta\left(\frac{\mu_0 v_0}{\tau_0 L_0}\right)\frac{\partial\bar{v}}{\partial\bar{x}}
\end{aligned} \tag{II.53}$$

Remarks:

(1) Dimensionless form of the mathematical models for one-dimensional wave propagation have been presented for hyper-elastic solid in the Lagrangian description and hypo-elastic solid in the Eulerian description with transport. The mathematical models for one-dimensional axial deformation of the Maxwell, Oldroyd-B, and Giesekus fluids are presented in the Eulerian description with transport. Care is taken to ensure to use same (or similar) dependent variables in all mathematical models so that if there is lack of interaction between these models, it can not be attributed to the choice of dependent variables in the mathematical models.

(2) We note that the mathematical models for hypo-elastic solid and polymeric liquid all have the same descriptions and the same dependent variables, hence in these models the interactions between these media is inherent in the mathematical models.

(3) The mathematical model for hyper-elastic solid is in the Lagrangian description, hence can not provide interaction with the remaining mathematical models.

(4) Dimensionless forms of the mathematical models are essential in the finite element processes due to varied magnitude of the dependent variables to ensure that in the resulting computational processes the coefficient matrices in the algebraic systems do not become ill-conditioned.

II.9 Numerical studies

II.9.1 Introduction

We present numerical studies for fluid-solid interaction using mathematical models presented in section II.8. Numerical solutions of the initial value problems describing fluid-solid interaction are computed using space-time finite element model. For an increment of time (Δt) the space-time strip is discretized using nine node p-version space-time elements (Fig. 11). The space-time local approximations are considered in higher order spaces $H^{k,p}(\bar{\Omega}^e_{xt})$, which permits higher order global differentiability in space and time. The space-time finite element processes are based on minimization of residuals resulting from the partial differential equations over the discretization for the space-time strip. Surana et. al. [10–12, 41–44] have shown that these processes result in unconditionally stable algebraic systems when the resulting non-linear algebraic equations are solved using Newton's linear method (or the Newton-Raphson method). This approach is used in the work presented here. Time evolution is computed by time marching using the computed solution for the current space-time strip to determine initial condition(s) for the next space-time strip corresponding to the next increment of time. Fig. 11 shows a schematic of the domain used for a single material wave propagation as well as a domain containing two materials (M1 and M2) with a bi-material interface at $x = L$. In both cases, the rigid end ($x = L$ or $x = 2L$) is subjected to a velocity pulse of $2\Delta t$ duration with maximum amplitude of v_{max} or $\bar{v}_{max}$. In numerical studies we choose different values of v_{max} or $\bar{v}_{max}$. A uniform discretization of ten space-time elements is shown in Fig. 11(d). Fig. 11(e) shows a non-uniform discretization of 25 elements used for bi-material studies.

We note that the mathematical models in section II.8.1 for the solid matter are a system of first-order partial differential equation (PDEs) in displacement u, velocity v and stress ${}_d\sigma_{xx}$. For viscoelastic fluids, the Maxwell model and the Giesekus model (section II.8.1 (A) and (C)) are also a system of first order PDEs in velocity $\bar{v}$ and deviatoric contravariant axial Cauchy stress ${}_d\bar{\sigma}^{(0)}_{xx}$. $\partial\bar{p}/\partial\bar{x}$ in these models is known pressure gradient driving the flow. Since the studies considered here involve wave propagation in stationary medium, $\partial\bar{p}/\partial\bar{x} = 0$ for all three viscoelastic liquids considered here. The Oldroyd-B model contains $\partial^2\bar{v}/\partial\bar{x}^2$ and $\partial^2\bar{v}/\partial t\partial\bar{x}$ terms in the constitutive equation for the deviatoric contravariant axial Cauchy stress ${}_d\bar{\sigma}^{(0)}_{xx}$.

Choice of approximation spaces:

Since the mathematical models for solids, Maxwell fluid, and Giesekus fluid are a system of first-order PDEs, we can choose approximation space of order 2 for all dependent variables, that is, $H^{k,p}(\bar{\Omega}^e_{xt})$; $k = (k_1 k_2) = (2, 2)$ for all dependent variables, where k_1 and k_2 are orders of the spaces in space and time giving rise to local space-time approximations of class C^1 in space and time. For this choice of k_1 and k_2, the space-time integrals over the space-time discretization ($\bar{\Omega}^T_{xt} = \cup_e \bar{\Omega}^e_{xt}$ of the space-time strip $\bar{\Omega}_{xt}$ in which $\bar{\Omega}^e_{xt}$ is a space-time element) are Riemann in the space-time finite element processes based on space-time least-squares residual functional I. When computed, I approaches zero (generally $O(10^{-8})$ or smaller), then the GDEs are satisfied in the pointwise sense (numerically) by the computed solution. Thus, such computed solutions truly have all the features of the theoretical

solution based on the orders of the derivatives in the GDEs in the mathematical model. This aspect of the computed solution is important in establishing validity and the accuracy of the solutions of the model problems for which theoretical solutions are not obtainable. In summary, when local approximations are of class C^1 in space and time and when residual functional I approaches zero, the computed solutions for solid medium, Maxwell fluid, and Giesekus fluid are virtually the same as the theoretical solutions. This indeed is the case in the numerical studies presented here. In case of Oldroyd-B fluid, the constitutive equations contain up to the second derivatives of velocity $\bar{v}$; hence, for this mathematical model, local approximations of class C^1 in space and time would yield space-time integrals over space-time discretizations in the Lebesgue sense. For this fluid, local approximations of class C^2 in space and time are needed to ensure Riemann integrals over the space-time discretization. Numerical studies for this fluid were performed using local approximations of class C^2 as well as C^1 in space and time. Comparisons of the residuals, computed solutions, their derivatives and the inter-element jumps in the derivatives confirm that between p-level of 9-11 in space and time, the solutions of class C^1 in space and time are converged (weakly) to the solutions of class C^2 in space and time. Thus, for the Oldroyd-B fluid also, it suffices to use local approximations of class C^1 in space and time but at p-levels of 9-11 in space and time. Hence, for all solids and fluids considered here, we can use local approximations of class C^1 in space and time at p-level of 11 in space and time with assurance that the computed solutions indeed are the true solutions of the PDEs in all cases. The I values are of the order of $O(10^{-8})$ or lower in all cases.

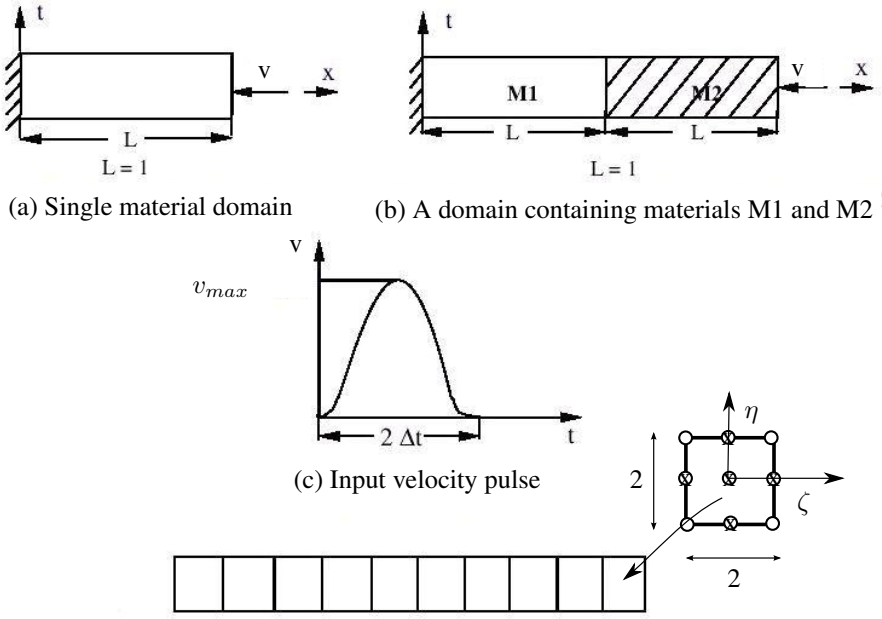

(a) Single material domain

(b) A domain containing materials M1 and M2

(c) Input velocity pulse

(d) 10 element uniform discritization for a single material domain

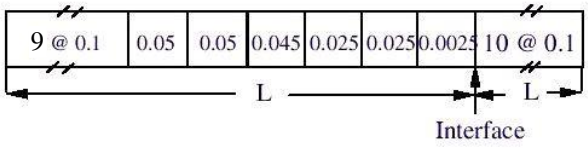

(e) 25 element non-uniform discretization for a domain consisting of material M1 and M2 (figure(b))

Figure 11: Model problem 1: schematic, applied disturbance and discretization

II.9.2 Material coefficients

In all numerical studies we choose the following material coefficients.

Hyper-elastic solid (S1):

$\hat{E} = 2.0 \times 10^{11} Pa\ \hat{\rho} = 7896\ kg/m^3$

Softer hyper-elastic solid (S2):

$\hat{E} = 4 \times 10^{2} Pa\ \hat{\rho} = 2170\ kg/m^3$

Maxwell fluid (F1) [72]:

$\hat{\rho} = 868\ kg/m^3,\ \lambda_1 = 0.1\ s,\ \hat{\eta_s} = 2.7 Pa \cdot s\ \hat{\eta_p} = 0.3 Pa \cdot s$

Oldroyd-B fluid (F2) [72]:

$\hat{\rho} = 868\ kg/m^3,\ \lambda_1 = 0.1\ s,\ \hat{\eta_s} = 2.7 Pa \cdot s\ \hat{\eta_p} = 0.3 Pa \cdot s\ \lambda_2 = 0.001\ s$

Giesekus fluid (F3) (PIB/C14) [73]:

$\hat{\rho} = 800\ kg/m^3,\ \lambda = 0.06\ s,\ \hat{\eta_s} = 0.002 Pa \cdot s\ \hat{\eta_p} = 1.424 Pa \cdot s\ \alpha = 0.15$

II.9.3 Wave propagation in a single material

In this section we present numerical studies for wave propagation in a single material to demonstrate that regardless of the type of description and material accurate numerical simulations of the evolution of wave propagation is possible. We consider elastic solid, softer elastic solid, Maxwell fluid, Oldroyd-B fluid and Giesekus fluid. These simulations are essential to demonstrate that the wave propagation in each one of these media can be simulated accurately. In the numerical computations, the space-time residual I for each space-time strip of the order of $O(10^{-8})$ or lower confirms (section II.9.1) that the computed solutions in fact are the true solutions of the PDEs in the mathematical models. This aspect is important to demonstrate for each media so that if there is a failure in simulating interaction between fluid and solid media, this failure cannot be attributed to failure of the wave propagation in individual media, but instead must be a consequence of the inadequate simulation of the interaction physics at the interface between the fluid and solid. It is for this reason that all wave propagation studies in single media are important to retain in this section. In all simulations, a uniform mesh of 10 elements with $p = 11$ in space and time, and solutions of class C^1 in space and time are used. Reference values used for the solids and fluids in the computations of evolutions are as follows.

Elastic solid (S1):

$\rho_0 = 7896\ kg/m^3,\ L_0 = 0.02\ m\ \ v_0 = 500\ m/s\ E_0 = 2.0 \times 10^{11}\ Pa\ \tau_0 = \rho_0 {v_0}^2 = 1.974 \times 10^9\ Pa$

Softer elastic solid (S2):

$\rho_0 = 868\ kg/m^3,\ L_0 = 0.02\ m\ \ v_0 = 0.05\ m/s\ E_0 = 4.0 \times 10^2\ Pa\ \tau_0 = \rho_0 {v_0}^2 = 2.17 Pa$

Maxwell fluid (F1):

$\rho_0 = 868\ kg/m^3,\ L_0 = 0.02\ m\ \ v_0 = 0.05\ m/s,\ \mu_0 = 3.0 Pa \cdot s\ ,\ p_0 = \tau_0 = \rho_0 {v_0}^2 = 2.17\ Pa$

Oldroyd-B fluid (F2):

$\rho_0 = 868\ kg/m^3,\ L_0 = 0.02\ m\ \ v_0 = 0.05\ m/s,\ \mu_0 = 3.0Pa \cdot s\ ,\ p_0 = \tau_0 = \rho_0 {v_0}^2 = 2.17\ Pa$

Giesekus fluid (F3):

$\rho_0 = 800\ kg/m^3,\ L_0 = 0.02\ m\ \ v_0 = 0.05\ m/s,\ \mu_0 = 1.426Pa \cdot s\ ,\ p_0 = \tau_0 = \rho_0 {v_0}^2 = 2.0\ Pa$

For the nonlinear initial value problems considered here, Newton's linear method with line search (see Surana et.al. [10–12, 41–44]) is used; solution is assumed to be converged when the absolute value of each component of the variation of residuals for the space-time strip is less than 10^{-6}. In all numerical studies in this section we chose v_{max} or $\bar{v}_{max}$ of 0.001. This choice yields displacement u (in case of hyper-elastic solid) of the order of $O(10^{-5})$, well within the range of infinitesimal deformation. In all computations, $\Delta t = 0.01$ is used. For figures 12-18 the blue color represents the evolution of incident wave and the red color represents the reflected wave. Figures 12-13 show evolutions of axial velocity, the deviatoric stress and displacement as a function of x for hyper-elastic solid.

We note that in the case of hyper and hypo-elastic solids (figures 12-14) there is no mechanism of dissipation; hence the amplitude and base of the velocity and stress waves do not change during evolution. Upon reflection the reflected positive velocity and negative stress is observed (as expected). Evolutions are smooth i.e. oscillation free. Residual values of the order of $O(10^{-8})$ or lower are obtained in all cases confirming that GDEs are satisfied accurately in the pointwise sense, hence the computed solutions are in fact true solutions of the GDEs in the mathematical models. In the case of Maxwell fluid we observe amplitude decay during evolution due to viscous dissipation but no significant base elongation, otherwise the behavior is similar to the solids. In the Oldroyd-B fluid significant base elongation and amplitude decay both are present. Base elongation in the model is due to dependence of the deviatoric Cauchy stress on $\boldsymbol{\gamma}_{(2)}$, second convected time derivative of the strain tensor. In this model amplitude decay is much more pronounced than Maxwell model. The Giesekus model (Fig. 18) also shows amplitude decay and base elongation. In this case the amplitude decay is more than the Maxwell model but not as pronounced as in the case of the Oldroyd-B model. Base elongation is also not as pronounced as in the case of the Oldroyd-B model. The wave propagation results for polymeric liquids confirm accurate and realistic simulations of the evolution using the mathematical models presented in earlier sections. These are important to confirm before we undertake fluid-solid interaction evolution studies using these mathematical models.

Similar graphs for softer hyper-elastic solids are shown in figures 14 and 15. Graphs of the evolutions of velocity $\bar{v}$ and the deviatoric Cauchy stress ${}_d\bar{\sigma}^{(0)}_{xx}$, for the Maxwell, Oldroyd-B and Giesekus fluid are shown in figures 16-18. From the results presented in figures 12-18 for wave propagation in a single medium we observe: (i) the wave propagation and its reflection from the impermeable left boundary are simulated without any difficulty (ii) the evolutions are smooth, that is, free of oscillations (iii) the evolution of the wave propagation is significantly different for each media, i.e. the speed of wave propagation, the reflection phenomena and the propagation of reflected waves. In case of solid media, the wave amplitude and its support do not change during evolutions as the media are considered non-dissipative.

Additionally, these results also confirm that the computational process used in practically free of numerical dispersion. In case of Maxwell, Oldroyd-B and Giesekus fluids we note: (a) Due to dissipative mechanism, the peak value of the wave progressively diminishes and its support elongates during evolution. (b) The evolution of the wave propagation is significantly different in the three fluids considered. (c) In all cases, the residual functional I of the order of $O(10^{-8})$ or lower confirms good accuracy of the computed solution. We reemphasize that these results for 1D wave propagation in single media and demonstration of their accuracy is essential in ensuring that any failures in fluid-solid interaction wave propagation cannot possibly be attributed to the failures of wave propagation in individual media.

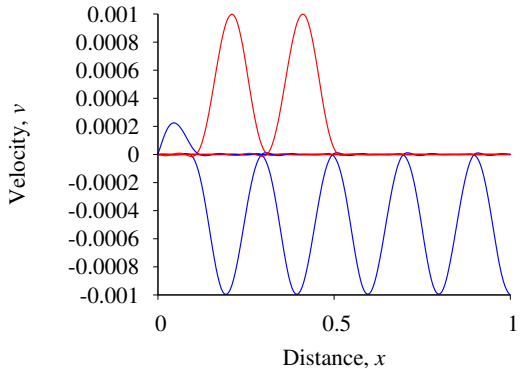

(a) Velocity v versus Distance x

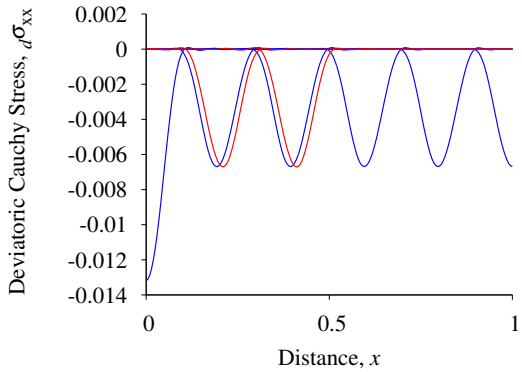

(b) Stress ${}_d\sigma_{xx}$ versus Distance x

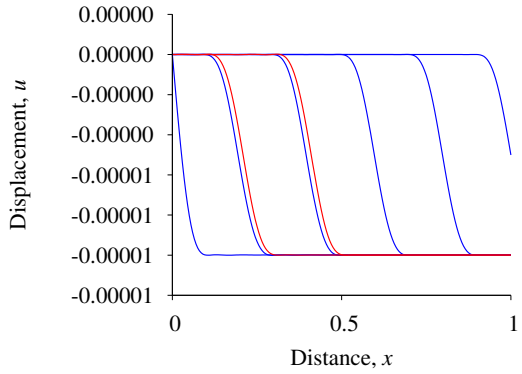

(c) Displacement u versus Distance x

Figure 12: Wave Propagation in Hyper-elastic solid: $v_{max} = 0.001$

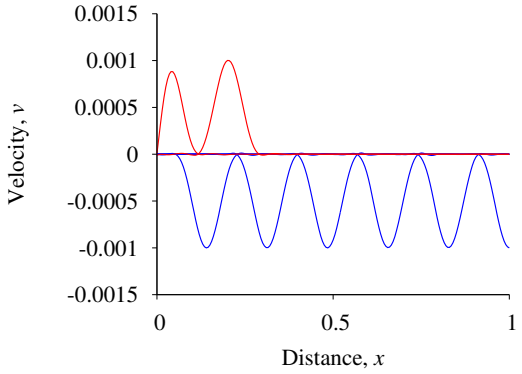

(a) Velocity v versus Distance x

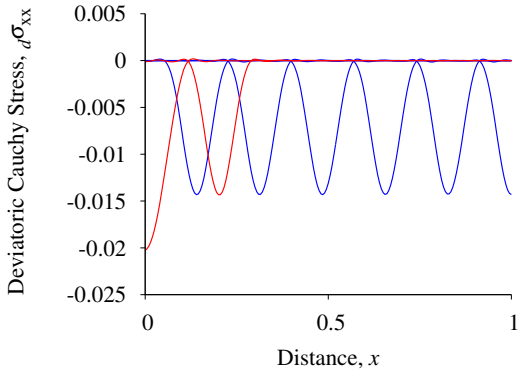

(b) Stress ${}_d\sigma_{xx}$ versus Distance x

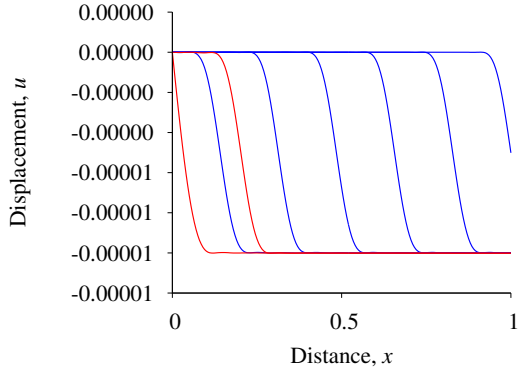

(c) Displacement u versus Distance x

Figure 13: Wave Propagation in Softer hyper-elastic solid: $v_{max} = 0.001$

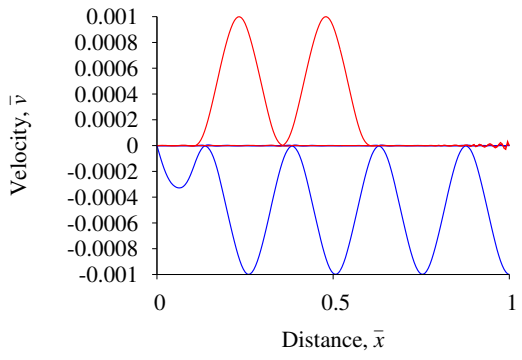

(a) Velocity $\bar{v}$ versus Distance $\bar{x}$

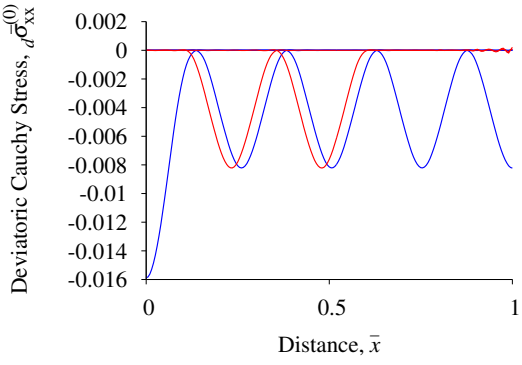

(b) Stress ${}_d\bar{\sigma}^{0}_{xx}$ versus Distance $\bar{x}$

Figure 14: Wave Propagation in hypo-elastic solid: $\bar{v}_{max} = 0.001$

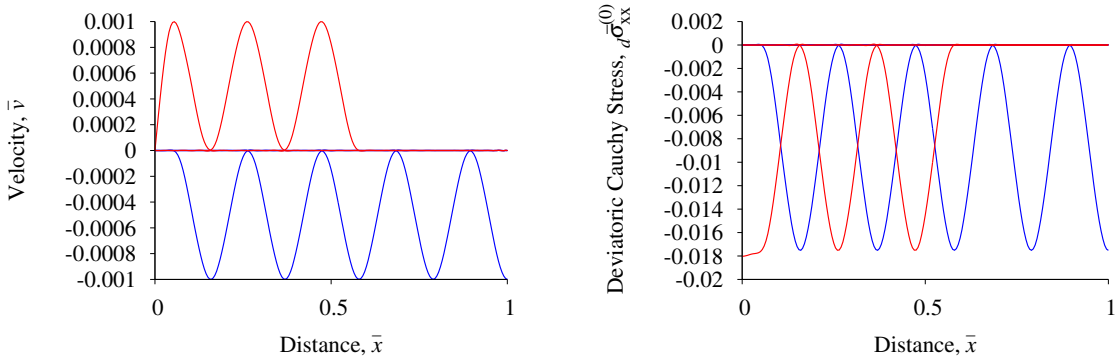

(a) Velocity $\bar{v}$ versus Distance $\bar{x}$ (b) Stress ${}_d\bar{\sigma}^0_{xx}$ versus Distance $\bar{x}$

Figure 15: Wave Propagation in Softer hypo-elastic solid: $\bar{v}_{max} = 0.001$

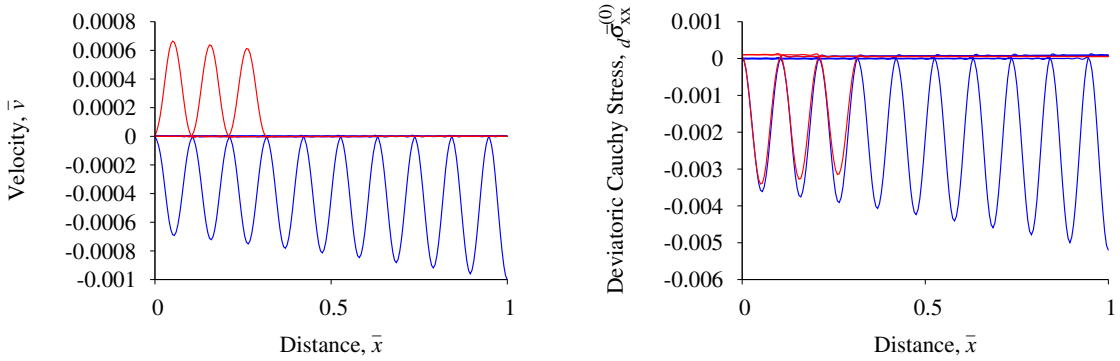

(a) Velocity $\bar{v}$ versus Distance $\bar{x}$ (b) Stress ${}_d\bar{\sigma}^0_{xx}$ versus Distance $\bar{x}$

Figure 16: Wave Propagation in Maxwell fluid: $\bar{v}_{max} = 0.001$

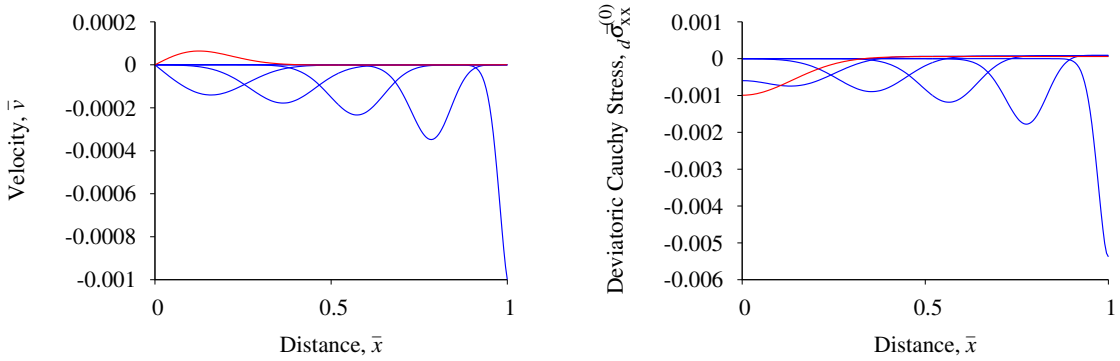

(a) Velocity $\bar{v}$ versus Distance $\bar{x}$ (b) Stress ${}_d\bar{\sigma}^0_{xx}$ versus Distance $\bar{x}$

Figure 17: Wave Propagation in Oldroyd-B fluid: $\bar{v}_{max} = 0.001$

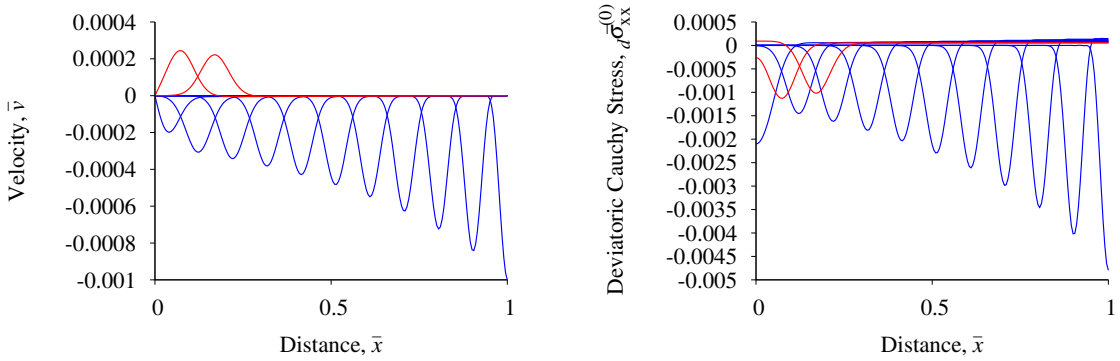

(a) Velocity $\bar{v}$ versus Distance $\bar{x}$

(b) Stress ${}_d\bar{\sigma}^0_{xx}$ versus Distance $\bar{x}$

Figure 18: Wave Propagation in the Giesekus Fluid: $\bar{v}_{max} = 0.001$

II.9.4 Wave propagation with bi-material interface using hyper-elastic solids and polymeric liquids

In this section we present fluid-solid interaction studies in which the solid is always hyper-elastic i.e. the mathematical model for the solid is in the Lagrangian description and the mathematical model for the polymeric liquid is in the Eulerian description with transport. We first give some details of reference quantities used in the numerical studies. Referring to Fig. 11 we choose M1 as a polymeric fluid and M2 to be hyper-elastic solid. The reference quantities for various combinations of M1 and M2 are listed in the following:

M1 - Maxwell fluid (F1) ; M2 - Hyper-elastic solid (S1):

$$\rho_0 = 7896\ kg/m^3,\ L_0 = 0.02\ m,\ v_0 = 500\ m/s,\ E_0 = 2 \times 10^{11}\ Pa,\ p_0 = \tau_0 = \rho_0 {v_0}^2 = 1.974 \times 10^9\ Pa$$

M1 - Oldroyd-B fluid (F2) ; M2 - Hyper-elastic solid (S1):

$$\rho_0 = 7896\ kg/m^3,\ L_0 = 0.02\ m,\ v_0 = 500\ m/s,\ E_0 = 2 \times 10^{11}\ Pa,\ p_0 = \tau_0 = \rho_0 {v_0}^2 = 1.974 \times 10^9\ Pa$$

M1 - Giesekus fluid (F3) ; M2 - Hyper-elastic solid (S1):

$$\rho_0 = 7896\ kg/m^3,\ L_0 = 0.02\ m,\ v_0 = 500\ m/s,\ E_0 = 2 \times 10^{11}\ Pa,\ p_0 = \tau_0 = \rho_0 {v_0}^2 = 1.974 \times 10^9\ Pa$$

For all numerical studies in this section we consider a non-uniform mesh of 25 nine node p-version elements for M1 and M2 with a p-level of 11 in space and time (Fig. 11(e)). We consider solutions of class C^1 in space and time we consider $\Delta t = 0.01$ for the entire evolution.

In this case, the mathematical model for solid is in Lagrangian description and for fluid in the Eulerian description with transport, same as in ALE and the deformation of the interface is infinitesimal, hence there is no need for moving mesh. Figures 19-21 show evolutions of axial velocity, axial stress and displacement when M1 is the Maxwell, Oldroyd-B and Giesekus fluid respectively and M2 is hyper-elastic solid (S1). In this particular case we note that the solid is a much stiffer material compared to the polymers, hence at the interface ($x = 1.0$) the polymer offer no resistance to the solid, hence at the solid-fluid interface the solid boundary behaves like a free boundary. This is confirmed by the reflected velocity wave being the same as the incident velocity wave while the reflected stress wave is tensile. For this case due to very high stiffness of the solid region the combined problem behaves as if the fluid is non existent, hence in this case it is difficult to judge the interaction of the solid model in Lagrangian description and the fluid model in the Eulerian description.

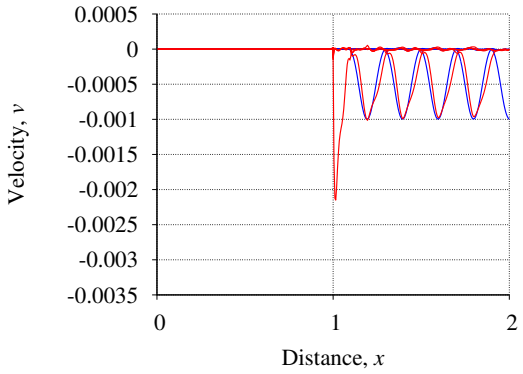

(a) Velocity v versus Distance x

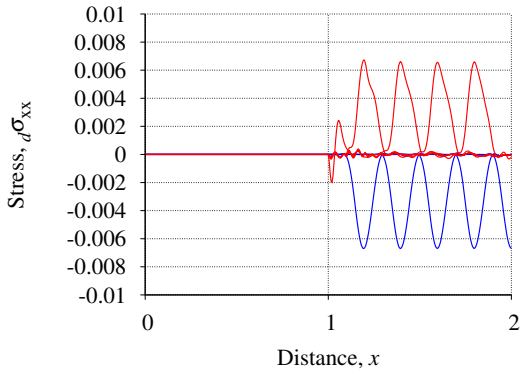

(b) Stress ${}_d\sigma_{xx}$ versus the distance x

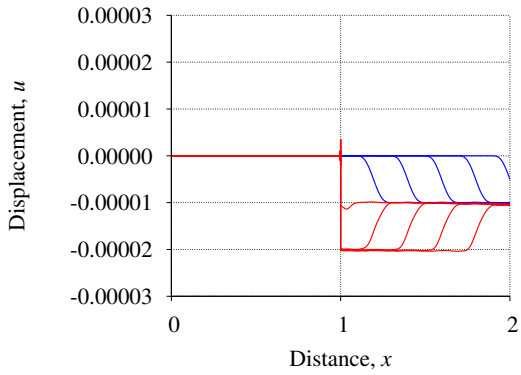

(c) Displacement u versus Distance x

Figure 19: Maxwell fluid (M1) - Hyper-elastic solid (M2): $v_{max} = 0.001$

Next, we consider interaction of polymeric liquids (M1) with softer hyper-elastic solid S2 (M2). In this case the stiffnesses of M1 and M2 are approximately in the same range. We should be able to see more clearly the influence of the fluid-solid interaction during evolution. We continue to use v_{max} or $\bar{v}_{max}$ of 0.001 which will keep the motion of the fluid solid interface in the infinitesimal range. With infinitesimal deformation of the fluid-solid interface our computed results should be exactly the same as those from ALE description due to the fact that no movement of the mesh(es) is needed due to the infinitesimal movement of the interface. Reference values are given in the following:

M1 - Maxwell fluid (F1) ; M2 - Softer hyper-elastic solid (S2):

$\rho_0 = 868\ kg/m^3,\ L_0 = 0.02\ m\ \ v_0 = 0.05\ m/s,\ \mu_0 = 3.0Pa \cdot s\ ,\ E_0 = 400\ Pa\ p_0 = \tau_0 = \rho_0 {v_0}^2 = 2.17\ Pa$

M1 - Oldroyd-B fluid (F2) ; M2 - Softer hyper-elastic solid (S2):

$\rho_0 = 868\ kg/m^3,\ L_0 = 0.02\ m\ \ v_0 = 0.05\ m/s,\ \mu_0 = 3.0Pa \cdot s\ ,\ E_0 = 400\ Pa\ p_0 = \tau_0 = \rho_0 {v_0}^2 = 2.17\ Pa$

M1 - Giesekus fluid (F3); M2 - Softer hyper-elastic solid (S2):

$\rho_0 = 868\ kg/m^3,\ L_0 = 0.02\ m\ \ v_0 = 0.05\ m/s,\ \mu_0 = 3.0Pa \cdot s\ ,\ E_0 = 400\ Pa\ p_0 = \tau_0 = \rho_0 {v_0}^2 = 2.17\ Pa$

Evolutions are compiled using 25 element non-uniform discretization for M1 and M2 with p-level of 11 in space and time. Local approximations of class C^1 in space and time are considered. Convergence tolerance for Newton's linear method is $O(10^{-6})$. In figures 22-31 the blue color represents incident waves and the red color represents reflected and transmitted waves. Evolution for axial velocity and axial stress of Maxwell fluid (M1) and softer hyper-elastic solid (M2) interaction are shown in in Fig. 22. Fig. 22(a) shows evolution of velocity for the first 15 time steps that consist of 12 time steps for the incident wave and 13-15 time steps related to the interaction of the wave at the interface located at $x = 1.0$. Fig. 22(a)-(e) show the first 12 time steps and time steps 13, 15, 17 and 19 respectively. We clearly observe that transmission, reflection and subsequent propagation of the velocity wave becomes progressively spurious with further evolution. Similar graphs for the evolution of axial deviatoric stress shown in figures 23(a)-(e) confirm the same observations as in the case of axial velocity in Fig. 22(a)-(e).

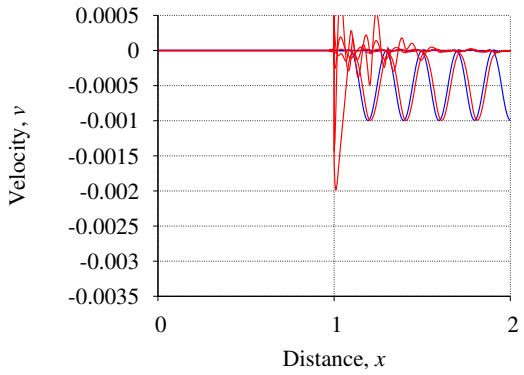

(a) Velocity v versus Distance x

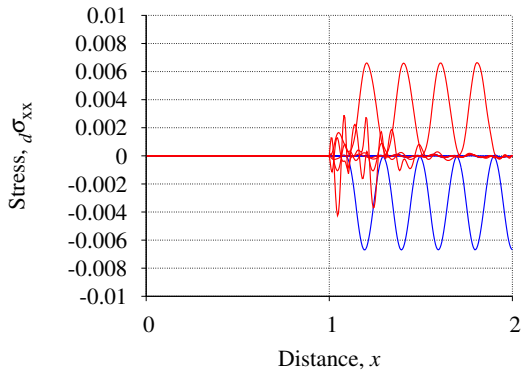

(b) Stress ${}_d\sigma_{xx}$ versus the distance x

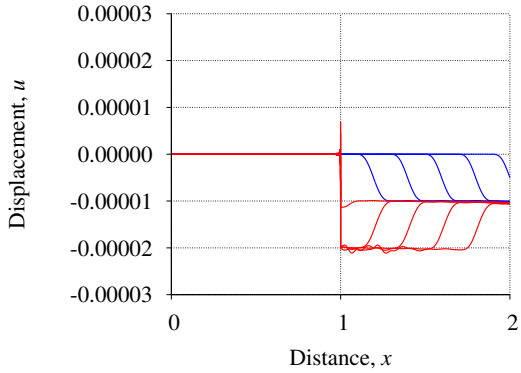

(c) Displacement u versus Distance x

Figure 20: Oldroyd-B fluid (M1) - Hyper-elastic solid (M2): $v_{max} = 0.001$

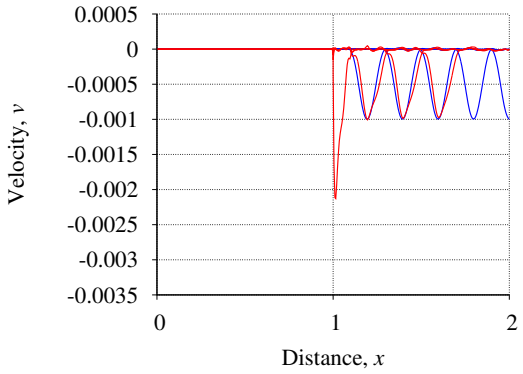

(a) Velocity v versus Distance x

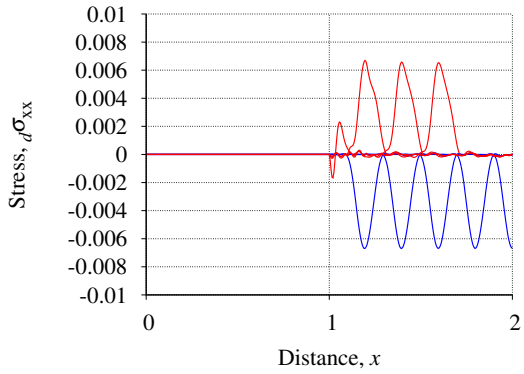

(b) Stress ${}_d\sigma_{xx}$ versus the distance x

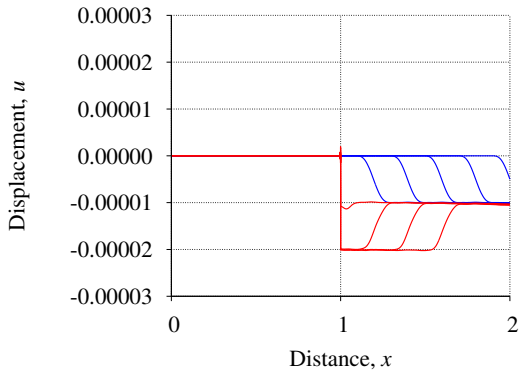

(c) Displacement u versus Distance x

Figure 21: Giesekus Fluid (M1) - Hyper-elastic solid (M2): $v_{max} = 0.001$

Similar graphs for axial velocity and axial stress for interaction of Oldroyd-B fluid (M1) and softer hyper-elastic solid (M2) are shown in figures 24(a)-(e) and 25(a)-(e). In this study, the evolution at the interface and in its neighborhood is not as oscillatory and spurious as in the case of Maxwell fluid and softer solid S2 but the spurious nature of reflected waves is quite apparent. In these studies $\bar{v}_{max}$ of 0.001 was used. Similar studies when performed using $\bar{v}_{max}$ of 0.1 produced quite spurious results as shown in Fig. 26(a)-(e) and 27(a)-(e). Interaction results for axial velocity and axial stress for Giesekus fluid (M1) and softer hyper-elastic solid (M2) for $\bar{v}_{max}$ of 0.001 are shown in figures 28(a)-(e) and 29(a)-(e). At a quick glance they may appear some what convincing but their spurious nature is quite obvious due to attenuating peaks of the reflected stress wave shown in Fig. 29(a). Evolutions of axial velocity and axial stress for $\bar{v}_{max}$ of 1.0 in figures 30(a)-(e) and 31(a)-(e) show complete breakdown of the interaction between M1 and M2 resulting in spurious evolution. We note that in all cases the computed evolution becomes spurious after the incidental wave reaches the fluid-solid interface. This holds regardless of the magnitude of $\bar{v}_{max}$, indicating the lack of correct physics at the interface in these mathematical models.

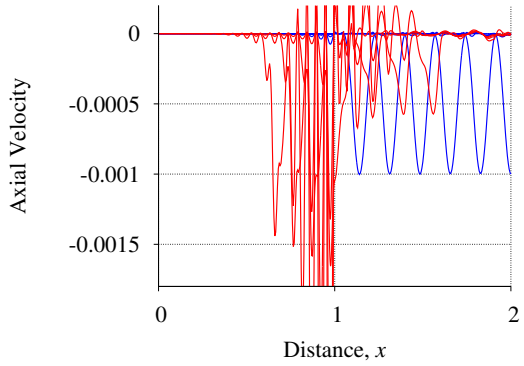

(a) Entire Evolution

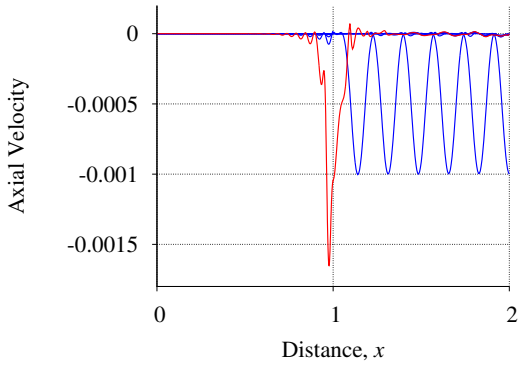

(b) Time Step 13

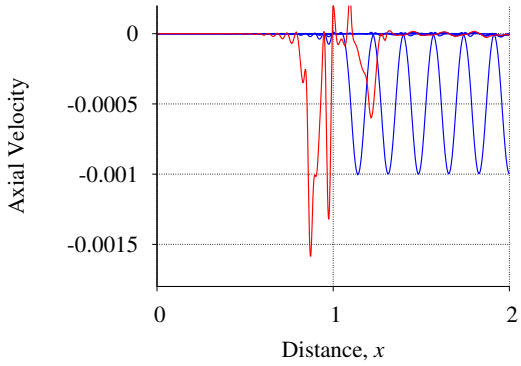

(c) Time Step 15

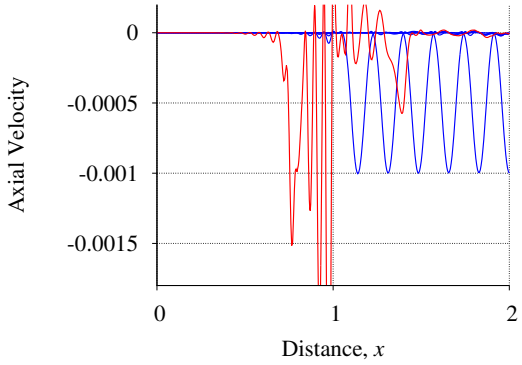

(d) Time Step 17

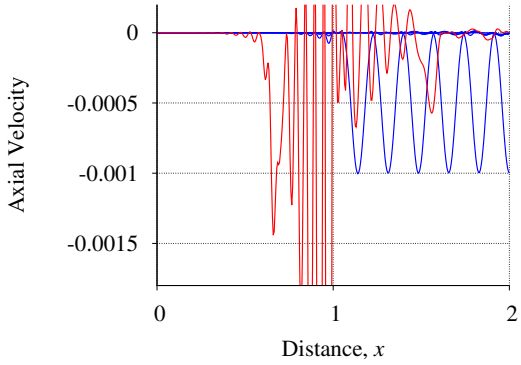

(e) Time Step 19

Figure 22: Maxwell fluid (M1) - Softer hyper-elastic solid (M2): $v_{max} = 0.001$; Evolution of the velocity

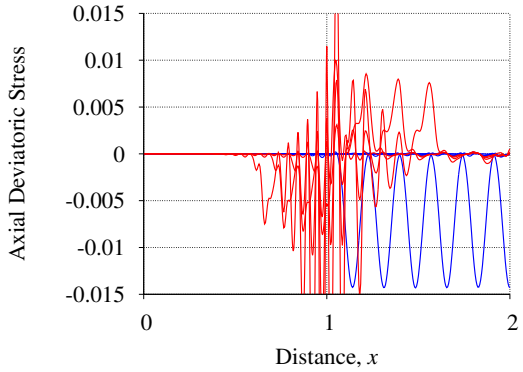

(a) Entire Evolution

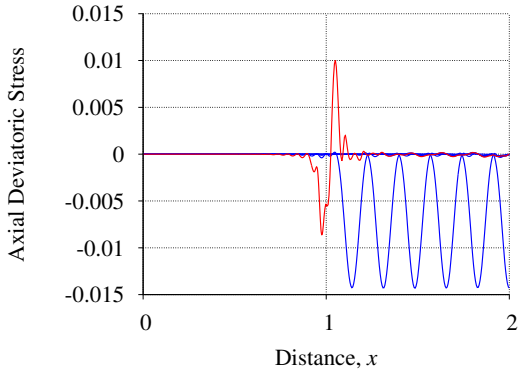

(b) Time Step 13

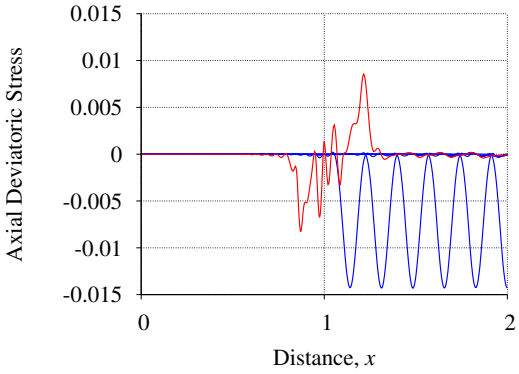

(c) Time Step 15

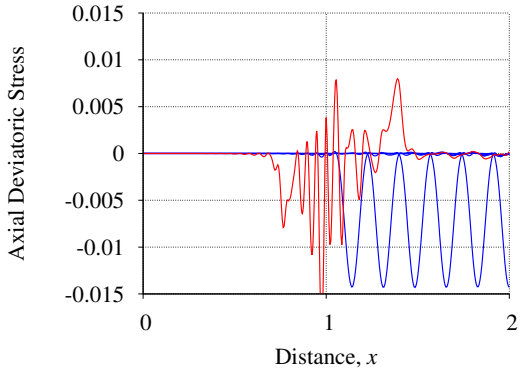

(d) Time Step 17

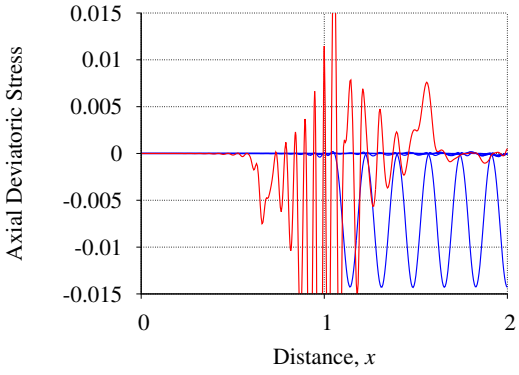

(e) Time Step 19

Figure 23: Maxwell fluid (M1) - Softer hyper-elastic solid (M2): $v_{max} = 0.001$; Evolution of the stress

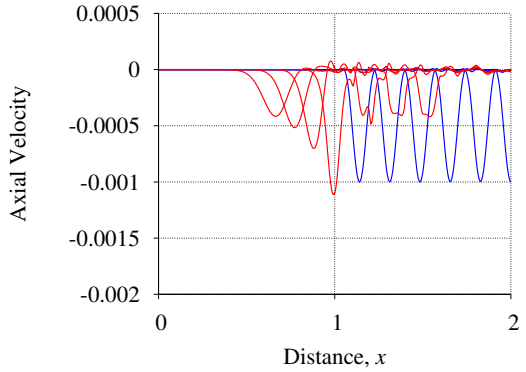

(a) Entire Evolution

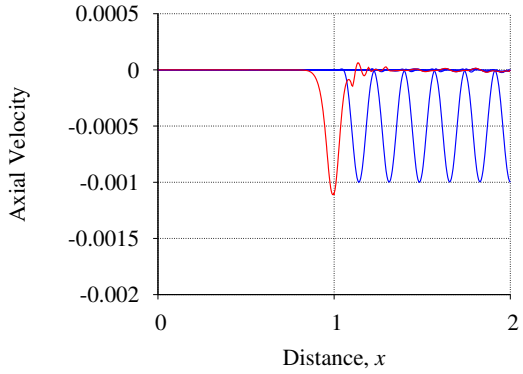

(b) Time Step 13

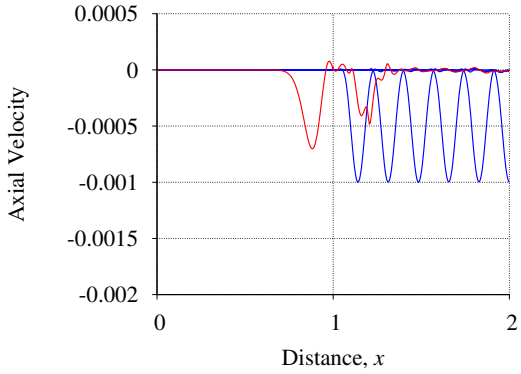

(c) Time Step 15

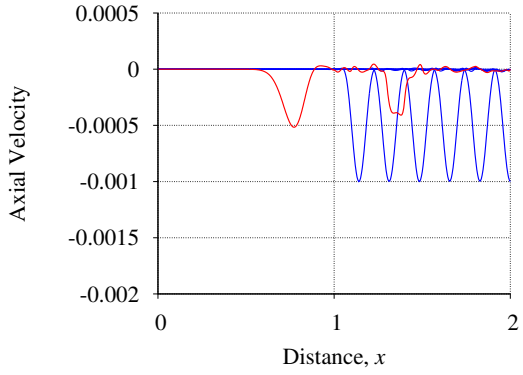

(d) Time Step 17

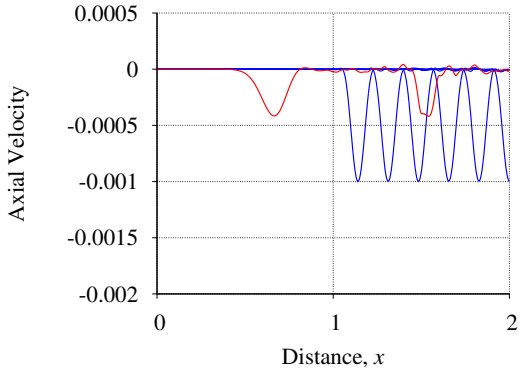

(e) Time Step 19

Figure 24: Oldroyd-B fluid (M1) - Softer hyper-elastic solid (M2): $v_{max} = 0.001$; Evolution of the velocity

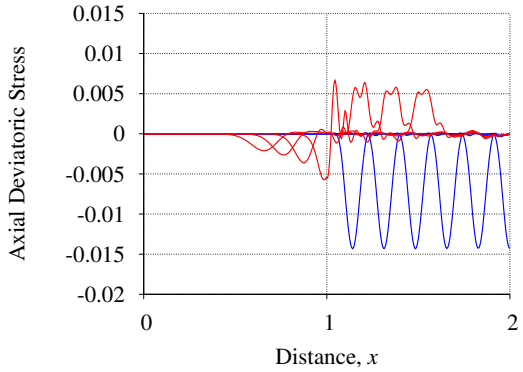

(a) Entire Evolution

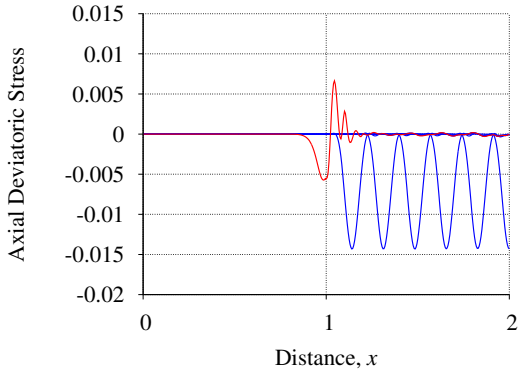

(b) Time Step 13

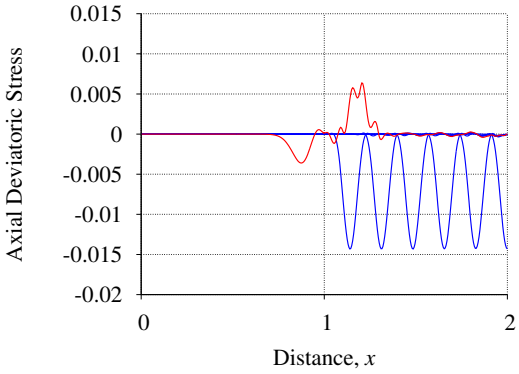

(c) Time Step 15

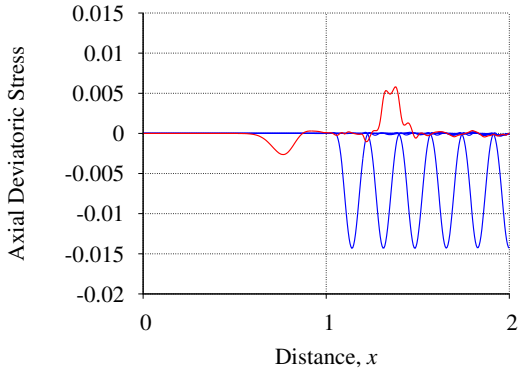

(d) Time Step 17

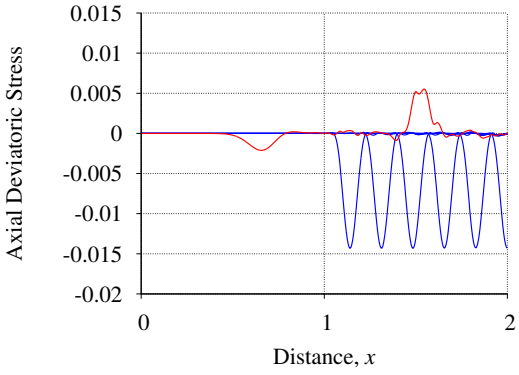

(e) Time Step 19

Figure 25: Oldroyd-B fluid (M1) - Softer hyper-elastic solid (M2): $v_{max} = 0.001$; Evolution of the stress

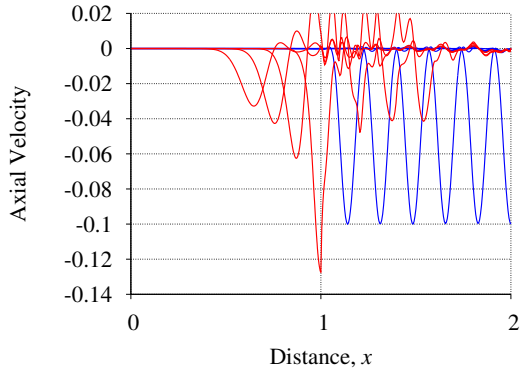

(a) Entire Evolution

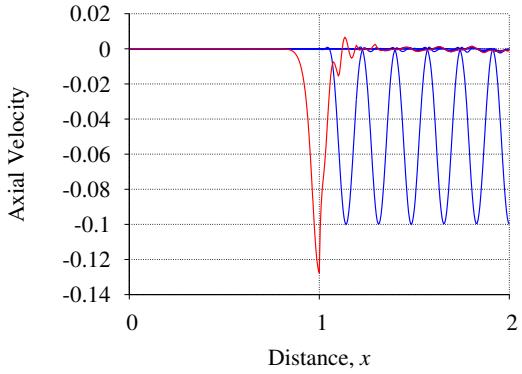

(b) Time Step 13

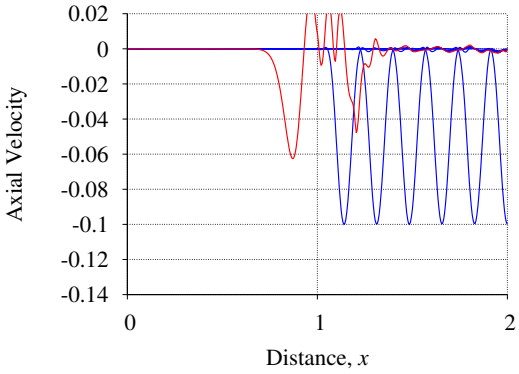

(c) Time Step 15

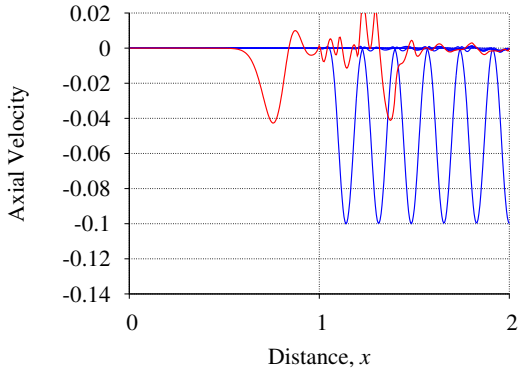

(d) Time Step 17

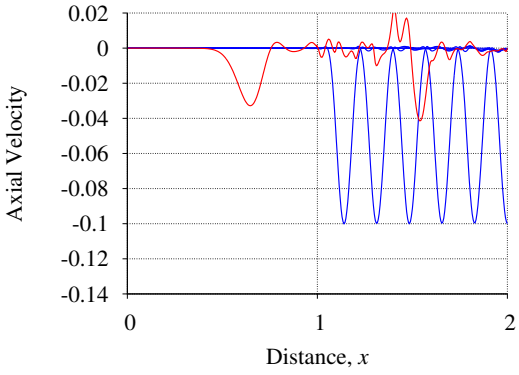

(e) Time Step 19

Figure 26: Oldroyd-B fluid (M1) - Softer hyper-elastic solid (M2): $v_{max} = 0.1$; Evolution of the velocity

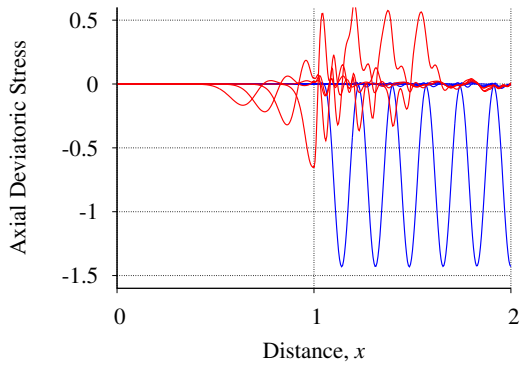

(a) Entire Evolution

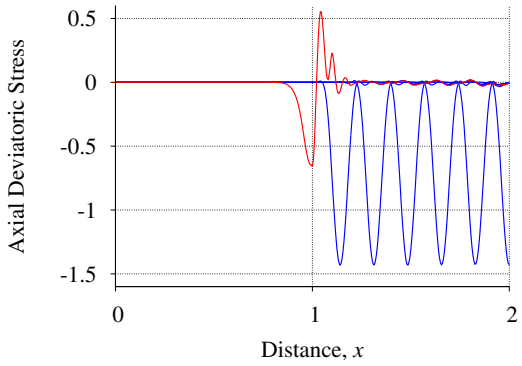

(b) Time Step 13

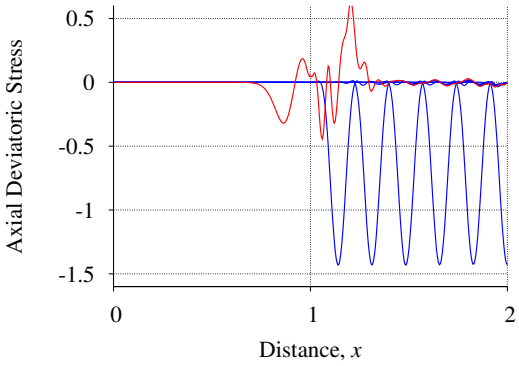

(c) Time Step 15

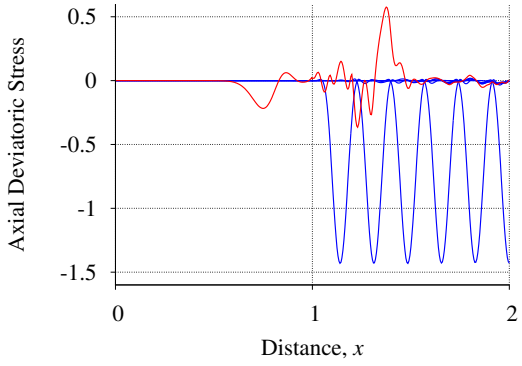

(d) Time Step 17

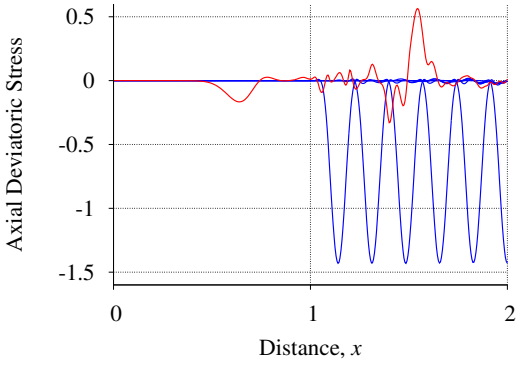

(e) Time Step 19

Figure 27: Oldroyd-B fluid (M1) - Softer hyper-elastic solid (M2): $v_{max} = 0.1$; Evolution of the stress

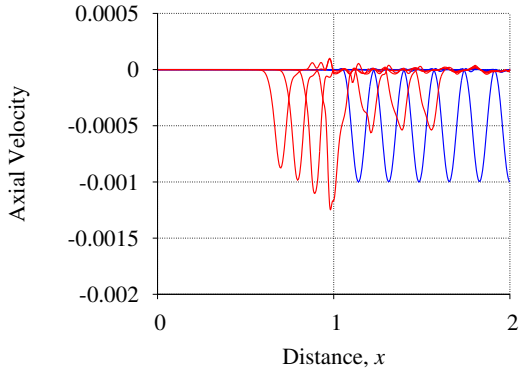

(a) Entire Evolution

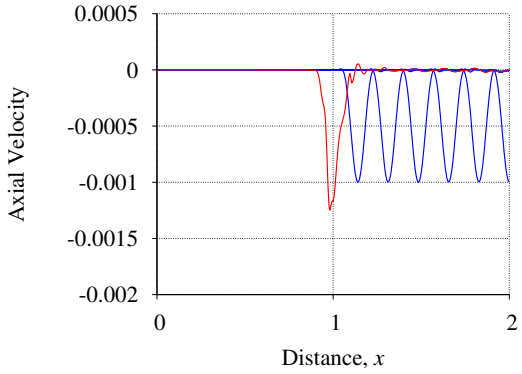

(b) Time Step 13

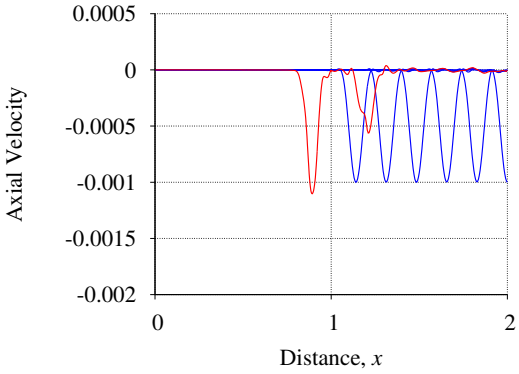

(c) Time Step 15

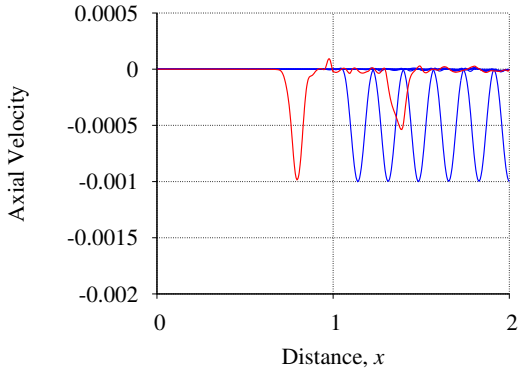

(d) Time Step 17

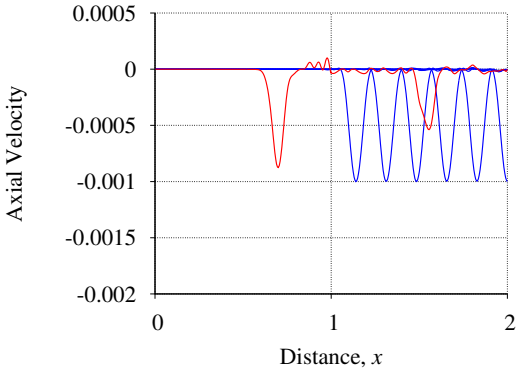

(e) Time Step 19

Figure 28: Giesekus Fluid (M1) - Softer hyper-elastic solid (M2): $v_{max} = 0.001$; Evolution of the velocity

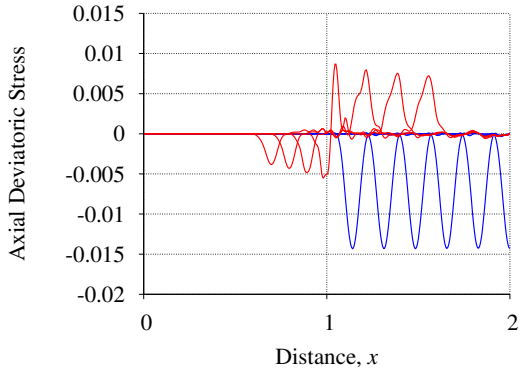

(a) Entire Evolution

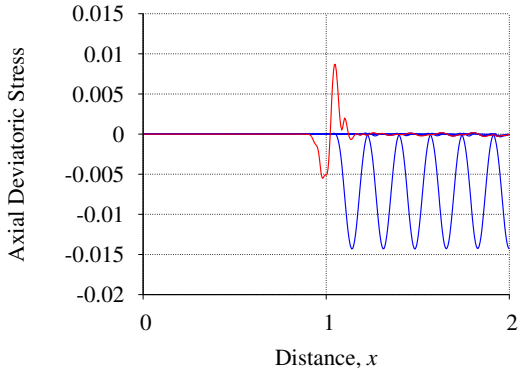

(b) Time Step 13

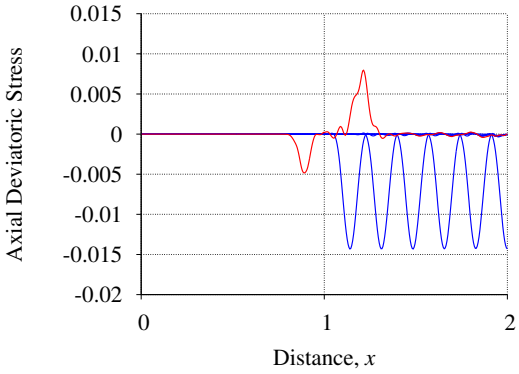

(c) Time Step 15

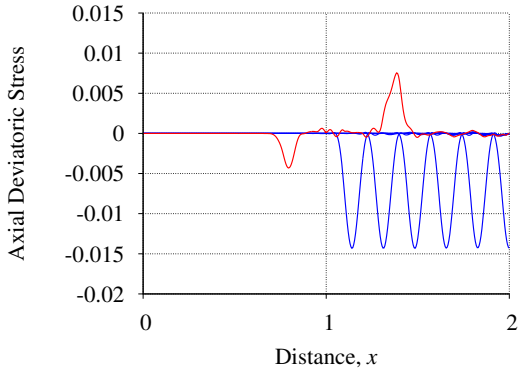

(d) Time Step 17

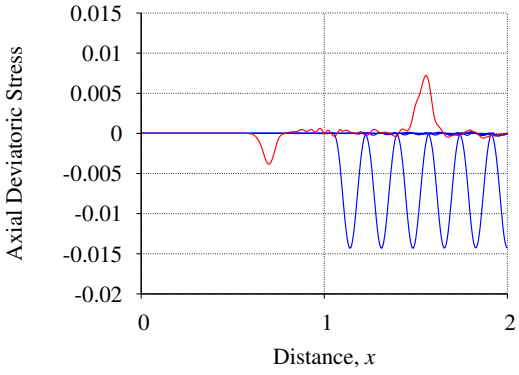

(e) Time Step 19

Figure 29: Giesekus Fluid (M1) - Softer hyper-elastic solid (M2): $v_{max} = 0.001$; Evolution of the stress

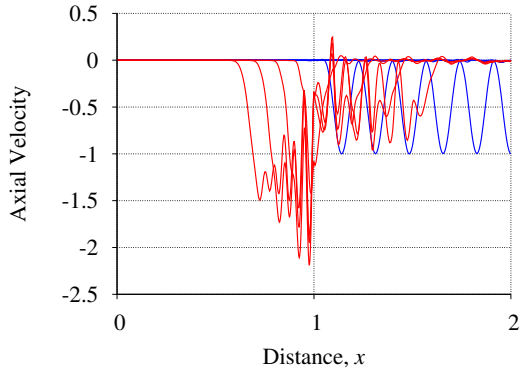

(a) Entire Evolution

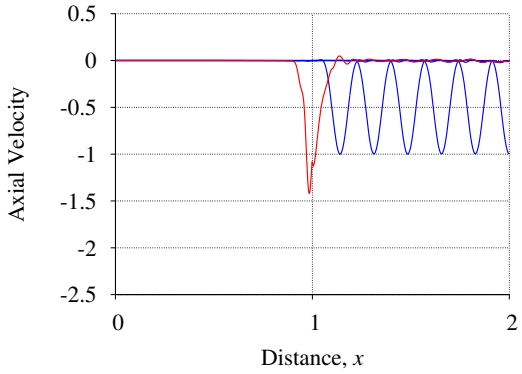

(b) Time Step 13

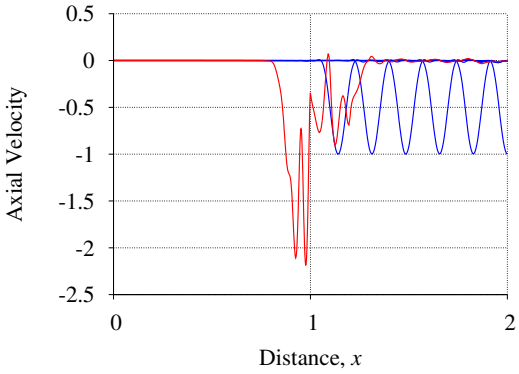

(c) Time Step 15

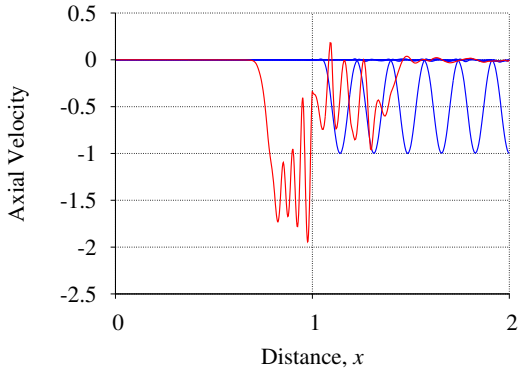

(d) Time Step 17

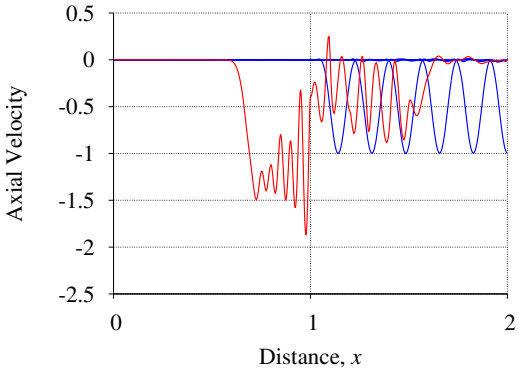

(e) Time Step 19

Figure 30: Giesekus Fluid (M1) - Softer hyper-elastic solid (M2): $v_{max} = 1.0$; Evolution of the velocity

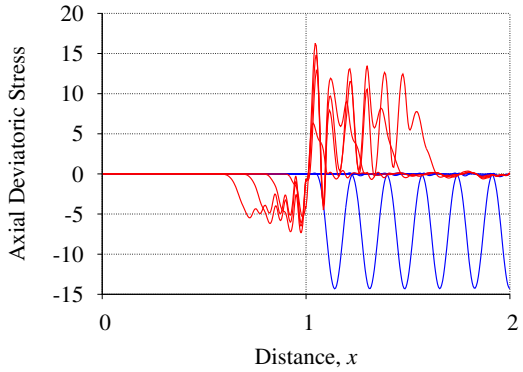

(a) Entire Evolution

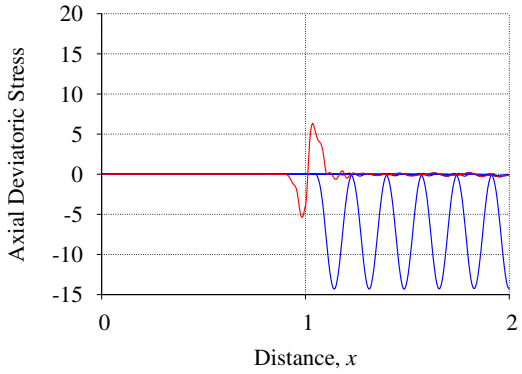

(b) Time Step 13

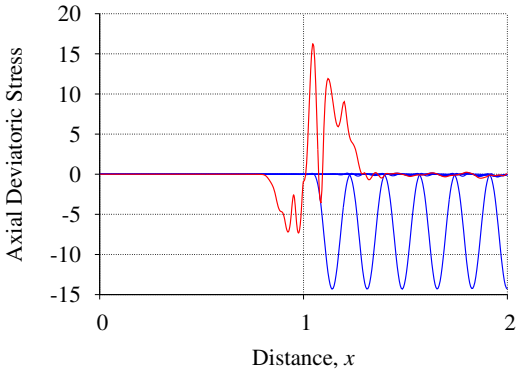

(c) Time Step 15

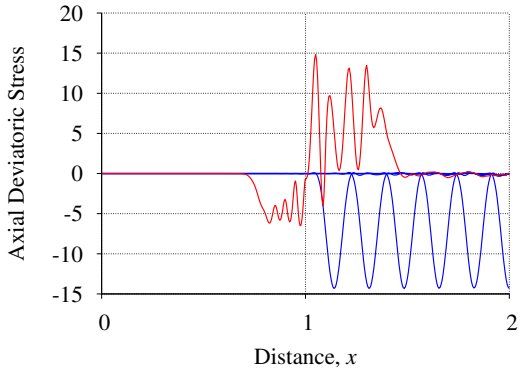

(d) Time Step 17

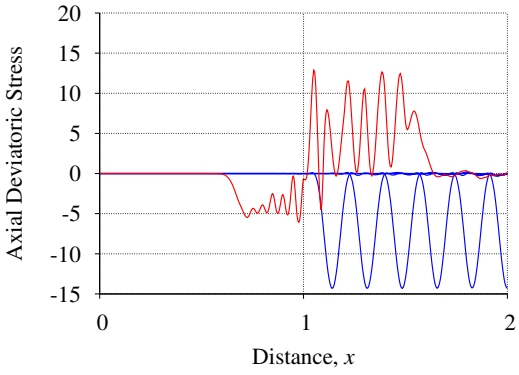

(e) Time Step 19

Figure 31: Giesekus Fluid (M1) - Softer hyper-elastic solid (M2): $v_{max} = 1.0$; Evolution of the stress

II.9.5 Wave propagation with bi-material interface using hypo-elastic solid and polymeric fluids

In these numerical studies we consider interaction between hypo-elastic solid and polymeric fluids. The mathematical models used for solid matter and polymers both utilize Eulerian description with transport. The dependent variables in both mathematical models are the same as well. Thus, the fluid-solid interaction is intrinsic in the mathematical models, hence we expect the computations of evolution to be non-spurious when converged. In these studies M1 is polymer and M2 is solid. The reference quantities for various combinations of M1 and M2 are:

M1 - Maxwell fluid (F1) ; M2 - Hypo-elastic solid (S1):

$\rho_0 = 7896\ kg/m^3,\ L_0 = 0.02\ m,\ v_0 = 500\ m/s,\ E_0 = 2 \times 10^{11}\ Pa,\ p_0 = \tau_0 = \rho_0 {v_0}^2 = 1.974 \times 10^9\ Pa$

M1 - Oldroyd-B fluid (F2) ; M2 - Hypo-elastic solid (S1):

$\rho_0 = 7896\ kg/m^3,\ L_0 = 0.02\ m,\ v_0 = 500\ m/s,\ E_0 = 2 \times 10^{11}\ Pa,\ p_0 = \tau_0 = \rho_0 {v_0}^2 = 1.974 \times 10^9\ Pa$

M1 -Giesekus fluid (F3) ; M2 - Hypo-elastic solid (S1):

$\rho_0 = 7896\ kg/m^3,\ L_0 = 0.02\ m,\ v_0 = 500\ m/s,\ E_0 = 2 \times 10^{11}\ Pa,\ p_0 = \tau_0 = \rho_0 {v_0}^2 = 1.974 \times 10^9\ Pa$

M1 - Maxwell fluid (F1); M2 - Softer hypo-elastic solid (S2):

$\rho_0 = 868\ kg/m^3,\ L_0 = 0.02\ m\ \ v_0 = 0.05\ m/s,\ \mu_0 = 3.0Pa \cdot s\ ,\ E_0 = 400\ Pa\ p_0 = \tau_0 = \rho_0 {v_0}^2 = 2.17\ Pa$

M1 - Oldroyd-B fluid (F2); M2 - Softer hypo-elastic solid (S2):

$\rho_0 = 868\ kg/m^3,\ L_0 = 0.02\ m\ \ v_0 = 0.05\ m/s,\ \mu_0 = 3.0Pa \cdot s\ ,\ E_0 = 400\ Pa\ p_0 = \tau_0 = \rho_0 {v_0}^2 = 2.17\ Pa$

M1 - Giesekus fluid (F3); M2 - Softer hypo-elastic solid (S2):

$\rho_0 = 868\ kg/m^3,\ L_0 = 0.02\ m\ \ v_0 = 0.05\ m/s,\ \mu_0 = 3.0Pa \cdot s\ ,\ E_0 = 400\ Pa\ p_0 = \tau_0 = \rho_0 {v_0}^2 = 2.17\ Pa$

For all numerical studies we consider non-uniform meshes of 25 nine node p-version elements for M1 and M2 with p-level of 11 in space and time. We consider solutions of class C^1 in space and time, we choose $\Delta t = 0.01$ for the entire evolution. Evolution of axial velocity and axial stress for various combination of fluids (M1) and solids (M2) are shown in figures 32-41. In figures 32-41 the blue color represents incident waves and the red color represents reflected and transmitted waves. A summary is given in the following:

M1: Maxwell fluid (F1) M2: Hypo-elastic solid (S1) ; Figures 32(a)-(b) for $\bar{v}_{max} = 0.001$

M1: Maxwell fluid (F1) M2: Hypo-elastic solid (S1) ; Figures 33(a)-(b) for $\bar{v}_{max} = 1.0$

M1: Giesekus fluid (F3) M2: Hypo-elastic solid (S1) ; Figures 34(a)-(b) for $\bar{v}_{max} = 0.001$

M1: Giesekus fluid (F3) M2: Hypo-elastic solid (S1) ; Figures 35(a)-(b) for $\bar{v}_{max} = 1.0$

M1: Maxwell fluid (F1) M2: Softer hypo-elastic solid (S2) ; Figures 36(a)-(b) for $\bar{v}_{max} = 0.001$

M1: Maxwell fluid (F1) M2: Softer hypo-elastic solid (S2) ; Figures 37(a)-(b) for $\bar{v}_{max} = 1.0$

M1: Oldroyd-B fluid (F2) M2: Softer hypo-elastic solid (S2) ; Figures 38(a)-(b) for $\bar{v}_{max} = 0.001$

M1: Oldroyd-B fluid (F2) M2: Softer hypo-elastic solid (S2) ; Figures 39(a)-(b) for $\bar{v}_{max} = 1.0$

M1: Giesekus fluid (F3) M2: Softer hypo-elastic solid (S2) ; Figures 40(a)-(b) for $\bar{v}_{max} = 0.001$

M1: Giesekus Fluid (F3) M2: Softer hypo-elastic solid (S2) ; Figures 41(a)-(b) for $\bar{v}_{max} = 1.0$

From Fig. 32 we note that due to the stiffness of the solid being much higher than the stiffness of the Maxwell fluid at the fluid-solid interface, the Maxwell fluid offers no resistance to the motion of the solid. As a consequence, the incident compressive stress wave is reflected as a tensile stress wave without any transmission in the fluid. The magnitude of $\bar{v}_{max}$ makes no difference (Fig. 33 for $\bar{v}_{max} = 1.0$). In the case of the Giesekus fluid, a dense polymer, the mismatch between the stiffness of this fluid and solid is not as large as in case of the Maxwell fluid, yet from Fig. 34(a)-(b) we still observe a reflected tensile stress wave without any transmission in the fluid at the interface. None the less the evolution is smooth and appears non-spurious in the interaction of polymers with softer hypo-elastic solid (S2) the mismatch in stiffnesses is not that drastic, hence we expect transmission and reflection of the incident wave at the interface in all three polymeric fluids. Figures 36(a)-(b) and 37(a)-(b) show evolutions of axial velocity and deviatoric stress along the length for $\bar{v}_{max}$ of 0.001 and 1.0. From Fig. 36(a)-(b) we observe reflection and transmission of velocity and stress waves. The reflected waves maintain amplitude and base as expected in elastic medium while the transmitted waves in the Maxwell fluid experience substantial amplitude decay during evolution. The evolution is smooth and oscillation free for both values of $\bar{v}_{max}$. Similar behaviors are observed in figures 38(a)-(b) and 39(a)-(b) for interaction of the Oldroyd-B fluid (M1) with softer hypo-elastic solid (M2) except that in this case the base elongation of the transmitted wave in the polymer is significant. The evolution of velocity and deviatoric stress for the Giesekus fluid (M1) and softer hypo-elastic solid (M2) for $\bar{v}_{max}$ of 0.001 and 1.0 are shown in 40(a)-(b) and 41(a)-(b). Evolutions are similar to those for the Maxwell and Oldroyd-B fluids and Softer hypo-elastic solids. Once again we observe that the reflected waves maintain their base and amplitude in the solid region as expected while the transmitted wave experiences amplitude decay during evolution. In all cases the evolutions are smooth. Reflections and transmissions of the waves at the fluid-solid interface are simulated smoothly. The reflected and the transmitted waves in all cases exhibit the expected physics in terms of their amplitude and base. The low values of the residuals ($O(10^{-6})$ or lower) in all calculations confirm that the reported evolutions indeed satisfy the governing differential equations quite well. Due to C^1 of local approximation the integrals are Lebesgue, however at high p-levels (11) used in the studies they are sufficiently close to their Riemann values.

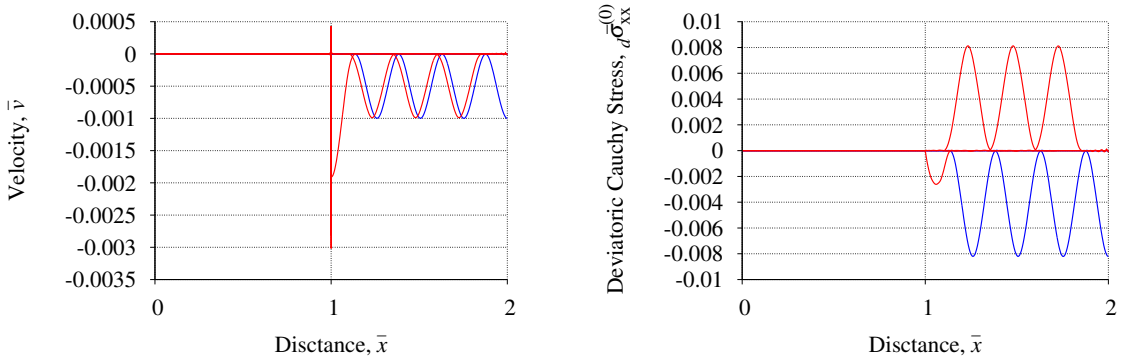

(a) Velocity $\bar{v}$ versus Distance $\bar{x}$ (b) Stress ${}_d\bar{\sigma}^{(0)}_{xx}$ versus Distance $\bar{x}$

Figure 32: Maxwell fluid (M1) - Hypo-elastic solid (M2): $\bar{v}_{max} = 0.001$

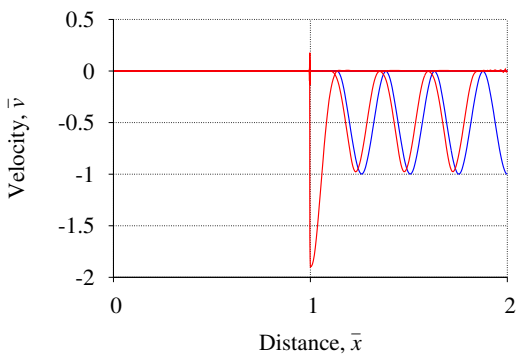

(a) Velocity $\bar{v}$ versus Distance $\bar{x}$

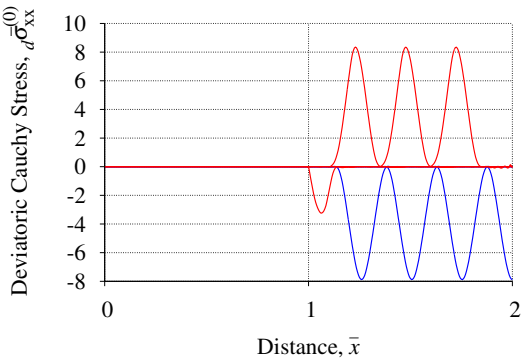

(b) Stress ${}_d\bar{\sigma}^{(0)}_{xx}$ versus Distance $\bar{x}$

Figure 33: Maxwell fluid (M1) - Hypo-elastic solid (M2): $\bar{v}_{max} = 1.0$

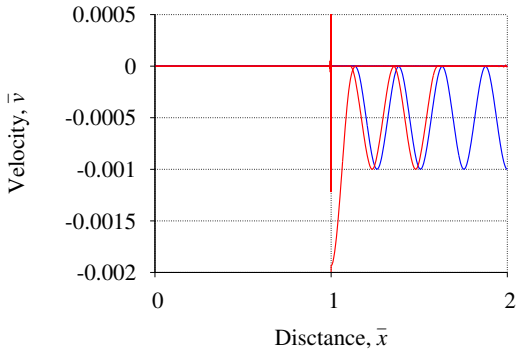

(a) Velocity $\bar{v}$ versus Distance $\bar{x}$

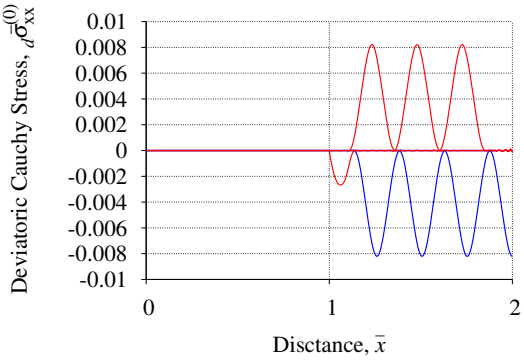

(b) Stress ${}_d\bar{\sigma}^{(0)}_{xx}$ versus Distance $\bar{x}$

Figure 34: Giesekus fluid (M1) - Hypo-elastic solid (M2): $\bar{v}_{max} = 0.001$

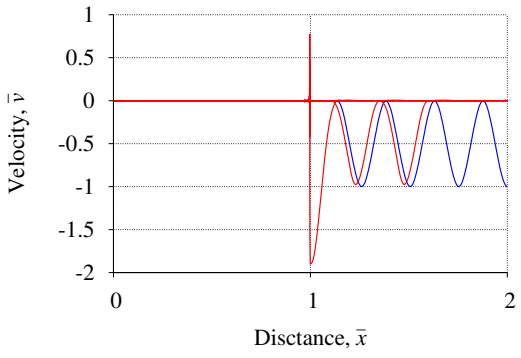

(a) Velocity $\bar{v}$ versus Distance $\bar{x}$

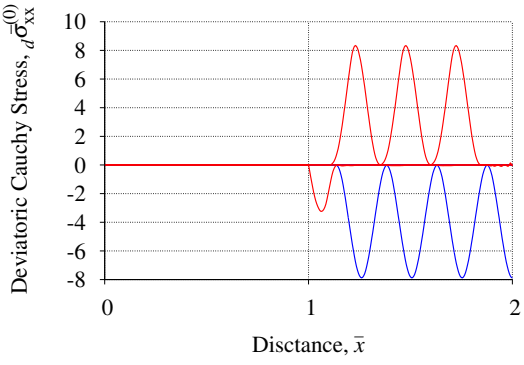

(b) Stress ${}_d\bar{\sigma}^{(0)}_{xx}$ versus Distance $\bar{x}$

Figure 35: Giesekus fluid (M1) - Hypo-elastic solid (M2): $\bar{v}_{max} = 1.0$

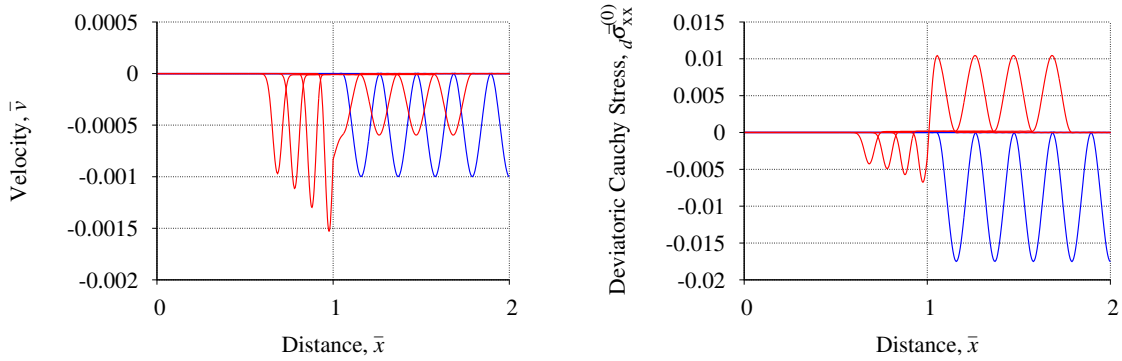

(a) Velocity $\bar{v}$ versus Distance $\bar{x}$ (b) Stress ${}_d\bar{\sigma}^{(0)}_{xx}$ versus Distance $\bar{x}$

Figure 36: Maxwell fluid (M1) - Softer hypo-elastic solid (M2): $\bar{v}_{max} = 0.001$

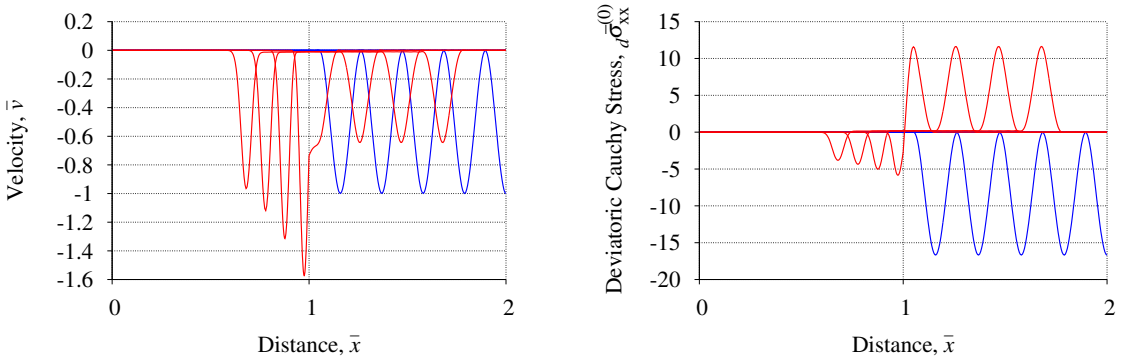

(a) Velocity $\bar{v}$ versus Distance $\bar{x}$ (b) Stress ${}_d\bar{\sigma}^{(0)}_{xx}$ versus Distance $\bar{x}$

Figure 37: Maxwell fluid (M1) - Softer hypo-elastic solid (M2): $\bar{v}_{max} = 1.0$

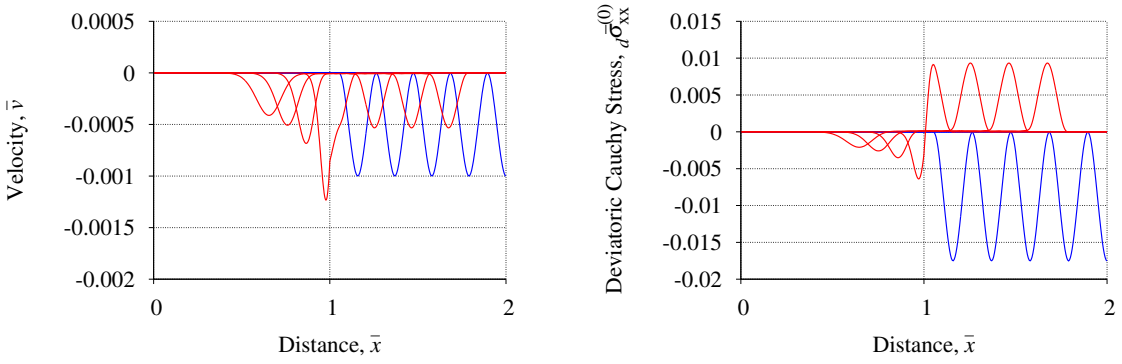

(a) Velocity $\bar{v}$ versus Distance $\bar{x}$ (b) Stress ${}_d\bar{\sigma}^{(0)}_{xx}$ versus Distance $\bar{x}$

Figure 38: Oldroyd-B fluid (M1) - Softer hypo-elastic solid (M2): $\bar{v}_{max} = 0.001$

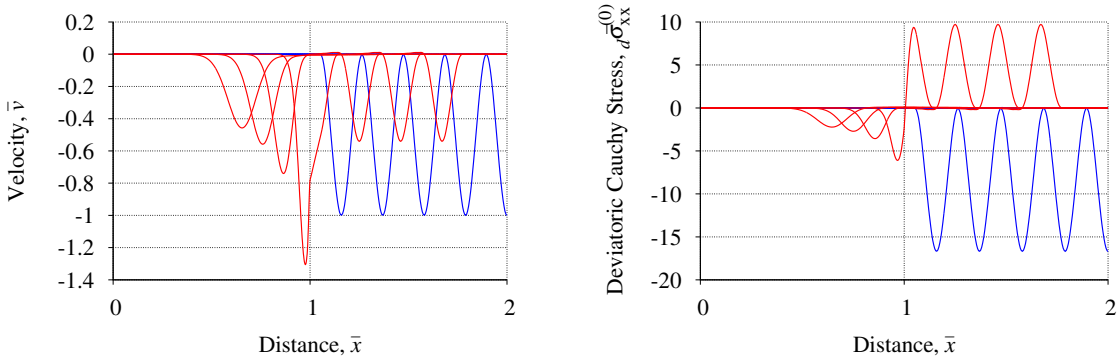

(a) Velocity $\bar{v}$ versus Distance $\bar{x}$ (b) Stress ${}_d\bar{\sigma}^{(0)}_{xx}$ versus Distance $\bar{x}$

Figure 39: Oldroyd-B fluid (M1) - Softer hypo-elastic solid (M2): $\bar{v}_{max} = 1.0$

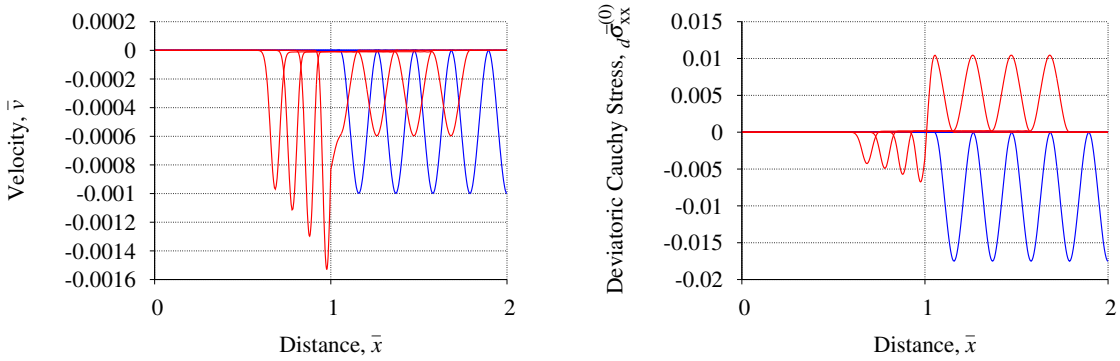

(a) Velocity $\bar{v}$ versus Distance $\bar{x}$ (b) Stress ${}_d\bar{\sigma}^{(0)}_{xx}$ versus Distance $\bar{x}$

Figure 40: Giesekus Fluid (M1) - Softer hypo-elastic solid (M2): $\bar{v}_{max} = 0.001$

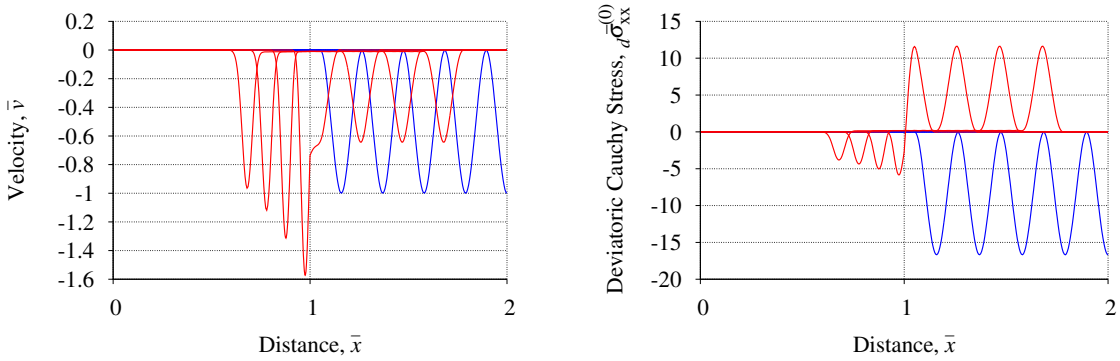

(a) Velocity $\bar{v}$ versus Distance $\bar{x}$ (b) Stress ${}_d\bar{\sigma}^{(0)}_{xx}$ versus Distance $\bar{x}$

Figure 41: Giesekus (M1) - Softer hypo-elastic solid (M2): $\bar{v}_{max} = 1.0$

These studies demonstrate that when the mathematical models for the fluid and the solid utilize the same mathematical description using the same dependent variables with the same physical meaning, the fluid-solid interaction is inherent or intrinsic in

the mathematical models. Such models easily permit delicate fluid-solid interaction numerical simulations like wave propagation shown here without any difficulty and without the use of any external means or conditions at the interface.

II.10 Summary, concluding remarks, significance and impact of this research

We presented various mathematical modeling approaches, including ALE, for fluid-solid interaction and associated computational methodologies for obtaining numerical solution of the initial value problems. The mathematical models for the thermoelastic solid matter are presented for two cases. (1) hyper-elastic solid matter using the Lagrangian and Eulerian descriptions without transport. In these mathematical models the grid point locations are indeed material point locations. During evolution we monitor displacements of the the material points. Material point displacements are required in kinematic description of a deforming solid matter. The constitutive theories for such material expresses stress tensor as a function of strain tensor thus precluding transport. (2) Hypo-elastic solid matter in the Eulerian description with transport. In this description the grid point locations are fixed during evolution. As the material flows through these locations during evolution, we monitor its state. Obviously, in this description the motion of individual material points, that is, displacements are not monitored. A fixed spatial location is occupied by different material particles for different values of time during evolution. In the constitutive theory for such materials we express convected time derivatives of stress tensor in terms of convected time derivatives of strain tensor excluding the strain tensor itself, thus permitting transport. We reiterate that in the case of hypo-elastic solids the material point displacements are not available. The mathematical model for fluids (viscoelastic polymeric liquids considered here) is derived using the Eulerian description with transport. This description is exactly same as the one used for hypo-elastic solid matter. Obviously, in this description also we do not identify material points and hence do not monitor their displacements; instead, we monitor the state of the deforming matter at fixed spatial location as different material points pass through these locations during evolution.

The ALE methodology based on the Lagrangian description for solid matter (hyper-elastic) and the Eulerian description for fluid is considered. The mathematical model used in the published works is considered equations (II.30)-(II.33). We note the following features of the formulation:

(a) When $\bar{\boldsymbol{C}} = \bar{\boldsymbol{v}}$ the model reduces to Eulerian description with transport, ideal for fluids.

(b) When $\bar{\boldsymbol{C}} = 0$, the mathematical model does not reduce to the Lagrangian description for solid matter that accounts for finite deformation. Firstly, the stress measure in (II.30)-(II.33) is not the same as in (II.1)-(II.5) or (II.34)-(II.37). Secondly, The velocity $\boldsymbol{v}$ for solid and $\bar{\boldsymbol{v}}$ for fluid have completely different meaning and physics. Thirdly, for solid matter considered here, the velocity field is not divergence free (obvious from (II.1)-(II.5) and (II.34)-(II.37)) when $\bar{\boldsymbol{C}} = 0$, the mathematical model reduces to (II.7) and (II.8), which is the mathematical model for infinitesimal deformation. Thus, the ALE mathematical model (II.30)-(II.33) does not have physics of finite motion or deformation of the fluid-solid interface.

(c) Choice of appropriate constitutive theories is another major concern in fluid-solid interaction, which is rarely addressed in the published studies on ALE.

From the derivations leading to the mathematical models for solids in the Lagrangian description and the Eulerian description without transport and fluids in the Eulerian description with transport, we have shown that the interaction between the fluid and the solid is not intrinsic in the mathematical models. At the interface between the solid and fluid, the Lagrangian description without transport and the Eulerian description with transport have nothing in common. The interface boundary pertaining to solid deforms during evolution while its mating position belonging to fluid remains fixed during the evolution. This physics is inherent in the mathematical models. In the published work on ALE the solid and fluid domain are discretized and the integral forms are constructed using the Lagrangian and Eulerian (with transport) descriptions (presented here) for the respective domains. It is advocated to introduce a "moving mesh" and the two discretizations are mapped on to the moving mesh resulting in the movement of the mesh in the fluid domain such that the separation between the fluid and solid domain boundaries similar to shown in Fig. 10 (b) does not occur. Forcing the interaction between solid and fluid by: (a) using discretized forms of the mathematical models (b) mapping the discretized forms on to a moving mesh so that the fluid and solid interfaces never separate even though mathematical models allow separation between the two media, lacks rationale and justification. The work presented here evaluates mathematical models for solids in the Lagrangian description (or the Eulerian description without transport) and for fluids in the Eulerian description with transport to determine whether the interaction between the solid and the fluid is intrinsic in the

mathematical model. If the interaction is intrinsic in the mathematical model, then the computation can proceed without any further regard or consideration of the interface between the fluid and the solid. On the other hand, if we establish that the physics of the fluid-solid interaction is not intrinsic or inherent in the two mathematical models, then regardless of the type of constraint equations describing interface behavior or any other means employed at the interface, the correct physics of interaction cannot be resolved through computational means. The work presented demonstrates several main aspects: (1) When the mathematical models for solid are in the Lagrangian description and for the fluid in the Eulerian description with transport, the fluid-solid interaction is not intrinsic in the mathematical model regardless of the magnitude of deformation or motion. The correct interaction physics cannot be defined using these models through any mathematically justifiable means. (2) The ALE approaches for fluid-solid interaction result in failure even in the case of infinitesimal deformation and are not justified based on continuum mechanics principles. (3) When the fluid-solid interaction is inherent in the mathematical model as in case of hypo-elastic solids and polymers, both using the Eulerian description with transport, computation of evolution for the fluid-solid interaction problems is a straight forward using space-time coupled or space-time decoupled approaches, as illustrated in the numerical studies for 1D wave propagation.

Many numerical studies are presented for simple one-dimensional wave propagation model problem to substantiate and illustrate the finding reported above. We summarize these in the following.

(1) Each mathematical model when used by itself simulates wave propagation accurately confirming the legitimacy of each mathematical model.

(2) Mathematical model for solid matter in the Lagrangian description and for fluid in the Eulerian description yield spurious evolutions and result in total failure in simulating interaction physics regardless of the magnitude of the deformation. Numerical studies in these one-dimensional wave propagation fluid-solid interaction studies are for infinitesimal deformation for which there is no need for a moving mesh in the ALE clearly show failure of these models and hence failure of the ALE methodology in fluid-solid interaction.

(3) When solid models are for hypo-elastic matter (the Eulerian description with transport) and the polymer models also in the Eulerian description with transport and use the same dependent variables with same physical meaning, the interaction between the solid and fluid is intrinsic in the mathematical models and hence accurate evolutions can be computed as reported here. We note that hypo-elastic solids can not describe common solids like metals (hyper-elastic) but are used in the represent work to demonstrate the intrinsic nature of the interaction physics in the mathematical model when used in interaction with polymers.

(4) We have shown that the mathematical models for hyper-elastic solids (most common) have no transport where as the mathematical models for fluids do. Presence or lack of transport in the mathematical model can be established by examining the constitutive theories for the stress tensor or the deviatoric stress tensor. When in the constitutive theory the stress tensor or deviatoric stress tensor is a function of strain tensor and strain rate tensors as in hyper-elastic solid material, the solid matter does not have physics of transport. On the other hand, if the constitutive theory for the stress tensor for a material is derived using strain tensor and its convected time derivatives as functions of strain rate tensor but not strain tensor itself, then the material can experience transport during deformation. Thus, thermoelastic solids have no transport but hypo-elastic solids and polymeric liquids do. For fluid-solid interaction to be inherent in the mathematical model, the mathematical models for both solid and fluid must either have transport or both should not have transport. We refer to this as same description for both fluid and solid. The choice of the Eulerian description is obvious due to interaction with fluids.

In the computations of evolution there are many other computational strategies possible [31]. The space-time coupled finite element approach in $H^{k,p}(\bar{\Omega}^e_{xt})$ based on space-time residual functional has been preferred here as [10–12, 41–44] it : (i) yields unconditionally stable algebraic systems (ii) has built in mechanism for adaptivity based on element residual functionals (iii) permits higher order global differentiability of local approximations in space and time.

Based on the work presented here we reached several conclusions. (1) The ALE methodologies have no theoretical bases and are in violation of basic physics for which the mathematical models for solid and fluid are derived. (2) Hypo-elastic solid models do not accommodate hyper-elasticity physics needed for most solid materials. The use of these mathematical models in fluid-solid interaction, as carried out in this work is only to demonstrate that correct interaction between the fluid and solid is only possible when the mathematical models for both media have same description and same dependent variables. (3) Since the

Eulerian description with transport does not permit displacements of material points, such models can not be used in applications requiring finite motion or deformation of the interface between fluid and solid. (5) Lastly, the mathematical models for solids (in the Lagrangian description) and fluids (in the Eulerian description), as exist at present, are not adequate for fluid-solid interaction studies. A single mathematical description in which fluid and solid descriptions coexist is essential for their interaction.

The work presented here investigates mathematical models for fluids and solids and their interactions. It is established that mathematical models for solids in Lagrangian description and for fluids in Eulerian description with zero displacements and strains are inadequate for use in fluid-solid interaction simulations in which discretization for both media are used concurrently in the computations. Solid mathematical models permit movement of the mesh (material points) whereas in case of fluid, the grid points (not material points) are fixed, hence cannot be moved. The work presented here demonstrates, mathematically as well as computationally, that ALE techniques used presently for fluid-solid interaction have no mathematical basis and in fact are incapable of describing th correct interaction physics, hence yield solutions that are not the solutions of the desired interaction problems. Based on the work presented here, FSI problems with currently available thermodynamic framework for fluids and solids can not be solved correctly using concurrent discretizations for solids and fluids as a single BVP and IVP. This is a significant finding that perhaps promotes alternative thinking: (1) Non-concurrent discretizations for solid and fluid with interaction through the interface boundary. (2) When the interface boundary moves due to motion of solid media, the discretization in the fluid cannot be moved, instead we must rediscretize. (3) This approach allows us to keep track of time history of solid media but not of the fluid, hence this approach can only be used for BVPs and not for IVPs. The research work on FSI using this approach for BVPs is in progress. (4) With the currently used mathematical models for fluids and solids, there does not appear to be a transparent and consistent methodology for their interaction for BVPs and IVPs if the combined interaction problem is to be considered as a single BVP or IVP.

III Mathematical models and numerical solutions of liquid-solid and solid-liquid phase change

This work presents numerical simulations of liquid-solid and solid-liquid phase change processes using mathematical models in Lagrangian and Eulerian descriptions. The mathematical models are derived by assuming a smooth interface or transition region between the solid and liquid phases in which the specific heat, density, thermal conductivity, and latent heat of fusion are continuous and differentiable functions of temperature. In the derivations of the mathematical models we assume the matter to be homogeneous, isotropic, and incompressible in all phases. The change in volume due to change in density during phase transition is neglected in all mathematical models considered in this work. This section describes various approaches of deriving mathematical models that incorporate phase transition physics in various ways, hence results in different mathematical models. In the present work we only consider the following two types of mathematical models: (i) We assume the velocity field to be zero i.e. no flow assumption, and free boundaries i.e. zero stress field in all phases. Under these assumptions the mathematical models reduce to first law of thermodynamics i.e. the energy equation, a nonlinear diffusion equation in temperature if we assume Fourier heat conduction law relating temperature gradient to the heat vector. These mathematical models are invariant of the type of description i.e. Lagrangian or Eulerian due to absence of velocities and stress field. (ii) The second class of mathematical models are derived with the assumption that stress field and velocity field are nonzero in the fluid region but in the solid region stress field is assumed constant and the velocity field is assumed zero. In the transition region the stress field and the velocity field transition in a continuous and differentiable manner from nonzero at the liquid state to constant and zero in the solid state based on temperature in the transition zone. Both of these models are consistent with the principles of continuum mechanics, hence provide correct interaction between the regions and are shown to work well in the numerical simulations of phase transition applications with flow. Details of other mathematical models, problems associated with them, and their limitations are also discussed. Numerical solutions of phase transition model problems in $\mathbb{R}^1$ and $\mathbb{R}^2$ are presented using these two types of mathematical models. Numerical solutions are obtained using h, p, k space-time finite element processes based on residual functional for an increment of time with time marching in which variationally consistent space-time integral forms ensure unconditionally stable computations during the entire evolution.

III.1 Introduction, literature review and scope of work

III.1.1 Introduction

The phase change phenomena in which the matter transitions and transforms from one state to another is of significant academic and industrial importance. Solid-liquid or liquid-solid phase transitions and their numerical simulation have been a subject of research and investigation for over a century. There are many sources of difficulties in the numerical simulation of phase change phenomena. Phase transition physics and its mathematical modeling is quite complex due to the fact that this phenomenon creates a transition region, a mixture of solid and liquid phases, in which the phase change occurs resulting in complex changes in transport properties such as density, specific heat, conductivity and the latent heat of fusion that are dependent on temperature. During evolution the phase transition region propagates in spatial directions, i.e. its location changes as the time elapses. Idealized physics of phase change, in which jumps in the transport properties are often assumed, results in singular interfaces. As a consequence the mathematical models describing such evolutions result in initial value problems that contain singularities at the interfaces. When solving such non-linear initial value problems, one must assume existence of the interface. Numerical simulation of the propagation of such fronts during evolution also presents many difficulties that cannot be resolved satisfactorily. Major shortcomings of this approach are that formation of the phase transition front cannot be simulated. Secondly, singular nature of the front is obviously not possible to simulate numerically.

In the second approach of phase transition physics and its mathematical modeling, one assumes that the phase transition region is of finite width, i.e. the phase transition occurs over a finite but small temperature range in which the transport properties such as density, specific heat, conductivity and latent heat are function of temperature and vary in a continuous and differentiable matter between the two states. Thus, the phase transition region is of finite width in temperature that propagates as time elapses. This approach is more realistic and more appealing from the point of view of numerical simulations of the resulting IVPs from the mathematical models as it avoids singularities present in the first approach. The phase-field approach utilizes this concept. A major source of difficulty in this approach is the physics of the transition region, often referred to as 'mushy region', that consists of liquid-solid mixture in varying volume fractions as one advances from one state to the other. Adequate mathematical modeling of the physics in the transition region may require use of mixture theory [74–76] or some similar approach, based on thermodynamic principles of continuum mechanics. Conservation of mass, balance of momenta, first law of thermodynamics and the constitutive theories for stress tensor and heat vector based on the second law of thermodynamics must all be reformulated assuming thermodynamic equilibrium in the transition region. This approach of mathematical modeling of the transition region has not been explored in the published literature (to our knowledge), but may be of benefit in accounting for the realistic physics in the transition region.

The third and perhaps another vital issue lies in the selection of the methods of approximation that are utilized to obtain numerical solutions of the initial value problems describing evolution. It is now well established in computational mathematics that methods of approximation such as finite difference, finite volume and finite element methods based on Galerkin Method (GM), Petrov-Galerkin method (PGM), weighted residual method (WRM), and Galerkin method with weak form (GM/WF) used in context with space-time decoupled or space-time coupled methodologies are inadequate for simulating time accurate evolutions of the non-linear IVPs describing phase change processes [44, 77–81].

Thus, in order to address numerical solutions of phase transition processes, in our view a simple strategy would be to: (i) Decide on a mathematical model with desired, limited physics. (ii) Employ a method of approximation that does not disturb the physics in the computational process, results in unconditionally stable computations and has inherent (built in) mechanism of the measure of error in the computed solution without the knowledge of theoretical solution as such solutions may not be obtainable for the problem of interest. The work presented in this thesis follows this approach. In the following we present literature review on mathematical modeling and methods of approximation for obtaining numerical solutions of the IVPs resulting from the mathematical models. This is followed by the scope of work undertaken in this work.

III.1.2 Literature Review

In this section we present some literature related to liquid-solid and solid-liquid phase transition phenomena. We group the literature review in two major categories: mathematical models and methods of approximation for obtaining numerical solutions of the initial value problems resulting from the mathematical models.

Mathematical Models

A large majority of published work on the mathematical models for phase change processes consider Lagrangian description only, with further assumptions of zero velocity field, i.e. no flow and free boundaries i.e. the medium undergoing phase change to be stress free. We first present literature review and a discussion of commonly used mathematical modeling methodologies in Lagrangian description based on the assumptions stated above. With the assumptions of no flow and stress free medium, the mathematical model of the phase change process is invariant of the type of description and reduces to the energy equation. In the published works there are three commonly used approaches: sharp-interface models, enthalpy models and phase field models.

In the mathematical models derived using sharp-interface the liquid and solid phases are assumed to be separated by a hypothetically and infinitely thin curve or surface called sharp interface or phase. The transport properties such as density, specific heat and conductivity are assumed to experience a jump at the interface. The latent heat of fusion is assumed to be instantaneously released or absorbed at the interface. This of course results in step (sharp) change in the transport properties and latent heat of fusion at the interface, hence the name sharp-interface models. The mathematical models for liquid and solid phases are derived individually. At the interface, the energy balance provides an additional relation (equation) that is used to determine the movement of the interface. The sharp-interface models are also called Stefan models, first derived by J. Stefan [82] to study freezing of ground. The derivation of this model is presented in Section III.2. The proof of existence and uniqueness of the classical solution of the Stefan mathematical model has been given by Rubinstein [83] in 1947. An analytical solution for temperature for one dimensional Stefan problem has been presented in reference [84]. The sharp-interface models have three major shortcomings: (*i*) Assumption of sharp-interface leads to mathematical model in which the initial value problem contains singularity at the interface. (*ii*) When obtaining solutions of the initial value problems based on sharp-interface assumption, the location of the interface is required a priori. That is sharp-interface models are unable to simulate initiation of the interface or front. (*iii*) Movement of the interface i.e. spatial location during evolution requires use of what are called front tracking methods.

Some mathematical models for phase change processes are called enthalpy models. In these models the energy equation is recast in terms of enthalpy and temperature with an additional equation describing enthalpy. Both enthalpy and temperature are retained as dependent variables in the mathematical model. Computations of the numerical solution of the resulting initial value problem are performed on a fixed discretization. This approach eliminates energy balance equation at the interface used in the sharp-interface models. These mathematical models have been derived using different approaches [85–87]. Enthalpy model is also presented in Section III.2. These models generally introduce a finite phase transition region (over a small temperature change) called mushy region between the liquid and the solid phases. The transport properties are assumed to vary in some manner from one phase to the other phase. The concept of liquid or solid fraction is generally introduced to account for the fact that the mushy region is a mixture of solid and liquid phases. Due to the assumption of the mushy region separating the solid and the liquid phases, sharp-interface and the problems associated with it are avoided in this approach.

Another category of mathematical models are called phase field models. These mathematical models are based on the work of Cahn and Hilliard [77]. In this approach the solid and liquid phases are also assumed to be separated by a finite width (in temperature) transition region in which the transport properties are assumed to vary with temperature between the two states. Landau-Ginzburg [78] theory of phase transition is used to derive the mathematical model. The basic foundation of the method lies in standard mean theories of critical phenomena based on free energy functional. Thus, the method relies on specification of free energy density functional which is the main driving force for the movement of the phase transition region. Details of phase field mathematical model in $\mathbb{R}^1$ are presented in section III.2. The method shows good agreement with the Stefan problem in $\mathbb{R}^1$. While the phase field models eliminate the sharp-interfaces and their tracking, the main disadvantages of this approach are: (*i*) It requires a priori knowledge of the free energy density functional for the application at hand. (*ii*)The mathematical model is incapable of simulating the initiation or formation of the solid-liquid interface, hence the liquid-solid phases and the transition region must be defined as initial conditions. This limitation is due to specific nature of the free energy function (generally a double well potential, see section III.2). However, if a liquid-solid interface is specified as initial condition, then the phase field models are quite effective in simulating the movement of the front during evolution. In most applications of interest, simulation of initiation of the transition region i.e. solid-liquid interface is essential as it may not be possible to know its location and the precise conditions under which it initiates a priori. These limitations have resulted in lack of wide spread use of these mathematical models in practical applications.

When the assumptions of stress free media and zero velocity are not valid (as in case of fluid flow), the mathematical models discussed above are not applicable. In such cases Eulerian description is necessary for the fluid while Lagrangian description is

essential for the solid region. The mathematical model in this case consists of conservation of mass, balance of momenta, first law of thermodynamics and constitutive theory for stress tensor and heat vector based on the second law of thermodynamics for each of the two phases (i.e. liquid and solid) as well as the transition region.

The published works on these mathematical models are rather sketchy, the models are not based on rigorous derivation and in most cases are aimed at solving a specific problem as opposed to developing a general infrastructure that addresses totality of a large group of applications. We present some account of the published works in the following. In almost all cases the fluid is treated as Newtonian fluid. In some cases [88] the fluid is also considered inviscid. Sharp-interface models generally force (set) the relative movement of the material particles to be zero in the solid phase [89, 90]. In case of enthalpy and phase field models the constitutive theory for the transition region is still unclear and published works in many instances are conflicting. There are three main ideas that are commonly found in the majority of the published works on mathematical models derived using Eulerian description. In the first approach both the liquid and the solid phases are assumed to be Newtonian fluids. The viscosity in the solid phase is artificially increased to a very high value and is assumed to vary along the interface between the two states in order to approximate no velocity condition in the solid phase [91]. In the second approach a varying interfacial force is employed such that it satisfies the no velocity condition in the solid phase [92]. The third approach assumes that the solid particles in the transition region form a porous medium through which the fluid flows. Voller and Cross [87] use Darcy model for flow in porous media in which the velocity field is assumed to be proportional to the pressure gradient in order to compare their results with variable viscosity model. Beckermann [93] assumed the average stress to be proportional to the gradient of superficial liquid viscosity in the porous media. There are other approaches [94] that utilize these three basic ideas in some manner or the other. In most cases, solid phase behavior is neglected by setting the velocity to zero. In general, our conclusion is that published phase change models that account for nonzero stress and velocity fields are crude, ad hoc and are aimed to obtain some numerical solutions for specific applications. A general theory of mathematical modeling based on thermodynamic and continuum mechanics principles is not available for phase transition modeling to our knowledge.

Computational Methodologies

Regardless of the type of mathematical model, the resulting mathematical models for phase change phenomena are non-linear partial differential equations in dependent variables, space coordinates and time, hence they are non-linear initial value problems. If we incorporate realistic physics of phase transition, the mathematical models become complex enough not to permit determination of theoretical solution, hence numerical solutions of these IVPs based on methods of approximation are necessary. The methods of approximation for IVPs can be classified in two broad categories [44, 79–81] : space-time decoupled methods and space-time coupled methods. In space-time decoupled methods, for an instant of time, the spatial discretization is performed by assuming the time derivatives to be constant. This approach reduces the original PDEs in space and time to ODEs in time which are then integrated using explicit or implicit time integration methods to obtain evolution. Almost all finite difference, finite volume and finite element methods (based on GM/WF) used currently [80] for initial value problems fall into this category. The assumption of constant time derivatives necessitates extremely small time increments during the integration of ODEs in time. The issues of stability, accuracy and lack of time accuracy of evolution are all well known in the space-time decoupled approaches. Majority of the currently used methods of approximation for phase change processes fall into this category. The non-concurrent treatment in space and time in space-time decoupled methods is contrary to the physics in which all dependent variables exhibit simultaneous dependence on space coordinates and time. In a large majority of published works on phase change processes, often the distinction between the mathematical models and the computational approaches is not clear either i.e. elements of the methods of approximation are often introduced during the development of the mathematical models. As a consequence, it is difficult to determine if the non-satisfactory numerical solutions are a consequence of the methods of approximation used or the deficiencies in the mathematical models.

The space-time coupled methods on the other hand maintain simultaneous dependence of the dependent variables on space coordinates and time [44, 79, 81]. In these methods the discretizations in space and time are concurrent as required by the IVPs. These methods are far superior to the space-time decoupled methods in terms of mathematical rigor as well as accuracy. Whether to choose space-time finite difference, finite volume or finite element method depends upon the mathematical nature of the space-time differential operator and whether the computational strategy under consideration will yield unconditionally stable computations, will permit error assessment, and will yield time accurate evolution upon convergence.

III.1.3 Scope of Work

The work presented here considers development of mathematical models and their numerical solutions for solid-liquid and liquid-solid phase transition of homogeneous, isotropic, and incompressible matter. In the phase transition region $[T_s, T_l]$ the matter is assumed to be homogeneous and isotropic and the transport properties are assumed to be continuous and differentiable with their respective values at the solid and liquid states. Three groups of mathematical models are considered for phase transition initial value problems. Numerical studies are presented using the mathematical models groups one and three.

The first group of mathematical models are based on the assumptions of stress free media and zero velocity in all phases. With these assumptions the mathematical models in Lagrangian and Eulerian descriptions are identical. We consider these mathematical models in $\mathbb{R}^1$ and $\mathbb{R}^2$. The mathematical models in this case consist of the energy equation and heat flux(es), a system of first order nonlinear PDEs in temperature and heat flux(es). By substituting heat flux(es) into the energy equation the mathematical model can be reduced to a single non-linear diffusion equation in temperature. In the derivation of the energy equation the specific total energy is expressed in terms of storage and latent heat of fusion. The Fourier heat conduction law is assumed to hold. In the solid and liquid phases the transport properties (ρ, c_p, k, L_f) are assumed to be constant. In the transition region the solid-liquid mixture is assumed to be isotropic and homogeneous. The transport properties are assumed to vary in a continuous and differentiable manner, described by a third or a fifth degree polynomial with continuous temperature derivatives at the boundaries of the transition region between the solid and liquid phases. With this approach the phase change process is a smooth process in which the transition region provides the smooth interface. We remark that if we assume both phases to be incompressible, then a change in density during phase change must be accompanied by a change in volume. In the present work we consider phase change studies in $\mathbb{R}^1$ and $\mathbb{R}^2$ assuming (*i*) the density ρ to be constant during the phase transition and (*ii*) the density to be a function of temperature i.e. variable with continuous and differentiable distribution between the states. Additionally, the influence of temperature dependent density in the transition region on the speed of propagation of the transition region is also investigated. Mathematical models and numerical studies are presented in $\mathbb{R}^1$ and $\mathbb{R}^2$ for solid-liquid and liquid-solid phase change when stress field and velocity field are zero.

In the second group of mathematical models stress and velocity fields are considered to be nonzero. In this case the mathematical models change drastically compared to the first group of models. This is due to the fact that in solid regions Lagrangian description is essential because we need to monitor displacements, have measures of strain, and restrict transport of material particles to describe solid continua. On the other hand the fluid media requires arbitrary transport which precludes displacement and strain measures. The transition region is even more complex. In general, the mathematical models must consist of complete Navier-Stokes equations: continuity equation, momentum equations, energy equation, and the constitutive equations for both solid and liquid phases. In the liquid phase, the Eulerian description with transport is ideally suited for deriving mathematical models using conservation and balance laws. In such descriptions material particle displacements are ignored and hence not monitored. Instead, the evolving state of the matter is monitored at fixed locations. In the case of fluids this approach is satisfactory as the stress field does not depend on strain, hence material point displacements are not needed. In the case of solid matter, the Lagrangian description is obviously ideal to derive the mathematical models. In this description the material points are the grid points that experience displacement during evolution. In the case of ice as a solid medium, it is reasonable to assume the matter to be hyperelastic and hence the use of constitutive theories based on strain energy density function (such as generalized Hooke's law) is appropriate. If we assume fluid to be Newtonian fluid then standard Newton's law of viscosity for incompressible media can be used as the constitutive theory for the liquid phase. In the transition region, a mushy zone of solid-liquid mixture, the mathematical model based on balance and conservation laws is not that straightforward to construct. In the present work we discuss various alternate approaches of deriving mathematical models for the transition region, their benefits, and shortcomings. Use of the mathematical models based on conservation and balance laws for solid-liquid and liquid-solid phase change and their validity are discussed and evaluated for solid and liquid, as well as the transition region.

The third group of mathematical models are derived based on the assumption that the stress field is constant and the velocity field is zero in the solid region but nonzero in the liquid region. In the transition zone, the stress and the velocities are assumed to make transition from nonzero state in the fluid to constant stress state and zero velocity in the solid phase based on the temperature in the transition zone. These mathematical models permit phase transition studies in the presence of flow, are consistent description based on continuum mechanics, and hence provide correct interaction between the solid and fluid media. Numerical studies are presented in $\mathbb{R}^1$ and $\mathbb{R}^2$ to demonstrate various features of the mathematical models presented here. Computed solutions in $\mathbb{R}^1$ are also compared with sharp-interface theoretical solution.

Computed mathematical solutions reported are always converged and are independent of mesh size and degree of local approximation. In all cases the integrated sum of squares of the residuals are small ($O(10^{-6})$ or lower), confirming good accuracy of the reported solutions.

III.2 Mathematical models

In this section we consider details of the three groups of mathematical models described in section III.1.3.

III.2.1 First group of mathematical models for phase change based on zero stress and velocity fields and free boundaries

These mathematical models constitute the first group of mathematical models. When the media are stress free, the velocity field is zero, and the boundaries are free the mathematical model for phase change reduces to linear or nonlinear diffusion equation regardless of the choice of dependent variables. In the published works there is a lot of confusion in the presentations of these models regarding the choice of conflicting notations, representation of physics, and even consistency of derivations. These models are generally classified as sharp-interface models, enthalpy models, phase field models, smooth-interface models, etc. We show that the energy equation resulting from the first law of thermodynamics is the same in all of these models. What differs is (*i*) the choice of dependent variable(s) and (*ii*) the manner in which the phase transition physics is incorporated. We present two basic forms of the energy equation that are used in the mathematical models mentioned above. Overbar on quantities indicates that the description is Eulerian with transport.

Energy Equation

Following [31] for a compressive and dissipative medium, we can derive the following energy equation from the first law of thermodynamics in Eulerian description with transport when the stress field and the velocity are not zero. Assuming sources and sinks to be absent

$$\bar{\rho}\frac{D\bar{e}}{Dt} + \bar{\boldsymbol{\nabla}}\cdot\bar{\boldsymbol{q}} - \mathrm{tr}\big(\big[\bar{\sigma}^{(0)}\big]\big[\bar{D}\big]\big) = 0 \qquad \forall(\bar{\boldsymbol{x}},t)\in\Omega_{\bar{\boldsymbol{x}}t}=\Omega_{\bar{\boldsymbol{x}}}\times\Omega_t \tag{III.1}$$

$\bar{\rho}$ is density, $\bar{e}$ is specific internal energy, $\bar{\boldsymbol{q}}$ is the heat vector, $[\bar{\sigma}^{(0)}]$ is the contravariant Cauchy stress tensor, and $[\bar{D}]$ is the symmetric part of the velocity gradient tensor, all in the current configuration at time t. Equation (III.1) can also be written in terms of specific enthalpy $\bar{h}$. Recall that

$$\bar{h} = \bar{e} + \frac{\bar{p}}{\bar{\rho}} \tag{III.2}$$

in which $\bar{p}$ is thermodynamic pressure. Thus

$$\begin{aligned} &\bar{\rho}\frac{D\bar{e}}{Dt} = \bar{\rho}\frac{D\bar{h}}{Dt} - \bar{\rho}\frac{D}{Dt}\big(\frac{\bar{p}}{\bar{\rho}}\big) \\ \text{or}\quad &\bar{\rho}\frac{D\bar{e}}{Dt} = \bar{\rho}\frac{D\bar{h}}{Dt} - \frac{D\bar{p}}{Dt} + \frac{\bar{p}}{\bar{\rho}}\frac{D\bar{\rho}}{Dt} \qquad \forall(\bar{\boldsymbol{x}},t)\in\Omega_{\bar{\boldsymbol{x}}t}=\Omega_{\bar{\boldsymbol{x}}}\times\Omega_t \end{aligned} \tag{III.3}$$

Consider decomposition of $[\bar{\sigma}^{(0)}]$ into equilibrium stress $\bar{p}[I]$ and deviatoric stress $[{}_d\bar{\sigma}^{(0)}]$

$$\bar{\boldsymbol{\sigma}}^{(0)} = -\bar{p}\boldsymbol{I} + {}_d\bar{\boldsymbol{\sigma}}^{(0)} \tag{III.4}$$

Using (III.4)

$$\mathrm{tr}\big(\big[\bar{\sigma}^{(0)}\big]\big[\bar{D}\big]\big) = -\mathrm{tr}\big(\bar{p}\big[\bar{D}\big]\big) + \mathrm{tr}\big(\big[{}_d\bar{\sigma}^{(0)}\big]\big[\bar{D}\big]\big) = -\bar{p}\bar{\boldsymbol{\nabla}}\cdot\bar{\boldsymbol{v}} + \mathrm{tr}\big(\big[{}_d\bar{\sigma}^{(0)}\big]\big[\bar{D}\big]\big) \tag{III.5}$$

Furthermore, from continuity

$$\frac{D\bar{\rho}}{Dt} + \bar{\rho}\bar{\boldsymbol{\nabla}}\cdot\bar{\boldsymbol{v}} = 0 \qquad \forall(\bar{\boldsymbol{x}},t)\in\Omega_{\bar{\boldsymbol{x}}t}=\Omega_{\bar{\boldsymbol{x}}}\times\Omega_t \tag{III.6}$$

Substituting from (III.6) for $\frac{D\bar{\rho}}{Dt}$ in (III.3)

$$\begin{aligned} \bar{\rho}\frac{D\bar{e}}{Dt} &= \bar{\rho}\frac{D\bar{h}}{Dt} - \frac{D\bar{p}}{Dt} + \frac{\bar{p}}{\bar{\rho}}\big(-\bar{\rho}\bar{\boldsymbol{\nabla}}\cdot\bar{\boldsymbol{v}}\big) \\ \text{or}\quad \bar{\rho}\frac{D\bar{e}}{Dt} &= \bar{\rho}\frac{D\bar{h}}{Dt} - \frac{D\bar{p}}{Dt} - \bar{p}\bar{\boldsymbol{\nabla}}\cdot\bar{\boldsymbol{v}} \qquad \forall(\bar{\boldsymbol{x}},t)\in\Omega_{\bar{\boldsymbol{x}}t}=\Omega_{\bar{\boldsymbol{x}}}\times\Omega_t \end{aligned} \tag{III.7}$$

Substituting from (III.5) and (III.7) into (III.1)

$$\bar{\rho}\frac{D\bar{h}}{Dt} - \frac{D\bar{p}}{Dt} - \bar{p}\bar{\boldsymbol{\nabla}}\cdot\bar{\boldsymbol{v}} + \bar{\boldsymbol{\nabla}}\cdot\bar{\boldsymbol{q}} + \bar{p}\bar{\boldsymbol{\nabla}}\cdot\bar{\boldsymbol{v}} - \mathrm{tr}\big(\big[{}_d\bar{\sigma}^{(0)}\big]\big[\bar{D}\big]\big)\forall(\bar{\boldsymbol{x}},t)\in\Omega_{\bar{\boldsymbol{x}}t}=\Omega_{\bar{\boldsymbol{x}}}\times\Omega_t \tag{III.8}$$

$$\bar{\rho}\frac{D\bar{h}}{Dt} - \frac{D\bar{p}}{Dt} + \bar{\boldsymbol{\nabla}}\cdot\bar{\boldsymbol{q}} - \mathrm{tr}\big(\big[{}_d\bar{\sigma}^{(0)}\big]\big[\bar{D}\big]\big) \qquad \forall(\bar{\boldsymbol{x}},t)\in\Omega_{\bar{\boldsymbol{x}}t}=\Omega_{\bar{\boldsymbol{x}}}\times\Omega_t \tag{III.9}$$

$\frac{D\bar{p}}{Dt}$ in (III.9) is often neglected if compressibility is not significant.

$$\bar{\rho}\frac{D\bar{h}}{Dt} + \bar{\boldsymbol{\nabla}}\cdot\bar{\boldsymbol{q}} - \mathrm{tr}\big(\big[{}_d\bar{\sigma}^{(0)}\big]\big[\bar{D}\big]\big) \qquad \forall(\bar{\boldsymbol{x}},t)\in\Omega_{\bar{\boldsymbol{x}}t}=\Omega_{\bar{\boldsymbol{x}}}\times\Omega_t \tag{III.10}$$

Equations (III.1) and (III.10) are two fundamental forms of the energy equation in specific internal energy $\bar{e}$ and specific enthalpy $\bar{h}$ when the medium is compressible and the stress field and the velocity field are not zero.

Stress free medium with zero velocities

When the medium is stress free and the velocity field is zero then

$$\frac{D}{Dt} = \frac{\partial}{\partial t} \qquad \text{and} \qquad {}_d\bar{\boldsymbol{\sigma}}^{(0)} = 0 = \bar{\boldsymbol{D}} \tag{III.11}$$

Furthermore, with these assumptions Eulerian and Lagrangian descriptions are the same, hence the overbar on all quantities can be omitted. Thus, (III.1) and (III.10) reduce to

$$\rho\frac{De}{Dt} + \boldsymbol{\nabla}\cdot\boldsymbol{q} = 0 \qquad \forall(\boldsymbol{x},t)\in\Omega_{\boldsymbol{x}t}=\Omega_{\boldsymbol{x}}\times\Omega_t \tag{III.12}$$

$$\rho\frac{Dh}{Dt} + \boldsymbol{\nabla}\cdot\boldsymbol{q} = 0 \qquad \forall(\boldsymbol{x},t)\in\Omega_{\boldsymbol{x}t}=\Omega_{\boldsymbol{x}}\times\Omega_t \tag{III.13}$$

For this case $h = e$ as obvious from (III.2) when $p = 0$. In the energy equations (III.12) and (III.13) the simplest constitutive theory for heat vector is of course Fourier heat conduction law.

$$\boldsymbol{q} = -k\boldsymbol{\nabla}T \qquad \forall(\boldsymbol{x},t)\in\Omega_{\boldsymbol{x}t}=\Omega_{\boldsymbol{x}}\times\Omega_t \tag{III.14}$$

in which k is the thermal conductivity for homogeneous isotropic matter. Equations (III.12) and (III.14) or (III.13) and (III.14) form the basis for phase transition mathematical models in the absence of stress field and velocity field. Various methods published in the literature differ in the manner in which the phase change physics is incorporated in (III.12) and (III.13).

Remarks

(1) First we note that since $h = e$, the specific enthalpy and the specific energy models are the same. From now onwards, we will use (III.12) to present further details.

(2) The fundamental issue is the physics for e we wish to consider during the phase change. We consider two possibilities.

(a) In the first class of mathematical models we assume that the release or absorption of latent heat during phase change occurs at a constant temperature. Referring to figure 42(a) when the temperature in the solid medium reaches T_s with specific internal energy e_s (point B), the addition of latent heat of fusion L_f at constant temperature T_s increases e_s to e_l (point C) at which the state of the matter has changed from solid to liquid. In case of freezing we go from the state of the matter at C to B by extracting latent heat of fusion L_f at constant temperature T_s.

In this physics of phase transition the interface between the solid and the liquid phases is sharp (step change), hence the mathematical models for e based on this approach are called "sharp-interface models." Step change in e is nonphysical even for the most idealized materials.

Secondly, its numerical simulation poses difficulties due to non-unique behavior of e at temperature T_s. We present details of sharp-interface models in a following section.

(b) In the second category of mathematical models for e we assume that phase transition from solid to liquid occurs over a finite but small range of temperature $[T_s, T_l]$ and that e is continuous and differentiable for $T_s \leq T \leq T_l$ (figure 42(b)). The range $[T_s, T_l]$ can be as narrow or as large as desired.

The obvious advantage in this approach is that the singular nature of e at T_s (as in figure 42(a)) is completely avoided. This is of immense benefit in numerical computations of evolution of phase change problems.

III.2.2 Sharp-interface models

As described earlier these models for e are based on its behavior during phase transition shown in figure 42(a). We have some alternative forms of the mathematical models.

Model (a)

In this model we consider

$$\rho \frac{\partial e}{\partial t} + \boldsymbol{\nabla} \cdot \boldsymbol{q} = 0 \qquad \forall (\boldsymbol{x}, t) \in \Omega_{\boldsymbol{x}t} = \Omega_{\boldsymbol{x}} \times \Omega_t \tag{III.15}$$

$$\boldsymbol{q} = -k \boldsymbol{\nabla} T \qquad \forall (\boldsymbol{x}, t) \in \Omega_{\boldsymbol{x}t} = \Omega_{\boldsymbol{x}} \times \Omega_t \tag{III.16}$$

$$e = e_s + \alpha L_f + c_p (T - T_s) \tag{III.17}$$

$$\alpha = \begin{cases} 0 & ; \quad e < e_s \\ \dfrac{e - e_s}{L_f} & ; \quad e_s \leq e \leq e_s + L_f \\ 1 & ; \quad e > e_s + L_f \end{cases} \tag{III.18}$$

Alternatively (III.16) can be substituted into (III.15) to obtain

$$\rho \frac{\partial e}{\partial t} - \boldsymbol{\nabla} \cdot (k \boldsymbol{\nabla} T) = 0 \qquad \forall (\boldsymbol{x}, t) \in \Omega_{\boldsymbol{x}t} = \Omega_{\boldsymbol{x}} \times \Omega_t \tag{III.19}$$

The mathematical model consists of (III.15) – (III.18) in dependent variables e, q, and T, or (III.17) – (III.19) in dependent variables e and T. In the published works specific heat c_p is generally considered as a function of temperature, but in general $\rho = \rho(T)$, $c_p = c_p(T)$, and $k = k(T)$ are permissible but can only be used outside the transition region. Consider equation (III.17) during phase change, i.e. change in e from e_s to e_l. When $\alpha = \frac{e - e_s}{L_f}$ and $T = T_s$, (III.17) is identically satisfied. $\alpha = 1$ for $e > e_s + L_f$ clearly indicates instantaneous addition of latent heat. Both models in e, q, T and e, T have been used in the published works [82–86].

Model (b)

If we assume that c_p, k, and ρ are constant in the solid and liquid regions and have values c_{ps}, k_s, ρ_s and c_{pl}, k_l, ρ_l, then we can write explicit forms of (III.19) for solid and liquid phases by using $e_s = c_{ps}T$ and $e_l = c_{pl}T$. These equations are augmented by a heat balance equation at the interface (BC, figure 42(a)).

Solid phase:

$$\rho_s c_{ps}\frac{\partial T}{\partial t} - \boldsymbol{\nabla}\cdot(k_s\boldsymbol{\nabla}T) = 0 \qquad \forall(\boldsymbol{x},t)\in\Omega^s_{\boldsymbol{x}t} = \Omega^s_{\boldsymbol{x}}\times\Omega_t \tag{III.20}$$

Liquid phase:

$$\rho_l c_{pl}\frac{\partial T}{\partial t} - \boldsymbol{\nabla}\cdot(k_l\boldsymbol{\nabla}T) = 0 \qquad \forall(\boldsymbol{x},t)\in\Omega^l_{\boldsymbol{x}t} = \Omega^l_{\boldsymbol{x}}\times\Omega_t \tag{III.21}$$

At the interface:

$$L_f v_n = \big((-k_s\boldsymbol{\nabla}T) - (-k_l\boldsymbol{\nabla}T)\big)\cdot\boldsymbol{n} \qquad \forall(\boldsymbol{x},t)\in\Gamma_{\boldsymbol{x}t} = \Gamma_{\boldsymbol{x}}\times\Omega_t \tag{III.22}$$

$\Omega^s_{\boldsymbol{x}}$ and $\Omega^l_{\boldsymbol{x}}$ are solid and liquid spatial domains. $\Gamma_{\boldsymbol{x}}(t) = \Omega^s_{\boldsymbol{x}}\bigcap\Omega^l_{\boldsymbol{x}}$ is the interface between the solid and liquid phases. L_f is the latent heat of fusion, $\boldsymbol{n}$ is the unit exterior normal from the solid phase at the interface, and v_n is the scalar normal velocity of the interface in the direction of $\boldsymbol{n}$. Subscripts and superscripts s and l stand for solid and liquid phases. When the mathematical model is posed as a system of integral equations, a complete proof of existence and uniqueness of the classical solution in $\mathbb{R}^1$ was given by Rubinstein in 1947 [83]. For the one dimensional case, analytical solutions to some specific problems are derived in reference [84] for the temperature distribution $T = T(x,t)$. When the properties are the same in both phases (i.e. $c_{ps} = c_{pl} = 1$, $k_s = k_l = 1$, $\rho_s = \rho_l = 1$), one example problem in reference [84] solves for T in the domain $x \geq 0$ with initial and boundary conditions:

$$T(0,t) = T_0 \qquad , \qquad T(x,0) = \Theta(x) \qquad , \qquad T(x,t)_{x\to\infty} = T_\infty \tag{III.23}$$

Then the solution to the sharp-interface model is given by

$$\begin{aligned} T(x,t) &= C_1\frac{\text{erf}\big(\beta/2\big) - \text{erf}\big(x/2\sqrt{t+t_0}\big)}{\text{erf}\big(\beta/2\big)} \quad ; \quad x \leq \Gamma_x(t) \\ T(x,t) &= C_2\frac{\text{erf}\big(\beta/2\big) - \text{erf}\big(x/2\sqrt{t+t_0}\big)}{\text{erfc}\big(\beta/2\big)} \quad ; \quad x > \Gamma_x(t) \end{aligned} \tag{III.24}$$

The interface location $\Gamma_x(t)$ is defined by

$$\Gamma_x(t) = \beta\sqrt{t+t_0} \tag{III.25}$$

The parameter β is obtained by solving the equation

$$\frac{2}{\sqrt{\pi}}\text{e}^{\frac{\beta^2}{4}}\Big[\frac{C_2}{\text{erfc}\big(\beta/2\big)} - \frac{C_1}{\text{erf}\big(\beta/2\big)}\Big] - \beta = 0 \tag{III.26}$$

Remarks

(1) One of the major disadvantages of the sharp-interface mathematical models is that the phase change is assumed to occur at a constant temperature T_s. Thus, e changes from e_s to e_l at constant $T = T_s$. This is true regardless of the form of the mathematical models.

(2) The sharp interface creates singularity of e at $T = T_s$ which poses many obvious difficulties in the computation of the numerical solutions of the associated initial value problem.

(3) It is meritorious to eliminate $\boldsymbol{q}$ as a dependent variable as done in case of (III.19) as it reduces the number of dependent variables in the mathematical model. But this reduction is at the cost of appearance of the second derivative of T with respect to spatial coordinates in the energy equation, which in context of finite element methods of approximation requires higher order regularity for the approximation of T.

(4) In addition to eliminating $\boldsymbol{q}$ as a dependent variable, the specific internal energy e can also be substituted in the energy equation yielding a single nonlinear diffusion equation in temperature T. We postpone details of this until a later section.

(5) It is critical to point out that all sharp-interface models are derived based on a priori existence of the transition front as initial condition. As a result these models cannot simulate initiation of the transition front. The models simply simulate propagation of this front during evolution. This is vital physics that is necessary in almost every phase change application and is missing in the sharp-interface approach.

(6) Finally, if one considers computations of the numerical solutions for phase change processes to be essential, then sharp-interface model of phase change processes are not meritorious.

III.2.3 Smooth-interface models

In smooth-interface models the phase change is assumed to take place over a finite temperature range $[T_s, T_l]$ (see figure 42(b)) during which e is continuous and differentiable in temperature T. The range $[T_s, T_l]$, referred to as transition region consisting of solid-liquid mixture i.e. a mushy region, can be as narrow or as wide as desired. At $T = T_s$ the state of the matter is solid whereas at $T = T_l$ it is pure liquid. Since the properties ρ, c_p, k have different values for solid and liquid phases, it is often meritorious to consider these as functions of temperature T with continuous and differentiable behavior for $T_s \leq T \leq T_l$ between their values ρ_s, c_{ps},k_s and ρ_l, c_{pl}, k_l for solid and liquid states respectively. In the following we present details of two smooth-interface mathematical models, one based on phase field approach and the other based on the energy equation (III.12) with transition region $[T_s, T_l]$ in which ρ, c_p, k and L_f are continuous and differentiable functions of the temperature T.

Phase field models

The phase field mathematical models of phase change also introduce a finite width variable transition region between the two states. These models are based on the work of Cahn and Hilliard [77] and are derived using Landau-Ginzberg theory of critical phenomena [78]. A phase field variable p is introduced which has a value of -1 for solid phase and $+1$ in the liquid phase. The length of the transition region between the solid and the liquid phases is controlled by choosing a value of ξ (figure 43) that corresponds to intermediate value of p.

The phase field approach avoids the explicit treatment of the interface conditions as employed in the sharp-interface models. Instead we use a coupled system of nonlinear evolution equations in temperature T and phase variable p [95]

$$\rho c_p \frac{\partial T}{\partial t} - \boldsymbol{\nabla}\boldsymbol{\cdot}(k\boldsymbol{\nabla}T) + \frac{1}{2}L_f \frac{\partial p}{\partial t} = 0 \quad \forall(\boldsymbol{x}, t) \in \Omega_{\boldsymbol{x}t} = \Omega_{\boldsymbol{x}} \times \Omega_t \tag{III.27}$$

$$\alpha\xi^2 \frac{\partial p}{\partial t} - \xi^2 \Delta p + \frac{\partial f}{\partial p} = 0 \qquad \forall(\boldsymbol{x}, t) \in \Omega_{\boldsymbol{x}t} = \Omega_{\boldsymbol{x}} \times \Omega_t \tag{III.28}$$

in which α is related to the kinetic parameter [95], $\Delta = \frac{\partial^2}{\partial x^2} + \frac{\partial^2}{\partial y^2} + \frac{\partial^2}{\partial z^2}$, and $f = f(p, T)$ is referred to as the restoring potential or free energy potential. Equations (III.27) and (III.28) can be interpreted in a simple way. Equation (III.28) is a linear time evolution of p governed by imbalance between the excess interface free energy and the restoring potential $f(p, T)$. The energy equation (III.27) has a source term $\frac{1}{2}L_f \frac{\partial p}{\partial t}$ to account for the latent heat release or absorption at the moving interface. When the phase field equations (III.27) and (III.28) are employed to simulate real solidification or melting problems, we expect that sharp-interface conditions are approached as the interface thickness $\xi \to 0$. The results in phase field models unfortunately depend largely on thermodynamic consistency of the potential $f(p, T)$. The work of Caginalp [96] provides a strong indication that the sharp-interface limit is attained for all forms of free energy potential $f(p, T)$ in which T and p coupling is linear i.e. $\frac{\partial^2 f(p,T)}{\partial p \partial T} = 0$. Given a specific form of $f(p, T)$, the entropy/energy/temperature scales must obey the relationships:

$$\Delta\eta = (\eta_{liquid} - \eta_{solid}) = \left.\frac{\partial f}{\partial T}\right|_{solid}^{liquid} \tag{III.29}$$

$$\Delta\eta\big|_{T=0} = \frac{L_f}{T_m} \tag{III.30}$$

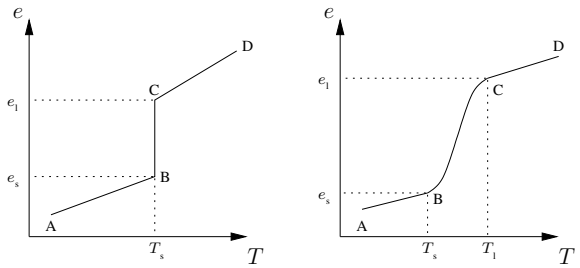

(a) e versus T for sharp interface

(b) e versus T for smooth interface

Figure 42: Sharp- and smooth-interface models for specific internal energy

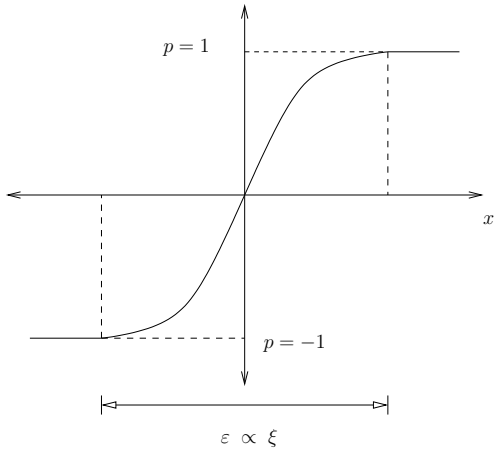

Figure 43: Expected spatial profile of phase field through a solid-liquid interface

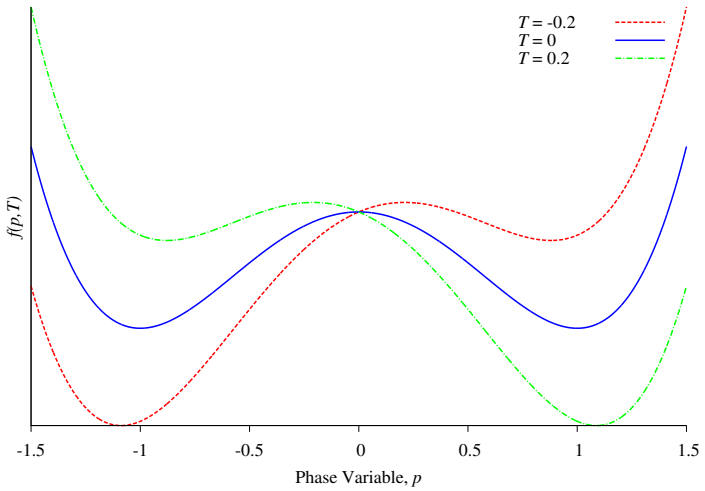

Figure 44: Double-well behavior of restoring potential for various values of temperature

in which η is entropy, $\Delta\eta$ is change in entropy, and T_m is mean temperature. In the Caginalp Potential (CP) model [95], dependence of f on T is taken into account by adding a simple linear term to the double well potential in p.

$$f(p,T) = \frac{1}{8a}(p^2-1)^2 - \frac{\Delta\eta}{2}pT \tag{III.31}$$

The parameter a is chosen such that $\frac{\partial f}{\partial p}$ exhibits three distinct roots, near 0 and ± 1. From (III.31) we note that minima of $f(p,T)$ at $p = \pm 1$ changes as T departs from zero. Figure 44 shows a plot of p versus $f(p,T)$ for $T = 0$, $T < 0$, and $T > 0$ (with $a = \Delta\eta = 1$).

For a finite value of a, a small amount of latent heat is released at positions away from the interface. This undesirable effect fades as $a \to 0$. Indeed, Caginalp et al. [96–99] have established that as $\xi \to 0$ and $a \to 0$ the phase field equations (III.27) and (III.28) with $f(p,T)$ defined by (III.31) produce solutions that approach sharp-interface limits.

Remarks

(1) The phase field models require free energy potential $f(p,T)$. There are some guidelines to establish this but for the most part the procedure is not deterministic.

(2) As in case of sharp-interface models, here also the interface must be defined as initial condition. The phase field models are not capable of initiating phase transition. Obviously, this is a major drawback of these models. This drawback is due to the use of double well function $f(p,T)$.

(3) When the spatial domain is either solid or liquid, the free energy density functions used presently do not allow initiation of the transition zone or front due to the presence of two distinct minima, regardless of the temperature. For example if the spatial domain is liquid and heat is removed from some boundary, the liquid will remain in the liquid state although the temperature may have fallen below the freezing temperature.

(4) This drawback of phase field models presents serious problems in simulating phase transition processes in which initiation and detection of the location of the transition zone is essential as it may not be known a priori.

(5) When the phase transition region is specified as initial condition, the phase field models predict accurate evolution i.e. movement of the transition region.

Mathematical models used in the present work: smooth-interface models (first group of models)

The mathematical models used in the present work presented in this section are derived based on the assumptions that the transition region between the liquid and solid phases occurs over a small temperature change (width of the transition region $[T_s, T_l]$) in which specific heat, thermal conductivity, density, and latent heat of fusion and hence specific internal energy change in a continuous and differentiable manner. Figures 45(a),(b),(c),(d),(e) show distributions of ρ, c_p, k, L_f, and e in the transition region $[T_s, T_l]$ between the solid and liquid phases. The range $[T_s, T_l]$ i.e. the width of the transition region, can be as narrow or as wide as desired by the physics of phase change in a specific application. The transition region is assumed to be homogeneous and isotropic. This assumption is not so detrimental as in this case the constitutive theory only consists of the heat vector due to the zero velocity field and zero stress assumptions.

The mathematical models derived and presented here are same in Lagrangian as well as Eulerian description, and are based on the first law of thermodynamics using specific total energy and the heat vector augmented by the constitutive equation for the heat vector (Fourier heat conduction law) and the statement of specific total energy incorporating the physics of phase transition in the smooth interface zone between liquid and solid phases.

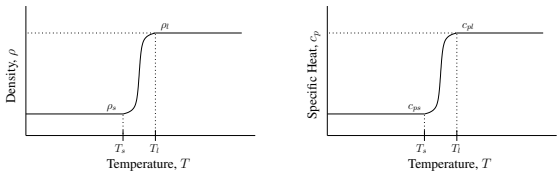

(a) Density ρ in the smooth interface

(b) Specific Heat c_p in the smooth interface

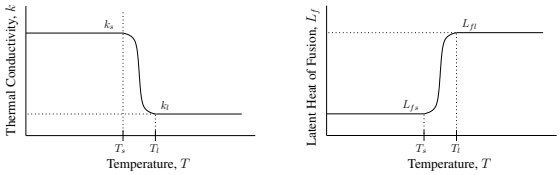

(c) Thermal Conductivity k in the smooth interface

(d) Latent Heat of Fusion L_f in the smooth interface

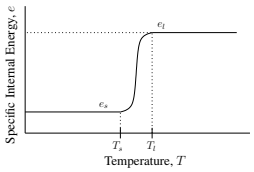

(e) Specific internal energy e in the smooth interface

Figure 45: ρ, c_p, k, L_f and e in the smooth interface transition region between the solid and liquid phases as functions of Temperature T

First Law of Thermodynamics

In the absence of sources and sinks we have

$$\rho \frac{De}{Dt} + \boldsymbol{\nabla} \cdot \boldsymbol{q} = 0 \qquad \forall (\boldsymbol{x}, t) \in \Omega_{\boldsymbol{x}} \times \Omega_t = \Omega_{\boldsymbol{x}} \times (0, \tau) \tag{III.32}$$

Assuming Fourier heat conduction law as constitutive theory for $\boldsymbol{q}$, we can write

$$\boldsymbol{q} = -k(T) \boldsymbol{\nabla} T \qquad \forall (\boldsymbol{x}, t) \in \Omega_{\boldsymbol{x}} \times \Omega_t = \Omega_{\boldsymbol{x}} \times (0, \tau) \tag{III.33}$$

The specific internal energy e is given by

$$e = \int_{T_0}^{T} c_p(T) dT + L_f(T) \tag{III.34}$$

Hence

$$\frac{\partial e}{\partial t} = \frac{\partial}{\partial T} \left(\int_{T_0}^{T} c_p(T) dT + L_f(T) \right) \frac{\partial T}{\partial t} = c_p(T) \frac{\partial T}{\partial t} + \frac{\partial L_f}{\partial t} \tag{III.35}$$

Substituting (III.35) into (III.32)

$$\begin{aligned} \rho(T) c_p(T) \frac{\partial T}{\partial t} + \rho(T) \frac{\partial L_f(T)}{\partial t} + \boldsymbol{\nabla} \cdot \boldsymbol{q} = 0 \\ \forall (\boldsymbol{x}, t) \in \Omega_{\boldsymbol{x}} \times \Omega_t = \Omega_{\boldsymbol{x}} \times (0, \tau) \end{aligned} \tag{III.36}$$

If $Q(T)$ represents any one of the quantities $\rho(T)$, $c_p(T)$, $k(T)$, and $L_f(T)$, then we define

$$Q(T) = \begin{cases} Q_s & ; \quad T < T_s \\ Q(T) & ; \quad T_s \le T \le T_l \\ Q_l & ; \quad T > T_l \end{cases} \tag{III.37}$$

We use the following for $Q(T)$

$$Q(T) = c_0 + \sum_{i=1}^{n} c_i T^i \qquad ; T_s \le T \le T_l \tag{III.38}$$

when $n = 3$, $Q(T)$ is a cubic polynomial in T. The coefficients c_0 and c_i, $i = 1, 2, 3$ in (III.38) are calculated using the conditions:

$$\begin{aligned} &\text{at} \quad T = T_s \ : \qquad Q(T_s) = Q_s \quad , \qquad \left.\frac{\partial Q}{\partial T}\right|_{T=T_s} = 0 \\ &\text{at} \quad T = T_l \ : \qquad Q(T_l) = Q_s \quad , \qquad \left.\frac{\partial Q}{\partial T}\right|_{T=T_l} = 0 \end{aligned} \tag{III.39}$$

when $n = 5$, $Q(T)$ is a 5^{th} degree polynomial in T. The coefficients c_0 and c_i, $i = 1, ..., 5$ in (III.38) are calculated using the conditions:

$$\begin{aligned} &\text{at} \quad T = T_s \ : \quad Q(T_s) = Q_s \ , \left.\frac{\partial Q}{\partial T}\right|_{T=T_s} = \left.\frac{\partial^2 Q}{\partial T^2}\right|_{T=T_s} = 0 \\ &\text{at} \quad T = T_l \ : \quad Q(T_l) = Q_s \ , \left.\frac{\partial Q}{\partial T}\right|_{T=T_l} = \left.\frac{\partial^2 Q}{\partial T^2}\right|_{T=T_l} = 0 \end{aligned} \tag{III.40}$$

Remarks

(1) By letting Q to be ρ, c_p, k and L_f, dependence of these properties on temperature can be easily established.

(2) In case of L_f we note that $L_f(T_s) = 0$ and $L_f(T_l) = L_f$ (value of latent heat of fusion).

(3) Thus all transport properties including latent heat of fusion are explicitly defined as functions of temperature T in the transition region.

We note that

$$\frac{\partial L_f(T)}{\partial t} = \left(\frac{\partial L_f(T)}{\partial T}\right)\left(\frac{\partial T}{\partial t}\right) \tag{III.41}$$

Hence, (III.36) can be written as

$$\left(\rho(T)c_p(T) + \rho(T)\frac{\partial L_f(T)}{\partial T}\right)\frac{\partial T}{\partial t} + \boldsymbol{\nabla \cdot q} = 0 \tag{III.42}$$

and

$$\boldsymbol{q} = -k(T)\boldsymbol{\nabla} T \qquad \forall(\boldsymbol{x}, t) \in \Omega_{\boldsymbol{x}} \times \Omega_t = \Omega_{\boldsymbol{x}} \times (0, \tau) \tag{III.43}$$

Equations (III.42) and (III.43) are smooth-interface mathematical model in dependent variables T and q. $\rho(T)$, $c_p(T)$, $k(T)$, and $L_f(T)$ are defined using (III.37)-(III.40). By substituting q from (III.43) into (III.42), we obtain a single nonlinear diffusion equation for smooth interface phase change model.

$$\left(\rho(T)c_p(T) + \rho(T)\frac{\partial L_f(T)}{\partial T}\right)\frac{\partial T}{\partial t} - \boldsymbol{\nabla \cdot}\big(k(T)\boldsymbol{\nabla}(T)\big) = 0 \tag{III.44}$$

or

$$\left(\rho(T)c_p(T) + \rho(T)\frac{\partial L_f(T)}{\partial T}\right)\frac{\partial T}{\partial t} - \frac{\partial k(T)}{\partial T}\sum_{i=1}^{3}\left(\frac{\partial T}{\partial x_i}\right)^2 - k(T)\Delta T = 0 \tag{III.45}$$

where $\Delta = \frac{\partial^2}{\partial x_1^2} + \frac{\partial^2}{\partial x_2^2} + \frac{\partial^2}{\partial x_3^2}$. $x_1 = x$, $x_2 = y$, and $x_3 = z$ have been used for convenience. Equation (III.45) is the final form of the mathematical model in temperature T.

Remarks

(1) The mathematical models presented in this section can be written in alternate forms. These are summarized in the following based on choice of dependent variables.

Model A: Dependent Variable T

If we consider T as the only dependent variable, then the mathematical model is given by (III.45) i.e.

$$\left(\rho(T)c_p(T) + \rho(T)\frac{\partial L_f(T)}{\partial T}\right)\frac{\partial T}{\partial t} - \frac{\partial k(T)}{\partial T}\sum_{i=1}^{3}\left(\frac{\partial T}{\partial x_i}\right)^2 - k(T)\Delta T = 0 \qquad \forall(\boldsymbol{x}, t) \in \Omega_{\boldsymbol{x}t} = \Omega_{\boldsymbol{x}} \times \Omega_t \tag{III.46}$$

This model requires higher order regularity of approximations of T in finite element processes of calculating numerical solutions for T. This is due to second order derivatives of the temperature with respect to spatial coordinates appearing in (III.46).

Model B: Dependent Variables T, $\boldsymbol{q}$

In this case the mathematical model consists of equations (III.42) and (III.43).

$$\left.\begin{aligned}\left(\rho(T)c_p(T) + \rho(T)\frac{\partial L_f}{\partial T}\right)\frac{\partial T}{\partial t} + \boldsymbol{\nabla}\cdot\boldsymbol{q} = 0 \\ \boldsymbol{q} = -k(T)\cdot\boldsymbol{\nabla}T\end{aligned}\right\} \tag{III.47}$$

This is a system of first order partial differential equations in T and q, hence lower order regularity on both q and T compared to T in Model A.

Model C: Dependent Variables T, L_f

In the mathematical model, rather than replacing $L_f(T)$ with an expression, a function of T, we could also consider L_f as a dependent variable and use $L_f(T) = G(T)$ as addition equation in which $G(T)$ is functional relationship of L_f on T.

$$\left.\begin{aligned}\left(\rho(T)c_p(T) + \rho(T)\frac{\partial L_f}{\partial T}\right)\frac{\partial T}{\partial t} - \frac{\partial k(T)}{\partial T}\sum_{i=1}^{3}\left(\frac{\partial T}{\partial x_i}\right)^2 - k(T)\Delta T = 0 \\ L_f = G(T)\end{aligned}\right\} \tag{III.48}$$

This model is second order in T but first order in L_f.

Model D: Dependent Variables T, $\boldsymbol{q}$, and L_f
In this case we consider the mathematical model (III.47), but also introduce L_f as a dependent variable.

$$\left.\begin{aligned} &\left(\rho(T)c_p(T)+\rho(T)\frac{\partial L_f}{\partial T}\right)\frac{\partial T}{\partial t}+\boldsymbol{\nabla}\cdot\boldsymbol{q}=0\\ &\boldsymbol{q}=-k(T)\boldsymbol{\nabla}T\\ &L_f=G(T)\end{aligned}\right\} \tag{III.49}$$

This is a first order model in T, q, and L_f.

(2) The mathematical models given in remark (1) are all valid models. We present more discussion on these models in the section on numerical studies.

III.2.4 Second group of mathematical models for phase change based on nonzero stress and velocity fields in all phases

When the media are not stress free and the velocity field is not zero, the mathematical models for phase change processes require use of all conservation and balance laws for solid and liquid phases, as well as the transition region. The mathematical models must incorporate the physics of solid, liquid, and transition regions and their interactions during the evolution of the phase change process. In the approach discussed here the mathematical models for all phases are strictly based on conservation and balance laws and the transition region is assumed to be a smooth interface between the solid and the liquid phases. We consider details of the models for all three phases and present discussion regarding their validity and use in determining phase change evolution.

III.2.5 Liquid Phase

If we assume (for simplicity) the liquid phase to be incompressible Newtonian fluid with constant properties, then the mathematical model for this phase is standard continuity, momentum equations, energy equation, and the constitutive theories for contravariant deviatoric Cauchy stress tensor and heat vector in Eulerian description with transport. In the absence of body forces, we have

$$\left.\begin{aligned} &\bar{\rho}_l\bar{\boldsymbol{\nabla}}\cdot\bar{\boldsymbol{v}}=0\\ &\bar{\rho}_l\left(\frac{\partial\bar{v}_i}{\partial t}+\bar{v}_j\frac{\partial\bar{v}_i}{\partial\bar{x}_j}\right)+\frac{\partial\bar{p}}{\partial\bar{x}_i}-\frac{\partial_d\bar{\sigma}^{(0)}_{ij}}{\partial\bar{x}_j}=0\\ &\bar{\rho}_l\bar{c}_{pl}\left(\frac{\partial\bar{T}}{\partial t}+\bar{\boldsymbol{v}}\cdot\bar{\boldsymbol{\nabla}}\bar{T}\right)+\bar{\boldsymbol{\nabla}}\cdot\bar{\boldsymbol{q}}-{}_d\bar{\sigma}^{(0)}_{ji}\bar{D}_{ij}=0\\ &{}_d\bar{\sigma}^{(0)}_{ij}=2\bar{\mu}\bar{D}_{ij}\\ &\bar{\boldsymbol{q}}=-\bar{k}_l\bar{\boldsymbol{\nabla}}\bar{T}\end{aligned}\right\} \tag{III.50}$$

$\bar{p}$ is mechanical pressure assumed positive when compressive. $\bar{\rho}_l$, $\bar{c}_{pl}$, $\bar{k}_l$, $\bar{\mu}$ are the usual constant transport properties of the medium. We remark that $\bar{\boldsymbol{x}}$ are fixed locations at which the state of the matter is monitored as time elapses i.e. $\bar{\boldsymbol{x}}$ location is occupied by different material particles for different values of time. In this mathematical model material point displacements are not monitored.

III.2.6 Solid Phase

In the solid phase the most appropriate form of the mathematical model can be derived using conservation and balance laws in Lagrangian description.

Hyperelastic Solid

If we assume the solid phase to be hyperelastic solid matter, homogeneous, isotropic, and incompressible with infinitesimal deformation and constant material coefficients, then we have the following for continuity, momentum equations in the absence of body forces, energy equation, and the constitutive equations (using $\boldsymbol{\sigma}$ for stress tensor).

$$\left.\begin{aligned}
&\rho_0 = \rho_s \quad \text{as} \quad |J| = 1 \\
&\rho_s \frac{\partial v_i}{\partial t} - \frac{\sigma_{ij}}{\partial x_j} = 0 \\
&\rho_s c_{ps} \frac{\partial T}{\partial t} + \boldsymbol{\nabla \cdot q} = 0 \\
&\sigma_{ij} = D_{ijkl} \varepsilon_{kl} \\
&\varepsilon_{ij} = \frac{1}{2}\left(\frac{\partial u_i}{\partial x_j} + \frac{\partial u_j}{\partial x_i}\right) \\
&v_i = \frac{\partial u_i}{\partial t} \\
&\boldsymbol{q} = -k_s \boldsymbol{\nabla} T
\end{aligned}\right\} \quad \forall (\boldsymbol{x}, t) \in \Omega_{\boldsymbol{x}t} = \Omega_{\boldsymbol{x}} \times \Omega_t \tag{III.51}$$

In this description the locations $\boldsymbol{x}$ are locations of material points, hence the deformation of the material points is monitored during evolution. We note that we can also introduce the stress decomposition $\boldsymbol{\sigma} = -p\boldsymbol{I} + {}_d\boldsymbol{\sigma}$ with $\text{tr}({}_d\boldsymbol{\sigma}) = 0$ in $\mathbb{R}^3$, $\text{tr}({}_d\boldsymbol{\sigma}) - p = 0$ in $\mathbb{R}^2$, and $\text{tr}({}_d\boldsymbol{\sigma}) - 2p = 0$ in $\mathbb{R}^1$ as additional equation relating mechanical pressure p to ${}_d\boldsymbol{\sigma}$. With this decomposition this mathematical model appears to have the same dependent variables (but not necessarily the same physical meaning) as the one for fluid in Section III.2.5.

Hypoelastic Solid

If we assume the solid phase to be hypo-thermoelastic solid matter, isotropic, homogeneous, and incompressible with constant material coefficients then the mathematical model can be derived in Eulerian description with transport. The constitutive theory for the stress tensor for such materials is a rate theory of order one in stress and strain rate tensors i.e. convected time derivative of order one of the stress tensor is related to the convected time derivative of order one of the conjugate strain tensor. If we consider $\bar{\boldsymbol{\sigma}}^{(0)} = -\bar{p}\boldsymbol{I} + {}_d\bar{\boldsymbol{\sigma}}^{(0)}$ decomposition then we have the following for continuity, momentum and energy equations, and the constitutive equations.

$$\left.\begin{aligned}
&\bar{\rho}_s \bar{\boldsymbol{\nabla}} \boldsymbol{\cdot} \bar{\boldsymbol{v}} = 0 \\
&\bar{\rho}_s \left(\frac{\partial \bar{v}_i}{\partial t} + \bar{v}_j \frac{\partial \bar{v}_i}{\partial \bar{x}_j}\right) + \frac{\partial \bar{p}}{\partial \bar{x}_i} - \frac{\partial_d \bar{\sigma}_{ij}^{(0)}}{\partial \bar{x}_j} = 0 \\
&\bar{\rho}_s \bar{c}_{ps} \left(\frac{\partial \bar{T}}{\partial t} + \bar{\boldsymbol{v}} \boldsymbol{\cdot} \bar{\boldsymbol{\nabla}} \bar{T}\right) + \bar{\boldsymbol{\nabla}} \boldsymbol{\cdot} \bar{\boldsymbol{q}} = 0 \\
&{}_d\bar{\sigma}_{ij}^{(1)} = \tilde{D}_{ijkl} \gamma_{kl}^{(1)} \\
&\bar{\boldsymbol{q}} = -\bar{k}_s \bar{\boldsymbol{\nabla}} \bar{T}
\end{aligned}\right\} \tag{III.52}$$

$\bar{\boldsymbol{\sigma}}^{(1)}$ is the first convected time derivative of the deviatoric contravariant Cauchy stress tensor and $\gamma^{(1)}$ is the first convected time derivative of the Almansi strain tensor, a contravariant measure of strain. It has been shown [100] that for thermo-hypoelastic solids the continuity equation in (III.52) must be replaced by $\text{tr}({}_d\bar{\boldsymbol{\sigma}}^{(0)}) = 0$ in $\mathbb{R}^3$, $\text{tr}({}_d\bar{\boldsymbol{\sigma}}^{(0)}) - \bar{p} = 0$ in $\mathbb{R}^2$, and $\text{tr}({}_d\bar{\boldsymbol{\sigma}}^{(0)}) - 2\bar{p} = 0$ in $\mathbb{R}^1$ as additional equation relating mechanical pressure $\bar{p}$ to ${}_d\bar{\boldsymbol{\sigma}}^{(0)}$. We note that in hypoelastic solids, strain rate produces stress as opposed to strain as in the case of hyperelastic solids. Secondly, such a model allows transport which is not present in the deformation of thermoelastic solids.

III.2.7 Transition Region

In the transition region the consideration of the physics of phase transformation and how we account for it in the development of the mathematical model determines the ultimate outcome of the details of the mathematical model. The following approaches are used or are possibilities.

(a) We can assume the transition region as a homogeneous, saturated mixture of fluid and solid constituents with appropriate volume fractions based on temperature. In this approach the solid particles are always mobile, which poses problems as we approach the solid phase. The choice of Lagrangian or Eulerian description (with transport) is also not straightforward. This approach has not been used in phase transition applications.

(b) We assume that freezing or melting in the transition region creates a porous media with variable permeability. This approach has been used but not in conjunction with the full Navier-Stokes equations.

(c) Some variations of mixture theory with various approximations are possible.

Remarks

It is perhaps more straightforward to illustrate the problems associated with these mathematical models and their use in phase transition if we consider sharp interface between solid and liquid regions. In this case purely solid phase is in contact with purely liquid phase. We consider the following:

(1) Lagrangian description with hyperelastic solid assumption is ideal for the solid phase and the Eulerian description with transport is suitable for the liquid phase. In the Lagrangian description the locations $\boldsymbol{x}$ are the positions of the material particles that undergo evolution and thus we have displacements of each material particle in time during evolution.

On the other hand, in Eulerian description with transport the locations $\bar{\boldsymbol{x}}$ are fixed locations that are occupied by different material particles for different values of time. Thus, in this approach we do not have displacement history of each material particle in time during evolution.

At the interface between the solid and the liquid regions, these two mathematical models do not provide interaction. This has been established by Surana et al. [101]. Forcing these mathematical models to interact will produce spurious behavior.

(2) We could consider hypoelastic solid description (Eulerian description with transport) for the solid phase and the Eulerian description with transport for the liquid phase. In this case, interaction between the two phases is intrinsic in the mathematical model and is mathematically consistent.

However the hypoelastic solids have transport which is not the case for solid phase and the first order rate constitutive theory is nonphysical for solid phase as it could yield zero stress in the absence of strain rates. The presence of transport for the solid phase is also problematic during the liquid to solid phase change.

Thus when the stress field and the velocity field are not zero the current mathematical models for solid and liquid phases do not permit interaction of the solid and liquid phases (see Surana et al. [101]).

III.2.8 Third group of mathematical models for phase change: the stress field is assumed to be constant and velocity field is assumed zero in the solid phase but both are nonzero in the liquid phase and transition region

The mathematical models in section III.2.4 fail to provide interaction between the phases. We note that the main source of this problem is that not all dependent variables in the two descriptions describe the same physics. For example velocities in Lagrangian description are time rate of change of displacements of a material point, whereas in Eulerian description the velocities at a location are velocities of different material points for different values of time. Since we want to consider phase transition in the presence of flow, the mathematical models for fluid derived based on conservation and balance laws must remain intact. In the solid region we have displacements, their time derivatives (velocities) and stress (dependent on displacements) in Lagrangian description. These quantities do not have the same physical meaning in case of fluid using Eulerian description with transport, thus must be eliminated

if we seek interaction the two media without changing the mathematical model for fluid. This gives rise to constant stress field and zero velocity field in the solid region. In the transition zone the velocity field must transition from nonzero state at the liquid boundary to zero state at the solid boundary, and the stress must assume a constant value. Thus in this approach only the energy equation provides the connecting link between the solid and transition regions. In the solid region, the energy equation has no transport terms (due to Lagrangian description) and no dissipation terms as the solid phase is thermoelastic, but these would have been zero even otherwise as the velocity field and divergence of the stress field are zero. In the liquid region we have energy equation with transport as well as dissipation, both of which approach zero in the transition region as the state evolves from liquid to solid and hence yields the desired energy equation for the solid phase.

Thus, in this approach we assume that the solid phase has constant stress field and the velocity field is zero in this phase but in the liquid phase we consider full Navier-Stokes equations based on conservation and balance laws. Some aspects of the approach discussed here are also found in [89, 91–93] but differ significantly in the specific details of the mathematical model and numerical computations of the evolution. We consider that the solid and liquid phases have smooth interface in which all transport properties vary in a continuous and differentiable manner as in Section III.2.3. We consider details of the mathematical models in the following.

Liquid Phase

For this phase we consider standard Navier-Stokes equations in Eulerian description (with transport) as used for fluids (constitutive theory for stress based on Newton's law of viscosity).

$$\left.\begin{aligned}
&\bar{\rho}_l \bar{\boldsymbol{\nabla}} \cdot \bar{\boldsymbol{v}} = 0 \\
&\bar{\rho}_l \left(\frac{\partial \bar{v}_i}{\partial t} + \bar{v}_j \frac{\partial \bar{v}_i}{\partial \bar{x}_j} \right) + \frac{\partial \bar{p}}{\partial \bar{x}_i} - \frac{\partial_d \bar{\sigma}^{(0)}_{ij}}{\partial \bar{x}_j} = 0 \\
&\bar{\rho}_l \bar{c}_{pl} \left(\frac{\partial \bar{T}}{\partial t} + \bar{\boldsymbol{v}} \cdot \bar{\boldsymbol{\nabla}} \bar{T} \right) + \bar{\boldsymbol{\nabla}} \cdot \bar{\boldsymbol{q}} - {}_d\bar{\sigma}^{(0)}_{ji} \bar{D}_{ij} = 0 \\
&{}_d\bar{\sigma}^{(0)}_{ij} = 2\bar{\mu} \bar{D}_{ij} \\
&\bar{\boldsymbol{q}} = -\bar{k}_l \bar{\boldsymbol{\nabla}} \bar{T}
\end{aligned}\right\} \tag{III.53}$$

Solid Phase

Since in the solid phase the stress field is assumed constant and the velocity field is assumed zero, the mathematical model for this phase only consists of the energy equation and the constitutive theory for heat vector. In the absence of the velocity field and stress field, there is no distinction between the Lagrangian and the Eulerian descriptions, but we use overbar to provide transparency between this description and the one given by (III.53).

$$\left.\begin{aligned}
&\bar{\boldsymbol{\nabla}} \cdot {}_d\bar{\boldsymbol{\sigma}}^{(0)} = 0 \\
&\bar{\rho}_s \bar{c}_{ps} \frac{\partial \bar{T}}{\partial t} + \bar{\boldsymbol{\nabla}} \cdot \bar{\boldsymbol{q}} = 0 \\
&\bar{\boldsymbol{q}} = -\bar{k}_s \bar{\boldsymbol{\nabla}} \bar{T}
\end{aligned}\right\} \quad \forall (\bar{\boldsymbol{x}}, t) \in \Omega_{\bar{\boldsymbol{x}}t} = \Omega_{\bar{\boldsymbol{x}}} \times \Omega_t \tag{III.54}$$

In this region we note that the momentum equations in (III.53) must be satisfied for zero velocity field with zero pressure gradient. From the first set of equations in (III.54) we note that a constant deviatoric Cauchy stress field is admissible. The values of the constant stresses in the solid region are determined by the values of the stresses at the solid-liquid interface. In other words, the constant of integration in the first set of equations in (III.54) is determined using the values of the stresses at the solid-liquid interface. Since the stress gradients are zero in the solid region, the stress values in the solid region remain constant and their values are same as those at the liquid-solid interface (see numerical studies in section III.3.13).

Transition Region

In the transition region from liquid to solid the mathematical model transitions from (III.53) to (III.54) or vice versa. As in Section III.2.3, we consider a transition region $[\bar{T}_s, \bar{T}_l]$ in temperature. In this region we assume that $\bar{k}$, $\bar{c}_p$, $\bar{\rho}$ transition from solid to liquid values in a continuous and differentiable manner as described in Section III.2.3. Let $\bar{f}_l$ and $\bar{f}_s$ be the liquid and solid fractions with $\bar{f}_s = 1 - \bar{f}_l$ and $0 \leq \bar{f}_l \leq 1$ in the transition region. We also assume that release or absorption of latent heat of fusion L_f is also continuous and differentiable in the transition region.

Combined Mathematical Model

The mathematical models for solid, liquid, and transition phases can be combined into a single mathematical model.

$$\left.\begin{aligned}
&\bar{f}_l \bar{\rho}(\bar{T}) \bar{\boldsymbol{\nabla}} \cdot \bar{\boldsymbol{v}} = 0 \\
&\bar{f}_l \bar{\rho}(\bar{T}) \left(\frac{\partial \bar{v}_i}{\partial t} + \bar{v}_j \frac{\partial \bar{v}_i}{\partial \bar{x}_j} \right) + \bar{f}_l \frac{\partial \bar{p}}{\partial \bar{x}_i} - \frac{\partial_d \bar{\sigma}_{ij}^{(0)}}{\partial \bar{x}_j} = 0 \\
&\bar{\rho}(\bar{T}) \left(\bar{c}_p(\bar{T}) + \frac{\partial \bar{L}_f(\bar{T})}{\partial \bar{T}} \right) \left(\frac{\partial \bar{T}}{\partial t} + \bar{f}_l \bar{\boldsymbol{v}} \cdot \bar{\boldsymbol{\nabla}} \bar{T} \right) \\
&\qquad\qquad + \bar{\boldsymbol{\nabla}} \cdot \bar{\boldsymbol{q}} - \bar{f}_l \left({}_d\bar{\sigma}_{ji}^{(0)} \bar{D}_{ij} \right) = 0 \\
&\bar{f}_l \left({}_d\bar{\sigma}_{ij}^{(0)} \right) = 2 \bar{\mu} \bar{D}_{ij} \\
&\bar{\boldsymbol{q}} = -\bar{k}(\bar{T}) \bar{\boldsymbol{\nabla}} \bar{T}
\end{aligned}\right\} \qquad \text{(III.55)}$$

where

$$\begin{aligned}
\bar{f}_l = 1 \quad &; \quad \text{liquid phase} \\
\bar{f}_l = 0 \quad &; \quad \text{solid phase} \\
0 \leq \bar{f}_l \leq 1 \quad &; \quad \bar{T}_s \leq \bar{T} \leq \bar{T}_l
\end{aligned} \qquad \text{(III.56)}$$

From (III.55) and (III.56) we note that in the solid phase $\bar{f}_l = 0$, hence continuity equation is identically zero, $\frac{\partial \bar{L}_f}{\partial \bar{T}} = 0$ and the others reduce to

$$\left.\begin{aligned}
&\frac{\partial_d \bar{\sigma}_{ij}^{(0)}}{\partial \bar{x}_j} = 0 \\
&\bar{\rho}_s \bar{c}_{ps} \frac{\partial \bar{T}}{\partial t} + \bar{\boldsymbol{\nabla}} \cdot \bar{\boldsymbol{q}} = 0 \\
&\bar{\boldsymbol{q}} = -\bar{k}_s \bar{\boldsymbol{\nabla}} \bar{T} \\
&\bar{D}_{ij} = 0
\end{aligned}\right\} \qquad \forall (\bar{\boldsymbol{x}}, t) \in \Omega_{\bar{\boldsymbol{x}}t} = \Omega_{\bar{\boldsymbol{x}}} \times \Omega_t \qquad \text{(III.57)}$$

Comparing (III.57) with (III.53) we note that $\bar{v} = 0$ and thus $\bar{D}_{ij} = 0$, and $\frac{\partial_d \bar{\sigma}_{ij}^{(0)}}{\partial \bar{x}_j} = 0$, therefore (III.53) reduces to (III.57), which is same as (III.54). Presence of the first equation in (III.57) is essential as it ensures that it is oscillation free so that $\frac{\partial_d \bar{\sigma}_{ij}^{(0)}}{\partial \bar{x}_j} = 0$ would hold precisely everywhere in the solid phase. Thus the challenge in the mathematical model (III.55),(III.56) is to ensure that $\bar{D}_{ij} = 0$ is achieved in the solid phase which would ensure that $\bar{v}$ and its gradients as well as the gradients of ${}_d\bar{\boldsymbol{\sigma}}^{(0)}$ are zero in the solid phase. The momentum equation in (III.55) (or (III.57)) when satisfied for zero velocity field ensures that $\bar{\boldsymbol{\nabla}} \cdot {}_d\bar{\boldsymbol{\sigma}}^{(0)}$ is identically zero and oscillation free in the solid phase.

This mathematical model is used in the present work to present numerical studies for phase change when the stress field and the velocity field in the liquid phase are not zero.

III.3 Numerical solutions of evolutions of phase change initial value problems

The mathematical models describing the phase change evolutions are nonlinear partial differential equations. Based on the work of Surana et al. [44,79,81], space-time least squares finite element processes for an increment of time with time marching are ideally suited for obtaining numerical solutions of phase change evolution. See [44, 79, 81, 102] for details. First we nondimensionalize the mathematical models derived in section III.2 (only those used in this work).

The numerical solutions presented here for all model problems are converged solutions that are independent of h and p for minimally conforming k [41–43]. For every increment of time, the integrated sum of squares of the residuals for the space-time discretization are always of the order of $O(10^-6)$ or lower, ensuring that the governing differential equations are satisfied in the pointwise sense as the space-time integrals are Riemann for the space-time discretizations.

III.3.1 Dimensionless form of the mathematical models used in the present work

In the following we present dimensionless form of the mathematical models of phase change based on: (*i*) the assumption that stress field and velocity field are zero in solid, liquid, and transition phases, and (*ii*) the assumption that in the solid phase the stress field and velocity field are zero but in the liquid phase full Navier-Stokes equations constitute the mathematical model.

In both models the transition zone of width $[T_s, T_l]$ in temperature is assumed homogeneous and isotropic in which ρ, c_p, k make transition from solid to liquid phase and vice versa in a continuous and differentiable manner.

In order to nondimensionalize the mathematical models we choose reference quantities to obtain dimensionless dependent and independent variables and other quantities. The quantities with hat (ˆ) are with their usual dimensions, quantities with zero subscript are reference quantities and the quantities without hat (ˆ) are dimensionless quantities. We define

$$\begin{aligned}
&x_i = \hat{x}_i/L_0 \quad , \quad v_i = \hat{v}_i/v_0 \\
&\mu = \hat{\mu}/\mu_0 \quad , \quad p = \hat{p}/p_0 \\
&{}_d\sigma_{ij}^{(0)} = {}_d\hat{\sigma}_{ij}^{(0)}/\tau_0 \quad , \quad L_f = \hat{L}_f/L_{f0} \\
&k = \hat{k}/k_0 \quad , \quad c_p = \hat{c}_p/c_{p0} \quad , \quad \rho = \hat{\rho}/\rho_0 \\
&T = (\hat{T} - T_0)/T_0 \quad , \quad t = \hat{t}/t_0 \quad , \quad \boldsymbol{q} = \hat{\boldsymbol{q}}/q_0
\end{aligned} \tag{III.58}$$

III.3.2 Mathematical model based on the assumption of zero stress and zero velocity field in all phases (first group of models)

Recall the following mathematical model presented in Section III.2.3.

$$\hat{\rho}\hat{c}_p \frac{\partial \hat{T}}{\partial \hat{t}} + \hat{\boldsymbol{\nabla}} \cdot \hat{\boldsymbol{q}} + \hat{\rho} \frac{\partial \hat{L}_f}{\partial \hat{t}} = 0 \qquad \forall \ (\hat{\boldsymbol{x}}, t) \ \in \ \Omega_{\hat{\boldsymbol{x}}t} \tag{III.59}$$

$$\hat{\boldsymbol{q}} = -\hat{k}\hat{\boldsymbol{\nabla}}\hat{T} \qquad \forall \ (\hat{\boldsymbol{x}}, t) \ \in \ \Omega_{\hat{\boldsymbol{x}}t} \tag{III.60}$$

Using (III.58) in (III.59) and (III.60), we obtain

$$\rho c_p \frac{\partial T}{\partial t} + \left(\frac{q_0 t_0}{L_0 \rho_0 c_{p0} T_0} \right) \boldsymbol{\nabla} \cdot \boldsymbol{q} + \left(\frac{L_{f0}}{c_{p0} T_0} \right) \rho \frac{\partial L_f}{\partial t} = 0 \tag{III.61}$$

$$\boldsymbol{q} = -\left(\frac{1}{q_0} \right) \left(\frac{k_0 T_0}{L_0} \right) k \boldsymbol{\nabla} T \tag{III.62}$$

If we choose

$$q_0 = k_0 T_0 / L_0 \tag{III.63}$$

Then, (III.61) and (III.62) can be written as

$$\rho c_p \frac{\partial T}{\partial t} + \left(\frac{t_0 k_0}{L_0^2 \rho_0 c_{p0}} \right) \boldsymbol{\nabla} \cdot \boldsymbol{q} + \left(\frac{L_{f0}}{c_{p0} T_0} \right) \rho \frac{\partial L_f}{\partial t} = 0 \tag{III.64}$$

$$\boldsymbol{q} = -k \boldsymbol{\nabla} T \tag{III.65}$$

Since the velocity field is assumed zero, t_0 cannot be defined using L_0 and v_0. We can choose the following:

$$t_0 = L_0^2 \rho_0 c_{p0} / k_0 \qquad , \qquad L_{f0} = c_{p0} T_0 \tag{III.66}$$

Using (III.66), the mathematical model (III.64) and (III.65) reduces to

$$\rho c_p \frac{\partial T}{\partial t} + \boldsymbol{\nabla} \cdot \boldsymbol{q} + \rho \left(\frac{\partial L_f}{\partial T} \right) \frac{\partial T}{\partial t} = 0 \tag{III.67}$$

$$\boldsymbol{q} = -k \boldsymbol{\nabla} T \tag{III.68}$$

Equations (III.67) and (III.68) are a system of first order PDEs in T and $\boldsymbol{q}$ in which reference time t_0 and reference latent heat of fusion L_{f0} are defined by (III.66). Alternatively, if we substitute $\boldsymbol{q}$ from (III.68) into (III.67), then we obtain a single PDE in temperature T.

$$\rho c_p \frac{\partial T}{\partial t} - \boldsymbol{\nabla} \cdot (k \boldsymbol{\nabla} T) + \rho \left(\frac{\partial L_f}{\partial T} \right) \frac{\partial T}{\partial t} = 0 \tag{III.69}$$

Equation (III.69) contains up to second order derivatives of temperature T in space coordinates. The mathematical models (III.67) and (III.68) as well as (III.69) can be used in numerical studies, but the choice of local approximations for minimally conforming approximation spaces differ in the two. Since $L_f = L_f(T)$, $\frac{\partial L_f}{\partial T}$ is strictly deterministic. Other mathematical models (Model C and Model D) presented in Section III.2.3 have similar dimensionless forms.

III.3.3 Mathematical model when the stress field is assumed constant and the velocity field is assumed zero in the solid phase but nonzero in both the liquid and transition regions (third group of models)

Recall the mathematical model given by (III.55) and (III.56)

$$\left.\begin{aligned}
&\bar{f}_l \hat{\bar{\rho}}(\hat{\bar{T}}) \hat{\boldsymbol{\nabla}} \cdot \hat{\boldsymbol{v}} = 0 \\
&\bar{f}_l \hat{\bar{\rho}}(\hat{\bar{T}}) \left(\frac{\partial \hat{\bar{v}}_i}{\partial \hat{t}} + \hat{\bar{v}}_j \frac{\partial \hat{\bar{v}}_i}{\partial \hat{\bar{x}}_j} \right) + \bar{f}_l \frac{\partial \hat{\bar{p}}}{\partial \hat{\bar{x}}_i} - \frac{\partial_d \hat{\bar{\sigma}}_{ij}^{(0)}}{\partial \hat{\bar{x}}_j} = 0 \\
&\hat{\bar{\rho}}(\hat{\bar{T}}) \left(\hat{\bar{c}}_p(\hat{\bar{T}}) + \frac{\partial \hat{\bar{L}}_f(\hat{\bar{T}})}{\partial \hat{\bar{T}}} \right) \left(\frac{\partial \hat{\bar{T}}}{\partial \hat{t}} + \bar{f}_l \hat{\boldsymbol{v}} \cdot \hat{\boldsymbol{\nabla}} \hat{\bar{T}} \right) \\
&\qquad\qquad + \hat{\boldsymbol{\nabla}} \cdot \hat{\boldsymbol{q}} - \bar{f}_l \left({}_d \hat{\bar{\sigma}}_{ji}^{(0)} \hat{\bar{D}}_{ij} \right) = 0 \\
&\bar{f}_l \left({}_d \hat{\bar{\sigma}}_{ij}^{(0)} \right) = 2 \hat{\bar{\mu}} \hat{\bar{D}}_{ij} \\
&\hat{\boldsymbol{q}} = -\hat{\bar{k}}(\hat{\bar{T}}) \hat{\boldsymbol{\nabla}} \hat{\bar{T}}
\end{aligned}\right\} \tag{III.70}$$

where

$$\begin{aligned}
\bar{f}_l = 1 \quad &; \quad \text{liquid phase} \\
\bar{f}_l = 0 \quad &; \quad \text{solid phase} \\
0 \le \bar{f}_l \le 1 \quad &; \quad \hat{\bar{T}}_s \le \hat{\bar{T}} \le \hat{\bar{T}}_l
\end{aligned} \tag{III.71}$$

Dimensionless forms of (III.70) and (III.71) can be obtained using (III.58):

$$\left.\begin{aligned}
&\bar{f}_l\bar{\rho}(\bar{T})\bar{\boldsymbol{\nabla}}\cdot\bar{\boldsymbol{v}}=0\\
&\bar{f}_l\bar{\rho}(\bar{T})\left(\frac{\partial\bar{v}_i}{\partial t}+\bar{v}_j\frac{\partial\bar{v}_i}{\partial\bar{x}_j}\right)+\bar{f}_l\left(\frac{p_0}{\rho_0 v_0^2}\right)\frac{\partial\bar{p}}{\partial\bar{x}_i}\\
&\qquad\qquad-\left(\frac{\tau_0}{\rho_0 v_0^2}\right)\frac{\partial_d\bar{\sigma}_{ij}^{(0)}}{\partial\bar{x}_j}=0\\
&\bar{\rho}(\bar{T})\left(\frac{1}{Ec}\bar{c}_p(\bar{T})+\frac{L_{f0}}{v_0^2}\frac{\partial\bar{L}_f(\bar{T})}{\partial\bar{T}}\right)\left(\frac{\partial\bar{T}}{\partial t}+\bar{f}_l\bar{\boldsymbol{v}}\cdot\bar{\boldsymbol{\nabla}}\bar{T}\right)\\
&\qquad+\frac{1}{ReBr}\bar{\boldsymbol{\nabla}}\cdot\bar{\boldsymbol{q}}-\bar{f}_l\left(\frac{\tau_0}{\rho_0 v_0^2}\right)\left({}_d\bar{\sigma}_{ji}^{(0)}\bar{D}_{ij}\right)=0\\
&\bar{f}_l\left({}_d\bar{\sigma}_{ij}^{(0)}\right)=\left(\frac{\mu_0 v_0}{L_0\tau_0}\right)2\bar{\mu}\bar{D}_{ij}\\
&\bar{\boldsymbol{q}}=-\bar{k}(\bar{T})\bar{\boldsymbol{\nabla}}\bar{T}
\end{aligned}\right\}\qquad\text{(III.72)}$$

where

$$\begin{aligned}
\bar{f}_l=1\quad &;\quad \text{liquid phase}\\
\bar{f}_l=0\quad &;\quad \text{solid phase}\\
0\le\bar{f}_l\le 1\quad &;\quad \bar{T}_s\le\bar{T}\le\bar{T}_l\\
Re=\frac{\rho_0 v_0 L_0}{\mu_0}\quad &;\quad \text{Reynolds Number}\\
Br=\frac{\mu_0 v_0^2}{k_0 T_0}\quad &;\quad \text{Brinkman Number}
\end{aligned}\qquad\text{(III.73)}$$

Remarks

(1) We keep in mind that in the solid phase the momentum equations must be satisfied for zero velocity field and constant stress field i.e. in the solid phase $\partial\bar{v}_i/\partial\bar{x}_j=0$ and $\partial_d\bar{\sigma}_{ij}^{(0)}/\partial\bar{x}_j=0$ must hold in the solid phase.

(2) Based on (1), it may be possible to redefine new dependent variables so that during numerical computations, conditions in (1) are also satisfied with this choice. This indeed is the case as shown in the model problems in section III.3.14.

III.3.4 Computational methodology for computing evolution of IVP describing phase change

The mathematical models describing phase change are a system of nonlinear partial differential equations. Numerical solutions are computed using space-time least squares finite element processes for a space-time strip (in $\mathbb{R}^1$) or a space-time slab (in $\mathbb{R}^2$) the with time marching. The mathematical models utilized in the computational studies are a system of PDEs. In case of $\mathbb{R}^1$, the space-time domain of a space-time strip for an increment of time is discretized using nine-node p-version space-time elements. In case of $\mathbb{R}^2$, the space-time slab is discretized using 27-node p-version space-time elements. Local approximations of class C^0 and C^1 in space and time are in the computations.

For an increment of time i.e. for a space-time strip or a slab, solution of the non-linear algebraic systems is obtained using Newton's linear method with line search. Newton's linear method is considered converged when the absolute value of each component of $\delta I=\{g\}$ is below a preset threshold Δ, numerically computed zero. $\Delta\le 10^{-6}$ has been used in all numerical studies. Discretization and p-levels (considered to be uniform in space and time) are chosen such that the least squares functional I resulting from the residuals for the entire space-time strip or slab is always of order of $O(10^{-6})$ or lower and hence good accuracy of the evolution is always ensured.

III.3.5 1D phase change model problems

We consider three model problems. In the first model problem we present a comparison of the smooth-interface solutions (present approach) with the theoretical solution obtained using the sharp-interface method. In the other two model problems we consider solid-liquid and liquid-solid phase change.

III.3.6 Model Problem 1: Comparison of Sharp- and Smooth-Interface Solutions

The sharp interface solution [84] has only been reported for constant material coefficients. When the material coefficients vary, i.e. are a function of temperature, the theoretical solution of the resulting mathematical model has not been reported, perhaps due to complexity. We choose $\rho = 1$, $c_p = 1$, $k = 1$, and $L_f = 1$. The spatial domain consists of $0 \leq x \leq 1$. Figure 46 shows a space-time strip $\Omega_{xt} = [0, 1] \times [0, \Delta t]$. The space-time domain Ω_{xt} is discretized using a uniform mesh of 500 p-version nine node space-time elements. The spatial domain $[1, 4] \times [0, \Delta t]$ is discretized using a 30 element uniform mesh. The spatial domain $1 \leq x \leq 4$ is added to $0 \leq x \leq 1$ to approximate the boundary condition at $x = \infty$ in the theoretical solution with $x = 4$ in the computed solution.

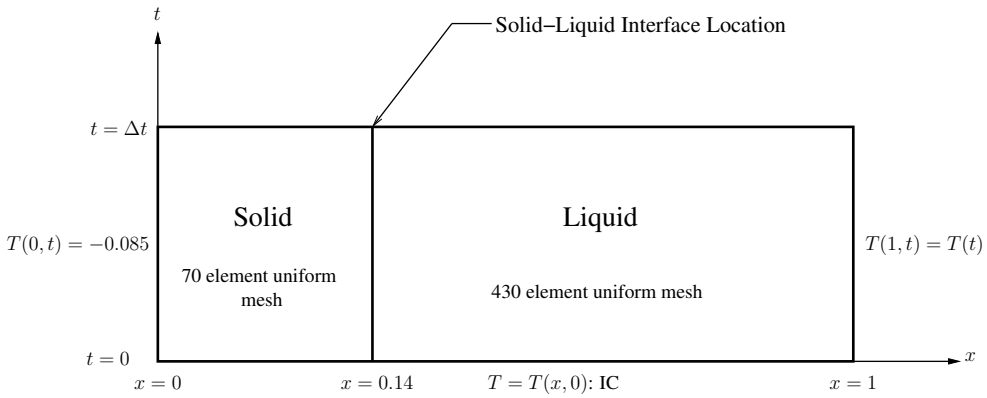

Figure 46: Schematic of first space-time strip, BCs, IC, and spatial discretization

The initial conditions on temperature T at $t = 0$ are defined piecewise by the following.

$$\begin{aligned} \Theta(x) &= C_1 \frac{\text{erf}\big(\beta/2\big) - \text{erf}\big(x/2\sqrt{t_0}\big)}{\text{erf}\big(\beta/2\big)} \quad ; \qquad x \leq \Gamma_x(0) \\ \Theta(x) &= C_2 \frac{\text{erf}\big(\beta/2\big) - \text{erf}\big(x/2\sqrt{t_0}\big)}{\text{erfc}\big(\beta/2\big)} \quad ; \qquad x > \Gamma_x(0) \end{aligned} \tag{III.74}$$

In the theoretical solution for sharp-interface (III.23)–(III.26), the following coefficients are used.

$$\begin{aligned} C_1 &= -0.085 \qquad C_2 = -0.015 \\ t_0 &= 0.1246 \qquad \beta = 0.396618 \end{aligned} \tag{III.75}$$

The mathematical model (III.69) is used for computing smooth-interface solutions. For smooth-interface solutions the transition region is defined by $[T_s, T_l] = [-0.001, 0.001]$. p-levels in space and time are chosen to be 7, with solutions of class C^1 in space and time. Figure 47 shows a plot of the initial condition at $t = 0$.

In the smooth-interface solutions we also use $\rho = 1$, $c_p = 1$, $k = 1$, and $L_f = 1$ i.e. constant material coefficients regardless of phase. The evolution is computed using $\Delta t = 0.01$ for 100 time steps i.e. up to $t = 1.0$. The latent heat L_f is expressed as a polynomial in temperature T in the transition zone. Generally a cubic or fifth degree polynomial in T for L_f is found adequate

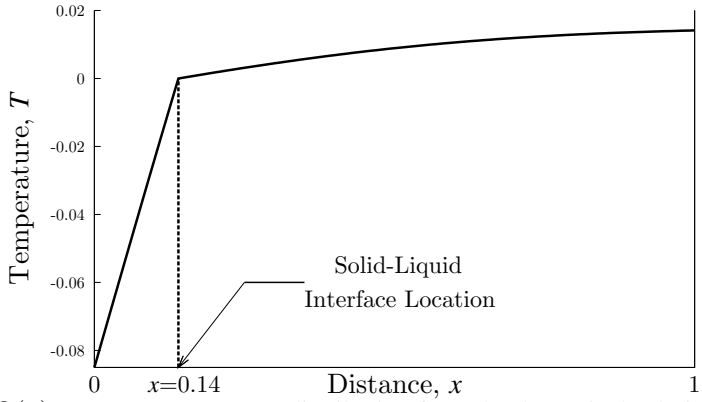

Figure 47: Initial condition $\Theta(x)$ at $t = 0$, temperature distribution from the theoretical solution of the sharp-interface model

(equations (III.37)–(III.40)). Evolution of temperature and latent heat for $0 \leq t \leq 1$ from smooth interface and comparison with sharp-interface solution are shown in figures 48 and 49. Interface location versus time t from smooth and sharp interface locations are compared in figure 50. Center of the transition region is considered as interface location in smooth interface solution.

From figures 48–50 we note that smooth-interface solutions are in good agreement with sharp-interface solutions. The sharp-interface theoretical solution is only possible for constant ρ, c_p, and k, whereas smooth-interface solutions are possible for variable ρ, c_p, and k. Smooth-interface solutions with transitions in material coefficients due to phase change describes physics of phase transitions more precisely.

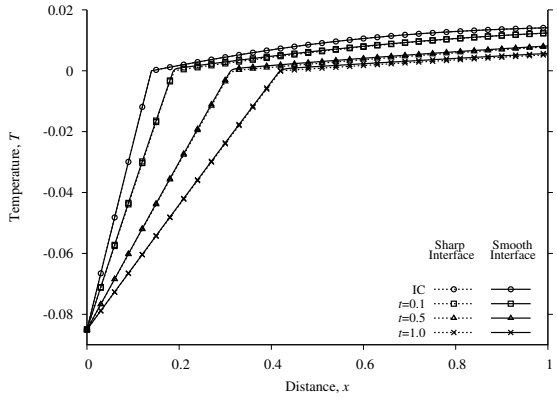

Figure 48: Model Problem 1: Evolution of temperature using smooth-interface model and sharp-interface theoretical solution, $C^{11}(\bar{\Omega}^e_{xt}), p = 7, \Delta t = 0.01$

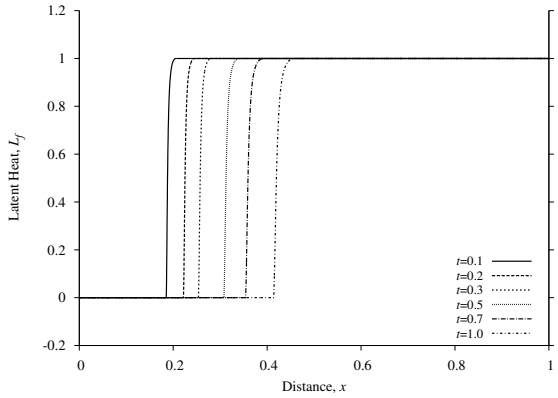

Figure 49: Model Problem 1: Evolution of latent heat (smooth interface), $C^{11}(\bar{\Omega}^e_{xt}), p = 7, \Delta t = 0.01$

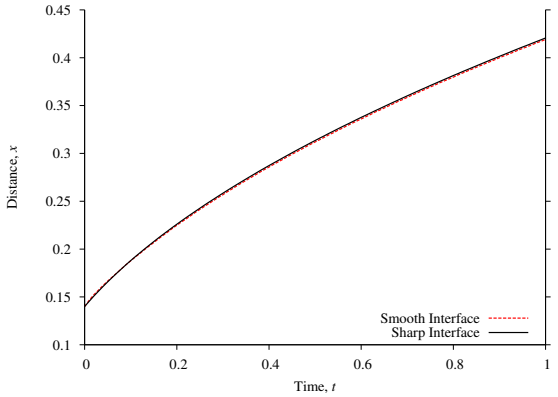

Figure 50: Model Problem 1: Interface location as a function of time, $C^{11}(\bar{\Omega}^e_{xt}), p = 7, \Delta t = 0.01$

III.3.7 Transport properties and reference quantities for liquid-solid and solid-liquid transition numerical studies with zero stress and velocity fields in all phases

In all numerical studies using zero velocity and zero stress field for the entire domain, we consider the liquid phase to be water and the solid phase to be ice with the following properties.

Water: $\hat{\rho}_l = 62.38\ lbm/ft^3$
$\hat{c}_{pl} = 1.006\ Btu/lbm\ R$
$\hat{k}_l = 9.01 \times 10^{-5}\ Btu/s\ ft\ R$
$\hat{L}_{fl} = 143.6\ Btu/lbm$
$\hat{\mu} = 0.12 \times 10^{-2}\ lbm/ft\ s$

Ice: $\hat{\rho}_s = 57.16\ lbm/ft^3$
$\hat{c}_{ps} = 0.4896\ Btu/lbm\ R$
$\hat{k}_s = 3.57 \times 10^{-4}\ Btu/s\ ft\ R$
$\hat{L}_{fs} = 0.000\ Btu/lbm$
$\hat{E} = 6.05 \times 10^6\ lbm/ft\ s^2$
$\nu = 0.33$

Transition region:

In the transition region $\rho(T)$, $c_p(T)$, $k(T)$ and $L_f(T)$ are assumed to vary in a continuous and differentiable manner between the temperatures T_s and T_l defining the transition region between solid and liquid phases.

Reference quantities:

Regardless of solid-liquid or liquid-solid phase transition we consider the following reference quantities:

$$\rho_0 = \hat{\rho}_s \quad , \quad k_0 = \hat{k}_s \quad , \quad c_{p0} = \hat{c}_{ps}$$
$$T_0 = (32^\circ F + 459.67) = 491.67\ R \quad , \quad L_0 = 0.25 ft$$
$$L_{f0} = c_{p0} T_0 = 240.72\ Btu/lbm$$
$$t_0 = \frac{L_0^2 \rho_0 c_{p0}}{k_0} = 4.899 \times 10^3\ s = 81.65 min$$

III.3.8 Model Problem 2: 1D Liquid-Solid Phase Change; Initiation and Propagation of Phase Transition

In this model problem we consider 1D liquid-solid phase change with variable material coefficients and to demonstrate the ability of the proposed formulation in initiating phase transition as well as in simulating its evolution as time elapses. Numerical solutions are calculated and compared for constant density ($\hat{\rho} = \hat{\rho}_l$ in all phases) as well as variable density. Figure 51 shows space-time strip $\bar{\Omega}_{xt} = [0,1] \times [0, \Delta t]$, initial conditions, and boundary conditions.

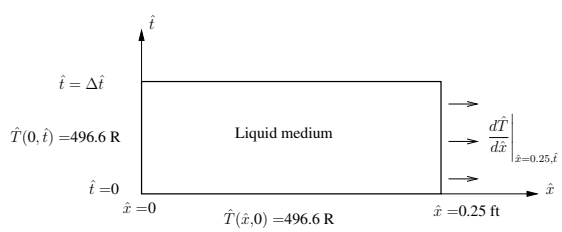

(a) Space-time strip

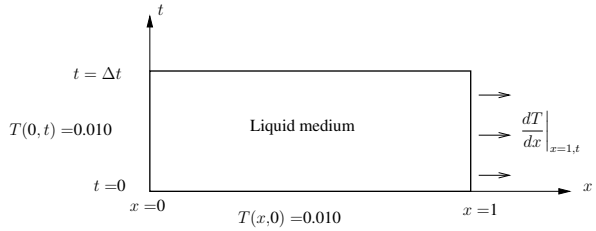

(b) Dimensionless space-time strip

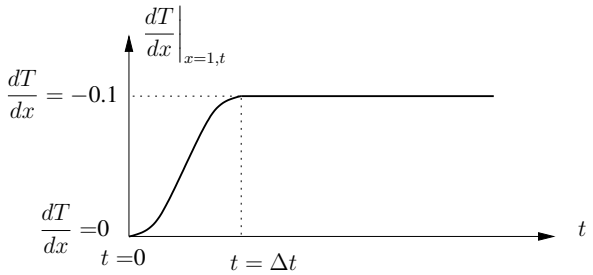

(c) Boundary condition $\frac{dT}{dx}$ at $x = 1$

Figure 51: Liquid-solid phase transition: space-time strip, boundary conditions, and initial condition

We consider solutions of class C^{11} with p-level of 9 in space and time. With this choice the space-time integrals are Riemann in time but Lebesgue in space. This choice functions quite well in simulating the evolution (low residuals). We choose the phase transition zone $[T_s, T_l]$ to be $[-0.001, 0.001]$. A different (smaller or larger) choice of transition zone width in temperature does not alter the location of the center of the transition region.

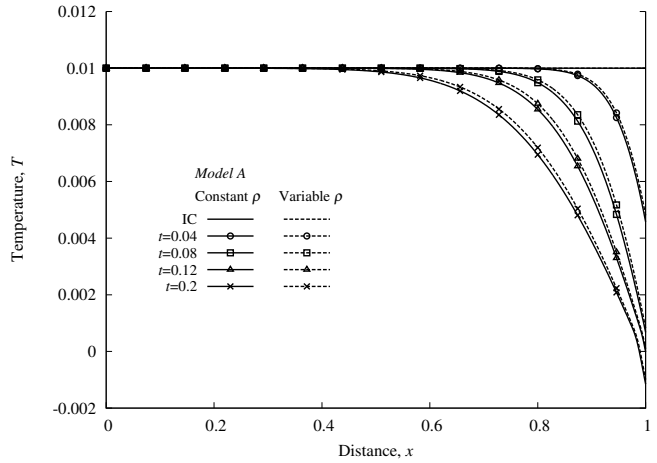

(a) Evolution of temperature, $0.0 \leq t \leq 0.2$

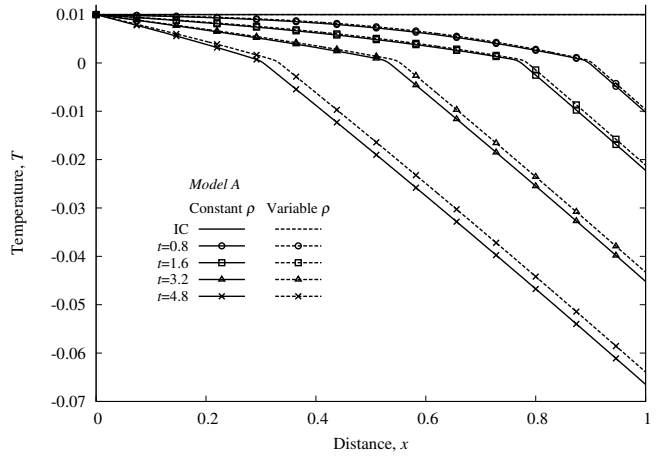

(b) Evolution of temperature, $0.0 \leq t \leq 4.8$

Figure 52: Model Problem 2: Evolution of temperature for liquid-solid phase change, $C^{11}(\bar{\Omega}^e_{xt}), p = 9, \Delta t = 0.04$

Computed numerical results are presented in figures 52–56. Figures 52(a), 53(a), 54(a), 55(a), 56(a) show plots of T, L_f, ρ, c_p, and k versus x during initial stages of the evolution ($0 \leq t \leq 0.2$). Continuous extraction of heat from the right boundary progressively lowers the temperature at the boundary and in the neighborhood of the boundary which eventually results in the initiation of phase change. Variations in $L_f(T)$, $c_p(T)$, $k(T)$ and $\rho(T)$ follow changes in temperature during evolution. From figure 52(a) we note that both constant and variable densities yield almost the same evolution of the temperature during initial stages of the evolution. Figures 53(a), 55(a), and 56(a) show differences in the evolution of L_f, c_p, and k for constant and variable densities even in the very early stages of the evolution. Constant density results lag variable density solutions.

Figures 52(b), 53(b), 54(b), 55(b), 56(b) show fully formed phase change transition region (liquid to solid) beginning with $t = 0.8$ and its propagation during evolution ($0.8 \leq t \leq 4.8$). For most space-time strips during time marching using $\Delta t = 0.04$, $I < O(10^{-6})$ and $|(g_i)|_{max} \leq 10^{-6}$ ensure accurate evolution that satisfies GDE quite well over the entire space-time domain of each space-time strip. Evolutions of all quantities are smooth and free of oscillations. The influence of variable density can be seen clearly in these graphs. The variable density results lead constant density evolution and the difference between them increases as

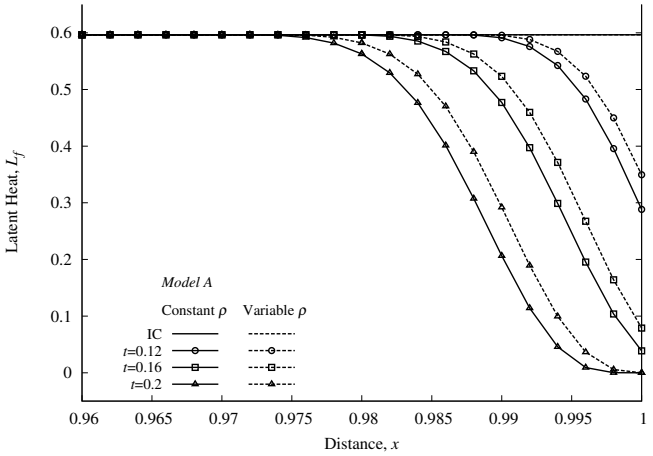

(a) Evolution of latent heat, $0.0 \leq t \leq 0.2$

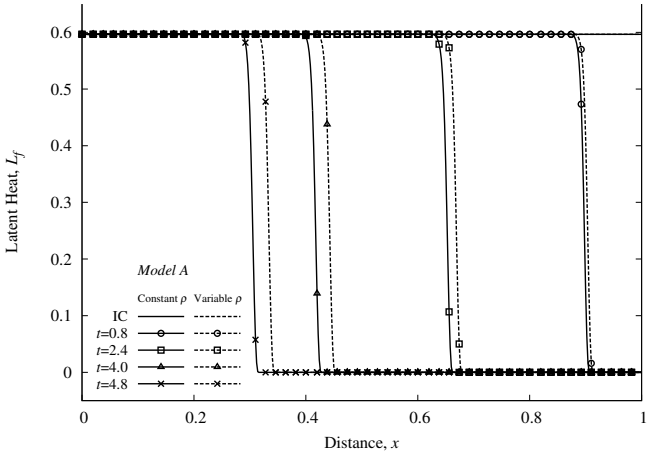

(b) Evolution of latent heat, $0.0 \leq t \leq 4.8$

Figure 53: Model Problem 2: Evolution of latent heat for liquid-solid phase change, $C^{11}(\bar{\Omega}^e_{xt}), p = 9, \Delta t = 0.04$

the evolution proceeds.

From figure 52(b) we clearly observe linear heat conduction in liquid and solid phases (constant but different slopes of T versus x) separated by smooth transition region.

If we define the center of the transition zone as the location x of the phase front, then using the results in figures 52–56 we can plot a graph of location x versus time t marking the location of the phase change front in time.

Figure 57 shows such a plot for the results presented in figures 52–56. The transition region width for these numerical studies consist of $[T_s, T_l] = [-0.001, 0.001]$. It is also obvious from figures 52–57 that the choice of constant density in all phases ($\rho = \rho_l$ used here), as is commonly used in the published works, will produce results that do not agree with the actual physics of phase change (variable density).

The differences in the computed solutions for constant and variable density are noticeable. We note that the center of the phase transition zone for variable density case is ahead of the constant density case during the entire evolution and the difference between the two increases as the evolution proceeds.

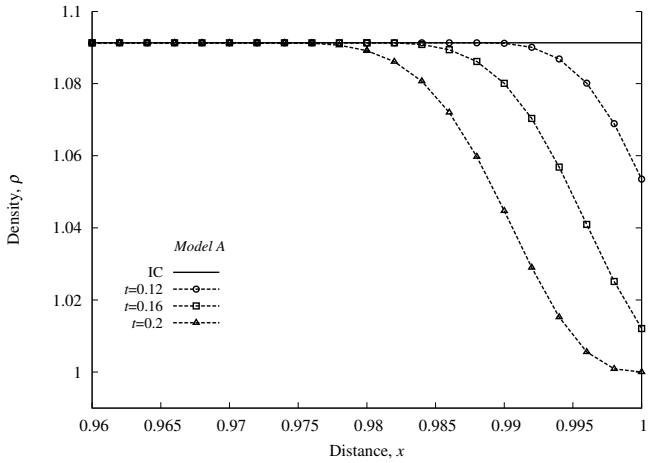

(a) Evolution of density, $0.0 \leq t \leq 0.2$

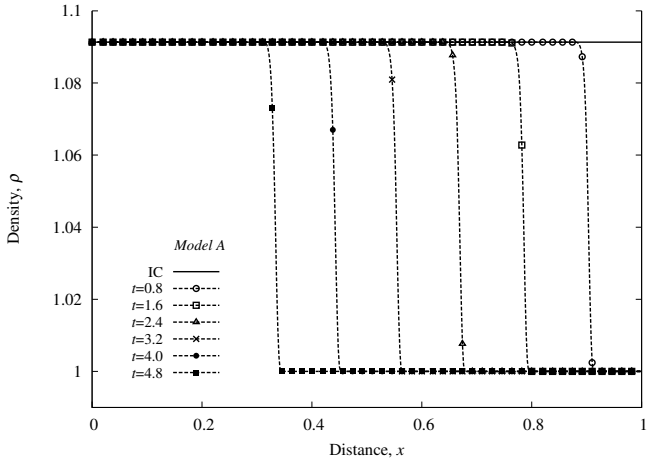

(b) Evolution of density, $0.0 \leq t \leq 4.8$

Figure 54: Model Problem 2: Evolution of density for liquid-solid phase change, $C^{11}(\bar{\Omega}^e_{xt}), p = 9, \Delta t = 0.04$

Similar studies were repeated for $[T_s, T_l] = [-0.002, 0.002]$ i.e. double the width of the transition zone, with virtually no change in the location of the center of the transition region.

The phase transition evolution for this model problem cannot be simulated using sharp-interface and phase field approaches as this model problem requires initiation of phase transition that is not possible in sharp-interface and phase field models.

III.3.9 Model Problem 3: 1D Solid-Liquid Phase Change; Initiation and Propagation of Phase Transition

In this section we present solid-liquid phase change studies using model A, similar to those presented in section III.3.8 for liquid-solid phase change. The space-time least squares formulation for a time strip (corresponding to an increment of time) with time marching is used to compute the evolution. Figure 58 shows a schematic of the space-time strip corresponding to the first increment of time, BCs and ICs, as well as dimensionless space-time domain and the dimensionless quantities.

Minimally conforming spaces are the same as described in section III.3.8. Due to smoothness of the evolution, we choose

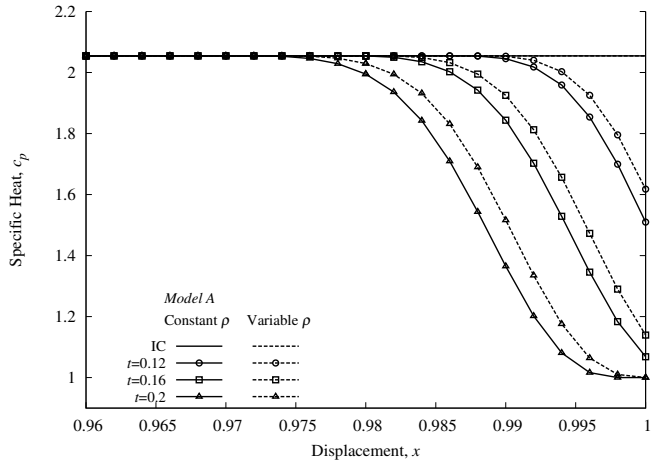

(a) Evolution of specific heat, $0.0 \leq t \leq 0.2$

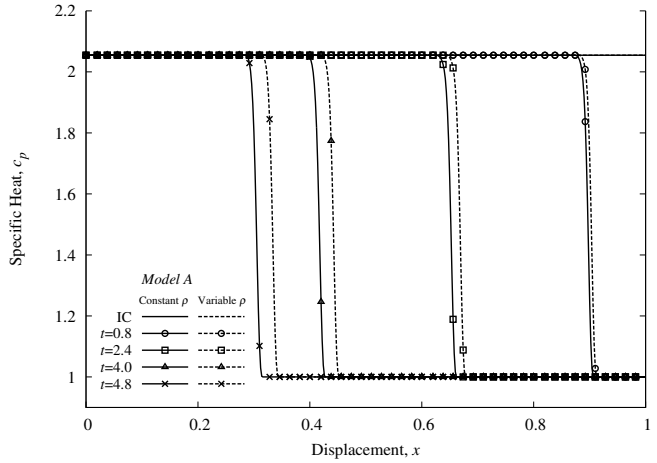

(b) Evolution of specific heat, $0.0 \leq t \leq 4.8$

Figure 55: Model Problem 2: Evolution of specific heat for liquid-solid phase change, $C^{11}(\bar{\Omega}^e_{xt}), p = 9, \Delta t = 0.04$

$k_1 = 2$ and $k_2 = 2$ i.e. T^e_h of class $C^{11}(\bar{\Omega}^e_{xt})$, therefore the integrals in the STLSP are Lebesgue in x but Riemann in t. The space-time strip ($\Delta t = 0.04$) is discretized using 100 nine node space-time $C^{11}(\bar{\Omega}^e_{xt})$ finite elements. Numerical studies were considered for the first space-time strip with phase change to determine adequate p-level for this discretization by starting with p-level of 3 (both in space and time) and incrementing it by two. At p-level of nine, I is of the order of 10^{-6} or lower and $|(g_i)|_{max} \leq 10^{-6}$ were achieved for all time steps.

This ensures converged Newton's linear method with line search as well as accurate evolution in the entire space-time domain. The numerical solutions computed using these values of *h*, *p* and *k* for $[T_s, T_l] = [-0.001, 0.001]$ are shown in figures 59–63. It may appear that presenting details of the evolutions of various quantities here is redundant in view of liquid-solid phase change model problem already considered, but this is not the case. In this case transition is from solid to liquid, thus evolutions of transport properties are quite different and hence essential to examine the resulting evolution of the solution.

Figures 59(a), 60(a), 61(a), 62(a), 63(a) show plots of T, L_f, ρ, c_p, and k versus x during the initial stages of the evolution ($0 \leq t \leq 0.8$). Continuous addition of heat from the right boundary progressively raises the temperature at the boundary and in

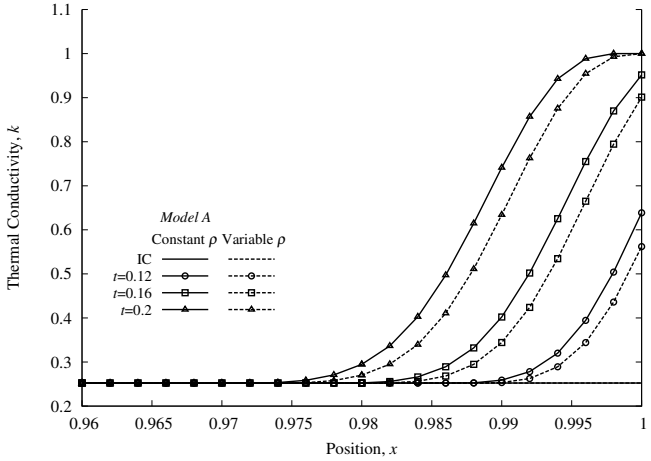

(a) Evolution of thermal conductivity, $0.0 \leq t \leq 0.2$

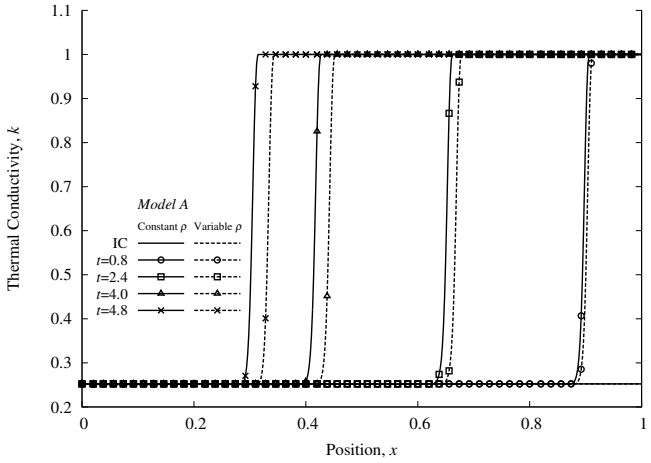

(b) Evolution of thermal conductivity, $0.0 \leq t \leq 4.8$

Figure 56: Model Problem 2: Evolution of thermal conductivity for liquid-solid phase change, $C^{11}(\bar{\Omega}^e_{xt}), p = 9, \Delta t = 0.04$

the neighborhood of the boundary which eventually results in the initiation of phase change. Variations in $L_f(T)$, $c_p(T)$, $k(T)$ and $\rho(T)$ follow changes in temperature during evolution. From figure 59(a) we note that both constant and variable densities yield almost the same temperature distribution in the initial stages of the evolution. Figures 60(a), 62(a), and 63(a) show differences in the evolutions of L_f, c_p, and k for constant and variable density cases. As expected, variable density solutions lag constant density results, opposite of liquid-solid phase transition in section III.3.8, model problem 2.

Figures 59(b), 60(b), 61(b), 62(b), 63(b) show fully formed phase change transition region (solid to liquid) beginning with $t = 3.2$ and its propagation during evolution ($3.2 \leq t \leq 19.2$). For each space-time strip during time marching using $\Delta t = 0.04$; $I < O(10^{-6})$ and $|(g_i)|_{max} \leq 10^{-6}$ ensure accurate evolution that satisfies GDE quite well over the entire space-time domain of each space-time strip. All evolutions are smooth and free of oscillations. The influence of variable density can be seen more clearly in these graphs. The variable density evolution lags the constant density evolution for all values of time, and the difference between them increases as evolution proceeds. Here also we clearly observe linear heat conduction in the solid and liquid phases (constant but different slopes of T versus x) separated by a smooth transition region.

Similar to the liquid-solid studies presented in section III.3.8, it is possible to use the solutions shown in figures 59–63 to follow

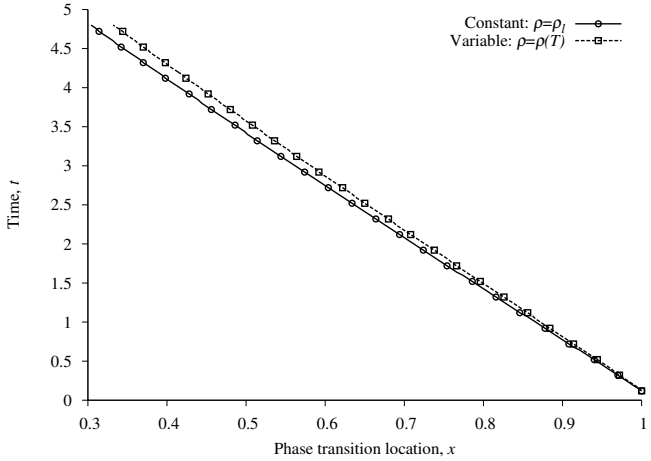

Figure 57: Model Problem 2: Interface location as a function of time, $C^{11}(\bar{\Omega}^e_{xt}), p = 9, \Delta t = 0.04$

the location of the phase transition front during the evolution. Figure 64 shows the location of the center of the transition zone for constant and variable densities. In contrast to similar results for liquid-solid phase transition shown in figure 57, here we note that the center of the phase transition zone for variable density case lags the constant density case during the entire evolution and the difference between the two increases as evolution proceeds.

The phase transition for this model problem also cannot be simulated using sharp-interface and phase field models as this model problem requires initiation of phase transition that is not possible in sharp-interface and phase field models.

III.3.10 2D Phase Change Model Problems

In this section we consider liquid-solid and solid-liquid phase change in $\mathbb{R}^2$ using the mathematical model (III.47) (Model B).

III.3.11 Model Problem 4: 2D Liquid-Solid Phase Change

In these numerical studies, we choose Model B, a system of first order PDEs that permits use of C^0 local approximation in space and time. We consider a two dimensional domain in $\mathbb{R}^2$ consisting of a one unit square. A schematic of the domain, boundary conditions, and initial conditions are shown in figure 65. A constant heat flux is applied to each boundary (heat removal), except for the first time step in which heat flux changes continuously from zero at $t = 0$ to the constant value at $t = \Delta t$.

A graded spatial discretization of the $[1 \times 1]$ spatial domain shown in figure 66 is constructed. Table 1 provides discretization details of regions A, B, C and D. All four boundaries contain uniform heat flux $q = -0.1$ (cooling) for $t \geq \Delta t$. Evolution is computed (56 time steps) using p-level of 3 in space and time with $\Delta t = 0.0025$ for the first 8 time steps and $\Delta t = 0.01$ for the remaining time steps. For this discretization, the C^{00} local approximation with p=3 yield I of $O(10^{-6})$ or lower, confirming good accuracy of the solution. $|g_i|_{max} \leq 10^{-6}$ is used for convergence check in the Newton's linear method. For most time increments Newton's linear method with line search converges in 5-10 iterations.

Evolution of temperature T and latent heat L_f calculated using variable density are shown in figures 67 and 68 using carpet plots for different values of time. Similar plots were generated for ρ, c_p, k but are not shown for the sake of brevity. The carpet plots show evolutions to be oscillation free. Evolution and propagation of phase transition is demonstrated more clearly by using x, y plots of temperature and latent heat at the centerline and at the boundary.

Figure 69(a) shows evolution of temperature at $x = 0.5$ (centerline) as a function of y for $t = 0.01$, 0.2, 0.5. Evolution of temperature T as a function of y at $x = 0.0$ (boundary) us shown in figure 69(b) for the same values of time. The evolution of latent heat L_f for the same locations and for the same values of time are shown in figures 70(a) and (b). From figure 69(a) we

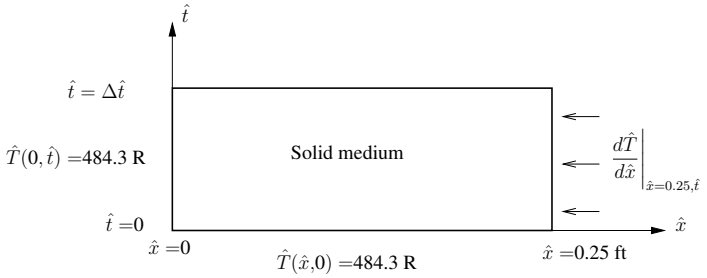

(a) Space-time strip

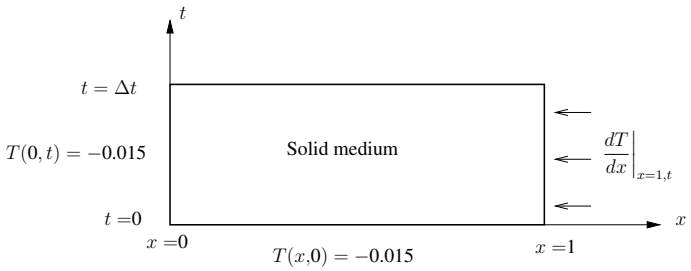

(b) Dimensionless space-time strip

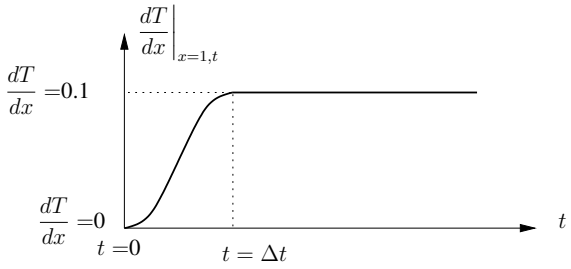

(c) Boundary condition $\frac{dT}{dx}$ at $x = 1$

Figure 58: Solid-liquid phase transition: space-time strip, boundary conditions, and initial condition

observe that at $t = 0.01$, the phase transition has not initiated along the centerline. At $t = 0.2$, the portions of the domain closer to the boundary are experiencing phase transition. At $t = 0.5$, a significant length along y near the boundaries is in the transition zone with some portion near freezing. At the boundary, the situation is quite different (figure 69(b)). At $t = 0.01$ the phase transition has not initiated yet. At $t = 0.2$ the entire boundary is in the transition zone except very small portions near $y = 0$ and $y = 1$ that have solidified. At $t = 0.5$ a significant portion of the boundary is completely frozen. Graphs of latent heat in figures 70(a) and (b) confirm these observations discussed here using figures 69(a) and (b). Graphs of the evolutions of ρ, c_p, and k confirm these observations made from figures 69 and 70 and hence are not included.

Evolutions are smooth and show that the differences between those with variable density and constant density are not as significant as for studies in $\mathbb{R}^1$ for the values of time reported here. As evolution proceeds, we expect more deviations between the two. As in the case of liquid-solid phase transition in $\mathbb{R}^1$, here also the evolution with variable density leads the constant density evolution (more visible in figure 69(b) and 70). These studies demonstrate the strength of the work in moving front in $\mathbb{R}^2$ without front tracking techniques. In these numerical studies we have used $[T_s, T_l] = [-0.004, 0.004]$.

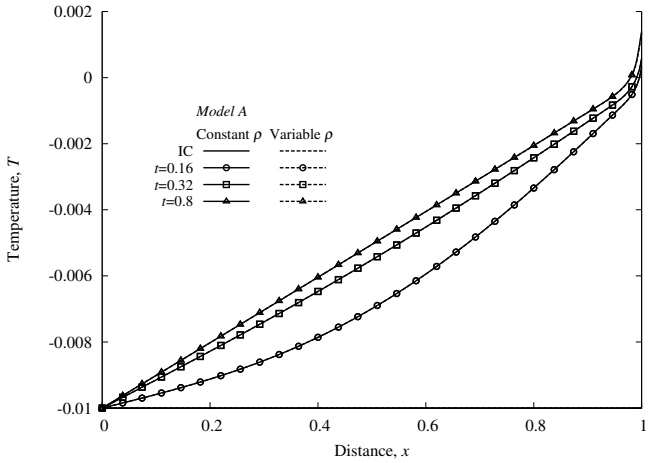

(a) Evolution of temperature, $0.0 \leq t \leq 0.8$

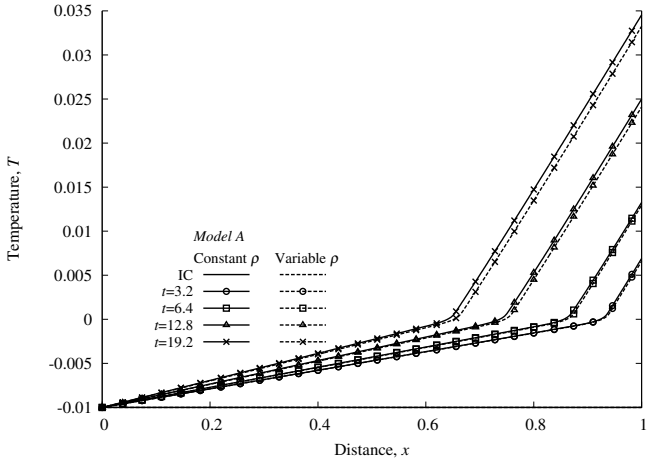

(b) Evolution of temperature, $0.0 \leq t \leq 19.2$

Figure 59: Model Problem 3: Evolution of temperature for solid-liquid phase change, $C^{11}(\bar{\Omega}^e_{xt}), p = 9, \Delta t = 0.04$

This model problem also cannot be simulated using phase field and sharp interface models due to the same reason as in the case of model problems in $\mathbb{R}^1$. Symmetry of the evolution is quite obvious from figures 67 and 68.

III.3.12 Model Problem 5: 2D Solid-Liquid Phase Change

Here we also consider a two dimensional domain in $\mathbb{R}^2$ consisting of a one unit square. A schematic of the domain, boundary conditions, initial conditions and reference quantities are shown in figure 71. A constant heat flux is applied to each boundary, except for the first time step in which the heat flux changes continuously from zero at $t = 0$ to the constant value at $t = \Delta t$.

The graded discretization for the $[1 \times 1]$ spatial domain is same as in section III.3.11, shown in figure 66, with details of regions A, B, C and D in Table 1. All four boundaries maintain uniform heat flux $q = 0.1$ (heating). Evolution is computed (50 time steps) using p-level of 3 in space and time with $\Delta t = 0.01$.

For this discretization, the C^{00} local approximations with p=3 yield I of $O(10^{-6})$ or lower, confirming good accuracy of the

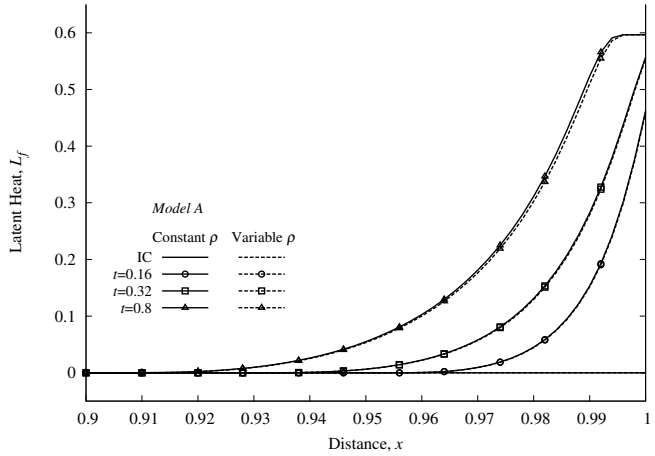

(a) Evolution of latent heat, $0.0 \leq t \leq 0.8$

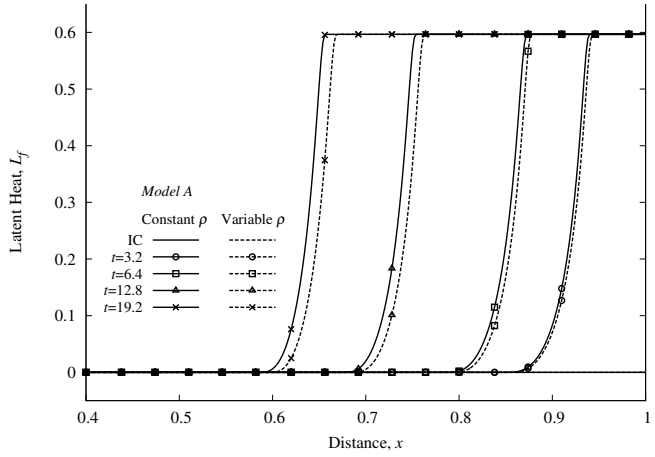

(b) Evolution of latent heat, $0.0 \leq t \leq 19.2$

Figure 60: Model Problem 3: Evolution of latent heat for solid-liquid phase change, $C^{11}(\bar{\Omega}^e_{xt}), p = 9, \Delta t = 0.04$

Table 1: Spatial discretization for model problems in $\mathbb{R}^2$

Region	Number of x elements	Number of y elements	Element length in x, h_{ex}	Element length in y, h_{ey}	Number of Total Elements
A	12	12	0.0167	0.0167	144
B	6	12	0.1000	0.0167	72
C	12	6	0.0167	0.1000	72
D	6	6	0.1000	0.1000	36

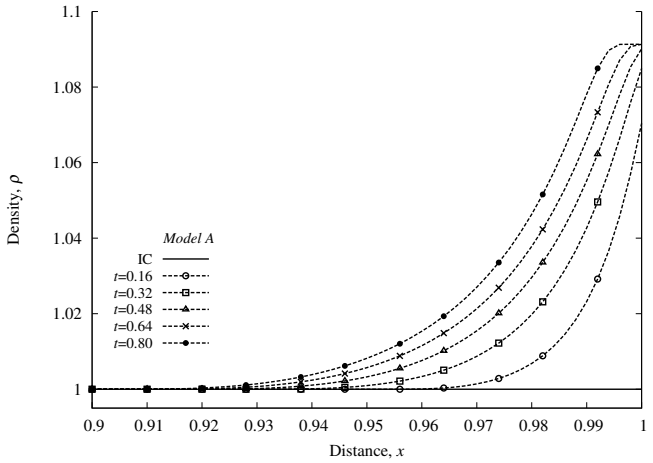

(a) Evolution of density, $0.0 \leq t \leq 0.8$

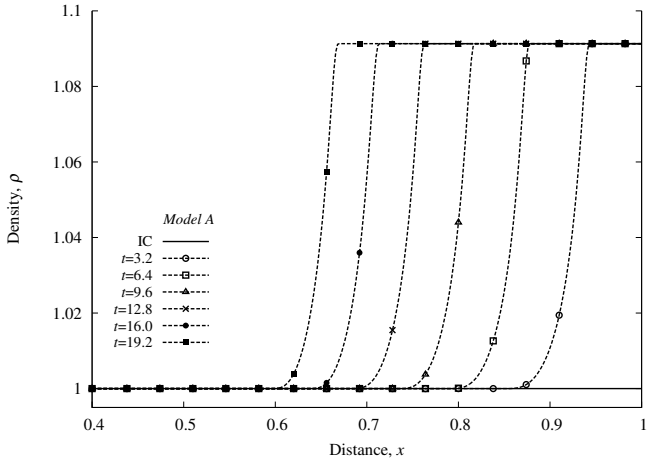

(b) Evolution of density, $0.0 \leq t \leq 19.2$

Figure 61: Model Problem 3: Evolution of density for solid-liquid phase change, $C^{11}(\bar{\Omega}^e_{xt}), p = 9, \Delta t = 0.04$

solution. $|g_i|_{max} \leq 10^{-6}$ is used for convergence check of the Newton's linear method. For most time increments Newton's linear method with line search converges in 5-10 iterations. In these studies we have used $[T_s, T_l] = [-0.004, 0.004]$.

Carpet plots similar to model problem 4 were also generated for this model problem with behaviors similar to model problem 4 and hence are not included here. Two dimensional line x, y plots of temperature T and latent heat L_f are presented to demonstrate the phase transition more clearly.

Figure 72(a) shows evolution of temperature at $x = 0.5$ (centerline) as a function of y for $t = 0.01$, 0.2, and 0.5. Evolution of temperature T as a function of y at $x = 0.0$ (boundary) is shown in figure 72(b) for the same values of time. The evolutions of latent heat L_f for the same locations and for the same values of time are shown in figures 73(a) and (b). From the evolution of temperature in figure 72(a) we note that at $t = 0.01$, the phase transition has not been initiated at the centerline. For $t = 0.2$ the entire region $0 \leq y \leq 1$ is in the transition zone $[T_s, 0]$. At $t = 0.5$ the entire zone $0 \leq y \leq 1$ is still in the transition zone, but some portions near the boundaries are in $[0, T_l]$. At the boundary ($x = 0$, $0 \leq y \leq 1$) the evolution of the temperature is quite different than at the centerline. From figure 72(b) we find that at $t = 0.01$, the phase transition has not commenced yet except in a

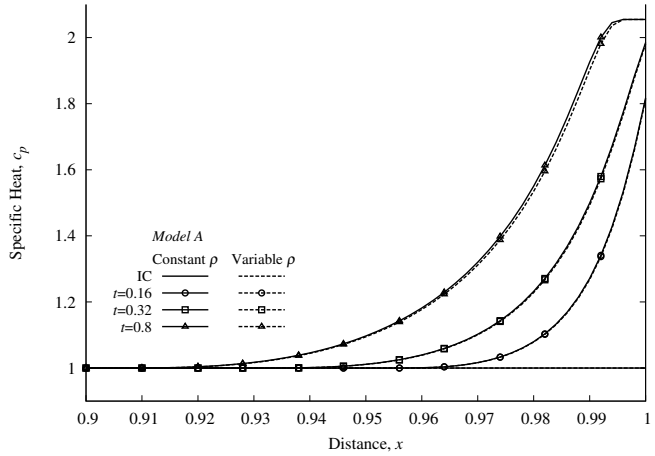

(a) Evolution of specific heat, $0.0 \leq t \leq 0.8$

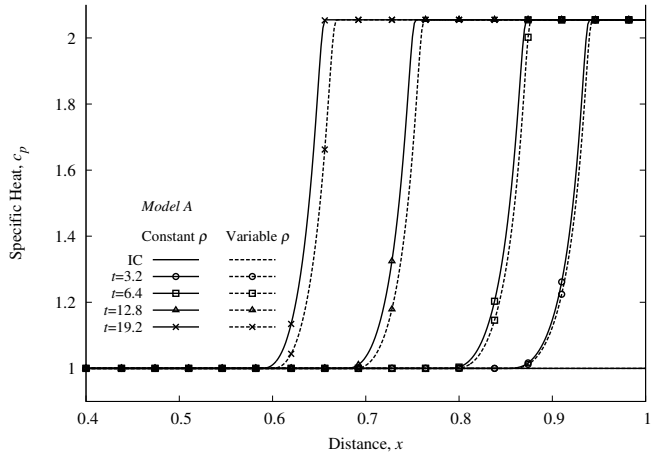

(b) Evolution of specific heat, $0.0 \leq t \leq 19.2$

Figure 62: Model Problem 3: Evolution of specific heat for solid-liquid phase change, $C^{11}(\bar{\Omega}^e_{xt}), p = 9, \Delta t = 0.04$

small portion near $y = 0$ and $y = 1$ (horizontal boundaries at $y = 0$ and $y = 1$). At $t = 0.2$ the entire length $0 \leq y \leq 1$ is in the transition zone $[0, T_l]$. At $t = 0.5$ a significant portion of $0 \leq y \leq 1$ near $y = 0$ and $y = 1$ is completely liquid.

Graphs of latent heat L_f in figures 73(a) and (b) confirm these observations. In figure 73(b) we note that at time $t = 0.5$ the straight line portions of the graph near $y = 0$ and $y = 1$ meaning constant L_f further confirm completely liquid state of the matter.

Graphs of the evolutions ρ, c_p, and k show evolutions that are in agreement with the evolutions of T and L_f shown in figures 72 and 73 and hence are omitted for the sake of brevity.

In this case also the evolutions are smooth and show that the differences between the evolutions with variable and constant density are not as significant as for studies in $\mathbb{R}^1$ for the values of time reported here. As evolution proceeds we expect more deviations between the two evolutions. As in case of solid-liquid phase transition in $\mathbb{R}^1$, here also the variable density evolution lags the constant density evolution (more visible in figures 72 and 73).

This model problem also cannot be simulated using sharp-interface or phase field approaches as it requires initiation of phase transition.

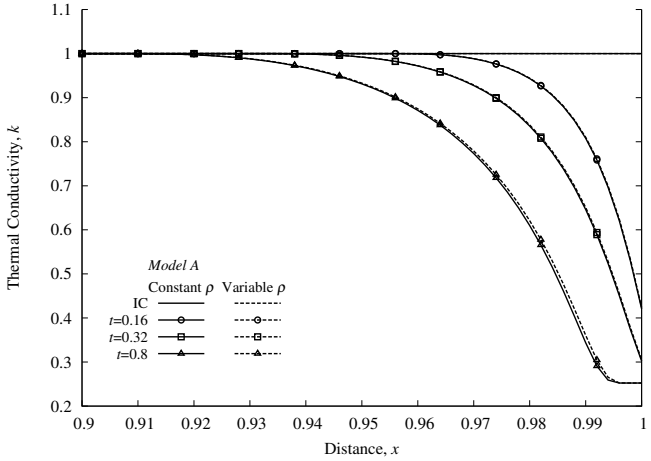

(a) Evolution of thermal conductivity, $0.0 \leq t \leq 0.8$

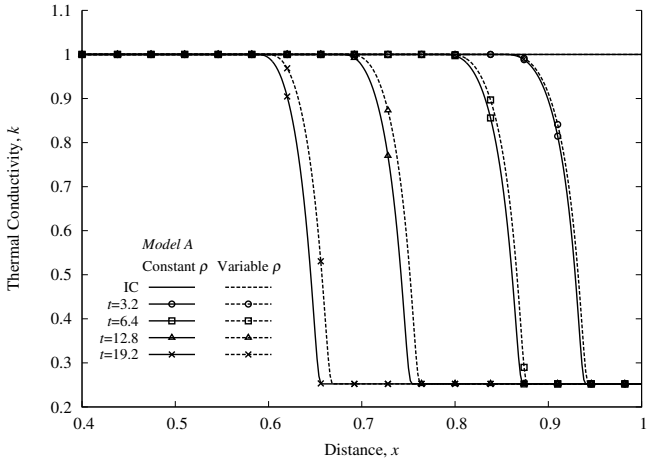

(b) Evolution of thermal conductivity, $0.0 \leq t \leq 19.2$

Figure 63: Model Problem 3: Evolution of thermal conductivity for solid-liquid phase change, $C^{11}(\bar{\Omega}^e_{xt}), p = 9, \Delta t = 0.04$

III.3.13 Phase Transition Numerical Studies in the Presence of Flow

In this section we present numerical studies using mathematical model based on constant stress and zero velocity in the solid phase but nonzero velocity and stress field in the liquid and transition regions. The details of the mathematical model are presented in Section III.2.8. In the following we present numerical results for fully developed flow between parallel plates in which the plates are being cooled to initiate and propagate liquid-solid phase transition.

III.3.14 Model Problem 6: Fully Developed Flow Between Parallel Plates

For this case we only need to consider evolution along any vertical line between the plates. The flow is pressure driven i.e. $\frac{\partial \bar{p}}{\partial \bar{x}_1}$ is given where $\bar{x}_1$ is the direction of the flow. If we choose $\bar{x}_1 = \bar{x}$ and $\bar{x}_2 = \bar{y}$, $\bar{v}_1 = \bar{u}$, ${}_d\bar{\sigma}^{(0)}_{x1x2} = {}_d\bar{\sigma}^{(0)}_{xy}$, then the dimensionless

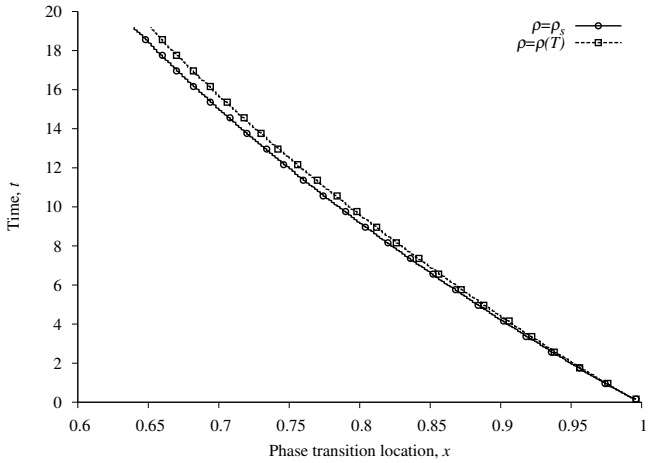

Figure 64: Model Problem 3: Interface location as a function of time, $C^{11}(\bar{\Omega}^e_{xt}), p = 9, \Delta t = 0.04$

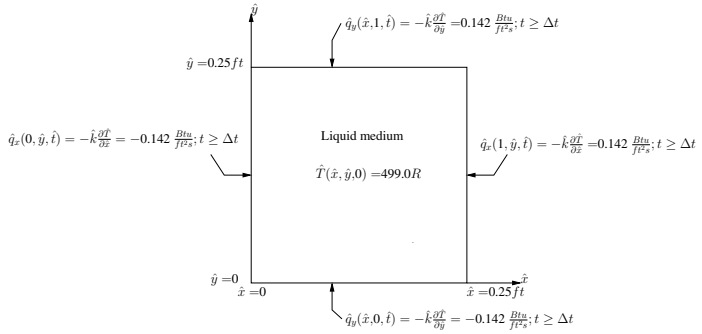

(a) Space-time slab

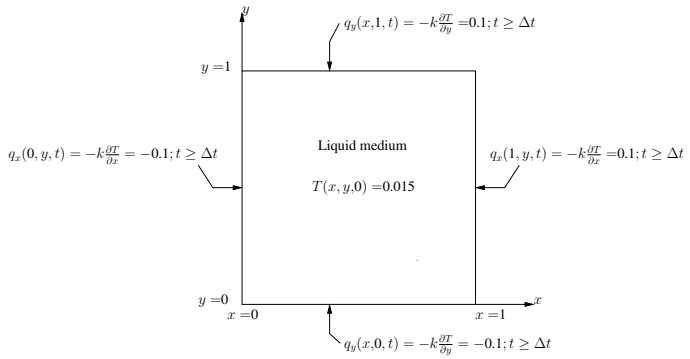

(b) Dimensionless space-time slab

Figure 65: 2D liquid-solid phase transition: space-time slab, boundary conditions, and initial condition

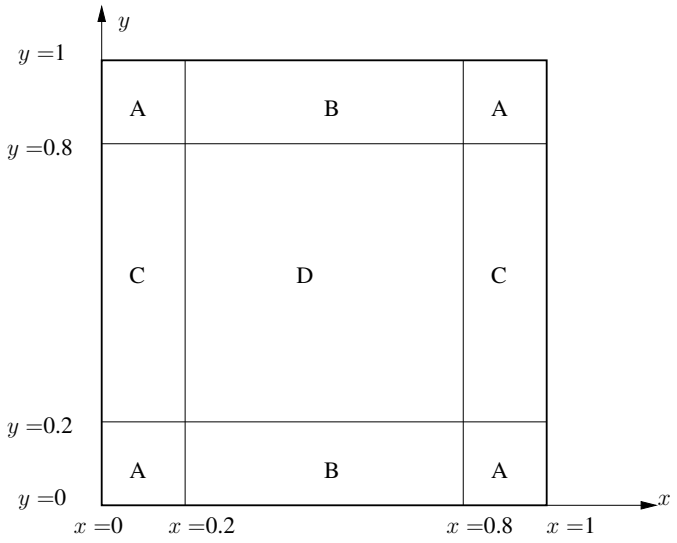

Figure 66: Spatial discretization for model problems in $\mathbb{R}^2$

form of the mathematical model presented in section III.72 (combined model) for this model problem reduces to

$$\left.\begin{aligned}
&\bar{f}_l\left(\frac{p_0}{\rho_0 v_0^2}\right)\frac{\partial \bar{p}}{\partial \bar{x}} - \left(\frac{\tau_0}{\rho_0 v_0^2}\right)\frac{\partial_d \bar{\sigma}_{xy}^{(0)}}{\partial \bar{y}} = 0 \\
&\bar{\rho}\left(\frac{\bar{c}_p(\bar{T})}{Ec} + \frac{L_{f0}}{v_0^2}\frac{\partial \bar{L}_f}{\partial \bar{T}}\right)\frac{\partial \bar{T}}{\partial t} + \frac{1}{ReBr}\frac{\partial \bar{q}_y}{\partial \bar{y}} = 0 \\
&\bar{f}_l\left({}_d\bar{\sigma}_{xy}^{(0)}\right) = \left(\frac{\mu_0 v_0}{L_0 \tau_0}\right)\bar{\mu}\frac{\partial \bar{u}}{\partial \bar{y}} \\
&\bar{q}_y = -\bar{k}(\bar{T})\frac{\partial \bar{T}}{\partial \bar{y}}
\end{aligned}\right\} \qquad \text{(III.76)}$$

where

$$\begin{aligned}
\bar{f}_l = 1 \quad &; \quad \text{liquid phase} \\
\bar{f}_l = 0 \quad &; \quad \text{solid phase} \\
0 \le \bar{f}_l \le 1 \quad &; \quad \bar{T}_s \le \bar{T} \le \bar{T}_l
\end{aligned} \qquad \text{(III.77)}$$

If we choose $\tau_0 = \rho_0 v_0^2$, characteristic kinetic energy, then (III.76) reduces to

$$\left.\begin{aligned}
&\bar{f}_l\frac{\partial \bar{p}}{\partial \bar{x}} - \frac{\partial_d \bar{\sigma}_{xy}^{(0)}}{\partial \bar{y}} = 0 \\
&\bar{\rho}\left(\frac{\bar{c}_p(\bar{T})}{Ec} + \frac{L_{f0}}{v_0^2}\frac{\partial \bar{L}_f}{\partial \bar{T}}\right)\frac{\partial \bar{T}}{\partial t} + \frac{1}{ReBr}\frac{\partial \bar{q}_y}{\partial \bar{y}} = 0 \\
&\bar{f}_l\left({}_d\bar{\sigma}_{xy}^{(0)}\right) = \frac{\bar{\mu}}{Re}\frac{\partial \bar{u}}{\partial \bar{y}} \\
&\bar{q}_y = -\bar{k}(\bar{T})\frac{\partial \bar{T}}{\partial \bar{y}}
\end{aligned}\right\} \qquad \text{(III.78)}$$

where

$$\begin{array}{rcl} \bar{f}_l = 1 & ; & \text{liquid phase} \\ \bar{f}_l = 0 & ; & \text{solid phase} \\ 0 \le \bar{f}_l \le 1 & ; & \bar{T}_s \le \bar{T} \le \bar{T}_l \end{array} \tag{III.79}$$

By substituting $\bar{q}_y$ in the energy equation we can eliminate $\bar{q}_y$ as a dependent variable. We designate this as Model (a).

Model (a)

$$\left.\begin{aligned} &\bar{f}_l \frac{\partial \bar{p}}{\partial \bar{x}} - \frac{\partial_d \bar{\sigma}^{(0)}_{xy}}{\partial \bar{y}} = 0 \\ &\bar{\rho}\left(\frac{\bar{c}_p(\bar{T})}{Ec} + \frac{L_{f0}}{v_0^2} \frac{\partial \bar{L}_f}{\partial \bar{T}} \right) \frac{\partial \bar{T}}{\partial t} \\ &\qquad - \frac{1}{ReBr}\left(\frac{\partial \bar{k}(\bar{T})}{\partial \bar{T}} \left(\frac{\partial \bar{T}}{\partial \bar{y}} \right)^2 + \bar{k}(\bar{T}) \frac{\partial^2 \bar{T}}{\partial \bar{y}^2} \right) = 0 \\ &\bar{f}_l \left({}_d\bar{\sigma}^{(0)}_{xy} \right) = \frac{\bar{\mu}}{Re} \frac{\partial \bar{u}}{\partial \bar{y}} \end{aligned}\right\} \tag{III.80}$$

The mathematical model consists of (III.80) and (III.79) with $\bar{u}$, ${}_d\bar{\sigma}^{(0)}_{xy}$, and $\bar{T}$ as dependent variables.

Model (b)

An alternate form of (III.80) can be derived by first substituting ${}_d\bar{\sigma}^{(0)}_{xy} = \dfrac{\bar{\mu}}{Re} \dfrac{\partial \bar{u}}{\partial \bar{y}}$ in the momentum equation and then recasting the momentum equation as a system of first order equations that enforce $\frac{\partial \bar{u}}{\partial \bar{y}} = 0$ in the solid region. We obtain the following:

$$\left.\begin{aligned} &Re \bar{f}_l \frac{\partial \bar{p}}{\partial \bar{x}} - \bar{\mu} \frac{\partial_d \bar{\tau}^{(0)}_{xy}}{\partial \bar{y}} = 0 \\ &\bar{\rho}\left(\frac{\bar{c}_p(\bar{T})}{Ec} + \frac{L_{f0}}{v_0^2} \frac{\partial \bar{L}_f}{\partial \bar{T}} \right) \frac{\partial \bar{T}}{\partial t} \\ &\qquad - \frac{1}{ReBr}\left(\frac{\partial \bar{k}(\bar{T})}{\partial \bar{T}} \left(\frac{\partial \bar{T}}{\partial \bar{y}} \right)^2 + \bar{k}(\bar{T}) \frac{\partial^2 \bar{T}}{\partial \bar{y}^2} \right) = 0 \\ &\bar{f}_l \left({}_d\bar{\tau}^{(0)}_{xy} \right) = \frac{\partial \bar{u}}{\partial \bar{y}} \end{aligned}\right\} \tag{III.81}$$

This mathematical model consists of (III.81) and (III.79). In this model ${}_d\bar{\tau}^{(0)}_{xy}$, hence $\frac{\partial \bar{u}}{\partial \bar{y}}$ and $\bar{f}_l \frac{\partial \bar{p}}{\partial \bar{x}} = 0$, and therefore $\frac{\partial_d \bar{\tau}^{(0)}_{xy}}{\partial \bar{y}} = 0$ holds in the solid region. This model is obviously an alternate way to achieve the desired physics of constant stress and zero velocity in the solid phase as in (III.80) and (III.79).

We consider both models (a) and (b) in the numerical calculations of the evolution.

From these mathematical models it is clear that $\frac{\partial_d \bar{\tau}^{(0)}_{xy}}{\partial \bar{y}} = 0$ in the solid region. This of course implies that ${}_d\bar{\tau}^{(0)}_{xy} = C_1$, a constant, in the solid region. We note that a constant ${}_d\bar{\tau}^{(0)}_{xy}$ with $\bar{f}_l = 0$ and $\frac{\partial \bar{u}}{\partial \bar{y}} = 0$ satisfies the last equation in the models (*a*) and (*b*) (i.e. last equation in (III.80) and (III.81)). Value of C_1 is dictated by the deviatoric shear stress at the solid-liquid interface. Only when the deviatoric shear stress at the liquid-solid interface becomes zero is ${}_d\bar{\tau}^{(0)}_{xy}$ in the solid region zero. In conclusion, a constant ${}_d\bar{\tau}^{(0)}_{xy}$ in the solidified region is supported by the mathematical model. Its magnitude is largest at the initiation of freezing and is progressively reduced upon continued growth of the solidified region, eventually becoming zero when the entire flow domain is solidified.

Transport Properties

Once again, the solid phase is considered to be ice and the liquid phase is water, with the same properties that are listed in section III.3.7. The reference and the dimensionless quantities are given as:

$$\rho_0 = \hat{\rho}_s \quad , \quad k_0 = \hat{k}_s \quad , \quad c_{p0} = \hat{c}_{ps}$$
$$L_0 = 0.25ft \quad , \quad v_0 = 1.0ft/s$$
$$q_0 = 1.42\ Btu/ft^2\, s \quad , \quad T_0 = (32^\circ F + 459.67) = 491.67\ R$$
$$t_0 = 0.25\ s \quad , \quad \Delta t = 50.0$$

$$\Delta\hat{t} = 12.5s \quad , \quad \mu_0 = \hat{\mu} \quad , \quad \tau_0 = E_0 = \rho_0 v_0^2 = 57.16\ lbm/ft\, s^2$$

in addition to:

$$Re = \frac{\rho_0 L_0 v_0}{\mu_0} \quad ; \quad \text{Reynolds number}$$

$$Ec = \frac{v_0^2}{c_{p0} T_0} \quad ; \quad \text{Eckert number}$$

$$Br = \frac{\mu_0 v_0^2}{k_0 T_0} \quad ; \quad \text{Brinkman number}$$

Figures 74(a)-(c) show a schematic of the problem and space-time strips for an increment of time Δt from the lower plate to the center of the flow. Boundary conditions and initial condition are also shown in figures 74(b),(c). The lower plate is subjected to a temperature gradient of 0 to 0.3 (continuous and differentiable; cubic) for the first increment of time and held fixed thereafter as shown in figure 74(d). Figure 74(e) shows a 40 element uniform discretization for the space-time strip. Evolution is computed using the space-time discretization of figure 74(e) with time marching using solutions of class C^{11} in space and time with uniform p-levels of 9 in space and time.

The temperature range for the transition zone is chosen to be $[\bar{T}_s, \bar{T}_l] = [-0.003, 0.003]$. $\bar{\rho}$, $\bar{c}_p$, $\bar{k}$, and $\bar{L}_f$ are assumed to be continuous and differentiable functions of temperature in the transition zone.

Fixed Δt of 50.0 is considered during time marching. For comparison purposes, evolution is also computed using constant density ($\bar{\rho} = \bar{\rho}_l$).

Numerical Results Using Model (b)

Figure 75 shows evolution of $\bar{u}$ for $t = 0$ (IC), $t = 1000$, 2500, and 4000 for constant as well as variable density. Progressive increase in the solid zone that initiates at the plate is clearly observed as the evolution proceeds. With progressively increasing solid zone the flow height is progressively reduced. Since the flow is pressure driven ($\frac{\partial \bar{p}}{\partial \bar{x}} = -6.7182 \times 10^{-5}$, constant), this results in the progressive reduction in the flow rate. In other words, as evolution proceeds, the effective $\frac{H}{2}$ is progressively reduced.

Similar plots of temperature $\bar{T}$ and ${}_d\bar{\tau}_{xy}^{(0)}$ are shown in figures 76 and 77. In the solidified region as expected we observe linear heat conduction and constant deviatoric Cauchy shear stress of the same magnitude as at the solid-liquid interface.

Figures 78-81 show evolutions of $\bar{L}_f$, $\bar{\rho}$, $\bar{c}_p$, $\bar{k}$ for variable as well as constant density for the same values of time. Smooth-interface approach in the transition region and the mathematical model work exceptionally well.

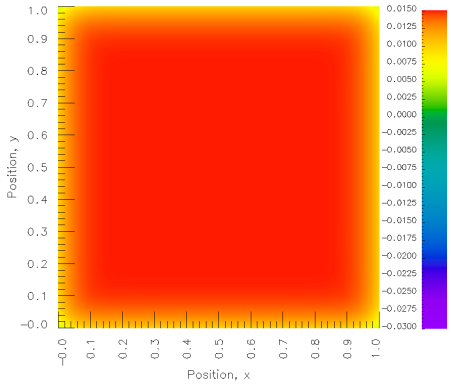

(a) $t = 0.02$

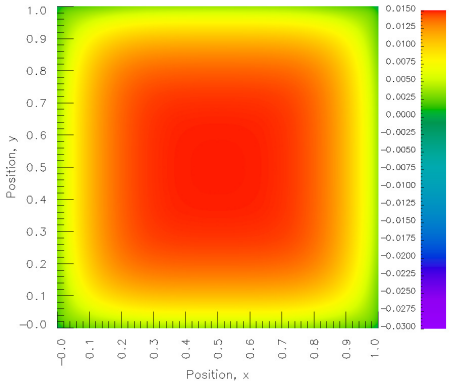

(b) $t = 0.1$

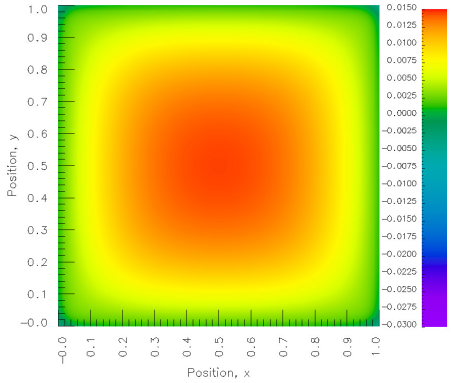

(c) $t = 0.2$

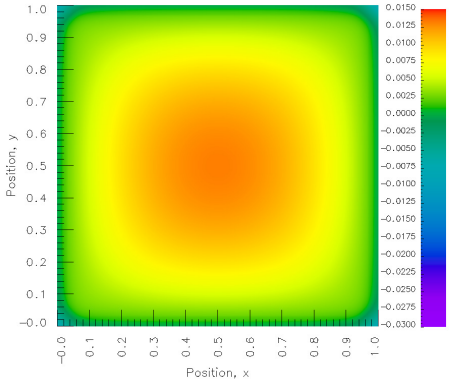

(d) $t = 0.3$

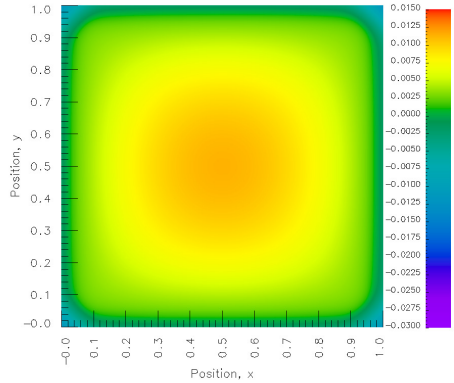

(e) $t = 0.4$

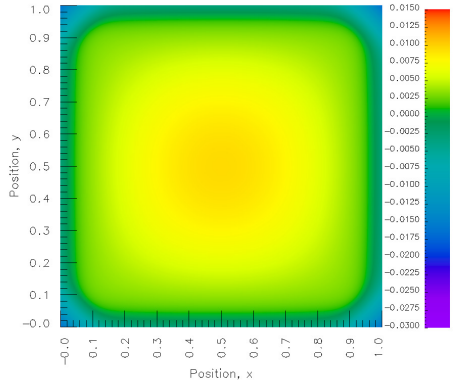

(f) $t = 0.5$

Figure 67: Model Problem 4: Evolution of temperature for liquid-solid phase change in $\mathbb{R}^2$, $C^{00}(\bar{\Omega}^e_{\boldsymbol{x}t})$, $p = 3$, $\Delta t = 0.0025$ for $0 \leq t \leq 0.02$ and $\Delta t = 0.01$ for $t \geq 0.02$

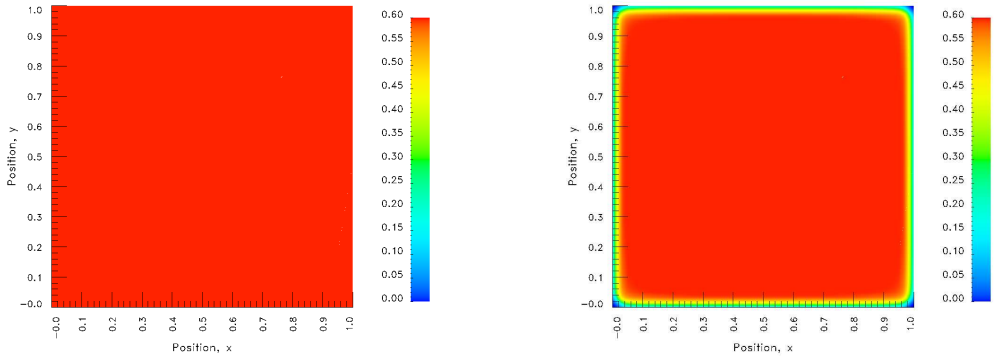

(a) $t = 0.02$

(b) $t = 0.1$

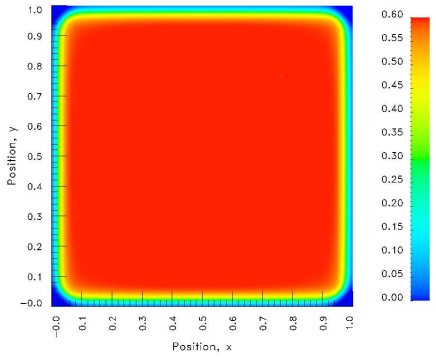

(c) $t = 0.2$

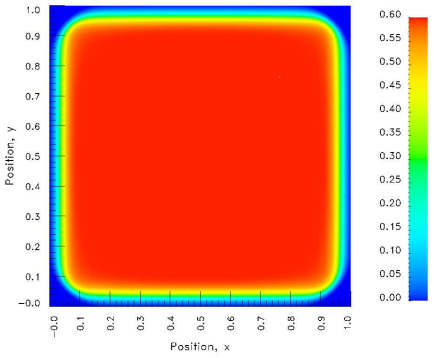

(d) $t = 0.3$

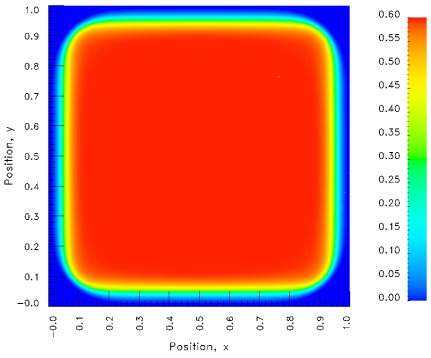

(e) $t = 0.4$

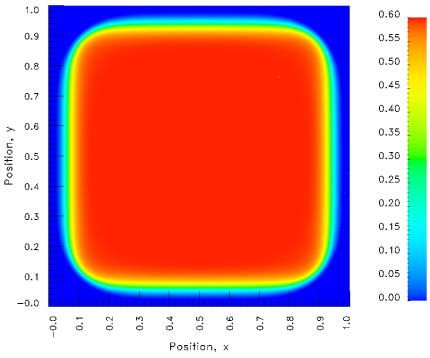

(f) $t = 0.5$

Figure 68: Model Problem 4: Evolution of latent heat for liquid-solid phase change in $\mathbb{R}^2$, $C^{00}(\bar{\Omega}^e_{\boldsymbol{x}t})$, $p = 3$, $\Delta t = 0.0025$ for $0 \leq t \leq 0.02$ and $\Delta t = 0.01$ for $t \geq 0.02$

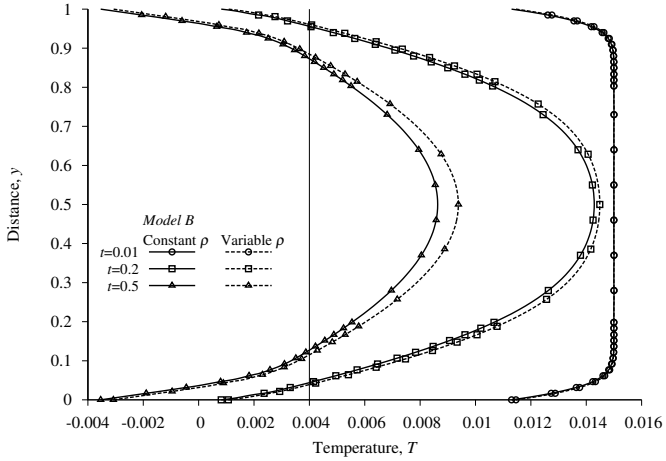

(a) Evolution of temperature at the centerline

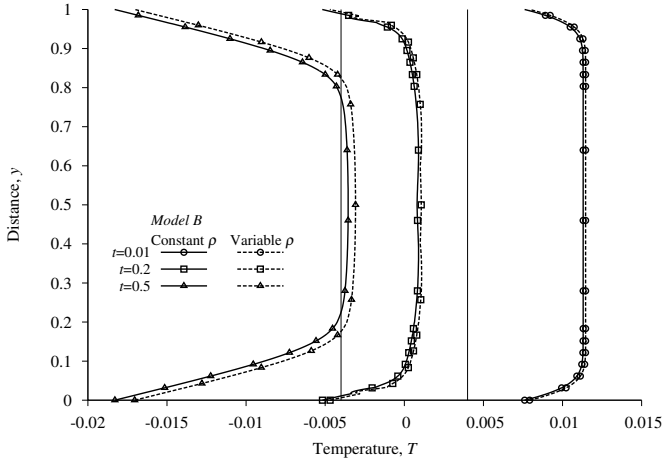

(b) Evolution of temperature at the boundary

Figure 69: Model Problem 4: Evolution of temperature for liquid-solid phase change in $\mathbb{R}^2$, $C^{00}(\bar{\Omega}^e_{xt})$, $p = 3$, $\Delta t = 0.0025$ for $0 \leq t \leq 0.02$ and $\Delta t = 0.01$ for $t \geq 0.02$

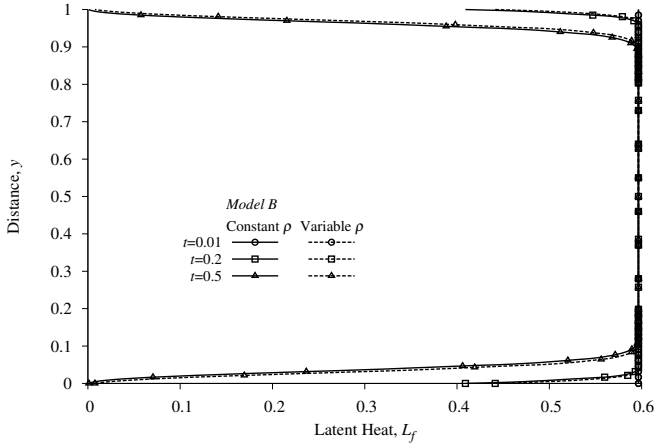

(a) Evolution of latent heat at the centerline

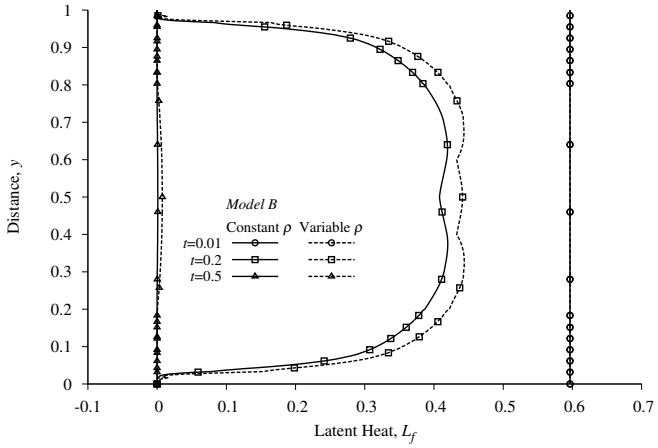

(b) Evolution of latent heat at the boundary

Figure 70: Model Problem 4: Evolution of latent heat for liquid-solid phase change in $\mathbb{R}^2$, $C^{00}(\bar{\Omega}^e_{\boldsymbol{x}t})$, $p = 3$, $\Delta t = 0.0025$ for $0 \leq t \leq 0.02$ and $\Delta t = 0.01$ for $t \geq 0.02$

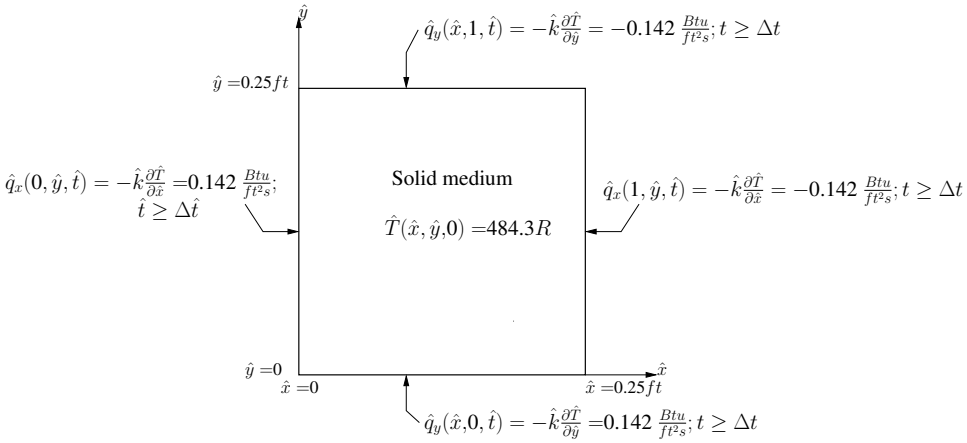

(a) Space-time slab

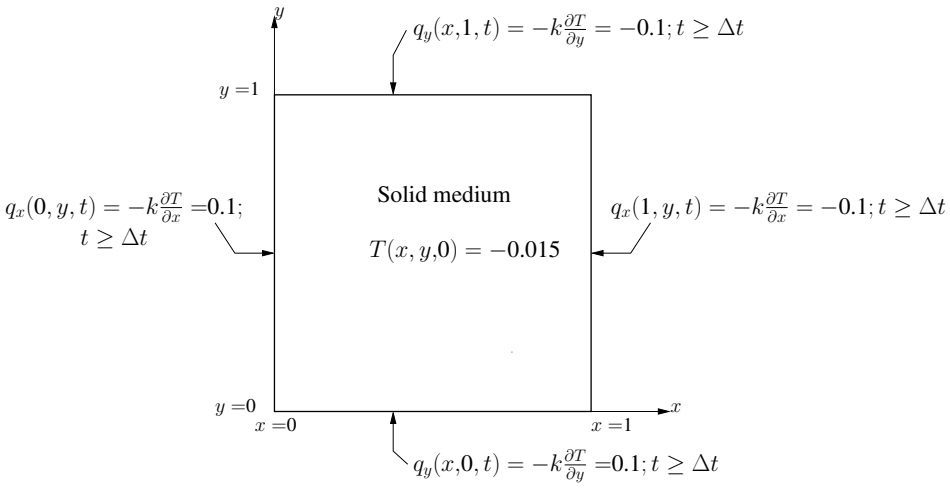

(b) Dimensionless space-time slab

Figure 71: 2D solid-liquid phase transition: space-time slab, boundary conditions, and initial condition

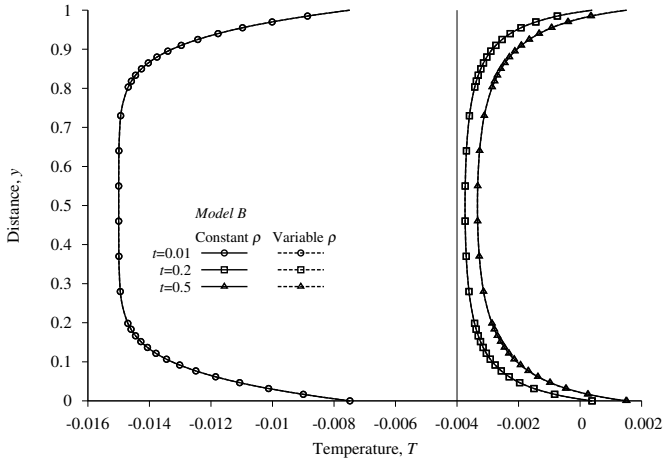

(a) Evolution of temperature at the centerline

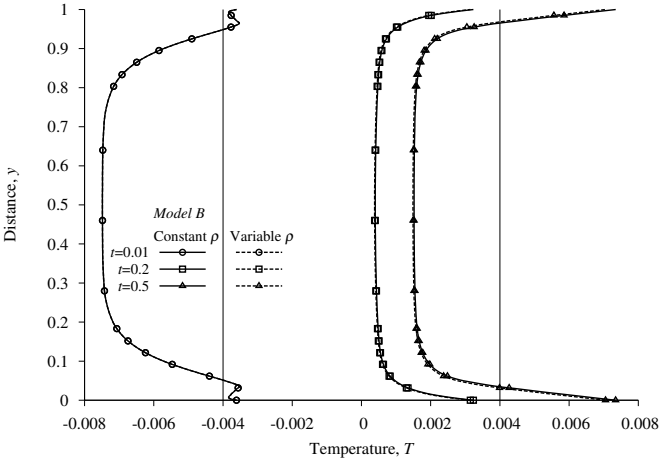

(b) Evolution of temperature at the boundary

Figure 72: Model Problem 5: Evolution of temperature for solid-liquid phase change in $\mathbb{R}^2$, $C^{00}(\bar{\Omega}^e_{\mathbf{x}t})$, $p = 3$, $\Delta t = 0.01$

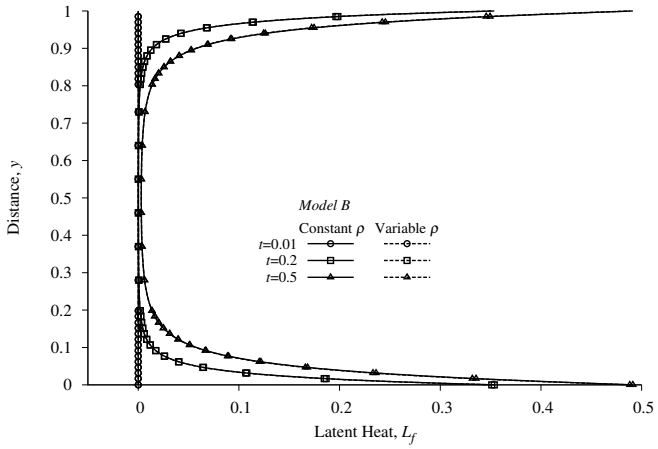

(a) Evolution of latent heat at the centerline

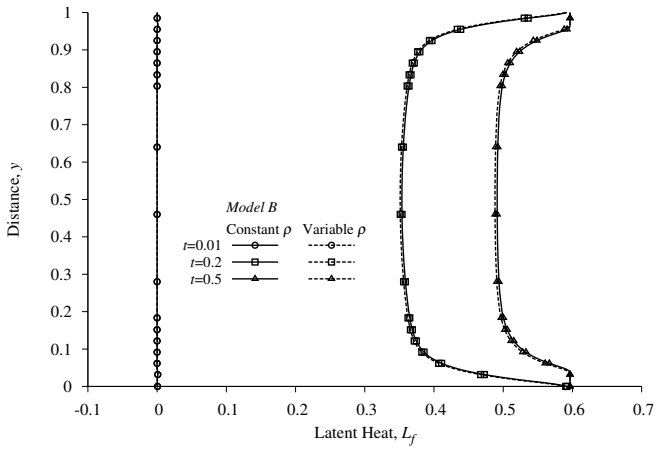

(b) Evolution of latent heat at the boundary

Figure 73: Model Problem 5: Evolution of latent heat for solid-liquid phase change in $\mathbb{R}^2$, $C^{00}(\bar{\Omega}^e_{\boldsymbol{x}t})$, $p = 3$, $\Delta t = 0.01$

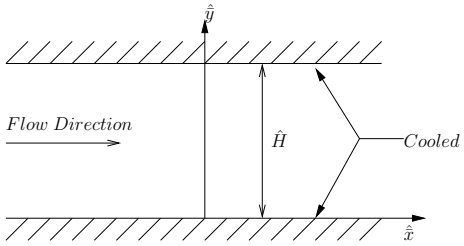

(a) Schematic of model problem 6

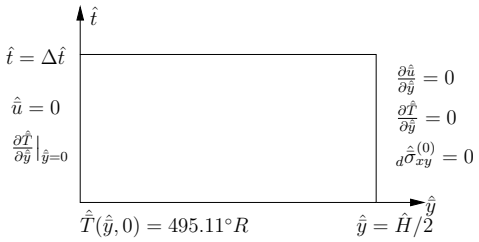

$\hat{H} = 0.25ft = 3in \qquad \Delta\hat{t} = 12.5sec$

(b) Space-time strip

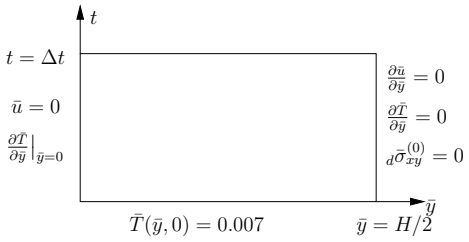

$H = 0.5 \qquad \Delta t = 50$

(c) Dimensionless space-time strip

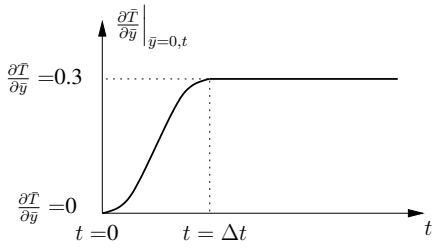

(d) Applied temperature gradient

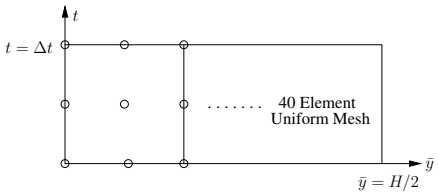

(e) Space-time discretization

Figure 74: 2D solid-liquid phase transition: space-time slab, boundary conditions, and initial condition

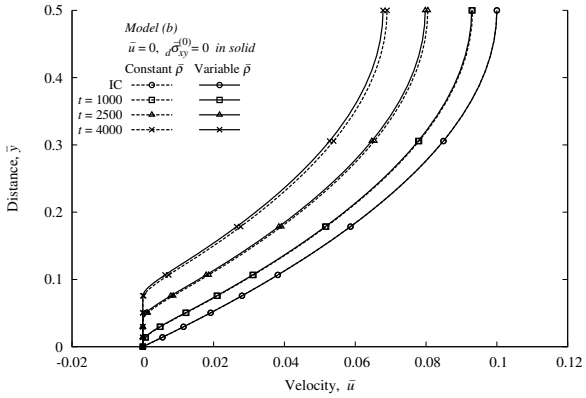

Figure 75: Model Problem 6: Evolution of velocity $\bar{u}$ versus $\bar{y}$ using model (b), $C^{11}(\bar{\Omega}^e_{xt}), p = 9, \Delta t = 50$

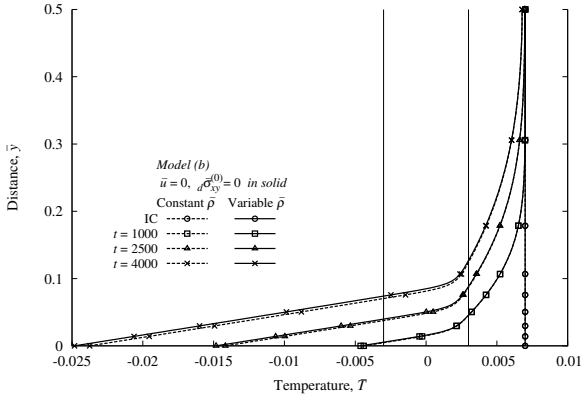

Figure 76: Model Problem 6: Evolution of temperature $\bar{T}$ versus $\bar{y}$ using model (b), $C^{11}(\bar{\Omega}^e_{xt}), p = 9, \Delta t = 50$

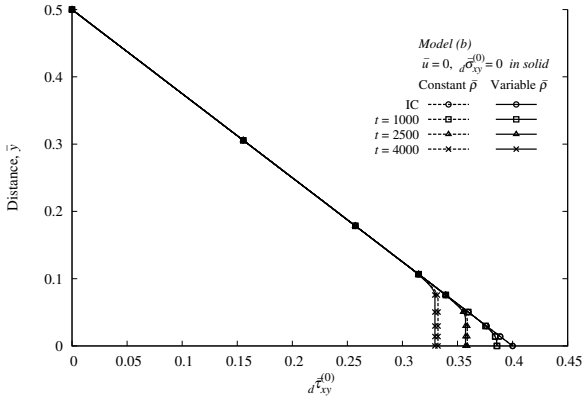

Figure 77: Model Problem 6: Evolution of ${}_d\bar{\tau}^{(0)}_{xy}$ versus $\bar{y}$ using model (b), $C^{11}(\bar{\Omega}^e_{xt}), p = 9, \Delta t = 50$

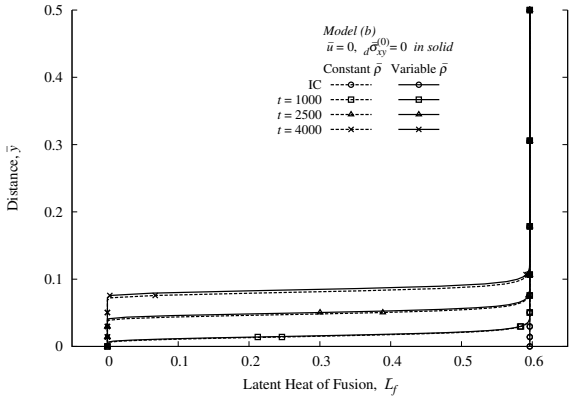

Figure 78: Model Problem 6: Evolution of latent heat $\bar{L}_f$ versus $\bar{y}$ using model (b), $C^{11}(\bar{\Omega}^e_{xt}), p = 9, \Delta t = 50$

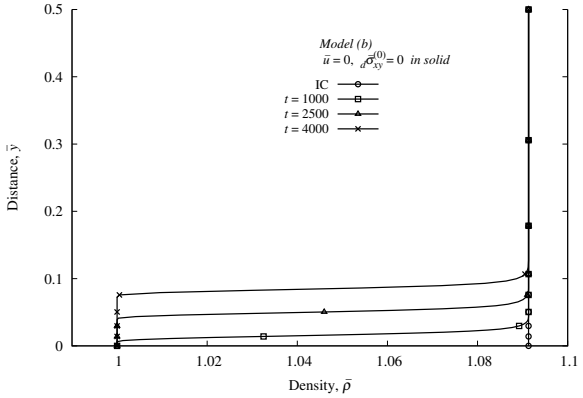

Figure 79: Model Problem 6: Evolution of density $\bar{\rho}$ versus $\bar{y}$ using model (b), $C^{11}(\bar{\Omega}^e_{xt}), p = 9, \Delta t = 50$

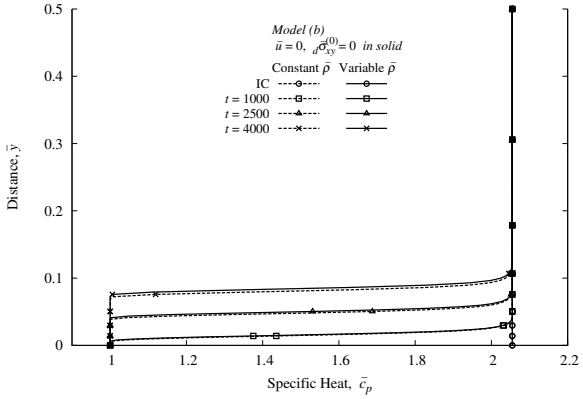

Figure 80: Model Problem 6: Evolution of specific heat $\bar{c}_p$ versus $\bar{y}$ using model (b), $C^{11}(\bar{\Omega}^e_{xt}), p = 9, \Delta t = 50$

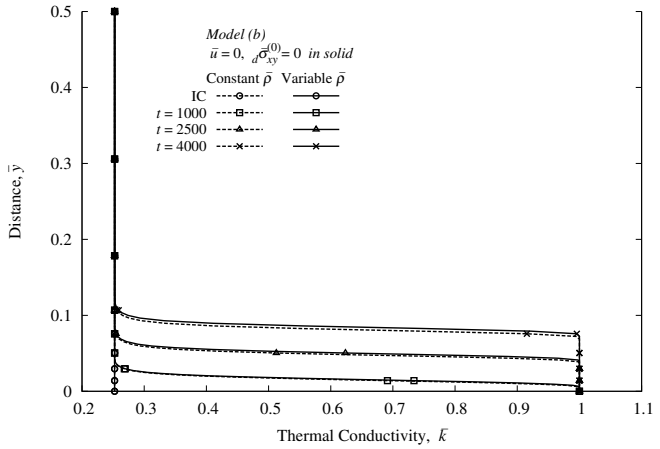

Figure 81: Model Problem 6: Evolution of thermal conductivity $\bar{k}$ versus $\bar{y}$ using model (b), $C^{11}(\bar{\Omega}^e_{xt}), p = 9, \Delta t = 50$

Evolutions are continuous and differentiable and are free of oscillations. As expected, variable density evolution leads constant density evolution.

Since in this model problem the flow is pressure driven, with continued evolution it is possible to freeze the entire height $\frac{H}{2}$ that corresponds to $\frac{\partial \bar{p}}{\partial \bar{x}} = 0$, zero velocity field, and zero flow rate.

Figures 82–84 show evolution of $\bar{u}$, $\bar{T}$, ${}_d\bar{\tau}^{(0)}_{xy}$ for $0 \leq t \leq 25000$. At $t = 25000$, the height $\frac{H}{2}$ is completely frozen with zero velocity and zero deviatoric Cauchy shear stress ${}_d\bar{\sigma}^{(0)}_{xy}$.

In figure 84, the graphs AA_1B_1, AA_2B_2, AA_3B_3, AA_4B_4, and AB_5 are shear stress distributions in the liquid-solid phases during evolution. The constant value of the stress in the solid region is dictated by the shear stress at the liquid-solid interface. As evolution proceeds the shear stress in the solid region progressively decreases (as expected due to reduced flow rate) and eventually becomes zero when the entire width $H/2$ solidifies.

It is interesting to observe the behavior of temperature $\bar{T}$ beyond $t = 23000$, at which the majority of $\frac{H}{2}$ is frozen but a small portion at the centerline still remains in the transition and liquid regions. Another six time increments ($t = 23300$) still show a very small portion of $\frac{H}{2}$ in the transition region. After another time step ($t = 23350$) the domain $\frac{H}{2}$ is completely frozen. $\frac{\partial \bar{T}}{\partial \bar{y}}$ condition at the centerline (due to symmetry) is responsible for the $\bar{T}$ versus $\bar{y}$ behavior (not a straight line as in linear heat conduction) at $t = 23350$ and beyond.

Figure 82 also shows a comparison of the calculated velocities with the theoretical solution for pressure-driven fully developed flow between parallel plates calculated using the same $\frac{\partial \bar{p}}{\partial \bar{x}}$ (-6.7182×10^{-5}) and the non-frozen part of $\frac{H}{2}$. Extremely minor deviations between the two are due to not being able to define the completely frozen height clearly as the transition region separates the liquid and solid regions.

Numerical Results using Model (a)

Numerical studies similar to those presented for model (b) are also conducted for model (a). A comparison of the results from models (b) and (a) is shown in figures 85 and 86. Evolution of deviatoric Cauchy shear stress ${}_d\bar{\sigma}^{(0)}_{xy}$ is shown in figure 87.

Results from the two mathematical models compare well.

Remarks

(1) Phase transition in the presence of flow is simulated quite accurately using Model (b) as well as Model (a) but requires assumption of constant stress field and zero velocity field in the solid medium. In the transition region, the stress field and

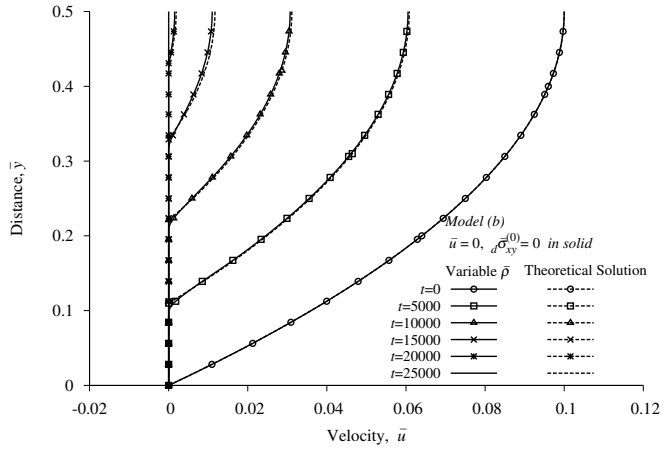

Figure 82: Model Problem 6: Evolution of velocity $\bar{u}$ versus $\bar{y}$ using model (b), $C^{11}(\bar{\Omega}^e_{xt}), p = 9, \Delta t = 50$

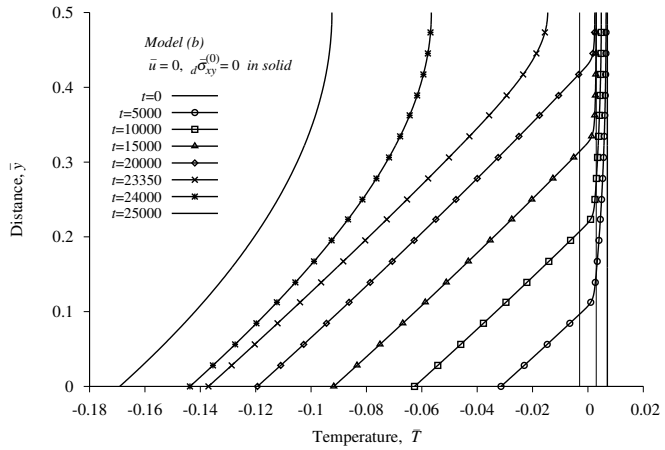

Figure 83: Model Problem 6: Evolution of temperature $\bar{T}$ versus $\bar{y}$ using model (b), $C^{11}(\bar{\Omega}^e_{xt}), p = 9, \Delta t = 50$

the velocity field transition from non-constant and nonzero values in the liquid region to constant and zero values in the solid region based on temperature $T \in [T_s, T_l]$. It is only with these assumptions that it is possible to establish interaction between different phases.

(2) Model (a) is preferable as in this case the mathematical model directly results from the conservation and balance laws and the constitutive theories for the deviatoric Cauchy stress tensor and heat vector from the second law of thermodynamics.

(3) It is noteworthy that even though phase transition physics in the transition region is quite complex, the assumption of homogeneity and isotropy with continuous and differentiable transition in the transport properties over the range $[\bar{T}_s, \bar{T}_l]$ is quite effective in simulating the evolutions of the expected physics.

(4) Application of the mathematical model in section III.3.3 (general case of Model (a)) is straightforward for phase transition studies in $\mathbb{R}^2$ and $\mathbb{R}^3$. The mathematical model and the computational procedure provide a straightforward means of phase transition initiation and its evolution in $\mathbb{R}^1$, $\mathbb{R}^2$, and $\mathbb{R}^3$ in the presence of nonzero stress and velocity fields in the liquid and transition regions but with the assumption of constant stress and zero velocity field in the solid region.

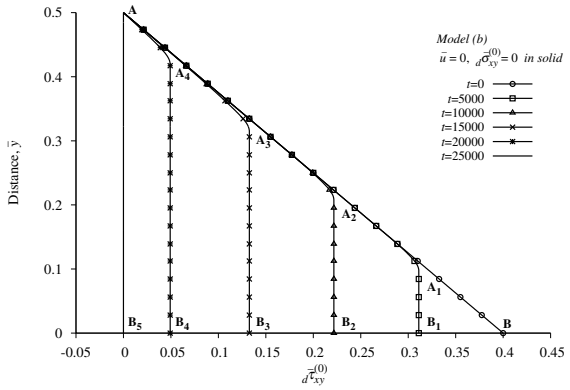

Figure 84: Model Problem 6: Evolution of ${}_d\bar{\tau}^{(0)}_{xy}$ using model (b), $C^{11}(\bar{\Omega}^e_{xt}), p = 9, \Delta t = 50$

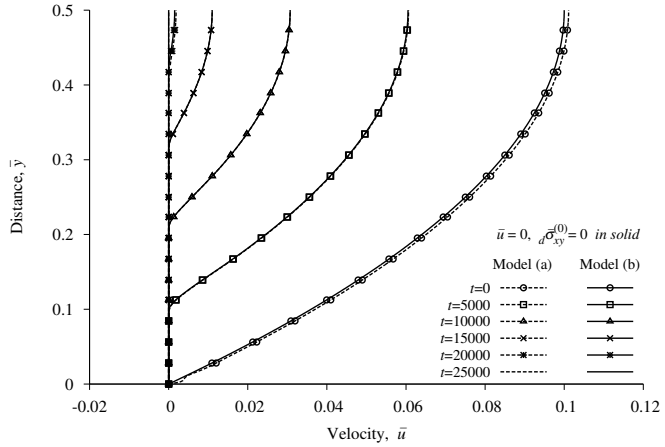

Figure 85: Model Problem 6: Evolution of velocity $\bar{u}$ versus $\bar{y}$ using model (a), $C^{11}(\bar{\Omega}^e_{xt}), p = 9, \Delta t = 50$

III.4 Summary, concluding remarks, significance and impact of this research

Summary and conclusions from the work presented are given in the following.

(1) Various modeling approaches have been discussed and the associated mathematical models have been presented.

(2) It is established that out of all the mathematical models presented here, the following two groups of mathematical models are in compliance with conservation and balance laws and provide correct interaction physics between all three phases.

   (a) The models derived based on zero stress and zero velocity fields in all phases.

   (b) The models derived based on constant stress field and zero velocity field in the solid region, complete conservation and balance laws in fluid region, and the stresses and velocities making transition based on temperature from the two states in the transition region.

(3) Numerical studies for model problems in $\mathbb{R}^1$ and $\mathbb{R}^2$ are presented based on space-time finite element method derived using space-time residual functional using the mathematical models described in (2). All numerical solutions reported in this section

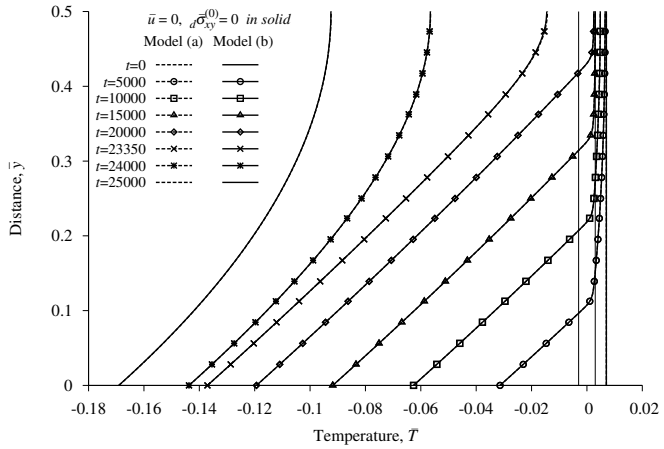

Figure 86: Model Problem 6: Evolution of temperature $\bar{T}$ versus $\bar{y}$ using model (a), $C^{11}(\bar{\Omega}^e_{xt}), p = 9, \Delta t = 50$

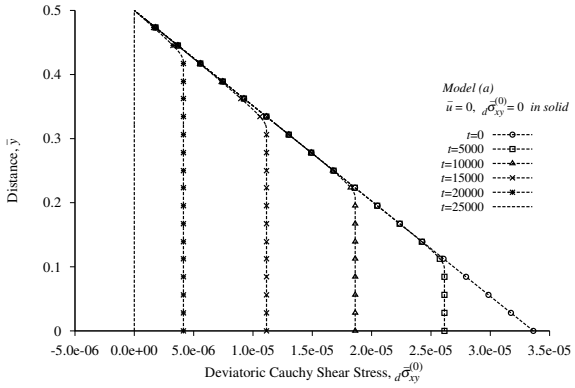

Figure 87: Model Problem 6: Evolution of deviatoric Cauchy shear stress ${}_d\bar{\sigma}^{(0)}_{xy}$ using model (a), $C^{11}(\bar{\Omega}^e_{xt}), p = 9, \Delta t = 50$

are converged solutions corresponding to space-time residual functionals of the order of $O(10^{-6})$ or lower. When the space-time integrals are Riemann, such low values of the space-time residuals ensure that the computed solutions satisfy GDEs in pointwise sense during the entire evolution.

(4) Smooth-interface approach avoids complex physics of transition region without affecting speed of propagation of the phase transition region. The transition region $[T_s, T_l]$ can be as narrow or as wide as desired.

(5) The smooth-interface approach presented here is highly meritorious over sharp-interface and phase field approaches as it permits initiation of phase transition and its subsequent evolution, whereas in sharp-interface and phase field methods a priori existence of phase transition is essential as initial condition i.e. these methods cannot simulate initiation of phase transition. This is a serious handicap in these methods. In most applications of interest, initiation of phase transition is essential as when and the precise conditions under which it occurs may not be known a priori.

(6) The published works on sharp-interface and phase field methods for phase transition generally consider constant density. The work presented here demonstrates that the variable density is necessary in the mathematical models to incorporate correct physics in the mathematical model. Incorporating $\rho = \rho_s$, $\rho = \rho_l$ in the liquid and solid regions and $\rho = \rho(T)$ in the transition region, as done in the case of variable density used in the present work, is more realistic description of actual physics. It is

demonstrated in the numerical studies that with variable density phase transition evolutions lead constant density evolutions for liquid-solid phase transition but lags for solid-liquid phase transition. It is shown in liquid-solid as well as solid-liquid phase transitions the distance between the locations of the center of the transition zones between variables and constant density cases increases as the evolution proceeds.

(7) Space-time finite element processes based on residual functionals with local approximation in $H^{k,p}(\bar{\Omega}^e_{xt})$ spaces for a space-time strip or slab with time marching work perfectly in computing accurate evolutions. This computational framework provides means of incorporating higher order global differentiability approximations in space and time as well as increasing p-levels for desired accuracy.

(8) The first group of mathematical models (2a) is ideal for phase transition studies in $\mathbb{R}^1$, $\mathbb{R}^2$, and $\mathbb{R}^3$ with zero stress, zero velocity, and free boundaries assumptions in all phases. Numerical studies and comparison with sharp-interface approach confirm this.

(9) The second group of models (2b) based on constant stress and zero velocities in the solid region are ideal for phase transition studies in the presence of flow without the assumption of constant stress and zero velocity fields in the liquid and transition regions. These groups of models are essential in establishing interaction between the solid, transition, and liquid phases such that the interaction is intrinsic and consistent (based on continuum mechanics principles) in the mathematical model. This model ensures that no artificial or external means are needed at the interface boundaries between the phases. Fully developed pressure-driven flow between parallel plates is an impressive illustration of the capabilities of these models that can be used in $\mathbb{R}^2$ and $\mathbb{R}^3$ to perform simulation of complex solidification (or melting) processes in phase transition applications.

(10) We remark that sharp-interface and phase field models do not permit initiation of phase transition but require its specification as initial condition. The models presented here permit initiation of liquid-solid and solid-liquid phase transition as well as its propagation during evolution without using any special or artificial means in the mathematical models or the numerical computations.

The fluid-solid or the solid-fluid phase transition obviously requires FSI. We know from the work presented in FSI research that at present with currently used mathematical models for solids and fluids, this is not possible without severe assumptions and limitations that only permit crude numerical solutions of a very isolated class of BVPs. In the present work, some important and realistic considerations are employed in such a way that the resulting mathematical models permit accurate solid-fluid and fluid-solid transition physics studies. Significant aspect of this work are described in (1)-(10) above and are not repeated for the same of brevity. Smooth interface approach used here is highly meritorious at it does not disturb the physics on either side of the transition zone. It is shown that when the stress field is assumed constant in the solid region and velocities are assumed zero, hence zero displacements with full thermodynamics model for fluid, liquid-solid phase transition studies can be performed accurately. This is demonstrated very well by the pressure driven flow between parallel plates in which the plates are cooled. The progressive cooling with evolution eventually freezes the entire flow domain between the plates.

IV A simple mixture theory for ν Newtonian and generalized Newtonian constituents

This work presents development of mathematical models based on conservation laws for a saturated mixture of ν homogeneous, isotropic, and incompressible constituents for isothermal flows. The constituents and the mixture are assumed to be Newtonian or generalized Newtonian fluids. Power law and Carreau-Yasuda models are considered for generalized Newtonian shear thinning fluids. The mathematical model is derived for a ν constituent mixture with volume fractions ϕ_α using principles of continuum mechanics: conservation of mass, balance of momenta, first and second laws of thermodynamics, and principles of mixture theory yielding continuity equations, momentum equations, energy equation, and constitutive theories for mechanical pressures and deviatoric Cauchy stress tensors in terms of the dependent variables related to the constituents. It is shown that for Newtonian fluids with constant transport properties, the mathematical models for constituents are decoupled. In this case one could use individual constituent models to obtain constituent deformation fields, and then use mixture theory to obtain the deformation field for the mixture. In the case of generalized Newtonian fluids, the dependence of viscosities on deformation field does not permit decoupling. Numerical studies are also presented to demonstrate this aspect. Using fully developed flow of Newtonian and generalized

Newtonian fluids between parallel plates as a model problem, it is shown that partial pressures p_α of the constituents must be expressed in terms of the mixture pressure p. In this work we propose $p_\alpha = \phi_\alpha p$ and $\sum_\alpha^\nu p_\alpha = p$ which implies $\sum_\alpha^\nu \phi_\alpha = 1$ which obviously holds. This rule for partial pressure is shown to be valid for a mixture of Newtonian and generalized Newtonian constituents yielding Newtonian and generalized Newtonian mixture. Modifications of the currently used constitutive theories for deviatoric Cauchy stress tensor are proposed. These modifications are demonstrated to be essential in order for the mixture theory for ν constituents to yield a valid mathematical model when the constituents are the same. Dimensionless form of the mathematical models are derived and used to present numerical studies for boundary value problems using finite element processes based on a residual functional i.e. least squares finite element processes in which local approximations are considered in $H^{k,p}\left(\bar{\Omega}^e\right)$ scalar product spaces. Fully developed flow between parallel plates and 1:2 asymmetric backward facing step are used as model problems for a mixture of two constituents.

IV.1 Introduction, Literature Review, and Scope of Work

IV.1.1 Introduction and Literature Review

The origin and the basis of the modern mixture theories seems to have begun in the late fifties. Papers by Truesdell et. al [103, 104] present equations of balance for a mixture based on balance of mass, momentum, and energy. This formulation has been generalized in many ways in references [105–107]. In a paper by Bowen [108], "Towards a Thermodynamic and Mechanics of Mixtures", a good historical development of the mixture theory is presented. Bowen's work in reference [108] is based on fundamental assumption that mixture stress is not the sum of the partial stresses of the constituent. This work is advocated to be a candidate for a general theory of mixtures. There are many works related to the incompressible porous media models that originate from thermodynamics of mixture theories. Work by Bowen [109] discusses incompressible porous media as a mixture where solid and fluid constituents are each incompressible. A review article by Boer [110] on porous media theories is a good source for a comprehensive list of published works in which porous media theories use mixture theory as an origin. Boer et. al. [111] discuss effects of uplift, friction, and capillarity for liquid-saturated porous solids by using general porous media theories that are based on mixture theories extended by the volume fraction concept. In another paper [112] Boer presents a brief historical review of the porous media theories. Thermodynamics of fluid saturated porous media with phase change is presented by Boer in reference [113]. In reference [114], Bluhm and Boer consider the volume fraction concept in porous media. The paper presents historical development of the theory and the development of transport theorem based on volume fraction. A history of mixture theory models can be found in the book by Boer [115].

Most of the recent literature on mixture theories can be divided into two major categories: theories based on volume averaging and theories based on the principles of continuum mechanics. The primary focus of this work is on mixture theories based on principles of continuum mechanics. Theories based on volume averaging involve applying volume and/or time integrals over a heterogeneous mixture to obtain "averaged" properties of the mixture. While these techniques may be useful due to their ability to reduce the number of dependent variables for a given problem, they generally lack a mechanism to recover meaningful information about the behavior of individual constituents. Because of this shortcoming, the primary focus of the majority of recently published works has been on continuum mechanics based theories. Information on averaged theories can be found in papers by Drew [116], Rubinow and Keller [117], Enlwald and Almstedt [118, 119], Terada et al [120], and Ahmadi et al [121].

Mixture theories based on continuum mechanics principles assume that each material point in the mixture is occupied simultaneously by each constituent [74]. This assumption is not physically accurate of course, but is necessary so that the quantities used to describe deformation are continuous and differentiable. This allows the development of the mathematical models that describe the behaviors of mixtures in a similar manner to those for homogeneous matter. Truesdell proposed a theory called a mechanical basis for diffusion. Author presents definitions for the basic kinematic relations as well as the continuity and momentum equations for mixtures of arbitrary constituents. This theory allows for the transfer of mass and momentum from one constituent to another, which is commonly referred to as the "interaction force" [74, 76, 122]. It is shown that Fick's Law of diffusion is a specific case of this theory.

Later Müller [123] presented the energy equation and entropy inequality for ν constituents, as well as a linear constitutive theory for a mixture of two Newtonian fluids. The author uses density gradients, the symmetric and anti-symmetric parts of the velocity gradient tensors, temperature gradient, and relative velocity between constituents as the arguments of the dependent variables in the constitutive theory. The author also shows that based on this theory, a mixture of two ideal gases is still an ideal gas with properties

that agree with the principle of partial pressures based classical thermodynamics. Green and Naghdi [124] propose a similar theory in which they use the energy equation and entropy inequality to derive the continuity and momentum equations. This is followed by the derivation of constitutive equations for the mixture of two Newtonian fluids including resulting thermodynamic restrictions. Atkin and Craine [125] derive continuity, momentum, and energy equations, and the entropy inequality for mixtures, as well as a constitutive theory for mixtures of ideal inviscid fluids. The authors show that the results agree with kinetic theory of gases. Bedford and Drumheller [126] present a survey of continuum theories of mixtures. The authors include constitutive examples for mixtures of immiscible fluids, solid particles suspended in fluids, fluids flowing through porous media, chemically reacting fluids, and composite materials. The authors also provide an overview of volume averaged theories, and micro-structure theories. The theory for mixtures of two fluids is restricted to mixtures of an inviscid and a viscous fluid.

In [74] authors derive the conservation laws for mixtures and provide details for several example problems including: diffusion of a fluid through a solid experiencing finite deformation, steady state diffusion problems, a diffusing singular surface, wave propagation, mixtures of Newtonian fluids, and solid particle suspensions. The main difference in these is the constitutive theory used for the stress tensor and the "interaction force". The authors derive the constitutive theory by selecting argument tensors based on the assumed physics of the problem and use the entropy inequality to determine appropriate restrictions on the material coefficients.

In reference [122] a review of interaction forces is given for fluid-solid mixtures. The authors compare constitutive theory for the interaction force to volume averaged theories based on results for single particle flows. The results include comparisons for drag, lift, buoyancy, and other effects. Johnson et al present numerical results for flow between parallel plates of solid particles suspended in a fluid [127]. The authors present a constitutive model for granular particles suspended in a fluid and simplify the governing equations to a system of ODE's which are then solved using a collocation method. Results are presented showing the effect of varying the volume fraction of the constituents and the coefficients of the interaction force terms. Massoudi et al [128] present results for a similar problem using pipe flow assumptions, and Massoudi and Rao [129] give results for flow between parallel plates. In [130] Massoudi et al show results for particulate flow down an inclined plane.

In references [131–133] authors present a series of studies for mixtures of fluids in a bearing. In [131] an oil-water mixture is considered. The authors give a mathematical model and results for 2D non-isothermal flow in a bearing. Portions of this mathematical model are used in section IV.2.10. The authors use a constitutive theory that includes relative velocity, volume fraction gradients, temperature gradient, and the symmetric part of the velocity gradient tensor as argument tensors of the dependent variables in the constitutive theories. Results are given for different volume fractions. In [132] a "bubbly oil" mixture is considered, and in [133] an oil-water mixture is studied in an elastohydrodynamic bearing. Similar results are given and the mathematical models only vary because of the different constitutive theory used for the gas phase. In all of the published work, the authors use finite difference method to obtain numerical results.

Massoudi [76] shows how the constitutive theory for solid particles suspended in a fluid (given previously in [122]) can be derived using the theory of invariants and generators. In [134] the author gives a method for applying boundary conditions when computing solutions to mixture problems. Massoudi [135] also shows that the constitutive theory used for a mixture of two fluids must reduce to the theory for a single fluid as the volume fraction approaches the limiting case of 0 or 1. The author also notes that the best way to ensure this is to have viscosity terms that are weighted by volume fraction. For more information on mixture theories see reference [74].

IV.1.2 Scope of Work and assumptions used

Mathematical models are derived based on mixture theory for ν homogeneous, isotropic, and incompressible constituents using conservation of mass, balance of momenta, and the first law of thermodynamics. For isothermal flows the constitutive theories for mechanical pressure and the deviatoric Cauchy stress tensor are presented for the constituents and the mixture based on the second law of thermodynamics. Currently used mixture theories are examined and essential modifications are suggested based on the physics. The resulting modified mixture theory is used in the numerical studies to demonstrate its validity.

In the following we state the assumptions used in deriving the mixture theory presented in this work. Constituents and mixture both are assumed incompressible. The fluids are assumed to be non-interacting. This assumption eliminates such features as relative drag, relative spin, or "Magnus effects" which could be significant near boundaries where there is high shear and hence high rotation. Thus, in applications where the mechanical interaction leads to "unmixing", segregation, etc, this theory is inadequate. In

the development of the mathematical model, specific heat is assumed to be constant. This assumption is obviously too restrictive for compressible constituents and compressible mixtures, but is adequate when the constituents and the mixture are incompressible. The volume additivity constraint is used throughout in the derivation. The incompressibility constraint is introduced in the entropy inequality through a Lagrange multiplier p representing mechanical pressure for the mixture. We further assume that contributions of p to partial pressures p_α of the constituents is through $\phi_\alpha p$ in which ϕ_α are volume fractions of the constituents. For the mixture theory presented here, this assumption reduces to $p_\alpha = -\phi_\alpha p$ where p_α are partial mechanical pressures for the constituents. Validity of this assumption is demonstrated and is also verified in the numerical results presented for the model problems. A thermodynamical way to split tractions is to prescribe total pressure and the chemical potential at the boundaries as discussed by Baek and Srinivasa in reference [136]. Whether this leads to the mechanical pressure assumptions used in the present work is not verified in this work. Throughout the derivations, the volume fractions of the constituents are assumed to be constant. The dissipation due to interaction of the constituents is neglected in the derivation of the entropy inequality.

The mixture theory presented in the work considers Newtonian and generalized Newtonian fluids. Power law and Carreau-Yasuda models for shear thinning fluids are used for the generalized Newtonian fluids. Dimensionless forms of the mathematical models are derived and used in the numerical studies. Numerical studies are given for Newtonian, power law, and Carreau fluids using fully developed flow between parallel plates and 1:2 asymmetric sudden expansion as model problems for a saturated mixture of two constituents.

Numerical solutions of the BVPs are computed using finite element processes based on a residual functional, i.e. least squares finite element processes, that ensure unconditionally stable computation. Local approximations are considered in $H^{k,p}\left(\bar{\Omega}^e\right)$ scalar product spaces.

IV.2 Development of Mathematical Model for a Mixture of ν Fluids

IV.2.1 Introduction

In this section we present derivations of continuity equation, momentum equations, energy equation, entropy inequality, and the constitutive theory derived from the entropy inequality for a saturated mixture of ν Newtonian and generalized Newtonian fluids. Some basic definitions of bulk densities of constituents, mixture density, mixture velocities, etc. are introduced based on basic physical principles that are used in the development of the mathematical model for the mixture. To avoid confusion in the notation used here and those commonly used in continuum mechanics we adopt the following convention. Greek letters such as α, β, γ, ν, etc. used as subscripts, superscripts, or indices refer to a quantity associated with an individual constituent and have no implied summation when the index is repeated. Any index using English letters i, j, k, etc. implies standard continuum mechanics summation conventions, i.e. summation over repeated indices. The derivation of the mathematical model presented in this section is strictly based on principles of continuum mechanics and thermodynamics.

IV.2.2 Preliminary Definitions

In this section we present basic definitions of bulk densities of constituents, mixture density, mixture velocity, material derivative for the constituents and the mixture etc. These are subsequently used in the conservation laws. We consider a saturated mixture of ν constituents with ϕ_α; $\alpha = 1, 2, \ldots, \nu$ volume fraction, and $\rho^{(\alpha)}$; $\alpha = 1, 2, \ldots, \nu$ constituent densities. We can give the following definitions:

IV.2.3 Definitions of densities

Consider an elemental volume dV of the mixture of Volume V. Then $\rho^{(\alpha)}\phi_\alpha dV$ is the mass of each constituent in the volume dV. If ρ_m is the bulk density of the mixture, then $\rho_m dV$ is also the total mass in the elemental volume dV. Hence, for volume V, we have

$$\int\limits_{V(t)} \rho_m dV = \sum_{\alpha=1}^{\nu} \int\limits_{V(t)} \rho^{(\alpha)}\phi_\alpha dV \tag{IV.1}$$

or

$$\int_{V(t)} \left(\rho_m - \sum_{\alpha=1}^{\nu} \rho^{(\alpha)} \phi_\alpha \right) dV = 0 \tag{IV.2}$$

Since $V(t)$ is arbitrary, we have

$$\rho_m = \sum_{\alpha=1}^{\nu} \rho^{(\alpha)} \phi_\alpha \tag{IV.3}$$

If we define bulk density of a constituent ρ_α as

$$\rho_\alpha = \rho^{(\alpha)} \phi_\alpha \tag{IV.4}$$

Then IV.3 can be written as

$$\rho_m = \sum_{\alpha=1}^{\nu} \rho_\alpha \tag{IV.5}$$

Additionally, for a saturated mixture, the volume additivity constraint must hold, i.e.

$$\sum_{\alpha=1}^{\nu} \phi_\alpha = 1 \tag{IV.6}$$

IV.2.4 Mixture velocities

Let $\mathbf{v}_\alpha$ be the velocities of the constituents at a material particle (simultaneously occupied by all constituents) and $\mathbf{v}$ the velocity of the mixture, then using the principle of balance of momentum, i.e. the momentum of the mixture must be equal to the sum of the momenta of the constituents, we have

$$\rho_m \mathbf{v} = \sum_{\alpha=1}^{\nu} \rho_\alpha \mathbf{v}_\alpha \tag{IV.7}$$

Equation IV.7 defines the mixture velocity at a material particle in terms of bulk densities of the constituents, their velocities, and the mixture density.

IV.2.5 Material derivative for the constituents and the mixture

Since the material derivative $\frac{D(\cdot)}{Dt}$ in Eulerian description uses the velocity of a material particle, it needs to be defined for each constituent. The material derivative of a dependent variable Q for constituent α is defined as

$$\frac{D_\alpha Q}{Dt} = \frac{\partial Q}{\partial t} + \mathbf{v}_\alpha \cdot \boldsymbol{\nabla} Q \tag{IV.8}$$

The material derivative of Q for the mixture is defined as

$$\rho_m \frac{DQ}{Dt} = \sum_{\alpha=1}^{\nu} \rho_\alpha \frac{D_\alpha Q}{Dt} = \sum_{\alpha=1}^{\nu} \rho_\alpha \left(\frac{\partial Q}{\partial t} + \mathbf{v}_\alpha \cdot \boldsymbol{\nabla} Q \right)$$

or

$$\rho_m \frac{DQ}{Dt} = \left(\sum_{\alpha=1}^{\nu} \rho_\alpha \right) \frac{\partial Q}{\partial t} + \left(\sum_{\alpha=1}^{\nu} \rho_\alpha \mathbf{v}_\alpha \right) \cdot \boldsymbol{\nabla} Q$$

$\therefore$

$$\rho_m \frac{DQ}{Dt} = \rho_m \frac{\partial Q}{\partial t} + \rho_m \mathbf{v} \cdot \boldsymbol{\nabla} Q \tag{IV.9}$$

IV.2.6 Conservation Laws

We use the definitions presented in section IV.2.2 to derive details of the mathematical model for the mixture using conservation laws. We assume the constituents and the mixture to be incompressible and the flows to be isothermal. The constituents and the mixture are considered to be Newtonian and generalized Newtonian fluids. The viscosities of the constituents and the mixture are described using the Carreau-Yasuda model. We present a general derivation which is made specific based on the assumptions stated above.

IV.2.7 Conservation of Mass

If we apply conservation of mass to an arbitrary volume containing ν constituents with bulk densities ρ_α and velocities $\mathbf{v}_\alpha$, then for each constituent we obtain

$$\frac{\partial \rho_\alpha}{\partial t} + \boldsymbol{\nabla} \cdot (\rho_\alpha \mathbf{v}_\alpha) = 0 \tag{IV.10}$$

Summing (IV.10) for the constituents

$$\sum_{\alpha=1}^{\nu} \frac{\partial \rho_\alpha}{\partial t} + \sum_{\alpha=1}^{\nu} \boldsymbol{\nabla} \cdot (\rho_\alpha \mathbf{v}_\alpha) = 0 \tag{IV.11}$$

or

$$\frac{\partial}{\partial t}\left(\sum_{\alpha=1}^{\nu} \rho_\alpha\right) + \boldsymbol{\nabla} \cdot \left(\sum_{\alpha=1}^{\nu} \rho_\alpha \mathbf{v}_\alpha\right) = 0 \tag{IV.12}$$

Using (IV.5) and (IV.7), (IV.12) can be written as

$$\frac{\partial \rho_m}{\partial t} + \boldsymbol{\nabla} \cdot (\rho_m \mathbf{v}) = 0 \tag{IV.13}$$

For the incompressible case (IV.10) and (IV.13) reduce to

$$\rho_\alpha \left(\boldsymbol{\nabla} \cdot \mathbf{v}_\alpha\right) = 0 \tag{IV.14}$$

$$\rho_m \left(\boldsymbol{\nabla} \cdot \mathbf{v}\right) = 0 \tag{IV.15}$$

IV.2.8 Balance of Momenta

Using the principle of balance of linear momentum to an arbitrary volume of mixture yields the following three equations for constituent α (in the absence of body forces)

$$\rho_\alpha \frac{D_\alpha \mathbf{v}_\alpha}{Dt} = \boldsymbol{\nabla} \cdot [\sigma_\alpha]^T + \boldsymbol{\pi}_\alpha \tag{IV.16}$$

Where $[\sigma_\alpha]^T$ is the contravariant Cauchy stress tensor and $\boldsymbol{\pi}_\alpha$ is the force exerted on the α^{th} constituent by each of the other constituents. In general

$$\sum_{\alpha=1}^{\nu} \boldsymbol{\pi}_\alpha = 0 \tag{IV.17}$$

must hold. In the case of a mixture of two constituents, IV.17 reduces to:

$$\boldsymbol{\pi}_1 = -\boldsymbol{\pi}_2 \tag{IV.18}$$

IV.2.9 Energy equation

In the derivation of the energy equation we assume that the sum of the constituent energies is the total energy of the mixture. For a constituent α, the rate of change of the total energy must be equal to the rate of heat added and the rate of work done.

$$\frac{D_\alpha E_t^\alpha}{Dt} = \frac{D_\alpha Q^\alpha}{Dt} + \frac{D_\alpha W^\alpha}{Dt} \tag{IV.19}$$

and for the mixture

$$\sum_{\alpha=1}^{\nu} \frac{D_\alpha E_t^\alpha}{Dt} = \sum_{\alpha=1}^{\nu} \frac{D_\alpha Q^\alpha}{Dt} + \sum_{\alpha=1}^{\nu} \frac{D_\alpha W^\alpha}{Dt} \tag{IV.20}$$

where (in the absence of body forces)

$$E_t^\alpha = \int\limits_{V(t)} \rho_\alpha \left(e_\alpha + \frac{1}{2}\mathbf{v}_\alpha \cdot \mathbf{v}_\alpha \right) dV \tag{IV.21}$$

$$\sum_{\alpha=1}^{\nu} \frac{D_\alpha Q^\alpha}{Dt} = -\int\limits_{\partial V} \mathbf{q} \cdot \mathbf{n} dS = -\int\limits_{V(t)} \boldsymbol{\nabla} \cdot \mathbf{q} dV \tag{IV.22}$$

$\mathbf{q}$ is total heat flux and $\mathbf{n}$ is the outward unit normal to the boundary dV of volume $V(t)$ in the current configuration.

$$\begin{aligned} \frac{D_\alpha W^\alpha}{Dt} &= \int\limits_{\partial V} \mathbf{P} \cdot \mathbf{v}_\alpha dS = \int\limits_{\partial V} \left([\sigma_\alpha]^T \cdot \mathbf{n} \right) \cdot \mathbf{v}_\alpha dS \\ &= \int\limits_{V} \boldsymbol{\nabla} \cdot \left(\mathbf{v}_\alpha \cdot [\sigma_\alpha]^T \right) dV \end{aligned} \tag{IV.23}$$

or

$$\frac{D_\alpha W^\alpha}{Dt} = \int\limits_{V} \left(\mathbf{v}_\alpha \cdot \left(\boldsymbol{\nabla} \cdot [\sigma_\alpha]^T \right) + (\sigma_\alpha)_{ij} \frac{\partial (v_\alpha)_i}{\partial x_j} \right) dV \tag{IV.24}$$

$$\frac{D_\alpha E_t^\alpha}{Dt} = \frac{D_\alpha}{Dt} \int\limits_{V(t)} \rho_\alpha \left(e_\alpha + \frac{1}{2}\mathbf{v}_\alpha \cdot \mathbf{v}_\alpha \right) dV \tag{IV.25}$$

for the α^{th} constituent

$$(\rho_\alpha)_0 \, dV_0 = (\rho_\alpha) \, dV \tag{IV.26}$$

$(\rho_\alpha)_0$ and dV_0 are densities and volumes in the reference configuration. Hence

$$\frac{D_\alpha E_t^\alpha}{Dt} = \int\limits_{V_0} \frac{D_\alpha}{Dt} \left(\left(e_\alpha + \frac{1}{2}\mathbf{v}_\alpha \cdot \mathbf{v}_\alpha \right) (\rho_\alpha)_0 \right) dV_0 \tag{IV.27}$$

Since $\frac{D(\rho_\alpha)_0}{Dt} = 0$, (IV.27) reduces to

$$\begin{aligned} \frac{D_\alpha E_t^\alpha}{Dt} &= \int\limits_{V_0} \frac{D_\alpha}{Dt} (e_\alpha + \frac{1}{2}\mathbf{v}_\alpha \cdot \mathbf{v}_\alpha) (\rho_\alpha)_0 \, dV_0 \\ &= \int\limits_{V(t)} \frac{D_\alpha}{Dt} (e_\alpha + \frac{1}{2}\mathbf{v}_\alpha \cdot \mathbf{v}_\alpha) \rho_\alpha dV \\ &= \int\limits_{V(t)} \left(\frac{D_\alpha e_\alpha}{Dt} + \frac{1}{2} \frac{D_\alpha}{Dt} (\mathbf{v}_\alpha \cdot \mathbf{v}_\alpha) \right) \rho_\alpha dV \end{aligned}$$

or

$$\frac{D_\alpha E_t^\alpha}{Dt} = \int\limits_{V(t)} \left(\frac{D_\alpha e_\alpha}{Dt} + \mathbf{v}_\alpha \cdot \frac{D_\alpha \left(\mathbf{v}_\alpha\right)}{Dt} \right) \rho_\alpha dV \tag{IV.28}$$

Thus, the energy equation for the α^{th} constituent can be written as

$$\int\limits_{V(t)} \rho_\alpha \left(\frac{D_\alpha e_\alpha}{Dt} + \mathbf{v}_\alpha \cdot \frac{D_\alpha(\mathbf{v}_\alpha)}{Dt} \right) dV = - \int\limits_{V(t)} \boldsymbol{\nabla} \cdot \mathbf{q}_\alpha dV + \int\limits_{V(t)} \left(\mathbf{v}_\alpha \cdot \left(\boldsymbol{\nabla} \cdot \left[\sigma_\alpha\right]^T \right) + \left(\sigma_\alpha\right)_{ij} \frac{\partial (v_\alpha)_i}{\partial x_j} \right) dV \tag{IV.29}$$

In (IV.29) we have used

$$\mathbf{q} = \sum_{\alpha=1}^{\nu} \mathbf{q}_\alpha \tag{IV.30}$$

Since the volume $V(t)$ is arbitrary, (IV.29) reduces to

$$\rho_\alpha \frac{D_\alpha e_\alpha}{Dt} + \rho_\alpha \mathbf{v}_\alpha \cdot \frac{D_\alpha(\mathbf{v}_\alpha)}{Dt} + \boldsymbol{\nabla} \cdot \mathbf{q}_\alpha - \left(\mathbf{v}_\alpha \cdot \left(\boldsymbol{\nabla} \cdot \left[\sigma_\alpha\right]^T \right) + \left(\sigma_\alpha\right)_{ij} \frac{\partial (v_\alpha)_i}{\partial x_j} \right) = 0 \tag{IV.31}$$

From the momentum equation for α^{th} constituent

$$\rho_\alpha \frac{D_\alpha \mathbf{v}_\alpha}{Dt} = \boldsymbol{\nabla} \cdot \left[\sigma_\alpha\right]^T + \boldsymbol{\pi}_\alpha \tag{IV.32}$$

Substituting from (IV.32) into (IV.31)

$$\rho_\alpha \frac{D_\alpha e_\alpha}{Dt} + \mathbf{v}_\alpha \cdot \left(\boldsymbol{\nabla} \cdot \left[\sigma_\alpha\right]^T + \boldsymbol{\pi}_\alpha \right) + \boldsymbol{\nabla} \cdot \mathbf{q}_\alpha - \left(\mathbf{v}_\alpha \cdot \left(\boldsymbol{\nabla} \cdot \left[\sigma_\alpha\right]^T \right) + \left(\sigma_\alpha\right)_{ij} \frac{\partial (v_\alpha)_i}{\partial x_j} \right) = 0 \tag{IV.33}$$

or

$$\rho_\alpha \frac{D_\alpha e_\alpha}{Dt} + \mathbf{v}_\alpha \cdot \boldsymbol{\pi}_\alpha + \boldsymbol{\nabla} \cdot \mathbf{q}_\alpha - \left(\sigma_\alpha\right)_{ij} \frac{\partial (v_\alpha)_i}{\partial x_j} = 0 \tag{IV.34}$$

Summing (IV.34) over the constituents and using (IV.30)

$$\sum_{\alpha=1}^{\nu} \rho_\alpha \frac{D_\alpha e_\alpha}{Dt} + \sum_{\alpha=1}^{\nu} \mathbf{v}_\alpha \cdot \boldsymbol{\pi}_\alpha + \boldsymbol{\nabla} \cdot \mathbf{q} - \sum_{\alpha=1}^{\nu} \left(\sigma_\alpha\right)_{ij} \frac{\partial (v_\alpha)_i}{\partial x_j} = 0 \tag{IV.35}$$

If we assume that for the α^{th} constituent

$$e_\alpha = c_{p_\alpha} \theta \tag{IV.36}$$

and further assume constant c_{p_α}, then (IV.35) reduces to

$$\sum_{\alpha=1}^{\nu} \rho_\alpha c_{p_\alpha} \frac{D_\alpha \theta}{Dt} + \sum_{\alpha=1}^{\nu} \mathbf{v}_\alpha \cdot \boldsymbol{\pi}_\alpha + \boldsymbol{\nabla} \cdot \mathbf{q} - \sum_{\alpha=1}^{\nu} \left(\sigma_\alpha\right)_{ij} \frac{\partial (v_\alpha)_i}{\partial x_j} = 0 \tag{IV.37}$$

This is the final form of the energy equation for ν constituents. If we consider only two constituents then (IV.37) becomes

$$\left(\rho_1 c_{p_1} \frac{D_1 \theta}{Dt} + \rho_2 c_{p_2} \frac{D_2 \theta}{Dt} \right) + \left(\mathbf{v}_1 \cdot \boldsymbol{\pi}_1 + \mathbf{v}_2 \cdot \boldsymbol{\pi}_2 \right) + \boldsymbol{\nabla} \cdot \mathbf{q} - \left(\sigma_1\right)_{ij} \frac{\partial (v_1)_i}{\partial x_j} - \left(\sigma_2\right)_{ij} \frac{\partial (v_2)_i}{\partial x_j} = 0 \tag{IV.38}$$

The theories based on (IV.37) and (IV.38) are much simplified as some interaction effects [74] are neglected. But in view of the fact that we only consider incompressible constituents and isothermal flows, these derivations are adequate.

IV.2.10 Constitutive theory

We follow the derivations in reference [131] based on the following notations

$$\begin{aligned} \mathbf{L}_{(\alpha)} &= \operatorname{grad} \mathbf{v}_\alpha(x,t) \qquad & \mathbf{D}_{(\alpha)} &= \frac{1}{2}\left(\mathbf{L}_{(\alpha)} + \mathbf{L}_{(\alpha)}^{\mathbf{T}}\right) \qquad & \mathbf{q} &= \sum_{\alpha=1}^{\nu} \mathbf{q}_\alpha \\ Q &= \frac{1}{\rho_m}\sum_{\alpha=1}^{\nu} \rho_\alpha Q_\alpha \qquad & \eta &= \frac{1}{\rho_m}\sum_{\alpha=1}^{\nu} \rho_\alpha \eta_\alpha(x,t) \qquad & \boldsymbol{\pi} &= -\boldsymbol{\pi}_1 = \boldsymbol{\pi}_2 \end{aligned} \tag{IV.39}$$

In which $\mathbf{q}$ is heat flux, Q is heat supply, η and η_α are entropy densities of the mixture and the constituents. We begin with the entropy inequality

$$\rho_m \frac{D\eta}{Dt} + \operatorname{div}\left(\frac{\mathbf{q}}{\theta}\right) - \rho\frac{Q}{\theta} \geq 0 \tag{IV.40}$$

We have assumed that entropy due to heat flux $\mathbf{q}_\alpha$ is $\frac{\mathbf{q}_\alpha}{\theta}$ where θ is the common temperature of the constituents and the entropy due to heat supply Q_α is $\frac{Q_\alpha}{\theta}$. The dissipation due to interaction of the constituents is neglected in (IV.40).

Let the partial Helmholtz free energy Φ_α for the constituent α be

$$\Phi_\alpha = e_\alpha - \theta\eta_\alpha \tag{IV.41}$$

Using (IV.40) and (IV.41) and the energy equation in e_α and the additivity constraint $\sum_{\alpha=1}^{\nu}\phi_\alpha = 1$ we can establish the following dependent variables in the constitutive theory for constituent α.

$$\Phi_\alpha, \eta_\alpha, \boldsymbol{\pi}, \mathbf{q}, \boldsymbol{\sigma}_\alpha \tag{IV.42}$$

The following argument tensors of the dependent variables in the constitutive theory are considered in the development of the constitutive theory.

$$\mathbf{v}^{(12)}, \mathbf{g}, \mathbf{h}^{(\alpha)}, \mathbf{D}_{(\alpha)}, w_{(12)} \tag{IV.43}$$

in which $\mathbf{v}^{(12)}$ is relative velocity, $\mathbf{h}^{(\alpha)} = \operatorname{grad}\phi_\alpha$, and $w_{(12)}$ is relative spin. We consider $\Phi_\alpha = \Phi_\alpha(\phi_\alpha, \theta)$, $\Phi = \Phi(\phi_\alpha, \theta)$. We have the following for the constitutive theory derived using the theory of generators and invariants [137, 138] based on the assumption of linear dependence of the constitutive variables on the argument tensors. We consider two constituents only.

$$\begin{aligned} \eta &= -\frac{\partial\Phi}{\partial\theta} \\ \pi &= \beta_1\mathbf{v}^{(12)} + \beta_4\mathbf{g} + \left(-\rho_2\frac{\partial\Phi_2}{\partial\phi_1} + \frac{\rho_2}{\rho_m}\pi\right)\mathbf{h}^{(1)} + \left(\rho_1\frac{\partial\Phi_1}{\partial\phi_2} + \frac{\rho_1}{\rho_m}\pi\right)\mathbf{h}^{(2)} \\ \mathbf{q} &= -k_1\mathbf{g} - k_2\mathbf{v}^{(12)} \\ \boldsymbol{\sigma}_1 &= -p_1[I] +_d \boldsymbol{\sigma}_1 \\ \boldsymbol{\sigma}_2 &= -p_2[I] +_d \boldsymbol{\sigma}_2 \end{aligned} \tag{IV.44}$$

in which p_1 and p_2 are mechanical pressures and ${}_d\boldsymbol{\sigma}_1$ and ${}_d\boldsymbol{\sigma}_2$ are deviatoric contravariant Cauchy stress tensors for constituents one and two. Determination of mixture pressure p is based on the assumption that the saturated mixture is incompressible. We introduce the incompressibility constraint in the entropy inequality through p as a Lagrange multiplier. We further assume that the mixture pressure p contributes $\phi_1 p$ and $\phi_2 p$ to the partial pressures p_1 and p_2 of the constituents.

$$\begin{aligned} p_1 &= \phi_1\left(\rho_1\frac{\partial\Phi_1}{\partial\phi_1} + \rho_2\frac{\partial\Phi_2}{\partial\phi_1} - p\right) = p_1^s - \phi_1 p \\ p_2 &= \phi_2\left(\rho_1\frac{\partial\Phi_1}{\partial\phi_2} + \rho_2\frac{\partial\Phi_2}{\partial\phi_2} - p\right) = p_2^s - \phi_2 p \\ {}_d\boldsymbol{\sigma}_1 &= \left(\lambda_1\mathrm{tr}\mathbf{D}_{(1)} + \lambda_3\mathrm{tr}\mathbf{D}_{(2)}\right)[I] + 2\mu_1\mathbf{D}_{(1)} + 2\mu_3\mathbf{D}_{(2)} + \lambda_5 w_{(12)} \\ {}_d\boldsymbol{\sigma}_2 &= \left(\lambda_4\mathrm{tr}r\mathbf{D}_{(1)} + \lambda_2\mathrm{tr}\mathbf{D}_{(2)}\right)[I] + 2\mu_4\mathbf{D}_{(1)} + 2\mu_2\mathbf{D}_{(2)} + \lambda_5 w_{(12)} \end{aligned} \tag{IV.45}$$

Based on reference [131] we have

$$\begin{aligned}
&\beta_1 \geq 0 \quad k_1 \geq 0 \quad \left(\rho_2\left(\eta_2 + \frac{\partial \Phi_2}{\partial \theta}\right) + \beta_4 + \frac{1}{\theta}k_2\right) \leq \frac{1}{\theta}4\beta_1 k_1 \\
&\lambda_5 \geq 0 \quad \mu_1 \geq 0 \quad \mu_2 \geq 0 \quad (\mu_3 + \mu_4)^2 \leq 4\mu_1\mu_2 \\
&\lambda_1 + \frac{2}{3}\mu_1 \geq 0 \quad \frac{2}{3}\mu_2 \geq 0 \\
&\left[\lambda_3 + \lambda_4 + \frac{2}{3}(\mu_3 + \mu_4)\right]^2 \leq 4\left(\lambda_1 + \frac{2}{3}\mu_1\right)\left(\lambda_2 + \frac{2}{3}\mu_2\right)
\end{aligned} \tag{IV.46}$$

The constitutive theory can be simplified for incompressible constituents and the mixture with further assumption of isothermal flow.

$$\mathbf{h}^{(1)} = 0, \quad \mathbf{h}^{(2)} = 0, \quad \mathbf{g} = 0, \quad \operatorname{tr}\mathbf{D}_{(1)} = 0, \quad \operatorname{tr}\mathbf{D}_{(2)} = 0$$

If we assume $\Phi_\alpha = \Phi_\alpha(\theta)$, then

$$\frac{\partial \Phi_\alpha}{\partial \phi_1} = 0, \quad \frac{\partial \Phi_\alpha}{\partial \phi_2} = 0$$

and if we ignore dependence of ${}_d\boldsymbol{\sigma}_\alpha$ on $w_{(12)}$, then the constitutive theory becomes

$$\begin{aligned}
\boldsymbol{\pi} &= \beta_1 \mathbf{v}^{(12)} \\
\boldsymbol{\sigma}_1 &= -p_1[I] +_d \boldsymbol{\sigma}_1 \\
\boldsymbol{\sigma}_2 &= -p_2[I] +_d \boldsymbol{\sigma}_2 \\
{}_d\boldsymbol{\sigma}_1 &= 2\mu_1\mathbf{D}_{(1)} + 2\mu_3\mathbf{D}_{(2)} \\
{}_d\boldsymbol{\sigma}_2 &= 2\mu_4\mathbf{D}_{(1)} + 2\mu_2\mathbf{D}_{(2)}
\end{aligned} \tag{IV.47}$$

and

$$\begin{aligned}
p_1 &= -\phi_1 p \\
p_2 &= -\phi_2 p
\end{aligned} \tag{IV.48}$$

$\mathbf{q}$ is not a dependent variable in this constitutive theory due to the assumption of isothermal flow. The validity of (IV.48) is demonstrated in the numerical studies presented in section IV.3.

IV.2.11 Complete mathematical model

If we consider two incompressible, homogeneous, and isotropic constituents with saturated mixture that is also incompressible, we have the following.

Continuity equations

$$\begin{aligned}
\rho_1 \boldsymbol{\nabla} \cdot \mathbf{v}_1 &= 0 \\
\rho_2 \boldsymbol{\nabla} \cdot \mathbf{v}_2 &= 0
\end{aligned} \tag{IV.49}$$

Momentum equations (in the absence of body forces)

$$\begin{aligned}
&\rho_\alpha \left((v_\alpha)_1 \frac{\partial (v_\alpha)_1}{\partial x_1} + (v_\alpha)_2 \frac{\partial (v_\alpha)_1}{\partial x_2} \right) + \frac{\partial p_\alpha}{\partial x_1} - \frac{\partial ({}_d\sigma_\alpha)_{11}}{\partial x_1} - \frac{\partial ({}_d\sigma_\alpha)_{21}}{\partial x_2} - (\pi_\alpha)_1 = 0 \\
&\rho_\alpha \left((v_\alpha)_1 \frac{\partial (v_\alpha)_2}{\partial x_1} + (v_\alpha)_2 \frac{\partial (v_\alpha)_2}{\partial x_2} \right) + \frac{\partial p_\alpha}{\partial x_2} - \frac{\partial ({}_d\sigma_\alpha)_{12}}{\partial x_1} - \frac{\partial ({}_d\sigma_\alpha)_{22}}{\partial x_2} - (\pi_\alpha)_2 = 0 \\
&\alpha = 1, 2
\end{aligned} \tag{IV.50}$$

Constitutive equations

$$\begin{aligned}
{}_d\boldsymbol{\sigma}_1 &= 2\mu_1 \mathbf{D}_{(1)} + 2\mu_3 \mathbf{D}_{(2)} \\
{}_d\boldsymbol{\sigma}_2 &= 2\mu_4 \mathbf{D}_{(1)} + 2\mu_2 \mathbf{D}_{(2)}
\end{aligned} \tag{IV.51}$$

Material coefficients μ_1, μ_2, μ_3, and μ_4 are functions of η_α, viscosities of the constituents and the volume fractions ϕ_α. This mathematical model has closure, twenty equations in twenty variables for 3D case and twelve equations in twelve variables for 2D case: $\mathbf{v}_\alpha$, $\alpha = 1, 2$; p_1, p_2; ${}_d\boldsymbol{\sigma}_\alpha$, $\alpha = 1, 2$.

Material coefficients

Based on references [131, 139], we consider the following:

$$\begin{aligned}
\mu_1 &= \phi_1^2 \eta_1 + \phi_1 \phi_2 \eta_{12} \\
\mu_2 &= \phi_2^2 \eta_2 + \phi_1 \phi_2 \eta_{12} \\
\mu_3 &= \mu_4 = \phi_1 \phi_2 \eta_{12} \\
\eta_{12} &= \sqrt{\eta_1 \eta_2}
\end{aligned} \tag{IV.52}$$

where η_1, η_2 are constituent viscosities. For Newtonian fluids these are constant. When the constituents are generalized Newtonian fluids, then $\eta_1 = \eta_1(I_2^1)$, $\eta_2 = \eta_2(I_2^2)$ in which I_2^α; $\alpha = 1, 2$ are second invariants of the strain rate tensors $\mathbf{D}_{(\alpha)}$; $\alpha = 1, 2$. Both Power Law and Carreau-Yasuda models are admissible in defining η_1 and η_2 when the constituents are generalized Newtonian fluids.

Remarks

1. We note that deviatoric Cauchy stress ${}_d\boldsymbol{\sigma}$ for the mixture is the sum of ${}_d\boldsymbol{\sigma}_1$ and ${}_d\boldsymbol{\sigma}_2$. The constitutive theories for ${}_d\boldsymbol{\sigma}_1$ and ${}_d\boldsymbol{\sigma}_2$ must satisfy this requirement. Using (IV.51) and (IV.52) we consider the following.

   Consider the two constituents to be the same (say constituent one), hence in this case $\eta_2 = \eta_1$. Thus

$$\begin{aligned}
\mu_1 &= \eta_1 \left(\phi_1^2 + \phi_1 \phi_2 \right) \\
\mu_2 &= \eta_1 \left(\phi_2^2 + \phi_1 \phi_2 \right) \\
\mu_3 &= \mu_4 = \phi_1 \phi_2 \eta_1
\end{aligned} \tag{IV.53}$$

   Therefore

$${}_d\boldsymbol{\sigma}_1 = 2\eta_1 \left(\phi_1^2 + \phi_1 \phi_2 \right) \mathbf{D}_{(1)} + 2\phi_1 \phi_2 \eta_1 \mathbf{D}_{(2)} \tag{IV.54}$$

$${}_d\boldsymbol{\sigma}_2 = 2\eta_1 \left(\phi_2^2 + \phi_1 \phi_2 \right) \mathbf{D}_{(2)} + 2\phi_1 \phi_2 \eta_1 \mathbf{D}_{(1)} \tag{IV.55}$$

Since constituent two is the same as constituent one

$$\rho^{(2)} = \rho^{(1)} \ , \quad \rho_1 = \phi_1 \rho^{(1)} \ , \quad \rho_2 = \phi_2 \rho^{(1)}$$

Since $\rho_m \mathbf{v} = \rho_1 \mathbf{v}_1 + \rho_2 \mathbf{v}_2$ and $\rho_m = \rho^{(1)}$

$$\begin{aligned} \rho^{(1)} \mathbf{v} &= \phi_1 \rho^{(1)} \mathbf{v}_1 + \phi_2 \rho^{(1)} \mathbf{v}_2 \\ \therefore \quad \mathbf{v} &= \phi_1 \mathbf{v}_1 + \phi_2 \mathbf{v}_2 \end{aligned}$$

Thus for the mixture we have

$$\mathbf{D} = \phi_1 \mathbf{D}_{(1)} + \phi_2 \mathbf{D}_{(2)} \tag{IV.56}$$

Now, going back to (IV.54) and (IV.55)

$$\begin{aligned} {}_d\boldsymbol{\sigma}_1 &= 2\eta_1 \left(\phi_1 + \phi_2\right) \phi_1 \mathbf{D}_{(1)} + 2\eta_1 \phi_1 \phi_2 \mathbf{D}_{(2)} \\ {}_d\boldsymbol{\sigma}_2 &= 2\eta_1 \left(\phi_1 + \phi_2\right) \phi_2 \mathbf{D}_{(2)} + 2\eta_1 \phi_1 \phi_2 \mathbf{D}_{(1)} \end{aligned} \tag{IV.57}$$

Since $\phi_1 + \phi_2 = 1$, using (IV.57) we can write

$${}_d\boldsymbol{\sigma} = {}_d\boldsymbol{\sigma}_1 + {}_d\boldsymbol{\sigma}_2 = 2\eta_1 \left(\phi_1 \mathbf{D}_{(1)} + \phi_2 \mathbf{D}_{(2)}\right) + 2\eta_1 \phi_1 \phi_2 \left(\mathbf{D}_{(1)} + \mathbf{D}_{(2)}\right) \tag{IV.58}$$

using (IV.56) in (IV.58), we can write

$${}_d\boldsymbol{\sigma} = 2\eta_1 \mathbf{D} + 2\eta_1 \phi_1 \phi_2 \left(\mathbf{D}_{(1)} + \mathbf{D}_{(2)}\right) \tag{IV.59}$$

But ${}_d\boldsymbol{\sigma} = 2\eta_1 \mathbf{D}$ must hold regardless of ϕ_1 and ϕ_2, hence the second term in (IV.59) must be zero which is only possible if $\mu_3 = \mu_4 = 0$.

Thus for saturated Newtonian and generalized Newtonian mixtures of two Newtonian and generalized Newtonian fluids we have the following constitutive equations

$$\begin{aligned} {}_d\boldsymbol{\sigma}_1 &= 2\mu_1 \mathbf{D}_{(1)} \\ {}_d\boldsymbol{\sigma}_2 &= 2\mu_2 \mathbf{D}_{(2)} \end{aligned} \tag{IV.60}$$

2. Generalized Newtonian fluids

If we consider both constituents and the mixture to be generalized Newtonian fluids, then

$$\eta_1 = \eta_1 \left(I_2^1\right), \qquad \eta_2 = \eta_2 \left(I_2^2\right) \tag{IV.61}$$

In which I_2^1 and I_2^2 are the second invariants of the tensors $\mathbf{D}_{(1)}$ and $\mathbf{D}_{(2)}$. We can use power law or Carreau-Yasuda model to define η_1 and η_2.

Power law

The viscosity of the α^{th} constituent is defined by

$$\eta_\alpha = \eta_\alpha^0 \left(I_2^\alpha\right)^{\frac{n_\alpha - 1}{2}} ; \quad \alpha = 1, 2 \tag{IV.62}$$

where η_α^0 is the zero shear rate viscosity, n_α is the power law index, and (I_2^α) is the second invariant of $\mathbf{D}_{(\alpha)}$. For example in $\mathbb{R}^2$ we have the following

$$I_2^\alpha = 2\left(\frac{\partial \left(v_\alpha\right)_1}{\partial x_1}\right)^2 + 2\left(\frac{\partial \left(v_\alpha\right)_2}{\partial x_2}\right)^2 + \left(\frac{\partial \left(v_\alpha\right)_1}{\partial x_2} + \frac{\partial \left(v_\alpha\right)_2}{\partial x_1}\right)^2 ; \quad \alpha = 1, 2 \tag{IV.63}$$

and η_α^0 and n_α are given data for a fluid.

Carreau-Yasuda model

$$\eta_\alpha = \eta_\alpha^\infty + \left(\eta_\alpha^0 + \eta_\alpha^\infty\right)\left(1 + \lambda_\alpha^2 I_2^\alpha\right)^{\frac{m_\alpha - 1}{2}} \quad ; \quad \alpha = 1, 2 \tag{IV.64}$$

η_α^0 and η_α^∞ are zero and infinite shear rate viscosity. η_α^0, η_α^∞, λ_α, and m_α are constants of the α^{th} constituent.

3. Mixture viscosity

The mixture viscosity μ_m can be determined using $\mathbf{D}_{(1)}$, $\mathbf{D}_{(2)}$, μ_1, μ_2, and ρ_1, ρ_2, ρ_m. For an isotropic, homogeneous, saturated mixture (Newtonian or generalized Newtonian) we can write

$$_d\boldsymbol{\sigma}_m = \mu_m \mathbf{D} \tag{IV.65}$$

in which

$$_d\boldsymbol{\sigma}_m = \sum_\alpha {}_d\boldsymbol{\sigma}_\alpha \tag{IV.66}$$

and

$$_d\boldsymbol{\sigma}_\alpha = \mu_\alpha \mathbf{D}_\alpha \tag{IV.67}$$

using (IV.7), we can write

$$\mathbf{D} = \sum_\alpha \frac{\rho_\alpha}{\rho_m} \mathbf{D}_\alpha \tag{IV.68}$$

using (IV.68) and (IV.65), we obtain

$$_d\boldsymbol{\sigma}_m = \mu_m \left(\sum_\alpha \frac{\rho_\alpha}{\rho_m} \mathbf{D}_\alpha \right) \tag{IV.69}$$

or

$$\left({}_d\sigma_m\right)_{ij} = \mu_m \left(\sum_\alpha \frac{\rho_\alpha}{\rho_m} \left(D_\alpha\right)_{ij} \right) \tag{IV.70}$$

also from (IV.65)

$$\left({}_d\sigma_m\right)_{ij} = \mu_m \left(D_{ij}\right) \tag{IV.71}$$

The mixture viscosity μ_m is deterministic from (IV.70) or (IV.71). For known volume fractions and constituent viscosities it is shown that for fully developed flow between parallel plates (IV.70) or (IV.71) holds.

IV.2.12 Dimensionless form of the mathematical models in $\mathbb{R}^2$

For convenience, we introduce more familiar notation. Let

$$\left(v_\alpha\right)_1 = u_\alpha \quad , \quad \left(v_\alpha\right)_2 = v_\alpha \quad , \quad x_1 = x \quad , \quad x_2 = y$$

In $\left({}_d\sigma_\alpha\right)_{ij}$; $i, j = 1, 2$ correspond to x and y. Velocities u and v are x and y components of $\mathbf{v}$. Likewise, $\mathbf{v}_\alpha$ has components u_α and v_α in the x and y directions.

Using this notation, the mathematical model in $\mathbb{R}^2$ for a two constituent, saturated, incompressible mixture of Newtonian or generalized Newtonian fluids can be written as (for isothermal flows).

$$\rho_\alpha = \phi_\alpha \rho^{(\alpha)} \quad , \quad \rho_m = \sum_{\alpha=1}^{2} \rho_\alpha \quad , \quad \sum_{\alpha=1}^{2} \phi_\alpha = 1 \quad , \quad \rho_m \mathbf{v} = \sum_{\alpha=1}^{2} \rho_\alpha \mathbf{v}_\alpha \tag{IV.72}$$

Continuity equations:

$$\rho_\alpha \left(\frac{\partial u_\alpha}{\partial x} + \frac{\partial v_\alpha}{\partial y} \right) = 0 \; ; \quad \alpha = 1, 2 \tag{IV.73}$$

Momentum equations:

$$\begin{aligned} \rho_\alpha \left(\frac{\partial u_\alpha}{\partial t} + u_\alpha \frac{\partial u_\alpha}{\partial x} + v_\alpha \frac{\partial u_\alpha}{\partial y} \right) + \frac{\partial p_\alpha}{\partial x} - \frac{\partial \left({}_d\sigma_\alpha \right)_{xx}}{\partial x} - \frac{\partial \left({}_d\sigma_\alpha \right)_{xy}}{\partial x} - \left(\pi_\alpha \right)_x = 0 \; ; \quad \alpha = 1, 2 \\ \rho_\alpha \left(\frac{\partial v_\alpha}{\partial t} + u_\alpha \frac{\partial v_\alpha}{\partial x} + v_\alpha \frac{\partial v_\alpha}{\partial y} \right) + \frac{\partial p_\alpha}{\partial y} - \frac{\partial \left({}_d\sigma_\alpha \right)_{xy}}{\partial x} - \frac{\partial \left({}_d\sigma_\alpha \right)_{yy}}{\partial x} - \left(\pi_\alpha \right)_y = 0 \; ; \quad \alpha = 1, 2 \end{aligned} \tag{IV.74}$$

Constitutive equations:

$${}_d\boldsymbol{\sigma}_\alpha = \mu_\alpha \mathbf{D}_{(\alpha)} \; ; \quad \alpha = 1, 2 \tag{IV.75}$$

where

$$\mu_1 = \phi_1^2 \eta_1 + \phi_1 \phi_2 \eta_{12} \quad ; \quad \mu_2 = \phi_2^2 \eta_2 + \phi_1 \phi_2 \eta_{12} \quad ; \quad \eta_{12} = \sqrt{\eta_1 \eta_2} \tag{IV.76}$$

η_1 and η_2 are the viscosities of the two constituents.

Power Law model:

$$\begin{aligned} \eta_\alpha = \eta_\alpha^0 \left(I_2^\alpha \right)^{\frac{n_\alpha - 1}{2}} \; ; \quad \alpha = 1, 2 \\ I_2^\alpha = 2 \left(\frac{\partial u_\alpha}{\partial x} \right)^2 + 2 \left(\frac{\partial v_\alpha}{\partial y} \right)^2 + \left(\frac{\partial u_\alpha}{\partial y} + \frac{\partial v_\alpha}{\partial x} \right)^2 \; ; \quad \alpha = 1, 2 \end{aligned} \tag{IV.77}$$

Carreau-Yasuda model:

$$\eta_\alpha = \eta_\alpha^\infty + \left(\eta_\alpha^0 + \eta_\alpha^\infty \right) \left(1 + \lambda_\alpha^2 I_2^\alpha \right)^{\frac{m_\alpha - 1}{2}} \; ; \quad \alpha = 1, 2 \tag{IV.78}$$

IV.2.13 Dimensionless form

First we introduce ' ˆ ' (hat) on all quantities in (IV.72) – (IV.78) indicating that the quantities have their usual dimensions or units and use the following reference quantities and the dimensionless variables

$$\begin{aligned} \hat{x} = x L_0, \qquad \hat{y} = y L_0, \qquad \hat{u}_\alpha = u_\alpha u_0, \qquad \hat{v}_\alpha = v_\alpha u_0 \\ \hat{\eta}_\alpha = \eta_\alpha \eta_0, \qquad \hat{p}_\alpha = p_\alpha p_0, \qquad {}_d\hat{\boldsymbol{\sigma}}_\alpha = {}_d\, \boldsymbol{\sigma}_\alpha \tau_0, \qquad \hat{\rho}_\alpha = \rho_\alpha \rho_0 \end{aligned} \tag{IV.79}$$

In which L_0 is the reference length, u_0 is the reference velocity, η_0 is the reference viscosity, p_0 is the reference pressure, τ_0 is the reference stress, and ρ_0 is reference density. For consistency we must use $p_0 = \tau_0$. We can use either characteristic kinetic energy or characteristic viscous stress to choose reference value τ_0. The reference time t_0 is given by

$$t_0 = \frac{L_0}{u_0} \tag{IV.80}$$

Using (IV.72) – (IV.78) with ' ˆ ' (hat) on all quantities and using (IV.79) and (IV.80), we can obtain the following dimensionless form of the GDEs for the two constituent mathematical model in $\mathbb{R}^2$. Equations (IV.72) and the continuity equations remain unchanged.

$$\rho_\alpha = \phi_\alpha \rho^{(\alpha)} \quad ; \quad \rho_m = \sum_{\alpha=1}^{2} \rho_\alpha \quad ; \quad \sum_{\alpha=1}^{2} \phi_\alpha = 1 \quad ; \quad \rho_m \mathbf{v} = \sum_{\alpha=1}^{2} \rho_\alpha \mathbf{v}_\alpha \tag{IV.81}$$

Continuity equations:

$$\rho_\alpha \left(\frac{\partial u_\alpha}{\partial x} + \frac{\partial v_\alpha}{\partial y} \right) = 0 \; ; \quad \alpha = 1, 2 \tag{IV.82}$$

Momentum equations:

$$\begin{aligned} &\rho_\alpha \left(\frac{\partial u_\alpha}{\partial t} + u_\alpha \, \frac{\partial u_\alpha}{\partial x} + v_\alpha \frac{\partial u_\alpha}{\partial y} \right) + \left(\frac{p_0}{\rho_0 u_0^2} \right) \frac{\partial p_\alpha}{\partial x} \\ &\qquad - \left(\frac{\tau_0}{\rho_0 u_0^2} \right) \left(\frac{\partial \left({}_d\sigma_\alpha \right)_{xx}}{\partial x} + \frac{\partial \left({}_d\sigma_\alpha \right)_{xy}}{\partial y} \right) - \left(\frac{L_0}{\rho_0 u_0^2} \right) \left(\pi_\alpha \right)_x = 0 \; ; \quad \alpha = 1, 2 \\ &\rho_\alpha \left(\frac{\partial v_\alpha}{\partial t} + u_\alpha \, \frac{\partial v_\alpha}{\partial x} + v_\alpha \frac{\partial v_\alpha}{\partial y} \right) + \left(\frac{p_0}{\rho_0 u_0^2} \right) \frac{\partial p_\alpha}{\partial y} \\ &\qquad - \left(\frac{\tau_0}{\rho_0 u_0^2} \right) \left(\frac{\partial \left({}_d\sigma_\alpha \right)_{xy}}{\partial x} + \frac{\partial \left({}_d\sigma_\alpha \right)_{yy}}{\partial y} \right) - \left(\frac{L_0}{\rho_0 u_0^2} \right) \left(\pi_\alpha \right)_y = 0 \; ; \quad \alpha = 1, 2 \end{aligned} \tag{IV.83}$$

IV.2.14 Power law for constituents and mixture

$$\hat{\eta}_\alpha = \hat{\eta}_\alpha^0 \left(\hat{I}_2^\alpha \right)^{\frac{n_\alpha - 1}{2}} \; ; \quad \alpha = 1, 2 \tag{IV.84}$$

where $\hat{\eta}_\alpha$ are the viscosities of the constituents. $\hat{\eta}_\alpha^0$, $\hat{I}_2^\alpha$, and n_α are zero shear rate viscosity, second invariant of the strain rate tensor, and power law index for constituent α. Using (IV.79), we can write (IV.84) as

$$\hat{\eta}_\alpha = \eta_0 \eta_\alpha^0 \left(\frac{u_0}{L_0} \right)^{n_\alpha - 1} \left(I_2^\alpha \right)^{\frac{n_\alpha - 1}{2}} = \left(\eta_0 \left(\frac{u_0}{L_0} \right)^{n_\alpha - 1} \right) \eta_\alpha^0 \left(I_2^\alpha \right)^{\frac{n_\alpha - 1}{2}} \; ; \quad \alpha = 1, 2 \tag{IV.85}$$

η_α^0 is dimensionless zero shear rate viscosity and I_2^α is the dimensionless second invariant of the strain rate tensor for constituent α.

or

$$\hat{\eta}_\alpha = \left(\eta_0 \left(\frac{u_0}{L_0} \right)^{n_\alpha - 1} \right) \eta_\alpha \quad ; \quad \eta_\alpha = \eta_\alpha^0 \left(I_2^\alpha \right)^{\frac{n_\alpha - 1}{2}} \; ; \quad \alpha = 1, 2 \tag{IV.86}$$

in which η_α is the dimensionless viscosity of constituent α. Using (IV.86) we can define $\hat{\mu}_1$ and $\hat{\mu}_2$ in (IV.76).

$$\begin{aligned} \hat{\mu}_1 &= \phi_1^2 \hat{\eta}_1 + \phi_1 \phi_2 \sqrt{\hat{\eta}_1 \hat{\eta}_2} \\ \hat{\mu}_2 &= \phi_2^2 \hat{\eta}_2 + \phi_1 \phi_2 \sqrt{\hat{\eta}_1 \hat{\eta}_2} \end{aligned} \tag{IV.87}$$

Consider $\hat{\mu}_1$. Substituting from (IV.86) for $\alpha = 1$.

$$\hat{\mu}_1 = \phi_1^2 \eta_0 \left(\frac{u_0}{L_0} \right)^{n_1 - 1} \eta_1 + \phi_1 \phi_2 \sqrt{\eta_0 \left(\frac{u_0}{L_0} \right)^{n_1 - 1} \eta_0 \left(\frac{u_0}{L_0} \right)^{n_2 - 1} \eta_1 \eta_2} \tag{IV.88}$$

Consider $\left({}_d\hat{\sigma}_1 \right)_{xx}$ in (IV.75). Substituting from (IV.88) and nondimensionalizing gives

$$\tau_0 \left({}_d\sigma_1 \right)_{xx} = 2 \left(\phi_1^2 \eta_0 \left(\frac{u_0}{L_0} \right)^{n_1 - 1} \eta_1 + \phi_1 \phi_2 \sqrt{\eta_0 \left(\frac{u_0}{L_0} \right)^{n_1 - 1} \eta_0 \left(\frac{u_0}{L_0} \right)^{n_2 - 1} \eta_1 \eta_2} \right) \frac{u_0}{L_0} \frac{\partial u_1}{\partial x}$$

or

$$\left({}_d\sigma_1\right)_{xx} = 2\left(\phi_1^2\left(\frac{u_0}{\tau_0 L_0}\right)\eta_0\left(\frac{u_0}{L_0}\right)^{n_1-1} + \phi_1\phi_2\sqrt{\left(\frac{u_0}{\tau_0 L_0}\eta_0\left(\frac{u_0}{L_0}\right)^{n_1-1}\right)\left(\frac{u_0}{\tau_0 L_0}\eta_0\left(\frac{u_0}{L_0}\right)^{n_2-1}\right)\eta_1\eta_2}\right)\frac{\partial u_1}{\partial x} \tag{IV.89}$$

If we use $\tau_0 = \rho_0 u_0^2$ (characteristic kinetic energy), then

$$\frac{u_0}{\tau_0 L_0}\left(\eta_0\left(\frac{u_0}{L_0}\right)^{n_1-1}\right) = \frac{\eta_0 u_0}{\rho_0 u_0^2 L_0}\left(\eta_0\left(\frac{u_0}{L_0}\right)^{n_1-1}\right) = \frac{\eta_0}{\rho_0\left(L_0\right)^{n_1}\left(u_0\right)^{2-n_1}} = \frac{1}{\left(R_{en}\right)_1} \tag{IV.90}$$

where $\left(R_{en}\right)_1$ is the Reynolds number for constituent one. Similarly

$$\frac{u_0}{\tau_0 L_0}\left(\eta_0\left(\frac{u_0}{L_0}\right)^{n_2-1}\right) = \frac{\eta_0}{\rho_0\left(L_0\right)^{n_2}\left(u_0\right)^{2-n_2}} = \frac{1}{\left(R_{en}\right)_2} \tag{IV.91}$$

Hence, we can write the following for $\left({}_d\sigma_1\right)_{xx}$

$$\left({}_d\sigma_1\right)_{xx} = 2\left(\phi_1^2\frac{\eta_1}{\left(R_{en}\right)_1} + \phi_1\phi_2\sqrt{\frac{1}{\left(R_{en}\right)_1\left(R_{en}\right)_2}\cdot\eta_1\eta_2}\right)\frac{\partial u_1}{\partial x} \tag{IV.92}$$

or

$$\left({}_d\sigma_1\right)_{xx} = 2\underset{\sim}{\mu}_1\frac{\partial u_1}{\partial x} \tag{IV.93}$$

where

$$\underset{\sim}{\mu}_1 = \phi_1^2\frac{\eta_1}{\left(R_{en}\right)_1} + \phi_1\phi_2\sqrt{\frac{1}{\left(R_{en}\right)_1\left(R_{en}\right)_2}\cdot\eta_1\eta_2} \tag{IV.94}$$

Similarly for $\left({}_d\sigma_2\right)_{xx}$, we have

$$\left({}_d\sigma_2\right)_{xx} = 2\underset{\sim}{\mu}_2\frac{\partial u_2}{\partial x} \tag{IV.95}$$

where

$$\underset{\sim}{\mu}_2 = \phi_2^2\frac{\eta_2}{\left(R_{en}\right)_2} + \phi_1\phi_2\sqrt{\frac{1}{\left(R_{en}\right)_1\left(R_{en}\right)_2}\cdot\eta_1\eta_2} \tag{IV.96}$$

Similar derivation holds for the other components of the deviatoric Cauchy stress components. In summary we have the following for the constitutive equations

$${}_d\boldsymbol{\sigma}_\alpha = \underset{\sim}{\mu}_\alpha\mathbf{D}_{(\alpha)}\ ; \quad \alpha = 1,2 \tag{IV.97}$$

and

$${}_d\boldsymbol{\sigma}_m = \underset{\sim}{\mu}_m\mathbf{D} \tag{IV.98}$$

Equations (IV.81)–(IV.83), (IV.97), (IV.94), (IV.96), and (IV.86) constitute the dimensionless form of the complete mathematical model in $\mathbb{R}^2$ for a power law mixture of two power law constituents.

IV.2.15 Carreau model for constituents and mixture

In the case of the Carreau model, the definitions of μ_1 and μ_2 change compared to power law. We consider details in the following.

Using (IV.78)

$$\hat{\eta}_\alpha = \hat{\eta}^0_\alpha + \left(\hat{\eta}^0_\alpha - \hat{\eta}^\infty_\alpha\right)\left(1+\lambda^2_\alpha \hat{I}^\alpha_2\right)^{\frac{m_\alpha-1}{2}} \quad ; \quad \alpha = 1,2 \tag{IV.99}$$

Using (IV.79) we can write the following for (IV.99)

$$\hat{\eta}_\alpha = \eta_0\left(\eta^0_\alpha + \left(\eta^0_\alpha - \eta^\infty_\alpha\right)\left(1+\lambda^2_\alpha\left(\frac{u_0}{L_0}\right)^2 I^\alpha_2\right)^{\frac{m_\alpha-1}{2}}\right) \quad ; \quad \alpha = 1,2 \tag{IV.100}$$

Let $\dfrac{\lambda_\alpha u_0}{L_0} = c_{u\alpha}$ be the Carreau number for constituent α.

$$\therefore \quad \hat{\eta}_\alpha = \eta_0\left(\eta^0_\alpha + \left(\eta^0_\alpha - \eta^\infty_\alpha\right)\left(1+(c_{u1})^2 I^\alpha_2\right)^{\frac{m_\alpha-1}{2}}\right) = \eta_0\eta_\alpha \; ; \quad \alpha = 1,2 \tag{IV.101}$$

where

$$\eta_\alpha = \eta^0_\alpha + \left(\eta^0_\alpha - \eta^\infty_\alpha\right)\left(1+(c_{u\alpha})^2 I^\alpha_2\right)^{\frac{m_\alpha-1}{2}} \quad ; \quad \alpha = 1,2 \tag{IV.102}$$

Using (IV.101) we can define $\hat{\mu}_1$ and $\hat{\mu}_2$ in (IV.76).

$$\begin{aligned}\hat{\mu}_1 &= \phi^2_1\hat{\eta}_1 + \phi_1\phi_2\sqrt{\hat{\eta}_1\hat{\eta}_2}\\ \hat{\mu}_2 &= \phi^2_2\hat{\eta}_2 + \phi_1\phi_2\sqrt{\hat{\eta}_1\hat{\eta}_2}\end{aligned} \tag{IV.103}$$

Consider $\hat{\mu}_1$. Substituting from (IV.101) we obtain

$$\hat{\mu}_1 = \phi^2_1\eta_0\eta_1 + \phi_1\phi_2\sqrt{\eta_0\eta_1\eta_0\eta_2} \tag{IV.104}$$

Consider $\left({}_d\sigma_1\right)_{xx}$ in (IV.75). Substituting from (IV.104) and nondimensionalizing gives

$$\tau_0\left({}_d\sigma_1\right)_{xx} = 2\left(\phi^2_1\eta_0\eta_1 + \phi_1\phi_2\sqrt{\eta_0\eta_1\eta_0\eta_2}\right)\frac{u_0}{L_0}\frac{\partial u_1}{\partial x} \tag{IV.105}$$

using $\tau_0 = \rho_0 u^2_0$ (characteristic kinetic energy)

$$\left({}_d\sigma_1\right)_{xx} = 2\left(\phi^2_1\left(\frac{\eta_0}{L_0\rho_0u_0}\right)\eta_1 + \phi_1\phi_2\sqrt{\left(\frac{\eta_0}{L_0\rho_0u_0}\right)\eta_1\left(\frac{\eta_0}{L_0\rho_0u_0}\right)\eta_2}\right)\frac{\partial u_1}{\partial x} \tag{IV.106}$$

or

$$\left({}_d\sigma_1\right)_{xx} = 2\left(\frac{1}{Re}\phi^2_1\eta_1 + \phi_1\phi_2\sqrt{\eta_1\eta_2}\right)\frac{\partial u_1}{\partial x} = 2\underset{\sim}{\mu}_1\frac{\partial u_1}{\partial x} \tag{IV.107}$$

where $Re = \frac{L_0\rho_0u_0}{\eta_0}$; Reynolds number. Similarly for constituent two we have

$$\left({}_d\sigma_2\right)_{xx} = 2\left(\frac{1}{Re}\phi^2_2\eta_2 + \phi_1\phi_2\sqrt{\eta_1\eta_2}\right)\frac{\partial u_2}{\partial x} = 2\underset{\sim}{\mu}_2\frac{\partial u_2}{\partial x} \tag{IV.108}$$

In summary, we have the following for the constitutive equations

$$ {}_d\boldsymbol{\sigma}_\alpha = \underset{\sim}{\mu}_\alpha \mathbf{D}_{(\alpha)} \ ; \quad \alpha = 1,2 \tag{IV.109} $$

and

$$ {}_d\boldsymbol{\sigma}_m = \underset{\sim}{\mu}_m \mathbf{D} \tag{IV.110} $$

Clearly, $\underset{\sim}{\mu}_1 = \dfrac{\mu_1}{Re}$ and $\underset{\sim}{\mu}_2 = \dfrac{\mu_2}{Re}$.

IV.2.16 Newtonian constituents and mixture

For this case $\hat{\eta}_\alpha \ ; \ \alpha = 1,2$ are constant, hence we have

$$ \begin{aligned} \hat{\mu}_1 &= \eta_0 \left(\phi_1^2 \eta_1 + \phi_1 \phi_2 \sqrt{\eta_1 \eta_2} \right) = \eta_0 \mu_1 \\ \hat{\mu}_2 &= \eta_0 \left(\phi_2^2 \eta_2 + \phi_1 \phi_2 \sqrt{\eta_1 \eta_2} \right) = \eta_0 \mu_2 \end{aligned} \tag{IV.111} $$

where

$$ \mu_1 = \phi_1^2 \eta_1 + \phi_1 \phi_2 \sqrt{\eta_1 \eta_2} \quad ; \quad \mu_2 = \phi_2^2 \eta_2 + \phi_1 \phi_2 \sqrt{\eta_1 \eta_2} \tag{IV.112} $$

Consider $\left({}_d\sigma_1\right)_{xx}$. Using (IV.111) and nondimensionalizing $\left({}_d\sigma_1\right)_{xx}$

$$ \left({}_d\sigma_1\right)_{xx} = 2\mu_1 \left(\frac{\eta_0 u_0}{\tau_0 L_0} \right) \frac{\partial u_1}{\partial x} \tag{IV.113} $$

when $\tau_0 = \rho_0 u_0^2$ (characteristic kinetic energy), we have

$$ \left({}_d\sigma_1\right)_{xx} = 2\mu_1 \left(\frac{\eta_0}{\rho_0 u_0 L_0} \right) \frac{\partial u_1}{\partial x} = 2 \frac{\mu_1}{Re} \frac{\partial u_1}{\partial x} = 2 \underset{\sim}{\mu}_1 \frac{\partial u_1}{\partial x} \tag{IV.114} $$

In summary, we have the following constitutive equations in the dimensionless form when the constituents and the mixture are Newtonian fluids.

$$ {}_d\boldsymbol{\sigma}_\alpha = \underset{\sim}{\mu}_\alpha \mathbf{D}_{(\alpha)} \ ; \quad \alpha = 1,2 \tag{IV.115} $$

and

$$ {}_d\boldsymbol{\sigma}_m = \underset{\sim}{\mu}_m \mathbf{D} \tag{IV.116} $$

IV.2.17 Remarks

1. If the constituents are Newtonian fluids and the mixture is also a Newtonian fluid and if we neglect $(\pi_1)_x$, $(\pi_2)_x$, $(\pi_1)_y$, and $(\pi_2)_y$, then the mathematical model for the constituents is decoupled. In this case we can use the continuity equation, momentum equations, and the constitutive equations for each constituent to obtain deformation fields and then use (IV.81) to obtain the mixture deformation field. The combined model will also function properly in the least squares computational process (see numerical studies). In the following we present details of the decoupled mathematical models in $\mathbb{R}^2$ for a two constituent mixture. For partial pressures p_α of the constituents we assume (based on (IV.45) and (IV.48)) $p_\alpha = \phi_\alpha p$ and $\sum_\alpha p_\alpha = p$ yielding $\sum_\alpha \phi_\alpha = 1$ which holds. Thus, for a two constituent mixture we can write

$$ p_\alpha = \phi_\alpha p \qquad , \qquad \frac{\partial p_\alpha}{\partial x_i} = \phi_\alpha \frac{\partial p}{\partial x_i} \ ; \quad \alpha, i = 1,2 \tag{IV.117} $$

Decoupled mathematical model (BVP): Newtonian constituents and mixture

The decoupled mathematical model for each constituent ($\alpha = 1, 2$) can easily be obtained using (IV.82), (IV.83), and (IV.115) with the definitions of $\underset{\sim}{\mu}_\alpha$ in (IV.114) and by neglecting $(\pi_\alpha)_x$ and $(\pi_\alpha)_y$. Additionally, we must use $p_\alpha = \phi_\alpha p$ in the momentum equations (IV.83). When using mathematical models for constituents 1 and 2 the calculated pressure p is p_α and the pressure field for the mixture is obtained from $p = p_1 + p_2$.

2. However, when the constituents are generalized Newtonian fluids and when the mixture is also a generalized Newtonian fluid, decoupling is not possible due to the fact that μ_1 and μ_2 are functions of deformation fields of both constituents.

3. In the numerical studies we neglect (π_1) and (π_2) in the momentum equations.

4. In section IV.2.18 that follows these remarks, we derive the mathematical model for fully developed flow between parallel plates. This model reveals some features that are not obvious from the mathematical model in $\mathbb{R}^2$.

IV.2.18 Mathematical model for fully developed flow between parallel plates: mixture of two constituents

In this case the mathematical model describes a BVP. For fully developed flow between parallel plates we only need to consider the one dimensional case i.e. a typical section **A**–**A** where the flow is fully developed.

For this case the continuity equation is satisfied identically. The dimensionless forms of the momentum equations and the constitutive equations reduce to (neglecting (π_1) and (π_2))

$$\left(\frac{p_0}{\rho_0 u_0^2}\right)\frac{\partial p_\alpha}{\partial x} - \left(\frac{\tau_0}{\rho_0 u_0^2}\right)\frac{\partial \left({}_d\sigma_\alpha\right)_{xy}}{\partial y} = 0 \quad ; \quad \left({}_d\sigma_\alpha\right)_{xy} = \underset{\sim}{\mu}_\alpha\left(\eta_1, \eta_2, \phi_1, \phi_2\right)\frac{\partial u_\alpha}{\partial y} \; ; \quad \alpha = 1, 2 \tag{IV.118}$$

Details of $\underset{\sim}{\mu}_1$ and $\underset{\sim}{\mu}_2$ are given in the following.

Newtonian constituents and mixture

$$\underset{\sim}{\mu}_\alpha = \frac{\mu_\alpha}{Re} \tag{IV.119}$$

μ_α is defined in (IV.114). If we assume the mixture to be a Newtonian fluid, then using (IV.70) or (IV.71) we have the following for the dimensionless case

$$\left({}_d\sigma\right)_{xy} = \underset{\sim}{\mu}_m \frac{\partial u_m}{\partial y} \tag{IV.120}$$

In which $\left({}_d\sigma\right)_{xy} = \left({}_d\sigma_1\right)_{xy} + \left({}_d\sigma_2\right)_{xy}$ and u_m is the mixture velocity in the x direction. Using (IV.120) we can determine $\underset{\sim}{\mu}_m$ for the mixture. However, since $\frac{\partial u}{\partial y} = 0$ at the center-line it is better to use

$$\underset{\sim}{\mu}_m = \left(\frac{\frac{\partial \left({}_d\sigma\right)_{xy}}{\partial y}}{\frac{\partial^2 u}{\partial y^2}}\right) \tag{IV.121}$$

to determine $\underset{\sim}{\mu}_m$.

Power law model for constituents and mixture

In this case $\underset{\sim}{\mu}_1$ and $\underset{\sim}{\mu}_2$ are given by

$$\underset{\sim}{\mu}_\alpha = \phi_\alpha^2 \frac{\eta_\alpha}{(R_{en})_\alpha} + \phi_1\phi_2 \sqrt{\frac{1}{(R_{en})_1 (R_{en})_2}\eta_1\eta_2}\ ; \quad \alpha = 1,2 \tag{IV.122}$$

where

$$\eta_\alpha = \eta_\alpha^0 \left(I_2^\alpha\right)^{\frac{n_\alpha - 1}{2}} \ ; \quad \alpha = 1,2 \tag{IV.123}$$

and

$$I_2^\alpha = \left(\frac{\partial u_\alpha}{\partial y}\right)^2 \ ; \quad \alpha = 1,2 \tag{IV.124}$$

For the mixture we can write

$$\left({}_d\sigma\right)_{xy} = \underset{\sim}{\mu}_m \frac{\partial u_m}{\partial y} \tag{IV.125}$$

Using (IV.125) we can determine $\underset{\sim}{\mu}_m$ for the mixture.

Carreau model for constituents and mixture

In this case $\underset{\sim}{\mu}_1$ and $\underset{\sim}{\mu}_2$ are given by (IV.107) and (IV.108) in which η_α are defined by (IV.102). The definition of I_2^α remains the same as in (IV.124). For the mixture we can write the following using (IV.70) or (IV.71).

$$\left({}_d\sigma\right)_{xy} = \underset{\sim}{\mu}_m \frac{\partial u_m}{\partial y} \tag{IV.126}$$

In this case also we can determine $\underset{\sim}{\mu}_m$ for the mixture using (IV.126).

Remarks:

1. We note that the mathematical model consists of four PDEs (IV.118) in u_1, u_2, $\left({}_d\sigma_1\right)_{xy}$, $\left({}_d\sigma_1\right)_{xy}$, p_1, and p_2. Thus, the mathematical model does not have closure. However, for this case (fully developed flow), if we assume the flow to be pressure driven, then $\frac{\partial p_1}{\partial x}$ and $\frac{\partial p_2}{\partial x}$ are known. p_1 and p_2 are partial pressures of the constituents, hence based on (IV.45) and (IV.48) we have

$$\begin{gathered} p_1 = \phi_1 p \quad , \quad p_2 = \phi_2 p \\ \text{ie} \quad p_1 + p_2 = p \end{gathered} \tag{IV.127}$$

   Since the volume fractions are constant, (IV.127) results in the following

$$\frac{\partial p_1}{\partial x} = \phi_1 \frac{\partial p}{\partial x} \quad , \quad \frac{\partial p_2}{\partial x} = \phi_2 \frac{\partial p}{\partial x} \tag{IV.128}$$

   Thus, knowing volume fractions ϕ_1, ϕ_2 and $\frac{\partial p}{\partial x}$ for the mixture, $\frac{\partial p_1}{\partial x}$ and $\frac{\partial p_2}{\partial x}$ are defined and the mathematical model has closure. Based on this (as stated earlier), $p_\alpha = \phi_\alpha p$ and $\sum_{\alpha=1}^{\nu} p_\alpha = p$ which implies $\sum_{\alpha=1}^{\nu} \phi_\alpha = 1$ which obviously holds regardless of the model problem as long as the constituents and the mixture are Newtonian or generalized Newtonian fluids. Validity of this assumption is demonstrated for this model problem as well as the backward facing step.

2. The validity of the assumption in remark (1) can be verified using the model problem in $\mathbb{R}^2$ using the combined model in which p_1 and p_2 remain dependent variables in the mathematical model.

3. Using (IV.127) and (IV.128) the mathematical model given by (IV.118) reduces to

$$\left(\frac{p_0}{\rho_0 u_0^2}\right)\phi_\alpha \frac{\partial p}{\partial x} - \left(\frac{\tau_0}{\rho_0 u_0^2}\right)\frac{\partial\left({}_d\sigma_\alpha\right)_{xy}}{\partial y} = 0 \quad ; \quad \left({}_d\sigma_\alpha\right)_{xy} = \underset{\sim}{\mu}_\alpha\left(\eta_1, \eta_2, \phi_1, \phi_2\right)\frac{\partial u_\alpha}{\partial y} \; ; \quad \alpha = 1, 2 \tag{IV.129}$$

   in which $\frac{\partial p}{\partial x}$ is known (pressure driven flow). This mathematical model has closure.

4. In the case of Newtonian constituents and mixture, $\underset{\sim}{\mu}_1$ and $\underset{\sim}{\mu}_2$ are not functions of the deformation field, hence the combined mathematical model can be decoupled for the constituents using (IV.129) we can obtain mathematical models for each constituent $(\alpha = 1, 2)$.

   Solutions from the combined mathematical model must be the same as the solutions obtained using decoupled models for constituents 1 and 2 and the mixture theory.

IV.3 Numerical studies

IV.3.1 Introduction

The mathematical models presented in Chapter IV.2 are a system of non-linear partial differential equations describing boundary value problems. The finite element processes derived using the residual functional (least squares process) yield variationally consistent integral forms when the second variation of the residuals are neglected in the second variation of the residual functional. Justifications for doing so are given in the references by the authors. Variationally consistent integral forms yield unconditionally stable computations. Hence, in the present work we use this approach for obtaining numerical solutions of the mixtures of Newtonian and generalized Newtonian fluids. The local approximations are considered in $H^{k,p}(\bar{\Omega}^e)$ scalar product spaces in which k is the order of the space defining global differentiability of approximations and p is the degree of local approximations for all dependent variables. With this choice the least squares processes remain convergent [140].

We consider two model problems consisting of fully developed flow between parallel plates and an asymmetric backward facing step. In both model problems we only consider a saturated mixture of two fluids. Both Newtonian and generalized Newtonian fluids are considered. In the case of generalized Newtonian fluids we consider power law and Carreau-Yasuda models for shear thinning fluids. In all numerical studies (both $\mathbb{R}^1$ and $\mathbb{R}^2$) $p_0 = \tau_0 = \rho_0 u_0^2$ (characteristic kinetic energy) is used to choose reference pressure and reference stress.

IV.3.2 Fully developed flow between parallel plates

In this model problem we consider fully developed flow between parallel plates. We only need to consider a typical section **A**–**A**. Furthermore, due to symmetry considerations only half of the domain **A**–**A** is considered (consider $0 < y < 1$ at **A**–**A**). We consider the distance between the plates to be $2\hat{H} = 2$ cm and if we choose $L_0 = 0.01$ m then the dimensionless distance $2H$ between the plates is 2 and our computational domain is $0 \leq y \leq 1$ at **A**–**A**. We consider saturated mixtures of two constituents. The properties of the constituents are given in the following.

Newtonian constituents [131]

Fluid 1 (or constituent 1)
$\hat{\rho}^{(1)} = 900 \qquad \hat{\eta}_1 = 0.0267$
Fluid 2 (or constituent 2)
$\hat{\rho}^{(2)} = 1000 \qquad \hat{\eta}_2 = 0.0018$

Power law constituents

Fluid 1 (or constituent 1)
$\hat{\rho}^{(1)} = 1001; \qquad \hat{\eta}_1^0 = 0.567$ (zero shear rate viscosity)
$n_1 = 0.854$ (power law index)

Fluid 2 (or constituent 2)
$\hat{\rho}^{(2)} = 1001$; $\hat{\eta}_2^0 = 0.332$ (zero shear rate viscosity)
$n_2 = 0.738$ (power law index)

Carreau model constituents

Fluid 1 (or constituent 1)
$\hat{\rho}^{(1)} = 1001 \quad , \quad \hat{\eta}_1^0 = 0.18 \quad , \quad \hat{\eta}_1^\infty = 0.0 \quad , \quad \lambda_1 = 0.048 \quad , \quad m_1 = 0.729$
Fluid 2 (or constituent 2)
$\hat{\rho}^{(2)} = 1001 \quad , \quad \hat{\eta}_2^0 = 0.450 \quad , \quad \hat{\eta}_2^\infty = 0.0 \quad , \quad \lambda_2 = 2.28 \quad , \quad m_2 = 0.756$
We consider a 5 element discretization of the domain $0 \leq y \leq 1$ (at **A**–**A**) using 3-node p-version elements with local approximation in $H^{k,p}(\bar{\Omega}^e)$ scalar product spaces.

IV.3.3 Newtonian constituents and Newtonian mixture

In this section we present a number of different numerical studies using the combined model for both constituents as well as using individual models for the constituents to demonstrate

1. that for Newtonian constituents and mixture the mathematical models for the constituents are decoupled
2. that the combined model produces exactly the same results as the individual models for the constituents.

In the numerical studies we choose $\dfrac{\partial p}{\partial x} = -0.2$, thus based on the assumption $p_1 = \phi_1 p$ and $p_2 = \phi_2 p$ we have

$$\begin{aligned} \frac{\partial p_1}{\partial x} &= \phi_1 \frac{\partial p}{\partial x} = -0.2\phi_1 \\ \frac{\partial p_2}{\partial x} &= \phi_2 \frac{\partial p}{\partial x} = -0.2\phi_2 \end{aligned} \tag{IV.130}$$

We use (IV.130) in the numerical studies using the combined model as well as the individual models for the constituents. The validity of assumption (IV.130) is also verified numerically in the section containing numerical studies in $\mathbb{R}^2$. We consider and present results for various numerical studies using the combined mathematical model based on assumption (IV.130) in the following. We consider a 5 element discretization using 3-node p-version elements. C^1 approximations at p-level 3 are used for the Newtonian studies, and C^2 approximations at p-level 9 are used for power law and Carreau model studies.

Case (a) when constituent 2 is the same as constituent 1 (combined model)

This is perhaps the simplest case for which the mixture theory must produce results that are obvious. We choose
$\eta_0 = \hat{\eta}_1^0 = 0.0267$; $\rho_0 = \hat{\rho}^{(1)} = 900$; and $\phi_1 = 0,\ 0.01,\ 0.1,\ 0.5,\ 0.9,\ 0.99$, and 1.

As expected the velocity u (figure 88) as a function of y is independent of volume fraction and the mixture velocity is the same as those of the constituents. Figure 89 shows plots of the mixture and constituent shear stresses for different volume fractions. $({}_d\sigma)_{xy} = ({}_d\sigma_1)_{xy} + ({}_d\sigma_2)_{xy}$ produces shear stress for the mixture that is in agreement with the theoretical solution. Figure 90 shows plots of $\underset{\sim}{\mu}_1$, $\underset{\sim}{\mu}_2$, and $\underset{\sim}{\mu}_m$ versus volume fraction ϕ_1. With progressively increasing ϕ_1, $\underset{\sim}{\mu}_1$ increases linearly while $\underset{\sim}{\mu}_2$ decreases linearly such that $\underset{\sim}{\mu}_1 + \underset{\sim}{\mu}_2 = \underset{\sim}{\mu}_m =$ constant (corresponding to $\hat{\eta}_1$). This study shows the validity of mixture theory when the two constituents are the same.

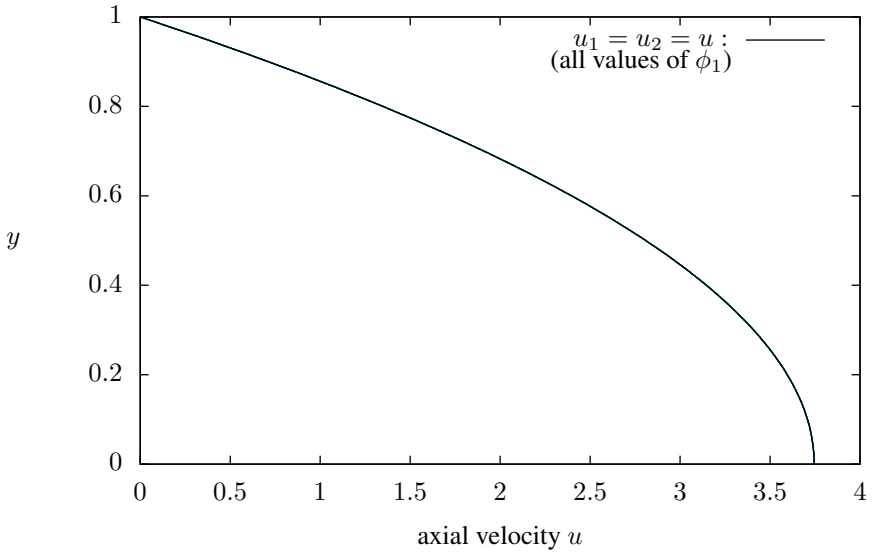

Figure 88: Velocity of constituents and mixture: Newtonian - fluid 2 same as fluid 1 (Combined Model)

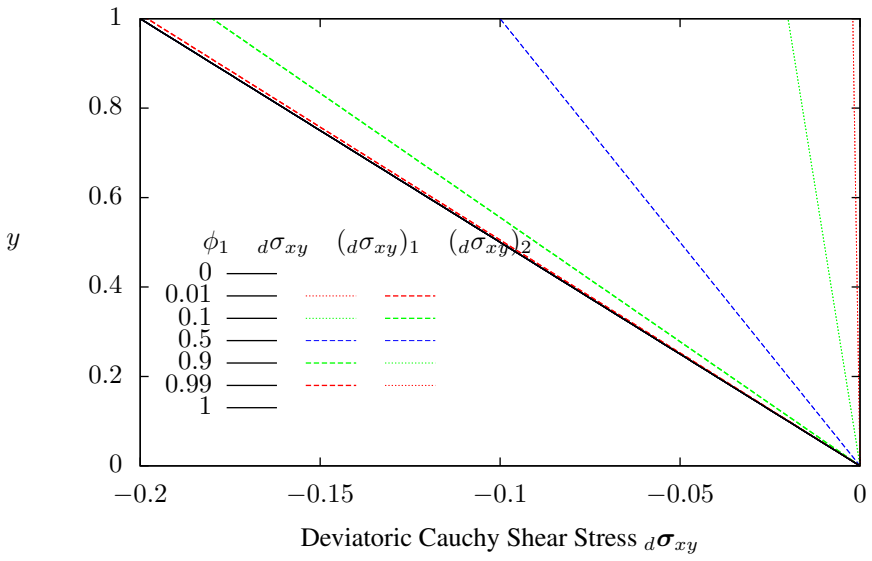

Figure 89: Deviatoric Cauchy shear stress for the constituents and the mixture: Newtonian - fluid 2 same as fluid 1 (combined model)

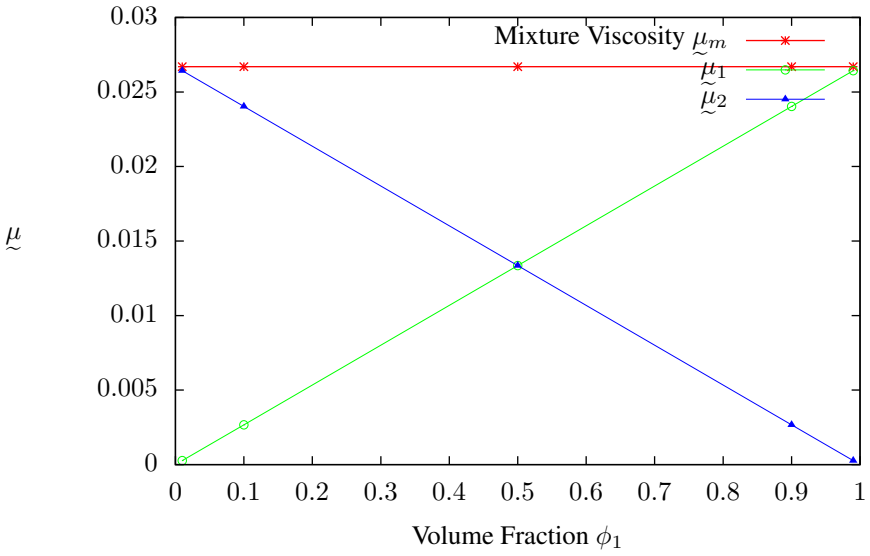

Figure 90: $\underset{\sim}{\mu}_1$, $\underset{\sim}{\mu}_2$, and $\underset{\sim}{\mu}_m$ versus y for different volume fractions

Case (b) mixture of constituent 1 and constituent 2 (combined model)

In this study we consider a saturated mixture of constituents one and two for different volume fractions. We choose $\rho_0 = \hat{\rho}^{(2)} = 1000$ and $\eta_0 = \hat{\eta}_1^0 = 0.0267$ as reference quantities. Figures (92) and (93) show plots of u_1, u_2, and u for different volume fractions. For $\phi_1 = 0$, the mixture consists of only constituent 2 and likewise for $\phi_1 = 1$, the mixture consists purely of constituent 1. The plots of u versus y for $\phi_1 = 0.0$ and $\phi_1 = 1.0$ confirm this. For $\phi_1 = 0.0$ and $\phi_1 = 1.0$, u versus y agrees precisely with the theoretical solutions for constituent 2 and constituent 1. u versus y for $\phi_1 = 0.0$ and $\phi_1 = 1.0$ obviously bracket the velocity profiles for different values of the volume fractions. Plots of shear stress for the constituents and the mixture are shown in figure 94. Plots of $\underset{\sim}{\mu}_1$, $\underset{\sim}{\mu}_2$, and $\underset{\sim}{\mu}_m$ for different volume fractions are shown in figure 91. For $\phi_1 = 1$ and $\phi_1 = 0$, $\underset{\sim}{\mu}_m$ corresponds to η_1 and η_2 as expected.

Remarks

1. The same numerical studies were repeated using decoupled models for the constituents. The results are identical to those reported above using the combined model.

2. The assumption (IV.130) regarding partial pressures p_1 and p_2 holds in the numerical studies. The validity of this assumption is further established numerically (see section IV.3.6).

IV.3.4 Carreau model for constituents and the mixture (combined model)

As described earlier, for generalized Newtonian fluids the decoupled model can not be used due to the fact that viscosities are deformation field dependent. In this section we present numerical studies similar to those presented in section IV.3.3 for the Newtonian case. In these studies the local approximations (equal order, equal degree) for all variables are of class $C^2(\bar{\Omega}^e)$ with p-level of 9. For this choice, I is $O(10^-8)$ or lower. The uniform discretization consists of five 3-node p-version elements.

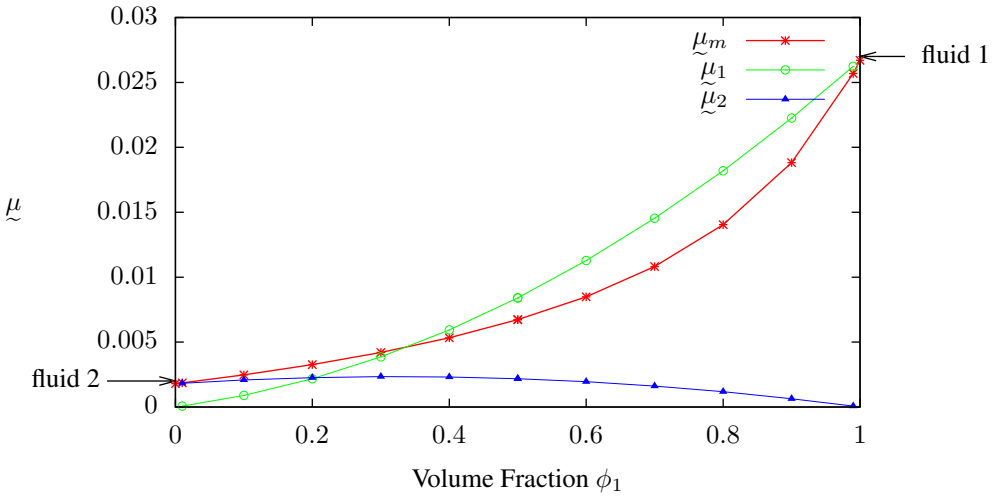

Figure 91: Mixture viscosity: Newtonian

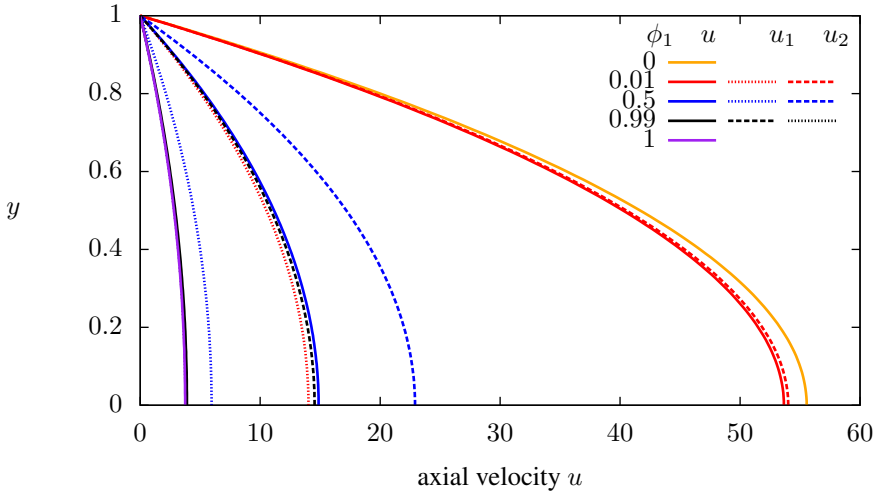

Figure 92: Velocity of constituents and mixture: Newtonian (combined model)

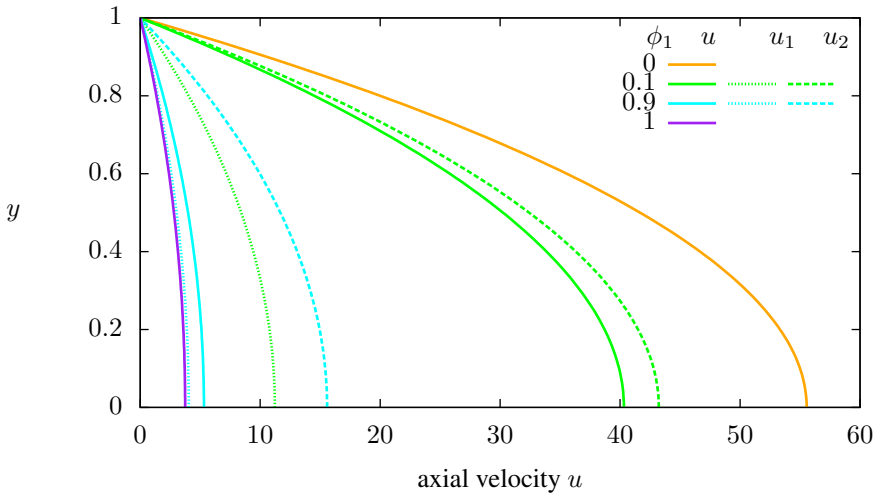

Figure 93: Velocity of constituents and mixture: Newtonian (combined model)

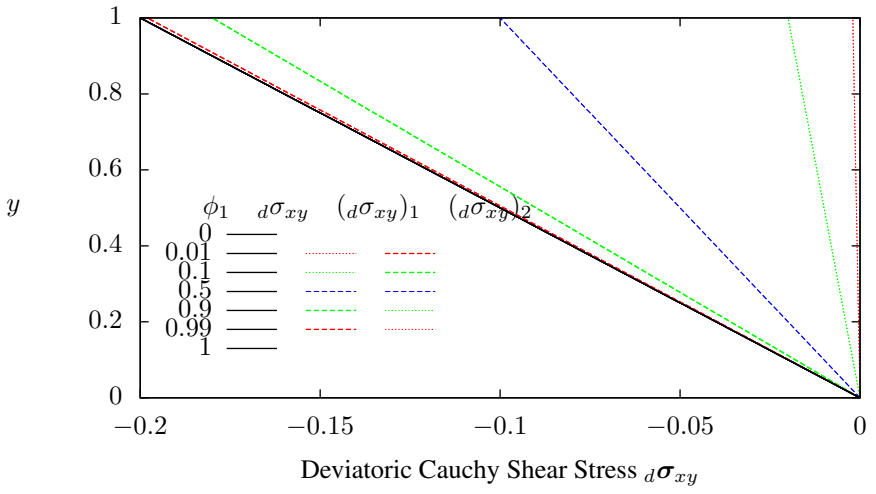

Figure 94: Deviatoric Cauchy shear stress for the constituents and the mixture: Newtonian (combined model)

Case (a): when constituent 2 is the same as constituent 1

For this case we choose $\rho_0 = \hat{\rho}^{(1)} = 1001$ and $\eta_0 = \hat{\eta}_1^0 = 0.18$ as reference values for density and viscosity. Axial velocity versus y confirms that $u_1 = u_2 = u$ holds for all volume fractions as expected. For $\phi_1 = \phi_2 = 0.5$ we observe that $({}_d\sigma_1)_{xy} = ({}_d\sigma_2)_{xy}$. For all volume fractions $({}_d\sigma_m)_{xy} = ({}_d\sigma_1)_{xy} + ({}_d\sigma_2)_{xy}$ holds. As expected, shear stresses are linear functions of the y coordinate. $\underset{\sim}{\mu}_m$ as a function of y is independent of the volume fraction due to the fact that the two constituents are the same. For all volume fractions $\underset{\sim}{\mu}_m = \underset{\sim}{\mu}_1 + \underset{\sim}{\mu}_2$ holds as $\frac{\partial u_1}{\partial y} = \frac{\partial u_2}{\partial y} = \frac{\partial u}{\partial y}$. Since findings are similar to the Newtonian case, graphs are omitted for the sake of brevity.

Case (b): Mixture of constituents 1 and 2 (combined model)

In this case we consider the same discretization with $k = 3$ (order of approximation space) and $p = 5$ as in case (a). We choose $\rho_0 = \hat{\rho}^{(1)} = 1001$ and $\eta_0 = \hat{\eta}_2^0 = 3.6$ as reference values of density and viscosity. Plots of velocities u_1, u_2, and u versus y for different volume fractions are shown in figures 95 and 96. Shear stresses for the constituents and the mixture as a function of y are shown in figure 97. These remain linear functions of y and are the same as those reported in case (a). Plots of μ_m as a function of I_2, second invariant of the strain rate tensor for different volume fractions are shown in figure 3.17. For $\phi_1 = 0.99$ and $\phi_2 = 0.01$, μ_m is close to η_1 and η_2 for constituents 1 and 2.

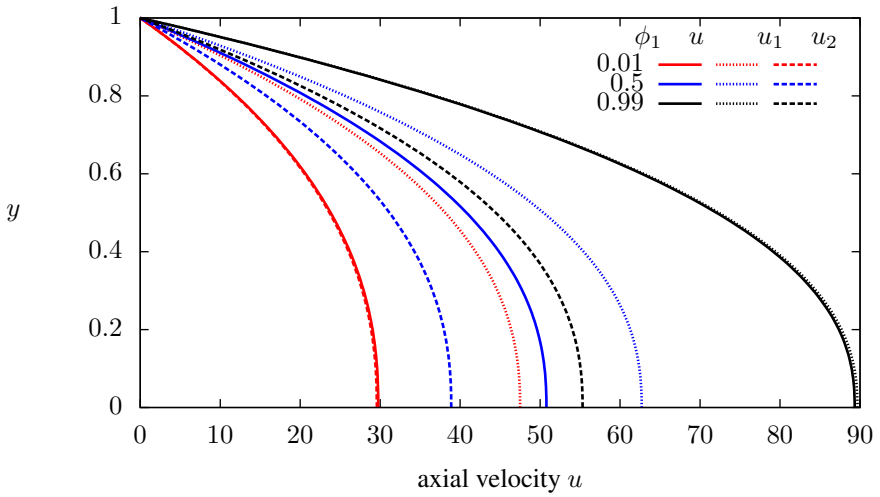

Figure 95: Velocity of constituents and mixture: Carreau fluid (combined model)

IV.3.5 Power law model for constituents and the mixture (combined model)

These studies are parallel to those for the Carreau model using the same discretization, k, and p.

Case (a): when constituent 2 is the same as constituent 1

We use $\rho_0 = \hat{\rho}^{(1)} = 1001$ and $\eta_0 = \hat{\eta}_1^0 = 0.332$ as reference values. Results and findings are similar to Carreau model, hence are omitted.

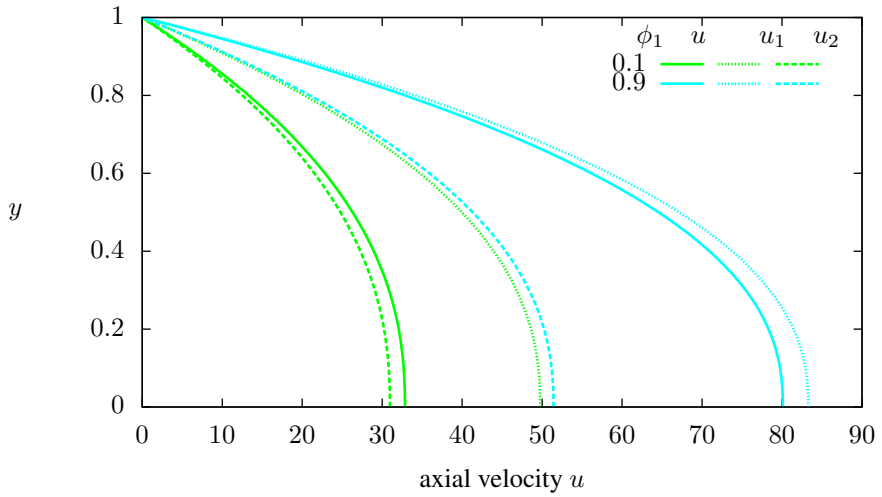

Figure 96: Velocity of constituents and mixture: Carreau fluid (combined model)

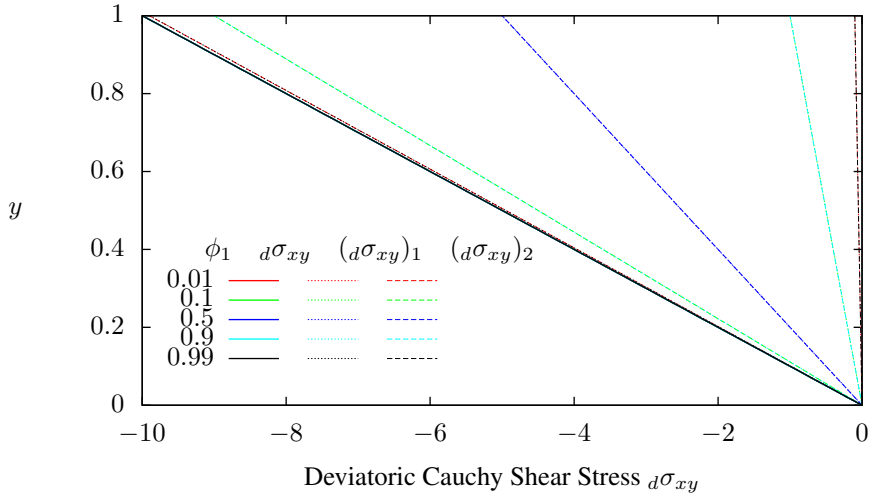

Figure 97: Deviatoric Cauchy shear stress for the constituents and the mixture: Carreau fluid (combined model)

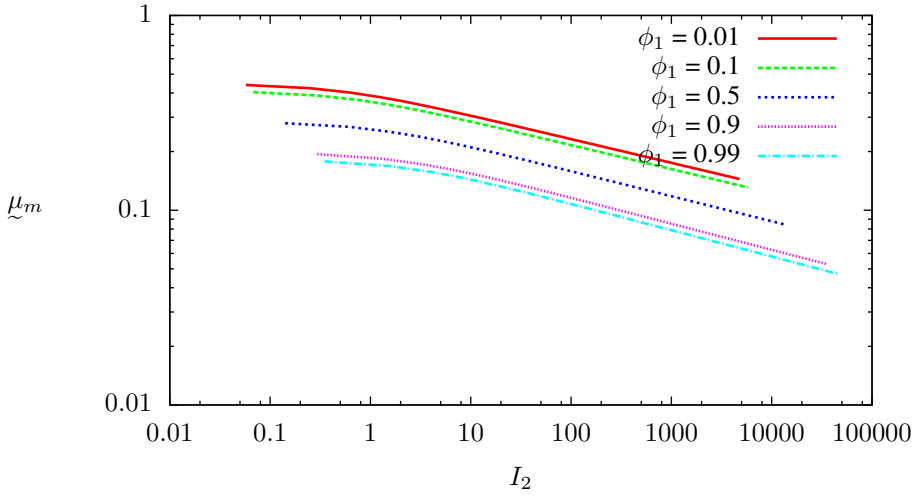

Figure 98: Viscosity of fluid mixtures: Carreau

Case (b): mixture of constituents 1 and 2 (combined model)

For these numerical studies we choose $\rho_0 = \hat{\rho}^{(1)} = 1001$ and $\eta_0 = \hat{\eta}_2^0 = 2.04$ as reference values. Graphs of $u_1 = u_2 = u$ versus y, and μ_m as a function of y for different volume fractions are shown in figures 99 – 102. Behaviors are similar to the Carreau model.

IV.3.6 1:2 backward facing asymmetric expansion

We consider a 1:2 backward facing asymmetric expansion. A schematic and the boundary conditions are shown in figure 103. Figure 104 shows a graded twenty element discretization using nine node p-version elements. In the numerical studies we only consider the constituents and the mixture to be Newtonian and use the same properties as listed for the Newtonian constituents for fully developed flow between parallel plates (section IV.3.2). At the inlet, the flow is assumed to be fully developed with a parabolic velocity field for both constituents with maximum value of one (figure 103). With this choice of axial velocities of the constituents, based on (IV.7), the axial velocity of the mixture is the same as the axial velocities of the constituents as $\phi_1 + \phi_2 = 1$ must hold. C^{00} local approximations at p-level 9 are used for all variables. For this choice, I values are $O(10^{-8})$ or lower confirming good accuracy of the solution. Characteristic kinetic energy is used for reference pressure and reference stress.

Case (a): constituent 2 same as constituent 1 (coupled model)

We choose $\rho_0 = \hat{\rho}^{(2)} = 1000$ and $\eta_0 = \hat{\eta}_1^0 = 0.0267$ as reference values. We consider two combinations of volume fractions, $\phi_1 = \phi_2 = 0.5$ and $\phi_1 = 1.0$, $\phi_2 = 0.0$. When $\phi_1 = \phi_2 = 0.5$ we expect the two constituent behaviors to be the same. The mixture response in this case is obviously the same as when $\phi_1 = 1.0$, $\phi_2 = 0.0$. As obvious in this case the mixture behavior is independent of the volume fractions. In this study p_1 and p_2, the constituent partial pressures, are dependent variables. Figures 105 and 106 show plots of pressures p_1, p_2, and p $(= p_1 + p_2)$ for $\phi_1 = 0.5$, $\phi_2 = 0.5$ and $\phi_1 = 1.0$, $\phi_2 = 0.0$ at the top and bottom boundaries (or plates). Results for pressure for volume fraction $\phi_1 = 0.2$ and $\phi_2 = 0.8$ and comparisons with $\phi_1 = 1.0$, $\phi_2 = 0.0$ are shown in figures 107 and 108. Plots of representative u_1, u_2, and u versus y at $x = 0.0$ and $x = 2.0$ are shown in figures 109 and 110. These are obviously independent of the volume fractions for the case when both constituents are the same.

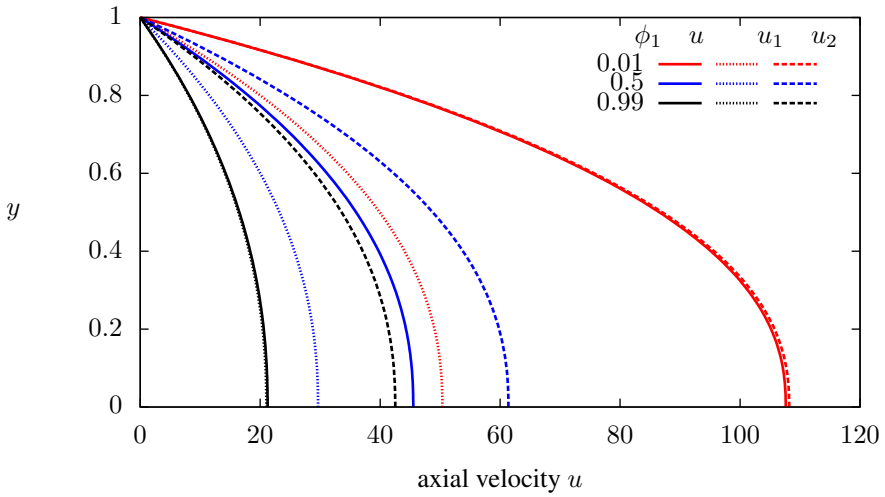

Figure 99: Velocity of constituents and mixture: Power Law fluid (combined model)

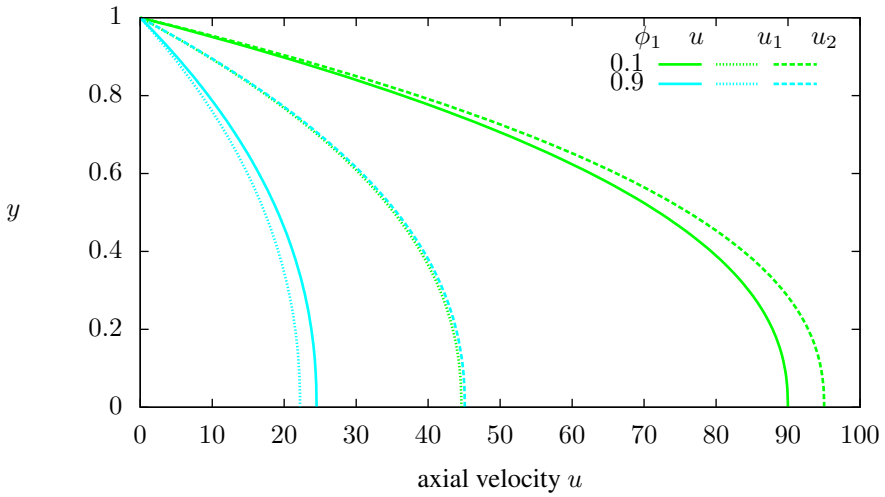

Figure 100: Velocity of constituents and mixture: Power Law fluid (combined model)

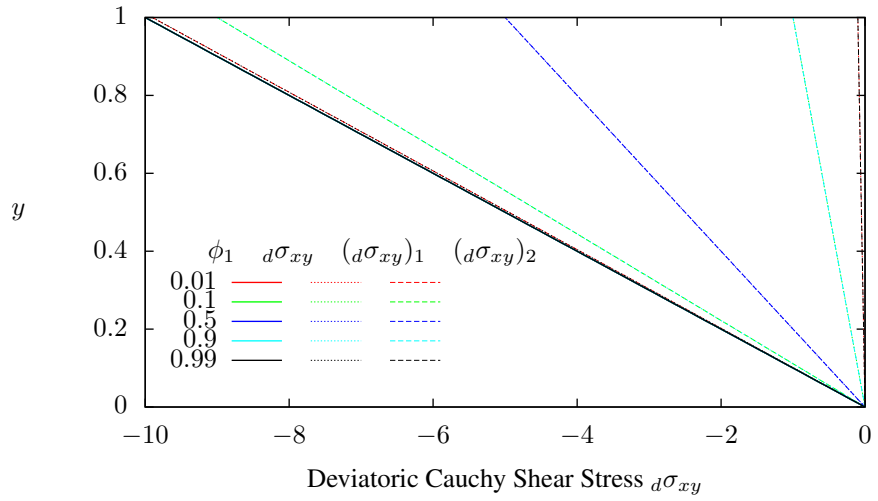

Figure 101: Deviatoric Cauchy shear stress of constituents and mixture: Power Law (combined model)

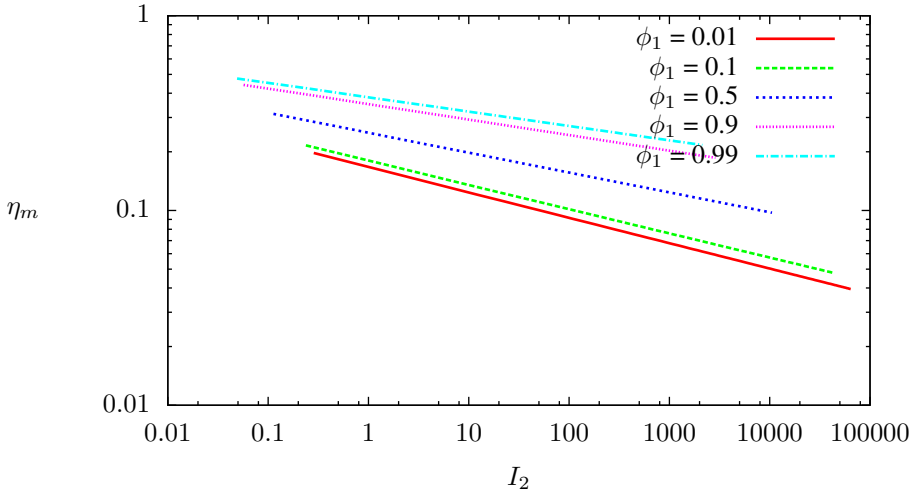

Figure 102: Viscosity of mixture of Power Law fluids

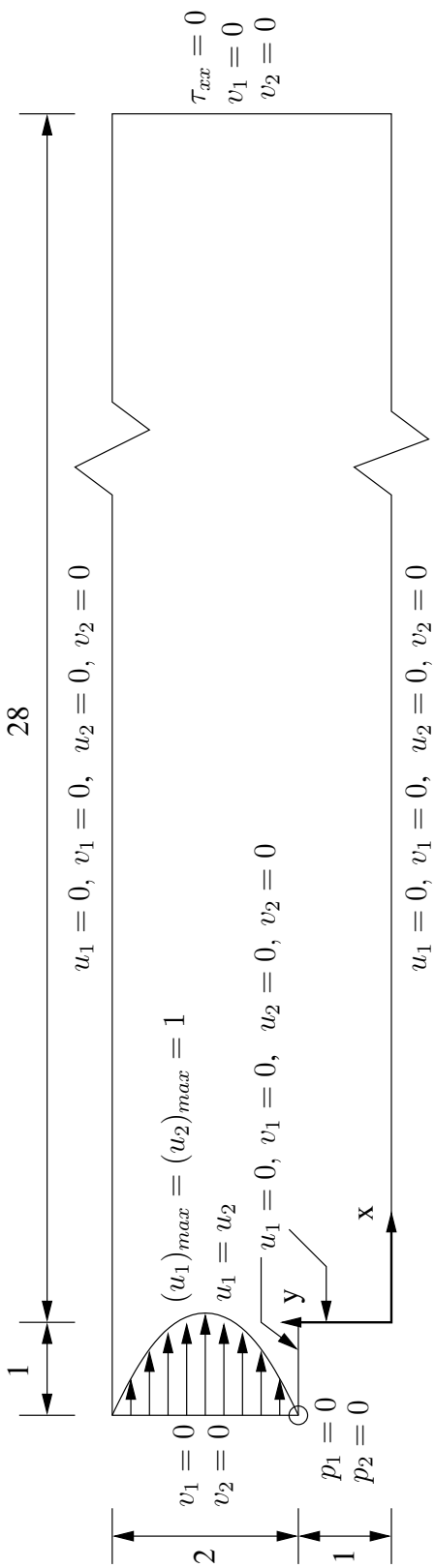

Figure 103: Schematic of boundary conditions

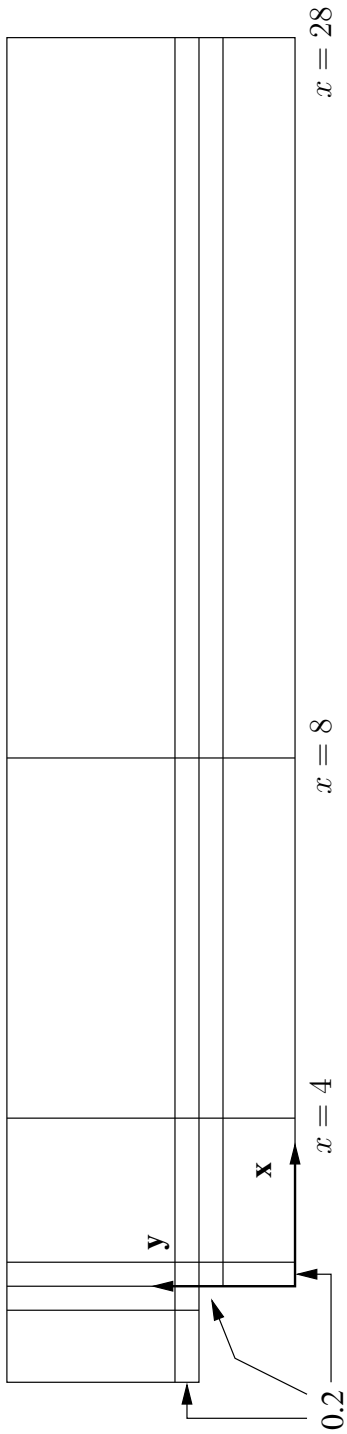

Figure 104: Graded discretization: 20 nine-node p-version elements

Numerical studies were also conducted using decoupled models for the constituents using $p_1 = \phi_1 p$ and $p_2 = \phi_2 p$. The results obtained from these studies are identical to those presented here using the combined model in which volume fractions are not used to describe partial pressures of the constituents. These studies confirm that the decoupled model used in section IV.2 and in the studies for fully developed flow between parallel plates is justified and the assumption of partial pressures of the constituents is valid as well.

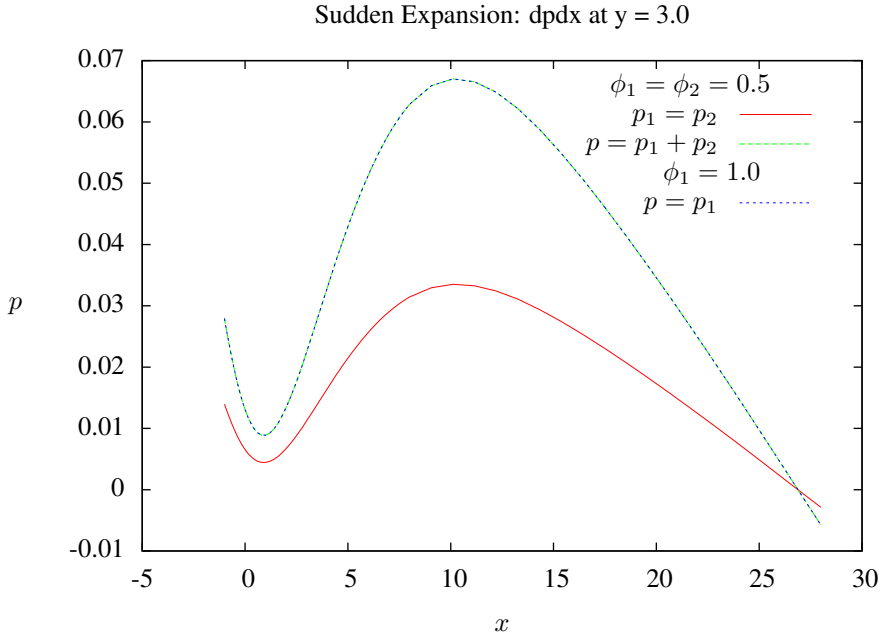

Figure 105: Pressure at top boundary ($y = 3, -1 \leq x \leq 28$): fluid 2 same as fluid 1, $\phi_1 = \phi_2 = 0.5$

Case (b): mixture of constituents 1 and 2

In this case we choose volume fractions $\phi_1 = 0.8$ and $\phi_2 = 0.2$. Figures 111 and 112 show plots of u_1, u_2, and u versus y at $x = 0.0$ and $x = 2.0$. Differences in u_1, u_2, and u are quite clear in figure 112. Figures 113 and 114 show plots of pressures p_1, p_2, and p at $y = 3$ and at $y = 0$.

Numerical studies were also conducted using decoupled models for the constituents using $p_1 = \phi_1 p$ and $p_2 = \phi_2 p$. The results obtained from these studies are identical to those presented in figures 111 – 114 using the combined model in which volume fractions are not used to define partial pressures of the constituents. These studies once again confirm the validity of the decoupled model.

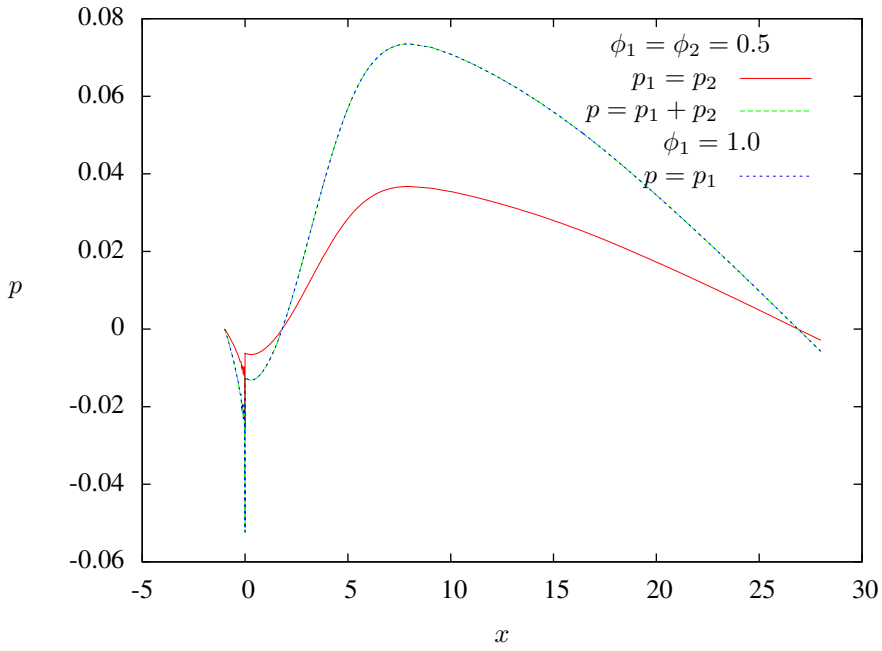

Figure 106: Pressure at bottom boundary ($y = 1, -1 \leq x \leq 0$; $y = 0, 0 \leq x \leq 28$): fluid 2 same as fluid 1, $\phi_1 = \phi_2 = 0.5$

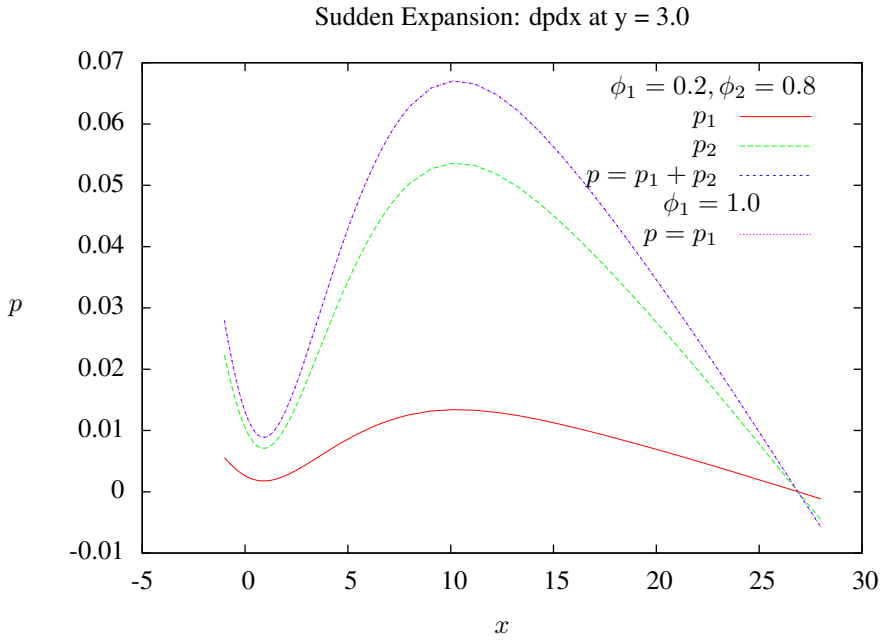

Figure 107: Pressure at top boundary ($y = 3, -1 \leq x \leq 28$): fluid 2 same as fluid 1, $\phi_1 = 0.2, \phi_2 = 0.8$

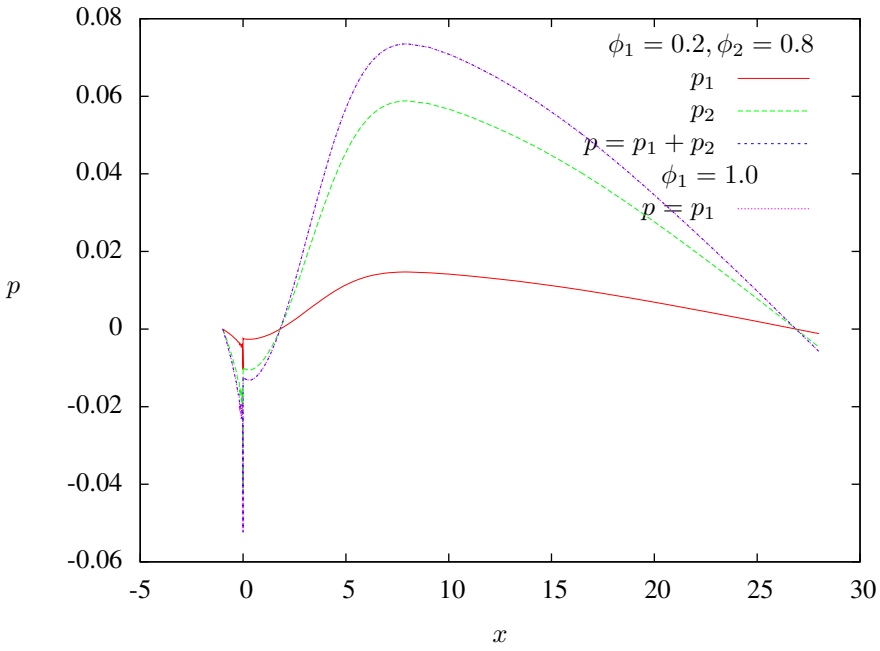

Figure 108: Pressure at bottom boundary ($y = 1, -1 \leq x \leq 0$; $y = 0, 0 \leq x \leq 28$): fluid 2 same as fluid 1, $\phi_1 = 0.2, \phi_2 = 0.8$

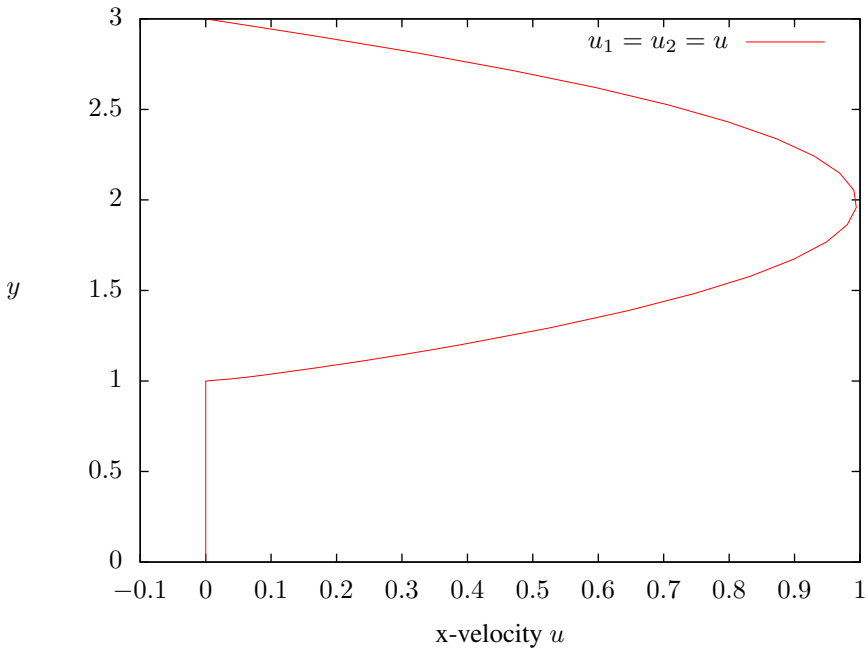

Figure 109: Velocity at $x = 0$: fluid 2 same as fluid 1

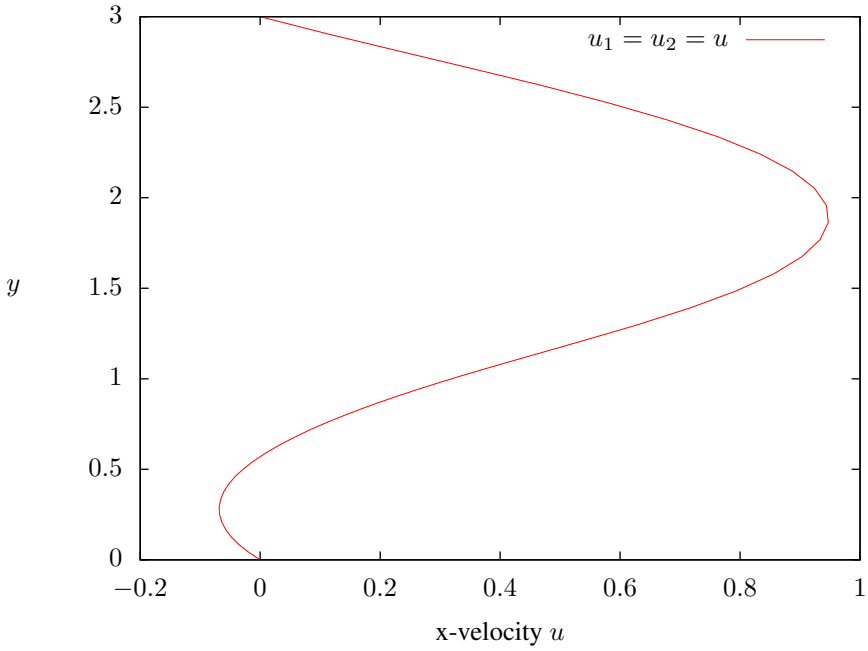

Figure 110: Velocity at $x = 2.0$: fluid 2 same as fluid 1

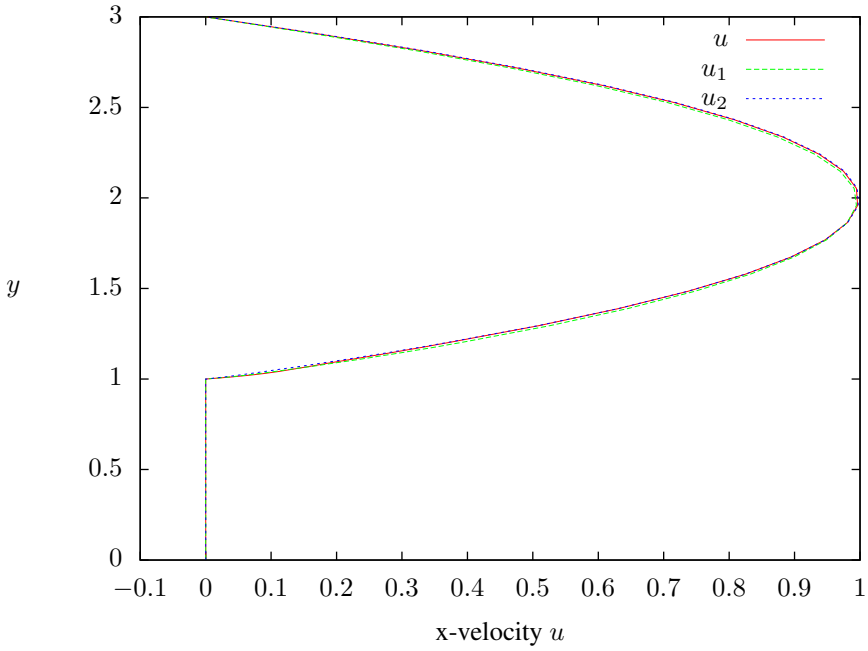

Figure 111: Velocity at $x = 0.0$: mixture of fluid 1 and fluid 2, $\phi_1 = 0.8, \phi_2 = 0.2$

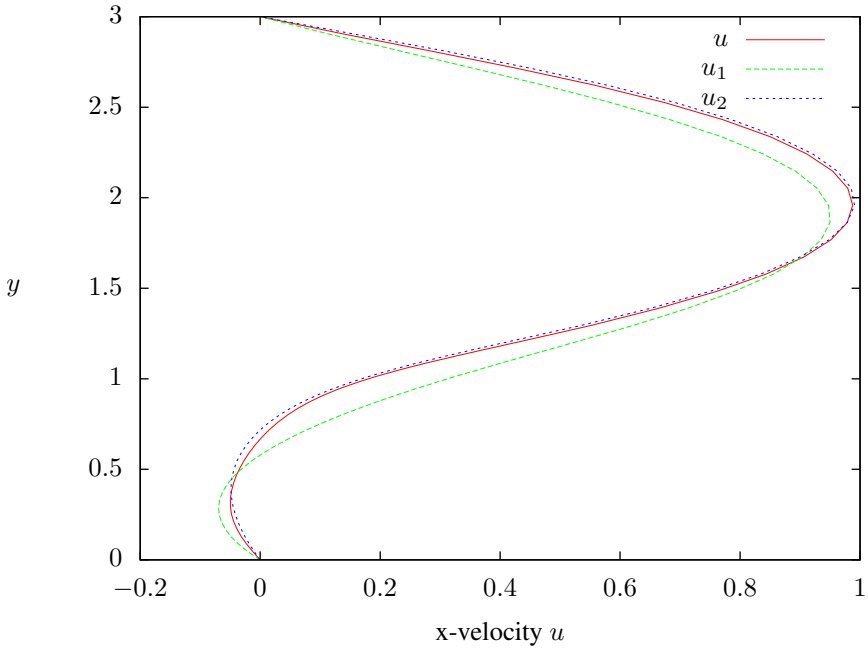

Figure 112: Velocity at $x = 2.0$: mixture of fluid 1 and fluid 2, $\phi_1 = 0.8, \phi_2 = 0.2$

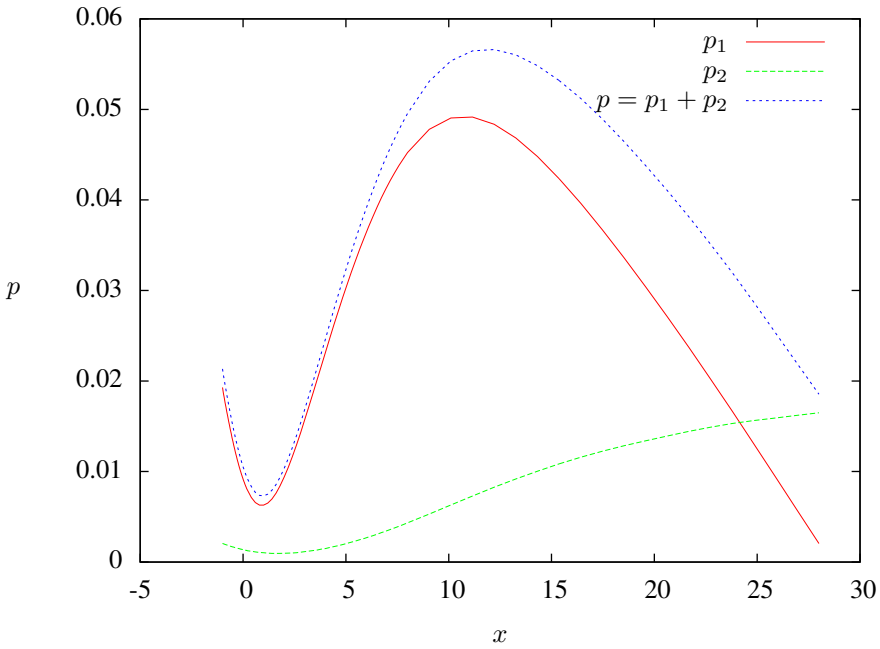

Figure 113: Pressure at top boundary ($y = 3, -1 \leq x \leq 28$): mixture of fluid 1 and fluid 2, $\phi_1 = 0.8, \phi_2 = 0.2$

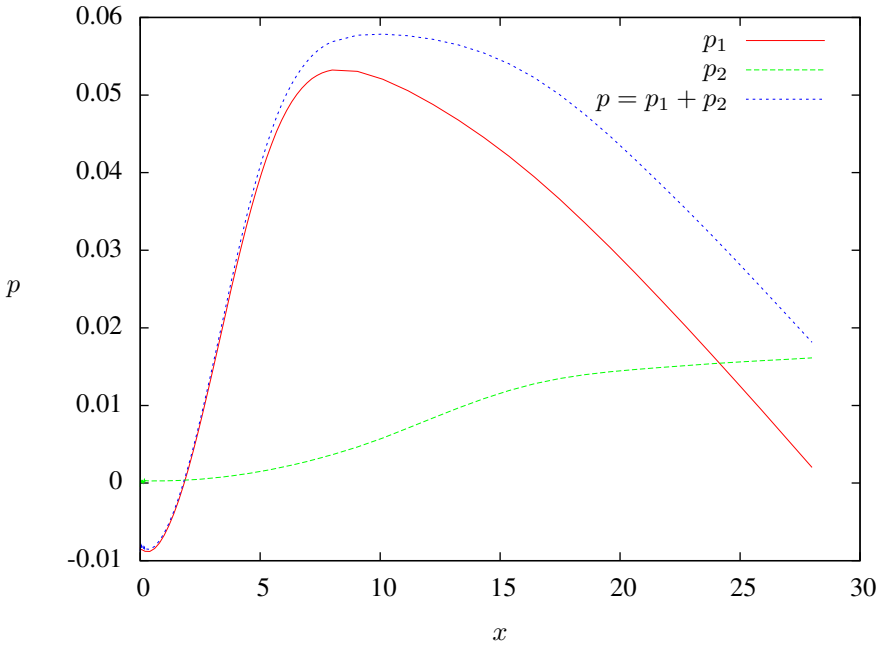

Figure 114: Pressure at bottom boundary ($y = 0, 0 \leq x \leq 28$): mixture of fluid 1 and fluid 2, $\phi_1 = 0.8, \phi_2 = 0.2$

IV.4 Summary, concluding remarks, significance and impact of this research

In this work, derivation of the mathematical model(s) for a homogeneous, isotropic, incompressible mixture of ν homogeneous, isotropic, and incompressible constituents using basic principles of mixture theory and continuum mechanics is presented. The deformation process is assumed to be isothermal, hence temperature effects due to viscous dissipation are assumed to be negligible. The basic definition of densities of the constituents, density of the mixture, mixture velocities, and the material derivative for the constituents and the mixture are presented and are utilized in the conservation laws: conservation of mass, balance of momenta for the constituents, and the energy equation for the mixture based on the first law of thermodynamics. The second law of thermodynamics (entropy inequality) and the theory of generators and invariants is used as a basis for the constitutive theories for the mechanical pressure and deviatoric Cauchy stress tensors for the constituents and the mixture. The constitutive theories borrow basic derivations from references [74, 131]; these are modified to account for the correct physics of the mixture for the constituents used in the present work. Specific forms of the complete mathematical models are presented in $\mathbb{R}^1$ and $\mathbb{R}^2$ using x–frame (x, y orthogonal coordinate system). The constituents and the mixture are assumed to be Newtonian or generalized Newtonian (power law and Carreau models). In $\mathbb{R}^2$, the mathematical model for two constituents indicated by subscripts 1 and 2 is presented in terms of velocities u_1, v_1, u_2, v_2, pressures p_1, p_2, and the deviatoric Cauchy stress tensors $({}_d\sigma_1)_{ij}$, $({}_d\sigma_2)_{ij}$; $i, j = x, y$ (total of 12 dependent variables). This constitutive model consists of twelve first order partial differential equations in twelve variables. The force π_α exerted on the α^{th} constituent by the other constituents are considered in the derivation of the momentum equations for the constituents but are neglected in the numerical studies and decoupled models. The constitutive theories presented here are based on [74, 131] and utilize material coefficients λ_i, $i = 1, 2, \ldots, 5$ and μ_i, $i = 1, 2, \ldots, 4$ which are shown to reduce to a much simplified form containing material coefficients $\mu_1, \mu_2, \ldots, \mu_4$ for the Newtonian and generalized Newtonian constituents and the mixture considered in the work.

The interaction forces π_α are much more significant in the case of liquid and solid particulate constituents, but are neglected in the present work. This mathematical model in various forms is commonly used for mixture theory in which the constituents are homogeneous, isotropic, incompressible fluids. In the present work we have shown that for the degenerated case when the two

constituents in a mixture are the same, μ_3 and μ_4 must be zero for the mixture constitutive theory to be meaningful. Hence, in the constitutive theory used in the present work we use $\mu_3 = \mu_4 = 0$. The final mathematical model in $\mathbb{R}^2$ with u_1, v_1, u_2, v_2, p_1, p_2, and $({}_d\sigma_1)_{ij}$, $({}_d\sigma_2)_{ij}$; $i, j = x, y$ as dependent variables with only $\mu_1(\phi_1, \phi_2, \eta_1, \eta_2)$ and $\mu_2(\phi_1, \phi_2, \eta_1, \eta_2)$ as material coefficients in the constitutive theory has closure and is used for numerical studies in $\mathbb{R}^2$. This model requires no assumptions regarding p_1 and p_2 and is used to compute numerical results for 1:2 backward facing step.

From the mathematical model presented in $\mathbb{R}^1$ for fully developed flow between parallel plates, it is obvious that p_1 and p_2 for the constituents must be expressed in terms of the pressure p for the mixture. The assumption $p_\alpha = \phi_\alpha p$, $\sum_{\alpha=1}^{\nu} p_\alpha = p$, which implies $\sum_{\alpha=1}^{\nu} \phi_\alpha = 1$ used in the mathematical model, is used to compute numerical results for fully developed flow between parallel plates. This assumption is verified using the second model problem in which the combined model is used to compute constituent pressure p_1 and p_2 and then compared with p_1 and p_2 obtained using the decoupled model to demonstrate that p_1 and p_2 obtained from this model are in precise agreement with those from the coupled model.

It is shown that the combined mathematical model proposed in this work can be decoupled when the constituents for the mixture are Newtonian fluids as for this case the viscosities are constant. However when the constituents and the mixture are generalized Newtonian fluids (power law and Carreau-Yasuda), the viscosities of the constituents are functions of the corresponding second invariant of the symmetric part of the velocity gradient tensors, hence the combined model can not be decoupled. The numerical studies presented for fully developed flow between parallel plates and 1:2 asymmetric backward facing step confirm the validity of the proposed mathematical model using $p_1 = \phi_1 p$, $p_2 = \phi_2 p$, and $p_1 + p_2 = p$ and the modifications proposed in the constitutive theory for the constituents.

The significant aspects of the work are described above. The mathematical model derived for ν constituents (isentropic, homogeneous and incompressible) fluids is based on conservation and balance laws in conjunction with basic principles of mixture theory. The constitutive theories are derived using entropy inequality. It is shown that when the transport properties are constant, the mixture model degenerates to individual constituent models, i.e. becomes decoupled. When the viscosity is a function of the second invariant of the symmetric part of the velocity gradient tensor (generalized Newtonian fluids), the mathematical model cannot be decoupled in terms of constituents. Approaches if deriving mixture properties are presented. The numerical examples clearly demonstrate the validity and usefulness of the proposed theory. The extension of this work accounting for interaction forces and for compressible constituents is important for real applications. This work is in progress.

V Riemann shock tube: 1D normal shocks in air, simulations and experiments

This work presents numerical simulation of the evolution of one-dimensional normal shocks, their propagation, reflection, and interaction in air using a single diaphragm Riemann shock tube and validate them using experimental results. Mathematical model is derived for one-dimensional compressible flow of viscous and conducting medium. Dimensionless form of the mathematical model is used to construct space-time finite element processes based on minimization of the space-time residual functional. The space-time local approximation functions for space-time p-version hierarchical finite elements are considered in higher order $H^{k,p}(\bar{\Omega}^e_{xt})$ spaces that permit desired order of global differentiability of local approximations in space and time. The resulting algebraic systems from this approach yield unconditionally positive-definite coefficient matrices, hence ensure unique numerical solution. The evolution is computed for a space-time strip corresponding to a time increment Δt and then time march to obtain the evolution up to any desired value of time. Numerical studies are designed using recently invented hand-driven shock tube (Reddy tube) parameters, high/low side density and pressure values, high and low pressure side shock tube lengths, so that numerically computed results can be compared with actual experimental measurements.

V.1 Introduction, literature review, and scope of work

In compressible flows, shocks naturally form due to the existence of the compression wave, and the process of piling up of these waves to eventually form a shock. Numerical simulation of flows with shocks can be viewed in many ways depending upon what outcome is of interest. The first group of numerical methods are shock fitting or shock capturing methods. In these methods one does not pay attention to the evolution of shock but are rather interested in the shock relations; hence, the name "shock fitting" or "shock capturing." The conditions behind and ahead of the shock are used to transition in some manner and then marched during evolution. Obviously, these methods can describe neither the evolution of the shock nor the physics in the shock region. The

second group of methods are those in which shock evolution is considered but with much higher viscosity than the actual viscosity of the medium so that extremely small shock widths with actual viscosity can be avoided. These methods work well in predicting shock relations and some aspects of other features like shock reflection, shock interaction, and so on, as long as the diffused shock width is much smaller than the spatial dimension of the domain. In this approach, with much increased shock width, one could study flows over large objects since shock structure is no longer a microprocess. In the third group of methods one studies the true evolution, propagation, reflection, and interaction of a shock. This, of course, requires actual values of viscosity and other transport properties. The shock width is generally of the same order of magnitude as viscosity. For example, for air the viscosity is $O(10^{-6})$ whereas the shock widths are also of the order of $O(10^{-6})$. Numerical simulations of the evolution of narrow shocks require local mesh refinements near the shock – behind and ahead of the shock. Thus, this approach is good in understanding the details of the shock physics but its use in large spatial domains could be prohibitively expensive due to extreme mesh refinement requirements in the entire spatial domain. There is extensive literature on the subject. A good literature review and discussion of various approaches, their merits, and shortcomings was done by [141–145]. In the following we only discuss the earlier published work that for most part provides the foundation for subsequently published works discussed in these references.

A thorough presentation of various relevant issues related to shock waves was first reported by [146] and [147]. They demonstrated on the basis of thermodynamic considerations that dissipation is by necessity present in shock waves. When viscosity is taken into account shocks are smeared and thus mathematical surfaces of discontinuity are replaced by thin layers in which pressure, velocity, density, and temperature are continuous. [148] used this idea to introduce artificial dissipation into the one-dimensional equations of hydrodynamics to give the shocks thickness comparable to the spacing of points in the discretization. With their special form of assumed dissipation, they demonstrated that the resulting equations in their finite difference numerical scheme satisfied the Rankine-Hugoniot relations, provided the thickness of the shock layers were small in comparison with the other dimensions of the system. The paper presents complete details of the proposed procedure, its limitations, and stability criterion (CFL condition as discussed by [149]) but lacks mathematical proofs of existence and uniqueness. Effects of nonlinearity and viscosity on the shock formation and shock structure was also investigated by [150] through analytical solutions of Burgers equations and other similar quasi-linear parabolic equations with findings similar to those reported by [146–149]. [151, 152] utilized the concepts by [149] and the hydrodynamics equations in conservation form to present a novel difference scheme in time for non-linear hyperbolic equations that incorporates artificial diffusion. Such solutions agreed with well known Rankine-Hugoniot shock relations in the limiting case.

The idea of generalized solutions of the differential and partial differential equations was first proposed by S. L. Sobolev and constitutes the mathematics and thus the backbone of the finite element method. In an important paper, [153] discussed the problem of generalized solutions of quasi-linear equations in gas dynamics. The author illustrated that for $\partial\phi/\partial t + \phi(\partial\phi/\partial x) = 0$ (Burgers equation), the theory of generalized solutions leads to non-uniqueness. This situation can be corrected by imposing additional restrictions on the weak form. For Burgers equation (and its generalization to quasi-linear systems) this restriction leads to the law of conservation of entropy. Thus, in gas dynamics equations describing reversible processes the law of conservation of entropy must hold in the theory of generalized solutions, whereas in irreversible processes there must be entropy production which in physical systems under adiabatic conditions is only possible through dissipative mechanisms. In other words, in the theory of generalized solutions of gas dynamics equations the law of increase in entropy must be replaced by the law of dissipation of energy to ensure uniqueness of generalized solutions. A rigorous mathematical exposition of the solutions of quasi-linear hyperbolic equations is presented by [154]. The findings are similar to those reported by Godunov and are summarized here:

1. The discontinuity of solutions (i.e. shocks) is a basic property of the solutions of quasi-linear equations. Independent of the smoothness of initial data, the solution is generally speaking continuous, and can be defined for arbitrarily large values of time t.

2. Systems of linear equations are always conservative, while the systems of non-linear equations, generally speaking, are conservative only for $n \leq 2$ (two conservation laws).

3. A discontinuous solution of a system of linear equations, satisfying conservation laws of the system, is unique; for quasi-linear systems additional 'stability conditions' have to be imposed to guarantee the uniqueness of the generalized solution.

4. Linear hyperbolic equations describe reversible physical processes while quasi-linear (strongly non-linear) systems generally describe irreversible processes.

5. Discontinuous solutions of a system of linear equations may be considered as the limits of smooth solutions with smooth initial data in the Cauchy problem.

6. For systems of quasi-linear equations, smoothness is not present in the solution even if the initial data are as smooth as we please. For this reason the method of generalized solutions is unsuited for systems of quasi-linear equations and hence 'method of viscosity' must be applied.

Solution of non-linear hyperbolic systems has also been reported by [155] and [156, 157]. Grimm proposed an existence theorem and provided its proof. Smoller reported general characteristics of these solutions with specific details and discussion of the Riemann problem and contact discontinuities. [158] presented a mathematical proof of the convergence of weak solutions of quasi-linear equations of first order with artificial viscosity to strong solutions as viscosity approaches zero. [159] discussed first order conservative systems of non-linear conservation laws which have as a consequence an additional conservation law. They show that if the additional conserved quantity is a convex function of the original ones, the original system can be put into symmetric hyperbolic form. They also derive an entropy inequality which has also been suggested by [160] for discontinuous solutions of the given system of conservation laws. Existence of discrete shocks, genuine non-linearity, and the use of fourth order dissipation in a single conservation law have been reported by [161, 162]. A thorough mathematical exposition with theorems and proofs for uniqueness of the solutions of hyperbolic conservation laws has been reported by [163]. Existence and uniqueness of entropy solutions to the Riemann problem for hyperbolic systems of two conservation laws has been reported by [164]. The paper presents proofs of existence and uniqueness of the solutions in one space variable. Only strictly hyperbolic and genuinely non-linear systems are investigated. [165] reported an investigation of the errors introduced in the calculation of strong shocks using artificial viscosity of the type discussed by [146] and artificial heat flux. Investigation of the errors introduced in the interaction of strong shocks due to the assumption of finite shock width has been reported by Menikoff [166]. [141–145] consider shock evolution, propagation, and reflection using actual values of transport properties and report shock relations, shock speed, and comparisons with Rankine-Hugoniot equation, but no comparisons are provided with any experimental data. In these numerical studies with reference length $L_0 = O(10^{-5})$ and Riemann shock tube dimensionless length of two units, the physical length of the shock tube is $O(10^{-5})$. This work demonstrates that if the evolution, propagation, and reflection of true shock is of interest, then such dimensions of the shock tube are essential in order to avoid the same discretization over the entire physical shock tube of length of several meters that would lead to millions of grid points and elements in case of just simple 1D normal shocks. Such discretizations in 2D and 3D are obviously prohibitive. In summary, simulations of an isolated sharp gradient solution and its propagation during evolution is what we are faced with here. Ongoing parallel research work done by [167] addresses this issue and will provide a practical alternative without compromise in the quality of the evolution. In the present work we wish to numerically simulate evolution of shock, its propagation, reïňĆection, and interaction using the parameters used in actual shock tube experiment performed by [168] using Reddy tube. The purpose obviously is to compare the numerically simulated results with the experiment. Even though the shock tube length in the experiment is 1.000 m and the numerical results are simulated for a shock tube length of 3.00696×10^{-6} m, still it is possible to compare the two. Two critical parameters in the shock tube experiments are the low pressure and the high pressure side lengths L_l and L_h of the shock tube. It is shown in the present work that the ratio L_l/L_h is important in the shock physics. This allows us to scale L_l and L_h to any desired length using the same scale factor thus providing a correspondence between the computed results and the actual experiment with the same L_l/L_h ratio. Consequences of different choices of the ratio L_l/L_h are investigated and demonstrated through numerical simulations of the evolutions.

There are two other important aspects in the numerical simulations and experiment that allow us to compare the two sets of results at selected locations. First, the process of shock evolution and its propagation after it is fully developed is same in the experiment and numerical simulation before the shock reaches the impermeable boundary. Thus the pressure measurement at a location in the vicinity of the diaphragm where shock is fully developed can be compared with the shock relations in the numerical simulation. Secondly, the fully developed shock propagates without change for a relatively short distance in the numerical simulation, whereas in the experiment this distance is half a meter. But this is of no consequence as there is no change in the shock relation during this propagation in both cases. Thus, the incident shocks on the impermeable boundary in both experiment and numerical simulation are identical. This allows us to conclude that pressure generated by the shock reflection in the two cases can be compared even thought shock tube lengths in the experiment and numerical simulations are different. We keep in mind that any deviations in the shock relations of incident shock wave between experiment and numerical simulations are bound to cause perhaps larger deviations in the two sets of pressure values at the impermeable boundary and in its vicinity due to shock reflection.

V.2 Mathematical model

The mathematical model for one dimensional compressible flow of a viscous conducting medium in Eulerian description with transport can be derived using conservation of mass, balance of momenta, first and second laws of thermodynamics. Conservation of mass, balance of momenta, and the first law of thermodynamics yield continuity equation, momentum equations, and the energy equation whereas the second law of thermodynamics yields entropy inequality which is used to derive constitutive theories for stress tensor and heat vector (see [31]). As well known in case of fluids, in order to derive constitutive theory(ies) for the Cauchy stress tensor (contravariant, see [31]) $\boldsymbol{\sigma}$, the Cauchy stress tensor must be decomposed into equilibrium Cauchy stress tensor ${}_e\boldsymbol{\sigma}$ and the deviatoric Cauchy stress tensor ${}_d\boldsymbol{\sigma}$ (or simply $\boldsymbol{\tau}$). The constitutive theory for ${}_e\boldsymbol{\sigma}$ establishes ${}_e\boldsymbol{\sigma} = -p(\rho,\theta)\boldsymbol{I}$ in which $p(\rho,\theta)$ is thermodynamic pressure (assumed positive when compressive) and the simplest form of the constitutive theory for $\boldsymbol{\tau}$ yields the well known Newton's law of viscosity. The constitutive theories for the heat vector $\boldsymbol{q}$ that are consistent with $\boldsymbol{\tau}$ can be derived in a number of ways (see [31]), however the simplest possible theory can be derived directly using the conditions resulting from the entropy inequality. This results in the well known Fourier heat conduction law. Using Newton's law of viscosity and Fourier heat conduction law as constitutive theories for stress tensor $\boldsymbol{\tau}$ and heat vector $\boldsymbol{q}$, we can derive the following mathematical model for 1D compressible flow of a viscous conducting medium directly from the conservation and balance laws (in the absence of body forces). We use hat (ˆ) on all quantities to indicate that they have their usual dimensions.

$$\frac{\partial\hat{\rho}}{\partial\hat{t}} + \frac{\partial(\hat{\rho}\hat{u})}{\partial\hat{x}} = 0 \tag{V.1}$$

$$\hat{\rho}\frac{\partial\hat{u}}{\partial\hat{t}} + \hat{\rho}\hat{u}\frac{\partial\hat{u}}{\partial\hat{x}} + \frac{\partial\hat{p}}{\partial\hat{x}} - \frac{\partial\hat{\tau}_{xx}}{\partial\hat{x}} = 0 \tag{V.2}$$

$$\hat{\rho}\frac{D\hat{e}}{D\hat{t}} + \frac{\partial\hat{q}_x}{\partial\hat{x}} - \hat{\sigma}_{xx}\frac{\partial\hat{u}}{\partial\hat{x}} = 0 \tag{V.3}$$

$$\hat{\sigma}_{xx} = -\hat{p}(\hat{\rho},\hat{\theta}) + \hat{\tau}_{xx} \tag{V.4}$$

$$\hat{\tau}_{xx} = 2\hat{\mu}\frac{\partial\hat{u}}{\partial\hat{x}} + \hat{\lambda}\frac{\partial\hat{u}}{\partial\hat{x}} = \hat{\mu}^*\frac{\partial\hat{u}}{\partial\hat{x}}; \qquad \hat{\mu}^* = 2\hat{\mu} + \hat{\lambda}; \qquad \hat{\lambda} = -\frac{2}{3}\hat{\mu} \tag{V.5}$$

$$\hat{q}_x = -\hat{k}_x\frac{\partial\hat{\theta}}{\partial\hat{x}} \tag{V.6}$$

The specific internal energy $\hat{e}$ is related to total energy $\hat{E}_t$ and kinetic energy.

$$\hat{E}_t = \hat{\rho}\left(\hat{e} + \frac{(\hat{u})^2}{2}\right) \tag{V.7}$$

We consider simple ideal gas law to define dependence of $\hat{p}$ on density $\hat{\rho}$ and temperature $\hat{\theta}$ and consider $\hat{e}$ to be proportional to $\hat{\theta}$

$$\hat{e} = \hat{c}_v\hat{\theta} \qquad ; \qquad \hat{p} = \hat{\rho}\hat{R}\hat{\theta} \tag{V.8}$$

in which $\hat{R}$ is the gas constant, $\hat{\mu}$ and $\hat{\lambda}$ are first and second viscosities, $\hat{k}_x$ is thermal conductivity, and $\hat{c}_v$ is specific heat. For constant $\hat{c}_v$ we can write

$$\hat{\rho}\frac{D\hat{e}}{D\hat{t}} = \hat{\rho}\hat{c}_v\frac{D\hat{\theta}}{D\hat{t}} = \hat{\rho}\hat{c}_v\left(\frac{\partial\hat{\theta}}{\partial\hat{t}} + \hat{u}\frac{\partial\hat{\theta}}{\partial\hat{x}}\right) \tag{V.9}$$

Substituting from (V.9) and (V.4) into (V.3) we obtain the following for the energy equation

$$\hat{\rho}\hat{c}_v\left(\frac{\partial\hat{\theta}}{\partial\hat{t}} + \hat{u}\frac{\partial\hat{\theta}}{\partial\hat{x}}\right) + \frac{\partial\hat{q}_x}{\partial\hat{x}} + \hat{p}\frac{\partial\hat{u}}{\partial\hat{x}} - \hat{\tau}_{xx}\frac{\partial\hat{u}}{\partial\hat{x}} = 0 \tag{V.10}$$

We can also substitute for $\hat{\tau}_{xx}$ from (V.5) into (V.10)

$$\hat{\rho}\hat{c}_v\left(\frac{\partial\hat{\theta}}{\partial\hat{t}} + \hat{u}\frac{\partial\hat{\theta}}{\partial\hat{x}}\right) + \frac{\partial\hat{q}_x}{\partial\hat{x}} + \hat{p}\frac{\partial\hat{u}}{\partial\hat{x}} - \hat{\mu}^*\left(\frac{\partial\hat{u}}{\partial\hat{x}}\right)^2 = 0 \tag{V.11}$$

The final mathematical model consists of (V.1), (V.2), (V.11), (V.5), (V.6), and $\hat{p}$ in (V.8). We summarize these in the following.

$$\left.\begin{aligned}
&\frac{\partial\hat{\rho}}{\partial\hat{t}}+\frac{\partial(\hat{\rho}\hat{u})}{\partial\hat{x}}=0\\
&\hat{\rho}\frac{\partial\hat{u}}{\partial\hat{t}}+\hat{\rho}\hat{u}\frac{\partial\hat{u}}{\partial\hat{x}}+\frac{\partial\hat{p}}{\partial\hat{x}}-\frac{\partial\hat{\tau}_{xx}}{\partial\hat{x}}=0\\
&\hat{\rho}\hat{c}_v\left(\frac{\partial\hat{\theta}}{\partial\hat{t}}+\hat{u}\frac{\partial\hat{\theta}}{\partial\hat{x}}\right)+\frac{\partial\hat{q}_x}{\partial\hat{x}}+\hat{p}\frac{\partial\hat{u}}{\partial\hat{x}}-\hat{\mu}^*\left(\frac{\partial\hat{u}}{\partial\hat{x}}\right)^2=0\\
&\hat{\tau}_{xx}=\hat{\mu}^*\frac{\partial\hat{u}}{\partial\hat{x}}\\
&\hat{q}_x=-\hat{k}_x\frac{\partial\hat{\theta}}{\partial\hat{x}}\\
&\hat{p}=\hat{\rho}\hat{R}\hat{\theta}
\end{aligned}\right\}\quad \forall(\hat{x},\hat{t})\in\Omega_{\hat{x}\hat{t}}=\Omega_{\hat{x}}\times\Omega_{\hat{t}} \tag{V.12}$$

V.3 Dimensionless form of the mathematical model

Dimensionless form of the mathematical model is helpful and many times necessary when constructing finite element processes for obtaining numerical solutions of the mathematical model.

We define the following dimensionless variables

$$\begin{aligned}
&L=\frac{\hat{L}}{L_0},\ x=\frac{\hat{x}}{L_0},\ u=\frac{\hat{u}}{v_0},\ \rho=\frac{\hat{\rho}}{\rho_0}\\
&\mu=\frac{\hat{\mu}}{\mu_0},\ \lambda=\frac{\hat{\lambda}}{\mu_0},\ \tau_{ij}=\frac{\hat{\tau}_{ij}}{\tau_0},\ p=\frac{\hat{p}}{p_o}\\
&\theta=\frac{\hat{\theta}}{\theta_0},\ k_x=\frac{\hat{k}_x}{k_o},\ c_v=\frac{\hat{c}_v}{c_{v0}},\ t=\frac{\hat{t}}{t_0}
\end{aligned} \tag{V.13}$$

The quantities with hat (ˆ) are with their usual dimensions and the quantities with the subscript zero are the reference values of the corresponding quantities. Using the reference quantities in (V.13), we define the following dimensionless parameters: Reynolds number, Re; Brinkman number, Br; and Eckert number, Ec.

$$Re=\frac{v_0\rho_0L_0}{\mu_0}\qquad,\qquad Br=\frac{\rho_0v_0^2}{k_0\theta_0}\qquad,\qquad Ec=\frac{v_0^2}{c_{v0}\theta_0} \tag{V.14}$$

Using (V.13) and (V.14) we can obtain the following dimensionless form of the mathematical model (V.12).

$$\left.\begin{aligned}
&\frac{\partial\rho}{\partial t}+\frac{\partial(\rho u)}{\partial x}=0\\
&\rho\frac{\partial u}{\partial t}+\rho u\frac{\partial u}{\partial x}+\left(\frac{p_0}{\rho_0v_0^2}\right)\frac{\partial p}{\partial x}-\left(\frac{\tau_0}{\rho_0v_0^2}\right)\frac{\partial\tau_{xx}}{\partial x}=0\\
&\frac{\rho c_v}{Ec}\left(\frac{\partial\theta}{\partial t}+u\frac{\partial\theta}{\partial x}\right)+\frac{1}{ReBr}\frac{\partial q_x}{\partial x}+\left(\frac{p_0}{\rho_0v_0^2}\right)p\frac{\partial u}{\partial x}-\frac{\mu^*}{Re}\left(\frac{\partial u}{\partial x}\right)^2=0\\
&\tau_{xx}=\left(\frac{\mu_0v_0}{L_0\tau_0}\right)\mu^*\frac{\partial u}{\partial x}\\
&q_x=-k_x\frac{\partial\theta}{\partial x}\\
&p=\rho R\theta
\end{aligned}\right\}\quad \forall(x,t)\in\Omega_{xt}=\Omega_x\times\Omega_t \tag{V.15}$$

If we choose

$$\tau_0 = p_0 = \rho_0 v_0^2 = \tau_{cke} \quad ; \quad \text{Characteristic kinetic energy} \tag{V.16}$$

then

$$\frac{\tau_0}{\rho_0 v_0^2} = 1 \quad and \quad \frac{\mu_0 v_0}{L_0 \tau_0} = \frac{1}{Re} \tag{V.17}$$

If we choose

$$\tau_0 = p_0 = \frac{\mu_0 v_0}{L_0} = \tau_{cvs} \quad ; \quad \text{Characteristic viscous stress} \tag{V.18}$$

then

$$\frac{\mu_0 v_0}{L_0 \tau_0} = 1 \quad and \quad \frac{p_0}{\rho_0 v_0^2} = \frac{\tau_0}{\rho_0 v_0^2} = \frac{1}{Re} \tag{V.19}$$

And

$$R = \frac{\hat{R}}{R_0} \quad ; \quad R_0 = \frac{p_0}{\rho_0 \theta_0} \tag{V.20}$$

Generally we use the greater of τ_{cke} and τ_{cvs} for p_0 and τ_0. In the present work $\tau_{cke} >> \tau_{cvs}$, hence we use (V.16) to nondimensionalize $\hat{p}$ and $\hat{\tau}_{xx}$. We note that

$$p = p(\rho, R, \theta) \tag{V.21}$$

hence

$$\frac{\partial p}{\partial x} = \left(\frac{\partial p}{\partial \rho}\right)\left(\frac{\partial \rho}{\partial x}\right) + \left(\frac{\partial p}{\partial \theta}\right)\left(\frac{\partial \theta}{\partial x}\right) \tag{V.22}$$

in which $\frac{\partial p}{\partial \rho}$ and $\frac{\partial p}{\partial \theta}$ are deterministic using (V.21) (ideal gas law as in (V.15) or real gas laws if needed). Thus, $\frac{\partial p}{\partial x}$ is (V.22) in the momentum equation in (V.15) and p in the energy equation can be replaced by (V.21), thereby eliminating p from the mathematical model. Thus, finally we have

$$\left.\begin{aligned}
&\frac{\partial \rho}{\partial t} + \frac{\partial (\rho u)}{\partial x} = 0 \\
&\rho \frac{\partial u}{\partial t} + \rho u \frac{\partial u}{\partial x} + \left(\frac{p_0}{\rho_0 v_0^2}\right)\left(\frac{\partial p}{\partial \rho}\frac{\partial \rho}{\partial x} + \frac{\partial p}{\partial \theta}\frac{\partial \theta}{\partial x}\right) - \left(\frac{\tau_0}{\rho_0 v_0^2}\right)\frac{\partial \tau_{xx}}{\partial x} = 0 \\
&\frac{\rho c_v}{Ec}\left(\frac{\partial \theta}{\partial t} + u\frac{\partial \theta}{\partial x}\right) + \frac{1}{ReBr}\frac{\partial q_x}{\partial x} + \left(\frac{p_0}{\rho_0 v_0^2}\right) p(\rho, R, \theta)\frac{\partial u}{\partial x} - \frac{\mu^*}{Re}\left(\frac{\partial u}{\partial x}\right)^2 = 0 \\
&\tau_{xx} = \left(\frac{\mu_0 v_0}{L_0 \tau_0}\right)\mu^* \frac{\partial u}{\partial x} \\
&q_x = -k_x \frac{\partial \theta}{\partial x}
\end{aligned}\right\} \forall (x,t) \in \Omega_{xt} = \Omega_x \times \Omega_t \tag{V.23}$$

where

$$\mu^* = 2\mu + \lambda \quad ; \quad \lambda = -\frac{2}{3}\mu \tag{V.24}$$

(V.23) is a system of five nonlinear time dependent partial differential equations in five dependent variables (ρ, u, θ, τ_{xx} and q_x), hence constitute initial value problem (IVP) describing evolution, propagation, reflection, and interactions of 1D normal shocks.

Generally the constitutive equations for τ_{xx} and q_x are called auxiliary equations and τ_{xx} and q_x are called auxiliary variables. This mathematical model only contains first order derivatives of ρ, u, θ, τ_{xx}, and q_x.

We note that τ_{xx} and q_x can be substituted in the momentum and energy equations and thereby the constitutive equations for τ_{xx} and q_x as dependent variables can be eliminated from the mathematical model and we obtain the following mathematical model from (V.23) in dependent variables ρ, u, and θ (assuming constant μ^* and k).

$$\left.\begin{aligned}
&\frac{\partial \rho}{\partial t}+\frac{\partial(\rho u)}{\partial x}=0\\
&\rho\frac{\partial u}{\partial t}+\rho u\frac{\partial u}{\partial x}+\left(\frac{p_0}{\rho_0 v_0^2}\right)\left(\frac{\partial p}{\partial \rho}\frac{\partial \rho}{\partial x}+\frac{\partial p}{\partial \theta}\frac{\partial \theta}{\partial x}\right)-\frac{\mu^*}{Re}\left(\frac{\partial^2 u}{\partial x^2}\right)=0\\
&\frac{\rho c_v}{Ec}\left(\frac{\partial \theta}{\partial t}+u\frac{\partial \theta}{\partial x}\right)-\frac{k_x}{ReBr}\frac{\partial^2\theta}{\partial x^2}\\
&\qquad\qquad+\left(\frac{p_0}{\rho_0 v_0^2}\right)p(\rho,R,\theta)\frac{\partial u}{\partial x}-\frac{\mu^*}{Re}\left(\frac{\partial u}{\partial x}\right)^2=0
\end{aligned}\right\}\ \forall (x,t)\in\Omega_{xt}=\Omega_x\times\Omega_t \tag{V.25}$$

We note that in (V.25) we have up to second order spatial derivatives of u and θ as opposed to only first order spatial derivatives of u and θ as in the mathematical model (V.23). Both mathematical models are suitable for numerical computations using finite element processes. Differences in the two processes for calculating numerical solutions obviously occur due to the second order spatial derivatives of u and θ in (V.25) and first order in (V.23). We discuss these in the following.

V.4 Space-time finite element processes: computation of evolution

The mathematical models (V.23) or (V.25) describe evolution, hence are initial value problems. Their numerical solutions can be calculated using either space-time coupled methods or space-time decoupled methods. In the present work we consider space-time coupled finite element processes. Details and benefits of using this approach can be found in [44, 81]. In this work we only present a brief summary. The choice of using (V.23) or (V.25) dictates the admissible choices for space-time approximations for a space-time element.

If we choose (V.23), then the local approximations of class C^1 in space and time ensure that all space-time integrals over the space-time discretization are Riemann. When the solutions are sufficiently smooth as in this case, the Lebesgue space-time integrals suffice. Thus when using (V.23) we could use space-time local approximations for all dependent variables of class C^0 in space and time. If we choose mathematical model (V.25), then the space-time local approximations for ρ can be of class C^1 in space and time but for u and θ we need C^2 in space and C^1 in time if the space-time integrals are to be Riemann. For the space-time integrals to be in Lebesgue sense the space-time local approximations of class C^0 for ρ in space and time and of classes C^1 and C^0 in space and time for u and θ are admissible. See [41–43] for more details.

Since (V.23) and (V.25) are nonlinear partial differential equations in space and time, the works presented by [41–44, 81] show that a space-time integral form based on space-time residual functional yields positive-definite coefficient matrix in the resulting algebraic system provided: (i) The second variations of the residuals are neglected in the second variation of the residual functional and (ii) the nonlinear conditions resulting from the first variation of the residual functional are satisfied using Newton's linear method (Newton-Raphson method). The space-time domain $\bar{\Omega}_{xt}$ is subdivided into space-time strips or slabs (figure 115(a) and (b)) corresponding to the time increments $\Delta t_i,\ i=1,2,...$ which can be uniform or non-uniform. We consider a typical space-time strip ${}^n\bar{\Omega}_{xt}$ corresponding to n^{th} time increment ($t_{n-1}\le t\le t_n$) and its discretization ${}^n\bar{\Omega}^T_{xt}$ using p-version nine-node space-time elements (figure 115(c)).

$${}^n\bar{\Omega}^T_{xt}=\bigcup_e {}^n\bar{\Omega}^e_{xt} \tag{V.26}$$

in which ${}^n\bar{\Omega}^e_{xt}$ is the space-time domain of a typical space-time element 'e' for n^{th} space-time strip. Consider the mathematical model (V.25) used in the present work and let

$$\{\phi\}=[\rho,u,\theta]^T \tag{V.27}$$

where ϕ is a list of dependent variables. Let ${}^n\{\phi\}^e_h$ be approximation of $\{\phi\}$ over ${}^n\bar{\Omega}^e_{xt}$

$${}^n\{\phi\}^e_h=[{}^n\rho^e_h,\ {}^nu^e_h,\ {}^n\theta^e_h]^T \tag{V.28}$$

In general for local approximations ${}^n\rho_h^e, {}^nu_h^e, {}^n\theta_h^e$, we can write the following.

$$\begin{aligned} {}^n\rho_h^e &= [N_\rho^{(k_1-1,k_2-1),(p_1,p_2)}]\{{}^n\rho^e\} \\ {}^nu_h^e &= [N_u^{(k_1-1,k_2-1),(p_1,p_2)}]\{{}^nu^e\} \\ {}^n\theta_h^e &= [N_\theta^{(k_1-1,k_2-1),(p_1,p_2)}]\{{}^n\theta^e\} \end{aligned} \tag{V.29}$$

in which $\{{}^n\rho^e\}$, $\{{}^nu^e\}$, and $\{{}^n\theta^e\}$ are nodal degrees of freedom for ${}^n\rho_h^e$, ${}^nu_h^e$, and ${}^n\theta_h^e$. By substituting (V.29) in (V.25) we obtain residual equations ${}^nE_i^e$, $i = 1, 2, 3\ \forall (x,t) \in {}^n\bar{\Omega}_{xt}^e$. We note that equal order, equal degree interpolations are admissible. We can write (V.29) in compact form

$${}^n\{\phi\}_h^e = [N_\phi^{(k_1-1,k_2-1),(p_1,p_2)}]\{{}^n\delta^e\} \tag{V.30}$$

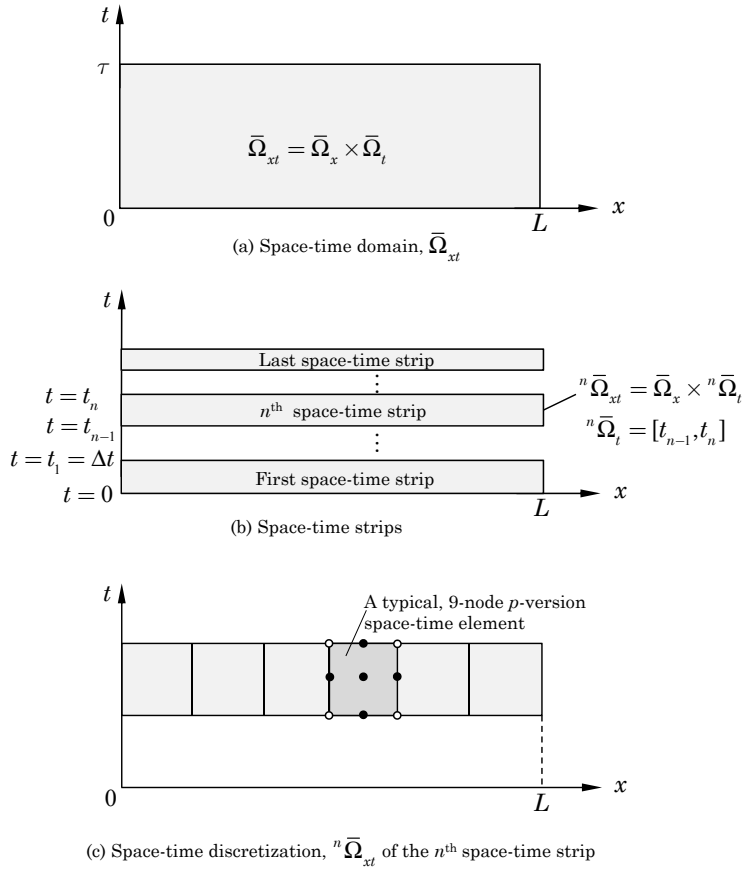

Figure 115: Space-time domain, space-time strips, and discretization for n^{th} space-time strip.

$[N_\phi^{(k_1-1,k_2-1),(p_1,p_2)}]$ are local approximation functions for ρ, u, and θ and $\{{}^n\delta^e\}$ are total degrees of freedom for all dependent variables. (k_1-1), (k_2-1) are orders of continuity in space and time and p_1, p_2 are corresponding p-levels. In general, k_1, k_2, p_1, p_2 can be different for each dependent variable if we so desire. Let $V_h({}^n\bar{\Omega}_{xt}^e)$ be the approximation space, then

$$V_h({}^n\bar{\Omega}_{xt}^e) \subset H^{k,p}({}^n\bar{\Omega}_{xt}^e) \quad ; \quad k = (k_1, k_2) \quad \forall \quad {}^n\bar{\Omega}_{xt}^e \subset {}^n\bar{\Omega}_{xt}^T \tag{V.31}$$

$$H^{(k_1,k_2),(p1_p2)}({}^n\bar{\Omega}^e_{xt}) = \{w : w\big|_{{}^n\bar{\Omega}^e_{xt}} \in C^{(k_1,k_2),(p1_p2)}({}^n\bar{\Omega}^e_{xt}),$$
$$w : w\big|_{{}^n\bar{\Omega}^e_{xt}} \in P^{p_1,p_2}({}^n\bar{\Omega}^e_{xt}); \tag{V.32}$$
$$p_1 \geq 2k_1 - 1,\ p_2 = 2k_2 - 1 \quad \forall \quad {}^n\bar{\Omega}^e_{xt} \subset {}^n\bar{\Omega}^T_{xt}\}$$

We note that for $k_1 = 2$, $k_2 = 2$ the space-time integrals over ${}^n\bar{\Omega}^T_{xt}$ are Lebesgue. When $k_1 = k_2 > 2$, the local approximations over ${}^n\bar{\Omega}^e_{xt}$ yield space-time integrals over ${}^n\bar{\Omega}^T_{xt}$ in Riemann sense. Due to smoothness of the evolutions we choose $k_1 = 2$ and $k_2 = 2$ i.e. local space-time approximations for all variables of class C^1 in space and time.

We construct space-time residual functional $I({}^n\phi_h)$ for the discretization ${}^n\bar{\Omega}^T_{xt}$ for n^{th} space-time strip containing M space-time elements using element residuals ${}^nE^e_i$; $i = 1, 2, 3$ obtained by substituting local approximations (V.29) into (V.25).

$$I({}^n\phi_h) = \sum_{e=1}^{M} I^e({}^n\phi^e_h) = \sum_{e=1}^{M}\sum_{i=1}^{3}\big({}^nE^e_i({}^n\phi^e_h), {}^nE^e_i({}^n\phi^e_h)\big) \tag{V.33}$$

First variation of $I({}^n\phi_h)$ set to zero gives necessary conditions provided $I(\bullet)$ is differentiable in its arguments.

$$\delta I({}^n\phi_h) = \sum_{e=1}^{M}\sum_{i=1}^{3}\big({}^nE^e_i, \delta({}^nE^e_i)\big) = \sum_{e=1}^{M} {}^ng^e({}^n\phi^e_h) = g({}^n\phi_h) = 0 \tag{V.34}$$

Sufficient condition or extremum principle is given by (see [43, 79, 81, 102])

$$\delta^2 I({}^n\phi_h) \cong \sum_{e=1}^{M}\sum_{i=1}^{3}\big(\delta({}^nE^e_i), \delta({}^nE^e_i)\big) > 0 \tag{V.35}$$

Let $({}^n\phi_h)_0$ be an assumed solution then improved solution ${}^n\phi_h$ is obtained using Newton's linear method with line search.

$${}^n\phi_h = ({}^n\phi_h)_0 + \alpha\Delta({}^n\phi_h) \tag{V.36}$$

$$\Delta({}^n\phi_h) = -\big[\delta^2 I({}^n\phi_h)\big]^{-1}_{({}^n\phi_h)_0} g\big(({}^n\phi_h)_0\big) \tag{V.37}$$

where α is determined such that $I({}^n\phi_h) \leq I\big(({}^n\phi_h)_0\big)$. Convergence of the iterative solution method is checked using $|g_i({}^n\phi_h)| \leq \Delta_1$, $i = 1, 2, ...$ in which Δ_1 is a preset tolerance for computed zero (generally 10^{-6} or lower).

Numerical computation of the evolution is commenced for the first space-time strip corresponding to the time increment Δt using BCs and ICs and then time marched by using the computed solution at $t = \Delta t$ as initial condition for the second space-time strip, thus obtaining solution for $\Delta t \leq t \leq 2\Delta t$. This procedure of time marching is continued until the desired time is reached.

V.5 Experimental setup and measurements

Experimental work on 1D Riemann shock tube has been reported by [168]. These experiments were conducted by Prof. KPJ Reddy's research group at Indian Institute of Science, Bangalore, India. Figure 116 shows a photograph of the Reddy tube (and schematic) that consists of a 29 mm diameter stainless steel shock tube divided into 490 mm long high pressure (driver) and 510 mm low pressure (driven) sides separated by a 0.1 mm thick aluminum or mylar diaphragm. The low pressure side is maintained at 0.88 bar and the pressure on the high pressure side is varied. The pressure measurements are conducted at two locations A and B. Pressure sensor at location A measures the fully developed shock pressure behind the fully developed shock wave. The pressure sensor at location B is used to measure the pressure behind the reflected shock wave (highest measured value listed in table 2). The measured values of pressures at location A and B for air reported by [168] are given in Table 2. The values of $\hat{p}_l$ and $\hat{p}_h$ corresponding to '*' are used in numerical simulations.

Using the experimental measurements in table 2 we chose three typical $\hat{p}_h$ values (high, medium, and low): 7.58, 5.38, 3.18 and $\hat{p}_l$ of 0.88 (for all three values of $\hat{p}_h$) for numerical simulations of the shock tube experiments. If these pressure values are nondimensionalized using reference pressure p_0, then we have $7.58/0.88$, $5.38/0.88$, and $3.28/0.88$ as pressure ratios of p_h/p_l (dimensionless). In the numerical studies we use these pressure ratios in the dimensionless form of the mathematical model for the Riemann shock tube.

Table 2: Measured pressure values (in bar)

	$\hat{p}_l$	$\hat{p}_h$	$\hat{p}_A$	$\hat{p}_B$	
	0.88	4.28	1.74	2.82	
*	0.88	7.58	2.31	4.0	
	0.88	7.18	2.35	4.18	
*	0.88	5.38	2.35	3.97	
	0.88	4.88	1.64	2.83	
	0.88	7.28	2.34	4.03	
*	0.88	3.18	1.72	3.23	
	0.88	3.38	1.76	3.48	
	0.88	3.48	1.81	3.64	

V.6 Considerations in the numerical simulation of shock evolution and comparisons with experimental results

As discussed earlier, shock width is generally of the same order of magnitude as the viscosity. Thus, in air, shock widths are $O(10^{-6})$. Resolution of the evolution of such a phenomenon obviously will require spatial discretization with element lengths of the order of $O(10^{-6})$. With such a refined discretization required for shock resolution, numerical simulation of 1D normal shocks in Riemann shock tube 1000 mm long as used in the experiment is virtually impossible using a fixed discretization. This may require millions of elements and the same number of time increments.

However, the pressure information at locations A and B related to fully developed propagating shock and the reflected shock can be generated numerically without modeling the entire shock tube of 1000 mm. Consider a shock tube of length $(L_h + L_l)$, L_h and L_l being the high pressure and low pressure side dimensionless lengths (figure 117(a)). We choose $L_h + L_l = 2$ and begin with $L_h = L_l = 1$. Upon rupture of the diaphragm at $t = 0$ the compression waves are initiated to the left of the diaphragm which pile up during evolution due to higher density behind the wave and hence higher wave speed and eventually form a fully developed shock at location $a - a$, a very small distance to the left of the diaphragm. We note that both the time and the distance from the diaphragm of location $a - a$ are extremely small and are same in the experiment and the simulations. The shock formation is rather quick and is in the proximity of the diaphragm. The fully developed shock propagates toward the left impermeable boundary. The pressure value at $a - a$ or other locations to the left of it during shock propagation but before the shock reaches the impermeable boundary can be compared to p_A (same as $\hat{p}_A$ in table 2) as both are pressures corresponding to fully developed shock. Upon reaching the impermeable boundary to the left, the shock wave with same shock relations in the experiment and in the simulation reflects. This results in higher pressure at the boundary and to the right of the boundary compared to the shock relation pressure corresponding to the incident fully developed shock. Thus, the larger pressure reading at location B (in the vicinity of the impermeable boundary) in the experiment corresponds to the pressure value at location $b - b$ in the numerical simulation after the shock reflection. Thus we see that numerical simulation for a shock tube of dimensionless length two units that correspond to approximately 3.127×10^{-6} m is sufficient to simulate the shock physics in the experiment.

V.7 Definition of a shock

We define a sustained wave that does not disperse or diffuse anymore during further evolution as a shock. In case of Riemann shock tube upon rupture of the diaphragm, compression waves with progressively increased speed pile up in the low density region. These processes result in steepening of the front or traveling wave. On the other hand, the mechanism of dispersion comes into play due to viscosity of the medium which results in elongation of the base of the wave or the front. If the steepening process is stronger than the base elongation process, then the wave begins to steepen as evolution proceeds and eventually we reach a time during evolution when both processes equilibrate. At this time we have a wave or a front that would neither steepen nor disperse during further evolution. We refer to this wave or front as 'shock'. This process can be quantified by examining the increase in entropy per unit volume for each space-time strip. The basic mechanism of entropy production in shocks is due to conversion of mechanical energy into heat due to viscous dissipation. Thus if S_r is the dimensionless rate of entropy production per unit volume then

$$S_r = \frac{1}{\theta}\left(\frac{\varphi}{Re} + \frac{1}{ReBr}\frac{k}{\theta}\left(\frac{\partial\theta}{\partial x}\right)^2\right) \tag{V.38}$$

where

$$\varphi = \big(2\mu + \lambda\big)\left(\frac{\partial u}{\partial x}\right)^2 \tag{V.39}$$

We note from the definition of a shock that S_r must be constant for a fully developed shock to exist during further evolution. S_r provides a thermodynamic map that quantitatively establishes when shocks are formed for the first time as well as their existence upon further evolution. Secondly, most numerical processes suffer from numerical dispersion in which case the presence of shock may be possible to establish but the shock structure would be in error. [44] have shown that the LSP and STLSP can be completely free of numerical dispersion with proper choices of h, p, and k. In the present work this aspect is critical in ensuring that shock structure and the S_r behavior reported have physical and true behavior based on the mathematical model.

V.8 Computations of 1D Normal Shocks Using Space-Time Finite Element Method

We consider a Riemann shock tube of two units (dimensionless) in length, as shown in Figure 117(a). The medium is air with the following properties at NTP:

$$\hat{\mu} = 1.983 \times 10^{-5} \text{ Pa-s}, \quad \hat{\rho} = 1.225412 \text{ kg/m}^3, \quad \hat{k} = 2.8854 \times 10^{-2} \text{ W/m-K}, \quad \hat{c}_v = 717.0 \text{ J/kg-K}$$

The following reference values are chosen:

$$L_0 = 1.50348 \times 10^{-6} \text{ m}, \quad \mu_0 = \hat{\mu}, \quad \rho_0 = \hat{\rho}, \quad k_0 = \hat{k}, \quad c_{v0} = \hat{c}_v, \quad \theta_0 = 410.52 \text{ K}$$
$$v_0 = 343.0 \text{ m/s}, \quad t_0 = L_0/v_0 = 4.4996 \times 10^{-9} \text{ s}, \quad p_0 = \tau_0 = \rho_0 v_0^2 = 1.4438 \times 10^5 \text{ Pa}$$

With these reference values, various characteristic numbers have the values

$$Re = \frac{\rho_0 v_0 t_0}{\mu_0} = 31.891, \quad Ec = \frac{v_0^2}{R_0\theta_0} = 0.40027$$
$$Br = \frac{\mu_0 v_0^2}{k_0\theta_0} = 0.19721, \quad Pr = \frac{c_{v0}\mu_0}{k_0} = 0.49276$$

We use the time interval $\Delta t = 0.02$ (a nondimensional value), which gives a dimensional time increment of $\Delta\hat{t} = 8.9592 \times 10^{-11}$ s. In this study, the following three pressure ratios are considered:

$$\frac{p_h}{p_l} = \frac{7.58}{0.88}, \quad \frac{5.38}{0.88}, \quad \text{and } \frac{3.18}{0.88}$$

The influence of the various values of lengths L_l and L_h on the evolution is also investigated. Between three pressure ratios and the various choices of L_l and L_h, we choose the following combinations:

(a) For $(p_h, p_l) = (7.58, 0.88)$ we choose
$(L_l, L_h) = (1.0, 1.0), (1.25, 0.75), (1.5, 0.5), (1.7, 0.3), (1.8, 0.2), (1.9, 0.1)$

(b) For $(L_l, L_h) = (1.0, 1.0)$ we consider
$(p_h, p_l) = (7.58, 0.88), (5.38, 0.88), (3.18, 0.88)$

Figure 117(b) shows boundary conditions at the two ends of the shock tube and the initial conditions at time $t = 0$ for the first space-time strip. Isothermal ICs are used at $t = 0$ ($\theta = 1.0$). The initial conditions for the second space-time strip ($[\Delta t, 2\Delta t]$) at $t = \Delta t$ are obtained from the computed evolution for the first space-time strip at Δt. The space-time domain $2 \times \Delta t$ is divided into a uniform discretization of 101 nine-node p-version space-time finite elements. The pressure ratio (same as density ratios as $p = \rho R\theta$ with $R = 1$, $\theta = 1$, hence $p = \rho$ at $t = 0$, ICs) or density ratio ρ_h/ρ_l is specified over an element centered at $x = 0$ in a continuous and differentiable manner from ρ_h to ρ_l. Numerical solutions are of class C^1 in space and time with equal p-level of 11 in space and time, thus local approximations for all dependent variables are in a scalar product subspace $H^{(2,2),(11,11)}({}^n\bar{\Omega}^e_{xt})$ and $\Delta t = 0.02$ is considered. With this choice of discretization, orders of the space, and p-levels in space and time, the integrated sum of squares of the residuals remain $O(10^{-6})$ or lower for the entire evolution for all numerical studies, confirming that the governing differential equations in the mathematical model are satisfied quite well. Newton's linear method in most cases converges in less than 5 iterations with $|g_i| \leq O(10^{-6})$ or lower.

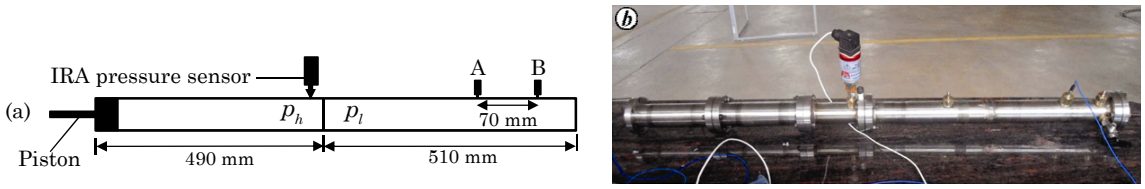

Figure 116: (a) Schematic diagram of the 29 mm internal diameter Reddy tube with pressure sensors located in the driven and driver sections. (b) Photograph of fully assembled Reddy tube with pressure gauges mounted for measuring the shock wave parameters and diaphragm rupture pressure.

V.8.1 1D normal shock for $(p_h, p_l) = (7.58, 0.88)$ with $(L_l, L_h) = (1.0, 1.0), (1.25, 0.75), (1.5, 0.5), (1.7, 0.3), (1.8, 0.2)$ and $(1.9, 0.1)$

Figures 118(a)-(f) show evolution of rate of entropy production S_r along the length of the shock tube for $0 \leq t \leq 150\Delta t$. For each ratio of L_l/L_h except $1.9/0.1$ we observe steady and nondiffusive S_r (constant width of S_r zone) during the entire evolution. The path of the shock (i.e. S_r) from the location of the diaphragm toward the left impermeable boundary is always straight as there is only constant low density air ahead of it in its path with the same value as in shock relations. The path of the reflected shock is not straight as it travels through the compressed medium and eventually reflects from the impermeable boundary on the right side of the diaphragm. These evolutions of S_r confirm that for each ratio of L_l/L_h (except $L_l/L_h = 1.9/0.1$) a shock is formed in the low density region that propagates, reflects, and interacts upon further evolution. For $L_l/L_h = 1.9/0.1$ lack of constant S_r indicates lack of steady propagating shock. These findings can be confirmed by examining evolution of pressure along the length of the shock tube.

Figures 119(a)-(f) show pressure evolution along the length of the shock tube for $\Delta t \leq t \leq 60\Delta t$ for all length ratios. Figures 119(a)-(e) show constant steady pressure wave propagation to the left of the diaphragm with pressure values of 0.88 and 2.36 ahead and behind the shock wave, confirming a steady shock for $1 \leq L_h \leq 0.2$. For L_h=0.1 we clearly observe lack of formation of a steady pressure wave, confirming lack of a steady shock wave as indicated by S_r evolution in figure 118(f). This is obviously due to inadequate length L_h that results in insufficient volume of high pressure air in the length L_h to form and sustain a shock.

Figures 119(a)-(f) also show reflection of the shock waves from the left impermeable boundary for $t \leq 60\Delta t$. Evolutions of pressure for $65\Delta t \leq t \leq 120\Delta t$ and $125\Delta t \leq t \leq 150\Delta t$ for all length ratios are shown in Figures 120(a)-(f) and 121(a)-(f). We observe the following:

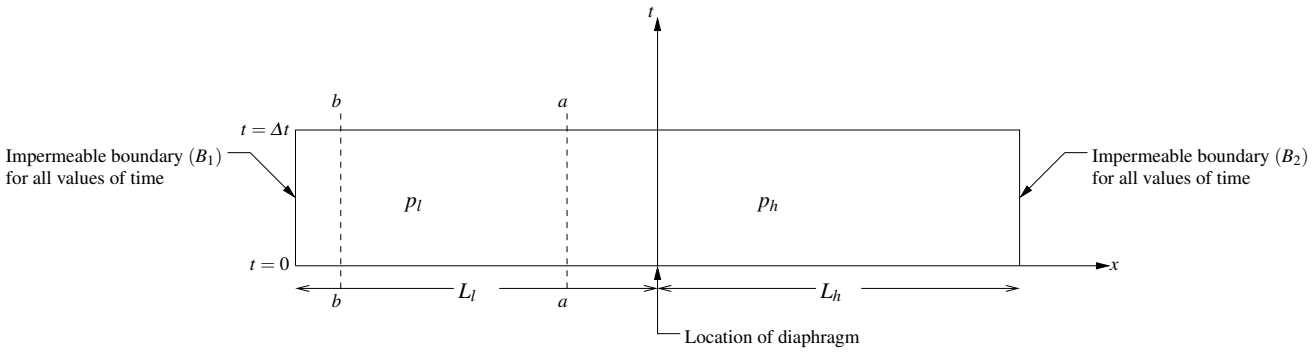

(a) Shock tube schematic for first increment of time for numerical simulation

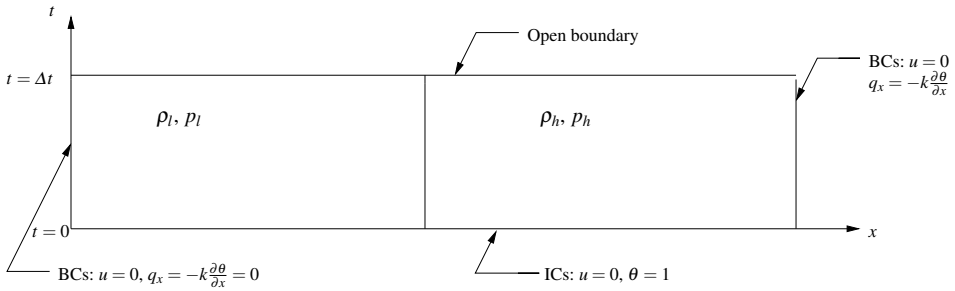

(b) Boundary conditions and initial conditions for the first space-time strip

Figure 117: Shock tube schematic, initial conditions, and boundary conditions

(i) The pressure of the left boundary continues to increase due to reflection of the shock wave for each length ratio until it reaches a maximum value and then begins to decrease upon further evolution.

(ii) The maximum pressure value at the left boundary upon shock reflection has the highest value for $(L_l, L_h) = (1, 1)$. This maximum value decreases with progressively reducing L_h. For $L_h = 1$, the length of the high pressure zone is the largest out of all values considered in the numerical studies, hence the reason for such behavior.

(iii) Progressively reducing length L_h of the high pressure zone has pronounced influence on the evolution of pressure for $t > 60\Delta t$.

(iv) Evolution of u and θ are not shown for the sake of brevity.

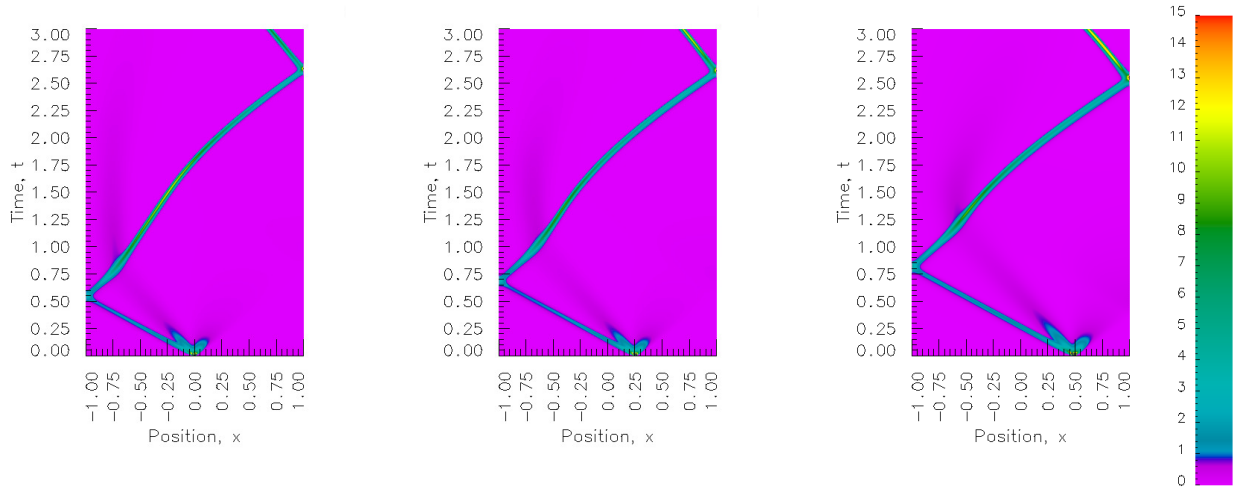

(a) Evolution of $S_r, (L_l, L_h) = (1.0, 1.0)$ (b) Evolution of $S_r, (L_l, L_h) = (1.25, 0.75)$ (c) Evolution of $S_r, (L_l, L_h) = (1.5, 0.5)$

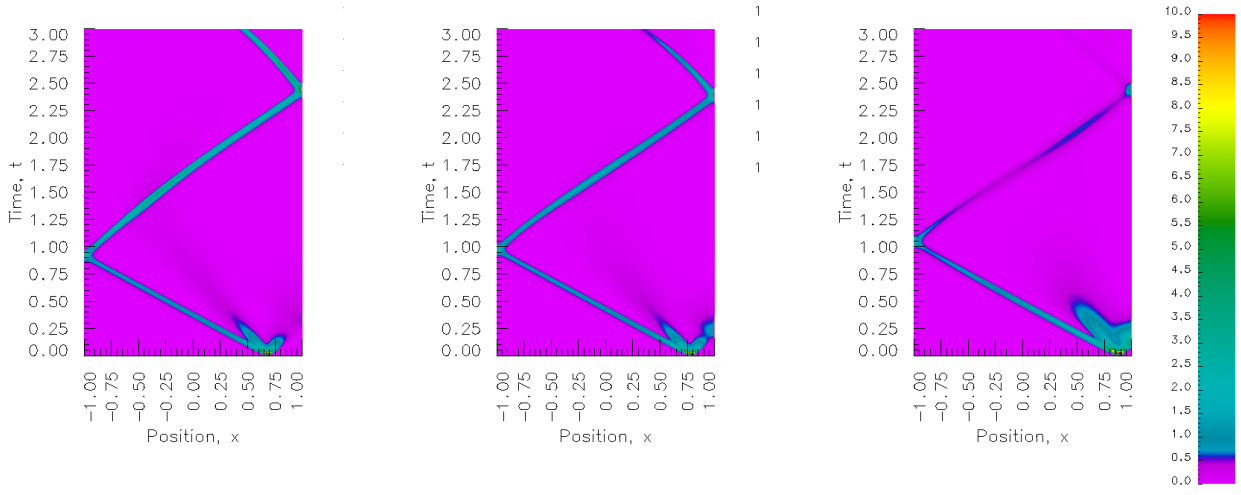

(d) Evolution of $S_r, (L_l, L_h) = (1.7, 0.3)$ (e) Evolution of $S_r, (L_l, L_h) = (1.8, 0.2)$ (f) Evolution of $S_r, (L_l, L_h) = (1.9, 0.1)$

Figure 118: Evolution of rate of entropy production for different values of L_l and L_h with $p_h = 7.58$ and $p_l = 0.88$

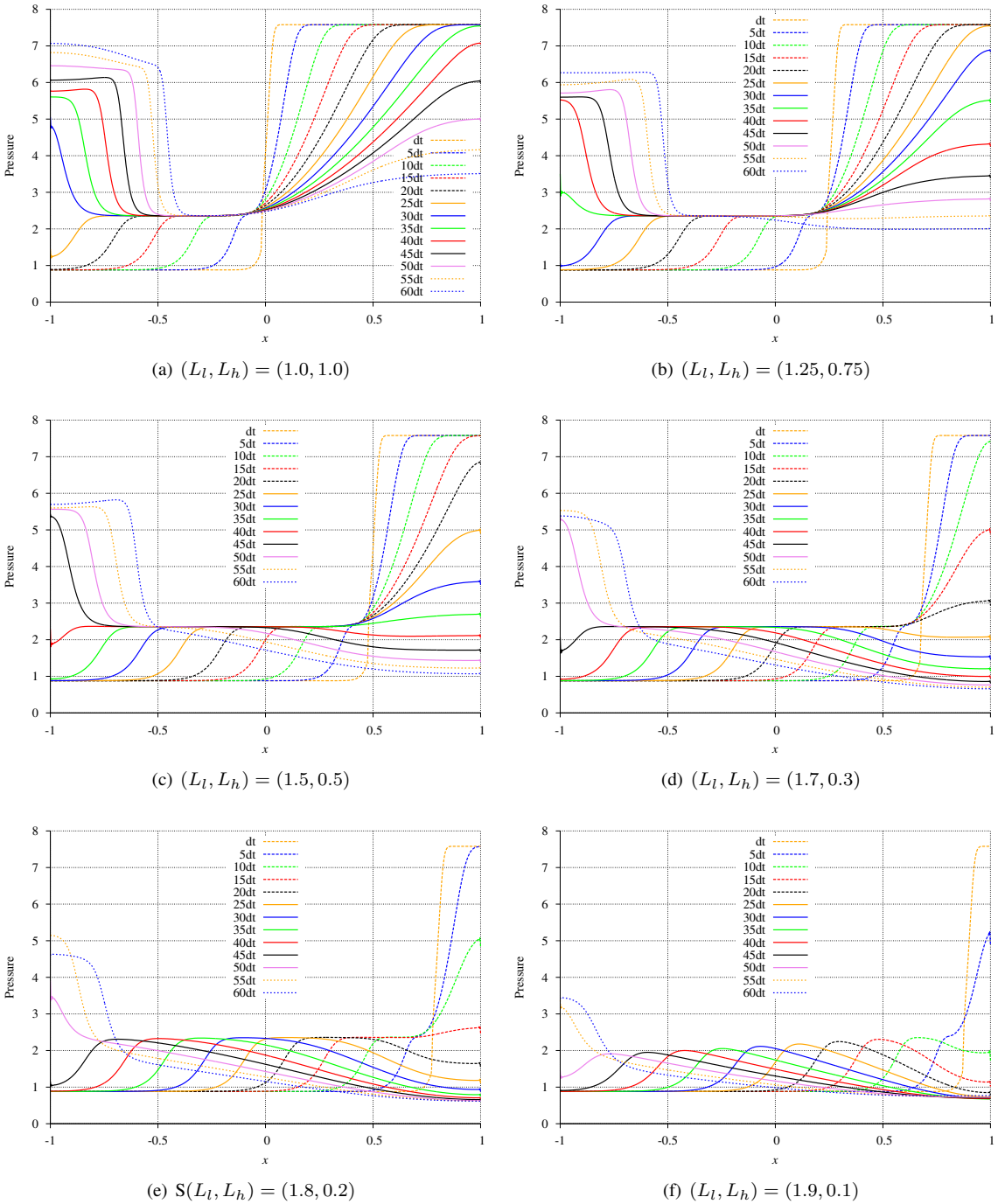

(a) $(L_l, L_h) = (1.0, 1.0)$

(b) $(L_l, L_h) = (1.25, 0.75)$

(c) $(L_l, L_h) = (1.5, 0.5)$

(d) $(L_l, L_h) = (1.7, 0.3)$

(e) $\mathrm{S}(L_l, L_h) = (1.8, 0.2)$

(f) $(L_l, L_h) = (1.9, 0.1)$

Figure 119: Evolution of pressure for different values of L_l and L_h; $\Delta t \leq t \leq 60\Delta t$

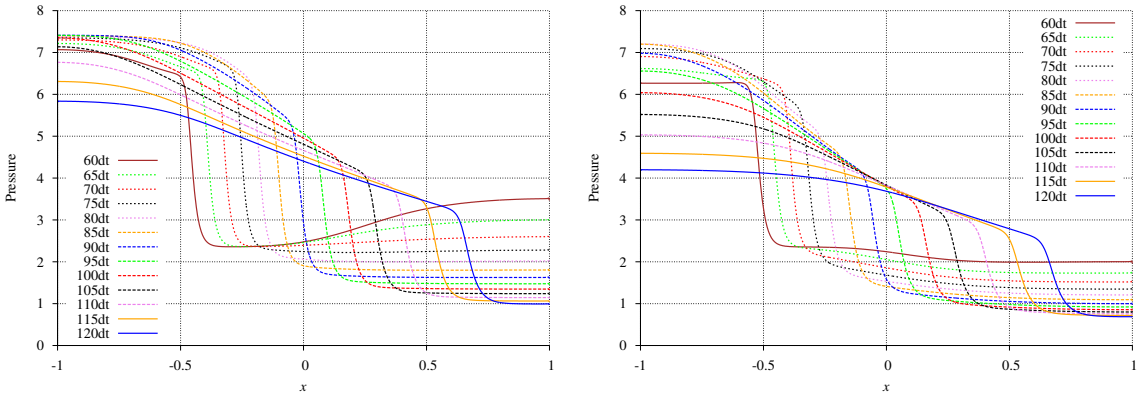

(a) $(L_l, L_h) = (1.0, 1.0)$ (b) $(L_l, L_h) = (1.25, 0.75)$

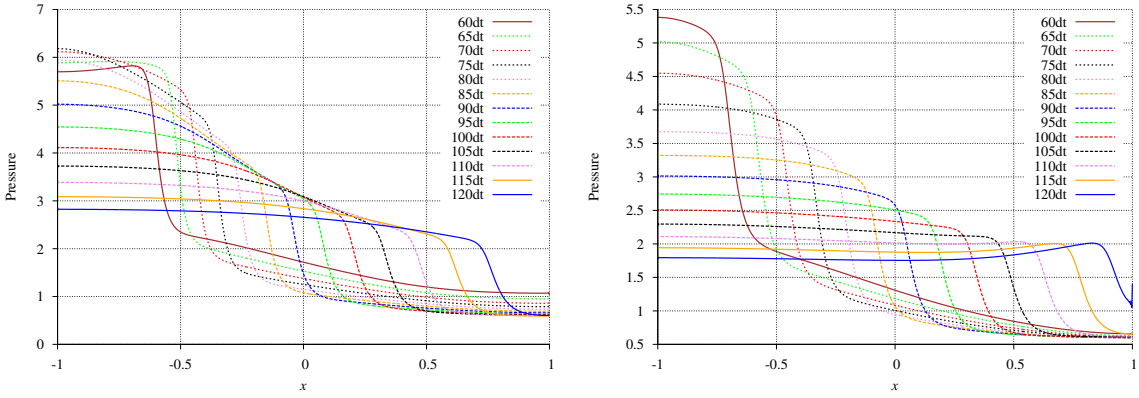

(c) $(L_l, L_h) = (1.5, 0.5)$ (d) $(L_l, L_h) = (1.7, 0.3)$

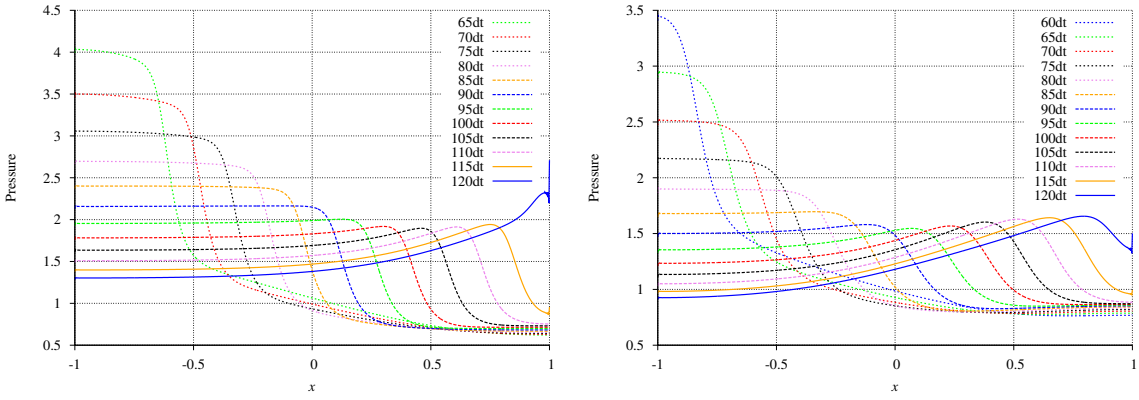

(e) S$(L_l, L_h) = (1.8, 0.2)$ (f) $(L_l, L_h) = (1.9, 0.1)$

Figure 120: Evolution of pressure for different values of L_l and L_h; $60\Delta t \leq t \leq 120\Delta t$

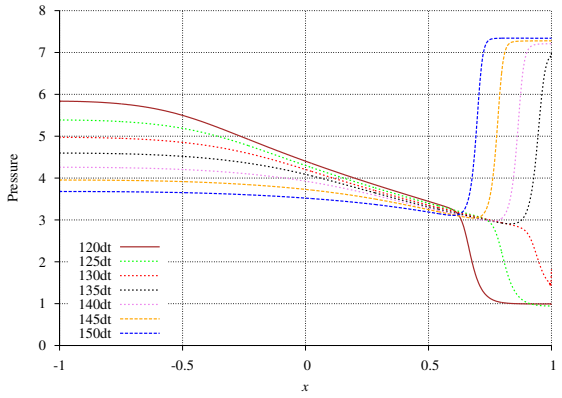

(a) $(L_l, L_h) = (1.0, 1.0)$

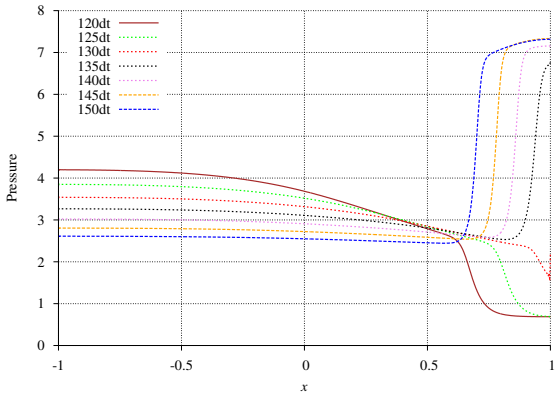

(b) $(L_l, L_h) = (1.25, 0.75)$

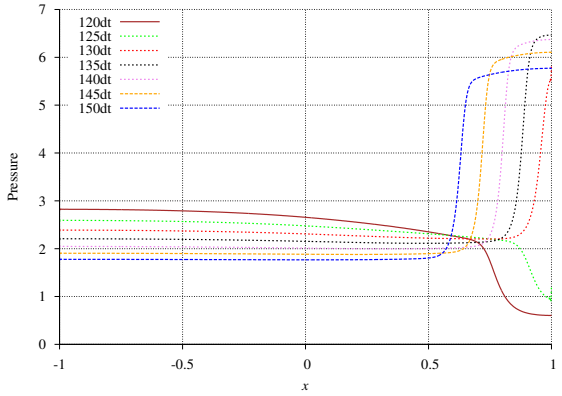

(c) $(L_l, L_h) = (1.5, 0.5)$

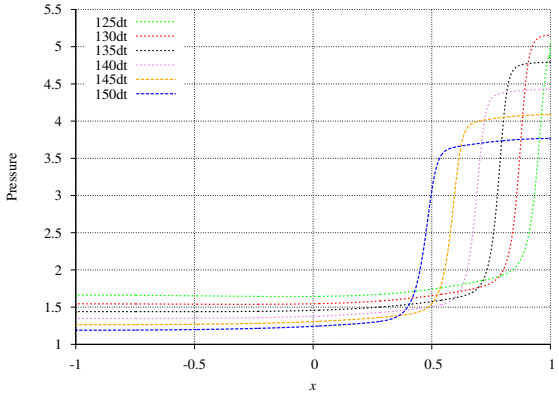

(d) $(L_l, L_h) = (1.7, 0.3)$

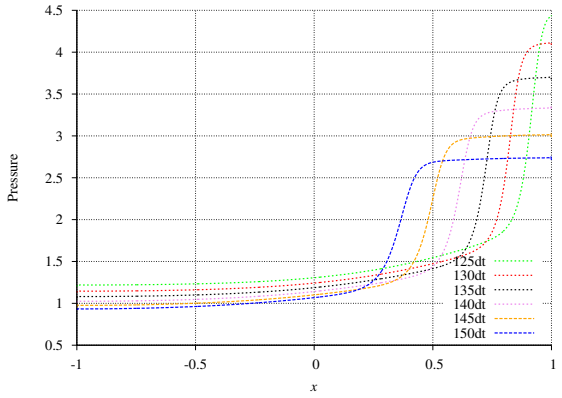

(e) S$(L_l, L_h) = (1.8, 0.2)$

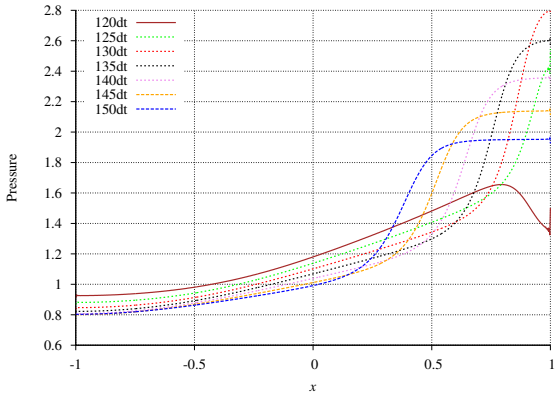

(f) $(L_l, L_h) = (1.9, 0.1)$

Figure 121: Evolution of pressure for different values of L_l and L_h; $120\Delta t \leq t \leq 150\Delta t$

V.8.2 1D normal shocks: $(L_l, L_h) = (1.0, 1.0)$ for $(p_h, p_l) = (7.58, 0.88)$, $(5.38, 0.88)$, $(3.18, 0.88)$ and comparison with experimental results

Figures 122(a)-(c) show evolution of S_r along the length of the shock tube for $0 \leq t \leq 150\Delta t$. For all three pressure ratios we observe formation of a steady shock that first reflects from the left boundary and then from the right boundary. From diaphragm to the left boundary, the shock path is a straight line whereas upon reflection the path of the shock is curved. Figures 123(a)-(c) show evolution of density along the length of the shock tube for $0 \leq t \leq 150\Delta t$. Similar evolutions of temperature θ and velocity u are shown in Figures 124(a)-(c) and 125(a)-(c). Figures 126(a)-(c), 127(a)-(c), 128(a)-(c) show evolution of pressure along the length of the tube for the three pressure ratios for $\Delta t \leq t \leq 150\Delta t$. For all three pressure ratios we have steady propagating shock that reflects from both boundaries. Table 2 presents a summary of the computed pressures and a comparison with the experimental data for the three pressure ratios. Shock relations in the table refer to pressure values ahead of the shock and behind the shock. The pressure values at the left boundary due to shock reflection result in evolution of pressure between p_{min} and p_{max} range for all three values of pressure ratios p_h/p_l. We note that the computed pressure values upon shock reflection are precisely at the left boundary whereas the measured values are away from the left boundary. We also remark that measured values may have a margin of error. For example, for p_h of 5.38 the measured pressure behind the shock is 2.35 whereas for p_h of 7.58 it is 2.31. This is inconsistent, as we expect the pressure behind the shock for $p_h = 5.38$ to be lower than that for $p_h = 7.58$. The computed values of the pressure behind the shock are consistent. They show progressively diminishing value of pressure behind the shock for progressively reduced p_h. The computed ranges of (p_{min}, p_{max}) for all these values of p_h are consistent as well. They show progressively reducing (p_{max}, p_{min}) range with progressively reducing p_h value.

Table 3: Computed and Measured Pressure Values

Pressure Ratio $(p_h, p_l) = (7.58, 0.88)$			
Shock relations		Pressure at left boundary	
Computed	Measured (Location A)	Computed	Measured (Location B)
(0.88, 2.36)	(0.88, 2.31)	$p_{max} = 7.41$ $p_{min} = 3.68$	4.00
Pressure Ratio $(p_h, p_l) = (5.38, 0.88)$			
Shock relations		Pressure at left boundary	
Computed	Measured (Location A)	Computed	Measured (Location B)
(0.88, 2.04)	(0.88, 2.35)	$p_{max} = 5.28$ $p_{min} = 2.70$	3.97
Pressure Ratio $(p_h, p_l) = (3.18, 0.88)$			
Shock relations		Pressure at left boundary	
Computed	Measured (Location A)	Computed	Measured (Location B)
(0.88, 1.62)	(0.88, 1.81)	$p_{max} = 3.12$ $p_{min} = 1.71$	3.64

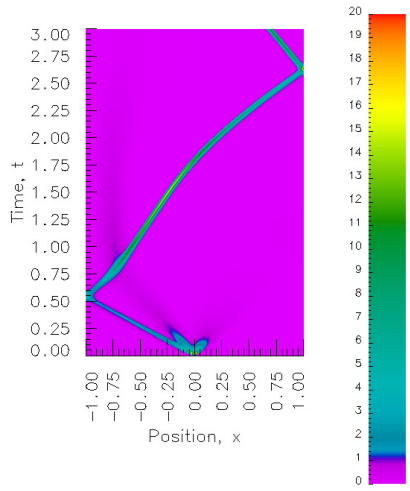

(a) $S_r, (L_l, L_h) = (1.0, 1.0), (p_h, p_l) = (7.58, 0.88)$

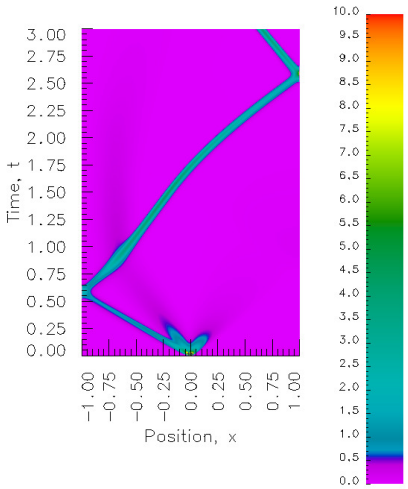

(b) $S_r, (L_l, L_h) = (1.0, 1.0), (p_h, p_l) = (5.38, 0.88)$

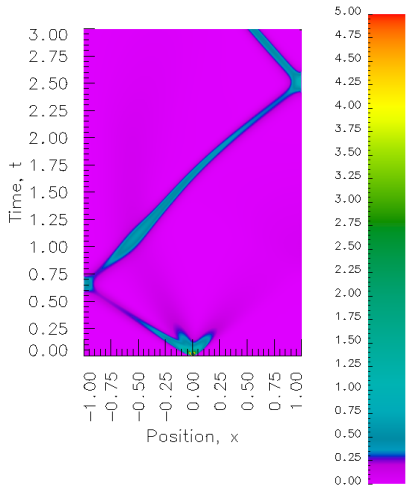

(c) $S_r, (L_l, L_h) = (1.0, 1.0), (p_h, p_l) = (3.18, 0.88)$

Figure 122: Evolution of rate of entropy production S_r for different pressure ratios

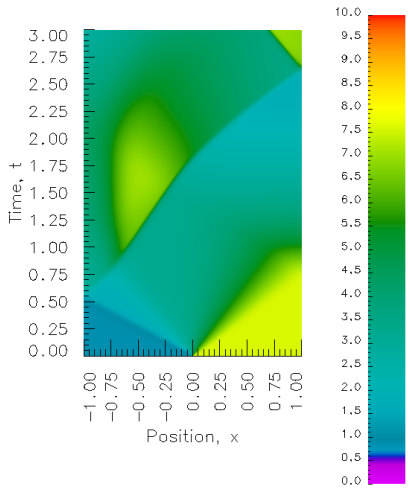

(a) $\rho, (L_l, L_h) = (1.0, 1.0)$,$(p_h, p_l) = (7.58, 0.88)$

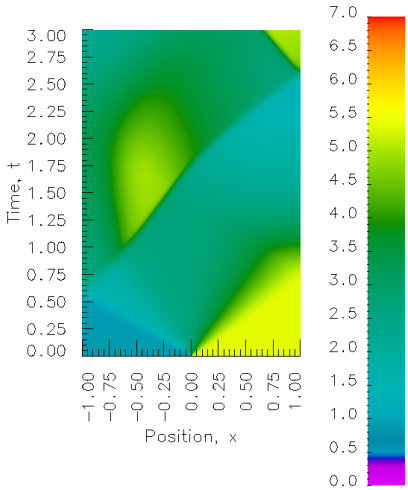

(b) $\rho, (L_l, L_h) = (1.0, 1.0)$,$(p_h, p_l) = (5.38, 0.88)$

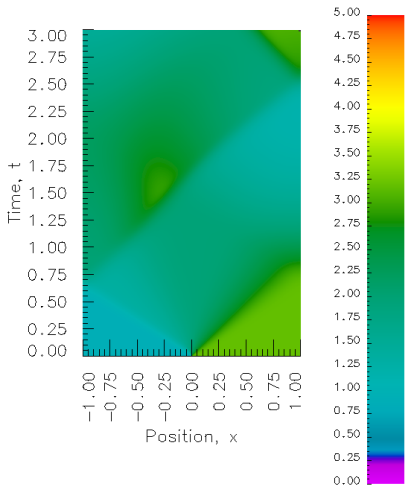

(c) $\rho, (L_l, L_h) = (1.0, 1.0)$,$(p_h, p_l) = (3.18, 0.88)$

Figure 123: Evolution of density ρ for different pressure ratios

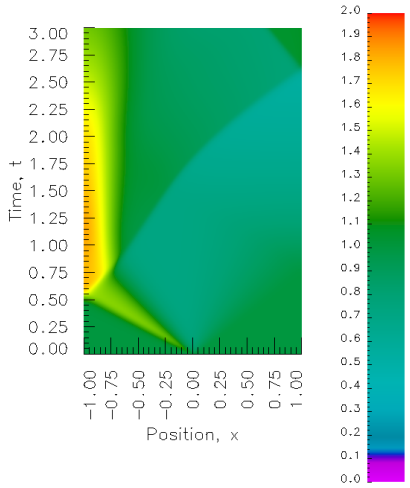

(a) $\theta, (L_l, L_h) = (1.0, 1.0)$,$(p_h, p_l) = (7.58, 0.88)$

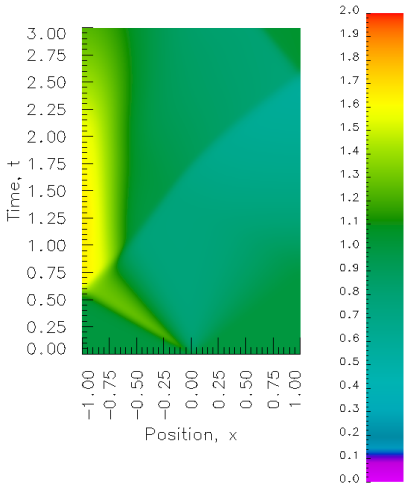

(b) $\theta, (L_l, L_h) = (1.0, 1.0)$,$(p_h, p_l) = (5.38, 0.88)$

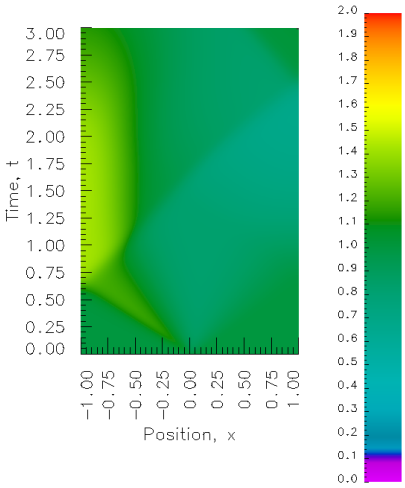

(c) $\theta, (L_l, L_h) = (1.0, 1.0)$,$(p_h, p_l) = (3.18, 0.88)$

Figure 124: Evolution of temperature θ for different pressure ratios

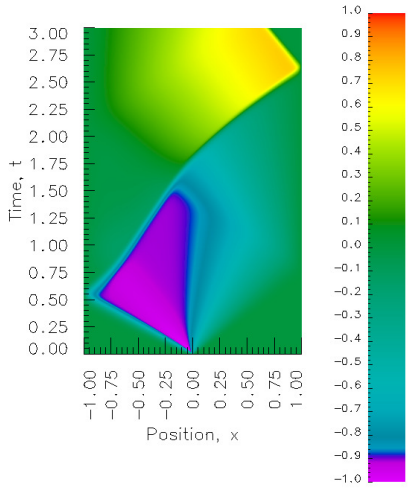

(a) $u, (L_l, L_h) = (1.0, 1.0)$,$(p_h, p_l) = (7.58, 0.88)$

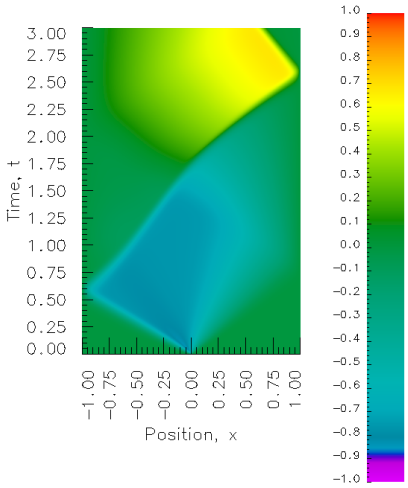

(b) $u, (L_l, L_h) = (1.0, 1.0)$,$(p_h, p_l) = (5.38, 0.88)$

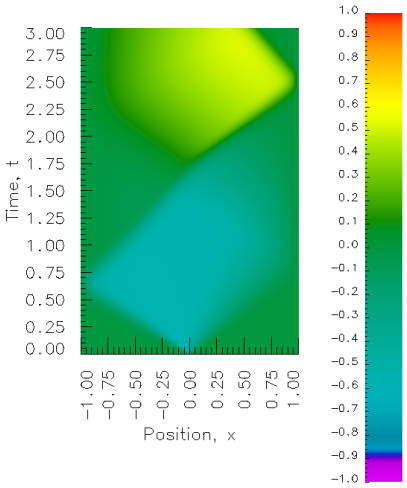

(c) $u, (L_l, L_h) = (1.0, 1.0)$,$(p_h, p_l) = (3.18, 0.88)$

Figure 125: Evolution of velocity u for different pressure ratios

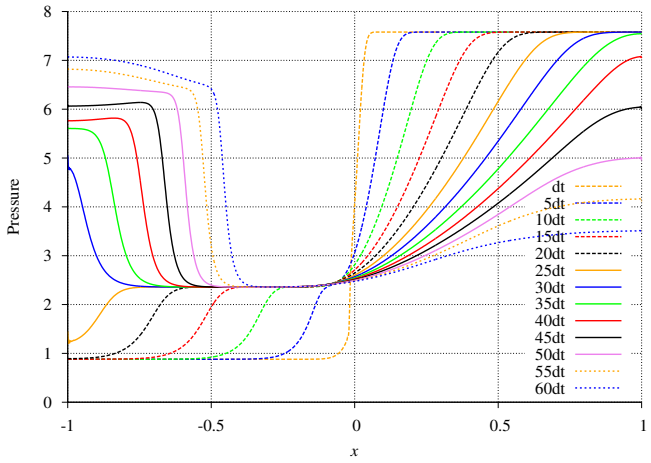

(a) $\Delta t \leq t \leq 60\Delta t$

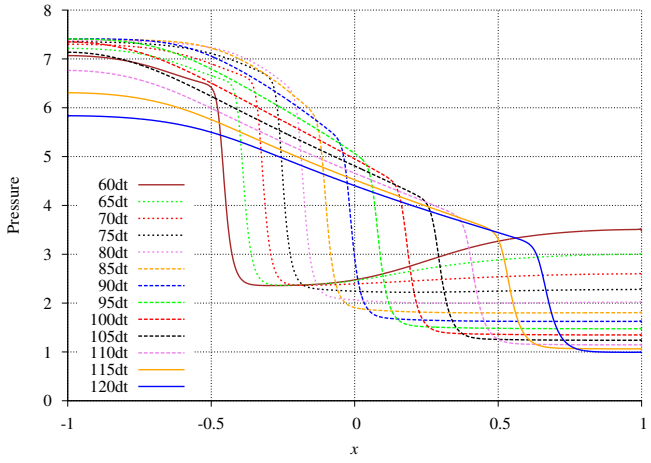

(b) $60\Delta t \leq t \leq 120\Delta t$

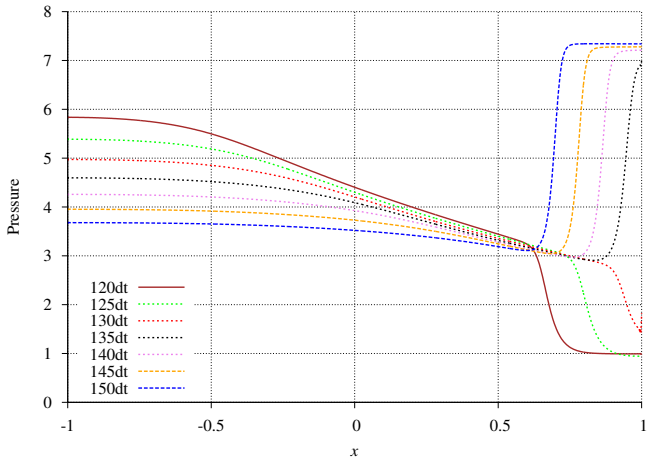

(c) $120\Delta t \leq t \leq 150\Delta t$

Figure 126: Evolution of pressure; $(p_h, p_l) = (7.58, 0.88)$, $(L_h, L_l) = (1, 1)$

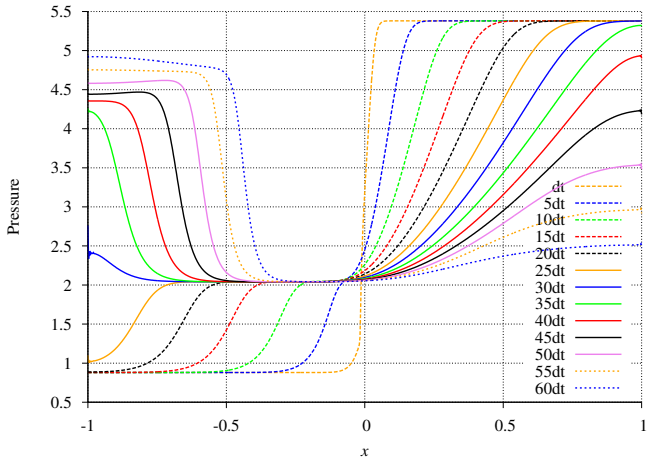

(a) $\Delta t \leq t \leq 60\Delta t$

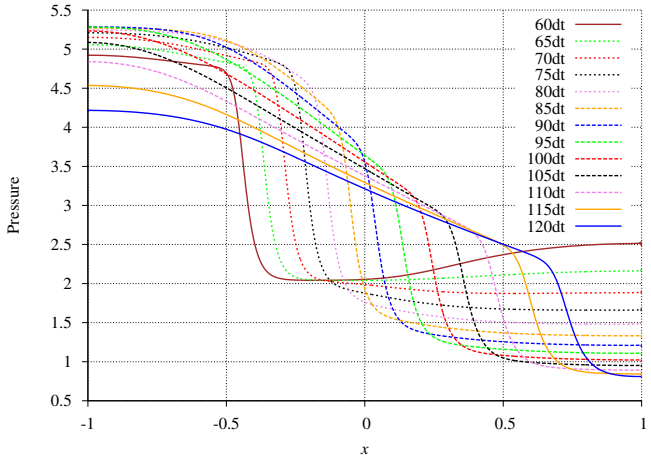

(b) $60\Delta t \leq t \leq 120\Delta t$

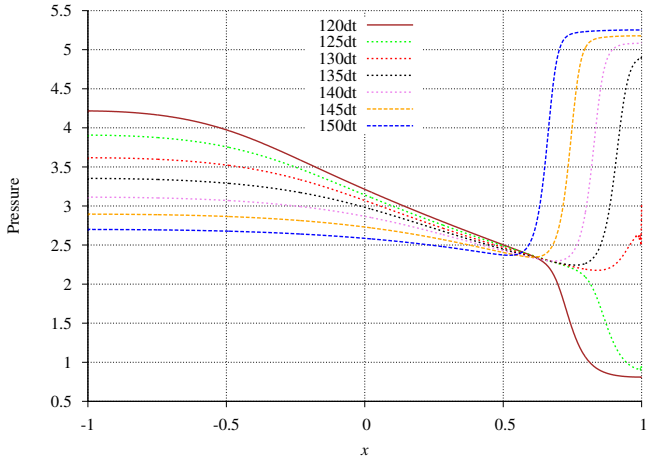

(c) $120\Delta t \leq t \leq 150\Delta t$

Figure 127: Evolution of pressure; $(p_h, p_l) = (5.38, 0.88)$, $(L_h, L_l) = (1, 1)$

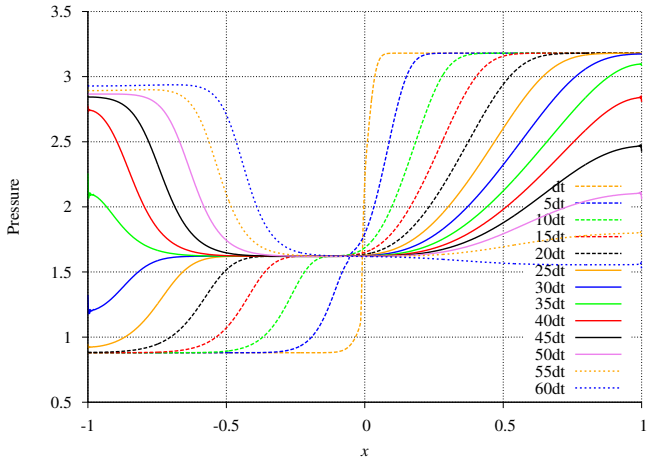

(a) $\Delta t \leq t \leq 60\Delta t$

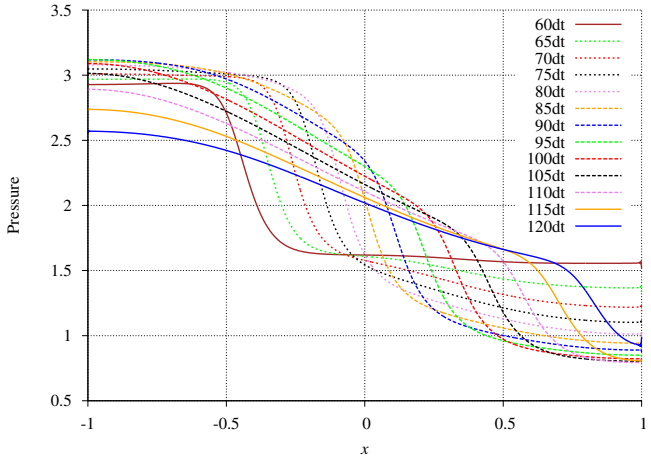

(b) $60\Delta t \leq t \leq 120\Delta t$

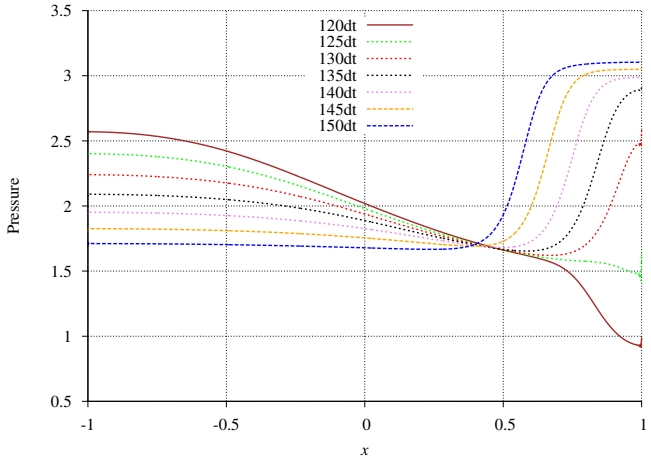

(c) $120\Delta t \leq t \leq 150\Delta t$

Figure 128: Evolution of pressure; $(p_h, p_l) = (3.18, 0.88)$, $(L_h, L_l) = (1, 1)$

We discuss computed solutions and correlation with experimental results.

(i) We note that in the numerical simulations the impermeable boundaries are theoretical. This is virtually impossible to achieve in the experimental set up, thus we expect the left and right boundary in the experimental setup to be compliant. This has the influence of lowering the maximum pressure values due to shock reflection.

(ii) We also observe some inconsistency in the experimental data. For example, the shock relation $(0.88, 2.35)$ for $p_h = 5.38$ is inconsistent with $(0.88, 2.31)$ for $p_h = 7.58$. Naturally, the pressure behind the shock wave for $p_h = 7.58$ should be greater than that for $p_h = 5.38$.

(iii) We also observe that the measured pressure at location B for $p_h/p_l = 3.18/0.88$ is 3.64 which is greater than 3.18. This is obviously not possible.

(iv) All computed solutions are consistent.

  (a) Shock relations $(0.88, 2.36)$, $(0.88, 2.04)$, $(0.88, 1.62)$ for $p_h = 7.58$, 5.38, and 3.18 show consistently reduced pressure $(2.36, 2.04, 1.62)$ behind the shock as expected.

  (b) Maximum pressure values at the left boundary due to shock reflection: 7.41, 5.28, 3.12 have progressively reduced values that are lower than corresponding pressure values in the high pressure region: $p_h = 7.58$, 5.38, and 3.18. This is consistent.

(v) Overall, the experimentally measured values are in reasonable agreement considering the extreme difficulty of achieving theoretical conditions in designing the experiment.

(vi) We remark that since the fully developed shock relations in the experiment and in the numerical simulations do not precisely agree, this naturally will influence the pressure values of the reflected shock waves in the experiment and the simulation as we note in Table 2.

V.9 Summary, concluding remarks, significance and impact of this research

In this work numerical simulation of 1D normal shocks in single diaphragm Riemann shock tube is studied and comparison with experimental measurements using Reddy tube is presented. The following conclusions can be drawn from the results obtained:

(1) Two mathematical models and their dimensionless forms are presented: Model 1 is based on (ρ, u, θ, τ_{xx}, q_x) and Model 2 is based on (ρ, u, θ) as dependent variables. Model 1 consists of a system of first-order nonlinear partial differential equations based on continuity of mass, balance of linear momentum, balance of energy, and constitutive equations for τ_{xx} (deviatoric Cauchy stress) and heat vector q_x. In Model 2, the constitutive equations are substituted in the momentum and energy equations resulting in three partial differential equations containing up to second-order spatial derivatives of u and θ. Model 2 is meritorious but it requires higher-order global differentiability of approximations used in space and time compared to Model 1.

(2) In the present work, Model 2 is used in space-time finite element formulation for a time strip corresponding to a time increment Δt based on minimization of the residual functional. Local approximations of class C^1 in space and time with p-level of 11 in space and time are used. Evolution is computed by time marching. With these choices of p-level and 101 element discretization for a dimensionless domain of two units, the maximum residual of the order of $O(10^{-6})$ or lower is obtained during the iterative solution procedure. The residual functional for each space-time strip is $O(10^{-6})$ or lower, confirming good accuracy of the computed solution.

(3) A number of numerical studies are presented for pressure ratios $(p_h, p_l) = (7.58, 0.88)$, $(5.38, 0.88)$, $(3.18, 0.88)$. For pressure ratio $(p_h, p_l) = (7.58, 0.88)$, the influence of the length of high pressure side on shock relations and the maximum pressure value upon shock reflection is investigated using $(L_l, L_h) = (1.0, 1.0)$, $(1.25, 0.75)$, $(1.5, 0.5)$, $(1.7, 0.3)$, $(1.8, 0.2)$, and $(1.9, 0.1)$. For $0.2 \leq L_h \leq 1.0$, the shock relations remain the same regardless of the choice of L_h. However, the

pressure evolution at the left boundary is affected significantly. As expected, larger values of L_h yield higher reflected pressures at the left boundary due to larger volume of high pressure air. For $L_h = 0.1$, we observe lack of shock formation as for this choice the steepening of compression wave can not overcome the diffusive process due to viscosity. The evolution of pressure differs significantly for different choices of L_h, specially for $t > 60\Delta t$. Rate of entropy production evolutions presented in the work ensure existence of a shock or lack of one.

(4) Three pressure ratios (high, medium, and low) are chosen based on experimental data. Numerical simulations show that for all three pressure ratios we have a sustained shock that propagates, reflects, and interacts for $(L_l, L_h) = (1.0, 1.0)$. This choice of lengths of low and high pressure sides are based on the experimental setup. The results shown graphically and in tabular form confirm that the numerical simulations are consistent i.e. high and low values of various quantities at various locations occur as expected.

(5) Overall the comparisons of the computed solutions with the measured pressure data for shock relations and pressure upon the first reflection are in good agreement. Minor inconsistencies in the measured pressure data are observed and are discussed. These are unavoidable in a sensitive and complex experiment in which it may not be possible to create precise theoretical conditions in the experimental set up or vice versa.

(6) Numerical studies were also conducted using Model 1, a system of first order partial differential equations with local approximations of class C^1 in space and time and p-level of 11 in space and time for all dependent variables. In this case, all space-time integrals are Riemann. The residual functional values of the order of $O(10^{-6})$ (similar to those for Model 2) confirm that in this case, the governing differential equations (GDEs) are satisfied in the the pointwise sense as the space-time integrals are Riemann. Hence, when the residual functional $I \to 0$, we are ensured that the residual function $E = A\phi_h - f \to 0$ in the pointwise sense $\forall(\boldsymbol{x}, t)$ in the space-time domain because only then $I \to 0$ can hold. An important point to note is that in Model 2 with local approximations of class C^1 in space and time, space-time integrals are Lebesgue, but in this case, I values of the same order of magnitude as in Model 1 confirm that the solutions computed using Model 2 also satisfy the GDEs in the pointwise sense. In other words, with I values of the order of $O(10^{-6})$ resulting from the discretization, p-levels and the orders of the approximation space used in Model 2, we are ensured that the space-time Lebesgue integrals approach space-time Riemann integrals. This deduction is critical in confirming that the solutions computed from Model 2 reported indeed satisfy the GDEs in the pointwise sense with good precision (due to residual functional of the order of $O(10^{-6})$).
The numerical solutions reported here are not compared with finite difference and finite volume solutions. Convergence of the numerically computed solutions (discretization and order of truncation error independence of the computed solutions) in these methods only implies that the computed solutions do not change any more with further mesh refinement or by increasing truncation error order. It is only by substituting the computed solutions in the non-discretized GDEs that we can be sure that the computed solutions indeed are the solutions of GDEs as well as establish their proximity to the theoretical solution. In these methods we have discrete numerical values at the grid points that are computed based on discretized form of the GDEs. Thus, in these methods, there is no mechanism to check if the computed solutions satisfy non-discretized GDEs $\forall(\boldsymbol{x}, t)$ in the space-time domain. In the STLSP presented and used in this work, we indeed show that GDEs are satisfied in the pointwise sense with high precision. Computations are time marched only when sufficiently high accuracy of the computed solution is achieved for the current space-time strip. This ensures accuracy of the solution for the entire evolution. Thus, comparisons with finite difference and finite volume solutions is not very meaningful, hence not included here.

In this research work, evolution, propagation, reflection, interaction and repeated reflection of 1D normal shocks in Riemann shock tube and comparisons with experimental data are presented. A very significant aspect of the work is that it simulates the first compression wave and piling up of subsequent compression waves behind it that eventually results in fully formed shock which then propagates, reflects, interacts and experiences repeated reflections. Space-time coupled finite element processes with time marching with local approximations in $H^{k,p}(\Omega^n_{xt})$ spaces permitting higher order global differentiability in space and time are used for each space-time strip. Integrals are maintained in Riemann sense by choosing appropriate order of the approximation space in space and time. This is an essential feature that ensures that when the integrated sum of squares residuals (I) for each space-time strip approaches zero, the GDEs are satisfied in the pointwise sense, hence ensure true solutions of the GDEs. This work shows the strength and significance of hpk framework and variationally consistent integral forms, for IVPs in this case (and

BVPs in other areas of research presented in this report) that has been part of the ongoing research in computational mathematics during this grant.

Final remarks

During this three year time period of the grant, five major areas listed under I–V have been investigated. Summary and conclusions resulting from this research, its impact and significance have been described at the end of each section in italics. Comments and in some cases, preliminary details, are also provided for future research. In each of the five major areas of research, model problems and their numerical solutions are presented to illustrate the features of the mathematical models and their applications. Computational mathematics frame for obtaining numerical solutions of the BVPs and IVPs in these areas is based on hpk finite element method with variationally consistent integral forms in which the space or space-time local approximations are in $H^{k,p}(\bar{\Omega}^e)$ or $H^{k,p}(\bar{\Omega}^e_{xt})$ scalar product spaces. These spaces permit higher order global differentiability local approximations that are necessary to ensure integrals over the discretizations in the Riemann sense, so that when the integrated sum of squares of the residuals (I) approaches zero for the whole discretization we are ensured that the GDEs are satisfied in the pointwise sense. Variationally consistent integral forms (in space or space-time) yield unconditionally stable computational processes for all BVPs and IVPs.

References

[1] K. S. Surana and P. W. Tenpas. k-version of Finite Element Method: A new Mathematical and Computational framework for BVPs and IVPs. *Report submitted to AFOSR / DEPSCoR: Computational Mathematics Division of AFOSR under Grant number: F49620-03-0298*, 2006.

[2] K. S. Surana, A. Romkes, and J. N. Reddy. Ordered Rate Constitutive Theories: Development of Rate Constitutive Equations for Solids, Liquids and Gases. *Report submitted to ARO: Mathematical Sciences Division under STIR Grant number: W911NF-09-1-0548(FED0065623)*, 2010.

[3] K. S. Surana, A. R. Ahmadi, , and J. N. Reddy. The k-Version of Finite Element Method for Self-Adjoint Operators in BVPs. *Int. J. Comp. Eng. Sci. and Sci.*, 3:155–218, 2002.

[4] K. S. Surana, A. R. Ahmadi, , and J. N. Reddy. The k-Version of Finite Element Method for Non-Self Adjoint Operators in BVPs. *Int. J. Comp. Eng. Sci. and Sci.*, 4:737–812, 2003.

[5] K. S. Surana, A. R. Ahmadi, , and J. N. Reddy. The k-Version of Finite Element Method for Non-Linear Operators in BVPs. *Int. J. Comp. Eng. Sci. and Sci.*, 5:133–207, 2004.

[6] K. S. Surana, S. Allu, P. W. Tenpas, and J. N. Reddy. k-Version of Finite Element Method in Gas Dynamics: Higher Order Global Differentiability Numerical Solutions. *Int. J. Numer. Meth in Engg.*, 69:1109–1157, 2006.

[7] K. S. Surana, S. Allu, , and J. N. Reddy. The k-Version of Finite Element Method for Initial Value Problems: Mathematical and Computational Framework. *Int. J. Comp. Eng. Sci. and Mech.*, 8:123–136, 2006.

[8] T. J. R. Hughes, M. Mallet, and A. Mizukami. A New Finite Element Formulation for Computational Fluid Dynamics: II. Beyond SUPG. *Comput. Meth. Appl. Mech. Eng.*, 54:341–355, 1986.

[9] T. J. R. Hughes and M. Mallet. A New Finite Element Formulation for Computational Fluid Dynamics: IV. A Discontinuity Capturing Operator for Multidimensional Advective-Diffusive Systems. *Comput. Meth. Appl. Mech. Eng.*, 58:329–336, 1986.

[10] Bell, B. and Surana, K. S. p-Version Least Squares Finite Element Formulation for Two-Dimensional, Incompressible, Non-Newtonian Isothermal and Non-Isothermal Fluid Flow. *International Journal for Numerical Methods in Fluids*, 18:127–162, 1994.

[11] Bell, B. and Surana, K. S. p-Version Space-Time Coupled Least Squares Finite Element Formulation for Two-Dimensional Unsteady Incompressible, Newtonian Fluid Flow. *ASME Winter Annual Meeting*, 1993.

[12] D. Winterscheidt and K. S. Surana. p-Version Least Squares Finite Element Formulation for Two-dimensional, Incompressible Fluid Flow. *Int. J. Numer. Methods Fluids*, 18:43–69, 1994.

[13] Todd, J. A. Ternary Quadratic Types. *Philosophical Transactions of the Royal Society of London. Series A: Mathematical and Physical Sciences*, 241:399–456, 1948.

[14] Prager, W. Strain Hardening under Combined Stresses. *Journal of Applied Physics*, 16:837–840, 1945.

[15] Reiner, M. A Mathematical Theory of Dilatancy. *American Journal of Mathematics*, 67:350–362, 1945.

[16] Rivlin, R. S. and Ericksen, J. L. Stress-Deformation Relations for Isotropic Materials. *Journal of Rational Mechanics and Analysis*, 4:323–425, 1955.

[17] Rivlin, R. S. Further Remarks on the Stress-Deformation Relations for Isotropic Materials. *Journal of Rational Mechanics and Analysis*, 4:681–702, 1955.

[18] Eringen, A. C. *Nonlinear Theory of Continuous Media*. McGraw-Hill, 1962.

[19] Eringen, A. C. *Mechanics of Continua*. John Wiley and Sons, 1967.

[20] Wang, C. C. On Representations for Isotropic Functions, Part I. *Archive for Rational Mechanics and Analysis*, 33:249, 1969.

[21] Wang, C. C. A New Representation Theorem for Isotropic Functions, Part I and Part II. *Archive for Rational Mechanics and Analysis*, 36:166–223, 1970.

[22] Wang, C. C. Corrigendum to 'Representations for Isotropic Functions'. *Archive for Rational Mechanics and Analysis*, 43:392–395, 1971.

[23] Spencer, A. J. M. and Rivlin, R. S. The Theory of Matrix Polynomials and its Application to the Mechanics of Isotropic Continua. *Archive for Rational Mechanics and Analysis*, 2:309–336, 1959.

[24] Spencer, A. J. M. and Rivlin, R. S. Further Results in the Theory of Matrix Polynomials. *Archive for Rational Mechanics and Analysis*, 4:214–230, 1960.

[25] Spencer, A. J. M. *Theory of Invariants*. Chapter 3 'Treatise on Continuum Physics, I' Edited by A. C. Eringen, Academic Press, 1971.

[26] Smith, G. F. On a Fundamental Error in two Papers of C.C. Wang, 'On Representations for Isotropic Functions, Part I and Part II'. *Archive for Rational Mechanics and Analysis*, 36:161–165, 1970.

[27] Smith, G. F. On Isotropic Functions of Symmetric Tensors, Skew-Symmetric Tensors and Vectors. *International Journal of Engineering Science*, 9:899–916, 1971.

[28] Boehler, J. P. On Irreducible Representations for Isotropic Scalar Functions. *Journal of Applied Mathematics and Mechanics / Zeitschrift für Angewandte Mathematik und Mechanik*, 57:323–327, 1977.

[29] Zheng, Q. S. On Transversely Isotropic, Orthotropic and Relatively Isotropic Functions of Symmetric Tensors, Skew-Symmetric Tensors, and Vectors. *International Journal of Engineering Science*, 31:1399–1453, 1993.

[30] Zheng, Q. S. On the Representations for Isotropic Vector-Valued, Symmetric Tensor-Valued and Skew-Symmetric Tensor-Valued Functions. *International Journal of Engineering Science*, 31:1013–1024, 1993.

[31] Surana, K. S. *Advanced Mechanics of Continua*. CRC/Tayler and Francis, 2014.

[32] Wang, C. C. On Representations for Isotropic Functions, Part II. *Archive for Rational Mechanics and Analysis*, 33:268, 1969.

[33] K. S. Surana, T. Moody, and J. N. Reddy. Ordered Rate Constitutive Theories in Lagrangian Description for Thermoviscoelastic Solids without Memory. *Acta Mechanica*, 224:2785–2816, 2013.

[34] K. S. Surana, T. Moody, and J. N. Reddy. Rate Constitutive Theories of Order Zero in Lagrangian Description for Thermoviscoelastic Solids. *Mechanics of Advanced Materials and Structures (DOI: 10.1080/15376494.2013.778617)*, 2014.

[35] K. S. Surana, J. N. Reddy, and D. Nunez. Ordered Rate Constitutive Theories for Thermoviscoelastic Solids without Memory in Lagrangian Description using Gibbs Potential. *Journal of Continuum Mechanics and Thermodynamics (DOI 10.1007/s00161-014-0366-5)*, 2015.

[36] Surana, K. S., Nunez, D., Reddy, J. N., and Romkes, A. Rate Constitutive Theory for Ordered Thermoviscoelastic Fluids - Polymers. *Journal of Continuum Mechanics and Thermodynamics*, 26:143–181, 2014.

[37] K. S. Surana, D. Nunez, and J. N. Reddy. Giesekus Constitutive Model for Thermoviscoelastic Fluids based on Ordered Rate Constitutive Theories. *Research Updates in Polymer Science*, 2:232–260, 2013.

[38] K. S. Surana, T. Moody, and J. N. Reddy. Ordered Rate Constitutive Theories in Lagrangian Description for Thermoviscoelastic Solids with Memory. *Acta Mechanica (DOI: 10.1007/s00707-014-1173-6)*, 2015.

[39] K. S. Surana, J. N. Reddy, and D. Nunez. Ordered Rate Constitutive Theories for Thermoviscoelastic Solids with Memory in Lagrangian Description using Gibbs Potential. *Journal of Continuum Mechanics and Thermodynamics (DOI 10.1007/s00161-014-0395-0)*, 2015.

[40] Adhikari, S. *Damping Models for Structural Vibration*. Ph.D. Dissertation, The University of Cambridge, 2000.

[41] Surana, K. S., Ahmadi, A. R. and Reddy, J. N. The k-Version of Finite Element Method for Self-Adjoint Operators in BVPs. *International Journal of Computational Engineering Science*, 3(2):155–218, 2002.

[42] Surana, K. S., Ahmadi, A. R. and Reddy, J. N. The k-Version of Finite Element Method for Non-Self-Adjoint Operators in BVPs. *International Journal of Computational Engineering Sciences*, 4(4):737–812, 2003.

[43] Surana, K. S., Ahmadi, A. R. and Reddy, J. N. The k-Version of Finite Element Method for Non-Linear Operators in BVPs. *International Journal of Computational Engineering Science*, 5(1):133–207, 2004.

[44] Surana, K. S., Reddy, J. N. and Allu, S. The k-Version of Finite Element Method for IVPs: Mathematical and Computational Framework. *International Journal for Computational Methods in Engineering Science and Mechanics*, 8(3):123–136, 2007.

[45] Surana, K. S., Allu, S. and Reddy, J. N. and Tenpas, P. W. Least Squares Finite Element Processes in h, p, k Mathematical and Computational Framework for a Non-Linear Conservation Law. *International Journal of Numerical Methods in Fluids*, 57(10):1545–1568, 2008.

[46] CW Hirt, Anthony A Amsden, and JL Cook. An arbitrary lagrangian-eulerian computing method for all flow speeds. *Journal of Computational Physics*, 14(3):227–253, 1974.

[47] W.F. Noh. Cel: A time-dependent, two-space dimensional coupled eulerian–lagrangian code. *Methods in Computational Physics*, page 117, 1964.

[48] J Donea, S Giuliani, and J Halleux. An arbitrary lagrangian-eulerian finite element method for transient dynamic fluid-structure interactions. *Computer Methods in Applied Mechanics and Engineering*, 33:689–723, 1982.

[49] Wing Kam Liu and Hsiu Guo Chang. A method of computation for fluid structure interaction. *Computers & Structures*, 20(1):311–320, 1985.

[50] Wing Kam Liu, Ted Belytschko, and Herman Chang. An arbitrary lagrangian-eulerian finite element method for path-dependent materials. *Computer Methods in Applied Mechanics and Engineering*, 58(2):227–245, 1986.

[51] Thomas JR Hughes, Wing Kam Liu, and Thomas K Zimmermann. Lagrangian-eulerian finite element formulation for incompressible viscous flows. *Computer methods in applied mechanics and engineering*, 29(3):329–349, 1981.

[52] T.E. Tezduyar, M. Behr, and J. Liou. A new strategy for finite element computations involving moving boundaries and interfaces: I. the concept and the preliminary numerical tests. *Computer Methods in Applied Mechanics and Engineering*, 94:339–351, 1992.

[53] TE Tezduyar, MITTAL Behr, S Mittal, and J Liou. A new strategy for finite element computations involving moving boundaries and interfacesâĂŤthe deforming-spatial-domain/space-time procedure: Ii. computation of free-surface flows, two-liquid flows, and flows with drifting cylinders. *Computer methods in applied mechanics and engineering*, 94(3):353–371, 1992.

[54] T Tezduyar and R Benney. Mesh Moving Techniques for Fluid-Structure Interactions with Large Displacements. *Journal of Applied Mechanics*, 70(1):58–63, 2003.

[55] Jean Donea, Antonio Huerta, J-Ph Ponthot, and Antonio Rodríguez-Ferran. Arbitrary lagrangian–eulerian methods. *Encyclopedia of computational mechanics*, 2004.

[56] Tayfun E Tezduyar, Sunil Sathe, Ryan Keedy, and Keith Stein. Space–time finite element techniques for computation of fluid–structure interactions. *Computer Methods in Applied Mechanics and Engineering*, 195(17):2002–2027, 2006.

[57] Wing Kam Liu, Chang Herman, Chen Jiun-Shyan, and Belytschko Ted. Arbitrary lagrangian-eulerian petrov-galerkin finite elements for nonlinear continua. *Computer Methods in Applied Mechanics and Engineering*, 68(3):259–310, 1988.

[58] Wing Kam Liu, Jiun-Shyan Chen, Ted Belytschko, and Yi Fei Zhang. Adaptive ale finite elements with particular reference to external work rate on frictional interface. *Computer methods in applied mechanics and engineering*, 93(2):189–216, 1991.

[59] S. Piperno and C. Farhat. Design and evaluation of staggered partitioned procedures for fluid-structure interaction simulations. *INRIA*, 3241, 1997.

[60] M Souli, A Ouahsine, and L Lewin. Ale formulation for fluid–structure interaction problems. *Computer methods in applied mechanics and engineering*, 190(5):659–675, 2000.

[61] Jing Li, Charbel Farhat, Philip Avery, and Radek Tezaur. A dual-primal feti method for solving a class of fluid–structure interaction problems in the frequency domain. *International Journal for Numerical Methods in Engineering*, 89(4):418–437, 2012.

[62] Marco Arienti, Patrick Hung, Eric Morano, and Joseph E Shepherd. A level set approach to eulerian–lagrangian coupling. *Journal of Computational Physics*, 185(1):213–251, 2003.

[63] V Sankaran, J Sitaraman, B Flynt, and C Farhat. Development of a coupled and unified solution method for fluid-structure interactions. In *Computational Fluid Dynamics 2008*, pages 147–152. Springer, 2009.

[64] C Farhat, A Rallu, K Wang, and T Belytschko. Robust and provably second-order explicit–explicit and implicit–explicit staggered time-integrators for highly non-linear compressible fluid–structure interaction problems. *International Journal for Numerical Methods in Engineering*, 84(1):73–107, 2010.

[65] Kevin Wang, Arthur Rallu, J-F Gerbeau, and Charbel Farhat. Algorithms for interface treatment and load computation in embedded boundary methods for fluid and fluid–structure interaction problems. *International Journal for Numerical Methods in Fluids*, 67(9):1175–1206, 2011.

[66] Jón Tómas Grétarsson, Nipun Kwatra, and Ronald Fedkiw. Numerically stable fluid–structure interactions between compressible flow and solid structures. *Journal of Computational Physics*, 230(8):3062–3084, 2011.

[67] David Amsallem and Charbel Farhat. On the stability of linearized reduced-order models: Descriptor vs non-descriptor form and application to fluid-structure interaction. *American Institute of Aeronautics and Astronautics*, 2012.

[68] K Wang, J Grétarsson, A Main, and C Farhat. Computational algorithms for tracking dynamic fluid–structure interfaces in embedded boundary methods. *International Journal for Numerical Methods in Fluids*, 70(4):515–535, 2012.

[69] Bird, R. B., Armstrong, R. C., and Hassager, O. *Dynamics of Polymeric Liquids, Volume 1, Fluid Mechanics, Second Edition*. John Wiley and Sons, 1987.

[70] Surana, K. S., MA, Y., Reddy, J. N. and Romkes, A. The Rate Constitutive Equations and their Validity for Progressively Increasing Deformation. *Mechanics of Advanced Materials and Structures*, 17:509–533, 2010.

[71] Bird, R. B., Armstrong, R. C., and Hassager, O. *Dynamics of Polymeric Liquids, Volume 2, Kinetic theory, Second Edition*. John Wiley and Sons, 1987.

[72] C. Bodart and M.J. Crochet. The Time Dependent Flow of a Viscoelastic Fluid Around a Sphere. *Journal of Non-Newtonian Fluid Mechanics*, 54:303–329, 1994.

[73] Quinzani, L. M., Armstrong, R. C. and Brown, R. A. Use of Coupled Birefringence and LDV Studies of Flow Through a Planar Contraction to Test Constitutive Equations for Concentrated Polymer Solutions. *Journal of Rheology*, 39(6):1201–1227, 1995.

[74] K. R. Rajagopal and L. Tao. *Mechanics of Mixtures*. World Scientific, River Edge, NJ, 1995.

[75] M. Massoudi and A. Briggs and C. C. Hwang. Flow of a dense particulate mixture using a modified form of the mixture theory. *Particulate Science and Technology*, 17:1–27, 1999.

[76] Mehrdad Massoudi. Constitutive relations for the interaction force in multicomponent particulate flows. *International Journal of Non-Linear Mechanics*, 38:313–336, 2003.

[77] John W. Cahn and John E. Hilliard. Free Energy of a Nonuniform System. I. Interfacial Free Energy. *The Journal of Chemical Physics*, 28(2):1015–1031, 1958.

[78] Lev D. Landau and Evgenij Michailovič Lifšic and Lev P. Pitaevskij. *Statistical Physics: Course of Theoretical Physics*. Pergamon Press plc, London, 1980.

[79] K.S. Surana and J.N. Reddy. *Mathematics of computations and finite element method for initial value problems*. Book manuscript in progress, 2014.

[80] T. Belytschko and T.J.R. Hughes. *Computational Methods in Mechanics*. North Holland, 1983.

[81] B.C. Bell and K.S. Surana. A space-time coupled p-version LSFEF for unsteady fluid dynamics. *International Journal of Numerical Methods in Engineering*, 37:3545–3569, 1994.

[82] J. Stefan. *Ober einige Probleme der Theorie der Warmeleitung*. Sitzungsber. Akad. Wiss. Wien, Math.-Naturwiss. Kl., 1889.

[83] L.I. Rubinstein. *The Stefan Problem*. American Mathematical Society, Providence, Twenty Seventh edition, 1994.

[84] H.S. Carslaw and J.S. Jaeger. *Conduction of Heat in Solids*. Oxford University Press, New York, second edition, 1959.

[85] K. Krabbenhoft and L. Damkilde and M. Nazem. An Implicit Mixed Enthalpy-Temperature Method for Phase-Change Problems. *Heat Mass Transfer*, 43:233–241, 2007.

[86] Sin Kim and Min Chan Kim and Won-Gee Chun. A Fixed Grid Finite Control Volume Model for the Phase Change Heat Conduction Problems with a Single-Point Predictor-Corrector Algorithm. *Korean J. Chem. Eng.*, 18(1):40–45, 2001.

[87] V.R. Voller and M. Cross and N. C. Markatos. An enthalpy method for convection/diffusion phase change. *International Journal for Numerical Methods in Engineering*, 24(1):271–284, 1987.

[88] R. A. Lambert and R. H. Rangel. Solidification of a supercooled liquid in stagnation-point flow. *International Journal of Heat and Mass Transfer*, 46(21):4013–4021, 2003.

[89] Nabeel Al-Rawahi and Gretar Tryggvason. Numerical Simulation of Dendritic Solidification with Convection: Two-Dimensional Geometry. *Journal of Computational Physics*, 180(2):471–496, 2002.

[90] E. Pardo and D. C. Weckman. A fixed grid finite element technique for modelling phase change in steady-state conduction–advection problems. *International Journal for Numerical Methods in Engineering*, 29(5):969–984, 1990.

[91] D. M. Anderson and G. B. McFadden and A. A. Wheeler. A phase-field model of solidification with convection. *Physica D: Nonlinear Phenomena*, 135(1-2):175–194, 2000.

[92] Y. Lu and C. Beckermann and J.C. Ramirez. Three-dimensional phase-field simulations of the effect of convection on free dendritic growth. *Journal of Crystal Growth*, 280(1-2):320–334, 2005.

[93] C. Beckermann and H. J. Diepers and I. Steinbach and A. Karma and X. Tong. Modeling Melt Convection in Phase-Field Simulations of Solidification. *Journal of Computational Physics*, 154(2):468–496, 1999.

[94] Curtis M. Oldenburg and Frank J. Spera. Hybrid model for solidification and convection. *Numerical Heat Transfer Part B: Fundamentals*, 21:217–229, 1992.

[95] M. Fabbri and V.R. Voller. The Phase-Field Method in Sharp-Interface Limit: A Comparison between Model Potentials. *Journal of Computational Physics*, 130:256–265, 1997.

[96] Caginalp, G. Stefan and Hele-Shaw type models as asymptotic limits of the phase-field equations. *Phys. Rev. A*, 39:5887–5896, 1989.

[97] Caginalp, G. An analysis of a phase field model of a free boundary. *Archive of Rational Mechanics and Analysis*, 92:205–245, 1986.

[98] G. Caginalp and J. Lin. A numerical analysis of an anisotropic phase field model. *IMA Journal of Applied Mathematics*, 39:51–66, 1987.

[99] G. Caginalp and E.A. Socolovsky. Computation of sharp phase boundaries by spreading: The planar and spherically symmetric cases. *Journal of Computational Physics*, 95:85–100, 1991.

[100] Surana, K. S., Ma, Y., Romkes, A., and Reddy, J. N. Development of Mathematicasl Models and Computational Framework for Multi-physics Interaction Processes. *Mechanics of Advanced Materials and Structures*, 17:488–508, 2010.

[101] Surana, K. S., Blackwell, B., Powell, M., and Reddy, J. N. Mathematical Models for Fluid-Solid Interaction and Their Numerical Solutions. *Journal of Fluids and Structures*, (already published online), 2014, DOI: 10.1016/j.jfluidstructs.2014.06.023.

[102] K.S. Surana and J.N. Reddy. *Mathematics of computations and finite element method for boundary value problems*. Book manuscript in progress, 2014.

[103] C. Truesdell. Sulle basi della termomeccanica. *Rend. Lincei*, 22:33–38, 158–166, 1957.

[104] C. Truesdell and R. Toupin. *Handbuch der Physik*, volume 3. Springer, Berlin–Göttingen–Heidelberg, 1960.

[105] P. D. Kelly. A reacting continuum. *International Journal of Engineering Science*, 2(2):129–153, 1964.

[106] A. C. Eringen and J. D. Ingram. A continuum theory of chemically reacting media. *International Journal of Engineering Science*, 3:231–242, 1965.

[107] A. E. Green and P. M. Naghdi. A dynamical theory of interacting continua. *International Journal of Engineering Science*, 3(2):231–241, 1965.

[108] R. M. Bowen. Toward a thermodynamics and mechanics of mixtures. *Archive for Rational Mechanics and Analysis*, 24(5):370–403, 1967.

[109] R. M. Bowen. Incompressible porous media models by use of the theory of mixtures. *International Journal of Engineering Science*, 18(9):1129–1148, 1980.

[110] R. de Boer and W. Ehlers. A historical review of the formulation of porous media theories. *Acta Mechanica*, 74(1):1–8, 1988.

[111] R. de Boer and W. Ehlers. Uplift, friction and capillarity: Three fundamental effects for liquid-saturated porous solids. *International Journal of Solids and Structures*, 26(1):43–57, 1990.

[112] R. de Boer. Development of porous media theories—a brief historical review. *Transport in Porous Media*, 9:155–164, 1992.

[113] R. de Boer and S. J. Kowalski. Thermodynamics of a fluid-saturated porous media with a phase change. *Acta Mechanica*, 109:167–189, 1995.

[114] J. Bluhm and R. de Boer. The volume fraction concept in porous media theory. *Journal of Applied Mathematics and Mechanics/Zeitschrift für Angewandte Mathematik und Mechanik*, 77(8):563–577, 1997.

[115] R. de Boer. *Porous Media: Theory and Experiments*. Springer, 1999.

[116] D. A. Drew. Mathematical modeling of two-phase flow. *Annual Review of Fluid Mechanics*, 15:261–291, 1983.

[117] S. I. Rubinow and Joseph B. Keller. The transverse force on a spinning sphere moving in a viscous fluid. *Journal of Fluid Mechanics*, 11(3):447–459, 1961.

[118] H. Enwald, E. Peirano, and A. E. Almstedt. Eulerian two-phase flow theory applied to fluidization. *International Journal of Multiphase Flow*, 22:21–66, 1996.

[119] H. Enwald and A. E. Almstedt. Fluid dynamics of a pressurized fluidized bed: comparison between numerical solutions from two-fluid models and experimental results. *Chemical Engineering Science*, 54:329–342, 1999.

[120] K. Terada, T. Ito, and N. Kikuchi. Characterization of the mechanical behaviors of solid-fluid mixture by the homogenization method. *Computer Methods in Applied Mechanics and Engineering*, 153:223–257, 1998.

[121] Goodarz Ahmadi, Jianfa Cao, Lukas Schneider, and Amsini Sadiki. A thermodynamical formulation for chemically active multiphase turbulent flows. *International Journal of Engineering Science*, 44:699–720, 2006.

[122] K. R. Rajagopal, Mehrdad Massoudi, and G. Johnson. A review of interaction mechanisms in fluid-solid flows. *DOE Report*, 90/9, 1991.

[123] Ingo Müller. A thermodynamic theory of mixtures of fluids. *Archive for Rational Mechanics and Analysis*, 28(1):1–39, 1968.

[124] A. E. Green and P. M. Naghdi. A theory of mixtures. *Archive for Rational Mechanics and Analysis*, 24(4):243–263, 1967.

[125] R.J. Atkin and R.E. Craine. Continuum theories of mixtures: basic theory and historical development. *Quarterly Journal of Mechanics and Applied Mathematics*, 29(2):209–243, 1976.

[126] A. Bedford and D.S. Drumheller. Theories of immiscible and structured mixtures. *International Journal of Engineering Science*, 21(8):863–960, 1983.

[127] G. Johnson, M. Massoudi, and K.R. Rajagopal. Flow of a fluid-solid mixture between flat plates. *Chemical Engineering Science*, 46(7):1713–1723, 1991.

[128] M. Massoudi, K.R. Rajagopal, and T.X. Phuoc. On the fully developed flow of a dense particulate mixture in a pipe. *Powder Technology*, 104:258–268, 1999.

[129] Mehrdad Massoudi and C. Lakshmana Rao. Vertical flow of a mutiphase mixture in a channel. *Mathematical Problems in Engineering*, 6:505–526, 2001.

[130] Mehrdad Massoudi, P. Ravindran, and N. K. Anand. Steady free surface flow of a fluid-solid mixture down and inclined plane. *Particulate Science and Technology*, 22:253–273, 2004.

[131] K.R. Rajagopal, A. Al-Sharif, K. Chamniprasart, and A.Z. Szeri. Lubrication with binary mixtures: liquid-liquid emulsion. *Journal of Tribology*, 115(1):46–55, 1993.

[132] K.R. Rajagopal, K. Chamniprasart, A. Al-Sharif, and A.Z. Szeri. Lubrication with binary mixtures: bubbly oil. *Journal of Tribology*, 115(2):253–260, 1993.

[133] K.R. Rajagopal, S.H. Wang, A. Al-Sharif, and A.Z. Szeri. Lubrication with binary mixtures: liquid-liquid emulsion in an ehl conjunction. *Journal of Tribology*, 115(3):515–522, 1993.

[134] Mehrdad Massoudi. Boundary conditions in mixture theory and in cfd applications of higher order models. *Computers and Mathematics with Applications*, 53:156–167, 2007.

[135] Mehrdad Massoudi. A note on the meaning of mixture viscosity using the classical continuum theories of mixtures. *International Journal of Engineering Science*, 46:677–689, 2008.

[136] S. Baek and A. R. Srinivasa. Diffusion of a fluid through an elastic solid undergoing large deformation. *International Journal of Non-linear Mechanics*, 39(2):201–218, 2004.

[137] A. C. Eringen. *Nonlinear Theory of Continuous Media*. McGraw-Hill, 1962.

[138] A. C. Eringen. *Mechanics of Continua*. John Wiley and Sons, 1967.

[139] R. Sampaio and W.O. Williams. On the viscosities of liquid mixtures. *Zeitschrift für angewandte Mathematik und Physik (Journal of Applied Mathematics and Physics)*, 28(4):607–614, 1977.

[140] Bo-Nan Jiang. *The Least-Squares Finite Element Method: Theory and Applications in Computational Fluid Dynamics and Electromagnetics*. Springer, River Edge, NJ, 1998.

[141] K. S. Surana and D. G. Van Dyne. Non-weak-strong Solutions in Gas Dynamics: A C^{11} p-Version STLSFEF in Langrangian Frame of Reference using ρ, u, T Primitive Variables. *International Journal of Computational Engineering Science*, 2:357–382, 2001.

[142] K. S. Surana and D. G. Van Dyne. Non-weak-strong Solutions in Gas Dynamics: A C^{11} p-Version STLSFEF in Eulerian Frame of Reference using ρ, u, T Primitive Variables. *International Journal of Computational Engineering Science*, 2:382–423, 2001.

[143] K. S. Surana and D. G. Van Dyne. Non-weak-strong Solutions in Gas Dynamics: A C^{11} p-Version STLSFEF in Langrangian Frame of Reference using ρ, u, P Primitive Variables. *International Journal for Numerical Methods in Engineering*, 53:1025–1050, 2002.

[144] K. S. Surana and D. G. Van Dyne. Non-weak-strong Solutions in Gas Dynamics: A C^{11} p-Version STLSFEF in Eulerian Frame of Reference using ρ, u, P Primitive Variables. *International Journal for Numerical Methods in Engineering*, 53:1051–1099, 2002.

[145] Surana, K. S., Allu, S. and Tenpas, P. W. and Reddy, J. N. k-Version of Finite Element Method in Gas Dynamics: Higher Order Global Differentiability Numerical Solutions. *International Journal Numerical Methods in Engineering*, 69:1109–1157, 2006.

[146] L. Rayleigh. Aerial Plane Waves of Finite Amplitude. *Proceedings of Royal Society*, A84:247–284, 1910.

[147] G. I. Taylor. Conditions Necessary for Discontinuous Motion in Gases. *Proceedings of Royal Society*, A84:371–377, 1910.

[148] J. von Neumann and R. D. Richtmyer. A Method for Calculation of Hydrodynamic Shocks. *Journal of Applied Physics*, 21:232–237, 1950.

[149] R. Courant, K. Friedrichs, and H. Lewy. Über die Partiellen Differenzengleichungen der Methematischen Physik. *Mathendtische Annalen*, 100:32–74, 1928.

[150] J. D. Cole. On a Quasi-Linear Parabolic Equation Occurring in Aerodynamics. *Quarterly of Applied Mathematics*, 9:225–236, 1951.

[151] P. D. Lax. Weak Solutions of Non-Linear Hyperbolic Equations and their Numerical Computation. *Communications on Pure and Applied Mathematics*, 7:159–193, 1954.

[152] P. D. Lax. Hyperbolic Systems of Conservation Laws II. *Communications on Pure and Applied Mathematics*, 10:537–566, 1957.

[153] S. K. Godunov. The Problem of a Generalized Solution in the Theory of Quasilinear Equations and in Gas Dynamics. *Russian Mathematical Surveys*, 17:145–156, 1962.

[154] S. K. Godunov. Discontinuous Solutions of Hyperbolic Systems of Quasilinear Equations. *Russian Mathematical Surveys*, 15:53–111, 1960.

[155] J. L. Grimm. Solutions in the Large for Non-Linear Hyperbolic Systems of Equations. *Communications on Pure and Applied Mathematics*, 18:697–715, 1965.

[156] J. A. Smoller. On the Solution of the Riemann Problem with General Step Data for an Extended Class of Hyperbolic Systems. *Communications of Pure and Applied Mathematics*, 23:791–801, 1970.

[157] J. A. Smoller. Contact Discontinuities in Quasi-Linear Hyperbolic Systems. *Communications of Pure and Applied Mathematics*, 23:791–801, 1970.

[158] E. Hopf. On the Right Weak Solution of Cauchy Problem for a Quasilinear Equation of First Order. *Journal of Mathematics and Mechanics*, 19:483–487, 1969.

[159] K. O. Friedrichs and P. D. Lax. Systems of Conservation Equations with a Convex Extension. *Proceedings of National Academic Science*, 68:1686–1688, 1971.

[160] S. N. Kruzhkov. First Order Quasilinear Equations in Several Variables. *Mathematics of USSR Sbornik*, 10, 1970.

[161] M. S. Mock. Discrete Shocks and Genuine Nonlinearity. *Mechanics and Mathematics Journal*, 25:131–146, 1978.

[162] M. S. Mock. On Fourth-Order Dissipation and Single Conservation Laws. *Communications on Pure and Applied Mathematics*, 29:383–388, 1976.

[163] R. J. Diperna. Uniqueness of Solutions to Hyperbolic Conservation Laws. *Indiana University Mathematics Journal*, 28:137–188, 1979.

[164] B. L. Keyfitz and H. C. Kranzer. Existence and Uniqueness of Entropy Solutions to the Riemann Problem for Hyperbolic Sysetems of Two Non-Linear Conservation Laws. *Journal of Differential Equations*, 27:444–476, 1978.

[165] W. F. Noh. Errors for Calculations of Strong Shocks Using an Artificial Viscosity and an Artificial Heat Flux. *Journal of Computational Physics*, 72:78–120, 1978.

[166] R. Menikoff. Errors When Shock Waves Interact Due to Numerical Shock Width. *Journal on Science and Computation*, 15:1227–1242, 1994.

[167] K. S. Surana, T. Stone, and J. N. Reddy. Moving Mesh Strategy for Initial Value Problems. (Manuscript of the article in preparation), 2014.

[168] K. P. J. Reddy and N. Sharath. Manually Operated Piston Driven Shock Tube. *Current Science*, 104, 2013.

Copies of technical reports not previously submitted to ARO: Not applicable